Mapping RAS: Biochemical Characterization of Small GTPases, Their Modulators, Effectors, and Mimics

Dissertation

This dissertation is submitted for the degree of Dr.rer.nat.

to the Faculty of Mathematics and Natural Sciences at the

Heinrich Heine University Düsseldorf

Presented by

Amin Mirzaiebadizi

From

Kerman, Iran

Düsseldorf, May 2025

From the Institute of Biochemistry and Molecular Biology II

At the Heinrich Heine University Düsseldorf

Published by permission of the

Faculty of Mathematics and Natural Sciences

At the Heinrich Heine University Düsseldorf

1st Supervisor: Prof. Dr. Reza Ahmadian

2nd Supervisor: Prof. Dr. Dieter Willbold

Date of the oral examination: 26. November 2025

Dedicated to my Father Hamid Mirzaiebadizi

Zusammenfassung

GTPasen der RAS-Superfamilie, zu der die RAS-, RHO- und ARF-Familien gehören, fungieren als zentrale molekulare Schalter. Sie koordinieren wichtige zelluläre Prozesse wie Proliferation, Migration, Differenzierung und intrazellulären Transport. Eine Fehlregulation dieser Proteine kann zu Krebs, Entwicklungsstörung und Infektionskrankheiten führen. In dieser Arbeit wird eine umfassende biochemische Untersuchung ausgewählter kleiner GTPasen, ihrer Modulatoren, Effektoren und pathogenen Mimikry in menschlichen, pflanzlichen und bakteriellen Systemen präsentiert. Der Schwerpunkt liegt auf der Aufklärung molekularer Mechanismen. Auf der Ebene einzelner GTPasen wurde zunächst das onkogene Potenzial der RAC1-P29S-Hotspot-Mutation untersucht, die häufig bei Melanomen auftritt. Detaillierte biochemische Analysen zeigten, dass RAC1-P29S einen beschleunigten intrinsischen Nukleotidaustausch aufweist und aufgrund einer starken Beeinträchtigung der GAP-vermittelten GTP-Hydrolyse überwiegend in seinem aktiven, GTP-gebundenen Zustand verbleibt. DOCK2 aktiviert es in erster Linie, während kanonische GEFs der DBL-Familie nur eine minimale Aktivität gegenüber dem Mutanten zeigen. Eine verstärkte Bindung an IQGAP1 anstelle von PAK1 fördert eine anhaltende onkogene Signalübertragung. Dies unterstreicht die Rolle von RAC1P29S als Melanomtreiber und zeigt potenzielle therapeutische Ansatzpunkte auf. Zweitens wurde TITAN5 (TTN5), eine pflanzenspezifische, ARF-ähnliche GTPase aus *Arabidopsis thaliana*, als nichtklassische kleine GTPase charakterisiert. Aufgrund seines schnellen Nukleotidaustauschs und seiner langsamen GTP-Hydrolyse reichert sich TTN5 im aktiven GTP-gebundenen Zustand an und ist an wichtigen Vesikeltransportprozessen beteiligt. Diese Ergebnisse deuten auf die evolutionäre Relevanz der Diversifizierung der GTPase-Funktion hin und unterstreichen deren Bedeutung für die Pflanzenentwicklung und -signalübertragung. Darüber hinaus hat diese Arbeit die einzigartige Regulation und Membrandynamik von RIT-GTPasen aufgeklärt, die für Krebs und RASopathien relevant sind. RIT1 weist einen sehr langsamen intrinsischen Nukleotidaustausch und eine sehr langsame GTP-Hydrolyse auf. Zudem ist es unempfindlich gegenüber SOS1-GEF und p120RASGAP. Aufgrund seiner geringen Affinität zu den meisten bekannten RAS-Effektoren besteht das Potenzial, neue GEFs, GAPs und Effektoren zu erforschen und somit die Aktivierungs- und Funktionsmechanismen von RIT besser zu verstehen. Zusammen mit seiner ausgeprägten Membranassoziation über eine basische C-terminale Region stützen diese Eigenschaften seine Einstufung als strukturell kanonisches, aber funktionell unterschiedliches Mitglied der RAS-Familie. In hepatischen Sternzellen wurde während der Ruhephase und Aktivierung ein reziprokes Regulationsmodell zwischen RAS- und RHO-GTPasen entdeckt. ERAS und RND3 definieren den Ruhezustand, während MRAS und RHOC die fibrogene Aktivierung fördern. Dies eröffnet neue therapeutische Ansätze für die Leberfibrose. In dieser Arbeit wurde darüber hinaus die regulatorische Komplexität kleiner GTPasen durch Modulatoren wie akzessorische Proteine und lange nichtkodierende RNAs (lncRNAs) untersucht. Dabei wurden die Proteine IQGAP1, Galectin-3, PDEδ, SHOC2 und NPM1 in der KRAS-gesteuerten Signalübertragung experimentell untersucht. Mithilfe einer systematischen Literaturanalyse haben wir jene lncRNAs überprüft und kategorisiert, die an der KRAS- und RHOA-Signalübertragung beteiligt sind. Dabei haben wir ihre neuen Funktionen in der transkriptionellen und posttranskriptionellen Regulation, der Sequestrierung von microRNAs (miRNAs) sowie der Gerüstbildung von Signalkomplexen hervorgehoben. Darüber hinaus haben wir eine literaturbasierte Übersicht über PAK1-Modulatoren erstellt, wobei der Schwerpunkt auf akzessorischen Proteinen lag, die deren räumliche und zeitliche Aktivierung steuern. Darüber hinaus ergab die Untersuchung der mit dem Noonan-Syndrom assoziierten LZTR1-L580P-Mutation, dass die LZTR1-Polymerisation die Ubiquitinierung von MRAS und RIT1 beeinträchtigt. Dies führt zu einer Hyperaktivierung von MAPK und einer Hypertrophie der Kardiomyozyten. In Kardiomyozyten von Patienten konnten die molekularen und phänotypischen Effekte bestätigt werden, und die Korrektur eines Allels stellte die normale Signalübertragung wieder her. Schließlich konnte gezeigt werden, dass der *Chlamydia-pneumoniae*-Effektor SemD strukturell und funktionell CDC42 nachahmt, indem er den CDC42-Effektor N-WASP direkt aktiviert. Dies fördert die Aktinpolymerisation und die Internalisierung von Pathogenen. Dies unterstreicht die evolutionären Strategien von Pathogenen und zeigt neue therapeutische Ansatzpunkte auf, die Infektionsmechanismen stören könnten. Zusammenfassend lässt sich sagen, dass diese Arbeit verschiedene experimentelle und literaturbasierte Ansätze integriert, um die Funktion und Regulation kleiner GTPasen in evolutionären Kontexten zu beleuchten. Sie betont sowohl konservierte Mechanismen als auch nicht-kanonische Modulatoren, um therapeutische Schwachstellen aufzudecken und unser Verständnis grundlegender biologischer Prinzipien zu vertiefen.

Summary

GTPases of the RAS superfamily, including the RAS, RHO, and ARF families, act as central molecular switches coordinating critical cellular processes such as proliferation, migration, differentiation, and intracellular trafficking. Dysregulation of these proteins contributes to cancer, developmental disorders, and infectious diseases. This thesis presents a comprehensive biochemical investigation of selected small GTPases, their modulators, effectors, and pathogen-derived mimics in human, plant, and bacterial systems. The focus is on elucidating molecular mechanisms. At the level of individual GTPases, the oncogenic potential of the RAC1 P29S hotspot mutation, prevalent in melanoma, was first addressed. Detailed biochemical analyses revealed that RAC1 P29S exhibits accelerated intrinsic nucleotide exchange and predominantly remains in its active GTP-bound state due to severe impairment in GAP-mediated GTP hydrolysis. DOCK2 primarily activates it, while canonical DBL family GEFs display minimal activity toward the mutant. Enhanced binding to IQGAP1 rather than to PAK1 promotes sustained oncogenic signaling, reinforcing the role of RAC1P29S as a melanoma driver and highlighting potential therapeutic targets. Second, TITAN5 (TTN5), a plant-specific ARF-like GTPase from *Arabidopsis thaliana*, was characterized as a non-classical small GTPase. TTN5 accumulates in the active GTP-bound state due to its rapid nucleotide exchange and slow GTP hydrolysis, and it is involved in key vesicle trafficking processes. These findings suggest the evolutionary relevance of GTPase function diversification and underscore its significance in plant development and signaling. Third, this thesis elucidated the unique regulation and membrane dynamics of RIT GTPases relevant to cancer and RASopathies. RIT1 exhibits very slow intrinsic nucleotide exchange and GTP hydrolysis, and it is insensitive to SOS1 GEF and p120RASGAP. Its low affinity for most known RAS effectors highlights the potential to explore novel GEFs, GAPs, and effectors to better understand RIT activation and function mechanisms. Together with its distinct membrane association via a basic C-terminal region, these characteristics support its classification as a structurally canonical but functionally distinct RAS family member. In hepatic stellate cells, a reciprocal regulatory model between RAS and RHO GTPases was uncovered during quiescence and activation. ERAS and RND3 define the quiescent state, whereas MRAS and RHOC promote fibrogenic activation, offering new therapeutic avenues for liver fibrosis. Furthermore, this work has explored the regulatory complexity of small GTPases through modulators such as accessory proteins and long noncoding RNAs (lncRNAs). This work experimentally investigates IQGAP1, galectin-3, PDEδ, SHOC2, and NPM1 in KRAS-driven signaling. Through systematic literature analysis, we reviewed and categorized lncRNAs involved in KRAS and RHOA signaling, highlighting their emerging roles in transcriptional and post-transcriptional regulation, microRNA (miRNA) sequestration, and scaffolding of signaling complexes. A literature-based review was conducted for PAK1 modulators, emphasizing accessory proteins that govern its spatial and temporal activation. Additionally, investigating the LZTR1 L580P mutation associated with Noonan syndrome revealed that LZTR1 polymerization impairs the ubiquitination of MRAS and RIT1. This leads to MAPK hyperactivation and cardiomyocyte hypertrophy. Patient-derived cardiomyocytes validated the molecular and phenotypic effects, and correcting one allele restored normal signaling. Finally, the *Chlamydia pneumoniae* effector SemD was shown to structurally and functionally mimic CDC42 by directly activating the CDC42 effector N-WASP, which promotes actin polymerization and pathogen internalization. This highlights the evolutionary strategies employed by pathogens and reveals novel therapeutic targets that could disrupt infection mechanisms. In conclusion, this thesis integrates diverse experimental and literature-based approaches to illuminate the function and regulation of small GTPases across evolutionary contexts. This work emphasizes both conserved mechanisms and noncanonical modulators to reveal therapeutic vulnerabilities and deepen our understanding of fundamental biological principles.

Table of contents

List of Abbreviations

A	
ACK1	Activated Cdc42-associated ki
AKT	Protein Kinase B
aPKC	Atypical Protein Kinase C
ARF	ADP-ribosylation Factor
ARL	ADP-ribosylation Factor-like
Arp2/3	Actin-related Protein 2/3 Complex
ASO	Antisense Oligonucleotide
ARAF	v-raf Murine Sarcoma 3611 Viral Oncogene Homolog A
B	
BCR-ABL	Breakpoint Cluster Region-Abelson Murine Leukemia Viral Oncogene
BCYRN1	Brain Cytoplasmic RNA 1
BRAF	v-raf Murine Sarcoma Viral Oncogene Homolog B
BTB	Broad-Complex, Tramtrack and Bric à Brac
C	
CAAX	C-terminal motif for Prenylation
CDC42	Cell Division Control Protein 42
CDK9	Cyclin-dependent Kinase 9
CDKN2B-AS1	Cyclin Dependent Kinase Inhibitor 2B Antisense RNA 1
CHD	Calponin Homology Domain
CIP4	Cdc42 Interacting Protein 4
CNK1	Connector Enhancer of KSR1
COPI	Coat Protein Complex I
COPII	Coat Protein Complex II
CRIB	Cdc42/Rac Interactive Binding
CRISPR	Clustered Regularly Interspaced Short Palindromic Repeats
CRAF	v-raf Murine Sarcoma Viral Oncogene Homolog C1
CUL3	Cullin 3
D	
DIRAS	Distinct Subgroup of RAS Proteins
DIRAS	Distinct Subgroup of RAS Proteins
DNA	Deoxyribonucleic Acid
DOCK	Dedicator of Cytokinesis
E	
ECM	Extracellular Matrix
EFA6	Exchange Factor for ARF6
ELK1	ETS-like Gene 1
EMT	Epithelial-Mesenchymal Transition
EPAC1	Exchange Protein Directly Activated by cAMP 1
ERAS	Embryonic Stem Cell Expressed Ras
ERK	Extracellular Signal-regulated Kinase
ERGIC	Endoplasmic Reticulum-Golgi Intermediate Compartment
ETS1	E26 Transformation-specific Sequence 1
F	
FHL1	Four and a Half LIM Domains 1
FMNL2	Formin-like Protein 2
FOXO1	Forkhead Box Protein O1
FRS2	Fibroblast Growth Factor Receptor Substrate 2
G	
GAP	GTPase-activating Protein
GAB1/2	GRB2-associated Binding Protein 1/2
GAL3	Galectin-3
GBD	GTPase Binding Domain
GDP	Guanosine Diphosphate
GDI	Guanine Nucleotide Dissociation Inhibitor
GEF	Guanine Nucleotide Exchange Factor
GFAP	Glial Fibrillary Acidic Protein
GPCR	G-protein-coupled Receptor
GRB2	Growth Factor Receptor-bound Protein 2
GTP	Guanosine Triphosphate
H	

HCM	Hypertrophic Cardiomyopathy
HES1	Hairy and Enhancer of Split-1
HIPPO	Mammalian Hippo Pathway
HRAS	Harvey Rat Sarcoma Viral Oncogene Homolog
HSPC300	Hematopoietic Stem/Progenitor Cell 300
HVR	Hyper-variable Region
I	
IL3	Interleukin 3
IQGAP	IQ Motif Containing GTPase Activating Protein
IRSp53	Insulin Receptor Substrate p53
IRS2	Insulin Receptor Substrate 2
J	
JAG1	Jagged Canonical Notch Ligand 1
JNK	c-Jun N-terminal Kinase
K	
KRAS	Kirsten Rat Sarcoma Viral Oncogene Homolog
KSR1	Kinase Suppressor of Ras 1
L	
LAT	Linker for Activation of T-cells
LATS	Large Tumor Suppressor Kinase
LIMK	LIM domain Kinase
lncRNA	Long Noncoding RNA
LLPS	Liquid-Liquid Phase Separation
LoF	Loss of Function
LZTR1	Leucine Zipper-like Transcription Regulator 1
M	
MALAT1	Metastasis Associated Lung Adenocarcinoma Transcript 1
MAPK	Mitogen-Activated Protein Kinase
MEK	MAPK/ERK Kinase
MLCK	Myosin Light Chain Kinase
MLK	Mixed-lineage Kinase
MLCP	Myosin Light Chain Phosphatase
mTORC1	Mechanistic Target of Rapamycin Complex 1
mTORC2	Mechanistic Target of Rapamycin Complex 2
MORG1	Mitogen-activated Protein Kinase Organizer 1
MVBs	multivesicular bodies
MRAS	Muscle RAS Oncogene Homolog
MMP	Matrix Metalloproteinase
MST	Mammalian Sterile 20-like Kinase
N	
NCK1	Non-catalytic Region of Tyrosine Kinase Adaptor Protein 1
NF1	Neurofibromatosis Type 1
NF2	Neurofibromin 2
NGF	Nerve Growth Factor
NPM1	Nucleophosmin 1
NTAL	Non-T cell Activation Linker
N-WASP	Neurales Wiskott-Aldrich Syndrome Protein
P	
PACAP38	Pituitary Adenylate Cyclase Activating Polypeptide 38
PAK	p21-Activated Kinase
PAR6	Partitioning-defective 6
PAX	Paxillin
PI3K	Phosphoinositide 3-Kinase
PI4P5K	Phosphatidylinositol 4-Phosphate 5-Kinase
PLCe	Phospholipase C epsilon
PKN	Protein Kinase N
PRK	Protein Kinase C-related Kinase
PROTACs	Proteolysis targeting chimeras
PTPN11	Protein Tyrosine Phosphatase Non-receptor Type 11
p120RASGAP	p120 Ras GTPase-activating Protein
R	
RAL	Ras-related Protein Ral
RAP	Ras-proximate Protein
RAS	Rat Sarcoma Viral Oncogene Homolog

RASSF	Ras Association Domain Family
RBPs	RNA-binding Proteins
RGCT	RasGAP C-terminal
RHEB	Ras Homolog Enriched in Brain
RGL3	Ral Guanine Nucleotide Dissociation Stimulator Like 3
RIT	Ras-like Without CAAX
S	
SemD	Secreted effector mimic D
SH3	Src Homology 3
SHOC2	Suppressor of Clear Homolog 2
SHP2	Src Homology Phosphatase 2
SOS1	Son of Sevenless 1
SPRED1	Sprouty-related EVH1 Domain-containing Protein 1
SPRED1	Sprouty-related EVH1 Domain-containing Protein 2
T	
TTN5	TITAN5 (ARF-like GTPase from *Arabidopsis thaliana*)

List of Amino Acids

Amino acid	**3-Letter code**	**1-Letter code**
Alanine	Ala	A
Arginine	Arg	R
Asparagine	Asn	N
Aspartic Acid	Asp	D
Cysteine	Cys	C
Glutamic acid	Glu	E
Glutamine	Gln	Q
Glycine	Gly	G
Histidine	His	H
Isoleucine	Ile	I
Leucine	Leu	L
Lysine	Lys	K
Methionine	Met	M
Phenylalanine	Phe	F
Proline	Pro	P
Serine	Ser	S
Selenocysteine	Sec	U
Threonine	Thr	T
Tryptophan	Trp	W
Tyrosine	Tyr	Y
Valine	Val	V

1 Introduction

1.1 RAS Superfamily of Small GTPases

The discovery of RAS oncogenes over 30 years ago prompted extensive research into small GTPases, leading to the identification of the RAS superfamily [1]. This superfamily comprises 167 human proteins and is evolutionarily conserved across diverse species, including plants, bacteria, *Drosophila*, *Caenorhabditis elegans*, *Saccharomyces cerevisiae*, and *Dictyostelium* [2]. It is divided into six major families: RAS, RHO, RAB, ARF, RAN, and RAG. Each family is associated with distinct cellular functions. The RAS family itself is further subdivided into groups, including RAL, RAP, RAD, RHEB, and RIT [1] (Figure 1A).

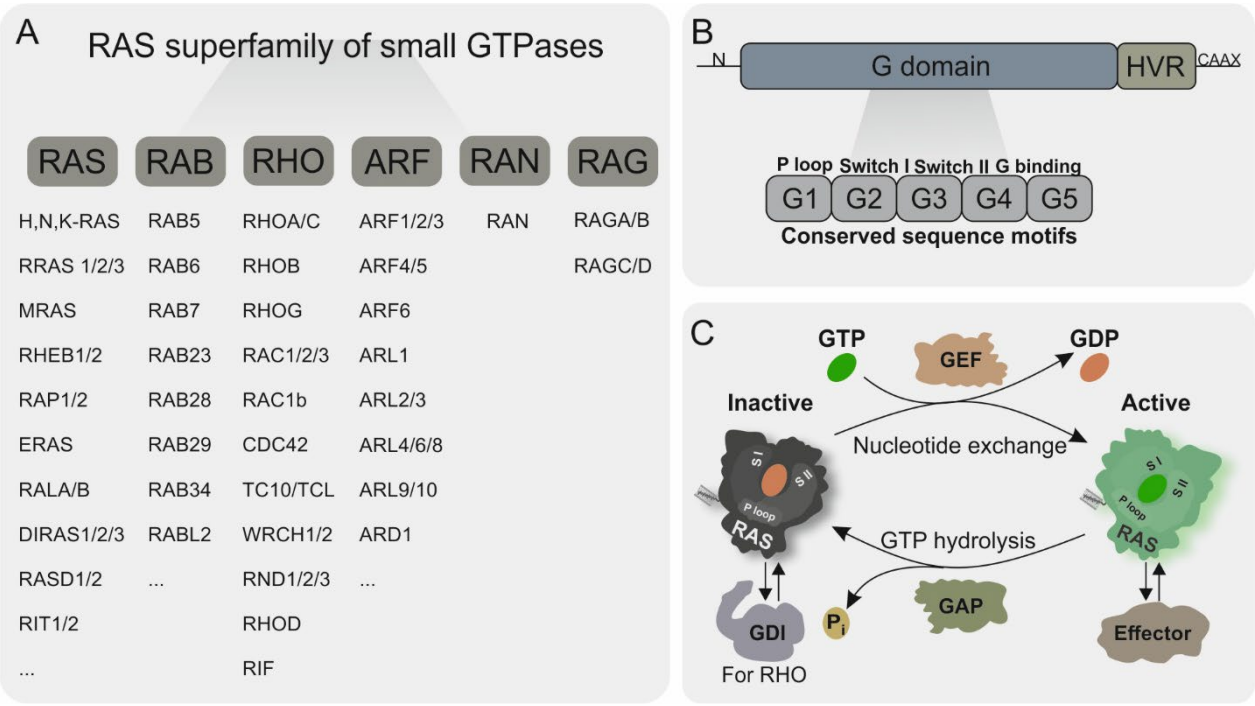

Figure 1. The RAS superfamily of small GTPases: classification, domain organization, and regulatory mechanism. (**A**) Overview of the six major subfamilies, including RAS (general signaling), RHO (cytoskeletal organization), ARF and RAB (vesicular trafficking), RAN (nuclear–cytoplasmic transport), and RAG (nutrient sensing), along with representative members of each group. (**B**) Schematic representation of the conserved domain architecture of RAS proteins. The core G domain includes five conserved sequence motifs (G1–G5), comprising the phosphate-binding loop (P-loop) and switch I and II regions, which undergo conformational changes during nucleotide exchange. This is followed by a hypervariable region (HVR), often modified post-translationally (e.g., prenylation at the CAAX motif) to promote membrane association. (**C**) General mechanism of small GTPase regulation. These proteins act as molecular switches, cycling between an inactive GDP-bound state and an active GTP-bound state. Activation is promoted by guanine nucleotide exchange factors (GEFs), while inactivation occurs through GTPase-activating proteins (GAPs), which stimulate GTP hydrolysis. Guanine nucleotide dissociation inhibitors (GDIs), specific to RHO and RAB family members, control the switch between the membrane-associated state of GTPases and their cytosolic pool. In the GTP-bound active state, small GTPases engage downstream effectors to induce signals to diverse cellular pathways.

Small GTPases are central regulators of signaling pathways controlling development, proliferation, differentiation, survival, and intracellular trafficking [1]. For example, RAS influences gene

expression and cell growth; RHO mediates actin cytoskeleton remodeling; RAB and ARF regulate vesicular transport; RAN governs nucleocytoplasmic trafficking; and RAG is involved in nutrient sensing and the recruitment of mTORC1 to lysosomes [1-4].

Typically ranging from 21 to 25 kDa, small GTPases share a conserved G domain of approximately 170 amino acids that allows them to function as molecular switches, cycling between an inactive GDP-bound state and an active GTP-bound state [1, 5]. This domain contains five conserved motifs (G1–G5), including the P-loop and switch I and II regions, which undergo conformational rearrangements upon nucleotide exchange to facilitate interaction with downstream effectors. The C-terminal HVR often undergoes post-translational modification, such as prenylation at the CAAX motif, to support subcellular targeting and membrane association [4] (Figure 1B).

Small GTPase activation is mediated by GEFs, which promote GDP-GTP exchange [6], while inactivation is facilitated by GAPs, which accelerate GTP hydrolysis. Inactivation is regulated by GTPase-activating proteins (GAPs), which accelerate GTP hydrolysis [7]. Additionally, guanine nucleotide dissociation inhibitors (GDIs) contribute to cytosolic sequestration and recycling of membrane-associated GTPases, particularly within the RHO and RAB families [8] (Figure 1C).

In their active, GTP-bound state, small GTPases bind specific effectors to initiate downstream signaling cascades [4, 9]. These pathways are tightly regulated in space and time to ensure precise cellular responses to internal and external cues [10].

1.1.1 RAS Family

The RAS protein family was first identified in the 1960s through the discovery of the oncogenic Harvey and Kirsten murine sarcoma viruses (Ha-MSV and Ki-MSV), which induced rapid tumor formation in rats [4, 11]. These viral oncogenes, HRAS, KRAS, and NRAS, encode 21-kDa proteins with guanine nucleotide-binding and GTPase activity. Subsequent studies revealed the importance of regulatory and effector proteins in RAS-mediated signaling [11].

As the founding members of the superfamily, HRAS, KRAS, and NRAS have been extensively studied for their roles in cell signaling and oncogenesis [11]. Phylogenetic analyses have identified 25 RAS family members, although some, such as RASL, RERG, and NKIRAS, are excluded due to significant sequence divergence [1]. Their tissue-specific functions are shaped by differences in the C-terminal hypervariable region, subcellular localization, and responsiveness to external stimuli, which collectively contribute to their functional diversity in both physiological and pathological contexts [1, 4].

Structural transitions during activation involve two flexible regions, switch I (residues 28–39) and switch II (residues 59–74), which mediate effector interactions. In the GTP-bound state, residues such as Tyr-32 and Thr-35 (switch I) and Gly-60 (switch II) form hydrogen bonds with the γ-phosphate of GTP. GTP hydrolysis triggers rearrangements that return RAS to the inactive state. The G domain contains five conserved motifs (G1–G5), responsible for nucleotide and magnesium binding [12]. Mutations at key residues like Gly-12 and Gln-61 impair GTP hydrolysis, leading to constitutive activation, a common feature in cancer [1, 4].

RAS proteins operate within intricate signaling networks shaped by regulatory proteins, effectors, and scaffolds [4]. GEFs and GAPs control the activation state of RAS with high precision. Certain RAS family members, including ERAS, DIRAS3, and RASD1/2, possess structural deviations that render them insensitive to GAP-mediated inactivation, resulting in persistent GTP-bound states and alternative regulatory mechanisms [13]. RAS proteins interact with a wide range of effectors,

including kinases, phospholipases, and scaffolding molecules, propagating signals through key pathways such as MAPK/ERK and PI3K/AKT (Figure 2A) [14]. Variations within the switch regions contribute to effector selectivity and functional specificity. Scaffold proteins like IQGAP1, SHOC2, and GAL1 further fine-tune signaling by stabilizing interactions or controlling subcellular distribution [10] (Figure 2A). For example, IQGAP1 amplifies BRAF and ERK1/2 activation, while SHOC2 promotes CRAF signaling in the MAPK cascade [10]. These complex networks underscore the central role of RAS in coordinating cellular processes such as proliferation, differentiation, and migration [4].

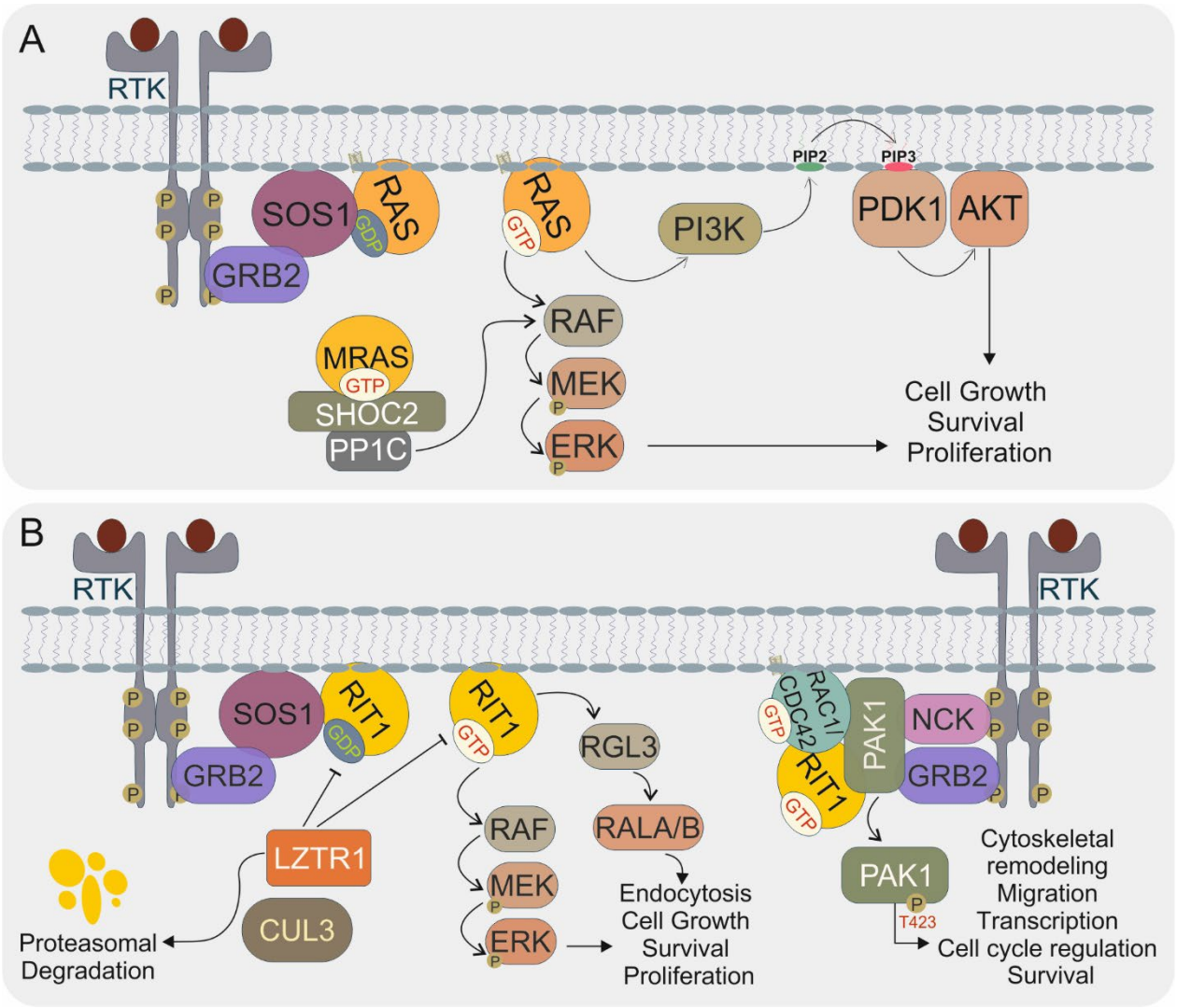

Figure 2. RAS signaling pathways from upstream activators to downstream effectors. (**A**) Schematic representation of canonical RAS signaling initiated by receptor tyrosine kinases (RTKs). Upon RTK phosphorylation, GRB2 recruits the GEF SOS1 to activate RAS. Activated RAS engages downstream pathways, including the RAF–MEK–ERK cascade and the PI3K–PDK1–AKT axis, the latter involving the conversion of PIP2 to PIP3. These cascades promote cell growth, survival, and proliferation. Additionally, the MRAS–SHOC2–PP1C complex facilitates RAF activation by dephosphorylating inhibitory serine residues on RAF kinases (e.g., p-CRAF S259 and p-BRAF S365), thereby enhancing MAPK signaling. (**B**) Overview of RIT1 signaling, a non-canonical RAS family GTPase. RIT1 is activated by SOS1 and degraded via the LZTR1–CUL3 complex through a proteasome-dependent mechanism. Active RIT1 initiates RAF–MEK–ERK and RGL3–RALA/B signaling, supporting endocytosis, proliferation, and survival. RIT1 also cooperates with RAC1 and CDC42 to stabilize PAK1 recruitment at the membrane, promoting PAK1

activation and downstream pathways involved in cytoskeletal remodeling, migration, transcription, and cell cycle regulation.

RAS family proteins function as essential molecular connectors that translate extracellular signals into precise intracellular responses [4]. Each paralog exhibits unique properties defined by upstream stimuli, subcellular localization, regulatory protein interactions, and downstream effectors. RAS activation is initiated by transmembrane receptors, including receptor tyrosine kinases (RTKs), G-protein-coupled receptors (GPCRs), ion channels, cytokine receptors, and adhesion molecules, which activate specific GEFs [15]. For example, KRAS4B and RRAS3 respond to IL3 and EGF in lymphocytes, while RIT1 and RIT2 are activated by NGF and PACAP38 in neuronal tissues [4, 15, 16]. GEFs such as SOS1/2 and EPAC1 help tailor the signaling response, while GAPs like p120RASGAP and NF1 ensure its timely termination [17, 18]. These regulatory layers provide precise spatiotemporal control over RAS activity [4].

By selectively engaging downstream effectors, RAS proteins direct distinct signaling pathways [4]. RAF kinases (ARAF, BRAF, and CRAF) are among the most studied RAS effectors, initiating the MAPK cascade that regulates gene expression, proliferation, apoptosis, and differentiation [19]. RAF activates MEK, which phosphorylates ERK, resulting in the induction of target genes such as *ELK1*, *ETS1*, *MYC*, and *FOS* [4, 20]. PI3K catalyzes the conversion of PIP2 to PIP3, activating AKT and regulating cellular metabolism, survival, and growth [21]. Other effectors, including RALGDS, PLCε, and RASSF, extend RAS signaling to processes such as vesicular trafficking, cytoskeletal organization, and apoptosis [4, 22]. Isoform-specific differences add further complexity: HRAS preferentially activates CRAF to promote proliferation, while KRAS4B interacts with calmodulin to modulate tumorigenic signaling [23]. These differences highlight the versatility and specificity of RAS signaling networks [4].

Aberrant RAS activity contributes to a broad spectrum of diseases, including cancer, developmental syndromes, metabolic disorders, and neurodegenerative conditions [4]. Somatic gain-of-function mutations in KRAS4B, HRAS, NRAS, and RIT1 lead to constitutive activation of MAPK and PI3K–AKT signaling, promoting unchecked cell proliferation and survival [24, 25]. Conversely, loss-of-function mutations in tumor suppressors such as DIRAS and NF1 impair RAS regulation and contribute to diseases such as neurofibromatosis [26, 27]. Germline mutations with partial gain-of-function are associated with RASopathies, developmental syndromes characterized by facial dysmorphisms, cognitive impairment, and congenital heart defects. Beyond these, RAS family proteins have been linked to neurological disorders such as Parkinson's disease, Huntington's disease, and schizophrenia [4]. For instance, RIT2 regulates dopamine signaling, while RASD2 modulates neurotoxicity in Huntington's disease by promoting SUMOylation of mutant huntingtin protein [28, 29]. These findings emphasize the importance of finely tuned RAS signaling and highlight its therapeutic potential [4].

1.1.1.1 RIT1

RIT1 is a unique member of the RAS family of small GTPases that regulates diverse cellular responses through tightly coordinated signaling networks [4]. While canonical RAS proteins such as HRAS, NRAS, and KRAS are established regulators of the RAF–MEK–ERK pathway and are implicated in cancer and RASopathies, RIT1 has emerged as an important contributor in similar contexts [30] (Figure 2B). Germline mutations in RIT1 are associated with Noonan syndrome (NS), a RASopathy characterized by developmental abnormalities and congenital heart defects. Somatic RIT1 mutations are increasingly linked to malignancies, including lung adenocarcinoma and myeloid cancers [31, 32]. Although initially studied in the context of neuronal differentiation and survival, RIT1 is now recognized for its broader roles in various tissues and disease states. A

deeper understanding of its biochemical properties, signaling mechanisms, and pathological associations is critical for the development of targeted therapies [33].

Structural and biochemical studies reveal distinct features that differentiate RIT1 from other RAS family members [33]. Structural and biochemical studies reveal distinct features that differentiate RIT1 from other RAS family members [33]. Its GDP-bound crystal structure shows a globular G-domain architecture with conserved G motifs required for nucleotide binding and hydrolysis. Unlike canonical RAS proteins, RIT1 lacks a CAAX box motif in its hypervariable region. Instead, membrane association is mediated by positively charged residues that interact with negatively charged phospholipids, and this interaction is influenced by the local lipid environment [34, 35]. Alternative splicing gives rise to three RIT1 isoforms, which may vary in localization and binding partners [36]. Specific substitutions in the effector-binding domain, including F82 and S43, limit RIT1's interaction with certain effectors such as PI3K isoforms [37]. These features underscore the specialization of RIT1 in cellular signaling and membrane dynamics [33].

RIT1 responds to upstream inputs such as growth factors, reactive oxygen species (ROS), and pathogenic mutations to modulate key signaling pathways [33]. In neuronal cells, it promotes differentiation and survival via the p38 MAPK and MEK/ERK pathways. Constitutively active RIT1 mutants enhance p38γ activation through MKK3, facilitating neurite initiation and branching [38]. Beyond neuronal contexts, RIT1 regulates cytoskeletal dynamics by interacting with actin-associated proteins such as PAR6, CDC42, RAC1, and PAK1, influencing morphology and motility [39, 40]. Notably, NS-associated RIT1 mutations enhance binding to the CRIB domain of PAK1, driving actin rearrangement and stress fiber dissolution [40]. RIT1 activity is also modulated by the LZTR1–CUL3 complex, which ubiquitinates and degrades RIT1 [41]. Pathogenic mutations impair LZTR1 interaction, stabilizing RIT1 and enhancing MEK/ERK signaling, a hallmark of Noonan syndrome and certain cancers [33, 41] (Figure 2B).

RIT1 mutations are implicated in NS and diverse cancers [32, 33, 35, 42]. In NS, mutations such as A57G, F82L, and G95A cluster near the switch II region, disrupting the GTPase cycle by increasing nucleotide exchange or reducing GTP hydrolysis. NS patients with RIT1 mutations exhibit distinctive phenotypes, including perinatal lymphatic abnormalities, congenital heart defects, and a high prevalence of hypertrophic cardiomyopathy (HCM). HCM is linked to MAPK hyperactivation, with MEK inhibitors like trametinib showing therapeutic promise [32]. In cancers, RIT1 mutations and amplifications drive oncogenesis [31]. RIT1 amplification correlates with poor prognosis in hepatocellular carcinoma and glioblastoma, promoting proliferation and metastasis [43, 44]. Conversely, reduced RIT1 expression in esophageal squamous cell carcinoma is associated with epithelial-to-mesenchymal transition (EMT) and poorer outcomes, reflecting tissue-specific roles [45]. These findings underscore RIT1’s complex contributions to pathophysiology and highlight its therapeutic potential [33].

While RIT1’s role in regulating neuronal growth, differentiation, and stress responses is established, its broader physiological and pathological functions remain incompletely understood. Its regulation of the RAF–MEK–ERK pathway and involvement in transient pro-survival responses suggest context-dependent functions. Future studies should focus on elucidating its regulatory mechanisms, identifying its GEFs and GAPs, and understanding its broader roles in cellular physiology and disease [33, 35, 46].

1.1.2 RHO Family

The RHO family of small GTPases is a subfamily within the Ras superfamily, comprising 20 canonical members classified into six subgroups based on sequence homology: RHO (RHOA,

RHOB, RHOC), RAC (RAC1, RAC1B, RAC2, RAC3, RHOG), CDC42 (CDC42, G25K, TC10, TCL, WRCH1, WRCH2), RHOD (RHOD, RIF), RND (RND1, RND2, RND3), and RHOH [9]. These proteins regulate critical cellular processes, including actin cytoskeleton remodeling, microtubule dynamics, gene expression, and enzymatic activity [9]. These proteins regulate critical cellular processes, including actin cytoskeleton remodeling, microtubule dynamics, gene expression, and enzymatic activity [9]. Among them, RHOA, RAC1, and CDC42 are the most extensively studied. They are key regulators of cell polarity, motility, proliferation, and adhesion. Their roles in actin remodeling, particularly in lamellipodia and filopodia formation and stress fiber assembly, are fundamental to many dynamic cellular functions [1, 2, 47] (Figure 3).

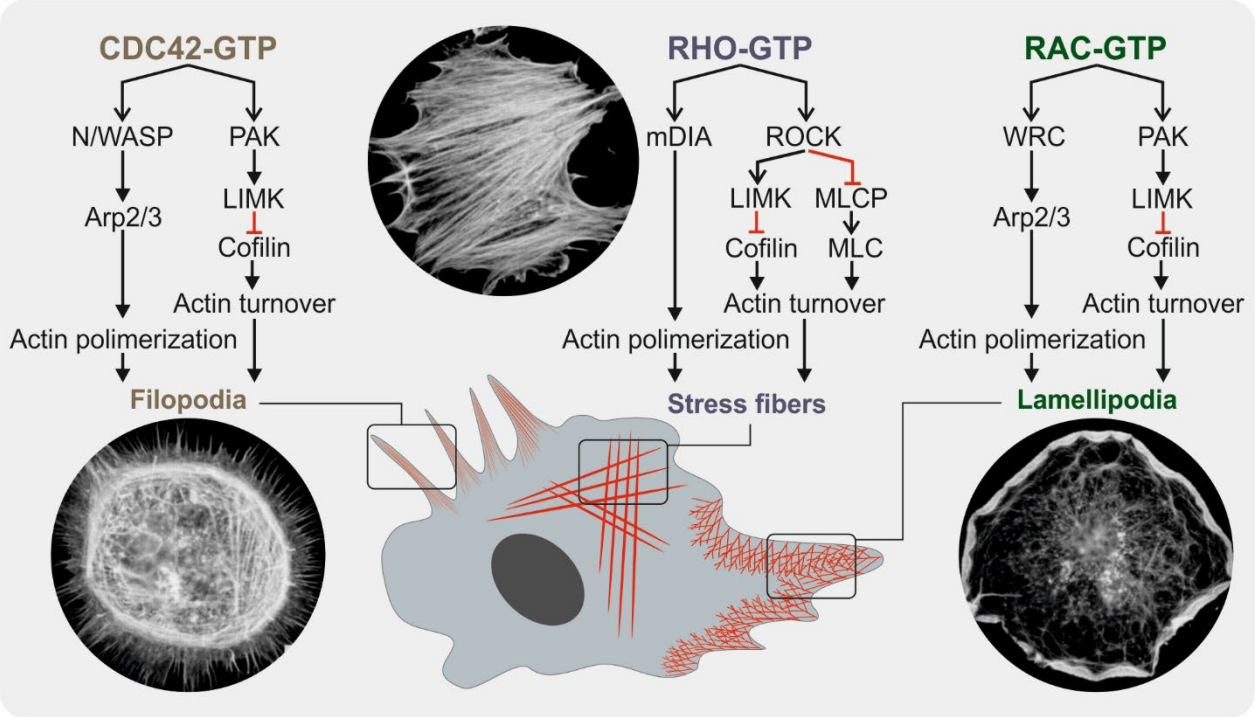

Figure 3. RHO family GTPases and their roles in actin cytoskeletal regulation. Schematic representation of the three major Rho GTPases: CDC42, RHOA, and RAC1, and their distinct signaling cascades involved in cytoskeletal dynamics. The central panel illustrates RHOA signaling through its effectors ROCK and mDIA, promoting actin polymerization and stress fiber formation. The right panel depicts RAC1 signaling via PAK1 and the WAVE regulatory complex (WRC), facilitating lamellipodia formation through branched actin polymerization and cofilin inactivation. The left panel shows CDC42 signaling via N-WASP and PAK1, which activate the Arp2/3 complex and LIMK to induce filopodia formation and regulate actin turnover. Electron microscopy images of filopodia, stress fibers, and lamellipodia were adapted from Hall (*Science*, 1998).

Rho GTPases are distinguished from other Ras superfamily members by a unique insert helix (residues 122–135, CDC42 numbering), a highly variable region that is critical for selective effector interactions. In addition to this structural feature, they undergo extensive post-translational modifications such as prenylation, palmitoylation, phosphorylation, and ubiquitylation, which collectively influence their membrane localization, subcellular distribution, and turnover [1].

Beyond their roles in cytoskeletal architecture, Rho GTPases also participate in complex signaling networks that influence cell cycle progression, hematopoiesis, vesicle trafficking, and noncanonical Wnt signaling. For instance, CDC42 contributes to microspike and filopodia formation; RAC1 promotes membrane ruffling and lamellipodia extension; and RHOA governs

stress fiber formation and focal adhesion assembly. These diverse roles have been explored through genetic, biochemical, and cell biological approaches, revealing the central importance of Rho GTPases in cellular plasticity, tissue morphogenesis, and disease progression [1, 47] (Figure 3).

1.1.2.1 RHO GTPases

Among Rho family GTPases, RHOA, RHOB, and RHOC exhibit functional specificity despite their high sequence similarity. RHOA is central to actomyosin contractility, facilitating stress fiber formation and focal adhesion turnover during cell migration. RHOB, primarily localized on endosomes, regulates receptor trafficking, cellular stress responses, and survival. In contrast, RHOC promotes cell motility and invasion, particularly in metastatic cancer cells, where its expression is frequently elevated. These isoforms achieve functional diversity through differences in subcellular localization, regulatory inputs, and effector interactions [48, 49].

Key downstream effectors include ROCK1 and ROCK2, which bind RHOA through C-terminal Rho-binding regions, driving actomyosin contractility and cytoskeletal reorganization [50]. Another effector, mDia, a diaphanous-related formin, stabilizes microtubules and contributes to cytoskeletal dynamics, particularly at the leading edge of migrating cells [51]. Additional effectors such as PRKs (also known as PKNs), Rhoteckin, and Rhophilin interact with RHOA via HR1 domains near their N-termini, influencing stress fiber assembly and focal adhesion turnover [52]. Citron kinase, with its unique Rho-binding domain, is essential for cytokinesis [53].

RHOB interacts with PRK1 on endosomal membranes to modulate growth factor receptor trafficking, while RHOC preferentially engages ROCK and Citron kinase to regulate cytoskeletal rearrangements critical for invasion and metastasis [48].

Post-translational modifications, such as differential prenylation, further regulate their membrane association and activity. Collectively, these distinct roles highlight the importance of RhoA, RhoB, and RhoC in cytoskeletal reorganization, cell migration, and cancer metastasis [48].

1.1.2.2 RAC GTPases

RAC GTPases, including RAC1, RAC2, RAC3, and RHOG, regulate a wide range of cellular processes such as cytoskeletal organization, cell migration, gene expression, and immune responses [49, 54]. While RAC1 and RHOG are widely expressed, RAC2 and RAC3 are predominantly found in hematopoietic and neural tissues, respectively. Despite sharing 89–93% sequence identity, these isoforms exhibit distinct biochemical properties and tissue-specific functions [49, 54].

RAC1, the best-characterized isoform, orchestrates actin remodeling, cell cycle progression, and transcriptional regulation. RAC2 contributes to oxidative bursts in hematopoietic cells [55], while RAC3 is involved in neural development and has been associated with tumor proliferation [56, 57]. RHOG, although less well-characterized, shares some effectors with RAC1 and can activate both RAC1 and CDC42, broadening its signaling potential [49]. I Unlike other RAC isoforms, RHOG shares only ~70% sequence identity with RAC1 and has been linked to cell growth and motility during the G1 phase [54, 58].

Biochemical studies reveal isoform-specific properties. For example, RAC2 shows distinct nucleotide-binding characteristics and enhanced activation by the RAC-specific GEF Tiam1 compared to RAC1 and RAC3 [59]. RAC1B, a splice variant of RAC1 containing a 19-amino-acid

insertion near the switch II region, exhibits impaired GTP hydrolysis and GEF-independent activation, linking it to tumorigenesis [54].

The functional diversity of RAC proteins underpins their involvement in various physiological and pathological processes. Their regulation of actin dynamics and interaction with effectors such as PAKs, IQGAP1/2, Ajuba, IRSp53, PI4P5K, CYFIP1/2, and WAVE regulatory complex positions them as central coordinators of lamellipodia formation, cell–cell and cell–matrix adhesion, cytoskeletal remodeling, immune responses, and tumor progression [9]. Among them, RAC1 has received particular attention due to its prominent role in cancer, especially through its oncogenic P29S hotspot mutation in melanoma [60, 61].

1.1.2.2.1 RAC1 P29S Hotspot Mutation in Melanoma

The proline 29 to serine (P29S) mutation in RAC1 is the third most frequent hotspot mutation in melanoma, following $BRAF^{V600E}$ and $NRAS^{Q61R}$ [62, 63]. Despite its prevalence, the mechanistic details of how RAC1P29S drives melanoma progression remain an active area of investigation[61]. The mutation has been associated with altered protein structure, enhanced effector interactions, immune evasion, resistance to targeted therapies, and tumorigenesis [63].

$RAC1^{P29S}$ is classified as a spontaneously activating GTPase. Structural studies, including those by Shimada and colleagues and Boggon and colleagues, have shown that the mutation increases GDP dissociation, elevates GTP-bound state levels, and retains GTP hydrolysis capability [64-66]. It induces conformational changes in the switch I region, increasing flexibility and accelerating nucleotide exchange. Shimada and colleagues also identified reduced Mg^{2+} affinity, shifting $RAC1^{P29S}$ toward an active state [65]. Gursoy and colleagues, through molecular dynamics simulations, demonstrated that $RAC1^{P29S}$ adopts an open GTP-bound conformation that enhances effector interactions [67] (Figure 4).

Functional studies have shown elevated binding of $RAC1^{P29S}$ to effectors such as PAK1 and MLK3. These findings were demonstrated in melanoma lysates and HEK293FT cells by Halaban and colleagues and Chin and colleagues [62, 68]. The resulting activation of downstream signaling promotes actin cytoskeletal remodeling, cell motility, and melanocyte proliferation. Danuser and colleagues further observed that $RAC1^{P29S}$ enhances lamellipodia formation and inactivates NF2/Merlin, enabling proliferation under growth-restrictive conditions [69]. The PAK1 axis also supports immune evasion and cell cycle progression through phosphorylation of Aurora A and PLK1 and inhibition of NF2/Merlin, contributing to metastasis and therapy resistance [69, 70] (Figure 4).

$RAC1^{P29S}$ has also been implicated in resistance to RAF inhibitors such as vemurafenib and dabrafenib, as shown by Chin and colleagues and Downward and colleagues [71, 72]. This resistance involves cytoskeletal remodeling and dedifferentiation of melanoma cells. This resistance is driven by cytoskeletal remodeling and dedifferentiation of melanoma cells. Dupuy and colleagues, using the Sleeping Beauty transposon system, found that $RAC1^{P29S}$ promotes resistance to MAPK inhibitors via transcriptional reprogramming through VAV1 [73].

Immune evasion is another hallmark of $RAC1^{P29S}$ activity. Aplin and colleagues reported that melanoma patients harboring this mutation exhibit higher PD-L1 expression compared to $RAC1^{WT}$ patients [74]. The $RAC1^{P29S}$–PAK1 signaling axis contributes to immune suppression by upregulating PD-L1, thereby reducing T cell-mediated antitumor responses [74]. Chernoff and colleagues demonstrated that CDK9 inhibition in $RAC1^{P29S}$-mutant melanoma reduces tumor growth and improves the efficacy of anti-PD-1 therapy [70].

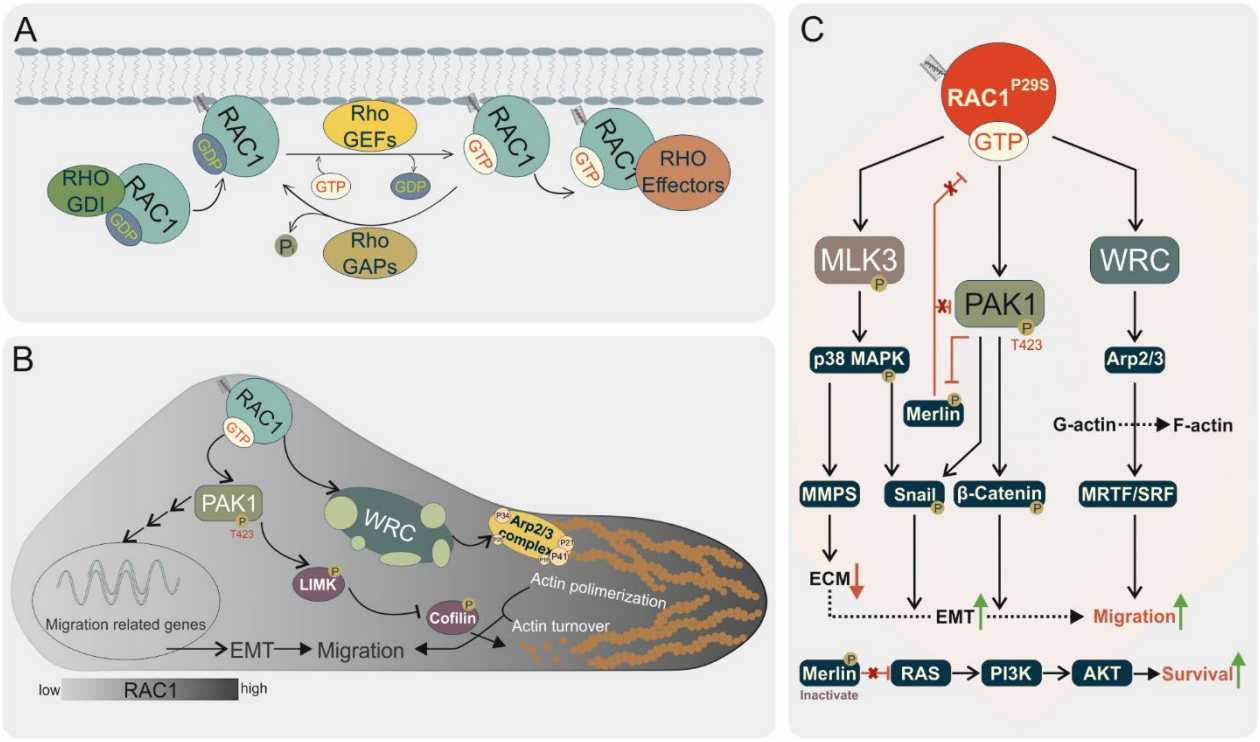

Figure 4. RAC1 signaling and oncogenic activation by the P29S hotspot mutation. (**A**) In resting cells, RAC1 is maintained in an inactive state through its association with RHO-GDI in the cytoplasm. Upon stimulation, RAC1 translocates to the membrane, dissociates from GDI, and is activated by RHO-specific GEFs. Active RAC1 binds downstream effectors, and its signaling is downregulated by RHO-GAPs that promote GTP hydrolysis. (**B**) In migrating cells, GTP-bound RAC1 localizes at the leading edge, where it activates PAK1 and the WAVE regulatory complex (WRC), inducing actin polymerization, lamellipodia formation, and cytoskeletal remodeling. PAK1 also phosphorylates LIMK, which inhibits cofilin to support actin turnover and regulate epithelial-to-mesenchymal transition (EMT). (**C**) In $RAC1^{P29S}$-expressing melanoma cells, the active P29S variant hyperactivates effectors such as MLK3, PAK1, and WRC. This hyperactivation disrupts feedback regulation, enhances cell motility and survival, and promotes oncogenesis, especially in cells co-harboring $BRAF^{V600E}$.

Although $RAC1^{P29S}$ is traditionally considered "undruggable," promising therapeutic strategies are emerging [75, 76]. Gomez and colleagues identified Rac1 inhibitor 1A-116, which binds $RAC1^{P29S}$ and inhibits its activity in silico and in SRE-luciferase assays [77]. Chernoff and colleagues demonstrated the efficacy of Group A PAK inhibitors, pan-PI3K inhibitors, and PI3Kβ-selective inhibitors in blocking $RAC1^{P29S}$-driven melanoma proliferation [75, 78]. Additional studies have shown that inhibitors of CDK9 and DOCK1 reduce invasion and growth in $RAC1^{P29S}$-positive cancers [79]. Willimsky and colleagues successfully employed adoptive T cell therapy targeting the $RAC1^{P29S}$ neoepitope. They also demonstrated that cross-reactive peptides such as $RAC2^{P29L}$ enhance therapeutic efficacy, resulting in tumor regression [80].

$RAC1^{P29S}$ has emerged as a key driver mutation in melanoma, influencing proliferation, motility, immune evasion, and drug resistance [61-63]. Its distinct structural and functional properties have made it a priority target for mechanistic studies and drug development [63]. Continued exploration of RAC1P29S-specific signaling and vulnerabilities may offer new opportunities for effective melanoma therapies [63].

1.1.2.3 CDC42 GTPases

CDC42, a member of the RHO family of small GTPases, is a master regulator of cell polarity and an integrator of cytoskeletal dynamics, vesicle trafficking, and signaling. It transitions between inactive GDP-bound and active GTP-bound states and interacts with downstream effectors to coordinate processes such as growth, division, and migration. Its role in establishing polarity is conserved across eukaryotes, from budding yeast to mammals, highlighting its importance in development and spatial organization [81-83].

In yeast, CDC42 localizes to the budding site, directing cytoskeletal reorganization and vesicle transport, with feedback mechanisms ensuring precise spatiotemporal activity during asymmetric division [81-83]. In multicellular organisms, CDC42 plays essential roles in epithelial polarity, immune cell chemotaxis, and neuronal pathfinding. It interacts with polarity complexes such as Par6–aPKC and CRB3 to establish apical–basal polarity in epithelial cells [81]. In immune cells, CDC42 governs leading-edge actin filament organization, coordinating chemotaxis and migration [83].

GTP binding induces conformational changes in CDC42, enabling interaction with numerous effectors. These include WASP/N-WASP, which promote Arp2/3-mediated actin nucleation; IQGAP1, a scaffolding protein linking CDC42 to cytoskeletal regulators; mDia, which regulates actin filament elongation; and PAK1 [9, 84-86]. Through these interactions, CDC42 integrates cytoskeletal remodeling with polarity and signal transduction.

The CDC42-like GTPases, including TC10, TCL, WRCH1, and CHP/WRCH2, share the ability to induce filopodia by binding WASP or N-WASP, although their broader roles remain less defined [49]. While CDC42 is essential for cell polarization, it remains unclear whether its subfamily members share this function. TC10 and TCL are implicated in insulin-mediated metabolic events [49]. TC10 and TCL are implicated in insulin signaling and membrane trafficking. WRCH1 is linked to Wnt signaling, while CHP/WRCH2 lacks a canonical prenylation signal yet still localizes to membranes via its C-terminal tail, reflecting functional diversity within this subfamily [49].

Aberrant CDC42 activity contributes to cancer progression, immune dysregulation, and neurological disease. In cancer, CDC42 promotes EMT, cell migration, and invasion by enhancing actin remodeling and enabling metastasis [83, 85]. IQGAP1 amplifies these oncogenic effects by stabilizing signaling complexes that promote MAPK pathway activation and therapeutic resistance [85, 86].

CDC42 is also exploited by pathogens. *Chlamydia pneumoniae*, for instance, uses the effector protein SemD to mimic active CDC42, thereby activating N-WASP and inducing actin polymerization to facilitate host cell entry [87]. This highlights the importance of CDC42 in host–pathogen interactions and its potential as a therapeutic target.

CDC42 serves as a central coordinator of polarity, cytoskeletal architecture, and signal integration. Although it represents a promising target in cancer and infectious diseases, the challenge lies in selectively modulating its activity without disrupting essential physiological functions. Future research into CDC42-specific effectors and regulatory mechanisms may enable more targeted and effective therapeutic approaches [83, 85].

1.1.2.4 RHO GTPases Signaling and Their Downstream Effectors

RHO family GTPases serve as essential molecular switches that coordinate an extensive array of intracellular signaling cascades [1]. Upon activation by extracellular stimuli, these proteins adopt a GTP-bound conformation and engage specific downstream effectors to precisely regulate key cellular processes, including actin cytoskeletal remodeling, polarity establishment, migration, proliferation, and differentiation [1, 9, 88, 89]. Among them, RHOA, RAC1, and CDC42 are the most studied, owing to their central roles in cytoskeletal regulation and cellular architecture [9, 89, 90].

Effector specificity is largely dictated by the GTP-bound state of each GTPase and the structural compatibility of effector-binding motifs, particularly within the switch I and II regions [9, 89, 90]. Downstream effectors fall into two major categories: serine/threonine kinases and scaffolding proteins [9]. Key kinases include ROCK [91], PAK [92], LIMK [93], CITRON [53], MLK1 [94], and PKN [95], while prominent scaffolding proteins include DIA [96], WASP/N-WASP [97], IRSp53 [98], Rhotekin [99], and IQGAP family members [9, 100, 101] .

RHOA primarily regulates actomyosin contractility and stress fiber formation through effectors such as ROCK [89, 91], DIA [96], CITRON kinase [53], and LIMK [9, 102]. ROCK increases myosin light chain (MLC) phosphorylation by inhibiting MLC phosphatase, thereby promoting contractile force generation [103]. It also activates LIMK, which phosphorylates and inhibits cofilin, stabilizing actin filaments [102]. DIA promotes linear actin polymerization and facilitates focal adhesion maturation, contributing to polarity and migration [96]. CITRON kinase plays a critical role in cytokinesis and cytoskeletal stabilization during cell division [53].

RAC1 controls membrane ruffling and lamellipodia extension via effectors such as PAK [92], the WAVE regulatory complex (WRC) [104], IRSp53 [98], IQGAP [100], PI4P5K [105], and MLK1 [9, 89, 94]. PAK activation through the CRIB motif leads to phosphorylation of LIMK and MLCK, enhancing local actin polymerization while modulating contractility [106]. WRC links RAC1 signaling to the Arp2/3 complex for branched actin nucleation [104]. IRSp53 facilitates membrane curvature and actin assembly [98], IQGAPs integrate polarity and adhesion signals [100]. PI4P5K modulates phosphoinositide levels at the membrane, supporting cytoskeletal remodeling [105]. MLK1 connects cytoskeletal remodeling to JNK-mediated stress responses and transcriptional regulation [94].

CDC42 promotes filopodia formation, cell polarity, and directional migration via its interactions with effectors such as N-WASP [97], PAR6 [107], CIP4 [108], ACK1 [109], and IQGAPs [9, 86, 89, 101]. N-WASP is activated through a conformational change induced by CDC42, enabling Arp2/3 complex recruitment for actin nucleation [97]. The PAR6–PAR3–aPKC polarity complex orchestrates microtubule orientation during asymmetric division and front–rear polarity [107]. CDC42 also engages CIP4 and intersectin to regulate N-WASP activity at membrane-cortical sites [108]. IQGAPs further integrate CDC42 signals with adhesion, trafficking, and morphogenesis [86, 100, 101].

Beyond actin regulation, Rho GTPases influence additional pathways. [9, 89]. For instance, RAC1 activates NADPH oxidase via p67phox, promoting ROS production for immune defense and signaling [110]. Both CDC42 and RAC1 regulate transcriptional responses through the JNK, p38 MAPK, SRF, and NF-κB pathways [111, 112]. Structural studies reveal that CRIB-containing effectors typically interact with conserved switch regions, while other effectors like ROCK and PKN engage additional surfaces, supporting effector diversity and spatial regulation [9, 113].

Together, these effectors form a highly adaptable and dynamic signaling network that enables Rho GTPases to orchestrate cell behavior with spatial and temporal precision [9, 89]. Understanding these modules not only enhances fundamental cell biology but also provides insight into therapeutic targets for diseases involving cytoskeletal dysfunction, such as cancer, fibrosis, and immune disorders.

1.1.2.5 The Mimicry Behavior of the *Chlamydia pneumoniae* Effector SemD to CDC42

Chlamydia pneumoniae is an obligate intracellular pathogen that initiates infection by invading non-phagocytic epithelial cells of the respiratory tract [114, 115]. This entry process is mediated by bacterial effector proteins that manipulate host signaling pathways and membrane structures [87]. One such early effector, SemD, anchors to the host plasma membrane through an N-terminal amphipathic helix with high specificity for phosphatidylserine, a phospholipid enriched in the inner leaflet of the membrane. This localization enables SemD to coordinate the recruitment and activation of host endocytic machinery involved in bacterial internalization [87].

SemD consists of multiple functional domains that engage distinct host targets. A central proline-rich region interacts with the SH3 domain of SNX9 [116], a membrane-remodeling protein involved in endocytic vesicle formation [87]. Two WH2 domains bind monomeric actin, while the C-terminal region interacts with the GTPase-binding domain (GBD) of N-WASP [97], a key actin nucleation-promoting factor [87]. Under normal conditions, N-WASP is activated by GTP-loaded CDC42, which relieves autoinhibition and exposes its VCA domain, leading to Arp2/3 complex activation and branched actin polymerization [117]. SemD mimics this mechanism by directly binding to the GBD of N-WASP, thereby inducing its activation in the absence of CDC42-GTP [87].

This structural mimicry is both functional and selective. SemD does not bind other CDC42 effectors, such as FMNL2 [118], highlighting its specific engagement of the N-WASP signaling axis [87]. Moreover, the modular structure of SemD, connected by flexible linker regions, allows it to simultaneously interact with the plasma membrane, SNX9 [116], and N-WASP [87]. This coordinated engagement integrates membrane curvature and localized actin polymerization, facilitating the rapid formation of a large endocytic vesicle that enables efficient internalization of the infectious elementary body into host cells [87].

1.1.3 ARF Family

The ARF (ADP-ribosylation factor) family of small GTPases, a subgroup of the RAS superfamily, regulates membrane trafficking, organelle identity, and lipid homeostasis. These proteins contain a conserved myristoylated N-terminal amphipathic helix that mediates membrane association. Like other GTPases, ARFs cycle between GDP- and GTP-bound states. Their activity is controlled by GEFs such as BIG1/2, GBF, Cytohesins, BRAGs, and EFA6, and by GAPs including ARFGAP1–3, ADAP1/2, ASAP1–3, ACAP1–3, and ARAP1–3, ensuring spatial and temporal regulation [119-121] (Figure 5A).

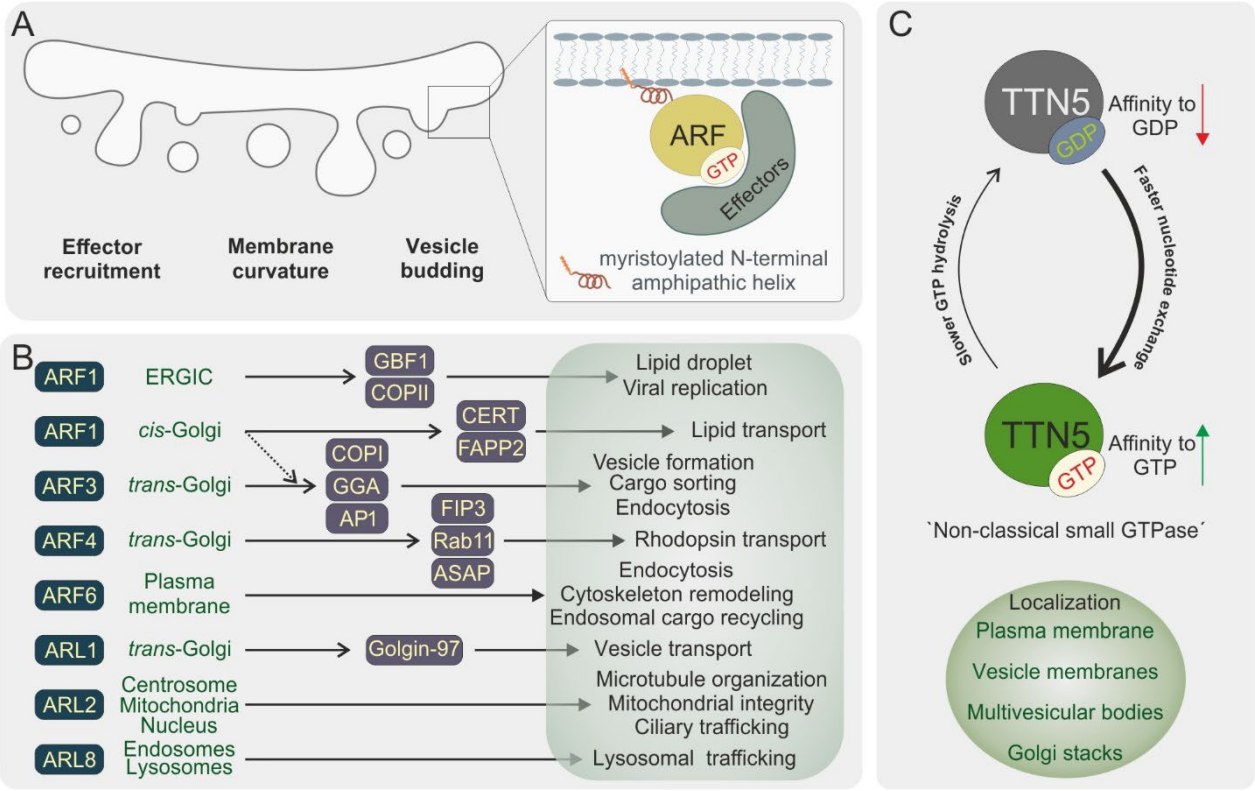

Figure 5. ARF GTPases: structure, localization, and functional diversity. (**A**) Schematic of ARF GTPase structure, highlighting the N-terminal myristoylated amphipathic helix responsible for membrane association. GTP binding promotes effector recruitment, membrane curvature, and vesicle budding. (**B**) Overview of ARF and ARL family members and their subcellular localization, including the ER-Golgi intermediate compartment (ERGIC), Golgi, plasma membrane, endosomes, and lysosomes, along with associated functions such as lipid transport, cargo sorting, endocytosis, vesicle formation, and cytoskeletal regulation. (**C**) TTN5 (TITAN5), a plant-specific ARL-like GTPase, is depicted as a non-classical member with reduced GDP affinity, accelerated nucleotide exchange, and delayed GTP hydrolysis, resulting in a predominantly active GTP-bound state. TTN5 localizes to the plasma membrane, Golgi stacks, multivesicular bodies, and vesicular membranes, linking its activity to plant-specific intracellular trafficking and membrane dynamics.

The ARF family includes six canonical members (ARF1–ARF6) and a structurally related group of ARF-like (ARL) GTPases. ARF1 and ARF3 function at the Golgi apparatus, where they recruit COPI and clathrin adaptor complexes (AP-1 and AP-3) to drive vesicle formation[120, 121]. ARF6, on the other hand, localizes to the plasma membrane, where it regulates endocytosis, cytoskeletal remodeling, and recycling of membrane components during cell migration and division [122, 123] (Figure 5B).

Although ARLs share structural homology with ARFs, their functions extend beyond classical vesicle trafficking. ARL1 promotes vesicle tethering at the trans-Golgi network through interactions with proteins such as Golgin-97. ARL2 contributes to microtubule organization, mitochondrial stability, and ciliary transport. ARL8 regulates lysosomal positioning and transport, supporting autophagy and innate immunity [119, 121, 122] (Figure 5B).

Beyond their roles in cellular physiology, ARF GTPases are also implicated in disease. ARF1 overactivation has been linked to cancer through the promotion of extracellular matrix remodeling and angiogenesis, while ARF6 enhances tumor invasiveness via cytoskeletal and trafficking

regulation [121, 122]. Pathogens such as *Legionella pneumophila* and *Salmonella* hijack ARF signaling to reprogram host cells during infection [119, 120, 123, 124]. ARL8 dysregulation has been associated with lysosomal defects in neurodegenerative disorders [119, 121, 123].

In plants, ARF and ARL proteins have evolved additional roles related to development, stress adaptation, and growth. For example, SAR1 and ARF1 facilitate ER-to-Golgi trafficking, while ARL1 regulates endosomal recycling to the Golgi. These adaptations underscore the versatility of ARF-family GTPases in coordinating membrane systems under diverse biological conditions [119, 121, 123, 125].

The next section introduces TITAN5 (TTN5), a plant-specific ARL protein in *Arabidopsis thaliana*, which illustrates this functional diversification. TTN5 exhibits distinctive localization and biochemical features, supporting its role in intracellular trafficking and plant development [125].

1.1.3.1 TITAN5 GTPase

TITAN5 (TTN5), also known as HALLIMASCH (HAL), ARL2, or ARLC1, is an essential ARL-type small GTPase in *Arabidopsis thaliana*. It was identified through genetic screens for embryo-defective mutants, where *ttn5* loss-of-function alleles caused early embryonic arrest, indicating its fundamental role in plant viability and development [125-128].

TTN5 shares significant sequence similarity with human ARL2 (hsARL2), a GTPase involved in microtubule dynamics, mitochondrial function, and intracellular signaling. While hsARL2 performs diverse cellular roles, TTN5 has diverged to fulfill plant-specific functions, particularly in vesicle trafficking and cytoskeletal organization [125, 127, 129] (Figure 5C).

Subcellular localization studies place TTN5 at the plasma membrane and throughout the endomembrane system, supporting its role in membrane remodeling and trafficking [125] (Figure 5C). These observations are consistent with the general functions of ARL proteins but highlight TTN5's specialization in plant developmental processes.

As a representative plant-specific ARL, TTN5 illustrates the functional expansion of the ARF family to meet the unique demands of plant cell architecture and growth. Its biochemical properties and developmental importance make TTN5 a valuable model for studying intracellular transport and cytoskeletal regulation in plants [125].

1.1.4 The Reciprocal Regulation of RAS and RHO Signaling

Hepatic stellate cells (HSCs) are liver-resident pericytes located in the space of Disse and play essential roles in liver development, immunoregulation, and tissue regeneration [130, 131]. In a healthy liver, HSCs remain in a quiescent state, storing vitamin A in lipid droplets and expressing ectodermal and mesodermal markers such as glial fibrillary acidic protein (GFAP) and desmin [130]. Upon liver injury, HSCs become activated, losing their quiescent phenotype and acquiring a contractile, myofibroblast-like state characterized by α-smooth muscle actin (α-SMA) expression and excessive extracellular matrix (ECM) production, which drive fibrosis progression [130, 132, 133]. This phenotypic switch is governed by multiple signaling pathways, including RAS–MAPK, PI3K–AKT, WNT, Hedgehog, NOTCH, and RHO–ROCK cascades [132, 134-138], with RAS and RHO GTPases acting as central regulators of HSC fate [4, 131, 132, 139, 140].

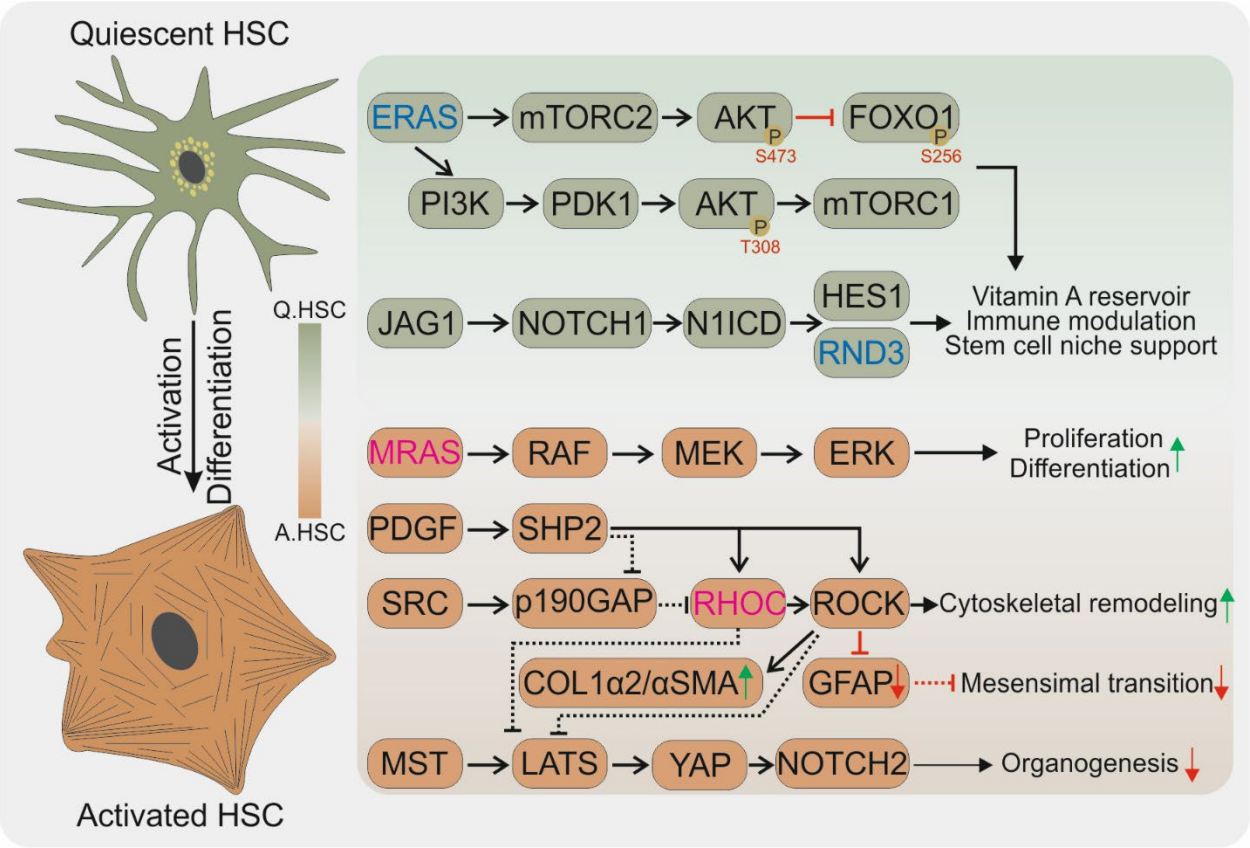

Figure 6. Reciprocal regulation of RAS and RHO signaling during hepatic stellate cell activation. This schematic illustrates the dynamic signaling transitions between quiescent and activated states of HSCs, emphasizing the context-dependent and reciprocal roles of RAS and RHO family members. In quiescent cells, ERAS signaling activates mTORC2 and the PI3K–PDK1–AKT axis, leading to FOXO1 inhibition and supporting immune modulation, vitamin A storage, and stem cell niche maintenance. RND3 and the NOTCH1–HES1 axis also contribute to maintaining quiescence. Upon activation, MRAS initiates RAF–MEK–ERK signaling, promoting proliferation and differentiation. Concurrently, PDGF–SHP2–SRC signaling activates p190GAP to suppress RHOC. However, RHOC-mediated ROCK activation drives cytoskeletal remodeling, COL1A2 and α-SMA expression, and downregulation of GFAP, contributing to fibrogenesis. The MST–LATS–YAP axis further activates NOTCH2, supporting HSC differentiation and organogenesis.

Recent studies have described a reciprocal regulatory network involving specific RAS and RHO family members that controls the transition between HSC quiescence and activation [131, 132, 140]. In quiescent HSCs, embryonic stem cell-expressed RAS (ERAS) is highly expressed and supports homeostasis by activating AKT, STAT3, mTORC2, and HIPPO pathways, while inhibiting FOXO1 and YAP [132, 141-143]. This signaling network maintains a non-fibrogenic phenotype by regulating metabolism, proliferation, and differentiation. Upon activation, ERAS expression is suppressed through promoter methylation, redirecting RAS signaling toward the RAF–MEK–ERK pathway, which promotes HSC proliferation and trans-differentiation into α-SMA–positive myofibroblasts [132]. MRAS expression is upregulated during this transition and contributes to the fibrogenic phenotype [131, 132] (Figure 6).

A similar regulatory switch occurs within the RHO family. In quiescent HSCs, RND3 (RHOE) is strongly expressed and acts as a negative regulator of cytoskeletal remodeling and contractility, limiting fibrotic activity [131]. However, upon activation, RND3 levels decrease, while RHOC expression is upregulated, promoting cytoskeletal reorganization, α-SMA expression, ECM deposition, and myofibroblast differentiation [131]. This functional switch is coupled to downstream

changes in signaling balance, particularly between NOTCH1 and RHO–ROCK activity, further modulating HSC activation and fibrotic progression [131, 134] (Figure 6).

The dynamic interplay between these signaling pathways underscores the complexity of HSC regulation and reveals potential therapeutic opportunities for antifibrotic intervention [131]. Strategies that preserve ERAS expression or block MRAS signaling may help maintain quiescence and prevent fibrotic activation [132]. Similarly, modulating RND3 levels or inhibiting RHOC activity could suppress α-SMA expression and limit HSC trans-differentiation [131]. Given the intricate crosstalk between these signaling modules, further research is needed to elucidate their roles in chronic liver disease and to evaluate their potential as therapeutic targets.

1.2 Modulators of Small GTPases

Small GTPases function as molecular switches that regulate critical cellular processes such as growth, differentiation, and migration. Their classical regulation involves GEFs, GAPs, and GDIs, which control nucleotide exchange, GTP hydrolysis, and membrane sequestration. These factors ensure proper cycling between active and inactive states, maintaining signaling fidelity [144].

Beyond these canonical regulators, a broader range of modulators has emerged. These modulators do not necessarily bind the switch regions but influence GTPase function by affecting expression, localization, turnover, or interaction networks. They include accessory proteins, scaffolding molecules, and long noncoding RNAs (lncRNAs), which regulate small GTPase signaling indirectly [10, 145-147].

Accessory proteins such as IQGAP1 and LZTR1 play important roles in fine-tuning GTPase pathways. IQGAP1 acts as a scaffold stabilizing GTPase-effector complexes, while LZTR1 controls GTPase stability through ubiquitination and proteasomal degradation [10, 147]. lncRNAs modulate the expression of small GTPases, influencing their downstream functions [145, 146]. These modulators add a further layer of regulation, coordinating spatiotemporal GTPase signaling in various cellular contexts.

This section focuses on such modulators, with particular attention to lncRNAs and accessory proteins. Their relevance in disease, especially cancer, highlights their potential as therapeutic targets.

1.2.1 Long Noncoding RNAs

Long noncoding RNAs (lncRNAs), transcripts longer than 200 nucleotides, contribute to the regulation of differentiation, gene expression, and chromatin architecture. Their structural diversity and cell type–specific expression enable functions in both the nucleus and cytoplasm. In the nucleus, lncRNAs interact with chromatin-modifying complexes and influence gene expression and nuclear compartmentalization. In the cytoplasm, they regulate translation, signaling, and metabolic activity [148, 149].

LncRNAs arise from diverse genomic sources, including intergenic, antisense, pseudogenes, and circular transcripts. Despite the annotation of over 100,000 lncRNAs, most remain functionally uncharacterized. Single-cell sequencing and spatial transcriptomics have uncovered their dynamic expression across tissues and conditions [148-150].

Through interactions with RNA, DNA, and proteins, lncRNAs regulate chromatin structure, histone modification, and transcription. Many associate with Polycomb repressive complexes or contribute to nuclear architecture by localizing to phase-separated compartments such as speckles and paraspeckles [148, 151].

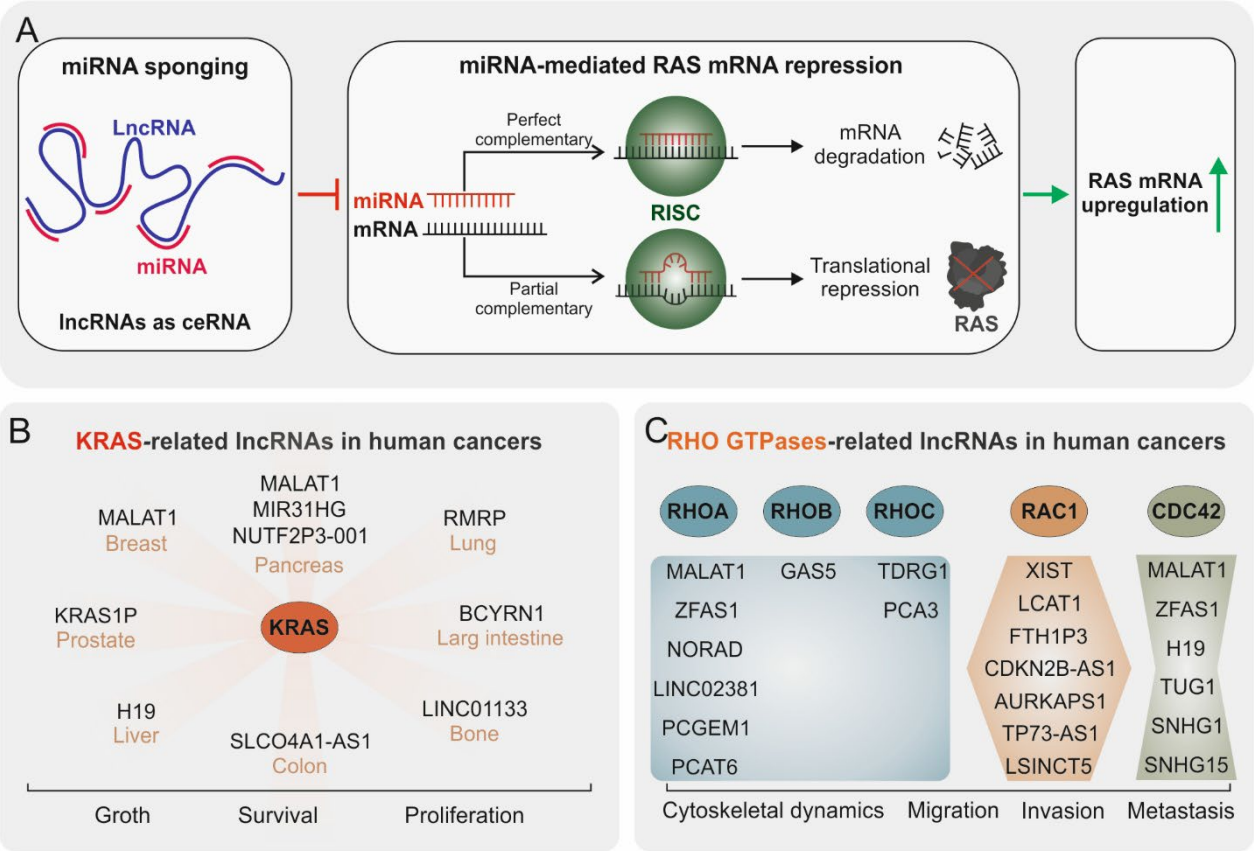

Figure 7. Regulatory roles of long noncoding RNAs (lncRNAs) in modulating RAS and RHO GTPase signaling via competing endogenous RNA (ceRNA) mechanisms. (**A**) Schematic representation of the ceRNA hypothesis, in which lncRNAs act as molecular sponges that bind and sequester microRNAs (miRNAs), thereby preventing them from targeting specific mRNAs. This interaction occurs through the RNA-induced silencing complex (RISC), which mediates either mRNA degradation or translational repression, depending on the degree of complementarity. Through this mechanism, lncRNAs can indirectly upregulate RAS mRNA expression by limiting miRNA-mediated repression. (**B**) Overview of KRAS-associated lncRNAs implicated in various human cancers, which have been shown to promote cancer cell growth, survival, and proliferation across different tissue types. (**C**) Summary of RHO GTPase-related lncRNAs, categorized by specific GTPase targets such as RHOA, RHOB, RHOC, RAC1, and CDC42. These lncRNAs regulate a range of cellular functions, including cytoskeletal dynamics, migration, invasion, and metastasis, thereby contributing to cancer progression.

LncRNAs also scaffold membraneless condensates like stress granules and paraspeckles by recruiting RNA-binding proteins (RBPs). Their dysregulation can disrupt phase separation, linking them to diseases including cancer and neurodegeneration [148, 152, 153]. Though nuclear functions are well documented, cytoplasmic lncRNA mechanisms, especially in signaling and translation regulation, require further investigation [149-152].

Among their mechanisms, lncRNAs can function as ceRNAs, regulating gene expression by sequestering miRNAs. This role is particularly significant in GTPase-driven signaling pathways such as KRAS and RHO GTPases [145, 146].

1.2.1.1 KRAS-Related Long Noncoding RNAs in Human Cancers

KRAS, a proto-oncogene frequently mutated in human cancers, promotes tumor progression primarily through MAPK and AKT pathways activation [11]. LncRNAs regulate KRAS at multiple levels, including miRNA sponging, mRNA stabilization, and transcriptional enhancement [145]. Some, like KRASIM, encode microproteins that suppress KRAS activity, while others harbor G-quadruplex structures that enhance KRAS transcription [154] (Figure 7A).

LncRNAs such as MALAT1 and MIR31HG promote KRAS expression by sponging miR-217, contributing to tumorigenesis in lung and pancreatic cancers [155, 156]. KRAS1P protects KRAS transcripts from degradation by sequestering miR-143 and let-7, while BCYRN1 and NUTF2P3-001 regulate KRAS through other miRNAs, enhancing metastatic behavior [157-159]. H19 also promotes KRAS-driven tumorigenesis by sponging let-7 miRNAs [145, 160] (Figure 7B).

In leukemia, KRAS mutations correlate with poor prognosis and altered transcriptional regulation. LncRNAs such as lnc-ACOT9-1 and MORRBID are differentially expressed in juvenile myelomonocytic leukemia and contribute to disease progression [161, 162]. Therapeutic strategies targeting lncRNAs include antisense oligonucleotides (ASOs), CRISPR/Cas9, and small-molecule inhibitors aimed at modulating lncRNA expression or structure. These approaches highlight the therapeutic relevance of lncRNAs in KRAS-driven cancers [145].

1.2.1.2 RHO GTPase-Related Long Noncoding RNAs in Human Cancers

RHO GTPases regulate adhesion, polarity, and migration. Although mutations are rare, aberrant activation and expression are common in cancer [9, 146]. LncRNAs influence RHO GTPase signaling by acting as ceRNAs that sequester miRNAs targeting GTPase transcripts such as RHOA, RHOB, RHOC, RAC1, and CDC42, thereby stabilizing expression in cancer cells[146].

Specific lncRNAs modulate individual RHO GTPase members. MALAT1 sponges miR-429 to elevate RHOA levels, promoting migration and invasion [163]. NORAD and ZFAS1 enhance RHOA signaling by binding miR-125a-3p and miR-3924, respectively [164, 165]. GAS5, a tumor-suppressive lncRNA, targets RHOB through miR-663a and inhibits proliferation [166]. TDRG1 and PCA3 promote RHOC-driven metastasis [167, 168]. RAC1 is regulated by CDKN2B-AS1 and AURKAPS1, while CDC42 is modulated by lncRNAs such as H19, which impact cytoskeletal remodeling and invasiveness [146, 169, 170] (Figure 7C).

Epigenetic modifications further contribute to lncRNA-mediated RHO GTPase regulation. TUG1 recruits EZH2 to the RND3 promoter, inducing H3K27me3-mediated repression [171]. RNA methylation (m6A) also affects lncRNA stability; for example, m6A-modified GAS5 enhances YAP degradation, while degradation via YTHDF3 promotes tumor progression [172].

Therapeutic targeting of lncRNAs regulating RHO GTPase signaling is an emerging strategy. Tools such as siRNAs, ASOs, and CRISPR/Cas9 offer promising avenues. MALAT1-targeting ASOs have demonstrated clinical efficacy, highlighting their translational potential [173]. Future efforts should aim to define tissue-specific lncRNA profiles and clarify their roles in spatial and temporal GTPase regulation, potentially leading to novel interventions for RHO GTPase-driven cancers [146].

1.2.2 Accessory Proteins

Accessory proteins regulate the spatiotemporal dynamics of signal transduction, ensuring efficiency, specificity, and strength in pathway activation. This group includes adaptors, anchors, docking proteins, and scaffolds, which assemble signaling components through modular multivalent interactions [174]. By facilitating physical interactions and promoting processes such as liquid–liquid phase separation (LLPS), they increase local concentrations of signaling molecules and enhance pathway efficiency. LLPS-driven condensates, for instance, can concentrate kinases while excluding phosphatases, enabling selective signal propagation. Though accessory proteins typically lack enzymatic activity, their protein–protein interaction domains, intrinsically disordered regions (IDRs), and lipid-binding motifs enable them to form macromolecular complexes essential for pathways such as RTK–RAS–MAPK and RAC1/CDC42–PAK1 [174, 175]. Targeting these proteins may allow modulation of signaling networks while preserving core physiological functions, making them promising therapeutic candidates [10].

Structurally and functionally diverse, accessory proteins include scaffold proteins like IQGAP1, KSR1, and FHL1, which coordinate multiple signaling elements; adaptor proteins such as GRB2, which link RTKs to downstream effectors like SOS1 [176-179] ; anchoring proteins such as CNK1 and flotillins, which localize signaling molecules to membranes; and docking proteins that stabilize RTK-effector interactions [180-182]. These proteins are involved in processes such as the organization of RAS nanoclusters at the plasma membrane and stabilization of RAF–MEK–ERK complexes, and they can influence RAS activation cycles [10]. Dysregulation of accessory proteins has been implicated in cancer, developmental disorders, and cardiovascular diseases, reinforcing their importance as therapeutic targets [10] (Figure 8A).

In cancer, accessory protein mutations and alterations can drive tumor growth and metastasis. [10]. For example, paxillin mutations enhance focal adhesion complex activity in non-small cell lung cancer, while SPRED1/2 downregulation in hepatocellular carcinoma contributes to hyperactive RAS signaling [183, 184]. IQGAP1 supports tumor progression by stabilizing RAS–MAPK complexes [185]. In RASopathies, mild gain-of-function mutations in SHOC2 cause Noonan-like and Mazzanti syndromes [186], germline mutations in *CBL* and *SPRED1* are linked to Legius syndrome and juvenile myelomonocytic leukemia [187, 188]. Additionally, SHP2 inhibits T-cell receptor (TCR) signaling, contributing to immune evasion, while FHL1/2 mutations are associated with hypertrophic cardiomyopathy [178, 189].

Targeting accessory proteins offers a compelling alternative to direct inhibition of core signaling molecules, which often leads to toxicity or resistance [10]. Examples include SHOC2, GIT1, CNK1, GRB2, and IQGAP1, which serve as therapeutic entry points by modulating signaling architecture [174]. SHOC2 knockout sensitizes RAS-mutant cancers to MEK inhibition, while CNK1 inhibitors such as PHT-7.3 block KRAS-driven tumor growth [190]. GRB2-targeted antisense oligonucleotides (ASOs) suppress oncogenic signaling in BCR-ABL–positive malignancies [191, 192]. Other strategies include APS-2-79, an inhibitor of KSR-mediated MEK phosphorylation, and SHP099, which stabilizes SHP2 in an inactive conformation to counteract resistance and promote anti-tumor immunity [193, 194].

Although promising, accessory proteins remain underexplored, and identifying context-specific modulators using technologies like CRISPR/Cas9 and live-cell imaging is essential to uncover their full therapeutic potential. Of particular interest is PAK1, whose modulation by accessory proteins governs cytoskeletal dynamics, migration, and oncogenic signaling [10, 174, 195].

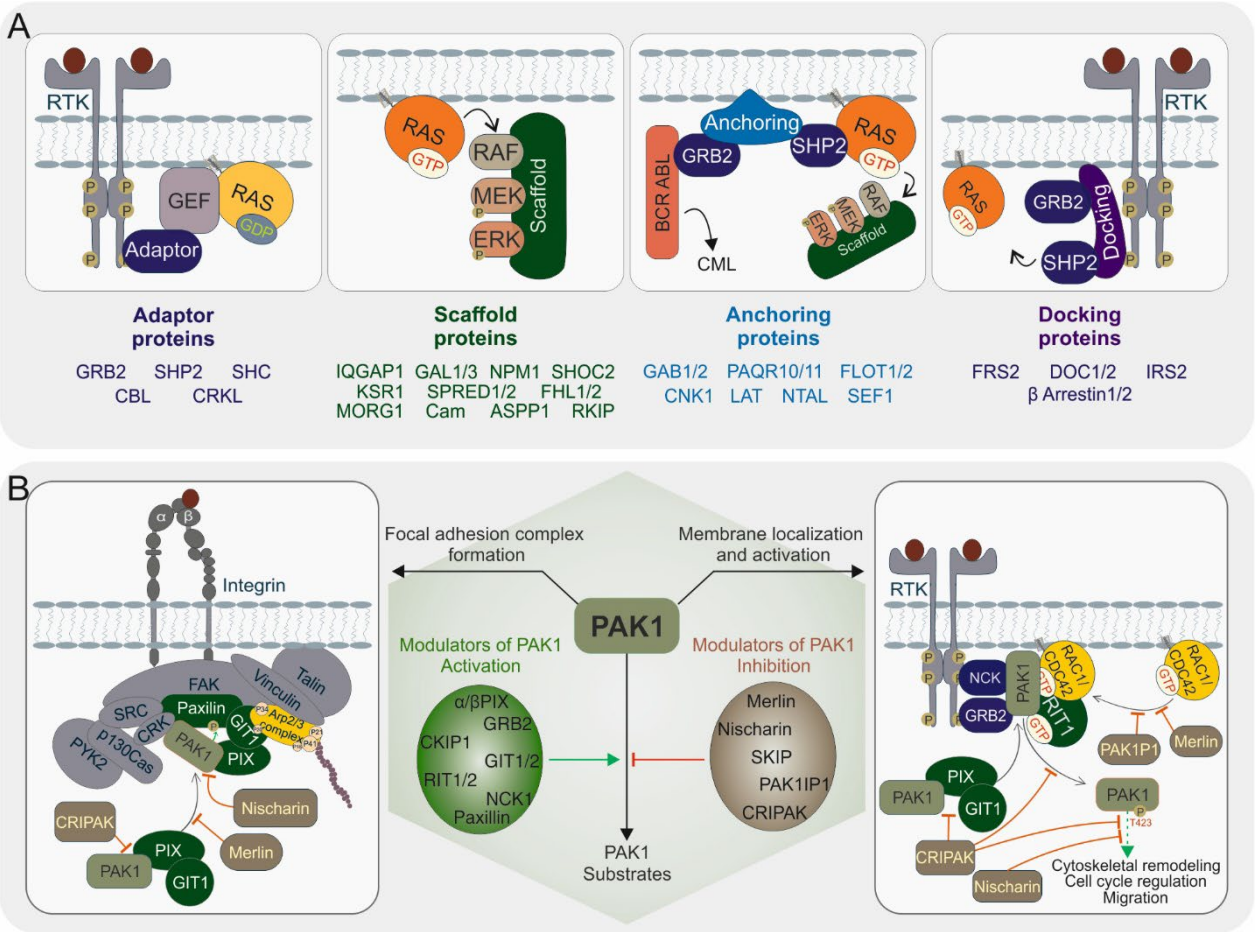

Figure 8. Classification and regulatory functions of accessory proteins in RAS and PAK1 signaling. (**A**) Schematic representation of accessory proteins classified based on their function within the KRAS signaling pathway. These include adaptor proteins (e.g., GRB2, SHP2, SHC), which link activated receptor tyrosine kinases (RTKs) to downstream signaling components via Src homology 2 (SH2) and typically SH3 domains; scaffold proteins (e.g., IQGAP1, GAL1/3, SHOC2), which organize signaling complexes to ensure spatial and temporal specificity; anchoring proteins (e.g., GAB1/2, CNK1, PAQR10/11), which tether signaling molecules to specific cellular compartments through pleckstrin homology (PH), prohibitin homology (PHB), or transmembrane (TM) domains; and docking proteins (e.g., FRS2, DOC1, IRS2), which facilitate the recruitment of effectors to activated receptors, often containing phosphotyrosine-binding (PTB) and membrane-targeting domains. (**B**) Schematic illustration of accessory modulators of PAK1 activity. Positive regulators of PAK1 activation include α/βPIX, GRB2, GIT1/2, RIT1/2, CKIP1, NCK, and paxillin, which collectively contribute to focal adhesion complex formation and membrane localization of PAK1. Negative modulators, including CRIPAK, SKIP, PAK1IP1, Merlin, and Nischarin, suppress PAK1 activity. This finely tuned balance regulates PAK1-dependent signaling pathways involved in cytoskeletal remodeling, cell cycle progression, and cellular migration.

1.2.2.1 Accessory Modulator of PAK1

PAK1 is a serine/threonine kinase that regulates cytoskeletal remodeling, adhesion, motility, and transcription [106, 196]. Activated by RHO GTPases, primarily RAC1 and CDC42, PAK1 is recruited to specific subcellular sites where it integrates signaling inputs. Its dysregulation is associated with tumor progression, therapy resistance, and poor outcomes in cancer [106]. Accessory proteins that modulate the spatiotemporal activity of PAK1 thus represent important therapeutic targets [106].

Positive regulators of PAK1 include scaffolds such as αPIX and βPIX, which interact with its proline-rich domain and guide localization to focal adhesions [197]. In complex with GIT1 and GIT2, these proteins stabilize PAK1 and promote cytoskeletal signaling [198]. CKIP1 enhances Ser223 phosphorylation in a PI3K-dependent manner, increasing kinase activity and promoting actin remodeling [199]. Adaptor proteins such as GRB2 and NCK1 connect PAK1 to RTKs and active RAC1/CDC42, facilitating migration and adhesion remodeling [200, 201]. Paxllin coordinates PAK1 with GIT1 and PIX in focal adhesion complexes [202], while RIT1 binds PAK1's CRIB domain, stabilizing interactions with RAC1 and CDC42 and promoting actin-driven motility [40] (Figure 8B).

Negative regulation is equally crucial to prevent aberrant signaling. CRIPAK binds PAK1's autoinhibitory domain, stabilizing its inactive state and blocking upstream activation [203]. Merlin inhibits PAK1 recruitment to focal adhesions and interferes with RAC1 and paxillin binding [204]. Nischarin binds the PAK1 kinase domain, suppressing downstream effectors such as LIMK [205]. Other inhibitory modulators, including PAK1IP1 and SKIP, act through distinct interference mechanisms to restrain PAK1 signaling [106, 206, 207] (Figure 8B).

In cancer, PAK1 hyperactivation promotes tumor invasiveness and therapeutic resistance [106]. Targeting accessory proteins offers a strategy to modulate PAK1 activity while preserving its physiological roles. Inhibiting GRB2, NCK1, or paxillin may limit PAK1 localization, while stabilizing its interactions with CRIPAK or Merlin could suppress hyperactivation [106]. Small molecules such as AX-024, which block NCK1–PAK1 interactions, exemplify this strategy [208]. Additionally, lncRNAs like H19 and MALAT1 regulate PAK1 pathways and represent emerging therapeutic targets [170, 209].

Further research is needed to clarify the dynamic regulation of PAK1 by accessory proteins. Advancing targeted approaches may enable the development of precise therapies that restore balance in PAK1-dependent pathways, minimizing off-target effects and improving outcomes in PAK1-driven diseases [106].

1.2.2.2 IQGAP1: A Versatile Scaffolding Protein

IQGAP1 is a multifunctional scaffolding protein that integrates diverse signaling pathways to regulate cytoskeletal organization, cell adhesion, and intracellular communication. Identified in 1994, IQGAP1 is widely expressed and structurally resembles RASGAPs but lacks intrinsic GAP activity. Instead, it binds and stabilizes RAC1 and CDC42 in their active GTP-bound states, thereby facilitating actin cytoskeletal remodeling, cell–cell adhesion, and signaling cascades, including the MAPK pathway [100].

IQGAP1 contains multiple domains critical for its regulatory roles. The calponin homology domain (CHD) binds F-actin, while the RasGAP-related domain (GRD) interacts with RAC1 and CDC42. This interaction is reinforced by the RASGAP C-terminal (RGCT) domain and further stabilized by the very C-terminal (CT) domain. Unlike classical GAPs that promote GTP hydrolysis and inactivation of small GTPases, IQGAP1 functions as a scaffold that maintains RAC1 and CDC42 in their active conformations, enhancing downstream signaling [210].

In cell adhesion, IQGAP1 localizes to junctional complexes where it modulates E-cadherin-mediated adhesion through interactions with β-catenin. This regulation is GTPase-dependent. When RAC1 and CDC42 are active, they inhibit IQGAP1–β-catenin binding, stabilizing adhesion. When inactive, IQGAP1 binds β-catenin, disrupting α-catenin interactions and weakening

adhesion, thereby promoting cell migration [210, 211]. This dual mechanism contributes to EMT and tumor cell invasion [212].

IQGAP1 is also essential for cytoskeletal remodeling. It crosslinks actin filaments and coordinates regulators such as N-WASP and Diaphanous-related formins to promote directional cell movement. At the leading edge of migrating cells, IQGAP1 connects actin and microtubule networks, ensuring coordinated cytoskeletal rearrangement [210, 213].

Beyond cytoskeletal regulation, IQGAP1 is a key component of the RAS–MAPK and Wnt/β-catenin pathways [185, 212]. It facilitates MAPK signaling by interacting with MEK and ERK, enhancing signal transduction in response to growth factors (Figure 8A). In Wnt signaling, IQGAP1 modulates β-catenin nuclear translocation and transcriptional activity, contributing to proliferation, differentiation, and oncogenesis [185, 210, 212].

Recent findings propose a multi-step mechanism for IQGAP1's interaction with RAC1 and CDC42. The RGCT domain initially binds the switch regions of GTP-bound GTPases, followed by GRD-mediated stabilization through adjacent residues, and further association via the CT domain. Interestingly, CDC42 binding promotes IQGAP1 dimerization and actin crosslinking, whereas RAC1 may interact through a distinct mechanism [86].

IQGAP1 is frequently overexpressed in various cancers, including glioblastoma, breast, colorectal, and gastric cancers, where it enhances proliferation, migration, and invasion [210]. High IQGAP1 expression correlates with aggressive tumor phenotypes, particularly in glioblastoma, breast, colorectal, and gastric cancers [214]. Functional studies show that silencing IQGAP1 reduces invasiveness, while overexpression enhances malignancy. IQGAP1 also contributes to invadopodia formation and extracellular matrix degradation, promoting metastasis [215]. Its interaction with RAC1/CDC42, the exocyst complex, and MT1-MMP trafficking underscores its role in cancer propagation [210, 216].

Overall, IQGAP1 serves as a central scaffolding protein coordinating cytoskeletal dynamics, adhesion, and signal transduction. Its interactions with RAC1 and CDC42 are fundamental to its role in cell migration and invasion. Through its integration into MAPK and Wnt signaling pathways, IQGAP1 contributes to tumor progression and represents a compelling target for therapeutic intervention [100, 210].

1.2.2.3 LZTR1: A Negative Modulator of the RAS-MAPK Signaling Pathway

Leucine zipper-like transcription regulator 1 (LZTR1) is a key modulator of the RAS–MAPK signaling pathway. It functions as a substrate-specific adaptor of the CUL3 (Cullin 3) E3 ubiquitin ligase complex and promotes the ubiquitination and degradation of RAS proteins, including KRAS, NRAS, HRAS, RIT1, and MRAS [217]. Through this regulatory mechanism, LZTR1 maintains balanced RAS signaling. Loss-of-function mutations in LZTR1 impair its ability to promote RAS turnover, resulting in RAS accumulation and sustained MAPK activation, which contributes to developmental disorders and malignancies [41, 218] (Figure 2B).

LZTR1 contains six N-terminal Kelch repeats responsible for substrate recognition and two C-terminal BTB-BACK domains required for dimerization and CUL3 interaction. Unlike other BTB-Kelch proteins, LZTR1 localizes to the Golgi complex, indicating potential roles in intracellular trafficking. Recent studies show that LZTR1 mediates MRAS degradation through non-proteasomal mechanisms, while RIT1 is degraded via both LZTR1-dependent and independent pathways [41, 218, 219].

Mutations in LZTR1 have been implicated in Noonan syndrome (NS), glioblastoma (GBM), chronic myeloid leukemia (CML), and schwannomatosis [217]. n NS, dominant mutations within the Kelch domains hinder substrate recognition, leading to hyperactivation of MAPK signaling. A homozygous L580P mutation in LZTR1 has been identified as a causative variant in early-onset hypertrophic cardiomyopathy. This mutation disrupts dimerization, induces linear polymerization of the protein, and results in accumulation of RAS GTPases [218]. In GBM, loss of LZTR1 prevents degradation of RIT1, contributing to tumor growth. In CML, LZTR1 inactivation is associated with MAPK hyperactivation and resistance to tyrosine kinase inhibitors [217]. Mutations linked to schwannomatosis are distributed more broadly across the protein and affect both substrate binding and interaction with CUL3 [217, 219].

Given its central role in negatively regulating RAS–MAPK signaling, LZTR1 represents a promising therapeutic target. Strategies aimed at restoring its function, stabilizing its interaction with CUL3, or suppressing downstream effectors may provide new treatment options for RASopathies and RAS-driven cancers [217]. Understanding the effects of specific pathogenic variants, such as L580P, is essential for advancing precision medicine approaches. Emerging technologies, including CRISPR-based therapies, offer potential for correcting LZTR1-associated disease phenotypes [218].

2 Aims and Objectives

This thesis primarily aims to elucidate the molecular mechanisms that regulate small GTPases of the RAS superfamily, including the RAS, RHO, and ARF families. These proteins act as molecular switches that control critical cellular processes, such as proliferation, migration, differentiation, and intracellular transport. Dysregulation of these proteins has been associated with various pathological conditions, including cancer, developmental disorders, and infections. This work integrates detailed biochemical characterization with cellular and interaction analyses to deepen our understanding of small GTPase regulation and identify novel modulators and interaction partners with therapeutic potential. A key objective is to define the oncogenic behavior of the melanoma-associated RAC1 P29S hotspot mutation. Through biochemical assays, effector binding studies, and regulatory profiling, this study aims to clarify how the mutation drives constitutive signaling and malignancy by elucidating its underlying molecular mechanisms. These insights will provide a mechanistic basis for developing targeted therapies. Another objective is to characterize the non-classical ARF-like GTPase TITAN5 (TTN5) in *Arabidopsis thaliana*. The study explores TTN5's atypical kinetic properties, membrane localization, and role in vesicular trafficking. This highlights the evolutionary adaptation of small GTPase functions in plants and their potential relevance to plant development and productivity. This thesis further investigates the regulatory and biochemical features of RIT GTPases. These are structurally canonical, yet functionally distinct, RAS-family members. Through the assessment of nucleotide exchange and hydrolysis rates, effector binding, and membrane interactions, the study aims to clarify the unique signaling roles of RIT GTPases in cancer and RASopathies while identifying candidate regulatory factors for further investigation. Additionally, the research explores the reciprocal regulation of RAS and RHO signaling in hepatic stellate cells to understand how specific GTPase members, including ERAS, RND3, MRAS, and RHOC, control the transition between quiescent and activated states. This analysis advances our understanding of liver fibrosis and opens opportunities for the therapeutic modulation of fibrogenic signaling. A key objective is to expand the current understanding of small GTPase regulation by investigating noncanonical modulators. Experimentally, the study assesses the influence of accessory proteins, such as IQGAP1, galectin-3, PDEδ, SHOC2, and NPM1, on KRAS-driven signaling and downstream pathway engagement. Concurrently, systematic literature-based reviews identify and classify long noncoding RNAs (lncRNAs) associated with KRAS and RHOA signaling and accessory modulators of PAK1. These reviews emphasize the roles of these modulators in spatial, temporal, and post-transcriptional regulation. This thesis investigates the pathogenic LZTR1 L580P mutation and its impact on RIT1 and MRAS degradation via the CUL3-LZTR1 complex. The study aims to clarify how LZTR1 polymerization impairs proteasomal targeting, leading to MAPK hyperactivation in Noonan syndrome-related cardiac pathology. This hypothesis is validated using patient-derived cardiomyocyte models. Lastly, the study examines the effect of the *Chlamydia pneumoniae* effector SemD as a structural and functional mimic of human CDC42. By analyzing SemD's selective activation of N-WASP and its interactions with host membrane-remodeling machinery, this research highlights a sophisticated pathogenic strategy and reveals novel intervention points in bacterial infection. Together, these objectives address conserved and context-specific principles of small GTPase signaling, providing an integrated framework for understanding their regulation and functional diversity across biological systems.

Chapter I. New insights into the classification of the RAC1 P29S hotspot mutation in melanoma as an oncogene

Authors: Amin Mirzaiebadizi, Mohammad Reza Ahmadian

DOI: 10.1101/2025.03.04.637030

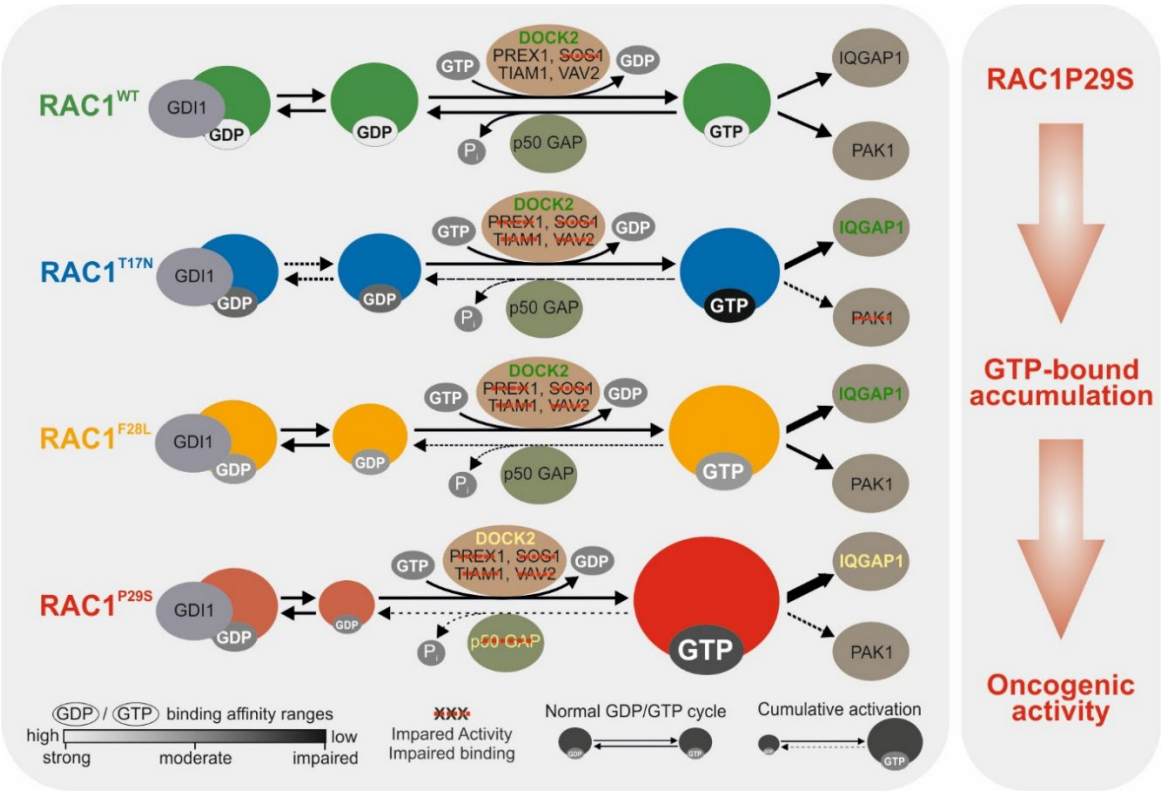

Status: Online Preprint, *bioRxiv*

Journal: -

JIF: -

Contribution: ≈95%

A.M. developed and optimized the experimental methods, performed all biochemical and cellular experiments, and assessed the results. He expressed and purified more than 14 RAC1 variants along with their regulators and effectors. He re-established and implemented a comprehensive biochemical workflow comprising HPLC-based nucleotide analysis, fluorescence polarization, stopped-flow fluorimetry, and GTPase activity pull-down assays. He integrated these methods with cell-based experiments, including transfection and Western blotting, to evaluate downstream signaling. A.M. and M.R.A. drafted and approved the final version of the manuscript.

New insights into the classification of the RAC1 P29S hotspot mutation in melanoma as an oncogene

Amin Mirzaiebadizi[1*], Mohammad Reza Ahmadian[1*]

[1] Institute of Biochemistry and Molecular Biology II, Medical Faculty and University Hospital Düsseldorf, Heinrich Heine University, 40225 Düsseldorf, Germany
[*]Corresponding authors: amin.mirzaiebadizi@hhu.de; reza.ahmadian@hhu.de

Running title: The gain-of-function mechanism of RAC1^{P29S}

Abstract
The RAC1^{P29S} hotspot mutation, prevalent in melanoma, drives tumorigenesis by enhancing molecular interactions and hyperactivating key signaling pathways, making it a compelling target for cancer therapy. This study provides a comprehensive biochemical characterization of RAC1^{P29S} compared to wild-type RAC1 and mutations T17N and F28L. The P29S mutation significantly impairs nucleotide binding to guanosine triphosphate (GTP) and guanosine diphosphate, accelerating intrinsic nucleotide exchange. While minimally affecting regulation by guanosine dissociation inhibitor 1, RAC1^{P29S} exhibits reduced activation via diffuse B-cell lymphoma family guanine nucleotide exchange factors but retains effective activation by dedicator of cytokinesis 2. Critically, the P29S mutation severely impairs GTPase-activating protein-stimulated GTP hydrolysis, most likely contributing to RAC1^{P29S} hyperactivation by prolonging its GTP-bound form. RAC1^{P29S} displays a stronger binding affinity for IQ motif-containing GTPase-activating protein 1 than for p21-activated kinase 1, highlighting the role of the former in scaffolding RAC1^{P29S}-driven signaling. In serum-starved cells, RAC1^{P29S} predominantly adopts an active GTP-bound state. RAC1^{P29S} overexpression activates key cancer-associated pathways, including extracellular signal-regulated kinase and p38 mitogen-activated protein kinase, reinforcing its role as an oncogenic driver in melanoma. These insights suggest potential therapeutic targets for melanoma treatment, including RAC1 regulators and modulators.

Keywords: Small GTPases, RAC1, P29S mutation, oncogene, gain of function, melanoma, drug resistance, DOCK2, p50GAP, IQGAP1

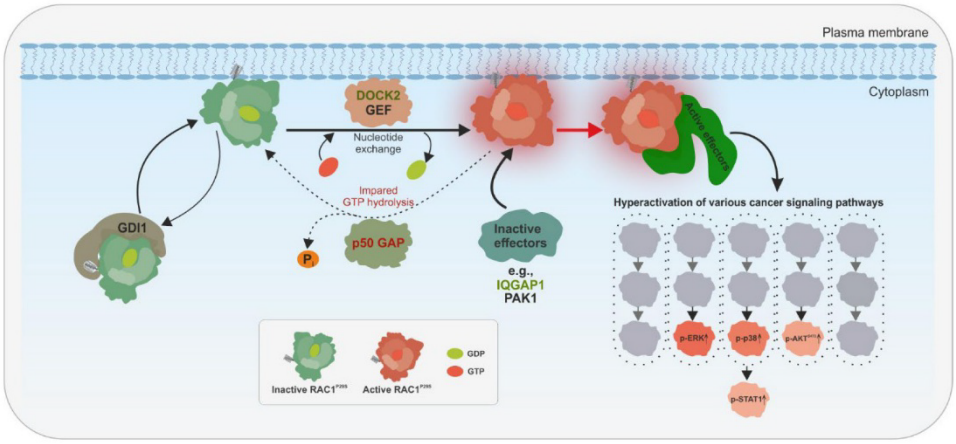

Graphical abstract. A model of RAC1^{P29S} activation and signaling in cancer cells. RAC1^{P29S} remains in an inactive GDP-bound state in the cytoplasm where GDI1 prevents its membrane association. Upon stimulation, GEFs, primarily DOCK2, activate RAC1^{P29S} by promoting GDP-GTP exchange, facilitating its transition to the active GTP-bound state and initiating

downstream signaling. RAC1^{P29S} binds preferentially to IQGAP1 over PAK1, reflecting a shift in effector interactions. IQGAP1 acts as a scaffolding protein, spatially modulating RAC1^{P29S}-driven signaling and amplifying its effects. Under normal conditions, GAPs such as p50GAP regulate RAC1 by accelerating GTP hydrolysis, thereby maintaining its dynamic activation cycle. However, the P29S mutation severely impairs p50GAP-mediated hydrolysis, leading to accumulation of RAC1^{P29S} in its GTP-bound state and loss of temporal regulation. This persistent activation hyperactivates downstream effectors and promotes cancer-associated pathways, including ERK and p38 MAPK, which drive cell growth, survival, invasion and metastasis.

Introduction

As a key member of the RHO guanosine triphosphatase (GTPase) family, RAC1 functions as a molecular switch, cycling between an inactive guanosine diphosphate (GDP)-bound form and an active guanosine triphosphate (GTP)-bound form (1). This switch relies on two essential processes—GDP/GTP exchange and GTP hydrolysis—which induce structural changes in the switch I (amino acids 29–42) and switch II (amino acids 62–68) regions (2). These functions are regulated by guanine nucleotide exchange factors (GEFs) and GTPase-activating proteins (GAPs) (3-5). The RHO GEF family includes the structurally distinct dedicator of cytokinesis (DOCK) and diffuse B-cell lymphoma (DBL) subfamilies (1, 6, 7). In addition, guanine nucleotide dissociation inhibitors (GDIs) selectively bind geranylgeranylated RAC1, controlling its membrane localization (8).

RAC1 and its isoform RAC1B (9) and paralogs RAC2 and RAC3 (10) activate diverse signaling pathways through direct interaction with effector proteins (1). These interactions regulate essential cellular processes, including motility, oxidative stress, and inflammation (11). GTP-bound RAC1 binds effectors, activating kinases like p21-activated kinase 1 (PAK1) and scaffolding proteins like IQ motif-containing GTPase-activating protein 1 (IQGAP1) (1). Dysregulation (12, 13) or gain-of-function mutations in RAC genes (14, 15) can hyperactivate RAC signaling, altering cellular responses and contributing to cancer. This dysregulation contributes to various pathological conditions, including cancer (16) , and other pathological conditions, including metabolic, neurodegenerative, cardiovascular, inflammatory, and infectious diseases (11).

The proline 29 to serine (P29S) mutation in RAC1 is the third most common hotspot mutation in melanoma, following BRAF V600E and NRAS Q61R (17). Despite its prevalence, the regulatory functions driving RAC1^{P29S} pro-tumorigenic effects remain poorly understood (18). Functional studies show that RAC1^{P29S} enhances effector binding, including PAK1 and mixed lineage kinase 3 (MLK3), promoting melanocyte proliferation and migration (19, 20). Additionally, RAC1^{P29S} inhibits invadopodia function (21), abolishes haptotaxis (22), drives dedifferentiation in melanoma, contributes to BRAF inhibitor resistance (23-25), and facilitates immune evasion via programmed death-ligand 1 (PD-L1) upregulation through the RAC1^{P29S}-PAK1 axis (17). This immune evasion is mediated by the RAC1^{P29S}-PAK1 axis, which promotes the G2/M cell cycle transition through phosphorylation of Aurora kinase A and polo-like kinase 1 (PLK1) (26) and inactivates neurofibromin 2 (NF2)/Merlin, promoting proliferation, metastasis, and drug resistance (27). Furthermore, while BRAF^{V600E} suppresses cell migration, extracellular signal-regulated kinase (ERK) pathway inhibition accelerates migration and invasion in BRAF^{V600E}- and mutant RAS-driven tumors (28). Although RAC1 is a critical therapeutic target in melanoma, its undruggable nature poses a significant challenge for targeting RAC1^{P29S} (11, 29-35).

Initial studies using radiolabeled nucleotide filter binding assays or thin-layer chromatography compared the basal GDP/GTP exchange and GTP hydrolysis of RAC1^{P29S} with RAC1^{WT}. Davis et al. reported increased GTP dissociation for RAC1^{P29S} (36), while Kawazu et al. observed increased GDP dissociation but not GTP dissociation (37). Both studies concluded that GTP hydrolysis remained unchanged. However, these and other overexpression studies alone cannot classify RAC1^{P29S} as spontaneously activating, self-activating, fast cycling,

constitutively active, or oncogenic (Box 1) (20, 21, 36, 38, 39). Some of these classifications are derived from assumptions about the phenylalanine 28 to leucine (F28L) mutant of RAC1. Although $RAC1^{F28L}$ is not extensively studied, it is described as a fast-cycling mutant, analogous to $CDC42^{F28L}$, capable of spontaneous nucleotide exchange without GEF activation while retaining full GTPase activity (40). Another widely studied mutant, threonine 17 to aspargine (T17N), is a dominant negative mutant with T17 in the phosphate-binding loop (P-loop), a region critical for nucleotide binding, while F28 and P29 reside at the N-terminus of switch I. The P-loop and switch I are essential for RAC1 nucleotide binding and hydrolysis (1). Biophysical and biochemical studies, supported by molecular dynamics simulations, indicate that the P29S mutation increases switch I flexibility, adopting an open conformation that facilitates rapid GDP/GTP exchange in RAC1 (20, 36, 41, 42).

This study comprehensively characterizes $RAC1^{P29S}$ at three levels: intrinsic properties, regulation, and effector interaction. At the intrinsic level, we analyzed its nucleotide exchange, GTP hydrolysis, and binding affinities for GDP and GTP. Studies on regulatory mechanisms examined its interaction with DBL and DOCK family GEFs, p50 Rho GTPase-activating protein (p50GAP)-mediated GTP hydrolysis, and GDI1-mediated regulation. Effector interactions focused on key proteins, including PAK1, a kinase, and IQGAP1, a scaffolding protein modulating RAC1 signaling. Active GTPase pull-down experiments under serum-stimulated and serum-starved conditions provided further insights into the GTP-bound state of $RAC1^{P29S}$ in cells. Comparative analyses with $RAC1^{WT}$, $RAC1^{T17N}$, and $RAC1^{F28L}$ revealed distinct properties of $RAC1^{P29S}$, including a fast intrinsic nucleotide exchange rate, DOCK2-mediated exchange facilitation, and severely impaired p50GAP-stimulated GTP hydrolysis. These biochemical and functional differences result in hyperactivation and preferential signaling through IQGAP1 rather than PAK1. Taken together, these findings highlight potential therapeutic targets in melanoma, including DOCK2, p50GAP, and IQGAP1.

Material and Methods

Constructs. Human RAC1 wild-type ($RAC1^{WT}$; accession no. P63000) and its mutants T17N, F28L, and P29S were expressed as N-terminal glutathione S-transferase (GST)-tagged fusion proteins using pGEX vectors (pGEX-2T and pGEX-4T-1). The same system was used to express regulators and effectors, including full-length GDI1, the Dbl homology-pleckstrin homology (DH-PH) tandem domains of T-lymphoma invasion and metastasis-inducing protein 1 (TIAM1), vav guanine nucleotide exchange factor 2 (VAV2), son of sevenless homolog 1 (SOS1), and phosphatidylinositol-3,4,5-trisphosphate-dependent Rac exchanger 1 (PREX1); the GAP domain of p50GAP; the C-terminal 794-amino acid region of IQGAP1; and the RAC1 binding domain (RBD) of PAK1. Additional constructs included His-tagged IQGAP1 (pET-23b+ vector) and His6-small ubiquitin-like modifier (SUMO)-tagged DOCK2 Dock homology region 2 (DHR2) domain (pOPINS vector). RAC1 constructs with N-terminal tandem decahistidine triple-flag tags were cloned into the pcDNA-3.1 vector for eukaryotic expression. Detailed deconstructs description including accession numbers and amino acid sequences, are available in the Supplementary information.

Proteins. All proteins were purified as described previously (3, 5, 9, 10, 43). Briefly, Escherichia coli strains were transformed for protein expression, lysed, and subjected to affinity purification using GST or His tags. GST tags were cleaved when necessary, and proteins were buffer-exchanged into optimized storage buffers. Purity was confirmed by SDS-PAGE and Coomassie staining (Supplementary Fig. S1), which shows the purified proteins used in this study. Proteins were stored at -80 °C. Detailed procedures are available in the Supplementary Materials.

Preparation of nucleotide-free and fluorescent nucleotide-bound GTPases. As previously described, nucleotide-free GTPases were prepared through sequential treatment with alkaline phosphatase and snake venom phosphodiesterase (44, 45). Fluorescent GDP- and GppNHp-bound GTPases were generated by incubating nucleotide-free proteins with mant-labeled nucleotides (mdGDP and mGppNHp). Protein concentrations were quantified by HPLC using

NAP-5 buffer exchange columns. Samples were stored at −80 °C. Detailed procedures are provided in the Supplementary Materials.

Fluorescence kinetic measurements. Fluorescence-based kinetic measurements for long-term and rapid reactions were performed using a Horiba Fluoromax-4 fluorimeter and a stopped-flow spectrophotometer (Applied Photophysics SX20), as described (43-46). Excitation and emission wavelengths were set according to the fluorophore-specific properties of mant- and tamra-labeled nucleotides. Detailed experimental conditions are provided in the Supplementary Materials.

Nucleotide-binding assay. The nucleotide-binding properties of RAC1 GTPases were assessed by stopped-flow fluorimetry, as described (47). Nucleotide association and dissociation rates were measured using fluorescent nucleotides (mdGDP and mGppNHp) and varying RAC1 concentrations. Association (k_{on}) and dissociation (k_{off}) rate constants were determined, and equilibrium dissociation constants (K_d) were calculated as described in Box 2. Detailed procedures are provided in the Supplementary Materials.

GEF-catalyzed nucleotide dissociation assay. The GEF-catalyzed nucleotide exchange reaction was monitored by stopped-flow fluorimetry, as described (45). Reactions were performed with mGDP-bound RAC1 and excess non-fluorescent nucleotide in the presence of GEFs from the DBL and DOCK families. Observed rate constants were analyzed using a single-exponential model in Origin software. Detailed procedures are provided in the Supplementary Materials.

Intrinsic and GAP-stimulated GTP-hydrolysis assays. The intrinsic GTP hydrolysis rate of RAC1 proteins was determined by high-performance liquid chromatography (HPLC), as described (45). Reactions were performed with nucleotide-free RAC1 and GTP in buffer C at 25 °C, and catalytic rate constants (k_{cat}) were calculated using Origin software. GAP-stimulated hydrolysis rates were measured by stopped-flow fluorimetry using tamra-GTP, as described (48). Detailed procedures are provided in the Supplementary Materials.

Protein-protein interaction kinetics. The interaction of RAC1 with GST-GDI1, GST-PAK1 RBD, and His-IQGAP1 C794 was analyzed by stopped-flow fluorimetry to determine k_{on}, k_{off}, and K_d values, as described (43). Binding assays were performed using mdGDP- and mGppNHp-bound RAC1 with varying protein concentrations, and rate constants were calculated using linear regression and single-exponential fits. Detailed procedures are provided in the Supplementary Materials.

Fluorescence polarization. Fluorescence polarization was used to determine the binding affinity between RAC1 and effector proteins, as described (43). Assays were performed with mGppNHp-bound RAC1 (1 µM) and titrated effectors in buffer containing 30 mM Tris-HCl (pH 7.5), 50 mM NaCl, 5 mM $MgCl_2$, and 3 mM DTT at 25 °C. K_d values were calculated by fitting binding curves to a quadratic ligand binding equation. Detailed procedures are provided in the Supplementary Materials.

Cell culture and transfection. HEK-293T cells were cultured under serum-stimulated and serum-starved conditions in DMEM supplemented with 10% FBS and 1% penicillin/streptomycin. RAC1 constructs with N-terminal 10 His-triple flag tags were transfected using TurboFect™ (Thermo Fisher Scientific) according to the manufacturer's protocol. Cells were harvested and lysed, and protein concentrations were measured using the Bradford assay. Detailed protocols, including buffer compositions, are provided in the supplementary information.

***In vitro* pull-down assays.** Pull-down assays were conducted to assess RAC1 binding to PAK1 RBD and IQGAP1 C794. GST-PAK1 RBD and His-IQGAP1 C794 were immobilized on glutathione-agarose and His-Mag Sepharose Ni beads, respectively. RAC1 proteins were

incubated with the beads, washed, eluted, and analyzed by SDS-PAGE followed by immunoblotting. Detailed protocols are provided in the Supplementary Materials.

Active GTPase pull-down assay. A pull-down assay was performed to assess GTP-bound active RAC1 levels in transiently transfected HEK-293T cells under serum-stimulated and serum-starved conditions, as described (49). GST-PAK1 RBD- and GST-IQGAP1 C794-coupled beads were prepared, incubated with lysates, washed, and analyzed by SDS-PAGE and immunoblotting. Detailed protocols are provided in the Supplementary Materials.

Antibodies and Immunoblotting. Primary and secondary antibodies were diluted in TBST with a blocking buffer. The antibodies included α-RAC1, α-6x-His, α-flag, α-γ-tubulin, α-p-ERK1/2, α-t-ERK1/2, α-p-AKT, α-t-AKT, α-p-p38 MAPK, α-p38 MAPK, α-p-STAT1, α-STAT1, α-GAPDH, and α-GST. Immunoblots were visualized using the Odyssey® XF Imaging System. Detailed antibody lists and protocols are provided in the Supplementary Materials.

Statistical Analysis. Data in bar graphs represent mean ± S.D., with replicate numbers detailed in figure legends. Immunoblot intensities were quantified using Image Studio Lite 5.2. For pull-down assays, data were normalized based on RAC1-to-effector ratios, and active RAC1 levels were calculated as described in Fig. 4B. Downstream signaling data were normalized to phosphorylated-to-total protein ratios and adjusted to GAPDH levels as a loading control. Statistical significance was determined using one-way ANOVA followed by Tukey's test (*P ≤ 0.05, **P ≤ 0.01, ***P ≤ 0.001, ****P ≤ 0.0001). Detailed normalization methods and calculations are provided in the Supplementary Materials.

Results

P29S significantly impairs the nucleotide binding of RAC1. Two sets of real-time kinetic measurements were performed to investigate the impact of the P29S mutation on nucleotide binding affinity. The first measured the association of mdGDP and mGppNHp with nucleotide-free (n.f.) RAC1 (Fig. 1A), while the second analyzed the dissociation of these nucleotides from RAC1 (Fig. 1B). The fluorescent analog mdGDP was used as a substitute for GDP, and the non-hydrolyzable mGppNHp replaced GTP. The RAC1 variants included WT, T17N, F28L, and P29S.

Binding of nucleotides to n.f. RAC1 induced a rapid fluorescence increase, with k_{obs} values rising proportionally with n.f. RAC1 concentrations (supplementary Fig. S2 and S3, left panels), which depict the interaction of mdGDP and mGppNHp with RAC1 at increasing concentrations. The k_{on} values for mdGDP and mGppNHp binding were derived from linear fits of kobs values across protein concentrations (supplementary Fig. S2 and S3, middle panels), where k_on was determined by plotting observed rate constants from exponential fits of association data against the corresponding RAC1 concentrations. A bar graph of kon values showed significant differences in nucleotide association among RAC1 variants (Fig. 1C). The P29S mutation notably reduced the association of mdGDP and mGppNHp with RAC1 by 14-fold and 27-fold, respectively, compared to $RAC1^{WT}$.

A decrease in fluorescence was observed during nucleotide dissociation from RAC1 proteins in the presence of excess free GDP (supplementary Fig. S2 and S3, right panels), which depict the dissociation kinetics of mdGDP and mGppNHp from RAC1 proteins. The k_{off} values, derived from single exponential fits of the dissociation data, are shown as bar graphs (Fig. 1C). $RAC1^{P29S}$ and $RAC1^{F28L}$ exhibited intrinsic nucleotide dissociation rates 10- and 20-fold faster than $RAC1^{WT}$, respectively. $RAC1^{T17N}$ showed the fastest mdGDP dissociation rate, 410-fold higher than $RAC1^{WT}$, resulting in a significantly reduced K_d and a 1346-fold decrease in binding affinity, highlighting its dominant-negative effect (see Box1 for Definitions). Additionally, due to extremely rapid association and dissociation rates, mGppNHp kinetics for $RAC1^{T17N}$ could not be determined using stopped-flow fluorimetry (supplementary Fig. S3, lower panel), which presents fluorescence spectrophotometry-based measurements confirming its rapid nucleotide exchange properties.

Nucleotide-binding affinity (K_d) was calculated using kinetic parameters for dissociation and association reactions. $RAC1^{WT}$ displayed tight binding affinities for mdGDP and mGppNHp, with Kd values of 0.3 nM and 0.6 nM, respectively. These affinities were significantly reduced for $RAC1^{T17N}$, followed by $RAC1^{P29S}$ and $RAC1^{F28L}$ (Fig. 1C). Due to rapid kinetics, the mGppNHp binding affinity for $RAC1^{T17N}$ could not be determined (supplementary Fig. S3, lower panel), where fluorescence measurements demonstrated its inability to be analyzed via standard stopped-flow techniques. $RAC1^{P29S}$ showed markedly impaired nucleotide binding, with 147-fold and 289-fold lower affinities for mdGDP and mGppNHp, respectively. These findings suggest that $RAC1^{P29S}$'s impaired binding properties likely drive its accelerated intrinsic nucleotide exchange, although further structural studies on its interactions with regulators and effectors are needed to elucidate its aberrant behavior.

Only the T17N mutation significantly impairs GDI1 activity. We recently developed a fluorescence-based method to monitor RAC1-GDI1 interactions (8). Our results showed that GDI1 binding, essential for GDI-mediated membrane translocation, does not differentiate between non-prenylated and prenylated RAC1. Real-time kinetic measurements evaluated the association and dissociation kinetics of GDI1 with mdGDP-bound RAC1 (Fig. 2A, left panel; supplementary Fig. S4), which presents the binding of RAC1 to GST-GDI1 across increasing concentrations, followed by kinetic analysis. Corresponding rate constants are shown in Figure 2A, right panel. $RAC1^{F28L}$ and $RAC1^{P29S}$ exhibited k_{on} and k_{off} values comparable to $RAC1^{WT}$, with slightly reduced GDI1 binding affinity for $RAC1^{P29S}$. In contrast, $RAC1^{T17N}$ displayed a 439-fold decrease in GDI association and an 18-fold reduction in dissociation, leading to a significantly decreased binding affinity compared to $RAC1^{WT}$.

$RAC1^{P29S}$ is mainly activated by DOCK2 and not by DBL family GEFs. To assess GEF-mediated nucleotide exchange, we evaluated mdGDP dissociation from $RAC1^{WT}$, $RAC1^{T17N}$, $RAC1^{F28L}$, and $RAC1^{P29S}$ in the presence of various RAC1-selective GEFs, including DBL family members (TIAM1, VAV2, SOS1, PREX1) (3, 4) and DOCK family member DOCK2 (7, 50) (Fig. 2B, left panel; supplementary Fig. S5), which presents kinetic measurements of GEF-catalyzed mdGDP dissociation from RAC1 proteins. Fluorescence decay curves were fitted to a single exponential function to determine k_{off} values in the presence of each GEF. Substantial GEF activity against $RAC1^{WT}$ was observed for the DH-PH domains of TIAM1, PREX1, and VAV2, but not SOS1, consistent with prior reports (3). This lack of SOS1 activity extended to RAC1 mutants. Our findings indicate that $RAC1^{P29S}$ has slow basal nucleotide exchange with DBL proteins and is primarily activated by DOCK2. The DHR2 domain of DOCK2 exhibited 40-fold greater activity than TIAM1 against $RAC1^{WT}$ and showed significant GEF activity for $RAC1^{P29S}$ and other mutants (Fig. 2B). This evidence positions DOCK2 as the primary potential activator of $RAC1^{P29S}$ in cancer cells, particularly in melanoma.

The P29S mutation significantly impairs the GAP activity. GTP hydrolysis was evaluated using HPLC for intrinsic hydrolysis and stopped-flow fluorimetry for GAP-stimulated hydrolysis (Fig. 2C; supplementary Fig. S6), which presents measurements of both basal and GAP-stimulated GTP hydrolysis of RAC1 proteins. Intrinsic hydrolysis was assessed by quantifying relative GTP content via HPLC, while real-time hydrolysis in the presence of p50GAP was analyzed using stopped-flow fluorescence. $RAC1^{WT}$ exhibited slow intrinsic GTP hydrolysis (k_{cat} = 0.001 s^{-1}), consistent across RAC1 mutants, including $RAC1^{P29S}$ (Fig. 2C). In contrast, $RAC1^{P29S}$ showed a dramatic reduction in GAP-stimulated hydrolysis, with k_{cat} dropping from 2.03 s^{-1} for $RAC1^{WT}$ to 0.0087 s^{-1}, a 233-fold decrease (Fig. 2C, right panel). T17N and F28L mutations also reduced GAP activity but to a lesser extent (14.5-fold and 50-fold, respectively). These results underscore the critical role of GAP in the temporal regulation of RAC1 activity, with diminished p50GAP activity prolonging $RAC1^{P29S}$'s GTP-bound state and enhancing its signaling capacity.

$RAC1^{P29S}$ shows a significantly stronger binding affinity to IQGAP1 compared to PAK1. The diverse signaling activities of RAC1 in human cells and cancers are primarily mediated

through its interactions with downstream effectors. To evaluate the impact of the P29S mutation on effector binding under cell-free conditions, we examined its interaction with two well-characterized RAC1 effectors: the RAC1 binding domain (RBD) of the serine/threonine kinase PAK1, a key downstream kinase, and the C-terminal 794 amino acids (C794) of the scaffolding protein IQGAP1, a critical accessory protein (9, 10, 51, 52).

The binding properties of RAC1 mutants to PAK1 RBD were assessed using a GST pull-down assay (Fig. 3A), revealing differential binding compared to $RAC1^{WT}$: weaker binding for $RAC1^{P29S}$, modestly stronger binding for $RAC1^{F28L}$, and no binding for $RAC1^{T17N}$ (Fig. 3B, 3C; supplementary Fig. S7A), which presents representative blots from the GST pull-down assay showing RAC1-PAK1 interactions, with statistical analyses displayed in Figure 3C. Fluorescence polarization further quantified these interactions, confirming no binding for $RAC1^{T17N}$, a modest increase in affinity for $RAC1^{F28L}$, and a 7.5-fold decrease in binding affinity for $RAC1^{P29S}$ relative to $RAC1^{WT}$ (Fig. 3D, 3E; supplementary Fig. S7B), which displays dissociation constants (K_d) derived from titrations of RAC1 mutants with GST-PAK1 RBD. The slightly enhanced affinity of $RAC1^{F28L}$ was attributed to its slower dissociation rate. Stopped-flow fluorimetry revealed that $RAC1^{P29S}$ and $RAC1^{F28L}$ exhibited 10- and 40-fold slower association rates, respectively, compared to $RAC1^{WT}$, while $RAC1^{F28L}$ displayed a 66-fold and 34-fold slower dissociation rate compared to $RAC1^{WT}$ and $RAC1^{P29S}$, respectively (Fig. 3F, 3G; supplementary Fig. S7C), which provides kinetic analyses of RAC1-PAK1 interactions, including association and dissociation rate constants. Overall, the binding affinity to PAK1 RBD increased slightly for $RAC1^{F28L}$ and decreased 5-fold for $RAC1^{P29S}$ compared to $RAC1^{WT}$ (Fig. 3G), consistent with the results of GST pull-down and fluorescence polarization assays (Fig. 3C, 3E).

The interaction of IQGAP1 C794 with RAC1 variants was assessed using a His-tag pull-down assay (Fig. 3A). Binding progressively increased in the order of $RAC1^{WT}$, $RAC1^{T17N}$, $RAC1^{F28L}$, and $RAC1^{P29S}$ (Fig. 3H; supplementary Fig. S8A), which presents representative blots from the pull-down assay showing RAC1-IQGAP1 interactions, with statistical analyses displayed in Figure 3I. This trend was confirmed by data from four independent pull-down experiments (Fig. 3I). Stopped-flow experiments further corroborated these findings, revealing a gradual increase in IQGAP1 binding affinity across the RAC1 variants in the same order (Fig. 3J; Supplementary Fig. S8B), which provides kinetic analyses of RAC1-IQGAP1 interactions, including association and dissociation rate constants. Notably, $RAC1^{P29S}$ exhibited significantly higher affinity for IQGAP1 C794 compared to PAK1 RBD, and IQGAP1 C794 bound more tightly to $RAC1^{T17N}$ than to $RAC1^{WT}$, providing new insights into the differential binding properties of RAC1 effectors.

$RAC1^{P29S}$ is found in its GTP-bound state in serum-starved cells. To evaluate active RAC1 levels under serum stimulation and starvation, $RAC1^{WT}$ and mutants were overexpressed in HEK-293T cells and pulled down in their GTP-bound states using GST-PAK1 RBD, GST-IQGAP1 C794, and GST as a negative control (supplementary Fig. S9), which provides a schematic representation of the pull-down assay used to determine the level of active, GTP-bound RAC1 from HEK-293T cell lysates.

The results showed significantly stronger binding of GTP-bound RAC1 proteins to IQGAP1 C794 compared to PAK1 RBD under serum-stimulated conditions (Fig. 4A, upper panel). $RAC1^{P29S}$ and $RAC1^{F28L}$ displayed stronger binding to GST-PAK1 RBD, while $RAC1^{T17N}$ exhibited minimal binding relative to $RAC1^{WT}$. In contrast, all RAC1 variants showed significantly higher binding to GST-IQGAP1 C794. Under serum starvation, high levels of $RAC1^{P29S}$•GTP were pulled down with GST-PAK1 RBD, corroborating in vitro findings and indicating temporal accumulation of $RAC1^{P29S}$ in its GTP-bound state (Fig. 4A, lower panel). Similarly, much higher levels of $RAC1^{P29S}$•GTP and $RAC1^{T17N}$•GTP were pulled down with GST-IQGAP1 C794. These findings were reproduced in triplicate, with no interaction observed for GST alone (supplementary Fig. S10), which presents western blot analyses of active

GTPase pull-down assays quantifying GTP-bound RAC1 in HEK-293T cell lysates under both serum-stimulated and serum-starved conditions.

Quantification of active, GTP-bound RAC1 levels was performed in three independent experiments for each condition (n = 3; supplementary Fig. S10A and S10B), where separate panels show pull-down results for GST-PAK1 RBD and GST-IQGAP1 C794 in both conditions. Results are presented as bar graphs (Fig. 4B). Under serum stimulation, in set 1 analysis, $RAC1^{F28L}$ and $RAC1^{P29S}$ displayed stronger binding to PAK1 RBD compared to $RAC1^{WT}$, which showed baseline interaction, whereas $RAC1^{T17N}$ demonstrated very weak binding, consistent with its K_d values. In set 2, $RAC1^{T17N}$ and $RAC1^{P29S}$ exhibited significantly stronger binding to IQGAP1 C794 compared to $RAC1^{WT}$, which showed baseline interaction, with $RAC1^{F28L}$ demonstrating intermediate binding. Notably, $RAC1^{T17N}$ exhibited binding levels to IQGAP1 C794 similar to $RAC1^{P29S}$. In set 3, all RAC1 variants bound more strongly to IQGAP1 C794 than PAK1 RBD, with $RAC1^{P29S}$ and $RAC1^{T17N}$ showing the highest binding levels.

Under serum starvation, set 4 showed that only $RAC1^{P29S}$ remained active and bound to PAK1 RBD, while $RAC1^{WT}$, $RAC1^{T17N}$, and $RAC1^{F28L}$ showed no significant binding. In set 5, $RAC1^{WT}$ completely lost activity, while $RAC1^{T17N}$ and $RAC1^{P29S}$ remained active and strongly interacted with IQGAP1 C794, although $RAC1^{F28L}$ activity was insufficient to achieve significance. In set 6, $RAC1^{WT}$ lost all activity, failing to bind either PAK1 RBD or IQGAP1 C794. $RAC1^{T17N}$ did not bind PAK1 RBD but bound strongly to IQGAP1 C794, while $RAC1^{F28L}$ showed no significant binding to either effector. $RAC1^{P29S}$, however, is bound more strongly to IQGAP1 C794 than to PAK1 RBD.

Sets 7 and 8 compared RAC1 activity between serum-stimulated and serum-starved conditions. $RAC1^{WT}$ lost all activity under serum starvation, failing to bind either effector. $RAC1^{T17N}$ retained tight binding to IQGAP1 C794 under both conditions, though binding strength decreased by 33.6% under starvation. $RAC1^{F28L}$ lost 93–97% of its binding to PAK1 RBD and IQGAP1 C794, reflecting its fast-cycling nature. In contrast, $RAC1^{P29S}$ retained 59% of its activity under serum starvation, binding strongly to PAK1 RBD and IQGAP1 C794, highlighting its constitutive gain-of-function properties.

$RAC1^{P29S}$ accumulates in its GTP-bound state in cells and hyperactivates cancer-related signaling pathways. To investigate the impact of RAC1 variants on key signaling pathways, HEK-293T cells were transiently transfected with constructs encoding Flag-tagged RAC1 variants. Western blot analysis revealed a significant increase in ERK1/2 phosphorylation (p-ERK1/2) in cells overexpressing $RAC1^{P29S}$ ($p < 0.001$, ***) and RAC1T17N ($p < 0.05$, *) (Figure 5). This increase was consistently observed across triplicate experiments (supplementary Fig. S11), which presents western blot analyses of phosphorylation levels of ERK1/2, AKT(S473), AKT(T308), p38 MAPK, and STAT1 α/β in serum-stimulated HEK-293T cells overexpressing RAC1 variants. The observed ERK hyperactivation aligns with its established role in promoting tumor growth and proliferation. $RAC1^{P29S}$ also significantly elevated p38 MAPK phosphorylation ($p < 0.01$, **) (Figure 5). Phosphorylation of AKT at serine 473 (S473), a target of mTORC2, and STAT1 α/β phosphorylation were statistically significant ($p < 0.05$, *) but less pronounced compared to ERK and p38 MAPK. AKT phosphorylation at threonine 308 (T308), a PDK1 target, remained non-significant (n.s.).

Discussion

This study provides a detailed biochemical characterization of $RAC1^{P29S}$ in comparison to $RAC1^{WT}$, $RAC1^{T17N}$, and $RAC1^{F28L}$ (Fig. 6). Our findings reveal that (i) $RAC1^{P29S}$ exhibits impaired nucleotide binding and accelerated intrinsic nucleotide exchange; (ii) its activation is primarily mediated by DOCK2 rather than DBL family GEFs; (iii) GAP-stimulated GTP hydrolysis is significantly impaired, enabling temporal accumulation of $RAC1^{P29S}$ in its GTP-bound active state; (iv) $RAC1^{P29S}$ exhibits a stronger binding affinity for IQGAP1 compared to PAK1, highlighting IQGAP1 as a spatial modulator of downstream activation; and (v) the accumulation of GTP-bound $RAC1^{P29S}$ leads to hyperactivation of key cancer-associated

signaling pathways, including ERK1/2, p38 MAPK. Taken together, these results classify $RAC1^{P29S}$ as a constitutively active mutant and an oncogene (Box 1) that transduces upstream signals to effectors such as IQGAP1, thereby driving processes such as proliferation, invasion, and epithelial-mesenchymal transition (53, 54).

Our biochemical data confirm that the P29S mutation increases the intrinsic nucleotide exchange rate, consistent with previous reports (36, 37). The slower GDP/GTP association rate results in reduced nucleotide binding affinity despite accelerated exchange. Shimada et al. demonstrated that RAC1P29S enhances GDP dissociation, favoring a GTP-bound state that drives oncogenic activity (55). Similarly, Gursoy et al. used molecular dynamics to show that this mutation increases switch I flexibility, facilitating rapid GDP/GTP exchange (20). Our findings suggest that the elevated exchange rate and activation of RAC1P29S arise from impaired nucleotide-binding affinity due to conformational changes induced by the P29S substitution. However, the intrinsic exchange rate of $RAC1^{P29S}$ remains insufficient for many cellular processes, emphasizing the importance of GEF-mediated exchange in its activation in cancer cells.

RHO-specific GDIs regulate RHO GTPase dynamics by extracting them from membranes, maintaining their inactive state, and preventing degradation through specific interactions (1). Despite progress in understanding GDI-mediated shuttling, some mechanisms remain unclear. We previously showed that GDI1 binds RAC1 regardless of its prenylation state (8). Our data suggest that $RAC1^{T17N}$ has impaired GDI1 activity, with decreased binding affinity, which may suggest persistent plasma membrane association. In contrast, $RAC1^{P29S}$ shows only a slight reduction in GDI1 affinity, indicating that GDI1 can still modulate its localization and translocation.

$RAC1^{P29S}$, like most oncogenes, requires repeated activation by RAC1-specific GEFs. Our data demonstrate that RAC1 mutants exhibit minimal activation by DBL family GEFs, such as TIAM1, PREX1, and VAV2, while DOCK2 significantly enhances the exchange rate for all RAC1 variants, including P29S. This observation aligns with the distinct mechanistic roles of the P-loop and switch I in RAC1, particularly in the functions of DBL and DOCK GEF families (7, 41, 56, 57). However, further analysis is needed to fully understand $RAC1^{P29S}$ activation in cancer cells. Uruno et al. showed that DOCK1 inhibition suppresses cancer cell invasion and macropinocytosis induced by $RAC1^{P29S}$ in melanoma and breast cancer cells (57). Notably, DOCK2 is a potent RAC1 activator in cancers, including melanoma and chronic lymphocytic leukemia (58-60), and regulates critical processes such as lymphocyte migration, T-cell differentiation, cell-cell adhesion, and bone marrow homing of immune cells (61). Although slight increases in TIAM1 activity were observed in our study, the TIAM1-RAC1 axis cannot be entirely excluded from $RAC1^{P29S}$ activation in cancers, including melanoma (62).

$RAC1^{T17N}$ did not show increased GEF-mediated nucleotide exchange via DBL proteins, consistent with its dominant-negative behavior. Overexpression of $RAC1^{T17N}$ in HEK-293T cells significantly increased ERK phosphorylation, though less than $RAC1^{P29S}$. Cool et al. showed that $HRAS^{D119N}$ exhibits dose-dependent dominant-negative and constitutively active effects by reducing nucleotide affinity, sequestering GEFs, binding GTP independently of GEFs, and activating downstream pathways at high concentrations (63). Similarly, $RAC1^{P29S}$ signaling may partially result from overexpression. $RAC1^{F28L}$ shares a GEF activity profile similar to $RAC1^{P29S}$, suggesting both mutations may similarly alter the RAC1 GEF-binding site. This hypothesis requires further structural investigation.

Among the analyzed DBL proteins, SOS1 showed no activity. Other DBL proteins, such as ABR, α-PIX, β-PIX, BCR, FGD4, and FGD6, contain pseudo-DH domains with functions yet to be determined (3). These domains, defined as globular structures performing specific roles like binding or catalysis independent of full-length protein context, may require posttranslational modifications (64-66) or interactions with specific binding partners (67) to become active.

RAC1 signaling is terminated by GTP hydrolysis to GDP, deactivating the protein (5). The intrinsic GTP hydrolysis rate of $RAC1^{WT}$ and its mutants is slow (~9,000 seconds), necessitating GAPs to catalyze hydrolysis and reduce deactivation time to just a second (48). Our findings confirm that $RAC1^{P29S}$ retains a similar intrinsic hydrolysis rate to $RAC1^{WT}$ (36, 37). However, this study reveals for the first time that the P29S mutation severely impairs GAP-mediated hydrolysis, with p50GAP activity reducing the inactivation time of $RAC1^{P29S}$ to ~1,000 seconds, a 233-fold decrease compared to $RAC1^{WT}$.

Previous studies have classified $RAC1^{P29S}$ as a spontaneously activating, self-activating, fast-cycling mutant (19, 36, 37) or an oncogenic driver (68) due to its rapid nucleotide exchange that maintains RAC1 in an active state (Box 1). due to its rapid nucleotide exchange that keeps RAC1 active. Our findings align with the latter, highlighting the critical role of p50GAP in regulating $RAC1^{P29S}$ activity. The severe impairment of GAP-stimulated GTP hydrolysis supports its classification as a constitutive gain-of-function mutant and oncogene, driven by defective GAP-mediated deactivation rather than just increased nucleotide exchange. This disruption in temporal regulation leads to the accumulation of active $RAC1^{P29S}$•GTP, as confirmed by its persistence in the GTP-bound state under serum-starved conditions, where most GTPases are typically inactive due to GAP sensitivity and lack of upstream GEF activation. As supported by prior studies, the sustained activation of $RAC1^{P29S}$ likely drives cancer-related processes, including proliferation, survival, invasion, metastasis, and therapy resistance (19, 23-25, 27, 36, 69-71).

The diverse signaling activities of RAC1 are mediated through interactions with specific effectors, which require RAC1 to adopt distinct conformations to function (1). RAC1 effectors include kinases such as PAK1/2/3, MLK1, PI4P5Ks, and accessory proteins like IQGAP1/2, IRSP53, AJUBA, p67phox, and CYFIP1/2 (1). This study examined the binding properties of PAK1, a major kinase, and IQGAP1, a critical scaffolding protein. IQGAP1 is involved in cytoskeletal reorganization processes, including polarity, adhesion, and migration (72, 73), and links RAC1 to the actin cytoskeleton via filamentous actin binding (74). Previous studies showed IQGAP1 interacts with RAC1 and CDC42 via switch regions and effector binding sites, with slight differences in mechanisms (2, 43, 51, 52) . Malliri et al. demonstrated that IQGAP1 exhibits increased RAC1 binding specifically upon TIAM1 expression but not other DBL GEFs, including PREX1 (75).

Our findings reveal that $RAC1^{P29S}$ interacts significantly more strongly with IQGAP1 than with PAK1, exhibiting a 30-fold higher binding affinity as measured by stopped-flow fluorimetry. This enhanced interaction was corroborated by a statistically significant increase in $RAC1^{P29S}$•GTP binding to IQGAP1 under both serum-stimulated and serum-starved conditions. In contrast, the stronger binding of $RAC1^{P29S}$ to GST-PAK1 RBD observed in human cell lysates, compared to in vitro pull-down assays using purified proteins, may be attributed to the presence of accessory proteins, modulators, and other cellular components that facilitate protein complex formation in the native environment. These findings suggest that IQGAP1 is a key effector downstream of $RAC1^{P29S}$, acting as an activated scaffolding protein to modulate pathways such as RAF/MEK/ERK (76-78). This underscores the pivotal role of scaffolding proteins, particularly IQGAP1, as spatial modulators facilitating $RAC1^{P29S}$-driven signaling and its downstream effects.

Hyperactivation of signaling pathways downstream of $RAC1^{P29S}$ highlights its oncogenic potential. Accumulated GTP-bound $RAC1^{P29S}$ robustly enhances ERK1/2 and p38 MAPK phosphorylation, suggesting these pathways play significant roles in $RAC1^{P29S}$-driven oncogenic transformation. ERK hyperactivation, a hallmark of uncontrolled tumor growth and proliferation, promotes unregulated cell cycle progression. Concurrently, p38 MAPK hyperactivation supports cellular adaptation to oxidative and inflammatory stress, contributing to tumor progression, invasion, and therapeutic resistance. These findings highlight ERK and p38 MAPK as important mediators of $RAC1^{P29S}$-driven oncogenic signaling, while acknowledging additional pathways may also contribute. Phosphorylation of AKTS473,

mediated by mTORC2, and STAT1 α/β, while statistically significant, was less pronounced and may represent secondary or context-specific effects. Selective AKTS473 activation could support cancer cell survival and metabolic adaptation, while STAT1 hyperactivation might facilitate immune evasion and survival under inflammatory conditions. This study focused on these pathways to illustrate GTP-bound RAC1^{P29S} hyperactivation and validate cell-free data highlighting its constitutive activation. However, many other signaling events remain unexplored, underscoring the need for future studies to fully elucidate RAC1^{P29S}-driven cancer mechanisms.

Conclusion

This study highlights the oncogenic potential of RAC1^{P29S} by demonstrating its accumulation in the GTP-bound state and the resulting hyperactivation of downstream signaling pathways (Fig. 6). The P29S mutation significantly impairs nucleotide binding, leading to accelerated intrinsic nucleotide exchange. It is primarily activated by DOCK2 and not by DBL family GEFs. The hyperactivation of RAC1^{P29S} is driven by severely impaired p50GAP-mediated GTP hydrolysis, which serves as a temporal regulatory mechanism facilitating the accumulation of GTP-bound RAC1^{P29S}. This accumulation enhances the activation of key cancer-associated signaling pathways, including ERK and p38 MAPK. RAC1^{P29S} exhibits altered binding characteristics that favor IQGAP1 as a critical scaffolding protein in the spatial modulation of downstream signaling. These findings position RAC1^{P29S} as a critical driver of tumorigenesis and suggest that targeting its regulators (DOCK2, p50GAP) and effectors (IQGAP1) may provide promising therapeutic strategies for melanoma.

Author Contributions Statement
A.M. developed the methods and designed, performed, and analyzed the experiments. A.M. and M.R.A. drafted and approved the final version of the manuscript.

Funding
This study was supported by the German Research Foundation (DFG; grant number: AH 92/8-3).

Acknowledgments
We are grateful to our colleagues at the Institute of Biochemistry and Molecular Biology II for their support, and fruitful discussions.

Conflict of Interest
The authors declare no conflict of interest.

Abbreveations:
AKT – Protein kinase B
BRAF – v-Raf murine sarcoma viral oncogene homolog B1
DBL – Diffuse B-cell lymphoma
DH-PH – Dbl homology-pleckstrin homology
DHR2 – Dock homology region 2
DOCK – Dedicator of cytokinesis
ERK – Extracellular signal-regulated kinase
GAP – GTPase-activating protein
GDP – Guanosine diphosphate
GEF – Guanine nucleotide exchange factor
GDI – Guanine nucleotide dissociation inhibitor
GSH – Glutathione
GST – Glutathione S-transferase
GTP – Guanosine triphosphate
IQGAP1 – IQ motif-containing GTPase-activating protein 1
MAPK – Mitogen-activated protein kinase
MLK3 – Mixed lineage kinase 3
NRAS – Neuroblastoma RAS viral oncogene homolog
PAK1 – p21-activated kinase 1
p50GAP – p50 Rho GTPase-activating protein
PD-L1 – Programmed death-ligand 1
PLK1 – Polo-like kinase 1
PREX1 – Phosphatidylinositol-3,4,5-trisphosphate-dependent Rac exchanger 1
RAC1 – Ras-related C3 botulinum toxin substrate 1
RBD – RAC1 binding domain
SOS1 – Son of sevenless homolog 1
STAT3 – Signal transducer and activator of transcription 3
SUMO – Small ubiquitin-like modifier
TIAM1 – T-lymphoma invasion and metastasis-inducing protein 1
VAV2 – Vav guanine nucleotide exchange factor 2

Box 1

The terminologies of the mutations and their effects on the intracellular regulation and function of small GTPases, using the example of RAC1:

- **Dominant negative mutations** impair nucleotide binding affinity to the extent that RAC1 forms a non-functional complex with its cognate GEFs in a nucleotide-free state. A dominant negative RAC1 prevents the activation of wild-type RAC1 when both are present in the same cell, leading to a loss of RAC1 activity and disruption of its downstream signaling pathways.
- **Spontaneous activation mutations** affect the basal activities of RAC1, including enhanced GDP/GTP exchange and reduced GTP hydrolysis. A spontaneously activated RAC1 bypasses normal regulatory mechanisms (without typical regulatory input from other cellular components) and initiates its function independently, leading to unregulated signaling and potentially contributing to cellular dysfunction and disease.
- **Self-activating mutations** refer to the ability of RAC1 to autonomously initiate its signaling function without requiring the usual activation by other cellular components or regulatory proteins. A self-activating RAC1 spontaneously binds GTP and hydrolyzes it to GDP without external regulatory input. This autonomous activation can lead to uncontrolled signaling pathways, potentially contributing to cellular dysfunctions and diseases such as cancer.
- **Fast cycling mutations** lead to the rapid turnover rates of the GDP/GTP exchange and GTP hydrolysis of RAC1. A fast-cycling GTPase rapidly cycles between the inactive, GDP-bound state and the active, GTP-bound state, allowing for quick and dynamic regulation of cellular processes.
- **Constitutively active mutations** affect the GTP hydrolysis reaction of RAC1, resulting in an increased proportion of its active, GTP-bound state, regardless of cellular signaling cues. A constitutively active RAC1 continuously promotes downstream signaling pathways, even when the cell is quiescent or upstream signaling is blocked.
- **Oncogenic mutations** lead to overactivation/hyperactivation of RAC1 and drive oncogenesis. The accumulation of oncogenic RAC1 in its GTP-bound state leads to uncontrolled cellular activities that may contribute to the initiation and progression of various types of cancer.

Box 2

The definition of various kinetic and equilibrium constants in the context of protein-ligand or protein-protein interactions are described as fallow:

- **Observed rate constants**: The observed rate constant ($\mathbf{k_{obs}}$) reflects the overall rate at which the interaction occurs, taking into account both the association of the proteins or the protein and ligand, as well as any potential subsequent reactions such as conformational changes or product formation. This is often used in cases where the binding is not at equilibrium and may vary with the concentration of the interacting partners.
- **Association rate constant**: The association rate constant ($\mathbf{k_{on}}$) measures the rate at which a protein and a ligand or two proteins come together to interact with each other and form a complex. It is defined as: k_{on} = [PL] / [P][L], Where [PL] is the concentration of the protein-ligand or protein-protein complex, and [P] and [L] are the concentration of free protein and free ligand. A higher k_{on} indicates a faster rate of complex formation.
- **Dissociation rate constant**: The dissociation rate constant ($\mathbf{k_{off}}$) quantifies how quickly the protein-ligand or protein-protein complex dissociates back into the free components. This constant It is important in determining the stability of the interaction; a higher k_{off} indicates a less stable complex. It can be measured experimentally by monitoring the concentration of the complex or over time after dilution or removal of the ligand.
- **Catalytic rate constant**: In the context of enzyme-ligand interactions, the catalytic rate constant ($\mathbf{k_{cat}}$) refers to the maximum rate of product formation for an enzyme when it is saturated with substrate. For protein-protein interactions, this term may not apply unless there is a specific enzymatic function associated with the interaction, such as in signaling complexes. This constant indicates how efficiently the enzyme catalyzes the reaction after the binding event.
- **Dissociation constants**: The dissociation constant ($\mathbf{K_d}$) is critical for understanding the affinity between a protein and its ligand or between two interacting proteins. It is defined as $K_d = k_{off} / k_{on}$. A lower K_d indicates a higher affinity between the protein and its partner, meaning they bind more tightly. It is often used to assess the strength of the interaction and is expressed in molar concentration units (M).
- **Equilibrium dissociation constants**: The equilibrium dissociation constant ($e\mathbf{K_d}$) measures the affinity between a protein and a ligand or between two proteins in a more complex or biochemical context. It represents the equilibrium state of a reversible binding interaction and is defined as the ratio of the rate constants of dissociation and association. This constant is particularly relevant when considering interactions that occur in environments where factors such as concentration, binding site availability, or the presence of other interacting partners may influence the overall binding dynamics. In a binding reaction where a ligand (L) binds to a protein (P) to form a complex (PL), It is given by the formula eK_d = [R][L] / [RL]. A low eK_d value indicates a high affinity between the proteins and its ligand, meaning they bind tightly, while a high eK_d value indicates low affinity, meaning they bind weakly.

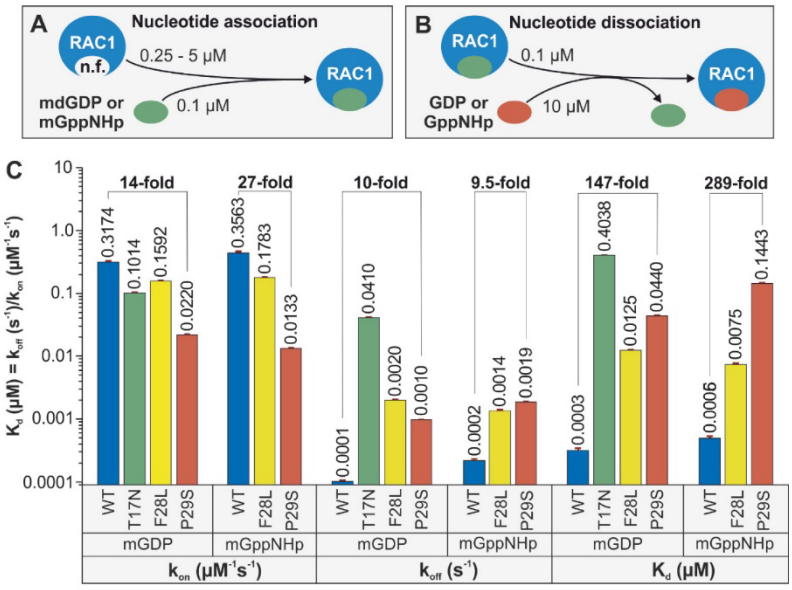

Figure 1. Severe impairment of the GDP/GTP binding properties of RAC1^{P29S}. The kinetics of association (**A**) and dissociation (**B**) of fluorescent mdGDP and mGppNHp with RAC1 proteins were measured as illustrated. (**C**) Kinetic rate constants for association (k_{on}) and dissociation (k_{off}), as well as the dissociation constant (K_d), calculated from the k_{off}/k_{on} ratio, reveal substantial effects of the P29S mutation on the binding of mdGDP and mGppNHp to RAC1. These effects differ markedly from those observed for the T17N and F28L substitutions. This impaired binding may contribute to the accelerated intrinsic nucleotide exchange observed in RAC1^{P29S}. All k_{on}, k_{off}, and K_d values, presented as bar graphs, represent the average of three to six measurements and are reported as means ± SD.

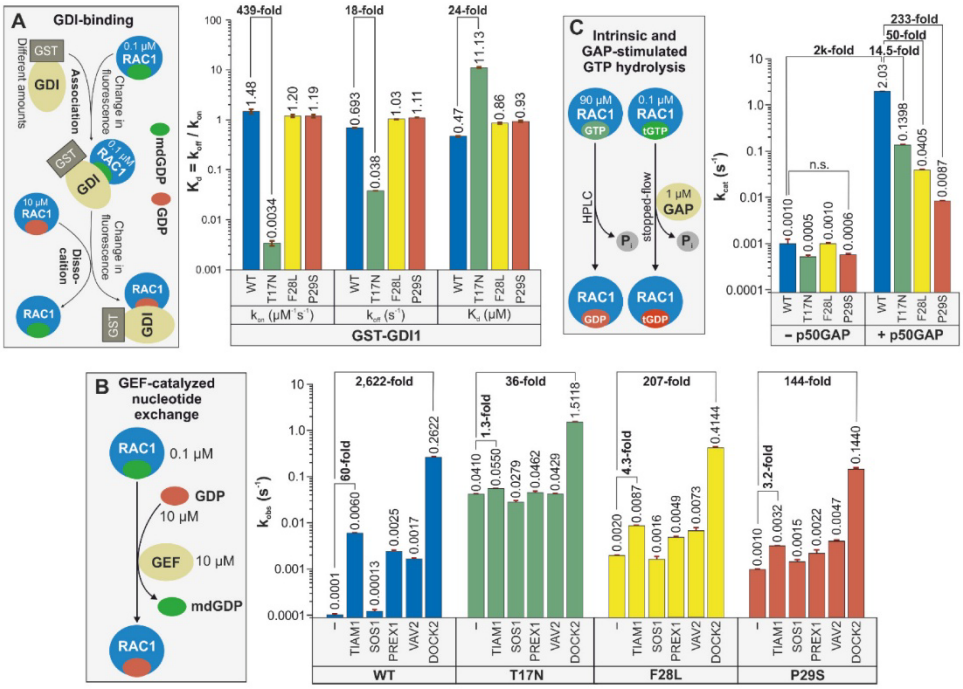

Figure 2. Effects of mutations on the regulation of RAC1 by GDI1, various GEFs, and p50GAP. (**A**) Minimal effect of the P29S mutation on the RAC1-GDI1 interaction. The principle behind the kinetic measurements of the association of GST-GDI1 with RAC1 proteins and its dissociation is illustrated using a stopped-flow instrument. In these experiments, 0.1 µM mdGDP-bound RAC1 was rapidly mixed with increasing concentrations of GST-GDI1 to monitor the association kinetics. Dissociation kinetics were measured by rapidly mixing a complex of RAC1•mdGDP•GST-GDI1 with excess GDP-bound RAC1. Bar graphs from the stopped-flow analysis depict the association rates (k_{on}) and dissociation rates (k_{off}) of the GDI1 interaction from/with RAC1 proteins, as well as the dissociation constant (K_d), calculated from the k_{off}/k_{on} ratio. The analysis revealed a substantial reduction in GDI1 binding affinity for $RAC1^{T17N}$ and a slight reduction for $RAC1^{P29S}$. All kinetic data are based on the average of three to six measurements and are presented as mean ± SD. (**B**) Impairment of the catalyzed nucleotide exchange of $RAC1^{P29S}$ by DBL proteins but not by DOCK2. The mdGDP-to-GDP exchange of RAC1 proteins was measured in the absence and presence of the DH-PH tandem of various DBL family members (TIAM1, SOS1, PREX1, and VAV2) and the DHR2 domain of DOCK2, a member of the DOCK family. The observed rate constants (k_{obs}), shown as bar graphs, represent the average of three to six measurements and are displayed as means ± SD. (**C**) Severely impaired GAP-stimulated GTP hydrolysis reaction of $RAC1^{P29S}$. The basal and p50GAP-stimulated GTP hydrolysis reactions were measured using HPLC and stopped-flow instruments, respectively. The determined catalytic rate constants (k_{cat}), presented as bar graphs, are based on duplicate measurements for HPLC data and three to six measurements for stopped-flow data and are reported as means ± SD.

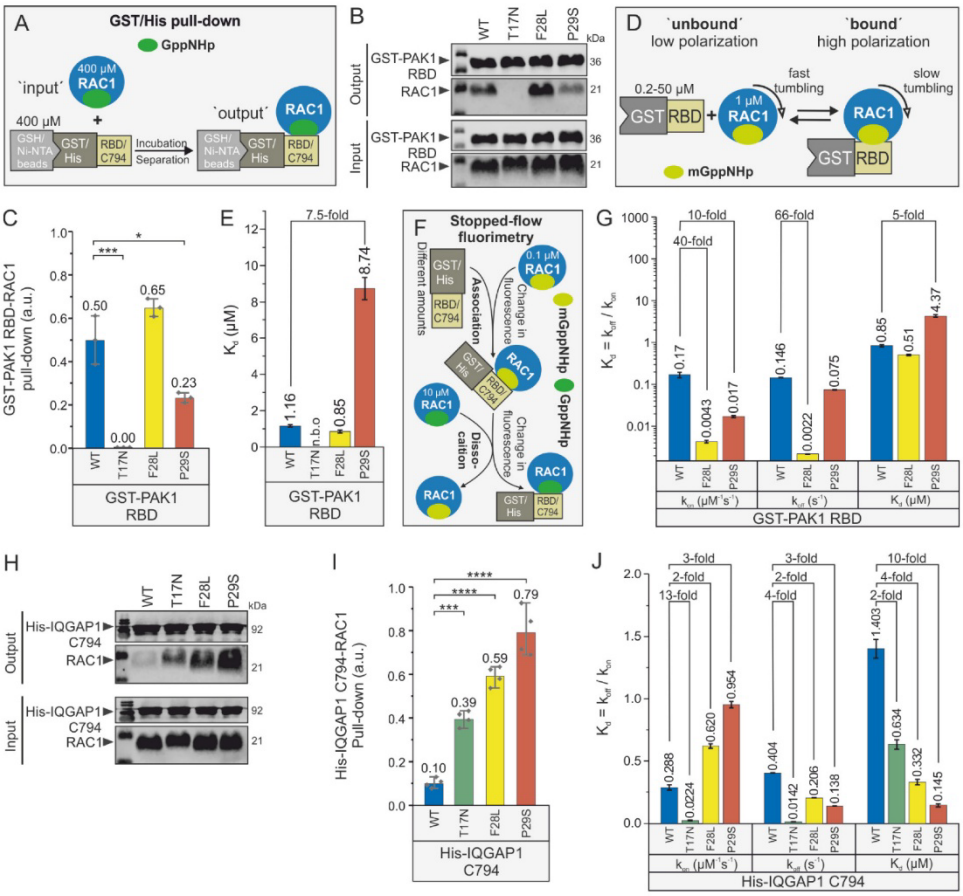

Figure 3. Reduced binding affinity of RAC1^{P29S} for PAK1 but increased for IQGAP1. (**A**) GST and His pull-down assays were performed to evaluate the binding strength of RAC1 variants to GST-PAK1 RBD and His-IQGAP1 C794, respectively. For each reaction, 50 µL of beads were incubated with 400 µM RAC1 proteins and 400 µM GST-PAK1 RBD or His-IQGAP1 C794. Input samples consisted of the protein mixtures before incubation, while output samples were the eluted fractions. (**B**) Western blot analysis of RAC1-PAK1 pull-down (output) was performed using anti-GST antibodies for GST-PAK1 and anti-RAC1 antibodies, with molecular weights indicated in kilodaltons (kDa). The input represents total protein mixtures before pull-down experiments. (**C**) Bar graphs quantify RAC1-PAK1 RBD interactions from 3 independent pull-down experiments analyzed using one-way ANOVA, with P values (* < 0.05; ** < 0.01; *** < 0.001; **** < 0.0001) and data expressed as means ± SD. (**D**) The principle behind the fluorescence polarization measurements for the interaction between GST-PAK1 RBD and RAC1 proteins is illustrated. Accordingly, 1 µM mGppNHp-bound RAC1 was titrated with increasing concentrations of GST-PAK1 RBD. (**E**) Bar graphs from fluorescence polarization analysis represent the dissociation constants (K_d) for PAK1 RBD binding to RAC1 proteins, with "n.b.o" indicating no binding observed and data expressed as means ± SD. (**F**) The principle behind the kinetic measurements of GST-PAK1 RBD association with and dissociation from RAC1 proteins is shown using a stopped-flow instrument. In these experiments, 0.1 µM mGppNHp-bound RAC1 was rapidly mixed with increasing concentrations of GST-PAK1 RBD to monitor association kinetics. Dissociation kinetics were measured by rapidly mixing a complex of RAC1•mGppNHp•GST-PAK1 RBD with excess GppNHp-bound RAC1. (**G**) Bar graphs from the stopped-flow analysis display the evaluated

association rates (k_{on}), dissociation rates (k_{off}), and dissociation constants (K_d, calculated as k_{off}/k_{on}) for the PAK1 RBD interaction with RAC1 proteins, with data presented as means ± SD. (**H**) Western blot analysis of RAC1-IQGAP1 pull-down (output) was performed using anti-His antibodies for His-IQGAP1 and anti-RAC1 antibodies, with molecular weights indicated in kilodaltons (kDa). The Input represents total protein mixtures before pull-down experiments. (**I**) Bar graphs quantify RAC1-IQGAP1 C794 interactions from 4 independent pull-down experiments analyzed using one-way ANOVA, with P values (* < 0.05; ** < 0.01; *** < 0.001; **** < 0.0001), and data expressed as mean ± SD. (**J**) Bar graphs from the stopped-flow analysis depict the k_{on} and the k_{off} values for the interaction between IQGAP1 C794 and RAC1 proteins, with K_d values calculated as the ratio of k_{off} to k_{on} and all kinetic data presented as means ± SD.

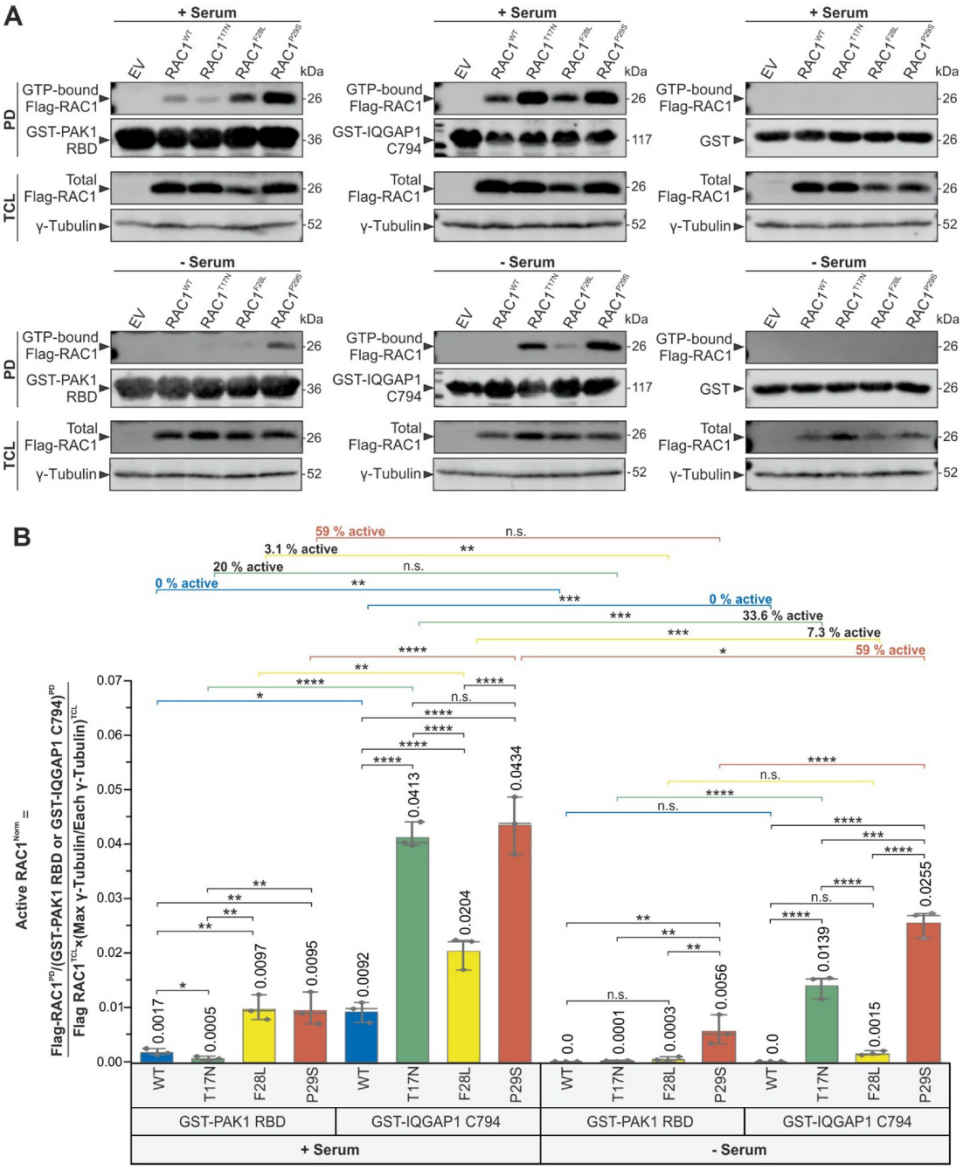

Figure 4. RAC1^{P29S} accumulates in its active, GTP-bound state in HEK-293T cells under serum-starved conditions. Active GTPase pull-down assays were performed to quantify GTP-bound RAC1 proteins (Supplementary Fig. S9). Lysis solutions from *E. coli* containing GST-PAK1 RBD or GST-IQGAP1 C794 were incubated with prewashed glutathione agarose beads to prepare bait-bound beads. Simultaneously, HEK-293T cells were transfected with Flag-RAC1 constructs and cultured under either serum-stimulated or serum-starved conditions for 24 hours. After harvesting, the cells were lysed, and the supernatants containing GTP-bound Flag-RAC1 proteins were collected. Equal amounts of HEK cell lysates were incubated with the bait-bound beads to facilitate protein-protein interactions. After three washes to remove unbound proteins, active GTP-loaded Flag-RAC1 proteins bound to GST-PAK1 RBD or GST-IQGAP1 C794 were eluted and analyzed by SDS-PAGE and Western blotting. (**A**)

Western blots of active GTPase pull-down assays were probed with anti-Flag, anti-GST, and anti-γ-tubulin antibodies to detect GTP-bound Flag-RAC1, GST-PAK1 RBD or GST-IQGAP1 C794, and γ-tubulin, respectively. Analyses were performed under serum-stimulated and serum-starved conditions using GST-PAK1 RBD, GST-IQGAP1 C794, and GST as negative controls. Molecular weights (in kDa) are indicated for each band corresponding to the target proteins. The pull-down (PD) lanes show the output signal representing the amount of GTP-bound Flag-RAC1 proteins captured by the bait-bound beads. GST-PAK1 RBD or GST-IQGAP1 C794 bands reflect the amount of bait protein available for RAC1 binding. Total cell lysate (TCL) lanes show Flag-RAC1 expression with γ-tubulin as a loading control. The figure consists of six Western blot panels: the first blot shows the levels of active $RAC1^{WT}$, $RAC1^{T17N}$, $RAC1^{F28L}$, and $RAC1^{P29S}$, with EV indicating the empty vector control. The upper panels show the serum-stimulated condition with GST-PAK1 RBD as bait protein (left panel), GST-IQGAP1 C794 (middle panel), and GST (right panel). The lower panels show the amount of active RAC1 after 24 hours of serum starvation with GST-PAK1 RBD, GST-IQGAP1 C794, and GST from left to right. (**B**) Bar graphs of normalized values from three independent experiments (n = 3), analyzed by one-way ANOVA, were used to quantify active RAC1 proteins. P values are indicated as follows: * < 0.05; ** < 0.01; *** < 0.001; **** < 0.0001, and ns = not significant. Data are expressed as mean ± SD, as detailed in Supplementary Figure 8 (A) and (B). Values for $RAC1^{WT}$, $RAC1^{T17N}$, $RAC1^{F28L}$, and $RAC1^{P29S}$ were compared and analyzed in eight different sets: Set 1 [GST-PAK1 RBD (+serum)], Set 2 [(GST-IQGAP1 C794 (+serum)], Set 3 [(GST-PAK1 RBD (+serum)) vs. (GST-IQGAP1 C794 (+serum))], Set 4 [GST-PAK1 RBD (-serum)], Set 5 [GST-IQGAP1 C794 (-serum)], Set 6 [(GST-PAK1 RBD (-serum)) vs (GST-IQGAP1 C794 (-serum))], Set 7 [(GST-PAK1 RBD (+serum) vs (-serum))], and Set 8 [(GST-IQGAP1 C794 (+serum) vs (-serum))], with the last two sets reporting the percentage of active GTP-loaded RAC1 proteins remaining from serum-stimulated to serum-starved conditions.

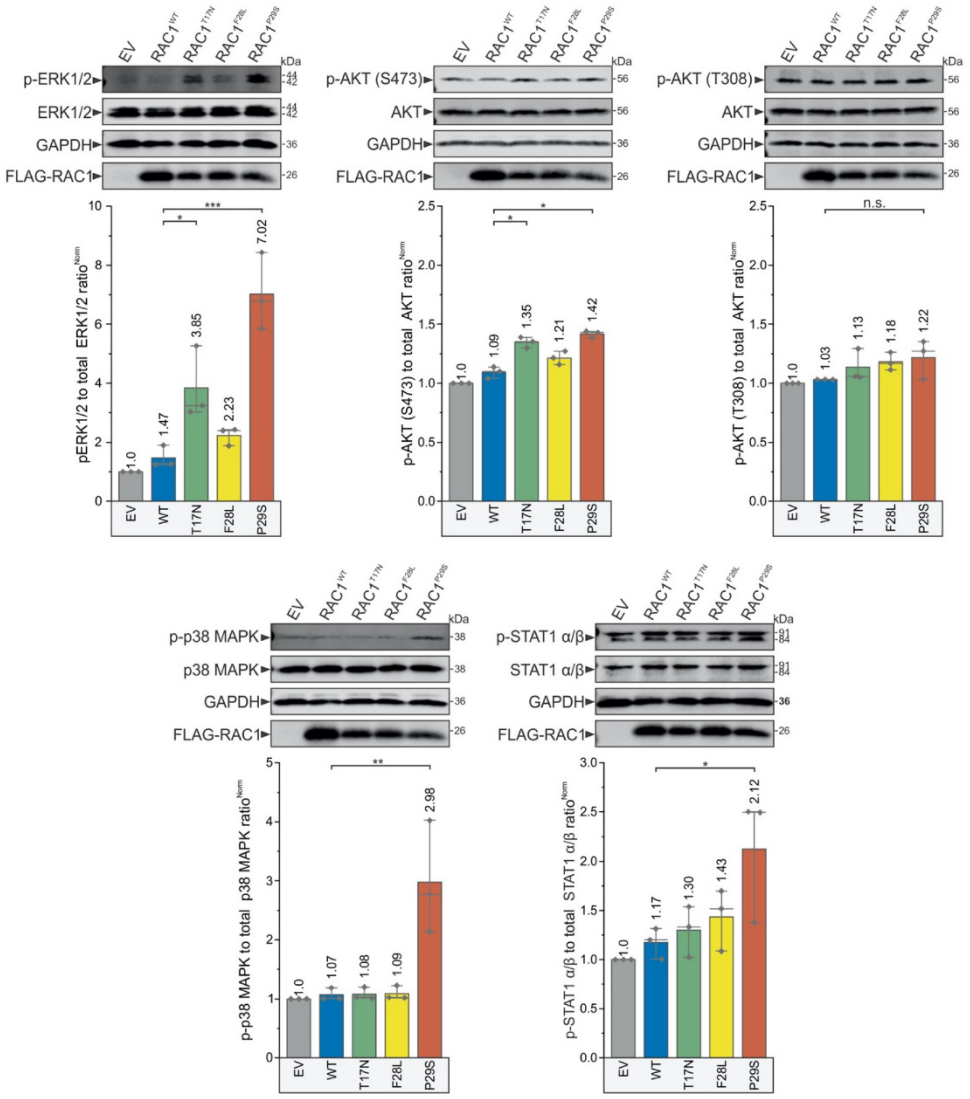

Figure 5. Accumulated GTP-bound RAC1^{P29S} hyperactivates various cancer signaling pathways. Immunoblot analysis was performed to evaluate the phosphorylation levels of several kinases, associated with the hallmarks of oncogenic transformation. Serum-stimulated HEK-293T cells transiently overexpressing Flag-tagged RAC1^{WT}, RAC1^{T17N}, RAC1^{F28L}, and RAC1^{P29S}, along with an empty vector (EV) control, were analyzed. The phosphorylation levels of ERK1/2 and AKT (at T308 and S473) were evaluated first. Additionally, the phosphorylation of p38 MAPK was examined as a marker of cellular adaptations that enhance survival under oxidative or inflammatory stress. Finally, the phosphorylation levels of STAT1 α/β, a transcription factor downstream of p38 that may promote immune evasion and support survival under inflammatory conditions, were assessed. Phosphorylation levels were quantified by calculating the ratio of phosphorylated target proteins to total proteins (e.g., p-ERK/t-ERK) and normalizing them to GAPDH as a loading control. Flag tag detection confirmed the expression of each RAC1 variant. Representative results were obtained from three independent experiments (Supplementary Fig. S11), and statistical significance was determined using one-

way ANOVA with P values (* $P \leq 0.05$; ** $P \leq 0.01$; and *** $P \leq 0.001$; **** $P \leq 0.0001$). Data are expressed as mean ± SD.

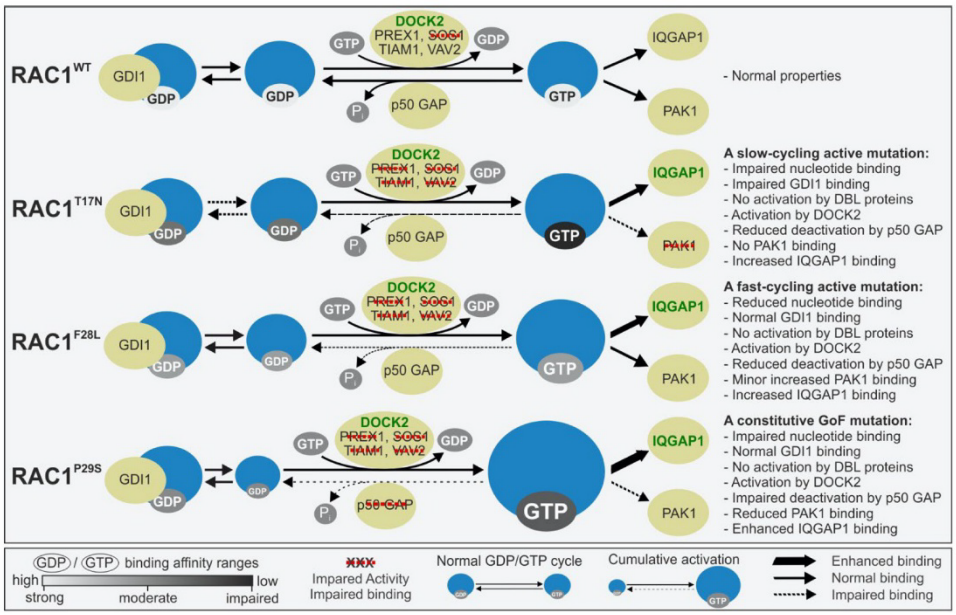

Figure 6. This schematic summarizes the findings of this study, which focuses on the biochemical characterization of RAC1^{T17N}, RAC1^{F28L}, and RAC1^{P29S} mutants in comparison to RAC1^{WT}. The middle section of the figure includes key guides illustrating the strength of GDP/GTP binding, impaired versus enhanced activity or binding to regulators and effectors, and the distinction between the normal GDP/GTP cycle and cumulative activation. Compared to RAC1^{WT}, the RAC1^{P29S} mutant significantly impairs nucleotide binding and exhibits a rapid intrinsic nucleotide exchange rate, while the RAC1^{T17N} mutant shows the most impaired nucleotide binding overall. The P29S mutation has a minimal effect on RAC1-GDI1 interaction, whereas the T17N mutation severely impairs GDI1 activity. The P29S mutation is predominantly activated by DOCK2 rather than DBL family GEFs, with GEF-mediated nucleotide exchange being impaired. A key finding of this study is that the P29S mutation significantly impairs GAP-stimulated GTP hydrolysis of RAC1, providing a temporal mechanism for the accumulation of RAC1^{P29S} in its GTP-bound active form and driving its hyperactivation. While the T17N variant shows no binding affinity for PAK1, the P29S mutation demonstrates a dual effect in vitro: reduced binding affinity for PAK1 but enhanced affinity for IQGAP1. This highlights the pivotal role of accessory proteins, particularly IQGAP1, in driving RAC1^{P29S}-mediated downstream activation. The rightmost section of the figure provides a detailed summary of the biochemical properties of the RAC1 proteins analyzed in this study.

References

1. Mosaddeghzadeh N, Ahmadian MR. The RHO family GTPases: mechanisms of regulation and signaling. Cells. 2021;10(7):1831.
2. Dvorsky R, Ahmadian MR. Always look on the bright site of Rho: structural implications for a conserved intermolecular interface. EMBO reports. 2004;5(12):1130-6.
3. Jaiswal M, Dvorsky R, Ahmadian MR. Deciphering the Molecular and Functional Basis of Dbl Family Proteins: A NOVEL SYSTEMATIC APPROACH TOWARD CLASSIFICATION OF SELECTIVE ACTIVATION OF THE Rho FAMILY PROTEINS*♦. Journal of Biological Chemistry. 2013;288(6):4486-500.
4. Koubek EJ, Santy LC. Actin Up: an overview of the Rac GEF Dock1/Dock180 and its role in cytoskeleton rearrangement. Cells. 2022;11(22):3565.
5. Amin E, Jaiswal M, Derewenda U, Reis K, Nouri K, Koessmeier KT, et al. Deciphering the molecular and functional basis of RHOGAP family proteins: a systematic approach toward selective inactivation of RHO family proteins. Journal of Biological Chemistry. 2016;291(39):20353-71.
6. Maldonado MDM, Medina JI, Velazquez L, Dharmawardhane S. Targeting Rac and Cdc42 GEFs in metastatic cancer. Frontiers in cell and developmental biology. 2020;8:201.
7. Boland A, Côté JF, Barford D. Structural biology of DOCK-family guanine nucleotide exchange factors. FEBS letters. 2023;597(6):794-810.
8. Mosaddeghzadeh N, Kazemein Jasemi NS, Majolée J, Zhang S-C, Hordijk PL, Dvorsky R, et al. Electrostatic forces mediate the specificity of RHO GTPase-GDI interactions. International Journal of Molecular Sciences. 2021;22(22):12493.
9. Fiegen D, Haeusler L-C, Blumenstein L, Herbrand U, Dvorsky R, Vetter IR, et al. Alternative splicing of Rac1 generates Rac1b, a self-activating GTPase. Journal of Biological Chemistry. 2004;279(6):4743-9.
10. Haeusler LC, Blumenstein L, Stege P, Dvorsky R, Ahmadian MR. Comparative functional analysis of the Rac GTPases. FEBS letters. 2003;555(3):556-60.
11. Bailly C, Beignet J, Loirand G, Sauzeau V. Rac1 as a therapeutic anticancer target: Promises and limitations. Biochemical pharmacology. 2022;203:115180.
12. Porter AP, Papaioannou A, Malliri A. Deregulation of Rho GTPases in cancer. Small GTPases. 2016;7(3):123-38.
13. Alan JK, Lundquist EA. Mutationally activated Rho GTPases in cancer. Small GTPases. 2013;4(3):159-63.
14. Hodge RG, Schaefer A, Howard SV, Der CJ. RAS and RHO family GTPase mutations in cancer: twin sons of different mothers? Critical reviews in biochemistry and molecular biology. 2020;55(4):386-407.
15. Priolo M, Zara E, Radio FC, Ciolfi A, Spadaro F, Bellacchio E, et al. Clinical profiling of MRD48 and functional characterization of two novel pathogenic RAC1 variants. European Journal of Human Genetics. 2023;31(7):805-14.
16. Kotelevets L, Chastre E. Rac1 signaling: from intestinal homeostasis to colorectal cancer metastasis. Cancers. 2020;12(3):665.
17. Vu HL, Rosenbaum S, Purwin TJ, Davies MA, Aplin AE. RAC 1 P29S regulates PD-L1 expression in melanoma. Pigment cell & melanoma research. 2015;28(5):590-8.
18. Foth M, Parkman G, Battistone B, McMahon M. RAC1mutation is not a predictive biomarker for PI3'-kinase-β-selective pathway-targeted therapy. Pigment Cell & Melanoma Research. 2020;33(5):719-30.
19. Krauthammer M, Kong Y, Ha BH, Evans P, Bacchiocchi A, McCusker JP, et al. Exome sequencing identifies recurrent somatic RAC1 mutations in melanoma. Nature genetics. 2012;44(9):1006-14.
20. Senyuz S, Jang H, Nussinov R, Keskin O, Gursoy A. Mechanistic differences of activation of Rac1P29S and Rac1A159V. The Journal of Physical Chemistry B. 2021;125(15):3790-802.

21. Revach O-Y, Winograd-Katz SE, Samuels Y, Geiger B. The involvement of mutant Rac1 in the formation of invadopodia in cultured melanoma cells. Experimental cell research. 2016;343(1):82-8.
22. King SJ, Asokan SB, Haynes EM, Zimmerman SP, Rotty JD, Alb Jr JG, et al. Lamellipodia are crucial for haptotactic sensing and response. Journal of cell science. 2016;129(12):2329-42.
23. Zhu EY, Schillo JL, Murray SD, Riordan JD, Dupuy AJ. Understanding cancer drug resistance with Sleeping Beauty functional genomic screens: Application to MAPK inhibition in cutaneous melanoma. Iscience. 2023;26(10).
24. Watson IR, Li L, Cabeceiras PK, Mahdavi M, Gutschner T, Genovese G, et al. The RAC1 P29S hotspot mutation in melanoma confers resistance to pharmacological inhibition of RAF. Cancer research. 2014;74(17):4845-52.
25. Lionarons DA, Hancock DC, Rana S, East P, Moore C, Murillo MM, et al. RAC1P29S induces a mesenchymal phenotypic switch via serum response factor to promote melanoma development and therapy resistance. Cancer cell. 2019;36(1):68-83. e9.
26. Cannon AC, Budagyan K, Uribe-Alvarez C, Kurimchak AM, Araiza-Olivera D, Cai KQ, et al. Unique vulnerability of RAC1-mutant melanoma to combined inhibition of CDK9 and immune checkpoints. Oncogene. 2024:1-15.
27. Mohan AS, Dean KM, Isogai T, Kasitinon SY, Murali VS, Roudot P, et al. Enhanced dendritic actin network formation in extended lamellipodia drives proliferation in growth-challenged Rac1P29S melanoma cells. Developmental cell. 2019;49(3):444-60. e9.
28. Gadal S, Boyer JA, Roy SF, Outmezguine NA, Sharma M, Li H, et al. Tumorigenesis driven by the BRAF V600E oncoprotein requires secondary mutations that overcome its feedback inhibition of migration and invasion. bioRxiv. 2024.
29. Immisch L, Papafotiou G, Gallarín Delgado N, Scheuplein V, Paschen A, Blankenstein T, et al. Targeting the recurrent Rac1P29S neoepitope in melanoma with heterologous high-affinity T cell receptors. Frontiers in Immunology. 2023;14:1119498.
30. Maldonado MdM, Dharmawardhane S. Targeting rac and Cdc42 GTPases in cancer. Cancer research. 2018;78(12):3101-11.
31. Liang J, Oyang L, Rao S, Han Y, Luo X, Yi P, et al. Rac1, a potential target for tumor therapy. Frontiers in oncology. 2021;11:674426.
32. Ma N, Xu E, Luo Q, Song G. Rac1: A regulator of cell migration and a potential target for cancer therapy. Molecules. 2023;28(7):2976.
33. Colón-Bolea P, García-Gómez R, Casar B. RAC1 activation as a potential therapeutic option in metastatic cutaneous melanoma. Biomolecules. 2021;11(11):1554.
34. Sauzeau V, Beignet J, Vergoten G, Bailly C. Overexpressed or hyperactivated Rac1 as a target to treat hepatocellular carcinoma. Pharmacological research. 2022;179:106220.
35. De P, Rozeboom BJ, Aske JC, Dey N. Active RAC1 promotes tumorigenic phenotypes and therapy resistance in solid tumors. Cancers. 2020;12(6):1541.
36. Davis MJ, Ha BH, Holman EC, Halaban R, Schlessinger J, Boggon TJ. RAC1P29S is a spontaneously activating cancer-associated GTPase. Proceedings of the National Academy of Sciences. 2013;110(3):912-7.
37. Kawazu M, Ueno T, Kontani K, Ogita Y, Ando M, Fukumura K, et al. Transforming mutations of RAC guanosine triphosphatases in human cancers. Proceedings of the National Academy of Sciences. 2013;110(8):3029-34.
38. Li A, Machesky LM. Rac1 cycling fast in melanoma with P29 S. Pigment cell & melanoma research. 2013;26(3).
39. Acuner SE, Sumbul F, Torun H, Haliloglu T. Oncogenic mutations on Rac1 affect global intrinsic dynamics underlying GTP and PAK1 binding. Biophysical journal. 2021;120(5):866-76.
40. Lin R, Bagrodia S, Cerione R, Manor D. A novel Cdc42Hs mutant induces cellular transformation. Current Biology. 1997;7(10):794-7.
41. Rajendran V, Gopalakrishnan C, Purohit R. Impact of point mutation P29S in RAC1 on tumorigenesis. Tumor Biology. 2016;37:15293-304.

42. Parise A, Magistrato A. Assessing the mechanism of fast-cycling cancer-associated mutations of Rac1 small Rho GTPase. Protein Science. 2024;33(4):e4939.
43. Nouri K, Fansa EK, Amin E, Dvorsky R, Gremer L, Willbold D, et al. IQGAP1 interaction with RHO family proteins revisited: kinetic and equilibrium evidence for multiple distinct binding sites. Journal of Biological Chemistry. 2016;291(51):26364-76.
44. Hemsath L, Ahmadian MR. Fluorescence approaches for monitoring interactions of Rho GTPases with nucleotides, regulators, and effectors. Methods. 2005;37(2):173-82.
45. Eberth A, Ahmadian MR. In vitro GEF and GAP assays. Current protocols in cell biology. 2009;43(1):14.9. 1-.9. 25.
46. Haeusler LC, Hemsath L, Fiegen D, Blumenstein L, Herbrand U, Stege P, et al. Purification and biochemical properties of Rac1, 2, 3 and the splice variant Rac1b. Methods in enzymology. 2006;406:1-11.
47. Mohr I, Mirzaiebadizi A, Sanyal SK, Chuenban P, Ahmadian MR, Ivanov R, et al. Characterization of the small Arabidopsis thaliana GTPase and ADP-ribosylation factor-like 2 protein TITAN 5. Journal of Cell Science. 2024;137(15).
48. Eberth A, Dvorsky R, Becker CF, Beste A, Goody RS, Ahmadian MR. Monitoring the real-time kinetics of the hydrolysis reaction of guanine nucleotide-binding proteins. Biological Chemistry. 2005;386(11):1105–1114.
49. Herbrand U, Reza Ahmadian M. p190-RhoGAP as an integral component of the Tiam1/Rac1-induced downregulation of Rho. Biological Chemistry. 2006;387(3):311–317.
50. Kulkarni K, Yang J, Zhang Z, Barford D. Multiple factors confer specific Cdc42 and Rac protein activation by dedicator of cytokinesis (DOCK) nucleotide exchange factors. Journal of Biological Chemistry. 2011;286(28):25341-51.
51. Nouri K, Timson DJ, Ahmadian MR. New model for the interaction of IQGAP1 with CDC42 and RAC1. Small GTPases. 2020;11(1):16-22.
52. Mosaddeghzadeh N, Nouri K, Krumbach OH, Amin E, Dvorsky R, Ahmadian MR. Selectivity determinants of RHO GTPase binding to IQGAPs. International Journal of Molecular Sciences. 2021;22(22):12596.
53. Hu W, Wang Z, Zhang S, Lu X, Wu J, Yu K, et al. IQGAP1 promotes pancreatic cancer progression and epithelial-mesenchymal transition (EMT) through Wnt/β-catenin signaling. Scientific reports. 2019;9(1):7539.
54. Liu J, Ni X, Li Y, Chen M, Chen W, Wu Y, et al. Downregulation of IQGAP1 inhibits epithelial-mesenchymal transition via the HIF1α/VEGF-A signaling pathway in gastric cancer. Journal of Cellular Biochemistry. 2019;120(9):15790-9.
55. Toyama Y, Kontani K, Katada T, Shimada I. Conformational landscape alternations promote oncogenic activities of Ras-related C3 botulinum toxin substrate 1 as revealed by NMR. Science advances. 2019;5(3):eaav8945.
56. Wu X, Ramachandran S, Lin M-cJ, Cerione RA, Erickson JW. A minimal Rac activation domain in the unconventional guanine nucleotide exchange factor Dock180. Biochemistry. 2011;50(6):1070-80.
57. Tomino T, Tajiri H, Tatsuguchi T, Shirai T, Oisaki K, Matsunaga S, et al. DOCK1 inhibition suppresses cancer cell invasion and macropinocytosis induced by self-activating Rac1P29S mutation. Biochemical and biophysical research communications. 2018;497(1):298-304.
58. Ji L, Xu S, Luo H, Zeng F. Insights from DOCK2 in cell function and pathophysiology. Frontiers in molecular biosciences. 2022;9:997659.
59. Hasan MK, Yu J, Widhopf GF, Rassenti LZ, Chen L, Shen Z, et al. Wnt5a induces ROR1 to recruit DOCK2 to activate Rac1/2 in chronic lymphocytic leukemia. Blood, The Journal of the American Society of Hematology. 2018;132(2):170-8.
60. Nishihara H, Maeda M, Oda A, Tsuda M, Sawa H, Nagashima K, et al. DOCK2 associates with CrkL and regulates Rac1 in human leukemia cell lines. Blood, The Journal of the American Society of Hematology. 2002;100(12):3968-74.
61. Wu M, Small D, Duffield AS. DOCK2: A novel FLT3/ITD leukemia drug target. Oncotarget. 2017;8(51):88253.

62. Uhlenbrock K, Eberth A, Herbrand U, Daryab N, Stege P, Meier F, et al. The RacGEF Tiam1 inhibits migration and invasion of metastatic melanoma via a novel adhesive mechanism. Journal of cell science. 2004;117(20):4863-71.
63. Cool RH, Schmidt G, Lenzen CU, Prinz H, Vogt D, Wittinghofer A. The Ras mutant D119N is both dominant negative and activated. Molecular and cellular biology. 1999;19(9):6297–6305.
64. Gerboth S, Frittoli E, Palamidessi A, Baltanas FC, Salek M, Rappsilber J, et al. Phosphorylation of SOS1 on tyrosine 1196 promotes its RAC GEF activity and contributes to BCR-ABL leukemogenesis. Leukemia. 2018;32(3):820-7.
65. Yamahashi Y, Lin Y-H, Mouri A, Iwanaga S, Kawashima K, Tokumoto Y, et al. Phosphoproteomic of the acetylcholine pathway enables discovery of the PKC-β-PIX-Rac1-PAK cascade as a stimulatory signal for aversive learning. Molecular Psychiatry. 2022;27(8):3479-92.
66. Feng Q, Baird D, Yoo S, Antonyak M, Cerione RA. Phosphorylation of the cool-1/β-Pix protein serves as a regulatory signal for the migration and invasive activity of Src-transformed cells. Journal of biological chemistry. 2010;285(24):18806-16.
67. Scita G, Tenca P, Areces LB, Tocchetti A, Frittoli E, Giardina G, et al. An effector region in Eps8 is responsible for the activation of the Rac-specific GEF activity of Sos-1 and for the proper localization of the Rac-based actin–polymerizing machine. The Journal of cell biology. 2001;154(5):1031-44.
68. Halaban R. RAC1 and melanoma. Clinical therapeutics. 2015;37(3):682-5.
69. Hodis E, Watson IR, Kryukov GV, Arold ST, Imielinski M, Theurillat J-P, et al. A landscape of driver mutations in melanoma. Cell. 2012;150(2):251-63.
70. Mar VJ, Wong SQ, Logan A, Nguyen T, Cebon J, Kelly JW, et al. Clinical and pathological associations of the activating RAC 1 P29S mutation in primary cutaneous melanoma. Pigment cell & melanoma research. 2014;27(6):1117-25.
71. Araiza-Olivera D, Feng Y, Semenova G, Prudnikova TY, Rhodes J, Chernoff J. Suppression of RAC1-driven malignant melanoma by group A PAK inhibitors. Oncogene. 2018;37(7):944-52.
72. Brown MD, Sacks DB. IQGAP1 in cellular signaling: bridging the GAP. Trends in cell biology. 2006;16(5):242-9.
73. Johnson M, Sharma M, Henderson BR. IQGAP1 regulation and roles in cancer. Cellular signalling. 2009;21(10):1471-8.
74. Ren J-G, Li Z, Crimmins DL, Sacks DB. Self-association of IQGAP1: characterization and functional sequelae. Journal of Biological Chemistry. 2005;280(41):34548-57.
75. Marei H, Carpy A, Macek B, Malliri A. Proteomic analysis of Rac1 signaling regulation by guanine nucleotide exchange factors. Cell Cycle. 2016;15(15):1961-74.
76. Ren J-G, Li Z, Sacks DB. IQGAP1 modulates activation of B-Raf. Proceedings of the National Academy of Sciences. 2007;104(25):10465-9.
77. Bardwell AJ, Lagunes L, Zebarjedi R, Bardwell L. The WW domain of the scaffolding protein IQGAP1 is neither necessary nor sufficient for binding to the MAPKs ERK1 and ERK2. Journal of Biological Chemistry. 2017;292(21):8750-61.
78. Caye A, Strullu M, Guidez F, Cassinat B, Gazal S, Fenneteau O, et al. Juvenile myelomonocytic leukemia displays mutations in components of the RAS pathway and the PRC2 network. Nature genetics. 2015;47(11):1334-40.

Supplementary information

New insights into the classification of the RAC1 P29S hotspot mutation in melanoma as an oncogene

Amin Mirzaiebadizi[1*], Mohammad Reza Ahmadian[1*]
Institute of Biochemistry and Molecular Biology II, Medical Faculty and University Hospital Düsseldorf, Heinrich Heine University, 40225 Düsseldorf, Germany

Detailed Material and Methods

Constructs. Different pGEX vectors (pGEX-2-T and pGEX-4T-1), encoding an N-terminal glutathione S-transferase (GST) fusion protein, were used to overexpress human RAC1 wild-type ($RAC1^{WT}$: accession number or acc. no. of P63000) and its mutants, including $RAC1^{T17N}$, $RAC1^{F28L}$, and $RAC1^{P29S}$, in *Escherichia coli.* The same expression system was also used to overexpress various regulators and effectors, including human guanosine dissociation inhibitor 1 (GDI1: acc. no. D13989), the Dbl homology-pleckstrin homology (DH-PH) tandem domains of T-lymphoma invasion and metastasis-inducing protein 1 (TIAM1: acc. no. Q13009; amino acids or aa 1033–1404), human vav guanine nucleotide exchange factor 2 (VAV2: acc. no. P52735; aa 168–543), human son of sevenless homolog 1 (SOS1: acc. no. Q07889; aa 189–551), and human phosphatidylinositol-3,4,5-trisphosphate-dependent Rac exchanger 1 (PREX1: acc. no. Q8TCU6; aa 34–415), as well as the GTPase-activating protein (GAP) domain of human p50GAP (acc. no. P85298; aa 198–439), the C-terminal part of human IQ motif-containing GTPase-activating protein 1 (IQGAP1: acc. no. P46940; C794; aa 863–1657), and the CDC42/RAC binding domains (RBD) of human p21-activated kinase 1 (PAK1: acc. no. Q13153; RBD, aa 57–141). In addition, the pET-23b(+) vector was used to overexpress human IQGAP1 (acc. no. P46940; C794; aa 863–1657) as a hexahistidine-tagged protein, and the pOPINS vector was used to express the Dock homology region 2 (DHR2) domain of human dedicator of cytokinesis 2 (DOCK2: acc. no. Q92608; aa 1211–1624) as an N-terminal His6-small ubiquitin-like modifier (SUMO)-tagged protein (1). For eukaryotic expression, all RAC1 constructs with N-terminal tandem decahistidine triple-flag tags were cloned into the pcDNA-3.1 vector.

Proteins. All proteins were purified according to previously described protocols (2-6). Briefly, *Escherichia coli* strains, including pLysS BL21(DE3), CodonPlusRIL, and BL21(Rosetta) were transformed to express the target proteins. For protein extraction, cells were incubated at 4 °C with DNase I (10 µg/mL), lysozyme (2 µg/mL), 1% Triton X-100, and a protease inhibitor cocktail (Roche) followed by sonication using a Branson Sonifier S-450A with a 3- to 19-mm titanium probe. Bacterial lysates were centrifuged at 20,000 g for 30 minutes and filtered to obtain soluble fractions. Tagged proteins were purified from the supernatant either as GST fusion proteins using a glutathione-Sepharose column or as His-tagged proteins using Talon cobalt affinity resin. If necessary, the GST tag was cleaved with thrombin (2 units/mg) overnight at 4 °C, followed by a second round of affinity chromatography to remove residual tags. The proteins were then concentrated and pooled after buffer exchange in a buffer containing 30 mM Tris-HCl or HEPES (adjusted to pH 1 unit above or below the isoelectric points of the proteins), 150-250 mM NaCl, 5-10 mM $MgCl_2$, 3 mM DTT, and 0.1 mM GDP for GTPases. Purified proteins were analyzed by SDS-PAGE and Coomassie staining (Supplementary Fig. S1) and stored at -80 °C.

Preparation of nucleotide-free and fluorescent nucleotide-bound GTPases. The preparation of nucleotide-free GTPase was performed in two steps, as described (7, 8). Free and bound GDP was degraded using alkaline phosphatase coupled to agarose beads (0.1-1 U per mg of GTPases) in the presence of a 1.5 molar excess of $Gpp(CH_2)p$, a non-hydrolyzable GTP analog that is resistant to alkaline phosphatase but sensitive to phosphodiesterase. After GDP was completely degraded and replaced by $Gpp(CH_2)p$, snake venom phosphodiesterase (0.002 U per mg of GTPases) was introduced to cleave the nucleotide into GMP, guanosine (G), and inorganic phosphate (Pi). The progress of the reaction was monitored by HPLC using a Beckman Gold instrument equipped with a C18 reversed-phase column and a buffer

consisting of 100 mM potassium phosphate (pH 6.5), 10 mM tetrabutylammonium bromide, and 7.5% acetonitrile. After complete degradation of Gpp(CH_2)p, the sample was centrifuged to remove the beads, snap frozen in liquid nitrogen, and immediately thawed to inactivate the phosphodiesterase. The nucleotide-free GTPases were then aliquoted and stored at −80 °C for subsequent analyses. Fluorescent GDP-bound (inactive) and GppNHp-bound (active) GTPases were prepared by incubating nucleotide-free proteins with a 1.2-fold molar excess of fluorescently labeled nucleotides (methylanthraniloyl or mant-labeled nucleotides: mdGDP and mGppNHp). mdGDP (methylanthraniloyl-2'-deoxy-guanosine 5′-diphosphate) was used instead of mGDP because of its simple monoexponential fluorescence signal, since mGDP equilibrates between the two 2'- and 3'-methylanthraniloyl isomers, resulting in a biphasic fluorescence signal. mGppNHp (methylanthraniloyl guanosine 5'-[beta,gamma-imido]triphosphate) is a non-hydrolyzable analog of GTP. Samples were passed through prepacked NAP-5 columns to exchange the buffer with one free of unbound nucleotides. In addition, GppNHp-bound GTPases were prepared by performing only the first step using alkaline phosphatase and GppNHp, eliminating the need for phosphodiesterase. The concentrations of the nucleotide-bound GTPases were quantified by HPLC under identical buffer conditions, with 25% acetonitrile for the fluorescently labeled nucleotides. The proteins were then stored at −80 °C. The nucleotides were purchased from Jena Bioscience Co.

Fluorescence kinetic measurements. Fluorescence-based kinetic measurements, including both long-term and rapid reactions, were performed using a Horiba Fluoromax-4 fluorimeter and a Hi-Tech Scientific stopped-flow spectrophotometer (Applied Photophysics SX20), respectively, as described (6-9). Excitation wavelengths of 355 nm for mdGDP/mGppNHp and 546 nm for tetramethylrhodamine-labeled GTP (tamra-GTP: tGTP) were used for the stopped-flow analysis. Fluorescence detection was facilitated by a photomultiplier equipped with cut-off filters that allowed the detection of wavelengths above 408 nm for mdGDP/mGppNHp and above 580 nm for tGTP. In addition, slow reactions were monitored using the Horiba fluorimeter in combination with quartz cuvettes (Hellma), with an excitation wavelength of 355 nm and an emission wavelength of 446 nm for mant labeled nucleotides.

Nucleotide-binding assay. The nucleotide-binding properties of the RAC1 GTPases were assessed using a stopped-flow fluorimetry approach, as described (10). ucleotide association was measured with 0.1 µM fluorescently labeled nucleotides, such as mdGDP and mGppNHp, and varying concentrations of nucleotide-free RAC1 proteins (0.25–5 µM). Measurements were conducted in a buffer containing 30 mM Tris-HCl, pH 7.5, 10 mM KH_2PO_4/K_2HPO_4, 5 mM $MgCl_2$, and 3 mM DTT, at 25 °C. The association rate constant (kon) was determined by plotting the observed rate constants (kobs) against the concentration of nucleotide-free RAC1 and analyzing the slope via linear regression using Origin software. The dissociation rate constant (koff) of the fluorescent nucleotide from RAC1 proteins (0.1 µM) was measured by adding a 200-fold excess of the non-fluorescent nucleotide (20 µM). The affinity of RAC1 proteins for GDP and GppNHp was calculated by dividing koff by kon, yielding the equilibrium dissociation constants (Kd), as defined in Box 2 of the main text.

GEF-catalyzed nucleotide dissociation assay. The rapid GEF-catalyzed nucleotide exchange reaction was monitored by stopped-flow fluorimetry, as described (8). In this assay, 0.1 µM mGDP-bound RAC1 protein in syringe 1 was rapidly mixed with 200-fold excess of non-fluorescent nucleotide (20 µM) and 10 µM of each GEF, including the DH-PH tandem domains of several DBL family members (TIAM1, SOS1, PREX1, and VAV2) and the DHR2 domain of DOCK2, a member of the DOCK family, separately, in syringe 2. The reactions were performed in a buffer containing 30 mM Tris-HCl, pH 7.5, 10 mM KH_2PO_4/K_2HPO_4, 5 mM $MgCl_2$, and 3 mM DTT, at 25 °C. The observed rate constants were determined by fitting the data to a single-exponential model using Origin software.

Intrinsic and GAP-stimulated GTP-hydrolysis assays. The intrinsic GTP hydrolysis rate of RAC1 proteins was determined by HPLC, a reliable method that has been successfully applied to various GTPases, as noted by Eberth and Ahmadian (8). Briefly, the GTPase reaction was

initiated by mixing 100 µM nucleotide-free RAC1 with 90 µM GTP in a GAP buffer containing 30 mM Tris-HCl (pH 7.5), 10 mM $KH_2PO_4/K2H_PO_4$, 10 mM $MgCl_2$, and 3 mM DTT at 25 °C. Nucleotide contents were monitored by injecting 30 µL of the reaction mixture onto a reverse phase column, with the total volume adjusted to allow for at least seven injections. The reaction was stopped when no further changes in GTP content were observed. The relative GTP content, determined as the ratio [GTP]/([GTP] + [GDP]), was plotted against time, and the data were fitted to a single exponential function using Origin software to calculate the catalytic rate constant (k_{cat}) for GTP hydrolysis. GAP-stimulated GTP hydrolysis rates of different RAC1 proteins were determined by stopped-flow fluorimetry using Tamra-GTP, as described (11). A 1 µM solution of nucleotide-free RAC1 was rapidly mixed with 0.8 µM Tamra-GTP in syringe 1, while 1 µM of the catalytic domains of p50 RhoGAP was added in syringe 2, all in the GAP buffer at 25 °C. After reaction initiation, real-time data were recorded and fitted to an exponential function to calculate k_{cat}.

Protein-protein interaction kinetics. The interaction of RAC1 with GST-GDI1, GST-PAK1 RBD, and His-IQGAP1 C794 was analyzed by stopped-flow fluorimetry to determine k_{on}, k_{off}, and K_d values, where K_d was calculated by dividing k_{off} by k_{on}, as described (6). For the GDI-binding assay, mdGDP-bound inactive RAC1 (0.1 µM) was incubated with varying concentrations of GST-GDI1 (0.25–2 µM). kon values were determined by plotting kobs versus GST-GDI1 concentrations and applying linear regression. koff values were measured by monitoring the release of GST-GDI1 (0.1 µM) from mdGDP-bound RAC1 in the presence of excess non-fluorescent GDP-bound RAC1 (10 µM) using a single-exponential fit. Similarly, mGppNHp-bound active RAC1 (0.1 µM) was used to study interactions with GST-PAK1 RBD and His-IQGAP1 C794. kon values were derived from kobs plots, and koff values were determined in the presence of excess non-fluorescent GppNHp-bound RAC1 (10 µM).

Fluorescence polarization. Fluorescence polarization was used to determine the binding affinity between RAC1 and various effector proteins in their three-dimensional state. Experiments were performed using a Fluoromax 4 fluorimeter in polarization mode according to a predefined protocol (6). Gradually increasing concentrations of different effectors were titrated against mGppNHp-bound RAC1 proteins (1 µM) in a buffer containing 30 mM Tris-HCl (pH 7.5), 50 mM NaCl, 5 mM $MgCl_2$, and 3 mM DTT. The total reaction volume was 200 µL, and assays were performed at a constant temperature of 25 °C. Dissociation constants (K_d) were determined by fitting the concentration-dependent binding curves to a quadratic ligand binding equation.

Cell culture and transfection. HEK-293T cells were cultured in DMEM supplemented with 10% fetal bovine serum (FBS) and 1% penicillin/streptomycin to support optimal growth and prevent contamination. For transfection, RAC1 constructs containing an N-terminal tandem 10 His-triple flag tag were introduced into the cells using TurboFect™ Transfection Reagent (Thermo Fisher Scientific) according to the manufacturer's protocol. After transfection, cells were harvested under both serum-stimulated and serum-starved conditions. Cell lysis was performed using FISH buffer (50 mM Tris-HCl, pH 7.5; 100 mM NaCl; 2 mM $MgCl_2$; 20 mM β-glycerophosphate; 1 mM Na_3VO_4; 10% glycerol; 1x protease inhibitor cocktail (Roche); and 1% IGEPAL (Thermo Fisher Scientific)). Lysis was performed on ice for 10 minutes, followed by centrifugation at 20,000 g for 5 minutes to remove debris. The resulting clear supernatants were used for subsequent analysis, and protein concentrations were determined using the Bradford assay.

***In vitro* pull-down assays.** Pull-down assays were performed to evaluate the ability and strength of RAC1 proteins to bind to PAK1 RBD and IQGAP1 C794. According to the manufacturer's protocols, these assays utilized GST-fused PAK1 RBD with glutathione agarose beads (Macherey-Nagel) and His-IQGAP1 C794 and His Mag Sepharose Ni beads (Cytiva). Briefly, 50 µL of beads per reaction were washed three times and equilibrated in an ice-cold pull-down buffer consisting 50 mM Tris/HCl (pH 7.5), 150 mM NaCl, 10 mM $MgCl_2$, 3 mM DTT, and 5% glycerol. Equimolar ratios of RAC1 protein to GST-PAK1 RBD and His-

IQGAP1 C794 were prepared in separate experiments, with small aliquots used as input controls. The remaining mixtures were incubated with the respective beads for 30 minutes at 4°C under gentle rotation. After three washes with ice-cold buffer, the glutathione-agarose beads were centrifuged at 700 g, while the His-Mag Sepharose Ni beads were magnetically separated using the MagRac6 device (Cytiva). Proteins were eluted from the His Mag pull-down using the buffer supplemented with 500 mM imidazole. The eluates from the His pull-down and protein-bound agarose beads from the GST pull-down were mixed with Laemmli loading buffer (100 mM Tris-HCl, pH 6.8; 33% glycerol; 300 mM dithiothreitol, 6.7% SDS; and 0.01% bromophenol blue), heated at 95°C to denature the proteins, and analyzed for protein-protein interactions using SDS-PAGE and immunoblotting.

Active GTPase pull-down assay. A GTPase pull-down assay was performed to assess GTP-bound active RAC1 levels under serum-stimulated and serum-starved conditions in transiently transfected HEK-293T cells (Supplementary Fig. S9), as described (12). Bacterial lysates containing GST-PAK1 RBD and GST-IQGAP1 C794 were prepared separately in 1 mL aliquots, snap frozen, and stored at -80°C. For bead coupling, based on the results of this pre-test, 25 µL of GST-PAK1 RBD lysate and 50 µL of GST-IQGAP1 C794 lysate were incubated with 50 µL of glutathione agarose beads in a total volume of 500 µL of an ice-cold pull-down buffer consisting 50 mM Tris/HCl (pH 7.5), 150 mM NaCl, 10 mM $MgCl_2$, 3 mM DTT, and 5% glyceroat 4°C. After 30 minutes, the beads were washed three times with the buffer and subsequently used for the assay (Supplementary Fig. S10C). HEK-293T lysates were clarified by centrifugation, normalized to equal protein concentrations, and incubated with GST-PAK1 RBD- and GST-IQGAP1 C794- coupled beads in a buffer containing 50 mM Tris-HCl, pH 7.5; 150 mM NaCl; 10 mM $MgCl_2$; 20 mM β-glycerophosphate; 1 mM Na_3VO_4; 3 mM DTT; 10% glycerol; protease inhibitor cocktail at 4°C for 20 minutes. The beads were washed three times, resuspended with SDS-Laemmli loading buffer, and heated at 95°C for 7 minutes. Samples were analyzed by SDS-PAGE and immunoblotting

Antibodies and Immunoblotting. Primary antibodies were diluted 1:1000 in TBST containing 0.2% Tween-20 and 30% Intercept® (TBS) blocking buffer (Li-Cor). The following antibodies in this study were as followa: α-RAC1 (Merck Millipore, Cat# 05-389), α-6x-His (Thermo Fisher Scientific, Cat# MA5-33032), α-flag (Sigma Aldrich, Cat# F3165), α-γ-tubulin (Sigma Aldrich, Cat# T5326), α-p-ERK1/2 (Thr202/Tyr204) (Cell Signaling Technology, Cat# 4370), α-t-ERK1/2 (Cell Signaling Technology, Cat# 4696), α-p-AKT(S473) (Cell Signaling Technology, Cat# 4060), α-p-AKT(T308) (Cell Signaling Technology, Cat# 2965), α-t-AKT (Cell Signaling Technology, Cat# 2920), α-p-p38 MAPK (Cell Signaling Technology, Cat# 9211), α-p38 MAPK (Cell Signaling Technology, Cat# 8690), α-p-STAT1 (Cell Signaling Technology, Cat# 8826), α-STAT1 (Cell Signaling Technology, Cat# 9176), and α-GAPDH (Cell Signaling Technology, Cat# 2118), α-GST (Cell Signaling Technology #2624). Secondary antibodies, IRDye® 680RD and 800CW donkey anti-rabbit IgG (Cat# 926-68073, 926-32213) and anti-mouse IgG (Cat# 926-68072, 926-32212), were purchased from Li-Cor. Immunoblots were visualized using the Odyssey® XF Imaging System.

Statistical Analysis. Data presented in bar graphs of Figures 1, 2, and 3 for all stopped-flow fluorescence measurements represent the average of 3–6 experiments and are expressed as the mean ± S.D. Intrinsic GTP hydrolysis assays (HPLC) and fluorescence polarization experiments were performed in duplicate, with results also expressed as the mean ± S.D. Immunoblot data were analyzed by quantifying the intensities of specific protein bands using Image Studio Lite version 5.2 software. For in vitro pull-down assays, data normalization was performed by dividing the output RAC1 protein by the output effector protein and then dividing this value by the corresponding input RAC1/effector ratio. Input bands were included to ensure the accuracy of the reaction setup. Representative images were obtained from three (supplementary Fig. S7A) or four (supplementary Fig. S8A) experiments. Data for pull-down assays are expressed as mean ± S.D. For active GTPase pull-down assays, normalization was performed according to the equation shown in Fig. 4B. Flag-RAC1 pull-down (PD) values were normalized to the beads-bound GST effector, while overexpressed Flag-RAC1 levels in

lysates were normalized to total cell lysate (TCL) levels using γ-tubulin as a loading control. Active RAC1 levels were calculated by dividing the PD values by the corresponding TCL values. Representative images were obtained from three independent experiments (Supplementary Fig. S10A and S10B). Data are expressed as mean ± S.D. For downstream signaling analyses using lysates from transfected HEK-293T cells, data were normalized by calculating the ratio of phosphorylated target proteins to total proteins (e.g., p-ERK/t-ERK), and further normalized to GAPDH signal as a loading control. To avoid false positives, Flag-RAC1 expression levels were excluded from normalization in these experiments. Data were analyzed by one-way ANOVA followed by Tukey's test, with results considered statistically significant at $P \leq 0.05$ (* $P \leq 0.05$; ** $P \leq 0.01$; and *** $P \leq 0.001$; **** $P \leq 0.0001$), Data are expressed as mean ± S.D.

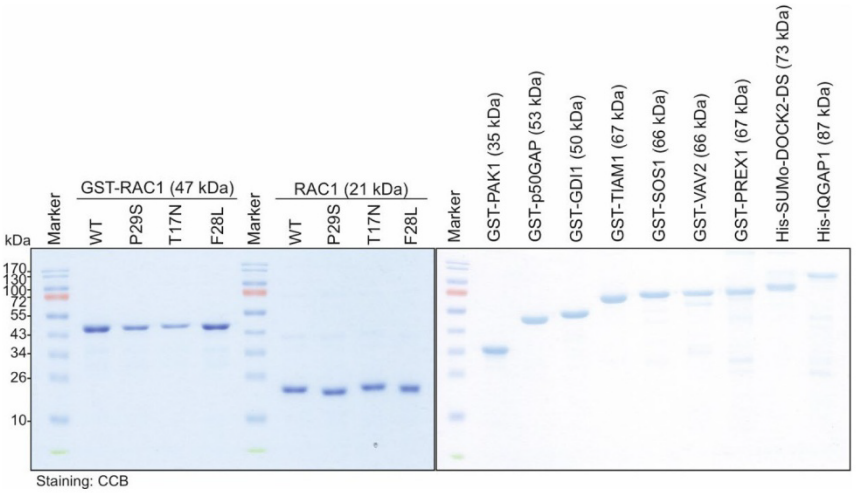

Figure S1. Purified proteins. SDS -PAGE gel stained with Coomassie Brilliant Blue (CBB) shows the purified proteins used in this study. For further details, please refer to the Materials and Methods section.

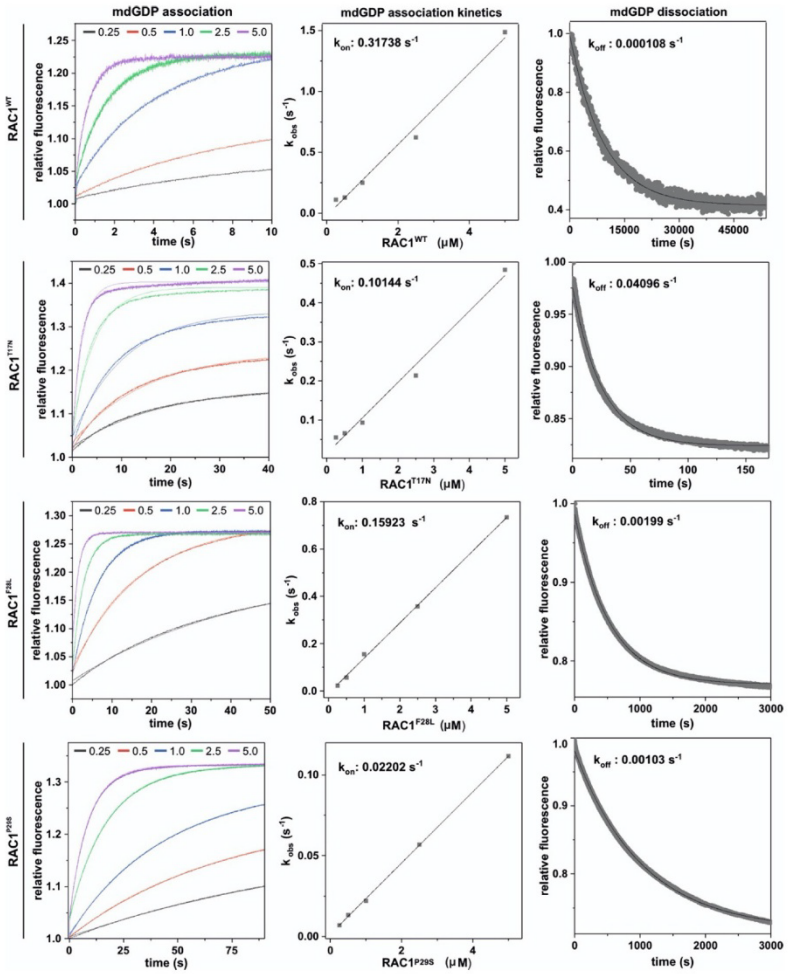

Figure S2. Kinetic measurements of mdGDP interaction with RAC1 proteins. The left panels show the interaction of mdGDP (0.1 μM) to RAC1 at increasing concentrations (0.25 to 5 μM). The middle panels illustrate the calculation of the association rate constant (k_{on}), derived by plotting the observed rate constants (k_{obs}) obtained from the exponential fits of the association data in the left panels against the corresponding RAC1 concentrations, followed by linear fitting. The right panels show the dissociation of mdGDP from RAC1 proteins (0.1 μM) in the presence of excess unlabeled GDP (10 μM). The dissociation rate constants (k_{off}) were determined using a single exponential fit. These results are presented as bar graphs in Figure 1.

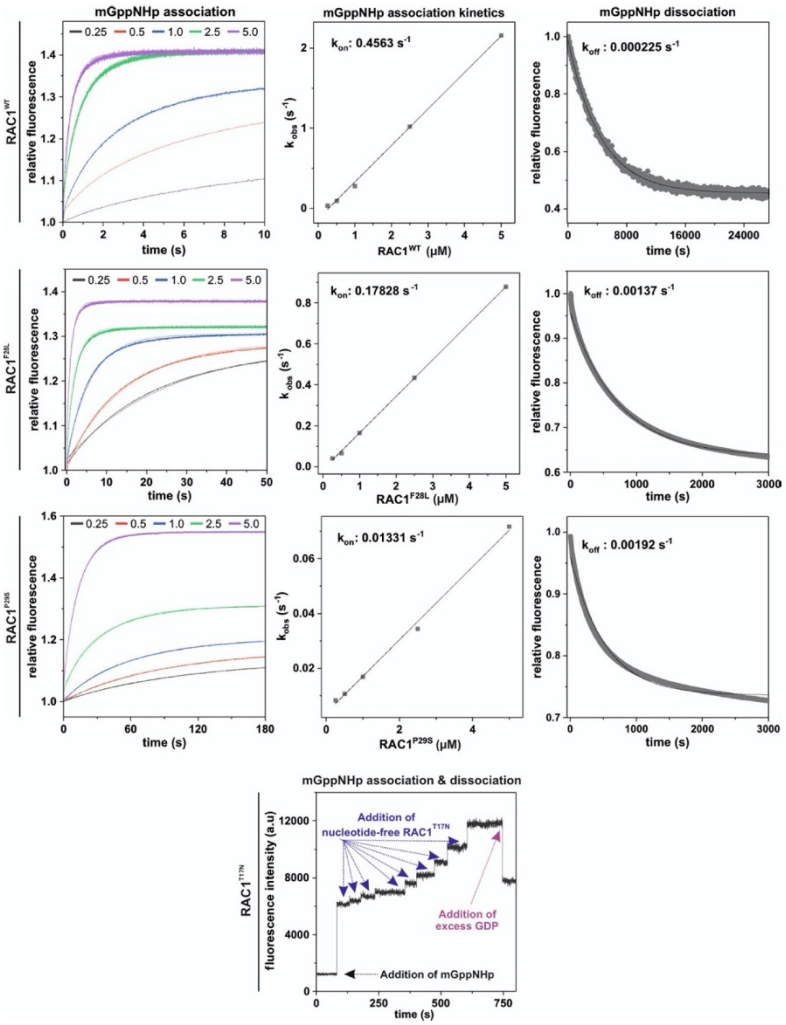

Figure S3. Kinetic measurements of mGppNHp interaction with RAC1 proteins. The left panels show the binding of mGppNHp (0.1 μM) to RAC1 over a range of concentrations (0.25-5 μM). In the middle panels, the association rate constant (k_{on}) is calculated by plotting the observed rate constants (k_{obs}) derived from the exponential fit of the association data in the left panels against the respective concentrations of RAC1, followed by a linear fit. The right panels show the dissociation of mGppNHp from RAC1 proteins (0.1 μM) in the presence of excess unlabeled GppNHp (10 μM). Dissociation rate constants (k_{off}) were calculated using a single exponential fit. The data are visually presented as bar graphs in Figure 1. The final lower panel shows fluorescence measurements taken using a standard fluorescence spectrophotometer to investigate the potential association and dissociation kinetics of the mGppNHp interaction with $RAC1^{T17N}$. These measurements could not be performed using stopped-flow fluorimetry. The experiment began with buffer alone, followed by the addition of 1 μM fluorescent mGppNHp, which caused an immediate increase in fluorescence intensity. The association was then assessed by sequentially adding nucleotide-free $RAC1^{T17N}$ in concentrations ranging from 0.05 μM to 1 μM and observing the increases in fluorescence signal. The potential dissociation of mGppNHp from the $RAC1^{T17N}$ was then examined by adding an excess of unlabeled nucleotide (200 μM GDP), which resulted in a rapid drop in signal intensity,

indicating dissociation of mGppNHp from nucleotide-free $RAC1^{T17N}$. This experiment demonstrated that the nucleotide-free $RAC1^{T17N}$ can bind to and dissociate from mGppNHp. However, k_{on} and k_{off} values could not be determined using stopped-flow fluorimetry because the association and dissociation rates of nucleotide-free $RAC1^{T17N}$ with mGppNHp were too fast, exceeding the detection capability of stopped-flow fluorescence measurement.

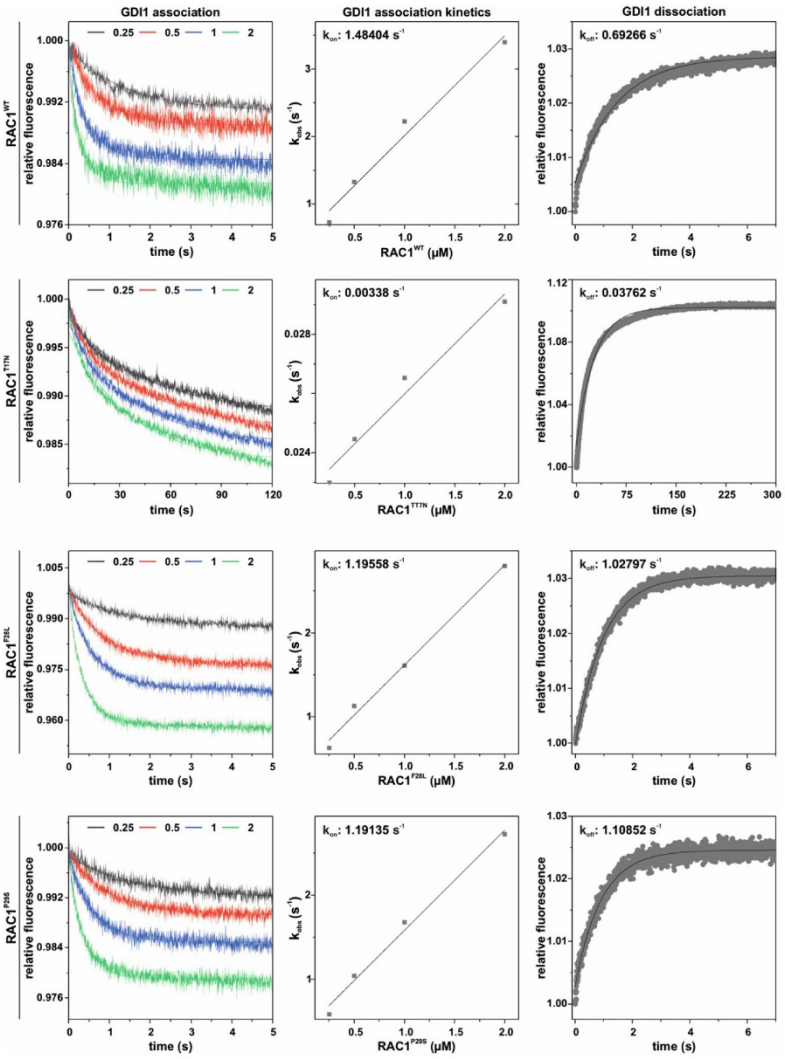

Figure S4. Kinetic measurements of GDI1 interaction with RAC1 proteins. The interaction between RAC1 and GST-GDI1 was examined using stopped-flow fluorimetry to determine the association (k_{on}) and dissociation (k_{off}) rate constants, as well as the dissociation constants (K_d) representing the affinity. The left panels show RAC1 binding (0.1 μM) to GST-GDI1 across concentrations ranging from 0.25 to 2 μM. The middle panels illustrate the calculation of k_{on} values, derived by plotting the observed rate constants (k_{obs}), obtained from exponential fits of the association data in the left panels, against GST-GDI1 concentrations, followed by linear regression. The right panels depict the dissociation of GST-GDI1 (0.1 μM) from RAC1 proteins (0.1 μM) in the presence of excess non-fluorescent GDP-bound RAC1 (10 μM). k_{off} values were determined through single-exponential fitting. The results are displayed as bar graphs in Figure 2A.

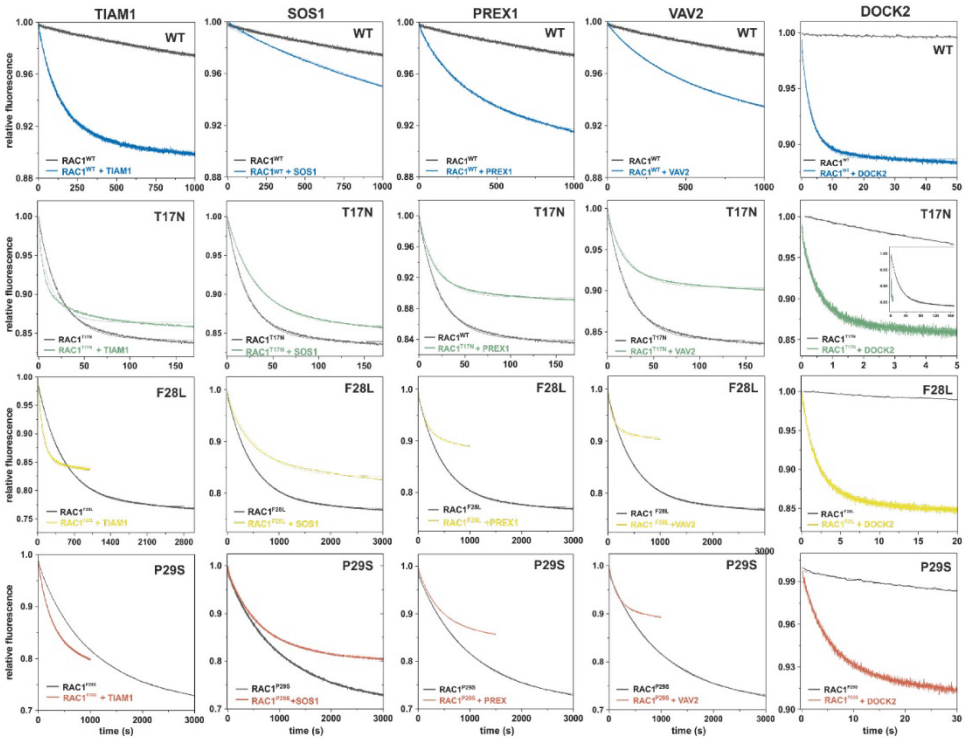

Figure S5. Kinetic measurements of GEF-catalyzed mdGDP dissociation from RAC1 proteins. The dissociation of mdGDP from RAC1 proteins (0.1 μM) was measured in the presence of 10 μM GEFs (DH-PH domains of TIAM1, SOS1, PREX1, and VAV2; DHR2 domain of DOCK2) and excess unlabeled GDP (10 μM). The inset show the full kinetics over time. All fluorescence decays were fitted to a single exponential function to calculate the dissociation rate constants (k_{off}). The results are presented as bar graphs in Figure 2B.

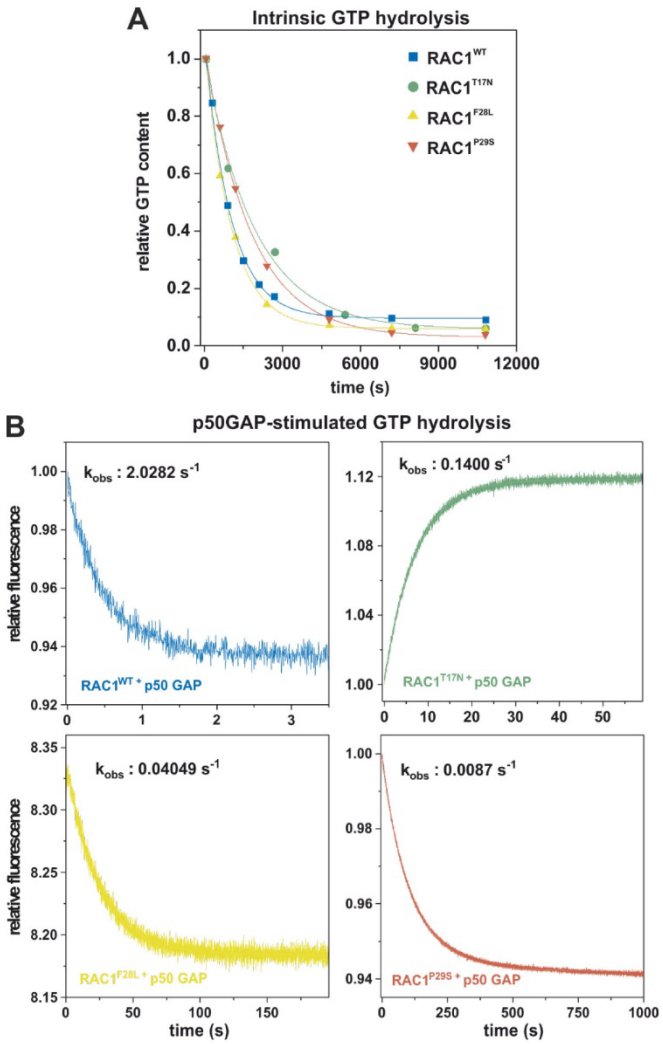

Figure S6. Measurements of the basal and GAP-stimulated GTP hydrolysis of RAC1 proteins. (**A**) The basal GTP hydrolysis of the RAC1 proteins was measured using GTP-bound RAC1 proteins and the HPLC method. The relative GTP content, determined as the ratio [GTP]/([GTP] + [GDP]), was used to describe the progress of the reaction. (**B**) Hydrolysis of tGTP (0.8 µM) by RAC1 proteins (0.1 µM) was measured in real-time in the presence of 1 µM p50GAP. All data sets, including HPLC and fluorescence curves, were fitted with a single exponential function to calculate the observed rate constants (kobs), which reflect the catalytic rate constants (k_{cat}). The results are presented as bar graphs in Figure 2C.

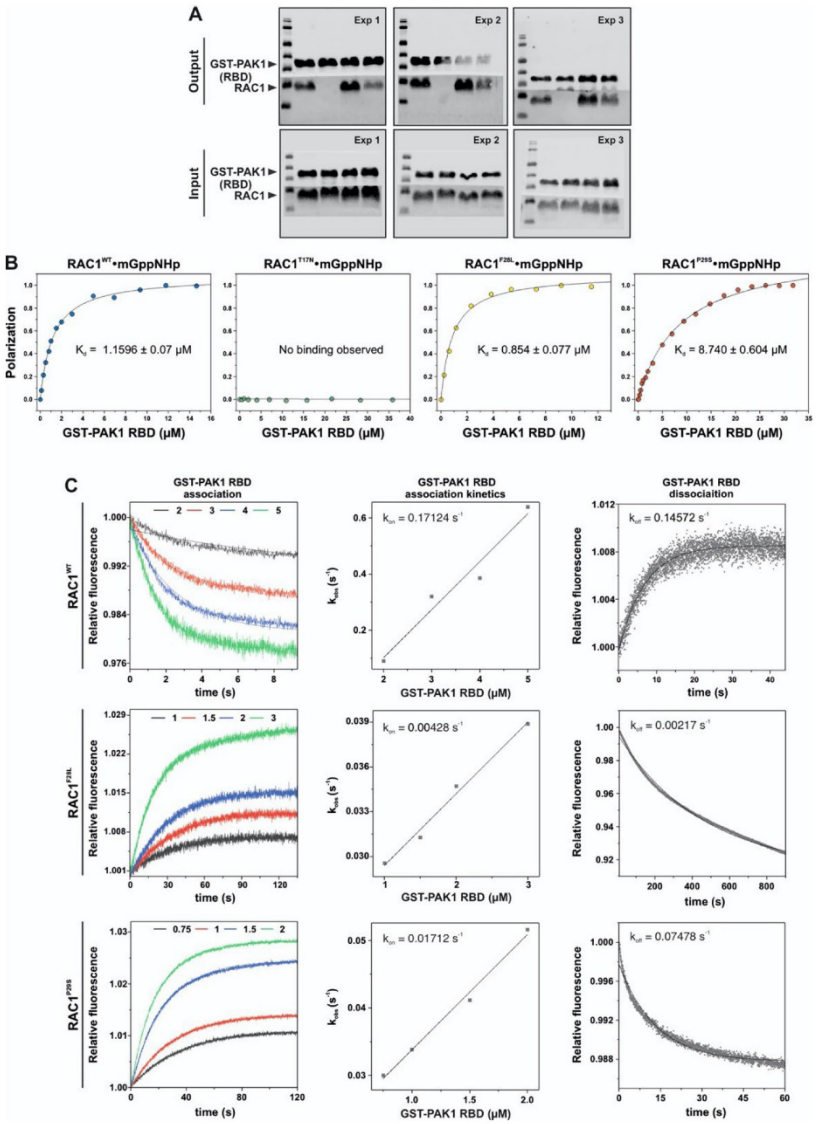

Figure S7. Measurements of PAK1 interaction with the RAC1 proteins. (**A**) A GST pull-down assay was performed in triplicate to assess the interaction between RAC1 mutants and GST-PAK1 RBD. The top blots show the pull-down signals (output), while the bottom blots show the input samples before bead incubation. GST-PAK1 RBD was detected with an anti-GST antibody, and RAC1 proteins were visualized with an anti-RAC1 antibody. The input blots confirm that identical amounts of protein were used before bead incubation, ensuring experiment accuracy. A cropped version of experiment 1 is shown in Figure 3B, with data points and statistical analyses displayed as bar graphs in Figure 3C. (**B**) Fluorescence polarization was used to calculate the dissociation constants (K_d) for each RAC1 mutant interacting with GST-PAK1 RBD. The mGppNHp-bound RAC1 proteins at 1 μM were titrated with increasing concentrations of GST-PAK1 RBD. Data are shown as bar graphs in Figure 3E. "n.b.o." indicates no binding was observed. (**C**) Stopped-flow fluorimetry was used to assess the affinity of the RAC1 proteins for GST-PAK1 RBD and to provide additional insight into the association (k_{on}) and dissociation (k_{off}) rate constants, complementing the data from

pull-down assays and fluorescence polarization. The left panels show the binding of RAC1 (0.1 μM) to GST-PAK1 RBD at different concentrations (μM). The middle panels show the calculation of the association rate constant (k_{on}) by plotting the observed rate constants (k_{obs}), derived from the exponential fits of the association data in the left panels, against GST-PAK1 concentrations, followed by linear regression. The right panels illustrate the dissociation of GST-PAK1 RBD (0.1 μM) from RAC1 proteins (0.1 μM) in the presence of excess non-fluorescent GppNHp-bound RAC1 (10 μM). Dissociation rate constants (k_{off}) were determined by single-exponential fitting. The results are plotted as bar graphs in Figure 3G.

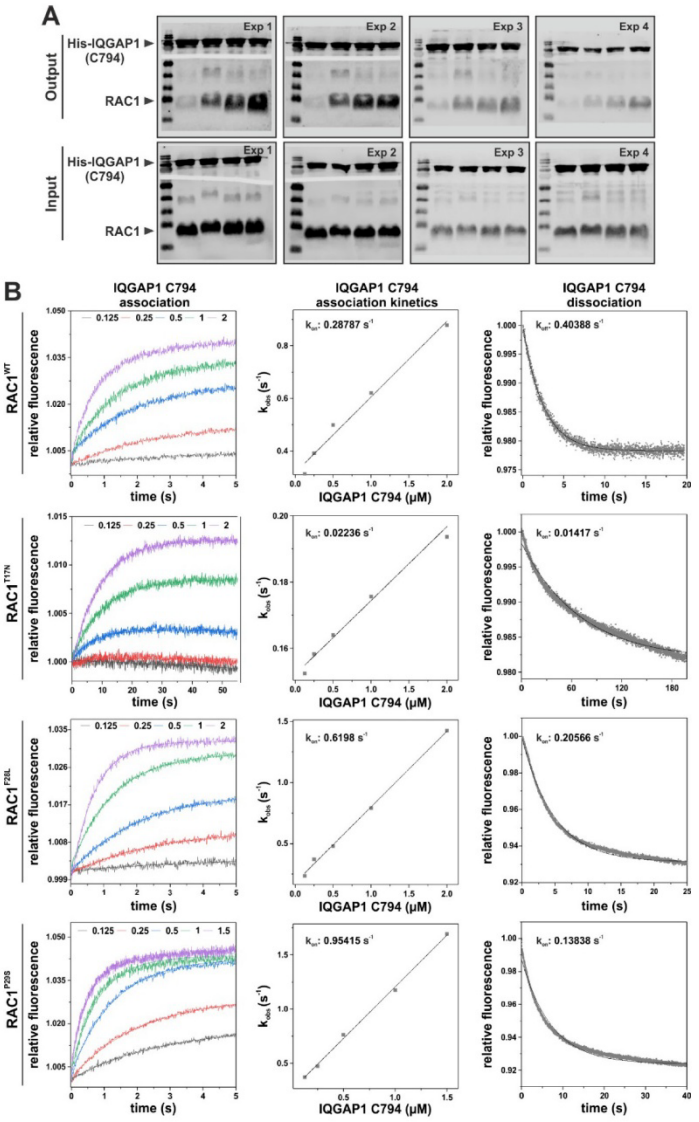

Figure S8. Measurements of IQGAP1 interaction with the RAC1 proteins. (**A**) The His pull-down assay was performed in quadruplicate to investigate the interaction between RAC1 mutants and His-IQGAP1 C794. The top blots show the pull-down signals (output), while the bottom blots show the input samples before incubation with His-Mag-Sepharose Ni beads. His-IQGAP1 C794 was detected with an anti-His antibody, and RAC1 proteins were visualized with an anti-RAC1 antibody. The input blots confirm that identical amounts of proteins were used before bead incubation, ensuring the reliability of the results. A cropped version of Experiment 1 is shown in Figure 3H, with data points and statistical analyses presented as bar graphs in Figure 3I. (**B**) Stopped-flow fluorimetry was used to study the interaction between RAC1 and His-IQGAP1 C794 to determine the association (k_{on}) and dissociation (k_{off}) rate constants, as well as the affinity represented by the dissociation constants (K_d). This analysis complements the data obtained from pull-down assays. The left panels show the binding of RAC1 (0.1 μM) to His-IQGAP1 C794 at varying concentrations in μM. The middle panels show the calculation

of the k_{on} values, derived by plotting the observed rate constants (k_{obs}), obtained from exponential fits of the association data in the left panels, against the concentrations of His-IQGAP1 C794, followed by linear regression. The right panels show the dissociation of His-IQGAP1 C794 (0.1 μM) from RAC1 proteins (0.1 μM) in the presence of excess non-fluorescent GppNHp-bound RAC1 (10 μM). The k_{off} values were determined using single-exponential fitting. The results are plotted as bar graphs in Figure 3J.

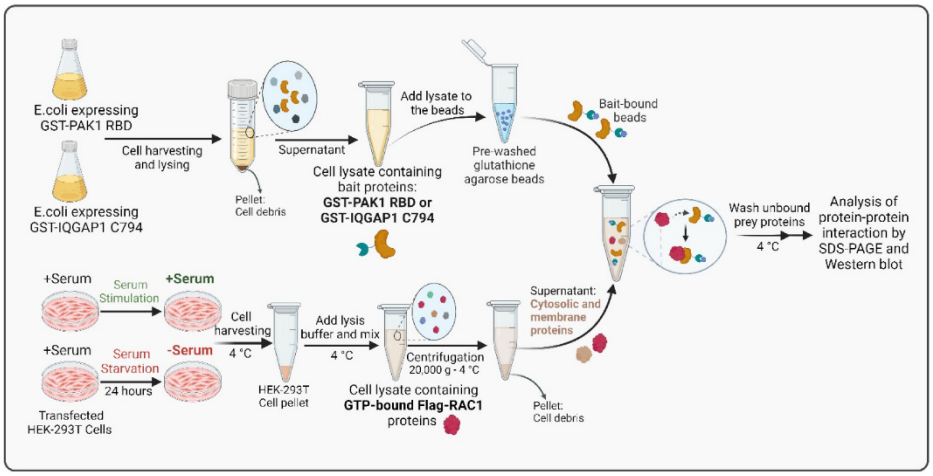

Figure S9. Schematic representation of the pull-down assay of active, GTP-bound RAC1 from HEK-293T cell lysates. See the Materials and Methods section for more details. This schematic was created in BioRender.

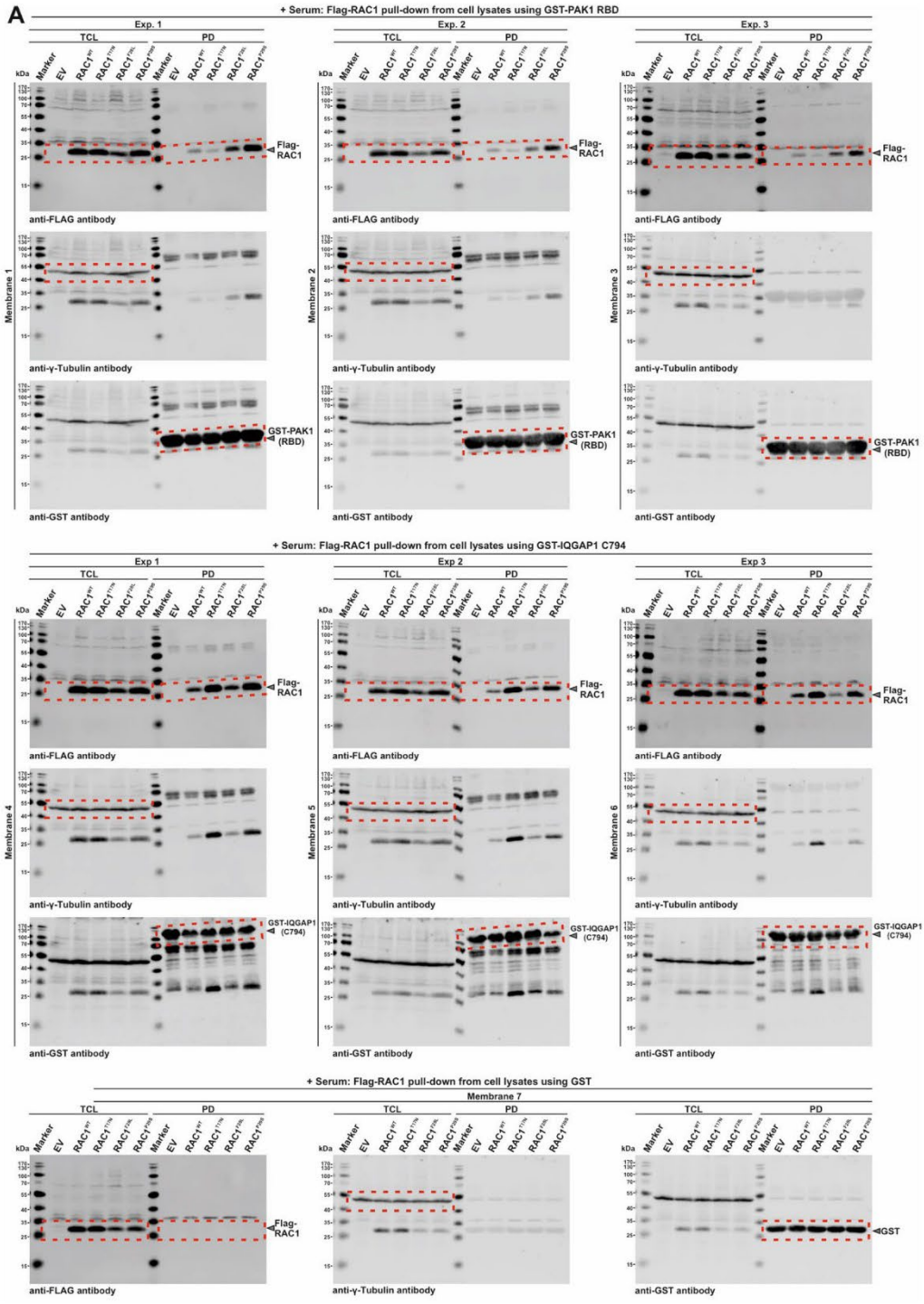
A
+ Serum: Flag-RAC1 pull-down from cell lysates using GST-PAK1 RBD
Exp. 1
Exp. 2
Exp. 3
TCL
PD
kDa
Marker
EV
RAC1WT
RAC1Y77A
RAC1P29L
RAC1P29S
Flag-RAC1
anti-FLAG antibody
Membrane 1
Membrane 2
Membrane 3
anti-γ-Tubulin antibody
GST-PAK1 (RBD)
anti-GST antibody
+ Serum: Flag-RAC1 pull-down from cell lysates using GST-IQGAP1 C794
Membrane 4
Membrane 5
Membrane 6
GST-IQGAP1 (C794)
+ Serum: Flag-RAC1 pull-down from cell lysates using GST
Membrane 7
GST

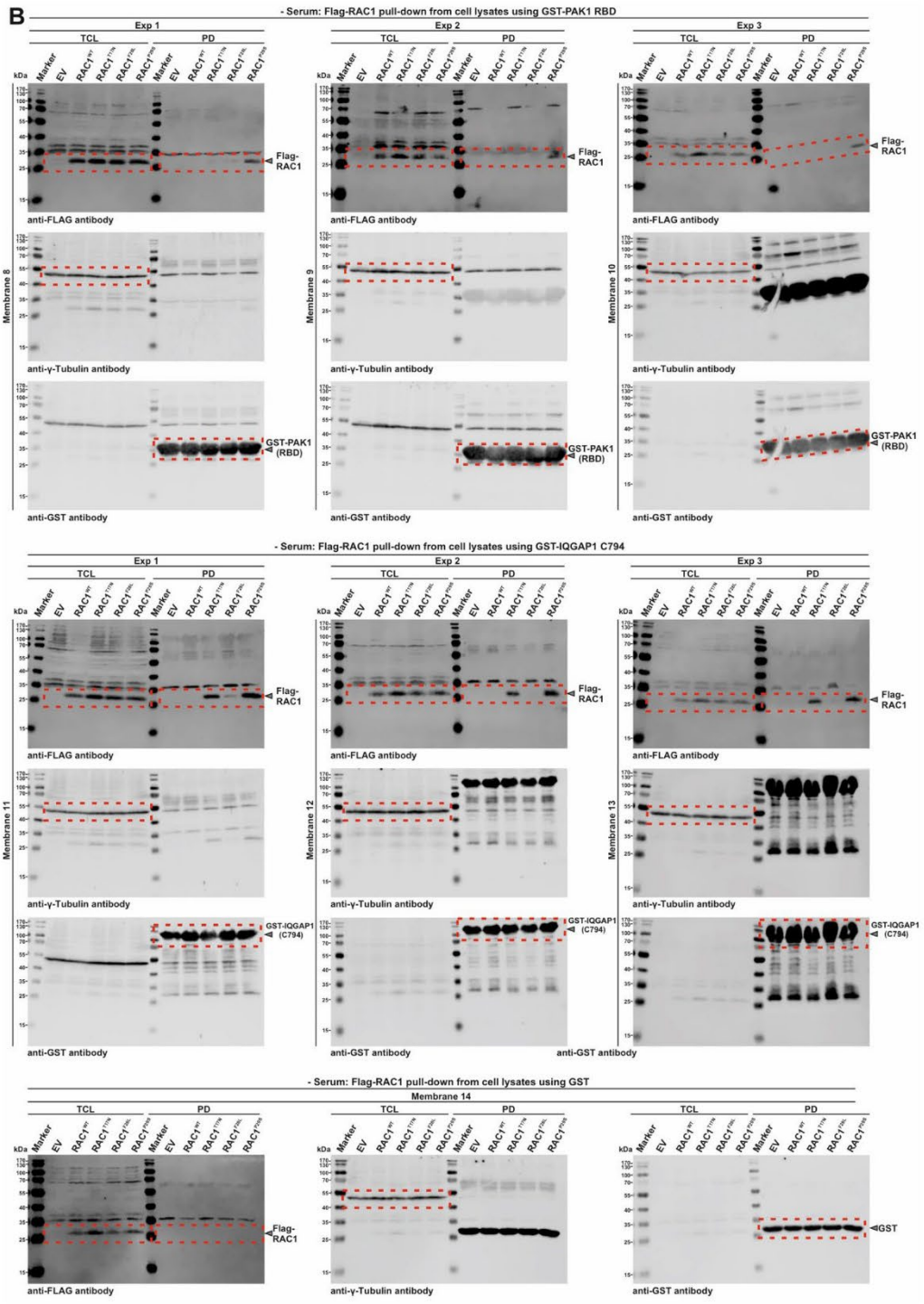
B
- Serum: Flag-RAC1 pull-down from cell lysates using GST-PAK1 RBD
Exp 1
Exp 2
Exp 3
TCL
PD
Marker
EV
RAC1WT
RAC1T17N
RAC1P29L
RAC1P29S
kDa
Flag-RAC1
anti-FLAG antibody
Membrane 8
Membrane 9
Membrane 10
anti-γ-Tubulin antibody
GST-PAK1 (RBD)
anti-GST antibody
- Serum: Flag-RAC1 pull-down from cell lysates using GST-IQGAP1 C794
Membrane 11
Membrane 12
Membrane 13
GST-IQGAP1 (C794)
- Serum: Flag-RAC1 pull-down from cell lysates using GST
Membrane 14
GST

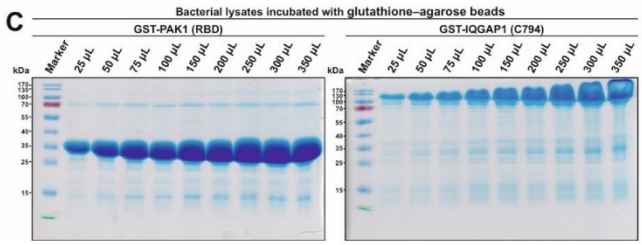

Figure S10. Active GTPase pull-down assays using GTP-bound Flag-RAC1 from HEK-293T cell lysates. Active GTPase pull-down assays were performed to quantify GTP-bound Flag-RAC1 from HEK-293T cell lysates with GST-PAK1 RBD, GST-IQGAP1 C794, and GST as negative controls. The assays were conducted under both serum-stimulated (**A**) and serum-starved (**B**) conditions. HEK-293T cells were transfected with RAC1 constructs, serum stimulated or starved for 24 hours, and then harvested and lysed for the pull-down assays. (**A**) shows three panels under serum-stimulated conditions (from top to bottom): the top panel represents GTP-bound Flag-RAC1 pull-down using GST-PAK1 RBD (performed in triplicate), the middle panel represents GST-IQGAP1 C794 (also in triplicate), and the bottom panel shows the negative control, GST, with no interaction observed with Flag-RAC1. (**B**) shows the same three panels under serum-starved conditions. Western blots were probed with anti-Flag, anti-GST, and anti-γ-tubulin antibodies to detect GTP-bound Flag-RAC1, the GST fusion proteins, and γ-tubulin, respectively. Molecular weights (in kDa) are indicated for each protein band. Pull-down (PD) lanes show GTP-bound Flag-RAC1 captured by the bait-bound beads, while total cell lysate (TCL) lanes show Flag-RAC1 expression levels, with γ-tubulin as a loading control. Each membrane contains samples from three independent experiments, labeled Exp1-3, with antibody incubations indicated by red dashed boxes. Membranes 1-3 represent GST-PAK1 RBD under serum stimulation; membranes 4-6, GST-IQGAP1 C794 under serum stimulation; membrane 7, GST under serum stimulation; membranes 8-10, GST-PAK1 RBD under serum starvation; membranes 11-13, GST-IQGAP1 under serum starvation; and membrane 14, GST under serum starvation. (**C**) Coomassie-stained SDS-PAGE Gels showing the bead saturation assay for GST-PAK1 RBD (left) and GST-IQGAP1 C794 (right). After IPTG induction and protein expression, varying amounts of bacterial lysate (25-350 µL) were incubated with 50 µL of GSH beads for one hour and washed three times. The beads were then mixed with SDS-Laemmli sample buffer, heated to 95°C, and analyzed by SDS-PAGE fallowed by Coomassie Brilliant Blue staining. Based on this pre-test, 25 µL of GST-PAK1 RBD lysate and 50 µL of GST-IQGAP1 C794 lysate were used for the active GTPase pull-down assays.

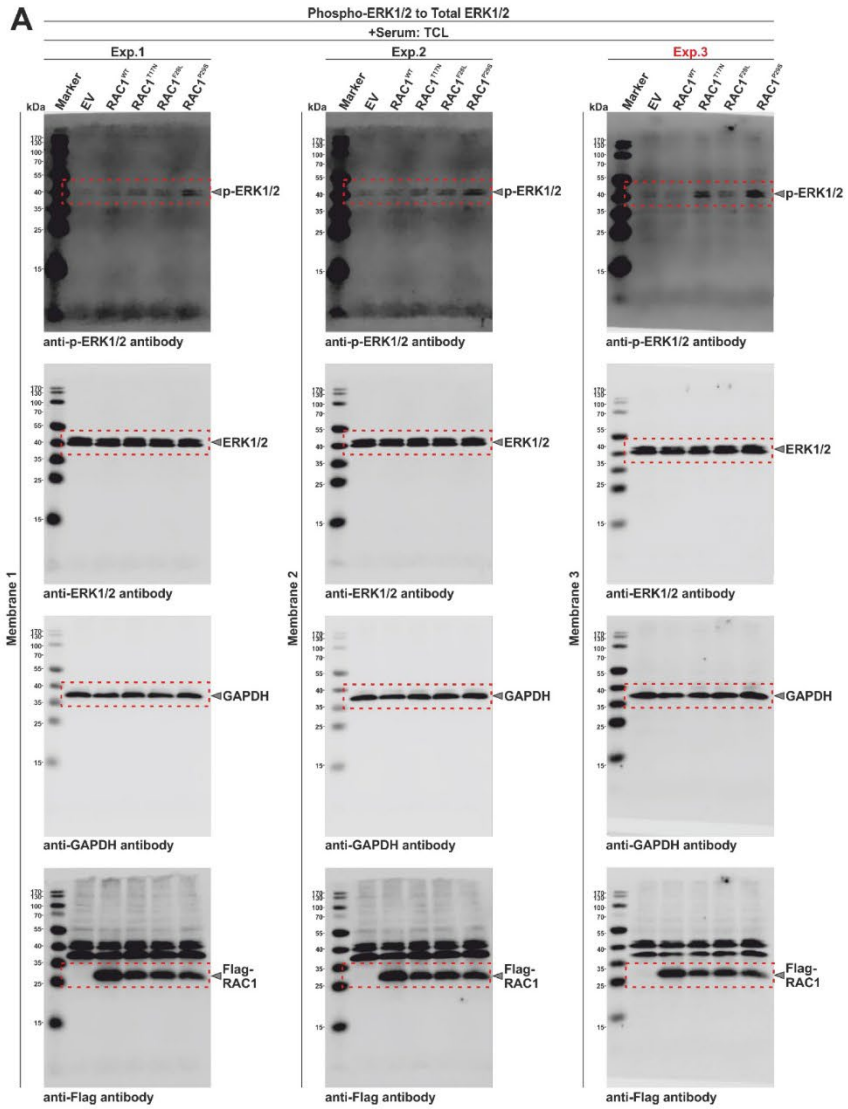
A
Phospho-ERK1/2 to Total ERK1/2
+Serum: TCL
Exp.1
Exp.2
Exp.3
Marker
EV
RAC1WT
RAC1T17N
RAC1F28L
RAC1P29S
kDa
p-ERK1/2
anti-p-ERK1/2 antibody
ERK1/2
anti-ERK1/2 antibody
GAPDH
anti-GAPDH antibody
Flag-RAC1
anti-Flag antibody
Membrane 1
Membrane 2
Membrane 3

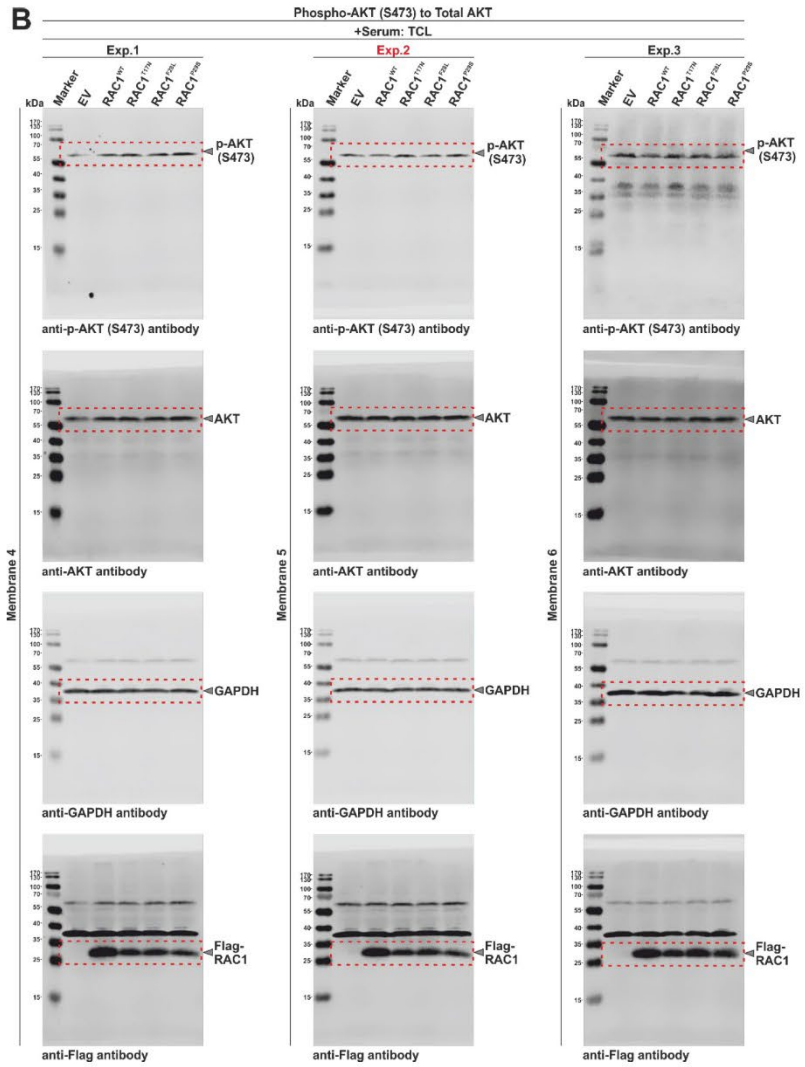
B
Phospho-AKT (S473) to Total AKT
+Serum: TCL
Exp.1
Exp.2
Exp.3
kDa
Marker
EV
RAC1 WT
RAC1 T17N
RAC1 P29L
RAC1 P29S
p-AKT (S473)
anti-p-AKT (S473) antibody
AKT
anti-AKT antibody
GAPDH
anti-GAPDH antibody
Flag-RAC1
anti-Flag antibody
Membrane 4
Membrane 5
Membrane 6

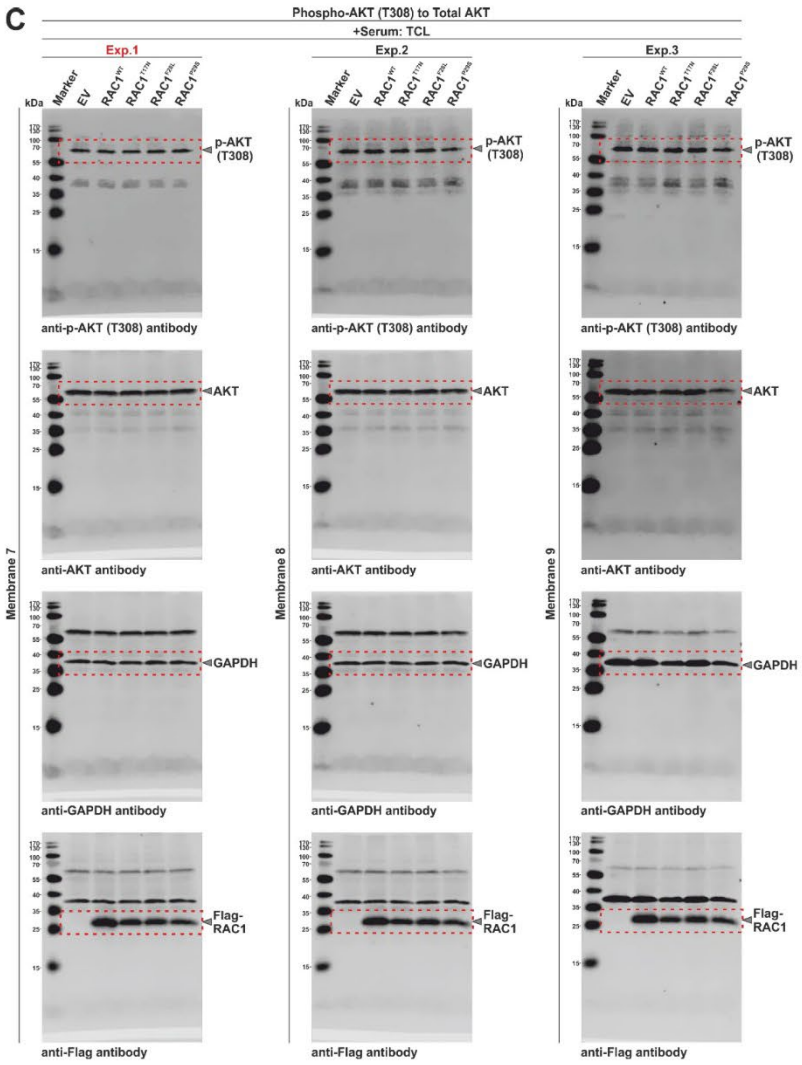
C
Phospho-AKT (T308) to Total AKT
+Serum: TCL
Exp.1
Exp.2
Exp.3
kDa
Marker
EV
RAC1WT
RAC1F77A
RAC1F28L
RAC1P29S
p-AKT (T308)
anti-p-AKT (T308) antibody
AKT
anti-AKT antibody
GAPDH
anti-GAPDH antibody
Flag-RAC1
anti-Flag antibody
Membrane 7
Membrane 8
Membrane 9

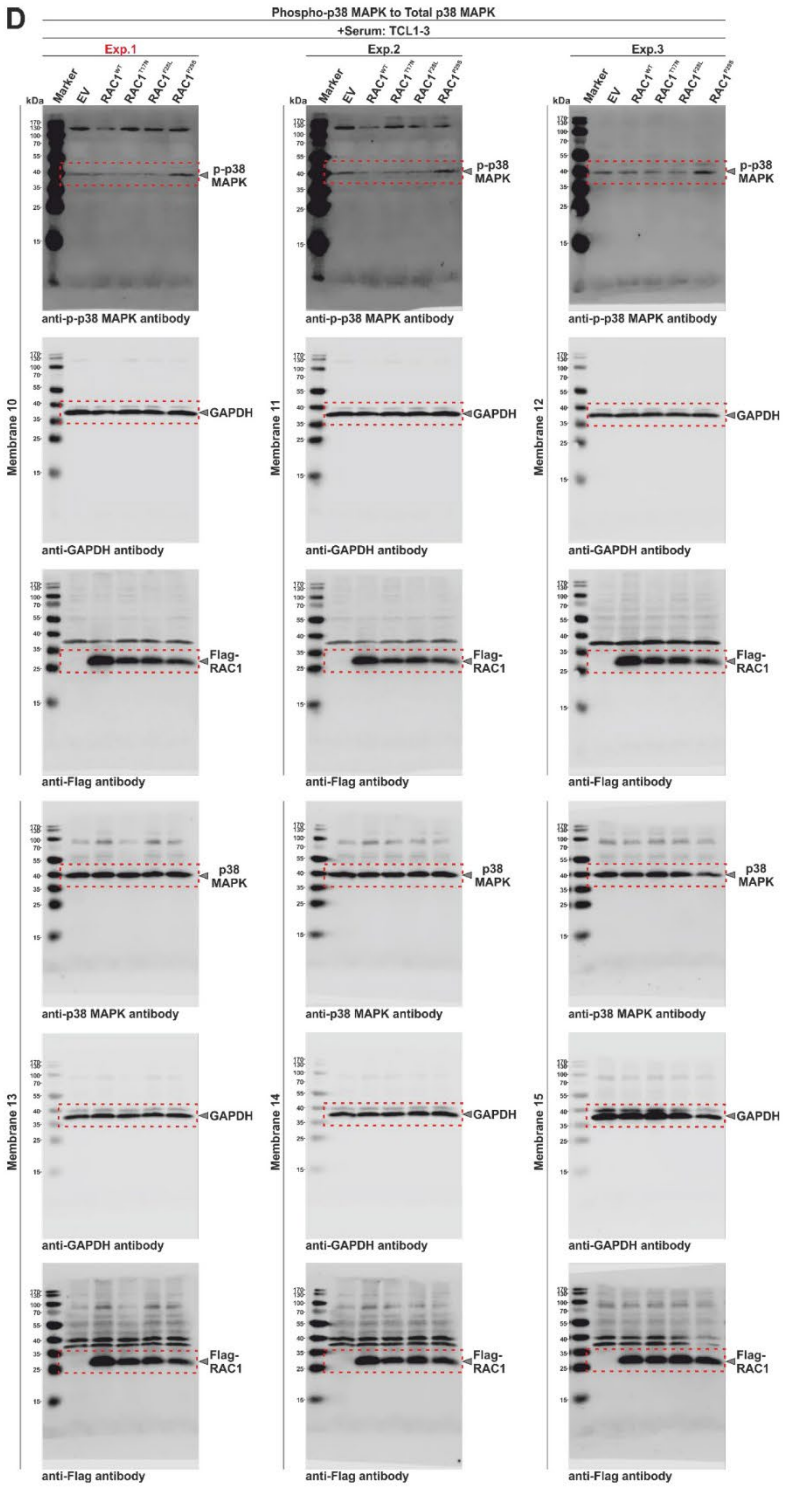
D
Phospho-p38 MAPK to Total p38 MAPK
+Serum: TCL1-3
Exp.1
Exp.2
Exp.3
kDa
Marker
EV
RAC1WT
RAC1T17N
RAC1F28L
RAC1P29S
p-p38 MAPK
anti-p-p38 MAPK antibody
GAPDH
anti-GAPDH antibody
Flag-RAC1
anti-Flag antibody
Membrane 10
Membrane 11
Membrane 12
p38 MAPK
Membrane 13
Membrane 14
Membrane 15

24

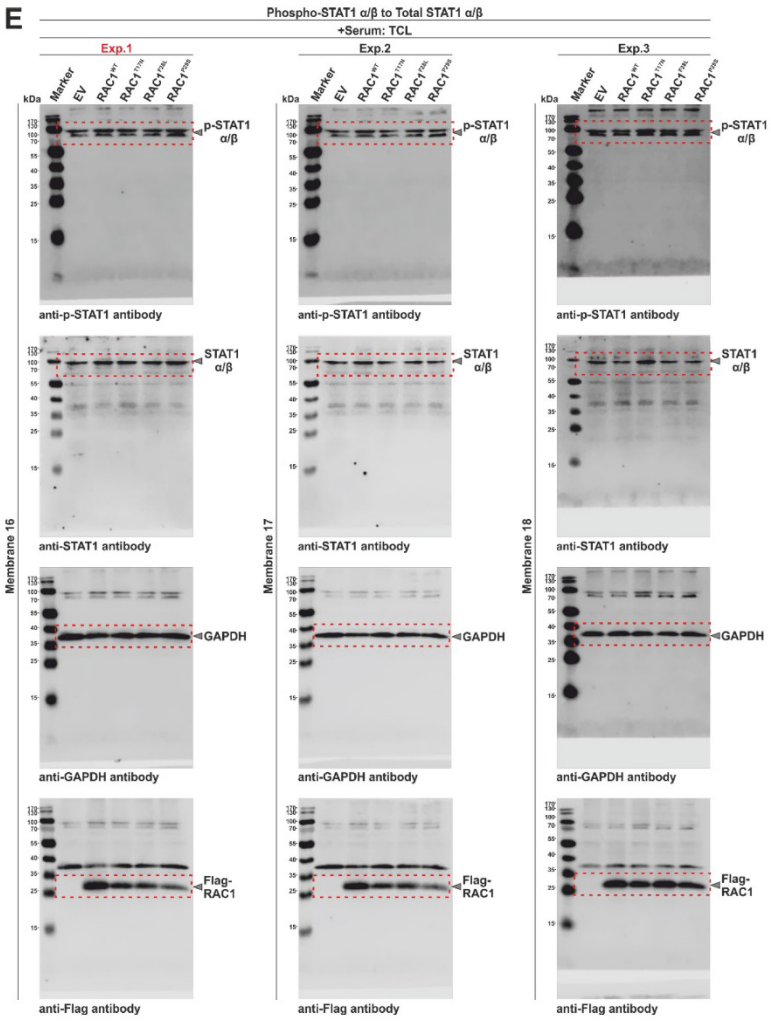

Figure S11. Western blotting and phosphorylation analysis of ERK1/2, AKT(S473), AKT(T308), p38 MAPK, and STAT1 α/β in HEK-293T cells overexpressing RAC1 variants. Western blot analysis was performed on serum-stimulated HEK-293T cells transiently transfected with pcDNA3.1 constructs encoding Flag-tagged RAC1 variants (WT, T17N, F28L, and P29S) alongside an empty vector (EV) control. Experiments were performed in triplicate, with each experiment visualized on nitrocellulose membranes and labeled as follows: (A) phospho-ERK1/2 to total ERK1/2 (membranes 1-3); (B) phospho-AKT (S473) to total AKT (membranes 4-6); (C) phospho-AKT (T308) to total AKT (membranes 7-9); (D) phospho-p38 MAPK to total p38 MAPK (membranes 10-15); and (E) phospho-STAT1 α/β to total STAT1 α/β (membranes 16-18). Cropped sections of the membrane shown in Figure 5 are as follows: Exp1 for AKT(T308), p38 MAPK, and STAT1 α/β; Exp2 for AKT(S473); Exp3 for ERK. Each membrane was probed sequentially, starting with the respective anti-phospho antibodies, followed by antibodies against ERK, AKT, p38 MAPK, STAT1 α/β, and GAPDH as loading controls, and the flag antibody to validate RAC1 variant expression. For p38 MAPK, separate membranes were used to detect phosphorylated and total form, as both antibodies are derived from the same host species. Detected protein bands are highlighted with dashed red boxes, and arrows indicate the corresponding molecular weight in kDa for each protein. Abbreviations:

TCL = total cell lysate; Serum+ = serum-stimulated HEK-293T cells. See the Materials and Methods section for further details.

References

1. Kulkarni K, Yang J, Zhang Z, Barford D. Multiple factors confer specific Cdc42 and Rac protein activation by dedicator of cytokinesis (DOCK) nucleotide exchange factors. Journal of Biological Chemistry. 2011;286(28):25341-51.
2. Haeusler LC, Blumenstein L, Stege P, Dvorsky R, Ahmadian MR. Comparative functional analysis of the Rac GTPases. FEBS letters. 2003;555(3):556-60.
3. Fiegen D, Haeusler L-C, Blumenstein L, Herbrand U, Dvorsky R, Vetter IR, et al. Alternative splicing of Rac1 generates Rac1b, a self-activating GTPase. Journal of Biological Chemistry. 2004;279(6):4743-9.
4. Jaiswal M, Dvorsky R, Ahmadian MR. Deciphering the Molecular and Functional Basis of Dbl Family Proteins: A NOVEL SYSTEMATIC APPROACH TOWARD CLASSIFICATION OF SELECTIVE ACTIVATION OF THE Rho FAMILY PROTEINS*♦. Journal of Biological Chemistry. 2013;288(6):4486-500.
5. Amin E, Jaiswal M, Derewenda U, Reis K, Nouri K, Koessmeier KT, et al. Deciphering the molecular and functional basis of RHOGAP family proteins: a systematic approach toward selective inactivation of RHO family proteins. Journal of Biological Chemistry. 2016;291(39):20353-71.
6. Nouri K, Fansa EK, Amin E, Dvorsky R, Gremer L, Willbold D, et al. IQGAP1 interaction with RHO family proteins revisited: kinetic and equilibrium evidence for multiple distinct binding sites. Journal of Biological Chemistry. 2016;291(51):26364-76.
7. Hemsath L, Ahmadian MR. Fluorescence approaches for monitoring interactions of Rho GTPases with nucleotides, regulators, and effectors. Methods. 2005;37(2):173-82.
8. Eberth A, Ahmadian MR. In vitro GEF and GAP assays. Current protocols in cell biology. 2009;43(1):14.9. 1-.9. 25.
9. Haeusler LC, Hemsath L, Fiegen D, Blumenstein L, Herbrand U, Stege P, et al. Purification and biochemical properties of Rac1, 2, 3 and the splice variant Rac1b. Methods in enzymology. 2006;406:1-11.
10. Mohr I, Mirzaiebadizi A, Sanyal SK, Chuenban P, Ahmadian MR, Ivanov R, et al. Characterization of the small Arabidopsis thaliana GTPase and ADP-ribosylation factor-like 2 protein TITAN 5. Journal of Cell Science. 2024;137(15).
11. Eberth A, Dvorsky R, Becker CF, Beste A, Goody RS, Ahmadian MR. Monitoring the real-time kinetics of the hydrolysis reaction of guanine nucleotide-binding proteins. Biological Chemistry. 2005;386(11):1105–1114.
12. Herbrand U, Reza Ahmadian M. p190-RhoGAP as an integral component of the Tiam1/Rac1-induced downregulation of Rho. Biological Chemistry. 2006;387(3):311–317.

Chapter II. Characterization of the small *Arabidopsis thaliana* GTPase and ADP-ribosylation factor-like 2 protein TITAN 5

Authors: Inga Mohr, Amin Mirzaiebadizi, Sibaji K Sanyal, Pichaporn Chuenban, Mohammad R Ahmadian, Rumen Ivanov, Petra Bauer

DOI: 10.1242/jcs.262315

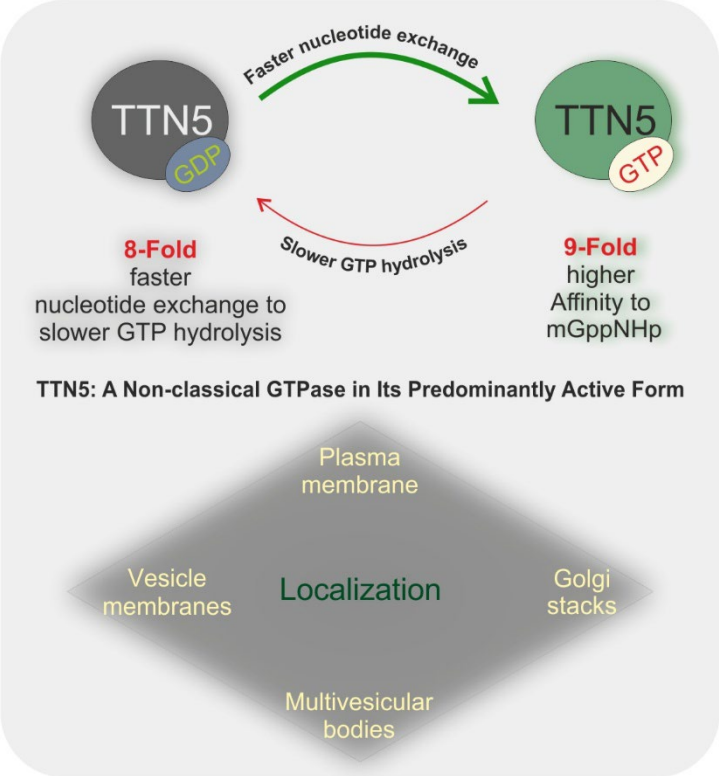

Status: Published

Journal: *Journal of Cell Science*
JIF: 3.3
Contribution: ≈30%

A.M. expressed and purified wild-type and mutant TTN5 proteins and generated both unlabeled and fluorescently labeled versions. He performed HPLC-based GTP hydrolysis experiments and conducted kinetic nucleotide-binding analyses using stopped-flow fluorimetry. He designed and carried out GST pull-down experiments, and addressed stability challenges of TTN5 variants by optimizing expression and purification conditions. A.M. analyzed the biochemical data, visualized the results, authored the corresponding *Materials and Methods* section, and contributed to interpreting and discussing the findings.

© 2024. Published by The Company of Biologists Ltd | Journal of Cell Science (2024) 137, jcs262315. doi:10.1242/jcs.262315

RESEARCH ARTICLE

Characterization of the small *Arabidopsis thaliana* GTPase and ADP-ribosylation factor-like 2 protein TITAN 5

Inga Mohr[1], Amin Mirzaiebadizi[2], Sibaji K. Sanyal[1], Pichaporn Chuenban[1,4], Mohammad R. Ahmadian[2], Rumen Ivanov[1,*] and Petra Bauer[1,3,*]

ABSTRACT

Small GTPases switch between GDP- and GTP-bound states during cell signaling. The ADP-ribosylation factor (ARF) family of small GTPases is involved in vesicle trafficking. Although evolutionarily well conserved, little is known about ARF and ARF-like GTPases in plants. We characterized biochemical properties and cellular localization of the essential small ARF-like GTPase TITAN 5 (TTN5; also known as HALLIMASCH, ARL2 and ARLC1) from *Arabidopsis thaliana*, and two TTN5 proteins with point mutants in conserved residues, TTN5^{T30N} and TTN5^{Q70L}, that were expected to be unable to perform nucleotide exchange and GTP hydrolysis, respectively. TTN5 exhibited very rapid intrinsic nucleotide exchange and remarkably low GTP hydrolysis activity, functioning as a non-classical small GTPase being likely present in a GTP-loaded active form. We analyzed signals from YFP–TTN5 and HA_3–TTN5 by *in situ* immunolocalization in *Arabidopsis* seedlings and through use of a transient expression system. Colocalization with endomembrane markers and pharmacological treatments suggests that TTN5 can be present at the plasma membrane and that it dynamically associates with membranes of vesicles, Golgi stacks and multivesicular bodies. Although TTN5^{Q70L} mirrored wild-type TTN5 behavior, the TTN5^{T30N} mutant differed in some aspects. Hence, the unusual rapid nucleotide exchange activity of TTN5 is linked with its membrane dynamics, and TTN5 likely has a role in vesicle transport within the endomembrane system.

KEY WORDS: TTN5, ARL2, Endomembrane, GTPase, Plasma membrane, Vesicle

INTRODUCTION

Regulatory processes in signal transduction rely heavily on guanine nucleotide-binding proteins of the GTPase family. After identifying oncogenes (*HRAS*, *KRAS* and *NRAS*), the RAS superfamily of small GTPases emerged, encompassing conserved members across eukaryotes. This family is divided into five mammalian subfamilies: the Rat sarcoma (RAS), RAS homologs (RHO), RAS-like proteins in the brain (RAB), Ras-related nuclear proteins (RAN) and ADP-ribosylation factor (ARF) subfamilies (Bos, 1988; Kahn et al., 1992; Ahmadi et al., 2017). In *Arabidopsis thaliana*, only four families exist, the Rho of plants (ROP), RAB, RAN and ARF subfamilies (Vernoud et al., 2003). These subfamilies are classified by sequence identity, with conserved sequence motifs playing essential regulatory roles in cells (Kahn et al., 1992). Many mammalian small GTPases act as molecular switches in signal transduction, switching from inactive GDP-loaded to active GTP-loaded forms, enabling differential protein complex formations or acting in tethering complexes to target membranes. With typically low intrinsic GDP-to-GTP exchange and GTP hydrolysis activity, small GTPases require guanine nucleotide exchange factors (GEFs) and GTPase-activating proteins (GAPs) for regulation. GEFs are potentially recruited to inactive GTPases to their site of action and accelerate GDP-GTP exchange leading to GTPase activation. The GTP-loaded GTPases exert their function via direct effector interaction (Sztul et al., 2019; Nielsen, 2020; Adarska et al., 2021) until inactivation occurs through GAP-stimulated GTP hydrolysis. ARF GTPases are often involved in vesicle-mediated endomembrane trafficking in mammalian cells and yeast (Just and Peränen, 2016). In plants, small GTPase activities and their cellular functions are not well understood. Although *Arabidopsis* has 12 ARF and seven ARF-like (ARL) and associated SAR1 proteins, plant ARF proteins are poorly described (Singh et al., 2018). The best-studied plant ARF GTPases, SAR1 and ARF1, act in anterograde and retrograde vesicle transport between the endoplasmic reticulum (ER) and the Golgi. SAR1 is involved in COPII-mediated trafficking from the ER to Golgi, whereas ARF1 participates in the COPI pathway (Singh et al., 2018; Nielsen, 2020). Another ARF-like protein, ARL1, might function in endosome-to-Golgi trafficking (Latijnhouwers et al., 2005; Stefano et al., 2006). These roles of ARF1 and SAR1 in vesicle formation are well conserved in eukaryotes, suggesting that other plant ARF members might also function in the endomembrane system. A recent study has shown Golgi-related localization for some ARF and ARF-like proteins (Niu et al., 2022), promoting a general involvement of ARF proteins in the endomembrane system.

TITAN 5 [TTN5; also known as HALLIMASCH (HAL), ARL2 and ARLC1] is essential for plant development, and was initially identified in two independent screens for abnormal embryo mutants. *ttn5* loss-of-function mutants arrest soon after cell division of the fertilized egg cell, indicating a fundamental, potentially housekeeping, role in cellular activities (Mayer et al., 1999; McElver et al., 2000; Lloyd and Meinke, 2012). The TTN5 sequence is closely related to that of human ARL2 (hsARL2), which has high nucleotide dissociation rates, up to 4000-fold faster than RAS (Hanzal-Bayer et al., 2005; Veltel et al., 2008). HsARL2 is associated with various cellular functions, including microtubule development (Bhamidipati et al., 2000; Fleming et al., 2000; Radcliffe et al., 2000; Antoshechkin and Han, 2002; Tzafrir et al., 2002; Mori and Toda, 2013), adenine nucleotide transport in mitochondria (Sharer

[1]Institute of Botany, Heinrich Heine University, 40225 Düsseldorf, Germany. [2]Institute of Biochemistry and Molecular Biology II, Medical Faculty and University Hospital Düsseldorf, Heinrich Heine University, 40225 Düsseldorf, Germany. [3]Cluster of Excellence on Plant Sciences, Heinrich Heine University, 40225 Düsseldorf, Germany. [4]Center for Plant Genome Engineering, Heinrich Heine University, 40225 Düsseldorf, Germany.

*Authors for correspondence (Rumen.Ivanov@hhu.de; Petra.Bauer@hhu.de)

A.M., 0000-0002-3340-586X; M.R.A., 0000-0002-2034-8894; R.I., 0000-0001-7909-4123; P.B., 0000-0002-0404-4532

Handling Editor: Michael Way
Received 31 May 2024; Accepted 3 June 2024

Journal of Cell Science (2024) 137, jcs262315. doi:10.1242/jcs.262315

et al., 2002) and control of phosphodiesterase activity in cilia (Ismail et al., 2011; Fansa and Wittinghofer, 2016), and yeast and *Caenorhabditis* homologs have been identified (Radcliffe et al., 2000; Antoshechkin and Han, 2002). With regard to TTN5, the cellular roles remain unknown. Its molecular function and the GTPase characteristics of TTN5 have not yet been demonstrated.

Here, we show, by means of stopped-flow fluorimetry kinetic assays, that TTN5 is a functional small GTPase with conserved GTP hydrolysis and rapid nucleotide exchange characteristics. Fluorescence microscopy combined with pharmacological treatments suggests that TTN5 might be located at the plasma membrane (PM) and within the endomembrane system. Our study enables future investigation of cellular and physiological functions of this small GTPase.

RESULTS

TTN5 exhibits the atypical characteristics of rapid nucleotide exchange and slow GTP hydrolysis

TTN5 has higher sequence similarity with HsARL2 than it does with *Arabidopsis* ARF or ARL proteins (Fig. 1A) (McElver et al., 2000; Vernoud et al., 2003). Its ubiquitous gene expression and regulation during plant development, particularly in the root epidermis, as revealed in public RNA-seq datasets of organ and single cell analysis of roots (Fig. S1A,B, and see Materials and Methods), reflect its crucial role. *TTN5* is strongly expressed during early embryo development where cell division, elongation and differentiation take place (Fig. S1C), suggesting that it has function in fundamental processes, especially when cells grow and divide.

Based on sequence similarity and structural predictions, TTN5 is presumed to function as a molecular switch. (Fig. 1B,C). Although HsARL2 shows fast GDP-GTP exchange characteristics (Hanzal-Bayer et al., 2005; Veltel et al., 2008), it was unclear whether plant TTN5 shared these characteristics. We here characterized the nucleotide binding and GTP hydrolysis properties of $TTN5^{WT}$ and two mutants, $TTN5^{T30N}$ and $TTN5^{Q70L}$, using heterologously expressed proteins and *in vitro* biochemical assays (experimental workflow illustrated in Fig. S2A–E), as previously established for human GTPases (Eberth and Ahmadian, 2009). $TTN5^{T30N}$ was chosen because it is assumed to preferentially bind GEFs, sequestering them from their proper context, whereas $TTN5^{Q70L}$ was chosen

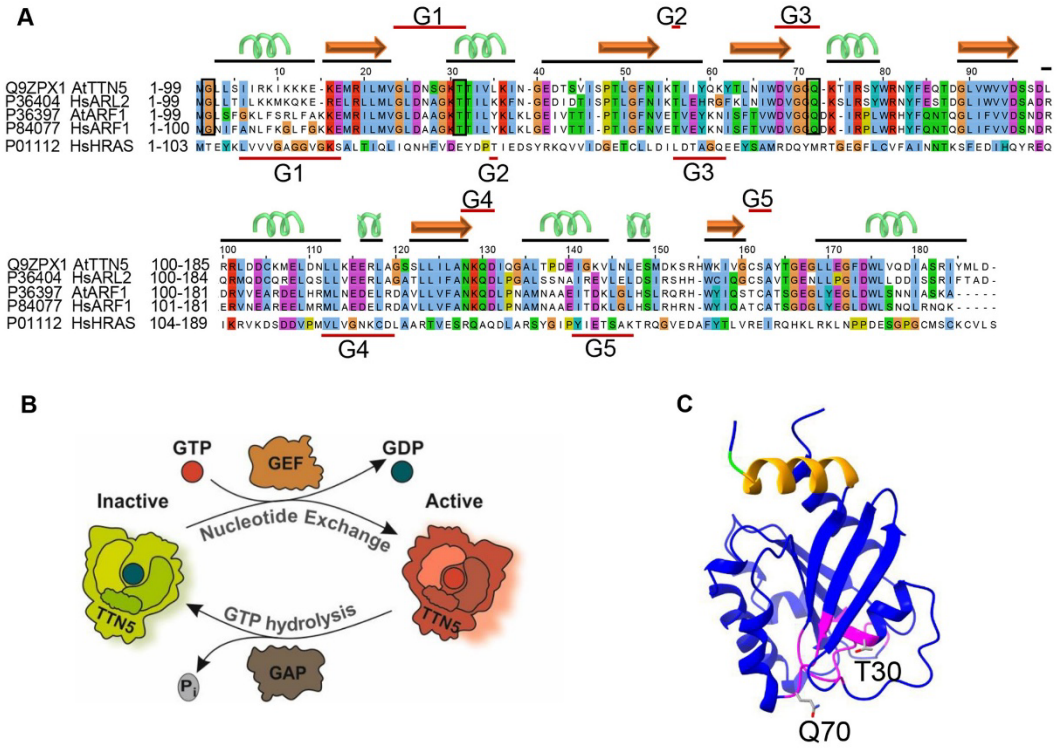

Fig. 1. TTN5 a predicted functional small ARF-like GTPase with nucleotide exchange capacity. (A) Sequence alignment of TTN5 with HsARL2, HsARF1, HsHRAS and AtARF1 created with Jalview (Waterhouse et al., 2009). Conserved G-motifs (G1–G5; red lines) are defined for TTN5 and HRAS. The TTN5 secondary structure is depicted by black lines and corresponding cartoon (α-helix green; β-sheet orange). Conserved residues in ARF and ARL proteins are highlighted by boxes (G2, and mutated T30 and Q70). $TTN5^{T30N}$ is expected to have a low nucleotide exchange capacity, whereas $TTN5^{Q70L}$ is expected to have a low GTPase hydrolysis activity. (B) Model of the predicted GTPase nucleotide exchange and hydrolysis cycle of TTN5. TTN5 switches from an inactive GDP-loaded to an active GTP-loaded form. GDP to GTP nucleotide exchange and GTP hydrolysis might be aided by GEFs and GAPs. (C) Predicted protein structural model of TTN5; GTP-binding pocket (magenta); N-terminal amphipathic helix (orange); conserved G2 (green); mutagenized T30 and Q70 (sticks). The model was generated with AlphaFold (Jumper et al., 2021), and adapted with UCSF ChimeraX 1.2.5 (Goddard et al., 2018).

Journal of Cell Science

because it is thought to be defective in hydrolyzing GTP; equivalent mutants have been frequently used and characterized dominant-negative and constitutively active (Scheffzek et al., 1997; Zhou et al., 2006; Newman et al., 2014). We monitored the real-time kinetics of interactions of fluorescent guanine nucleotides using stopped-flow fluorimetry suited for very rapid enzymatic reactions (Fig. 2A–C). 2-deoxy-3-O-N-methylanthraniloyl-deoxy-GDP (mdGDP) and GppNHp (mGppNHp), a non-hydrolyzable GTP analog, were used to mimic GDP and GTP binding to TTN5. This approach allowed us to monitor real-time kinetics and determine and quantify nucleotide association (k_{on}) and dissociation (k_{off}) characteristics of small GTPases, such as has been done for HsARL2 and HsARL3 (Hillig et al., 2000; Hanzal-Bayer et al., 2005; Veltel et al., 2008; Zhang et al., 2018). The k_{on} value is defined as the rate of nucleotide binding to GTPases, to form the GTPase–nucleotide complex (Fig. 2B), whereas the k_{off} value describes the rate of nucleotide dissociation from GTPases (Fig. 2C). TTN5 proteins were able to bind both nucleotides, except for mGppNHp binding by $TTN5^{T30N}$ (Figs S3A–F, S4A–E). $TTN5^{Q70L}$ revealed the highest k_{on} value for mGDP binding (0.401 $\mu M^{-1}s^{-1}$), being 9-fold higher compared to that of $TTN5^{WT}$ (0.044 $\mu M^{-1}s^{-1}$) and $TTN5^{T30N}$ (0.048 $\mu M^{-1}s^{-1}$), respectively (Fig. 2D, Fig. S3D–F). k_{on} values for mGppNHp binding were about half for $TTN5^{WT}$ (0.029 $\mu M^{-1}s^{-1}$) and $TTN5^{Q70L}$ (0.222 $\mu M^{-1}s^{-1}$) compared to those for mGDP binding (Fig. 2E; Fig. S4C,D). The differences in k_{on} for the respective nucleotide binding were small. However, $TTN5^{Q70L}$ showed a 7.5-fold faster mGppNHp binding than $TTN5^{WT}$. Remarkably, we were not able to monitor mGppNHp association with $TTN5^{T30N}$ but observed its dissociation (k_{off}=0.026 s^{-1}; Fig. 2E). To confirm the binding capability of $TTN5^{T30N}$ with mGppNHp, we measured the mGppNHp fluorescence in real-time before and after titration of nucleotide-free $TTN5^{T30N}$ and binding occurred too fast to resolve the association rate (Fig. S4B).

We next measured the dissociation (k_{off}) of mdGDP and mGppNHp from TTN5 proteins with excess amounts of GDP and GppNHp, respectively (Fig. 2C) with interesting differences (Fig. 2D,E; Figs S3G–I,S4F–H). First, $TTN5^{WT}$ showed a 100-fold faster k_{off} value (mGDP, 0.012 s^{-1}) (Fig. 2D; Fig. S3G), compared to classical small GTPases, including RAC1 (Haeusler et al., 2006) and HRAS (Gremer et al., 2011), but very similar to the k_{off} value of HsARF3 (Fasano et al., 2022). Second, k_{off} values for mGDP and mGppNHp were in a similar range for $TTN5^{WT}$ (mGDP, 0.012 s^{-1}; mGppNHp, 0.001 s^{-1}) and $TTN5^{Q70L}$ (mGDP, 0.025 s^{-1}; mGppNHp, 0.006 s^{-1}), but k_{off} values differed 10-fold between the two nucleotides in $TTN5^{WT}$ (Fig. 2D,E; Figs S3G,I, S4F,H). Thus, mGDP dissociated from proteins 10-fold faster than mGppNHp. Third, mGDP dissociation from $TTN5^{T30N}$ (0.149 s^{-1}) was 12.5-fold faster than that of $TTN5^{WT}$ and 37-fold faster than mGppNHp dissociation of $TTN5^{T30N}$ (0.004 s^{-1}; Fig. 2D,E; Figs S3H, S4G). Mutants of CDC42, RAC1, RHOA, ARF6, RAD, GEM and RAS GTPases that are equivalent to $TTN5^{T30N}$ display decreased nucleotide binding affinity and therefore tend to remain in a nucleotide-free state, complexed with their cognate GEFs (Erickson et al., 1997; Ghosh et al., 1999; Radhakrishna et al., 1999; Jung and Rösner, 2002; Kuemmerle and Zhou, 2002; Wittmann et al., 2003; Nassar et al., 2010; Huang et al., 2013; Chang and Colecraft, 2015; Fisher et al., 2020; Shirazi et al., 2020). Given that $TTN5^{T30N}$ exhibited fast nucleotide dissociation, these results suggest that $TTN5^{T30N}$ might act in either a dominant-negative or fast-cycling manner as reported for other GTPase mutants (Fiegen et al., 2004; Wang et al., 2005; Fidyk et al., 2006; Klein et al., 2006; Soh and Low, 2008; Sugawara et al., 2019; Aspenström, 2020).

The dissociation constant (K_d) is calculated from the ratio k_{off}/k_{on}, which inversely indicates the affinity of interactions between proteins and nucleotides (higher K_d=lower affinity). Interestingly, $TTN5^{WT}$ binds mGppNHp (0.029 µM) 10-fold tighter than mGDP (0.267 µM), a difference, which was not observed for $TTN5^{Q70L}$ (mGppNHp, 0.026 µM; mGDP, 0.061 µM; Fig. 2D,E). The lower affinity of $TTN5^{WT}$ for mdGDP compared to mGppNHp brings us closer to the hypothesis that classifies TTN5 as a non-classical GTPase prone to remain in the active, GTP-bound state (Jaiswal et al., 2013). The K_d value for the $TTN5^{T30N}$–mGDP interaction was 11.5-fold higher (3.091 µM) than for $TTN5^{WT}$, suggesting that this mutant exhibited faster nucleotide exchange and lower affinity for nucleotides and might behave in a dominant-negative manner in signal transduction, similar to what occurs with other GTPases with a T30N exchange (Vanoni et al., 1999).

To get hints on TTN5 functionalities during the GTPase cycle, it is crucial to determine its ability to hydrolyze GTP. Accordingly, the catalytic rate of intrinsic GTP hydrolysis (k_{cat}), was determined by incubating GTP-bound TTN5 proteins and analyzing the samples at various time points (Fig. 2F; Fig. S5). Determined k_{cat} values were quite remarkable in two respects (Fig. 2G). First, all TTN5 proteins, $TTN5^{WT}$, $TTN5^{T30N}$ and $TTN5^{Q70L}$, showed quite similar k_{cat} values (0.0015 s^{-1}, 0.0012 s^{-1}, 0.0007 s^{-1}; Fig. 2G; Fig. S5). $TTN5^{Q70L}$ GTP hydrolysis activity was unexpectedly high given that such glutamine mutations typically impair hydrolysis and result in constitutively active GTPases (Hodge et al., 2020; Matsumoto et al., 2021). Second, the k_{cat} value of $TTN5^{WT}$ (0.0015 s^{-1}) although comparatively low to other GTPases (Jian et al., 2012; Esposito et al., 2019), was 8-fold lower than the determined k_{off} value for mGDP dissociation (0.012 s^{-1}; Fig. 2E). This means that a fast intrinsic GDP/GTP exchange versus a slow GTP hydrolysis can have drastic effects on TTN5 activity in resting cells, given that TTN5 can accumulate in its GTP-bound form, unlike classical GTPases (Jaiswal et al., 2013). To investigate this scenario, we pulled down GST–TTN5 protein in the presence of an excess amount of GppNHp and measured the nucleotide-bound form of GST–TTN5. Isolated GST–TTN5 bound to increasing amounts of GppNHp, indicating that the bound nucleotide is rapidly exchanged for free nucleotide (here GppNHp; Fig. 2H), which is in contrast to what is seen for classical GTPases, which remain in their inactive GDP-bound forms under the same experimental conditions (Walsh et al., 2019; Hodge et al., 2020).

In summary, TTN5 contains conserved regions required for nucleotide binding and binds nucleotides. Interestingly, the slow intrinsic GTP hydrolysis rates in combination with high GDP dissociation rates indicates that TTN5 tends to exist in a GTP-loaded form, as opposed to the classical GTPases. This might have drastic effects on TTN5 activity in cells under resting conditions (Jaiswal et al., 2013). By contrast, the $TTN5^{Q70L}$ mutant, which we originally suspected would be constitutively active, still has intrinsic GTPase activity, whereas the T30N variant exhibits a low affinity for mGDP. Therefore, we propose that TTN5 exhibits typical functions of a small GTPase based on *in vitro* biochemical activity studies, including guanine nucleotide association and dissociation, and emphasize its divergence among the ARF GTPases because of its kinetics.

TTN5 may be a highly dynamic protein and localize to different intracellular compartments

Several eukaryotic ARF GTPases function in vesicle transport and are located at various membranous sites linked with the endomembrane compartments (Vernoud et al., 2003). Localization had not been comprehensively studied for TTN5. To obtain hints as to where in a cell TTN5 localizes to, we first created transgenic *Arabidopsis* lines

Journal of Cell Science (2024) 137, jcs262315. doi:10.1242/jcs.262315

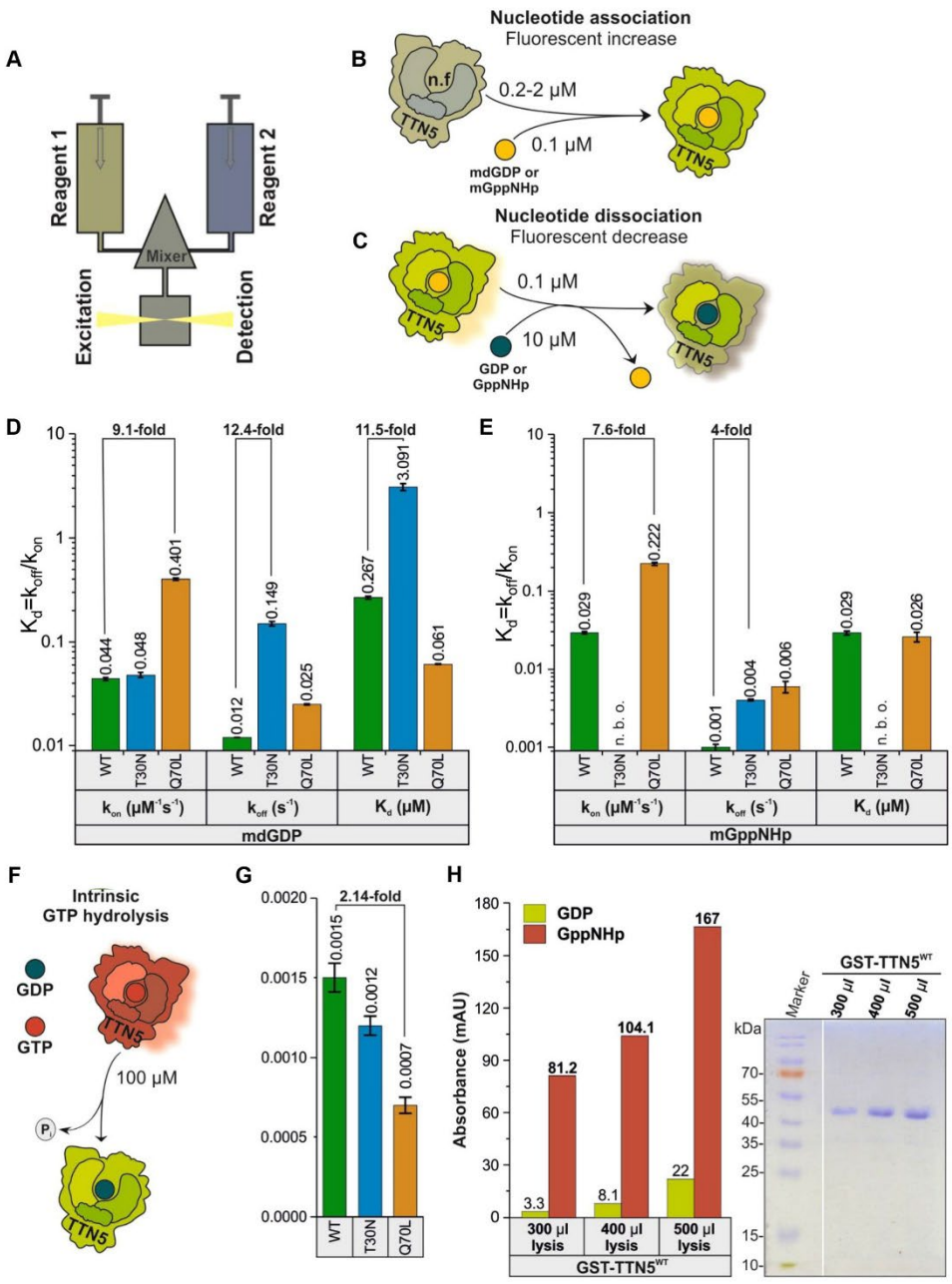

Fig. 2. See next page for legend.

constitutively expressing YFP-tagged TTN5 (pro35S::YFP–TTN5) and its two mutant forms (pro35S::YFP–TTN5^{T30N}, pro35S::YFP–TTN5^{Q70L}) and investigated the localization in 6-day-old seedlings in the epidermis of cotyledons, hypocotyls, root hair zone and in root tips (Fig. 3A; Fig. S6A). Microscopy observations were made in different planes of the tissues, for example, inside the cells across the vacuoles

Fig. 2. Biochemical properties of TTN5 suggest its presence in a GTP-loaded active form in cells. (A) Schematic illustration of the stopped-flow fluorescence device for monitoring nucleotide-binding kinetics of heterologously expressed and purified TTN5 protein (Fig. S2A–D). It consists of two motorized thermostated syringes, a mixing chamber and a fluorescence detector. Two different reagents, 1 and 2, with one containing a fluorescent reporter group (mdGDP or mGppNHp to mimic GDP and GTP) are rapidly mixed and transferred to a fluorescence detection cell. (B) Schematic illustration of nucleotide association. Nucleotide-free TTN5 (for preparation see Fig. S2E) was rapidly mixed with mdGDP. A fluorescence increase is expected upon association of mdGDP with TTN5. Similar measurements were performed with mGppNHp. (C) Schematic illustration of intrinsic nucleotide dissociation. mdGDP-bound TTN5 is mixed with a molar excess of GDP. A fluorescence decrease is expected upon mdGDP dissociation from TTN5 and binding of free unlabeled GDP. Similar measurements were performed with mGppNHp. (D,E) Kinetics of association and dissociation of fluorescent nucleotides mdGDP (D) or mGppNHp (E) with TTN5 proteins (WT, $TTN5^{T30N}$, $TTN5^{Q70L}$). Association rate constants (k_{on} in $\mu M^{-1}s^{-1}$) were determined from the plot of increasing observed rate constants (k_{obs} in s^{-1}) against corresponding TTN5 protein concentrations (as denoted in A,B; for full data, see Figs S3A–F, S4A–E). Intrinsic dissociation rates (k_{off} in s^{-1}) were determined from the plot of fluorescent decrease upon exchange from mdGDP-bound or mGppNHp-bound TTN5 to GDP-bound TTN5 (as denoted in A,C; for full data, see Figs S3G–I, S4F–H). The nucleotide affinity (dissociation constant K_d in μM) of the corresponding TTN5 proteins was calculated from the k_{off}/k_{on} ratio. When mixing mGppNHp with nucleotide-free $TTN5^{T30N}$, no binding was observed (n.b.o.) under these experimental conditions. k_{on} and k_{off} values presented as bar graphs are calculated from the average of four to six measurements and presented as mean±s.d. (F,G) GTP hydrolysis of TTN5 proteins determined by HPLC. (F) Schematic illustration of GTP hydrolysis measurement. (G) GTP-bound TTN5 proteins incubated at different time points before injecting them on a reversed-phase HPLC system. Evaluated data (Fig. S5) resulted in determination of GTP hydrolysis rates (k_{cat} in s^{-1}). Each bar represents the k_{cat} value obtained from a single experiment per condition, comprising six data points. Error bars indicate the standard errors of the fitted values as determined by Origin software. (H) TTN5 accumulation in a GTP-loaded form by HPLC values and Coomassie Blue-stained SDS-PAGE. GST–$TTN5^{WT}$ (46.5 kDa) was purified from bacterial cell lysates at three different volumes in the presence of free GppNHp. Presence of much higher amounts of GppNHp-bound versus GDP-bound GST-TTN5 protein indicates that TTN5 rapidly exchanged bound nucleotide and accumulated in this state. This was a confirmatory experiment performed once.

(Fig. S6) and underneath the PM at the cell peripheries (Fig. 3). We chose to investigate YFP–TTN5 in the epidermis, as *TTN5* transcripts were detected there in plants (Fig. S1B). YFP signals in epidermal cotyledon cells of YFP–TTN5 seedlings were detected in nuclei and cytoplasm and/or in close proximity to the PM (Fig. S6B). Similar localization patterns were found for mutant YFP–TTN5 signals (Fig. S6C,D). YFP signals in YFP–TTN5, YFP–$TTN5^{T30N}$ and YFP–$TTN5^{Q70L}$ seedlings were also present in a similar pattern in stomata (Fig. 3B–D). In hypocotyls, an intracellular YFP signal was observed in nuclei and in close proximity to or at the PM with all three YFP–TTN5 forms (Fig. S6E–G). Investigation of the root hair zone showed YFP signals in the cytoplasm and at the PM of root hairs (Fig. S6H–J). In the root tip, YFP signal was detectable inside the cytoplasm and in nuclei (Fig. S6K). The pattern was similar for YFP–$TTN5^{T30N}$ and YFP–$TTN5^{Q70L}$ (Fig. S6L,M). Fluorescence signal in YFP–TTN5, YFP–$TTN5^{T30N}$ and YFP–$TTN5^{Q70L}$ seedlings inside the cytoplasm was confined to punctate structures, indicating that fluorescence was present in vesicle-like structures together with free signal. This localization pattern was also present in leaf epidermal cells of the cotyledons (Fig. 3B–D), in the hypocotyls (Fig. 3E–G) and in cells of the root hair zones and in root hairs (Fig. 3H–J). These observed structures point to an association of TTN5 with vesicle and endomembrane trafficking. A closer inspection of the dynamics of these structures in the leaf epidermis of cotyledons showed high mobility of fluorescent signals (Movies 1–3) as well as in hypocotyl cells (Movie 4). Interestingly, the mobility of these punctate structures differed within the YFP–$TTN5^{T30N}$ hypocotyl cells, but not in the leaf epidermis cells (Movie 5, compare with Fig. S2), which was not the case for the YFP–$TTN5^{Q70L}$ mutant (Movie 6, compare with Fig. S5). We detected that movement of YFP–$TTN5^{T30N}$ was slow or completely arrested for approximately half of the cells within the hypocotyl epidermis compared to movements for YFP–TTN5 and YFP–$TTN5^{Q70L}$ (Movies 4–6). This loss of fluorescence signal mobility in YFP–$TTN5^{T30N}$ seedlings might be a consequence of a missing effector interaction. We did not observe the blocked mobility for fluorescence signals in cells expressing YFP–TTN5, YFP–$TTN5^{T30N}$ or YFP–$TTN5^{Q70L}$ in the root elongation zone (Movies 7–9). No mobility of YFP fluorescence signal was visible in root tip cells for any YFP–TTN5 form (Movies 10–12).

To evaluate the *Arabidopsis* data and to better visualize YFP–TTN5, we expressed YFP–TTN5 constructs transiently in *Nicotiana benthamiana* leaf epidermis cells. Fluorescence signals in YFP–TTN5-, YFP–$TTN5^{T30N}$- and YFP-$TTN5^{Q70L}$-expressing cells were all localized at or in close proximity to the PM and in several cytosolic punctate structures, apart from nuclei, similar to what was seen in *Arabidopsis* cotyledons, hypocotyls and root hair zones (Fig. 3K–N; Fig. S6N–Q). Additionally, YFP signals were detected in a net-like pattern typical for ER localization (Fig. 3M,N). This indicates that the fluorescent signal localization is similar in both *Arabidopsis* epidermis cells and *N. benthamiana* leaf epidermis.

It should be noted that the 35S promoter-driven YFP–TTN5 constructs did not complement the *ttn5-1* embryo-lethal phenotype (Fig. S7A,B). Western blot analysis with anti-GFP antibody using YFP–TTN5 *Arabidopsis* seedlings revealed three weak YFP bands ranging between 26 and 35 kDa, besides the expected and strong 48 kDa YFP–TTN5 band (Fig. S7C). We cannot explain the presence of these small protein bands. They might correspond to free YFP, proteolytic products or potentially to proteins produced from aberrant transcripts with perhaps alternative translation start or stop sites. On the other hand, a 35S promoter-driven triple hemagglutinin-tagged HA_3–TTN5 did complement the *ttn5-1* embryo-lethal phenotype (Fig. S7D,E). Western blot analysis with anti-HA antibody performed with HA_3–TTN5 seedlings showed a single, correctly sized band, but no band that was 13 to 18 kDa smaller (Fig. S7D). Hence, the inability of YFP–TTN5 to complement the embryo-lethal phenotype is presumably due to the relatively large YFP tag in comparison with the small GTPase and smaller HA_3 tag. Interestingly, HA_3–$TTN5^{T30N}$ seedlings presented a shorter root length phenotype, which might be due to the atypical biochemical $TTN5^{T30N}$ characteristics, whereas HA_3–TTN5 and HA_3–$TTN5^{Q70L}$ seedlings had no obvious phenotypic difference from wild-type (Fig. 3O).

To verify that the localization patterns observed with YFP–TTN5 constructs are representative of a functional TTN5, we performed immunofluorescence staining against the HA_3 tag in HA_3–TTN5 roots and compared the localization patterns (Fig. 3P). Alexa Fluor 488-labeled anti-HA antibody staining reflected HA_3–TTN5 localization, and signals were visible in root cells and root hairs as expected. Signals were mostly present in punctate structures close to the PM and in the cytosol (Fig. 3P), fitting the fluorescence signals obtained with YFP–TTN5.

For a more detailed investigation of the HA_3–TTN5 subcellular localization, we performed co-immunofluorescence staining with an Alexa Fluor 488-labeled anti-ARF1 antibody, which recognizes the Golgi and trans-Golgi network (TGN), together with Alexa Fluor 555-labeled HA_3–TTN5 (Robinson et al., 2011; Singh et al., 2018)

Journal of Cell Science (2024) 137, jcs262315. doi:10.1242/jcs.262315

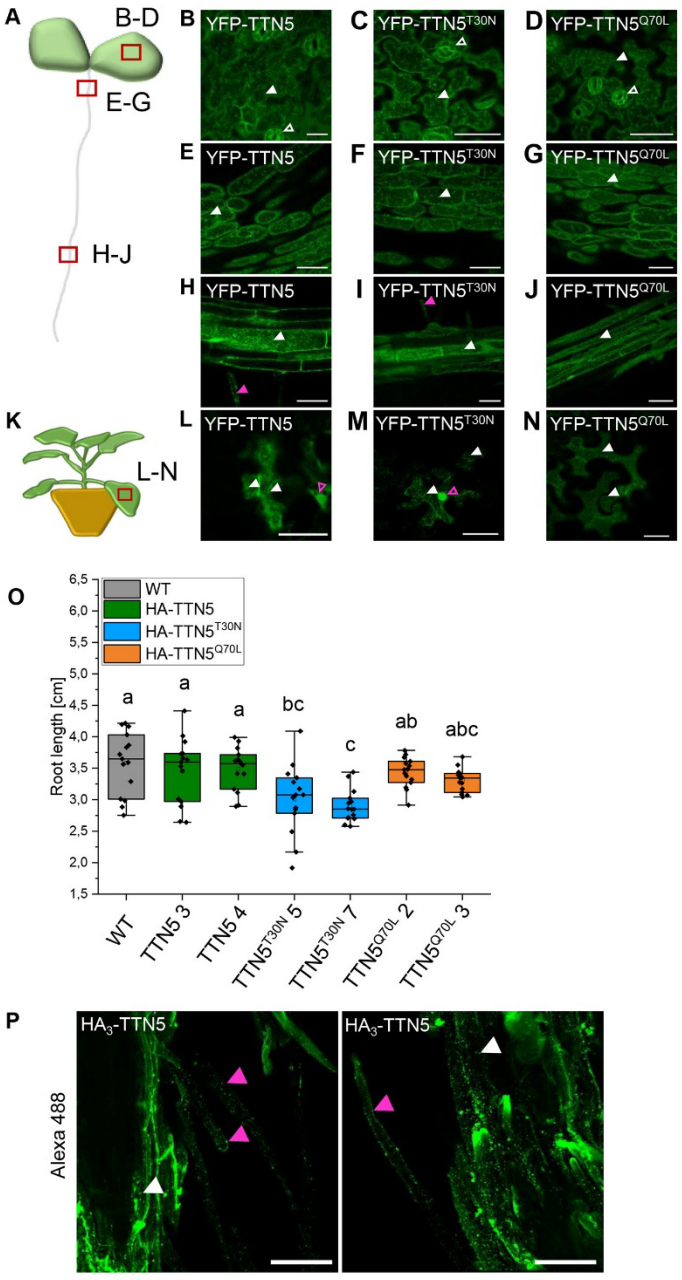

Fig. 3. TTN5 might be present in punctate structures in seedlings. Microscopy observations of YFP fluorescence were made in a plane underneath the PM at the cell peripheries. (A) Schematic representation of an *Arabidopsis* seedling with indicated imaged positions (red rectangle). (B–J) Analysis of YFP–TTN5, YFP–TTN5^{T30N} and YFP-TTN5^{Q70L} Arabidopsis seedlings via fluorescent confocal microscopy. (B–D) Fluorescence signals observed in stomata (empty white arrowhead) and in the epidermis of cotyledons in punctate structures (filled white arrowhead). (E–G) Localization in hypocotyls showed a similar pattern of punctate structures. (H–J) Signals were present in punctate structures in the root hair zone and root hairs (filled magenta arrowhead). (K) Schematic representation of a *N. benthamiana* plant, used for transient expression with indicated imaged position (red rectangle). (L–N) YFP signals in *N. benthamiana* leaf epidermal cells expressing YFP–TTN5, YFP–TTN5^{T30N} and YFP–TTN5^{Q70L}. Signals were present in punctate structures (white arrowheads) and in nuclei (empty magenta arrowheads). Experiments were repeated twice with two seedlings (n=2) or one plant (n=1). (O) Root length measurement of 10-day-old HA$_3$–TTN5, HA$_3$–TTN5^{T30N} and HA$_3$–TTN5^{Q70L} *Arabidopsis* seedlings in comparison with wild-type (WT). Only HA$_3$–TTN5^{T30N} showed slightly reduced root length compared to WT. Analysis was conducted in replicates (n=14). The box represents the 25–75th percentiles, and the median is indicated. The whiskers show the 5–95th percentiles. One-way ANOVA with Tukey post-hoc test was performed. Different letters indicate groups that have a statistical significance difference at P<0.05. (P) Maximum intensity projection of whole-mount immunostaining of HA$_3$–TTN5 roots in the differentiation zone (anti-HA primary antibody, Alexa-488-labeled secondary antibody). Alexa Fluor 488 signals were present in punctate structures in root cells (filled white arrowhead) and root hairs (filled magenta arrowhead), which is comparable to what was seen for YFP signals (H–J). Experiment was repeated three times with two seedlings (n=2). Scale bars: 50 µm.

(Fig. 4A). ARF1–Alexa Fluor 488 staining was clearly visible in punctate structures representing presumably Golgi stacks (Fig. 4A) (Singh et al., 2018). Similar structures were seen with HA$_3$–TTN5–Alexa Fluor 555 staining, but these did not colocalize with the ARF1-labeled structures, although they were in close proximity to each other (Fig. 4A). We hypothesized that the HA$_3$–TTN5 structures might be connected to intracellular trafficking steps and performed brefeldin A (BFA) treatment, a commonly used tool in cell biology for

preventing dynamic membrane trafficking events and vesicle transport involving the Golgi. BFA is a fungal macrocyclic lactone that leads to a loss of cis-cisternae and accumulation of Golgi stacks, known as BFA-induced compartments, and Golgi–ER fusion (Ritzenthaler et al., 2002; Wang et al., 2016). For better BFA body identification, we simultaneously used the membrane dye FM4-64, which can emit fluorescence in a lipophilic membrane environment. FM4-64 marks the PM only a few minutes after application to the cell, and can then be endocytosed; in the presence of BFA, accumulates in BFA bodies (Bolte et al., 2004). We observed BFA bodies positive for both HA_3–TTN5–Alexa Fluor 488 and FM4-64 signals (Fig. 4B). Similar patterns were observed for YFP–TTN5-derived signals in YFP–TTN5-expressing roots (Fig. 4C). Hence, HA_3–TTN5 and YFP–TTN5 are present in similar subcellular membrane compartments.

In HA_3–TTN5 immunostaining, we did not observe any staining in nuclei or ER (Figs 3P, 4A,B), in contrast to the fluorescence signals in YFP–TTN5-expressing cells. This might indicate that either the nuclear and ER signals seen with YFP–TTN5 correspond to the smaller proteins detected, or that immunostaining was not suited to detect this localization. Hence, we focused on analysis of the area where there were overlapping localization patterns between fluorescence with YFP-labeled TTN5 and HA_3-TTN5 immunostaining, such as the specific signal patterns seen for punctate membrane structures.

Taken together, our results show that signals of YFP–TTN5 and HA_3–TTN5 were located in multiple membrane compartments in the epidermis of different *Arabidopsis* organs and of *N. benthamiana* leaves, including particular ring-like punctate structures and vesicles. Fluorescence signals in YFP–TTN5- and YFP-$TTN5^{Q70L}$-expressing seedlings displayed high mobility in cells, as expected from an active GTPase functioning in dynamic processes, such as vesicle trafficking. In contrast, fluorescence signals for YFP–$TTN5^{T30N}$ were less mobile, consistent with the root length phenotype conferred by HA_3–$TTN5^{T30N}$, speaking in favor of the observed $TTN5^{T30N}$ kinetics, with a very fast nucleotide exchange rate and nucleotide affinity loss. Altogether, the TTN5 intracellular localization indicates that TTN5 might have multiple cellular functions as an active GTPase as it can associate with different intracellular structures of the endomembrane system.

TTN5 might associate with components of the cellular endomembrane system

The overlapping localization of HA_3–TTN5 and YFP–TTN5 signals prompted us to better resolve the membrane structures and compartments of the highly dynamic endomembrane system. Well-established fluorescent markers and pharmacological treatments help to determine the nature of individual components in cells in parallel to colocalization studies with proteins of interest, such as TTN5. We conducted colocalization experiments in *N. benthamiana* leaf epidermis as the fluorescence signals were comparable to those for *Arabidopsis* cotyledons and root epidermis. Moreover, it represents an established system for functional association of fluorescent proteins with multiple endomembrane components and optimal identification of membrane structures (Brandizzi et al., 2002; Hanton et al., 2009).

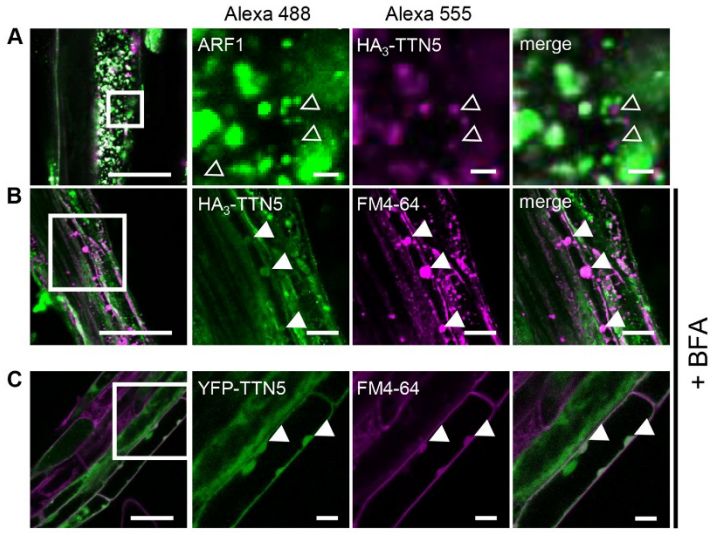

Fig. 4. Whole-mount immunolocalization hints at TTN5 presence in BFA bodies. (A,B) Colocalization of HA_3–TTN5 seedlings by whole-mount immunostaining. (A) Detection of HA_3–TTN5 (anti-HA primary antibody, Alexa Fluor 555-labeled secondary antibody) with Golgi and TGN marker ARF1 (anti-ARF1 primary antibody, Alexa Fluor 488-labeled secondary antibody). Both fluorescence signals were detected in vesicle-like structures in root cells in close proximity to each other but mostly not colocalizing. The experiment was repeated twice with three seedlings (n=3). (B) Detection of HA_3–TTN5 (anti-HA primary antibody, Alexa Fluor 488-labeled secondary antibody) and staining with membrane dye FM4-64 after BFA treatment (10 mM FM4-64 FX and 72 µM BFA for 1 h). Alexa Fluor 488 signals colocalized with FM4-64 in BFA bodies in root cells. The experiment was repeated three times with three seedlings (n=3). (C) YFP fluorescence in YFP–TTN5 seedlings, co-analyzed with FM4-64 after BFA treatment. YFP fluorescence signals colocalized with FM4-64 in BFA bodies similar to what was seen in B. The experiment was performed once with three independent YFP–TTN5 lines (n=3). Colocalization indicated by filled white arrowheads, non-colocalized HA_3–TTN5 Alexa Fluor 488-labeled signals is indicated with empty white arrowheads. Scale bars: 50 µm (overview images on left), 10 µm (magnifications).

Journal of Cell Science (2024) 137, jcs262315. doi:10.1242/jcs.262315

At first, we further investigated the ER–Golgi connection as a characteristic site of association with small GTPases, like the tested ARF1, involved in COPI vesicle transport (Just and Peränen, 2016). We used the soybean (*Glycine max*) protein α-1,2 mannosidase 1 (GmMan1) as a marker; this protein is a glycosidase that acts on glycoproteins at the cis-Golgi, facing the ER (Fig. 5A) and is visible as nearly round punctuate structures throughout the whole cell (Nelson et al., 2007; Wang et al., 2016). Fluorescence signals in leaf discs transiently expressing YFP–TTN5 and its mutant variants partially colocalized with GmMan1–mCherry signals at Golgi

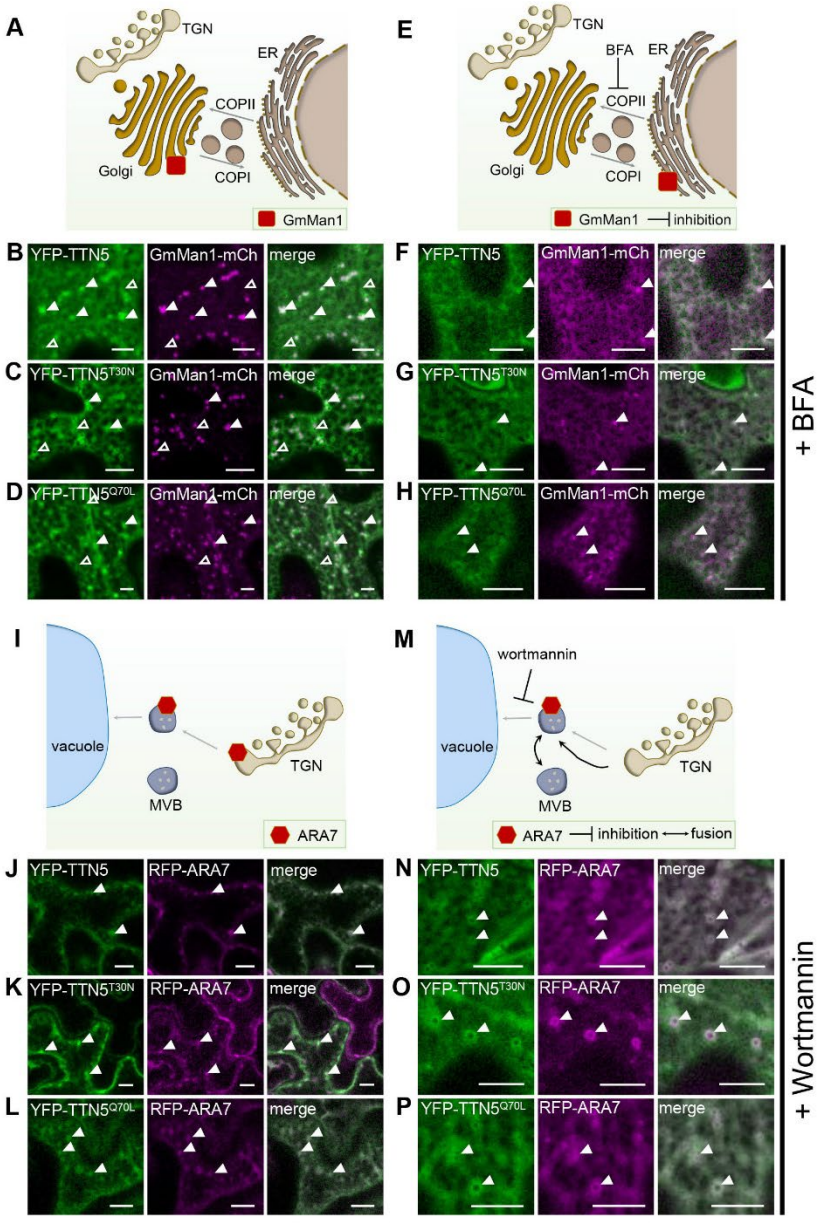

Fig. 5. See next page for legend.

Fig. 5. TTN5 might be associated with the endomembrane system in *N. benthamiana* pavement cells. YFP signals were detected in *N. benthamiana* pavement cells transiently expressing YFP–TTN5, YFP–TTN5^{T30N} and YFP–TTN5^{Q70L} with specific endomembrane markers via fluorescence confocal microscopy. (A) Schematic representation of GmMan1 localization at the cis-Golgi site. (B–D) Partial colocalization of the YFP signal with the Golgi marker GmMan1–mCherry at cis-Golgi stacks (filled white arrowheads). Additionally, YFP fluorescence signals were detected in non-colocalizing punctate structures with depleted fluorescence in the center (empty white arrowheads). (E) Schematic representation of GmMan1 localization at the ER upon BFA treatment. BFA blocks ARF GEF proteins, leading to a loss of Golgi cis-cisternae and formation of BFA-induced compartments due to an accumulation of Golgi stacks up to redistribution of the Golgi to the ER by fusion (Renna and Brandizzi, 2020). (F–H) GmMan1–mCherry and YFP fluorescence were present in the ER and in colocalizing punctate structures upon BFA treatment (36 µM for ~30–60 min). (I) Schematic representation of ARA7 localization at the TGN and MVBs. (J–L) Colocalization of YFP signals with the MVB marker RFP–ARA7. (M) Schematic representation of ARA7 localization in swollen MVBs upon wortmannin treatment. Wortmannin inhibits PI3K function leading to TGN/EE fusion to swollen MVBs (Renna and Brandizzi, 2020). (N–P) ARA7-RFP colocalized with YFP signal in swollen MVBs upon wortmannin treatment (10 µM for ~30–10 min). Colocalization indicated with filled arrowheads; non-colocalized YFP signal is indicated with with empty arrowheads. Corresponding colocalization analysis data is presented in Fig. S8. Experiments were repeated three times with two plants (n=2). Scale bars: 10 µm.

stacks (Fig. 5B–D). We also observed YFP fluorescence in form of circularly shaped ring structures with a fluorescence-depleted center; such structures can be of vacuolar origin as described for similar fluorescent rings for ANNI–GFP (Tichá et al., 2020). Furthermore, quantitative analysis reflected the visible colocalization of GmMan1 marker and YFP fluorescence with Pearson coefficients 0.63 (YFP–TTN5), 0.65 (YFP–TTN5^{T30N}) and 0.68 (YFP–TTN5^{Q70L}) (Fig. S8A; similar obtained overlap coefficients), indicating a strong correlation between the signals. We performed an additional object-based analysis to compare overlapping YFP fluorescence in YFP–TTN5-expressing leaves with GmMan1–mCherry signals (YFP/mCherry ratio) and vice versa (mCherry/YFP ratio). We detected 24% overlapping YFP fluorescence signals for TTN5 with Golgi stacks, whereas in YFP-TTN5^{T30N} and YFP-TTN5^{Q70L}-expressing leaves, signals only shared 16 and 15% overlap with GmMan1–mCherry-positive Golgi stacks (Fig. S8B). Some YFP signals did not colocalize with the GmMan1 marker; these signals were more prominent in leaves expressing YFP–TTN5^{T30N} and less prominent for leaves expressing YFP-TTN5^{Q70L} compared to YFP–TTN5 expression (Fig. 5B–D). Indeed, we identified 48% GmMan1–mCherry signal overlapping with YFP-positive structures in YFP–TTN5^{Q70L} leaves, whereas this was 43% and 31% for YFP fluorescence signals in YFP–TTN5 and YFP–TTN5^{T30N}-expressing leaves, respectively (Fig. S8B), indicating a smaller amount of GmMan1-positive Golgi stacks colocalizing with YFP signals for YFP–TTN5^{T30N}. Hence, the GTPase-active TTN5 forms are likely present at cis-Golgi stacks at higher levels compared to TTN5^{T30N}.

Next, we evaluated the Golgi localization by BFA treatment, resulting in a corresponding redistribution of GmMan1–mCherry (Ritzenthaler et al., 2002; Wang et al., 2016) (Fig. 5E). We found that upon BFA treatment, the GmMan1–mCherry signal was present in the ER and in BFA-induced compartments with partially matching localization of YFP signal of YFP–TTN5 constructs, suggesting a connection of TTN5 to Golgi localization (Fig. 5F–H). Hence, colocalization with GmMan1–mCherry and BFA treatment is indicative of YFP signals localizing to Golgi stacks upon YFP–TTN5 expression, whereas there was lower association of the YFP–TTN5^{T30N} mutant form with this membrane compartment.

Second, we investigated localization to the endocytic compartments, endosomes of the TGN and multivesicular bodies (MVBs) using RFP–ARA7 (RABF2B), a small RAB-GTPase present there (Kotzer et al., 2004; Lee et al., 2004; Stierhof and El Kasmi, 2010; Ito et al., 2016) (Fig. 5I). These compartments play a role in sorting proteins between the endocytic and secretory pathways, with MVBs developing from the TGN and representing the final stage in transport to the vacuole (Valencia et al., 2016; Heucken and Ivanov, 2018). Colocalization studies revealed that the YFP signal in YFP–TTN5-expressing leaves was present at RFP–ARA7-positive MVBs (Fig. 5J). Noticeably, overlaps between RFP–ARA7 and YFP fluorescence signals upon TTN5^{T30N} expression were lower than for the other TTN5 forms (Fig. 5J–L; Fig. S8C,D). We obtained a Pearson coefficient for YFP fluorescence from YFP–TTN5 or YFP–TTN5^{Q70L} expression with RFP–ARA7 of 0.78, whereas a coefficient of only 0.59 was obtained with YFP–TTN5^{T30N}, confirming the visual observation (Fig. S8C; similar obtained overlap coefficients). Object-based analysis showed that, RFP–ARA7-positive structures had an overlap with YFP fluorescence in YFP–TTN5-expressing leaves of 29%, and even more with YFP–TTN5^{Q70L} (75%) unlike with YFP–TTN5^{T30N} (21%) (Fig. S8D). Based on this, signals of YFP–TTN5^{Q70L} and YFP–TTN5 tended to colocalize better with ARA7-positive compartments than YFP–TTN5^{T30N}.

To test MVB localization, we treated plant cells with wortmannin, a fungal metabolite that inhibits phosphoinositide 3-kinase (PI3K) function and thereby causes swelling of the MVBs (Cui et al., 2016), a common approach to study endocytosis events (Fig. 5M). RFP–ARA7-expressing cells showed the typical wortmannin-induced formation of doughnut-like shaped MVBs (Jaillais et al., 2008). YFP fluorescence in YFP–TTN5-expressing leaves partially colocalized with these structures (Fig. 5N–P) indicating that fluorescence signals from expression of YFP–TTN5 and its two mutants are present in MVBs. YFP signals in YFP–TTN5^{Q70L}-expressing leaf discs were located even to a greater extent to MVBs than for YFP–TTN5 and much more than for YFP–TTN5^{T30N}-expressing cells, suggesting an active role for YFP–TTN5^{Q70L} in MVBs, for example in the lytic degradation pathway or the recycling of proteins, similar to the role of ARA7 (Kotzer et al., 2004).

Finally, to investigate a possible connection of TTN5 with the PM, we determined the colocalization of YFP signals from YFP–TTN5 constructs with FM4-64 (Fig. 6A). Fluorescence signals for all three YFP–TTN5 forms colocalized with FM4-64 at the PM in a similar manner (Fig. 6B–D). To further investigate PM localization, we performed mannitol-induced plasmolysis. YFP signals for all YFP–TTN5 constructs were located similarly to FM4-64-stained Hechtian strands, thread-like structures attached to the apoplast visible upon plasmolysis and surrounded by PM (Fig. 6E–G).

In summary, these colocalization experiments show that YFP signals upon YFP–TTN5 expression are found in different membrane sites of the endomembrane system, including the Golgi, MVBs and PM. We hypothesize that, similar to other ARF proteins, this pattern indicates that TTN5 participates in a highly dynamic vesicle trafficking process. Indeed, recorded dynamic YFP signal movement of YFP–TTN5 and YFP–TTN5^{Q70L} in *N. benthamiana* pavement cells colocalized with GmMan1–mCherry signals, and revealed high motion over time, whereas this was less the case for the YFP–TTN5^{T30N} construct (Movies 13–15).

One potential cellular trafficking route is the degradation pathway to the vacuole. We, therefore, investigated fluorescence localization upon transient expression of YFP–TTN5 together with FM4-64 in

Journal of Cell Science (2024) 137, jcs262315. doi:10.1242/jcs.262315

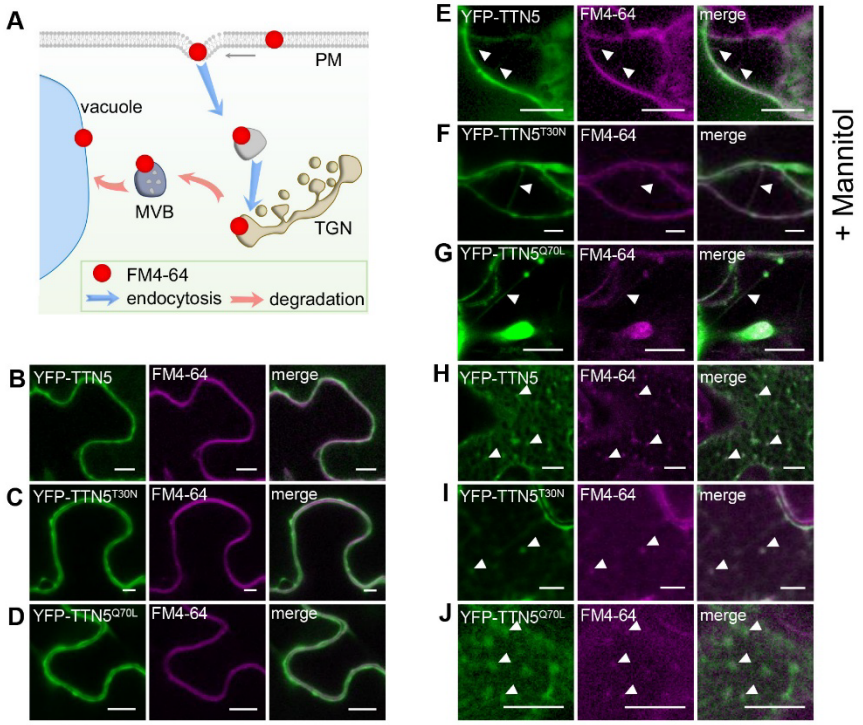

Fig. 6. TTN5 might colocalize with endocytosed PM material. (A) Schematic representation of the progressive stages of lipophilic membrane dye FM4-64 localization and internalization in cells. After infiltration, it first localizes in the PM, and later in intracellular vesicles and membrane compartments, reflecting the endocytosis process (Bolte et al., 2004). (B–J) YFP fluorescence colocalized with FM4-64 in *N. benthamiana* leaf epidermal cells as observed by confocal microscopy, following transient expression of YFP–TTN5, YFP–TTN5^{T30N} and YFP–TTN5^{Q70L}. (B–D) YFP signals colocalized with FM4-64 at the PM. (E–G) PM localization of YFP fluorescence was evaluated after mannitol-induced plasmolysis (1 M for ~15–30 min). Formation of Hechtian strands is a sign of PM material and fluorescence staining there (filled arrowheads). (H–J) Internalized FM4-64 was present in vesicle-like structures that showed YFP signals. Colocalization indicated with filled arrowheads. Experiments were repeated three times with two plants (n=2). Scale bars: 10 µm.

late endosomal compartments, which might be involved in vacuolar targeting. FM4-64 is used as a marker for membranes of late endosomal compartment and vacuole targeting, because following PM visualization FM4-64-stained endocytic vesicles become apparent at later stages, as well as tonoplast staining (Ueda et al., 2001; Emans et al., 2002; Dhonukshe et al., 2007; Ivanov and Vert, 2021). Next to YFP colocalization in YFP–TTN5-expressing leaves with FM4-64 at the PM, we detected colocalization with intracellular fluorescent compartments; a similar expression was seen for both mutant forms (Fig. 6H–J). This indicates that YFP–TTN5 might be involved in targeting of endocytosed PM material, irrespective of the mutations.

In summary, YFP signals upon YFP–TTN5 and YFP–TTN5^{Q70L} expression were dynamic and colocalized with endomembrane structures, whereas fluorescence signal in YFP–TTN5^{T30N}-expressing leaf discs tended to be less mobile and dynamic and colocalized less with such structures.

DISCUSSION

This work provides evidence that the small ARF-like GTPase TTN5 has very rapid intrinsic nucleotide exchange capacity with a conserved nucleotide-switching mechanism. TTN5 might primarily be present in a GTP-loaded active form in cells as a dynamic protein with respect to its localization to membrane structures, potentially associating it with vesicle transport and different endomembrane processes (Fig. 7). The active TTN5^{Q70L} mutant was capable of nucleotide switching and appeared to be mostly similarly localized to wild-type TTN5. The TTN5^{T30N} mutant, on the other hand, has a lower nucleotide exchange capacity, and differed significantly in localization properties and its dynamics, albeit depending on cell types, and conferred a root length phenotype. Therefore, the GTP-bound state that we presume for TTN5 is most likely crucial for correct protein localization and dynamics.

TTN5 exhibits characteristic GTPase functions

TTN5 is classified as an ARL2 homolog based on its high sequence identity with human HsARL2 (McElver et al., 2000), which is reinforced by structural prediction of a nucleotide-binding pocket. TTN5, TTN5^{T30N} and TTN5^{Q70L} can all bind guanine nucleotides. k_{on} values for TTN5^{T30N} and TTN5 were nearly identical, indicating that the mutation has no effect on GDP-binding characteristics, as would usually expected in the absence of a GEF. The TTN5^{Q70L}

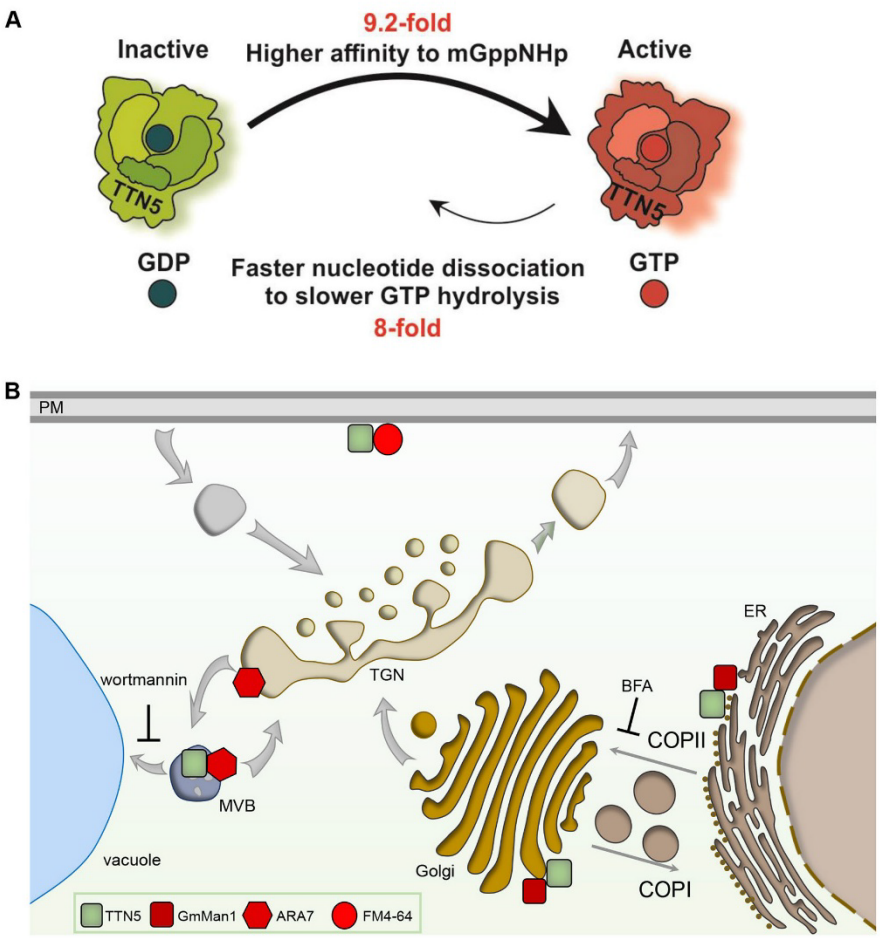

Fig. 7. Schematic models summarizing TTN5 kinetic GTPase activities and potential localization within cells. (A) Model of the predicted GTPase nucleotide exchange and hydrolysis cycle of TTN5 based on the biochemical investigation. The TTN5 affinity for mGppNHp is 9.2-fold higher than it is for mGDP resulting in fast switching from inactive GDP-loaded to active GTP-loaded form. mGppNHp dissociation is 8-fold faster than GTP hydrolysis, but both processes were much slower than nucleotide association. TTN5 kinetics identified TTN5 as a non-classical GTPase that tends to stay in a GTP-loaded form even under resting conditions. (B) Presumed TTN5 locations within the cell. TTN5 (green square) can be present at the PM similar as FM4-64 (red circle) or in the endomembrane compartments of the TGN or MVB as found by ARA7-colocalization (red hexagon). Additionally, TTN5 might colocalize with GmMan1-positive (red square) Golgi stacks.

k_{on} value was clearly higher compared to that of the wild type, indicating that this mutant can bind GDP faster. Compared to other Ras superfamily members, these values are in the range of HRAS (Hanzal-Bayer et al., 2005) and around ten times slower than the fast association of RAC1 (Jaiswal et al., 2013). Well-studied RAS proteins, like RAC1, RAC2 and RAC3, have an intrinsic nucleotide exchange reaction rates of ~40,000 s^{-1} (Haeusler et al., 2006), whereas TTN5 has a remarkably fast rate of nucleotide exchange that is very similar to that of HsARL2 (Hanzal-Bayer et al., 2005; Veltel et al., 2008). This suggests that TTN5 quickly replaces GDP for GTP and transforms from an inactive to an active state presumably without the need of GEF interaction. This could also be an explanation for what is seen with $TTN5^{Q70L}$. Small GTPases with mutations in the glutamine residue of switch II region (e.g. Q71 for HsARF1 and ARL1, and Q61 for HRAS) are constitutively active (Zhang et al., 1994; Van Valkenburgh et al., 2001; Karnoub and Weinberg, 2008). Accordingly, $TTN5^{Q70L}$ is likely to exchange GDP rapidly to GTP and switch itself to stay in an active form, as suggested by the fast-intrinsic nucleotide exchange rate. Interestingly, $TTN5^{T30N}$ resulted in an even higher dissociation rate constant (k_{off}). The calculated K_d confirmed the higher nucleotide-binding affinity for GDP of TTN5 and $TTN5^{Q70L}$ compared with $TTN5^{T30N}$. Reports on HsARL2, HsARF6 and HsARL4D show that their corresponding T30N mutants led to a

similar decreased affinity for GDP (Macia et al., 2004; Hanzal-Bayer et al., 2005; Li et al., 2012).

Interestingly, a comparison of mdGDP with mGppNHp revealed that all three versions had higher GTP affinity than with GDP, with the highest for TTN5^{Q70L}. These high GTP affinities in combination with fast GDP exchange rates and extremely slow hydrolysis pinpoint TTN5 as being GTP-loaded, even in resting conditions, which is very unusual. This atypical behavior has already been reported for a few non-classical RHO GTPases like RHOD and RIF (Jaiswal et al., 2013). This unusual GTP-bound active state along with it lacking *N*-myristoylation and the phylogenetic distance (Boisson et al., 2003; Vernoud et al., 2003) strengthens that there are major differences between TTN5 and other ARF proteins. The similarity in binding affinity between wild-type and TTN5^{Q70L} is consistent with a previous report on HsARL2 (Hanzal-Bayer et al., 2005). Additionally, an equivalent ratio of nucleotide affinity was found between HRAS and HRAS^{Q61L}, but with a much higher affinity, more typical for small GTPases (Der et al., 1986). Given that Q70 is important for GAP-stimulated GTP hydrolysis (Cherfils and Zeghouf, 2013), we assume nucleotide exchange activity is unaffected.

The *Arabidopsis* genome encodes only the two large of five mammalian ARF-GEF subgroups, BFA-inhibited GEF (BIG) and the Golgi BFA-resistance factor 1 (GBF/GNOM) family (Memon, 2004; Wright et al., 2014; Brandizzi, 2018), but no TTN5 GEF protein has been reported. Potential interactions with GEFs are of high interest given the potential role of TTN5 as a co-GEF, similar to what is seen for HsARL3 and HsARL2, where their effector BART stabilizes the active GTPase (ElMaghloob et al., 2021). Especially, interactions at the nucleotide-binding site, which are prevented in the TTN5^{T30N} mutant, will be of great interest to study further for TTN5.

Taken together, the categorization as a non-classical GTPase has three implications. First, very slow hydrolysis rates predict the existence of a TTN5 GAP. Second, TTN5^{T30N} might function as a dominant-negative mutant and, in the presence of a GEF, it cannot bind GDP. Third, the TTN5^{Q70L} hydrolysis rate is not decreased.

TTN5 might act in the endomembrane system

The localization data on YFP– and HA_3–TTN5 suggest that it might be localized at different cellular membrane compartments, typical for the ARF-like family (Memon, 2004; Sztul et al., 2019), and supports potential involvement of TTN5 in endomembrane trafficking. Even though YFP–TTN5 did not complement the *ttn5-1* embryonic lethality, we made several observations that suggest that the YFP–TTN5 signals seen at various membrane sites are meaningful. YFP–TTN5 might not complement due to differences in TTN5 levels and interactions in some cell types, which were hindered specifically for YFP–TTN5 but not HA_3–TTN5. In a previous study, overexpression of ARF1 did not affect the intracellular localization compared to endogenous tagged-ARF1 but did cause the formation of tubulated structures (Bottanelli et al., 2017). Alhough constitutively driven, YFP–TTN5 expression might be delayed or insufficient at early embryonic stages resulting in the lack of embryonic lethal complementation. On the other hand, the fast nucleotide exchange activity might be hindered by the large YFP compared to the small HA_3 tag, given that HA_3–TTN5 rescued the embryo lethality. The lack of complementation represents a challenge for determining the localization of small GTPases with rapid nucleotide exchange in plants. Despite these limitations, we made relevant observations that made us believe that YFP signals in YFP–TTN5-expressing cells at membrane sites are meaningful. First, using pharmacological treatments and colocalization with organellar markers, we noted that various particular membrane compartments showed YFP signals, such as the punctate small ring-like structures, resembling previously reported ANNI–GFP staining (Tichá et al., 2020), the large wortmannin-induced ring-like structures and the BFA bodies, all of which are meaningful for vesicle transport and PM protein regulation processes (Wang et al., 2009; Suo et al., 2021). Furthermore, fluorescence signals obtained with YFP–TTN5 constructs also depended on T30 and Q70 residues; particularly YFP–TTN5^{T30N} had partly quite distinct fluorescence localization patterns, reduced mobility in certain cells and differing degrees of colocalization with the utilized markers. Next to this, HA_3–TTN5^{T30N} seedlings showed reduced root growth which might be due to similar reasons. Given that TTN5^{T30N} has a very fast nucleotide exchange rate and less affinity to nucleotides compared to TTN5, these differing YFP fluorescence patterns of YFP–TTN5^{T30N} at membrane sites and the effect on root growth are not unexpected. Hence, we considered these specific YFP localizations at membrane sites as valid, especially when supported by HA_3–TTN5 immunodetection.

Following up, colocalization analysis showed that both cis-Golgi and MVB-positive structures colocalized with a higher proportion with YFP signals from YFP–TTN5^{Q70L} than from YFP–TTN5^{T30N}. This could indicate the site of TTN5 action, considering our knowledge of ARF family activation in other organisms with high TTN5 sequence similarity. Small GTPases are usually recruited or move to their place of action upon interaction with their specific GEF and nucleotide exchange-dependent activation (Sztul et al., 2019; Nielsen, 2020; Adarska et al., 2021). Although our biochemical data implies no need for a typical GTPase–GEF interaction for activation, it can be still important for localization. Most of effector–GTPase interactions take place with GTPases in their GTP-bound form (Sharer and Kahn, 1999; Hanzal-Bayer et al., 2005). One exception is the role of ARL2–Alp41-GDP in microtubule dynamics by interaction with Cofactor D–Alp1^{D} (Bhamidipati et al., 2000; Mori and Toda, 2013). Another possibility is a hindrance of dimerization by the T30N mutation. ARF1 protein dimer formation is important for the formation of free vesicles (Beck et al., 2009; Beck et al., 2011) and is associated with cell mobility, which was disturbed in YFP–TTN5^{T30N}-expressing cells. Colocalization of YFP fluorescence upon YFP–TTN5 expression with ARA7-positive structures, even in the wortmannin-induced swollen state, might indicate that TTN5 has similar functions to ARA7. ARA7 is involved in endocytic cargo transport to the vacuole, for example, endocytosis of PM material (Ueda et al., 2001; Sohn et al., 2003; Kotzer et al., 2004; Ebine et al., 2011). Colocalization of FM4-64-labeled intracellular structures with fluorescence in YFP–TTN5-expressing cells might indicate the TTN5 has a role in endocytosis and the possible degradation pathway into the vacuole. Our data on colocalization with the different markers support the hypothesis that TTN5 might have functions in vesicle trafficking.

A potential explanation of YFP localization to similar compartments upon YFP–TTN5 and YFP–TTN5^{Q70L} expression compared to fluorescence signal of YFP–TTN5^{T30N} expression can be made based on a special feature of TTN5 in the ARF family. ARF GTPases are mostly myristoylated on G2, which is essential for their membrane binding. TTN5, as well as HsARL2 and HsARL3, lack this myristoylation, although G2 is present (Boisson et al., 2003; Kahn et al., 2006). HsARL2 and HsARL3 are still able to bind membranes, probably only through their N-terminal amphipathic helix, as was established for SAR1, with HsARL2 membrane binding efficiency being nucleotide independent (Lee et al., 2005; Kapoor et al., 2015). We suggest similar behavior for TTN5, as detected YFP signals localized to membranous compartments. Based on the varying

colocalization degrees, with signals of YFP–TTN5^{T30N} construct being less prominent at the Golgi and MVBs compared to YFP–TTN5 and YFP–TTN5^{Q70L}, we hypothesize that different membrane localization could be associated with a nucleotide- or nucleotide exchange-dependent process. In a nucleotide-free or GDP-bound state, TTN5 might be predominantly present close to the PM, whereas in an active GTP-bound state, which according to enzyme kinetics is expected to be predominant, it would be dynamically linked with the endomembrane system. Interestingly, with respect to the intracellular dynamics, we observed that the TTN5^{T30N} mutant had a different behavior in different organ types. This could be due to differing GEFs. Likewise, it is conceivable that constitutively expressed TTN5 has different effector binding partners.

The broad diversity of biological functions for proteins that have related sequences to TTN5, such that they are associated with a variety of signaling cascades, is also reflected by these related proteins having very different protein partners. Few orthologs of HsARL2 interaction partners are present in *Arabidopsis*. It is therefore exceedingly interesting to identify interacting proteins to determine whether TTN5 performs similar functions to HsARL2 or what other role it might play, especially with regard to the potential GTP dependence of TTN5 essential function, which fits with already known functions of other ARF GTPases (Sztul et al., 2019; Nielsen, 2020; Adarska et al., 2021). In addition, ARF proteins are affected by a similar set of GEFs and GAPs, indicating an interconnected network of ARF signaling. ARF double knockdowns have revealed specific phenotypes, suggesting redundancy in the ARF family (Volpicelli-Daley et al., 2005; Kondo et al., 2012; Nakai et al., 2013; Adarska et al., 2021). Investigation of the role of TTN5 within the ARF family might reveal a missing link in ARF signaling and cell traffic.

Conclusion

In this study, we identified TTN5 as a functional ARF-like GTPase that not only shares sequence similarity with HsARL2, but also the very fast nucleotide exchange capacity, in contrast to other characterized ARF and ARL proteins. TTN5 has a fast nucleotide dissociation and a slow GTP hydrolysis rate, and a higher affinity for GTP than GDP. Thus, TTN5 is a non-classical GTPase that most likely accumulates in a GTP-bound state in cells in line with certain cellular phenotypes and protein localization data. The nucleotide exchange capacity affected the localization and dynamics of YFP-tagged TTN5 forms, and the association of TTN5 with the endomembrane system. In the future, identification of a potential TTN5 GEF, GAP and effector proteins as well as other interaction partners, and particularly potential PM target proteins as cargo for vesicle transport, will be of great interest to clarify potential roles of TTN5 in endomembrane trafficking and whole-plant physiological contexts.

MATERIALS AND METHODS

Arabidopsis plant material and plant growth conditions

The *Arabidopsis ttn5-1* (Stock Number: CS16077) mutant was previously described (McElver et al., 2000). Heterozygous seedlings were selected by genotyping using the primers TTN5 intron1 fwd and pDAP101 LB1 (Table S1). For pro35S::YFP-TTN5 and pro35S::HA_3-TTN5 constructs, *TTN5* coding sequences was amplified with B1 and B2 attachment sites for Gateway cloning (Life Technologies) using the primer TITAN5 n-ter B1 and TITAN5 stop B2 (Table S1). The obtained PCR fragments were cloned via BP reaction (Life Technologies) into pDONR207 (Invitrogen). pro35S::YFP-TTN5 and pro35S::HA_3-TTN5 constructs were created via LR reaction (Life Technologies) with the destination vector pH7WGY2 (Karimi et al., 2005) (VIB-UGent Center for Plant Systems Biology, Vector ID:1_48) and pALLIGATOR2 (Bensmihen et al., 2004), respectively. Agrobacteria were transformed with obtained constructs and used for stable *Arabidopsis* transformation (method adapted from Clough and Bent, 1998). *Arabidopsis* seeds were sterilized with sodium hypochlorite solution (6% sodium hypochlorite and 0.1% Triton X-100) and stored for 24 h at 4°C for stratification. Seedlings were grown upright on half-strength Hoagland agar medium [1.5 mM $Ca(NO_3)_2$, 0.5 mM KH_2PO_4, 1.25 mM KNO_3, 0.75 mM $MgSO_4$, 1.5 µM $CuSO_4$, 50 µM H_3BO_3, 50 µM KCl, 10 µM $MnSO_4$, 0.075 µM $(NH_4)_6Mo_7O_{24}$, 2 µM $ZnSO_4$, 50 µM FeNaEDTA and 1% sucrose, pH 5.8, supplemented with 1.4% Plant agar (Duchefa)] in growth chambers (CLF Plant Climatics) under long-day conditions (16 h light at 21°C, 8 h darkness at 19°C). Seedlings were grown for 6 days (6-day system) or 10 days (10-day system) or 17 days with the last 3 days on fresh plates (2-week system).

Seed clearing was undertaken by incubating seeds in a chloral hydrate-glycerol clearing solution [chloral hydrate:glycerol:water, 8:1:2 (g:ml:ml)] for 4 h up to overnight. Imaging was done using an Axio Imager.M2 (Zeiss).

Root length measurement were performed using JMicroVision with the image analysis toolbox for measuring and quantifying components of high-definition images [version 1.3.4; https://jmicrovision.github.io; Roduit, N.]

Nicotiana benthamiana plants were grown on soil for 2–4 weeks in a greenhouse facility under long-day conditions (16 h of light, 8 h of darkness).

Point mutant generation of *TTN5*

pDONR207:TTN5 was used as a template for site-directed *TTN5* mutagenesis. Primers T5T30Nf and T5T30Nr (Table S1) were used to amplify the entire vector generating the TTN5^{T30N} coding sequence and primers TQ70Lf and T5Q70Lr (Table S1) were used to amplify the entire vector generating the TTN5^{Q70L} coding sequence. The PCR amplifications were run using the following conditions: 95°C, 30 s; 18 cycles of 95°C for 30 s, 55°C for 1 min, and 72°C for 8 min; then 72°C for 7 min. The completed reaction was treated with 10 units of DpnI endonuclease for 1 h at 37°C and then used for *Escherichia coli* transformation. Successful mutagenesis was confirmed by Sanger sequencing.

In vitro GTPase activity assays

An overview of protein expression and purification is shown in Fig. S2A. Recombinant pGEX-4T-1 bacterial protein expression vectors (Amersham, Germany) containing coding sequences for *TTN5*, *TTN5^{T30N}* and *TTN5^{Q70L}* were transferred into *E. coli* BL21 (DE3) Rosetta strain (Invitrogen, Germany). Following induction of GST–TTN5 fusion protein expression according to standard procedures (Hemsath et al., 2005), cell lysates were obtained after cell disruption with a probe sonicator (Bandelin sonoplus ultrasonic homogenizer, Germany) using a standard buffer [300 mM NaCl, 3 mM dithiothreitol (DTT), 10 mM $MgCl_2$, 0.1 mM GDP, 1% glycerol and 50 mM Tris-HCl, pH 7.4]. GST fusion proteins were purified by loading total bacterial lysate on a precquilibrated glutathione Sepharose column (Sigma, Germany) using fast performance liquid chromatography system (Cytiva, Germany) (Step 1, affinity-purified GST-TTN5 protein fraction). GST-tagged protein fractions were incubated with thrombin (Sigma, Germany) at 4°C overnight for cleavage of the GST tag (Step 2, GST cleavage) and applied again to the affinity column (Step 3, yielding TTN5 protein fraction). Purified proteins were concentrated using 10 kDa ultra-centrifugal filter Amicon (Merck Millipore, Germany). The quality and quantity of proteins were analyzed by SDS-PAGE (Bio-Rad), a UV/Vis spectrometer (Eppendorf, Germany) and high-performance liquid chromatography (HPLC) using a reversed-phase C18 column (Sigma, Germany) and a pre-column (Nucleosil 100 C18, Bischoff Chromatography) as described previously (Eberth and Ahmadian, 2009) (Fig. S2B–D).

Nucleotide-free TTN5 protein was prepared from the TTN5 protein fraction (Eberth and Ahmadian, 2009) as illustrated in Fig. S2E. 0.5 mg TTN5 protein was combined with 1 U of agarose bead-coupled alkaline phosphatase (Sigma-Aldrich, Germany) for degradation of bound GDP to GMP and Pi in the presence of a 1.5-fold molar excess of non-hydrolyzable GTP analog GppCp (Jena Bioscience, Germany). After confirmation of GDP degradation by HPLC, 0.002 U snake venom phosphodiesterase (Sigma-Aldrich, Germany) per mg TTN5 was added to cleave GppCp to

GMP, G and Pi. The reaction progress of degradation of nucleotides was analyzed by HPLC using 30 µM TTN5 in a 30 µl injection volume (Beckman Gold HPLC, Beckman Coulter). After completion of the reaction, in order to remove the agarose bead-coupled alkaline phosphatase, the solution was centrifuged for 10 min at 10,000 ***g***, 4°C, which was followed by snap freezing and thawing cycles to inactivate the phosphodiesterase. mdGDP (2-deoxy-3-O-N-methylanthraniloyl GDP)- and mGppNHp 2′/3′-O-(N-methyl-anthraniloyl)-guanosine-5′-[(β,γ)-imido]triphosphate)-bound TTN5, $TTN5^{T30N}$ and $TTN5^{Q70L}$ were prepared by incubation of nucleotide-free forms with fluorescent nucleotides (Jena Bioscience, Germany) in a molar ratio of 1 to 1.2. The solution was purified from the excess amount of mdGDP and mGppNHp by using prepacked gel-filtration NAP-5 Columns (Cytiva, Germany) to remove unbound nucleotides. Protein and nucleotide concentration were determined using the Bradford reagent (Sigma-Aldrich, Germany) and HPLC, respectively.

All kinetic fluorescence measurements including nucleotide association and dissociation reactions were monitored on a stopped-flow instrument system SF-61, HiTech Scientific (TgK Scientific Limited, UK) and SX20 MV (Applied Photophysics, UK) at 25°C using nucleotide exchange buffer (10 mM K_2HPO_4/KH_2PO_4, pH 7.4, 5 mM $MgCl_2$, 3 mM DTT, 30 mM Tris-HCl, pH 7.5) (Eberth and Ahmadian, 2009). Fluorescence was detected at 366 nm excitation and 450 nm emission using 408 nm cut-off filter for mant-nucleotides (Hemsath and Ahmadian, 2005).

To determine the intrinsic nucleotide exchange rate, k_{off}, 0.2 µM mdGDP- and mGppNHp-bound proteins were combined with a 200-fold molar excess of 40 µM non-fluorescent GDP in two different set of experiments, respectively. The decay of the fluorescence intensity representing mdGDP and mGppNHp dissociation and replacement by non-fluorescent nucleotide were recorded over time (Fig. S2G). Moreover, to determine the nucleotide association rate, k_{on}, of mdGDP and mGppNHp to the nucleotide-free GTPase, 0.2 µM fluorescent nucleotides were mixed with different concentrations of nucleotide-free TTN5 variants. The increase in the fluorescent intensity was obtained by analyzing the conformational change of fluorescent nucleotides after binding to the proteins (Fig. S2H).

The data provided by the stopped-flow assay, were applied to obtain the observed rate constants. Dissociation rate constants or nucleotide exchange rates (k_{off} in s^{-1}) and pseudo-first-order rate constants or observed rate constants (k_{obs} in s^{-1}) at the different concentrations of the protein were obtained by non-linear curve fitting using Origin software (version 2021b). The slopes obtained from plotting k_{obs} against respective concentrations of proteins were used as the second-order association rate constants (k_{on} in $\mu M^{-1}s^{-1}$). The equilibrium constant of dissociation (K_d in µM) was calculated from the ratio of k_{off}/k_{on}. In order to investigate the intrinsic GTP-hydrolysis rate of TTN5 variants, the HPLC method is used as described previously (Eberth and Ahmadian, 2009). As an accurate strategy, HPLC provides the nucleotide contents over time. The GTPase reaction rates were determined by mixing 100 µM nucleotide-free GTPase and 100 µM GTP at 25°C in a standard buffer without GDP. The GTP contents were measured at different times and the data were fitted with Origin software to get the observed rate constant.

Nicotiana benthamiana leaf infiltration

N. benthamiana leaf infiltration was performed with the Agrobacterium (*Agrobacterium radiobacter*) strain C58 (GV3101) carrying the respective constructs for confocal microscopy (LSM 780, Zeiss). Agrobacteria cultures were grown overnight at 28°C, centrifuged for 5 min at 4°C at 5000 ***g***, resuspended in infiltration solution (5% sucrose, a pinch of glucose, 0.01% Silwet Gold, 150 µM Acetosyringone) and incubated for 1 h at room temperature. The bacterial suspension was adjusted to an OD_{600}–0.4 and infiltrated into the abaxial side of *N. benthamiana* leaves.

Subcellular localization of fluorescent protein fusions

Cloning of YFP-tagged TTN5 constructs is described in the section '*Arabidopsis* plant material and growth conditions' above. Localization studies were carried out by laser-scanning confocal microscopy (LSM 780 or LSM880, Zeiss) with a 40× C-Apochromat water immersion objective. YFP constructs and Alexa Fluor 488 stainings were excited at 488 nm and detected at 491–560 nm. mCherry, Alexa 555 and FM4-64 fluorescence was excited at 561 nm and detected at 570–633 nm.

Wortmannin (10 µM, Sigma-Aldrich), BFA (36 µM, Sigma-Aldrich) and plasma membrane dyes FM4-64 (165 µM, Thermo Fisher Scientific) were infiltrated into *N. benthamiana* leaves or used for incubation bath of *Arabidopsis* seedlings. FM4-64 was detected after 5 min incubation. Wortmannin and BFA were incubated for 25 min before checking the treatment effect. Plasmolysis was induced by incubating leaf discs in 1 M mannitol solution for 15 min. Signal intensities were increased for better visibility.

RFP–ARA7 clones were a gift from Dr Thierry Gaude (Ecole Normale Supérieure, Lyon, France).

Whole-mount immunostaining

Whole-mount immunostaining by immunofluorescence was performed according to Pasternak et al. (2015). Briefly, *Arabidopsis* seedlings were grown in the standard condition in Hoagland medium for 4–6 days. Methanol or formaldehyde (4%) was used to fix the seedlings. The seedlings were transferred to a glass slide and resuspended in 1× microtubule-stabilizing buffer (MTSB). Seedlings were digested with 2% Driselase dissolved in 1× MTSB at 37°C for 40 mins. Following digestion, a permeabilization step was performed by treating the seedlings with permeabilization buffer (3% IGEPAL C630, 10% DMSO in 1× MTSB buffer) at 37°C for 20 mins. Then blocking was performed with a buffer consisting of 5% BSA for 30 min at room temperature. They were incubated overnight with different primary antibodies (detailed information is listed below). After two washes with 1× MTSB, seedlings were incubated with a respective Alexa Fluor secondary antibody for 2 h at 37°C. After five steps of washing with 1x PBS, coverslips were mounted on slides with the antifade reagent (Prolong glass Antifade Mountant with NucBlue Stain, Invitrogen, P36985). Fluorescence microscopy was conducted as described in the previous section.

Immunodetection was conducted with following antibody combinations: HA detection was performed using anti-HA antibody (1:100 dilution, rabbit Abcam ab9110 or chicken AGRISERA, AS20 4463, Lot: 2303) followed by Alexa Fluor 488 or Alexa Fluor 555-labeled secondary antibodies (1:200 anti-rabbit-IgG, Thermo Fisher Scientific, A32731, Lot: 2541675 and 1:500 goat anti-chicken-IgY, Thermo Fisher Scientific A32932). ARF1 (Golgi and TGN marker) was detected using primary anti-ARF1 antibody (1:200 dilution, rabbit, Agrisera, AS08 325, Lot: 2208), in combination with Alexa Fluor™ Plus 488-labeled secondary antibody.

For initiation of BFA bodies, seedlings were first treated with BFA (72 µM, Sigma-Aldrich) and fixable plasma membrane dye FM4-64 FX (10 mM, Thermo Fisher Scientific, F34653) for 1 h, before formaldehyde fixation.

Immunoblot detection

After total protein extraction from *Arabidopsis* plants grown for 6 days or in the 2-week system, sample separation by SDS-PAGE and immunodetection were performed as previously described (Le et al., 2015). In brief, plant material was ground under liquid nitrogen and proteins were extracted with SDG buffer (62 mM Tris-HCl, pH 8.6, 2.5% SDS, 2% DTT, 10% glycerol). Samples were separated on 12% SDS-PAGE gels. Following electrophoresis, the proteins were transferred to a Protran nitrocellulose membrane (Amersham).

Membranes were blocked for 1 h in 5% milk-TBST solution (20 mM Tris-HCl, pH 7.4, 180 mM NaCl and 0.1% Tween 20), followed by 1 h antibody incubation (anti-GFP, monoclonal mouse antibody, Roche, catalog no. 11814460001, 1:1000). After three washes with TBST for 10 min each, membranes were incubated in secondary antibody (anti-mouse-IgG conjugated to HRP, polyclonal goat antibody, Sigma-Aldrich, cat. no. SAB3701159, 1:5000) for 1 h. HA detection was performed with a directly coupled anti-HA antibody (anti-HA–HRP, high-affinity monoclonal rat antibody, 3F10, Roche, catalog no. 12013819001, 1:1000). Immunodetection was performed after three washes with TBST for 10 min each, using the enhanced chemiluminescence system (GE Healthcare) and the FluorChem Q System for quantitative western blot

imaging (ProteinSimple) with the AlphaView software. Full images of uncropped western blot from this study can be found in Fig. S9.

JACoP based colocalization analysis

Colocalization analysis was carried out with the ImageJ (Schneider et al., 2012) Plugin Just Another Colocalization Plugin (JACoP) (Bolte and Cordelières, 2006) and a comparison of Pearson's and Overlap coefficients was performed. Object-based analysis was performed for punctate structures (method adapted from Ivanov et al., 2014). Colocalization for both channels was calculated based on the distance between geometrical centers of signals and presented as a percentage. Analysis was done in three replicates each (n=3).

Structure prediction

TTN5 structure prediction was performed by AlphaFold (Jumper et al., 2021). The molecular graphic was edited with UCSF ChimeraX (1.2.5, Goddard et al., 2018), developed by the Resource for Biocomputing, Visualization and Informatics at the University of California, San Francisco, with support from the National Institutes of Health R01-GM129325 and the Office of Cyber Infrastructure and Computational Biology, National Institute of Allergy and Infectious Diseases.

In silico tool for gene expression analysis

RNA-seq data was analyzed from previously published studies and was visualized with the AtGenExpress eFP at https://bar.utoronto.ca/eplant/ (Nakabayashi et al., 2005; Schmid et al., 2005; Ryu et al., 2019; Waese et al., 2017).

Accession numbers for sequence data

Sequence data used in this article can be found in the TAIR and GenBank data libraries under accession numbers: *ARA7* (TAIR: AT4G19640), *ARF1* (TAIR: AT1G23490), *GmMan1* (Uniprot: Q0PKY2) and *TTN5* (TAIR: AT2G18390).

Statistical analysis

One-way ANOVA was used for statistical analysis and performed in OriginPro 2019. Fisher's least significant difference or a Tukey's test was chosen as a post-hoc test with P<0.05.

Acknowledgements

We thank Gintaute Matthäi and Elke Wieneke for excellent technical and Natalie Köhler for experimental assistance. Thanks to Anna Sergeeva, Madhumita Narasimhan and Alexander Hertle for advice and help with whole-mount immunolocalization. We thank Stefanie Weidtkamp-Peters and Sebastian Hänsch for assistance and Ksenia Krooß (NFDI4BIOIMAGE, DFG project ID 501864659) for help with microscopy, metadata annotation and upload to the BioImage Archive repository, all members of the Center for Advanced Imaging (CAi) at Heinrich Heine University. Funding for instrumentation was through Zeiss LSM780+4channel FLIM extension (Picoquant): DFG-INST 208/551-1 FUGG and Zeiss LSM 880 Airyscan Fast DFG-INST 208/746-1 FUGG.

Competing interests

The authors declare no competing or financial interests.

Author contributions

Conceptualization: I.M., M.R.A., R.I., P.B.; Formal analysis: I.M., A.M., M.R.A., R.I.; Investigation: I.M., A.M., S.K.S., P.C., R.I.; Writing - original draft: I.M.; Writing -review & editing: I.M., A.M., M.R.A., R.I., P.B.; Visualization: I.M., A.M.; Supervision: M.R.A., R.I., P.B.; Funding acquisition: M.R.A., P.B.

Funding

This work was supported by the Deutsche Forschungsgemeinschaft (DFG, German Research Foundation) Project no. 267205415-SFB 1208, project B05 to P.B.; Ba1610/7-2 to P.B.; Germany's Excellence Strategy – EXC-2048/1 – project ID 390686111. Support was provided by DFG AH 92/8-3 to A.M. and M.R.A. Open access funding provided by Heinrich Heine University Duesseldorf. Deposited in PMC for immediate release.

Data availability

Microscopic images are available at BioImage Archive with the accession number S-BIAD1241 (doi:10.6019/S-BIAD1241).

First Person

This article has an associated First Person interview with the first author of the paper.

Peer review history

The peer review history is available online at https://journals.biologists.com/jcs/lookup/doi/10.1242/jcs.262315.reviewer-comments.pdf

References

Adarska, P., Wong-Dilworth, L. and Bottanelli, F. (2021). ARF GTPases and their ubiquitous role in intracellular trafficking beyond the Golgi. *Front. Cell Dev. Biol.* **9**, 679046. doi:10.3389/fcell.2021.679046

Ahmadi, Y., Ghorbanihaghjo, A. and Argani, H. (2017). The balance between induction and inhibition of mevalonate pathway regulates cancer suppression by statins: a review of molecular mechanisms. *Chem. Biol. Interact.* **273**, 273-285. doi:10.1016/j.cbi.2017.06.026

Antoshechkin, I. and Han, M. (2002). The C. elegans evl-20 gene is a homolog of the small GTPase ARL2 and regulates cytoskeleton dynamics during cytokinesis and morphogenesis. *Dev. Cell* **2**, 579-591. doi:10.1016/S1534-5807(02)00146-6

Aspenström, P. (2020). Fast-cycling Rho GTPases. *Small GTPases* **11**, 248-255. doi:10.1080/21541248.2017.1391365

Beck, R., Adolf, F., Weimer, C., Bruegger, B. and Wieland, F. T. (2009). ArfGAP1 activity and COPI vesicle biogenesis. *Traffic* **10**, 307-315. doi:10.1111/j.1600-0854.2008.00865.x

Beck, R., Prinz, S., Diestelkötter-Bachert, P., Röhling, S., Adolf, F., Hoehner, K., Welsch, S., Ronchi, P., Brügger, B., Briggs, J. A. G. et al. (2011). Coatomer and dimeric ADP ribosylation factor 1 promote distinct steps in membrane scission. *J. Cell Biol.* **194**, 765-777. doi:10.1083/jcb.201011027

Bensmihen, S., To, A., Lambert, G., Kroj, T., Giraudat, J. and Parcy, F. (2004). Analysis of an activated ABI5 allele using a new selection method for transgenic Arabidopsis seeds. *FEBS Lett.* **561**, 127-131. doi:10.1016/S0014-5793(04)00148-6

Bhamidipati, A., Lewis, S. A. and Cowan, N. J. (2000). ADP ribosylation factor-like protein 2. (Arl2) regulates the interaction of tubulin-folding cofactor D with native tubulin. *J. Cell Biol.* **149**, 1087-1096. doi:10.1083/jcb.149.5.1087

Boisson, B., Giglione, C. and Meinnel, T. (2003). Unexpected protein families including cell defense components feature in the N-myristoylome of a higher eukaryote. *J. Biol. Chem.* **278**, 43418-43429. doi:10.1074/jbc.M307321200

Bolte, S. and Cordelières, F. P. (2006). A guided tour into subcellular colocalization analysis in light microscopy. *J. Microsc.* **224**, 213-232. doi:10.1111/j.1365-2818.2006.01706.x

Bolte, S., Talbot, C., Boutte, Y., Catrice, O., Read, N. D. and Satiat-Jeunemaitre, B. (2004). FM-dyes as experimental probes for dissecting vesicle trafficking in living plant cells. *J. Microsc.* **214**, 159-173. doi:10.1111/j.0022-2720.2004.01348.x

Bos, J. L. (1988). The ras gene family and human carcinogenesis. *Mutat. Res.* **195**, 255-271. doi:10.1016/0165-1110(88)90004-8

Bottanelli, F., Kilian, N., Ernst, A. M., Rivera-Molina, F., Schroeder, L. K., Kromann, E. B., Lessard, M. D., Erdmann, R. S., Schepartz, A., Baddeley, D. et al. (2017). A novel physiological role for ARF1 in the formation of bidirectional tubules from the Golgi. *Mol. Biol. Cell* **28**, 1676-1687. doi:10.1091/mbc.e16-12-0863

Brandizzi, F. (2018). Transport from the endoplasmic reticulum to the Golgi in plants: where are we now? *Semin. Cell Dev. Biol.* **80**, 94-105. doi:10.1016/j.semcdb.2017.06.024

Brandizzi, F., Snapp, E. L., Roberts, A. G., Lippincott-Schwartz, J. and Hawes, C. (2002). Membrane protein transport between the endoplasmic reticulum and the golgi in tobacco leaves is energy dependent but cytoskeleton independent: evidence from selective photobleaching. *Plant Cell* **14**, 1293-1309. doi:10.1105/tpc.001586

Chang, D. D. and Colecraft, H. M. (2015). Rad and Rem are non-canonical G-proteins with respect to the regulatory role of guanine nucleotide binding in Ca(V)1.2 channel regulation. *J. Physiol.* **593**, 5075-5090. doi:10.1113/JP270889

Cherfils, J. and Zeghouf, M. (2013). Regulation of small GTPases by GEFs, GAPs, and GDIs. *Physiol. Rev.* **93**, 269-309. doi:10.1152/physrev.00003.2012

Clough, S. J. and Bent, A. F. (1998). Floral dip: a simplified method for Agrobacterium-mediated transformation of Arabidopsis thaliana. *Plant J.* **16**, 735-743. doi:10.1046/j.1365-313x.1998.00343.x

Cui, Y., Shen, J., Gao, C., Zhuang, X., Wang, J. and Jiang, L. (2016). Biogenesis of plant prevacuolar multivesicular bodies. *Mol. Plant* **9**, 774-786. doi:10.1016/j.molp.2016.01.011

Der, C. J., Finkel, T. and Cooper, G. M. (1986). Biological and biochemical properties of human rasH genes mutated at codon 61. *Cell* **44**, 167-176. doi:10.1016/0092-8674(86)90495-2

Dhonukshe, P., Aniento, F., Hwang, I., Robinson, D. G., Mravec, J., Stierhof, Y.-D. and Friml, J. (2007). Clathrin-mediated constitutive endocytosis of PIN auxin efflux carriers in Arabidopsis. *Curr. Biol.* **17**, 520-527. doi:10.1016/j.cub.2007.01.052

Eberth, A. and Ahmadian, M. R. (2009). In vitro GEF and GAP assays. *Curr. Protoc. Cell Biol.* **43**, 14.19.11-14.19.25. doi:10.1002/0471143030.cb1409s43

Ebine, K., Fujimoto, M., Okatani, Y., Nishiyama, T., Goh, T., Ito, E., Dainobu, T., Nishitani, A., Uemura, T., Sato, M. H. et al. (2011). A membrane trafficking pathway regulated by the plant-specific RAB GTPase ARA6. *Nat. Cell Biol.* **13**, 853-859. doi:10.1038/ncb2270

ElMaghloob, Y., Sot, B., McIlwraith, M. J., Garcia, E., Yelland, T. and Ismail, S. (2021). ARL3 activation requires the co-GEF BART and effector-mediated turnover. *Elife* **10**, e64624. doi:10.7554/eLife.64624

Emans, N., Zimmermann, S. and Fischer, R. (2002). Uptake of a fluorescent marker in plant cells is sensitive to brefeldin A and wortmannin. *Plant Cell* **14**, 71-86. doi:10.1105/tpc.010339

Erickson, J. W., Cerione, R. A. and Hart, M. J. (1997). Identification of an actin cytoskeletal complex that includes IQGAP and the Cdc42 GTPase. *J. Biol. Chem.* **272**, 24443-24447. doi:10.1074/jbc.272.39.24443

Esposito, A., Ventura, V., Petoukhov, M. V., Rai, A., Svergun, D. I. and Vanoni, M. A. (2019). Human MICAL1: activation by the small GTPase Rab8 and small-angle X-ray scattering studies on the oligomerization state of MICAL1 and its complex with Rab8. *Protein Sci.* **28**, 150-166. doi:10.1002/pro.3512

Fansa, E. K. and Wittinghofer, A. (2016). Sorting of lipidated cargo by the Arl2/Arl3 system. *Small GTPases* **7**, 222-230. doi:10.1080/21541248.2016.1224454

Fasano, G., Muto, V., Radio, F. C., Venditti, M., Mosaddeghzadeh, N., Coppola, S., Paradisi, G., Zara, E., Bazgir, F., Ziegler, A. et al. (2022). Dominant ARF3 variants disrupt Golgi integrity and cause a neurodevelopmental disorder recapitulated in zebrafish. *Nat. Commun.* **13**, 6841. doi:10.1038/s41467-022-34354-x

Fidyk, N., Wang, J. B. and Cerione, R. A. (2006). Influencing cellular transformation by modulating the rates of GTP hydrolysis by Cdc42. *Biochemistry* **45**, 7750-7762. doi:10.1021/bi060365h

Fiegen, D., Haeusler, L. C., Blumenstein, L., Herbrand, U., Dvorsky, R., Vetter, I. R. and Ahmadian, M. R. (2004). Alternative splicing of Rac1 generates Rac1b, a self-activating GTPase. *J. Biol. Chem.* **279**, 4743-4749. doi:10.1074/jbc.M310281200

Fisher, S., Kuna, D., Caspary, T., Kahn, R. A. and Sztul, E. (2020). ARF family GTPases with links to cilia. *Am. J. Physiol. Cell Physiol.* **319**, C404-C418. doi:10.1152/ajpcell.00188.2020

Fleming, J. A., Vega, L. R. and Solomon, F. (2000). Function of tubulin binding proteins in vivo. *Genetics* **156**, 69-80. doi:10.1093/genetics/156.1.69

Ghosh, P. M., Ghosh-Choudhury, N., Moyer, M. L., Mott, G. E., Thomas, C. A., Foster, B. A., Greenberg, N. M. and Kreisberg, J. I. (1999). Role of RhoA activation in the growth and morphology of a murine prostate tumor cell line. *Oncogene* **18**, 4120-4130. doi:10.1038/sj.onc.1202792

Goddard, T. D., Huang, C. C., Meng, E. C., Pettersen, E. F., Couch, G. S., Morris, J. H. and Ferrin, T. E. (2018). UCSF ChimeraX: meeting modern challenges in visualization and analysis. *Protein Sci.* **27**, 14-25. doi:10.1002/pro.3235

Gremer, L., Merbitz-Zahradnik, T., Dvorsky, R., Cirstea, I. C., Kratz, C. P., Zenker, M., Wittinghofer, A. and Ahmadian, M. R. (2011). Germline KRAS mutations cause aberrant biochemical and physical properties leading to developmental disorders. *Hum. Mutat.* **32**, 33-43. doi:10.1002/humu.21377

Haeusler, L. C., Hemsath, L., Fiegen, D., Blumenstein, L., Herbrand, U., Stege, P., Dvorsky, R. and Ahmadian, M. R. (2006). Purification and biochemical properties of Rac1, 2, 3 and the splice variant Rac1b. *Methods Enzymol.* **406**, 1-11. doi:10.1016/S0076-6879(06)06001-0

Hanton, S. L., Matheson, L. A., Chatre, L. and Brandizzi, F. (2009). Dynamic organization of COPII coat proteins at endoplasmic reticulum export sites in plant cells. *Plant J.* **57**, 963-974. doi:10.1111/j.1365-313X.2008.03740.x

Hanzal-Bayer, M., Linari, M. and Wittinghofer, A. (2005). Properties of the interaction of Arf-like protein 2 with PDEdelta. *J. Mol. Biol.* **350**, 1074-1082. doi:10.1016/j.jmb.2005.05.036

Hemsath, L. and Ahmadian, M. R. (2005). Fluorescence approaches for monitoring interactions of Rho GTPases with nucleotides, regulators, and effectors. *Methods* **37**, 173-182. doi:10.1016/j.ymeth.2005.05.014

Hemsath, L., Dvorsky, R., Fiegen, D., Carlier, M. F. and Ahmadian, M. R. (2005). An electrostatic steering mechanism of Cdc42 recognition by Wiskott-Aldrich syndrome proteins. *Mol. Cell* **20**, 313-324. doi:10.1016/j.molcel.2005.08.036

Heucken, N. and Ivanov, R. (2018). The retromer, sorting nexins and the plant endomembrane protein trafficking. *J. Cell Sci.* **131**, 2. doi:10.1242/jcs.203695

Hillig, R. C., Hanzal-Bayer, M., Linari, M., Becker, J., Wittinghofer, A. and Renault, L. (2000). Structural and biochemical properties show ARL3-GDP as a distinct GTP binding protein. *Structure* **8**, 1239-1245. doi:10.1016/S0969-2126(00)00531-1

Hodge, R. G., Schaefer, A., Howard, S. V. and Der, C. J. (2020). RAS and RHO family GTPase mutations in cancer: twin sons of different mothers? *Crit. Rev. Biochem. Mol. Biol.* **55**, 386-407. doi:10.1080/10409238.2020.1810622

Huang, X., Shen, Y., Zhang, Y., Wei, L., Lai, Y., Wu, J., Liu, X. and Liu, X. (2013). Rac1 mediates laminar shear stress-induced vascular endothelial cell migration. *Cell Adh. Migr.* **7**, 472-478. doi:10.4161/cam.27171

Ismail, S. A., Chen, Y. X., Rusinova, A., Chandra, A., Bierbaum, M., Gremer, L., Triola, G., Waldmann, H., Bastiaens, P. I. and Wittinghofer, A. (2011). Arl2-GTP and Arl3-GTP regulate a GDI-like transport system for farnesylated cargo. *Nat. Chem. Biol.* **7**, 942-949. doi:10.1038/nchembio.686

Ito, E., Uemura, T., Ueda, T. and Nakano, A. (2016). Distribution of RAB5-positive multivesicular endosomes and the trans-Golgi network in root meristematic cells of Arabidopsis thaliana. *Plant Biotechnol.* **33**, 281-286. doi:10.5511/plantbiotechnology.16.0218a

Ivanov, R. and Vert, G. (2021). Endocytosis in plants: peculiarities and roles in the regulated trafficking of plant metal transporters. *Biol. Cell* **113**, 1-13. doi:10.1111/boc.202000118

Ivanov, R., Brumbarova, T., Blum, A., Jantke, A.-M., Fink-Straube, C. and Bauer, P. (2014). SORTING NEXIN1 is required for modulating the trafficking and stability of the Arabidopsis IRON-REGULATED TRANSPORTER1. *Plant Cell* **26**, 1294-1307. doi:10.1105/tpc.113.116244

Jaillais, Y., Fobis-Loisy, I., Miège, C. and Gaude, T. (2008). Evidence for a sorting endosome in Arabidopsis root cells. *Plant J.* **53**, 237-247. doi:10.1111/j.1365-313X.2007.03338.x

Jaiswal, M., Fansa, E. K., Dvorsky, R. and Ahmadian, M. R. (2013). New insight into the molecular switch mechanism of human Rho family proteins: shifting a paradigm. *Biol. Chem.* **394**, 89-95. doi:10.1515/hsz-2012-0207

Jian, X., Gruschus, J. M., Sztul, E. and Randazzo, P. A. (2012). The pleckstrin homology (PH) domain of the Arf exchange factor Brag2 is an allosteric binding site. *J. Biol. Chem.* **287**, 24273-24283. doi:10.1074/jbc.M112.368084

Jumper, J., Evans, R., Pritzel, A., Green, T., Figurnov, M., Ronneberger, O., Tunyasuvunakool, K., Bates, R., Žídek, A., Potapenko, A. et al. (2021). Highly accurate protein structure prediction with AlphaFold. *Nature* **596**, 583-589. doi:10.1038/s41586-021-03819-2

Jung, A. and Rösner, H. (2002). RAC1-dependent regulation of cholinergically induced lamellar protrusive activity is independent of MAPKinase and attenuated by active p-JNK. *Neuroreport* **13**, 2443-2446. doi:10.1097/00001756-200212200-00014

Just, W. W. and Peränen, J. (2016). Small GTPases in peroxisome dynamics. *Biochim. Biophys. Acta. – Mol. Cell Res.* **1863**, 1006-1013. doi:10.1016/j.bbamcr.2016.01.004

Kahn, R. A., Der and G, C. J. and Bokoch, M. (1992). The ras superfamily of GTP-binding proteins: guidelines on nomenclature. *FASEB J.* **6**, 2512-2513. doi:10.1096/fasebj.6.8.1592203

Kahn, R. A., Cherfils, J., Elias, M., Lovering, R. C., Munro, S. and Schurmann, A. (2006). Nomenclature for the human Arf family of GTP-binding proteins: ARF, ARL, and SAR proteins. *J. Cell Biol.* **172**, 645-650. doi:10.1083/jcb.200512057

Kapoor, S., Fansa, E. K., Möbitz, S., Ismail, S. A., Winter, R., Wittinghofer, A. and Weise, K. (2015). Effect of the N-Terminal Helix and Nucleotide Loading on the Membrane and Effector Binding of Arl2/3. *Biophys. J.* **109**, 1619-1629. doi:10.1016/j.bpj.2015.08.033

Karimi, M., De Meyer, B. and Hilson, P. (2005). Modular cloning in plant cells. *Trends Plant Sci.* **10**, 103-105. doi:10.1016/j.tplants.2005.01.008

Karnoub, A. E. and Weinberg, R. A. (2008). Ras oncogenes: split personalities. *Nat. Rev. Mol. Cell Biol.* **9**, 517-531. doi:10.1038/nrm2438

Klein, S., Franco, M., Chardin, P. and Luton, F. (2006). Role of the Arf6 GDP/GTP cycle and Arf6 GTPase-activating proteins in actin remodeling and intracellular transport. *J. Biol. Chem.* **281**, 12352-12361. doi:10.1074/jbc.M601021200

Kondo, Y., Hanai, A., Nakai, W., Katoh, Y., Nakayama, K. and Shin, H. W. (2012). ARF1 and ARF3 are required for the integrity of recycling endosomes and the recycling pathway. *Cell Struct. Funct.* **37**, 141-154. doi:10.1247/csf.12015

Kotzer, A. M., Brandizzi, F., Neumann, U., Paris, N., Moore, I. and Hawes, C. (2004). AtRabF2b (Ara7) acts on the vacuolar trafficking pathway in tobacco leaf epidermal cells. *J. Cell Sci.* **117**, 6377-6389. doi:10.1242/jcs.01564

Kuemmerle, J. F. and Zhou, H. (2002). Insulin-like growth factor-binding protein-5. (IGFBP-5) stimulates growth and IGF-I secretion in human intestinal smooth muscle by Ras-dependent activation of p38 MAP kinase and Erk1/2 pathways. *J. Biol. Chem.* **277**, 20563-20571. doi:10.1074/jbc.M200885200

Latijnhouwers, M., Hawes, C., Carvalho, C., Oparka, K., Gillingham, A. K. and Boevink, P. (2005). An Arabidopsis GRIP domain protein locates to the trans-Golgi and binds the small GTPase ARL1. *Plant J.* **44**, 459-470. doi:10.1111/j.1365-313X.2005.02542.x

Le, C. T. T., Brumbarova, T., Ivanov, R., Stoof, C., Weber, E., Mohrbacher, J., Fink-Straube, C. and Bauer, P. (2015). ZINC FINGER OF ARABIDOPSIS THALIANA12. (ZAT12) interacts with FER-LIKE IRON DEFICIENCY-INDUCED TRANSCRIPTION FACTOR. (FIT) linking iron deficiency and oxidative stress responses. *Plant Physiol.* **170**, 540-557.

Lee, G. J., Sohn, E. J., Lee, M. H. and Hwang, I. (2004). The Arabidopsis rab5 homologs rha1 and ara7 localize to the prevacuolar compartment. *Plant Cell Physiol.* **45**, 1211-1220. doi:10.1093/pcp/pch142

Lee, M. C., Orci, L., Hamamoto, S., Futai, E., Ravazzola, M. and Schekman, R. (2005). Sar1p N-terminal helix initiates membrane curvature and completes the fission of a COPII vesicle. *Cell* **122**, 605-617. doi:10.1016/j.cell.2005.07.025

Li, C.-C., Wu, T.-S., Huang, C.-F., Jang, L.-T., Liu, Y.-T., You, S.-T., Liou, G.-G. and Lee, F.-J. S. (2012). GTP-binding-defective ARL4D alters mitochondrial morphology and membrane potential. *PLoS One* **7**, e43552. doi:10.1371/journal.pone.0043552

Lloyd, J. and Meinke, D. (2012). A comprehensive dataset of genes with a loss-of-function mutant phenotype in Arabidopsis. *Plant Physiol.* **158**, 1115-1129. doi:10.1104/pp.111.192393

Macia, E., Luton, F., Partisani, M., Cherfils, J., Chardin, P. and Franco, M. (2004). The GDP-bound form of Arf6 is located at the plasma membrane. *J. Cell Sci.* **117**, 2389-2398. doi:10.1242/jcs.01090

Matsumoto, S., Taniguchi-Tamura, H., Araki, M., Kawamura, T., Miyamoto, R., Tsuda, C., Shima, F., Kumasaka, T., Okuno, Y. and Kataoka, T. (2021). Oncogenic mutations Q61L and Q61H confer active form-like structural features to the inactive state. (state 1) conformation of H-Ras protein. *Biochem. Biophys. Res. Commun.* **565**, 85-90. doi:10.1016/j.bbrc.2021.05.084

Mayer, U., Herzog, U., Berger, F., Inzé, D. and Jürgens, G. (1999). Mutations in the PILZ group genes disrupt the microtubule cytoskeleton and uncouple cell cycle progression from cell division in Arabidopsis embryo and endosperm. *Eur. J. Cell Biol.* **78**, 100-108. doi:10.1016/S0171-9335(99)80011-9

McElver, J., Patton, D., Rumbaugh, M., Liu, C.-M., Yang, L. J. and Meinke, D. (2000). The TITAN5 gene of Arabidopsis encodes a protein related to the ADP ribosylation factor family of GTP binding proteins. *Plant Cell* **12**, 1379-1392. doi:10.1105/tpc.12.8.1379

Memon, A. R. (2004). The role of ADP-ribosylation factor and SAR1 in vesicular trafficking in plants. *Biochim. Biophys. Acta* **1664**, 9-30. doi:10.1016/j.bbamem.2004.04.005

Mori, R. and Toda, T. (2013). The dual role of fission yeast Tbc1/cofactor C orchestrates microtubule homeostasis in tubulin folding and acts as a GAP for GTPase Alp41/Arl2. *Mol. Biol. Cell* **24**, 1713-1718. doi:10.1091/mbc.e12-11-0792

Nakabayashi, K., Okamoto, M., Koshiba, T., Kamiya, Y. and Nambara, E. (2005). Genome-wide profiling of stored mRNA in Arabidopsis thaliana seed germination: epigenetic and genetic regulation of transcription in seed. *Plant J.* **41**, 697-709. doi:10.1111/j.1365-313X.2005.02337.x

Nakai, W., Kondo, Y., Saitoh, A., Naito, T., Nakayama, K. and Shin, H. W. (2013). ARF1 and ARF4 regulate recycling endosomal morphology and retrograde transport from endosomes to the Golgi apparatus. *Mol. Biol. Cell* **24**, 2570-2581. doi:10.1091/mbc.e13-04-0197

Nassar, N., Singh, K. and Garcia-Diaz, M. (2010). Structure of the dominant negative S17N mutant of Ras. *Biochemistry* **49**, 1970-1974. doi:10.1021/bi9020742

Nelson, B. K., Cai, X. and Nebenführ, A. (2007). A multicolored set of in vivo organelle markers for co-localization studies in Arabidopsis and other plants. *Plant J.* **51**, 1126-1136. doi:10.1111/j.1365-313X.2007.03212.x

Newman, L. E., Zhou, C. J., Mudigonda, S., Mattheyses, A. L., Paradies, E., Marobbio, C. M. and Kahn, R. A. (2014). The ARL2 GTPase is required for mitochondrial morphology, motility, and maintenance of ATP levels. *PLoS One* **9**, e99270. doi:10.1371/journal.pone.0099270

Nielsen, E. (2020). The small GTPase superfamily in plants: a conserved regulatory module with novel functions. *Annu. Rev. Plant Biol.* **71**, 247-272. doi:10.1146/annurev-arplant-112619-025827

Niu, F., Ji, C., Liang, Z., Guo, R., Chen, Y., Zeng, Y. and Jiang, L. (2022). ADP-ribosylation factor D1 modulates Golgi morphology, cell plate formation, and plant growth in Arabidopsis. *Plant Physiol.* **190**, 1199-1213. doi:10.1093/plphys/kiac329

Pasternak, T., Tietz, O., Rapp, K., Begheldo, M., Nitschke, R., Ruperti, B. and Palme, K. (2015). Protocol: an improved and universal procedure for whole-mount immunolocalization in plants. *Plant Methods* **11**, 50. doi:10.1186/s13007-015-0094-2

Radcliffe, P. A., Vardy, L. and Toda, T. (2000). A conserved small GTP-binding protein Alp41 is essential for the cofactor-dependent biogenesis of microtubules in fission yeast. *FEBS Lett.* **468**, 84-88. doi:10.1016/S0014-5793(00)01202-3

Radhakrishna, H., Al-Awar, O., Khachikian, Z. and Donaldson, J. G. (1999). ARF6 requirement for Rac ruffling suggests a role for membrane trafficking in cortical actin rearrangements. *J. Cell Sci.* **112**, 855-866. doi:10.1242/jcs.112.6.855

Renna, L. and Brandizzi, F. (2020). The mysterious life of the plant trans-Golgi network: advances and tools to understand it better. *J. Microsc.* **278**, 154-163. doi:10.1111/jmi.12881

Ritzenthaler, C., Nebenführ, A., Movafeghi, A., Stussi-Garaud, C., Behnia, L., Pimpl, P., Staehelin, L. A. and Robinson, D. G. (2002). Reevaluation of the effects of brefeldin A on plant cells using tobacco Bright Yellow 2 cells expressing Golgi-targeted green fluorescent protein and COPI antisera. *Plant Cell* **14**, 237-261. doi:10.1105/tpc.010237

Robinson, D. G., Scheuring, D., Naramoto, S. and Friml, J. (2011). ARF1 localizes to the golgi and the trans-golgi network. *Plant Cell* **23**, 846-849. doi:10.1105/tpc.110.082099

Ryu, K. H., Huang, L., Kang, H. M. and Schiefelbein, J. (2019). Single-Cell RNA Sequencing Resolves Molecular Relationships Among Individual Plant Cells. *Plant Physiol.* **179**, 1444-1456. doi:10.1104/pp.18.01482

Scheffzek, K., Ahmadian, M. R., Kabsch, W., Wiesmüller, L., Lautwein, A., Schmitz, F. and Wittinghofer, A. (1997). The Ras-RasGAP complex: structural basis for GTPase activation and its loss in oncogenic Ras mutants. *Science* **277**, 333-339. doi:10.1126/science.277.5324.333

Schmid, M., Davison, T. S., Henz, S. R., Pape, U. J., Demar, M., Vingron M., Schölkopf, B., Weigel, D. and Lohmann J. U. (2005). A gene expression map of Arabidopsis thaliana development. *Nat Genet.* **37**, 501-506. doi:10.1038/ng1543

Schneider, C. A., Rasband, W. S. and Eliceiri, K. W. (2012). NIH Image to ImageJ: 25 years of image analysis. *Nat. Methods* **9**, 671-675. doi:10.1038/nmeth.2089

Sharer, J. D. and Kahn, R. A. (1999). The ARF-like 2. (ARL2)-binding protein, BART. Purification, cloning, and initial characterization. *J. Biol. Chem.* **274**, 27553-27561. doi:10.1074/jbc.274.39.27553

Sharer, J. D., Shern, J. F., Van Valkenburgh, H., Wallace, D. C. and Kahn, R. A. (2002). ARL2 and BART enter mitochondria and bind the adenine nucleotide transporter. *Mol. Biol. Cell* **13**, 71-83. doi:10.1091/mbc.01-05-0245

Shirazi, F., Jones, R. J., Singh, R. K., Zou, J., Kuiatse, I., Berkova, Z., Wang, H., Lee, H. C., Hong, S., Dick, L. et al. (2020). Activating KRAS, NRAS, and BRAF mutants enhance proteasome capacity and reduce endoplasmic reticulum stress in multiple myeloma. *Proc. Natl. Acad. Sci. USA* **117**, 20004-20014. doi:10.1073/pnas.2005052117

Singh, M. K., Richter, S., Beckmann, H., Kientz, M., Stierhof, Y.-D., Anders, N., Fäßler, F., Nielsen, M., Knöll, C., Thomann, A. et al. (2018). A single class of ARF GTPase activated by several pathway-specific ARF-GEFs regulates essential membrane traffic in Arabidopsis. *PLoS Genet.* **14**, e1007795. doi:10.1371/journal.pgen.1007795

Soh, U. J. and Low, B. C. (2008). BNIP2 extra long inhibits RhoA and cellular transformation by Lbc RhoGEF via its BCH domain. *J. Cell Sci.* **121**, 1739-1749. doi:10.1242/jcs.021774

Sohn, E. J., Kim, E. S., Zhao, M., Kim, S. J., Kim, H., Kim, Y. W., Lee, Y. J., Hillmer, S., Sohn, U., Jiang, L. et al. (2003). Rha1, an Arabidopsis Rab5 homolog, plays a critical role in the vacuolar trafficking of soluble cargo proteins. *Plant Cell* **15**, 1057-1070. doi:10.1105/tpc.009779

Stefano, G., Renna, L., Hanton, S. L., Chatre, L., Haas, T. A. and Brandizzi, F. (2006). ARL1 plays a role in the binding of the GRIP domain of a peripheral matrix protein to the Golgi apparatus in plant cells. *Plant Mol. Biol.* **61**, 431-449. doi:10.1007/s11103-006-0022-y

Stierhof, Y. D. and El Kasmi, F. (2010). Strategies to improve the antigenicity, ultrastructure preservation and visibility of trafficking compartments in Arabidopsis tissue. *Eur. J. Cell Biol.* **89**, 285-297. doi:10.1016/j.ejcb.2009.12.003

Sugawara, R., Ueda, H. and Honda, R. (2019). Structural and functional characterization of fast-cycling RhoF GTPase. *Biochem. Biophys. Res. Commun.* **513**, 522-527. doi:10.1016/j.bbrc.2019.04.018

Suo, Y., Hu, F., Zhu, H., Li, D., Qi, R., Huang, J. and Wu, W. (2021). BIG3 and BIG5 redundantly mediate vesicle trafficking in Arabidopsis. *Biomolecules* **11**, 732. doi:10.3390/biom11050732

Sztul, E., Chen, P.-W., Casanova, J. E., Cherfils, J., Dacks, J. B., Lambright, D. G., Lee, F.-J. S., Randazzo, P. A., Santy, L. C., Schürmann, A. et al. (2019). ARF GTPases and their GEFs and GAPs: concepts and challenges. *Mol. Biol. Cell* **30**, 1249-1271. doi:10.1091/mbc.E18-12-0820

Tichá, M., Richter, H., Ovečka, M., Maghelli, N., Hrbáčková, M., Dvořák, P., Šamaj, J. and Šamajová, O. (2020). Advanced microscopy reveals complex developmental and subcellular localization patterns of ANNEXIN 1 in Arabidopsis. *Front. Plant Sci.* **11**, 1153. doi:10.3389/fpls.2020.01153

Tzafrir, I., McElver, J. A., Liu, C.-M., Yang, L. J., Wu, J. Q., Martinez, A., Patton, D. A. and Meinke, D. W. (2002). Diversity of TITAN functions in Arabidopsis seed development. *Plant Physiol.* **128**, 38-51. doi:10.1104/pp.010911

Ueda, T., Yamaguchi, M., Uchimiya, H. and Nakano, A. (2001). Ara6, a plant-unique novel type Rab GTPase, functions in the endocytic pathway of Arabidopsis thaliana. *EMBO J.* **20**, 4730-4741. doi:10.1093/emboj/20.17.4730

Valencia, J. P., Goodman, K. and Otegui, M. S. (2016). Endocytosis and endosomal trafficking in plants. *Annu. Rev. Plant Biol.* **67**, 309-335. doi:10.1146/annurev-arplant-043015-112242

Van Valkenburgh, H., Shern, J. F., Sharer, J. D., Zhu, X. and Kahn, R. A. (2001). ADP-ribosylation factors. (ARFs) and ARF-like 1. (ARL1) have both specific and shared effectors: characterizing ARL1-binding proteins. *J. Biol. Chem.* **276**, 22826-22837. doi:10.1074/jbc.M102359200

Vanoni, M., Bertini, R., Sacco, E., Fontanella, L., Rieppi, M., Colombo, S., Martegani, E., Carrera, V., Moroni, A., Bizzarri, C. et al. (1999). Characterization and properties of dominant-negative mutants of the ras-specific guanine nucleotide exchange factor CDC25(Mm). *J. Biol. Chem.* **274**, 36656-36662. doi:10.1074/jbc.274.51.36656

Veltel, S., Kravchenko, A., Ismail, S. and Wittinghofer, A. (2008). Specificity of Arl2/Arl3 signaling is mediated by a ternary Arl3-effector-GAP complex. *FEBS Lett.* **582**, 2501-2507. doi:10.1016/j.febslet.2008.05.053

Vernoud, V., Horton, A. C., Yang, Z. and Nielsen, E. (2003). Analysis of the small GTPase gene superfamily of Arabidopsis. *Plant Physiol.* **131**, 1191-1208. doi:10.1104/pp.013052

Volpicelli-Daley, L. A., Li, Y., Zhang, C. J. and Kahn, R. A. (2005). Isoform-selective effects of the depletion of ADP-ribosylation factors 1-5 on membrane traffic. *Mol. Biol. Cell* **16**, 4495-4508. doi:10.1091/mbc.e04-12-1042

Waese, J., Fan, J., Pasha, A., Yu, H., Fucile, G., Shi, R., Cumming, M., Kelley, L. A., Sternberg, M. J., Krishnakumar, V. et al. (2017). ePlant: visualizing and exploring multiple levels of data for hypothesis generation in plant biology. *Plant Cell* **29**, 1806-1821. doi:10.1105/tpc.17.00073

Walsh, T. G., Li, Y., Wersäll, A. and Poole, A. W. (2019). Small GTPases in platelet membrane trafficking. *Platelets* **30**, 31-40. doi:10.1080/09537104.2018.1535703

Wang, J. B., Wu, W. J. and Cerione, R. A. (2005). Cdc42 and Ras cooperate to mediate cellular transformation by intersectin-L. *J. Biol. Chem.* **280**, 22883-22891. doi:10.1074/jbc.M414375200

Wang, J., Cai, Y., Miao, Y., Lam, S. K. and Jiang, L. (2009). Wortmannin induces homotypic fusion of plant prevacuolar compartments*. *J. Exp. Bot.* **60**, 3075-3083. doi:10.1093/jxb/erp136

Wang, Y., Liu, F., Ren, Y., Wang, Y., Liu, X., Long, W., Wang, D., Zhu, J., Zhu, X., Jing, R. et al. (2016). GOLGI TRANSPORT 1B regulates protein export from the endoplasmic reticulum in rice endosperm cells. *Plant Cell* **28**, 2850-2865. doi:10.1105/tpc.16.00717

Waterhouse, A. M., Procter, J. B., Martin, D. M., Clamp, M. and Barton, G. J. (2009). Jalview Version 2–a multiple sequence alignment editor and analysis workbench. *Bioinformatics* **25**, 1189-1191. doi:10.1093/bioinformatics/btp033

Wittmann, T., Bokoch, G. M. and Waterman-Storer, C. M. (2003). Regulation of leading edge microtubule and actin dynamics downstream of Rac1. *J. Cell Biol.* **161**, 845-851. doi:10.1083/jcb.200303082

Wright, J., Kahn, R. A. and Sztul, E. (2014). Regulating the large Sec7 ARF guanine nucleotide exchange factors: the when, where and how of activation. *Cell. Mol. Life Sci.* **71**, 3419-3438. doi:10.1007/s00018-014-1602-7

Zhang, C. J., Rosenwald, A. G., Willingham, M. C., Skuntz, S., Clark, J. and Kahn, R. A. (1994). Expression of a dominant allele of human ARF1 inhibits membrane traffic in vivo. *J. Cell Biol.* **124**, 289-300. doi:10.1083/jcb.124.3.289

Zhang, H., Yang, Z., Lin, T., Wu, Y., Zou, T., yang, J. and Zhang, Y. (2018). ARL2 regulates trafficking and expression of isoprenylated proteins and is crucial for development of photoreceptor outer segments. *Invest. Ophthalmol. Vis. Sci.* **59**, 963-963.

Zhou, C., Cunningham, L., Marcus, A. I., Li, Y. and Kahn, R. A. (2006). Arl2 and Arl3 regulate different microtubule-dependent processes. *Mol. Biol. Cell* **17**, 2476-2487. doi:10.1091/mbc.e05-10-0929

Chapter III. Mutation-induced LZTR1 polymerization provokes cardiac pathology in recessive Noonan syndromes

Authors: Alexandra Viktoria Busley*, Óscar Gutiérrez-Gutiérrez*, Elke Hammer, Fabian Koitka, Amin Mirzaiebadizi, Martin Steinegger, Constantin Pape, Linda Böhmer, Henning Schroeder, Mandy Kleinsorge, Melanie Engler, Ion Cristian Cirstea, Lothar Gremer, Dieter Willbold, Janine Altmüller, Felix Marbach, Gerd Hasenfuss, Wolfram-Hubertus Zimmermann, Mohammad Reza Ahmadian, Bernd Wollnik, Lukas Cyganek

*These authors equally contributed to this study

DOI: 10.1016/j.celrep.2024.114448

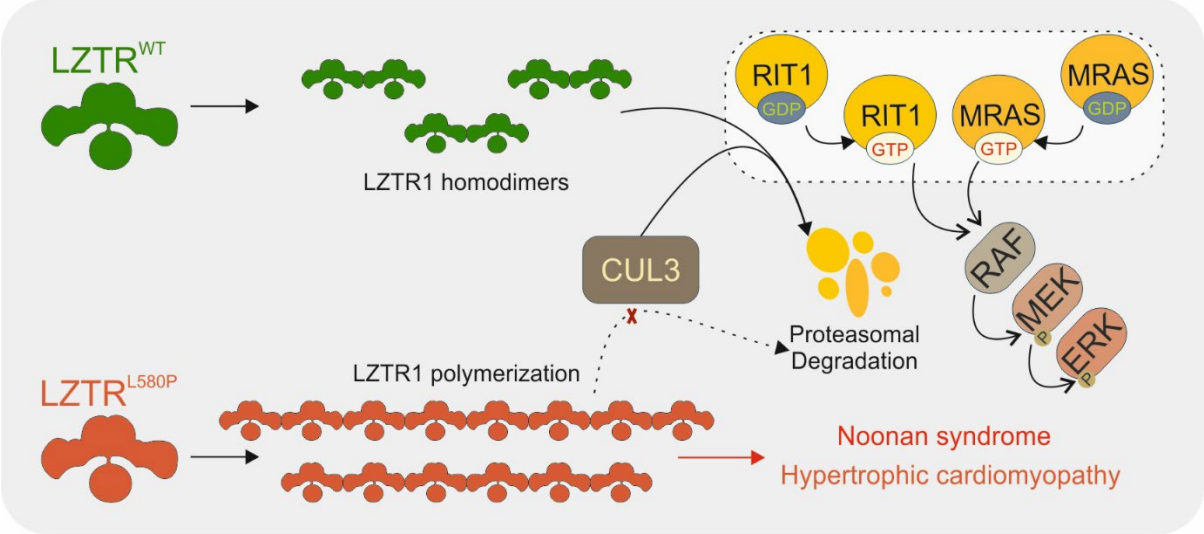

Status: Published

Journal: *Cell reports*
JIF: 7.5
Contribution: ≈13-15%

A.M. expressed and purified LZTR1 wild-type and L580P variant proteins from Expi293F cells for molecular mass analysis. He conducted analytical size-exclusion chromatography and confirmed oligomeric states via TCA precipitation and Western blotting. He expressed and purified KRAS, MRAS, and RIT1 GTPases and prepared their labeled forms. He performed pull-down assays to evaluate the binding of LZTR1 variants to MRAS and RIT1 in both GDP- and GppNHp-bound states. A.M. analyzed the biochemical data, contributed to result visualization, authored the relevant *Materials and Methods* section, and and assisted in interpreting findings and addressing related reviewer comments.

Cell Reports

Article

Mutation-induced LZTR1 polymerization provokes cardiac pathology in recessive Noonan syndrome

Graphical abstract

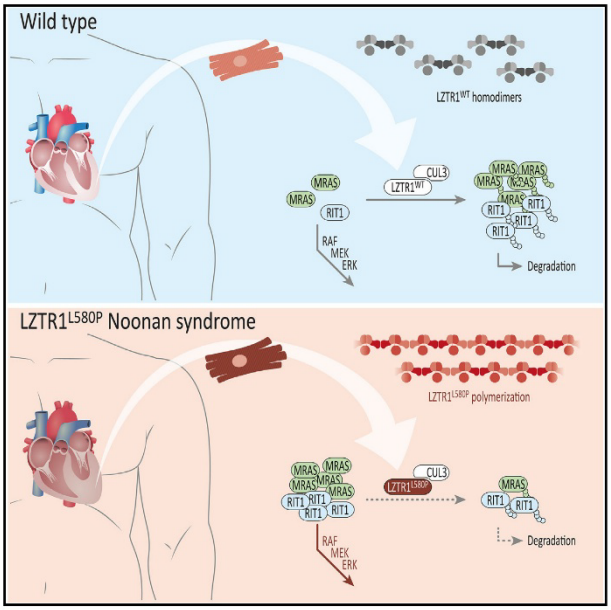

Highlights

- LZTR1^{L580P} in homozygosity is causative for Noonan syndrome and hypertrophic cardiomyopathy
- LZTR1^{L580P} fosters assembly of LZTR1 polymers, resulting in complex dysfunction
- Pathological LZTR1 results in impaired RAS GTPase degradation, causing cellular hypertrophy
- CRISPR correction of one allele is sufficient to normalize cardiac disease phenotype

Authors

Alexandra Viktoria Busley, Óscar Gutiérrez-Gutiérrez, Elke Hammer, ..., Mohammad Reza Ahmadian, Bernd Wollnik, Lukas Cyganek

Correspondence

lukas.cyganek@gwdg.de

In brief

Using patient-specific and CRISPR-Cas9-corrected iPSC cardiomyocytes, Busley et al. describe an *LZTR1*^{L580P}-specific disease mechanism provoking Noonan syndrome-associated cardiac hypertrophy. Mutation-induced polymerization of LZTR1 complexes results in the accumulation of RAS GTPases, leading to molecular and cellular impairments associated with cardiac hypertrophy, whereas CRISPR correction of the missense variant rescues the disease phenotype.

Busley et al., 2024, Cell Reports *43*, 114448
July 23, 2024
https://doi.org/10.1016/j.celrep.2024.114448

CellPress

Cell Reports

CellPress
OPEN ACCESS

Article

Mutation-induced LZTR1 polymerization provokes cardiac pathology in recessive Noonan syndrome

Alexandra Viktoria Busley,[1,2,4,20] Óscar Gutiérrez-Gutiérrez,[1,2,20] Elke Hammer,[3,5] Fabian Koitka,[1,2,4] Amin Mirzaiebadizi,[6] Martin Steinegger,[7] Constantin Pape,[4,8] Linda Böhmer,[1] Henning Schroeder,[9] Mandy Kleinsorge,[1,2] Melanie Engler,[10] Ion Cristian Cirstea,[10] Lothar Gremer,[11,12] Dieter Willbold,[11,12] Janine Altmüller,[13,14] Felix Marbach,[15,16] Gerd Hasenfuss,[1,2,4] Wolfram-Hubertus Zimmermann,[2,4,17,18] Mohammad Reza Ahmadian,[6] Bernd Wollnik,[2,4,19] and Lukas Cyganek[1,2,4,18,21,*]

[1]Stem Cell Unit, Clinic for Cardiology and Pneumology, University Medical Center Göttingen, Göttingen, Germany
[2]DZHK (German Center for Cardiovascular Research), Göttingen, Germany
[3]DZHK (German Center for Cardiovascular Research), Greifswald, Germany
[4]Cluster of Excellence "Multiscale Bioimaging: from Molecular Machines to Networks of Excitable Cells" (MBExC), University of Göttingen, Göttingen, Germany
[5]Interfaculty Institute of Genetics and Functional Genomics, University Medicine Greifswald, Greifswald, Germany
[6]Institute of Biochemistry and Molecular Biology II, Medical Faculty and University Hospital Düsseldorf, Heinrich Heine University Düsseldorf, Düsseldorf, Germany
[7]School of Biological Sciences, Seoul National University, Seoul, South Korea
[8]Institute of Computer Science, Georg-August University Göttingen, Göttingen, Germany
[9]NMR Signal Enhancement Group, Max Planck Institute for Multidisciplinary Sciences, Göttingen, Germany
[10]Institute of Applied Physiology, University of Ulm, Ulm, Germany
[11]Institute of Physical Biology, Heinrich Heine University Düsseldorf, Düsseldorf, Germany
[12]Institute of Biological Information Processing, Structural Biochemistry (IBI-7), Forschungszentrum Jülich GmbH, Jülich, Germany
[13]Cologne Center for Genomics, University of Cologne, Faculty of Medicine, and University Hospital Cologne, Cologne, Germany
[14]Genomics Platform, Berlin Institute for Medical Systems Biology, Max Delbrück Center for Molecular Medicine–Berlin, Berlin, Germany
[15]Institute of Human Genetics, University Hospital Cologne, Cologne, Germany
[16]Institute of Human Genetics, Heidelberg University, Heidelberg, Germany
[17]Institute of Pharmacology and Toxicology, University Medical Center Göttingen, Göttingen, Germany
[18]Translational Neuroinflammation and Automated Microscopy, Fraunhofer Institute for Translational Medicine and Pharmacology ITMP, Göttingen, Germany
[19]Institute of Human Genetics, University Medical Center Göttingen, Göttingen, Germany
[20]These authors contributed equally
[21]Lead contact
*Correspondence: lukas.cyganek@gwdg.de
https://doi.org/10.1016/j.celrep.2024.114448

SUMMARY

Noonan syndrome patients harboring causative variants in *LZTR1* are particularly at risk to develop severe and early-onset hypertrophic cardiomyopathy. In this study, we investigate the mechanistic consequences of a homozygous variant *LZTR1*^{L580P} by using patient-specific and CRISPR-Cas9-corrected induced pluripotent stem cell (iPSC) cardiomyocytes. Molecular, cellular, and functional phenotyping in combination with *in silico* prediction identify an *LZTR1*^{L580P}-specific disease mechanism provoking cardiac hypertrophy. The variant is predicted to alter the binding affinity of the dimerization domains facilitating the formation of linear LZTR1 polymers. LZTR1 complex dysfunction results in the accumulation of RAS GTPases, thereby provoking global pathological changes of the proteomic landscape ultimately leading to cellular hypertrophy. Furthermore, our data show that cardiomyocyte-specific MRAS degradation is mediated by LZTR1 via non-proteasomal pathways, whereas RIT1 degradation is mediated by both LZTR1-dependent and LZTR1-independent pathways. Uni- or biallelic genetic correction of the *LZTR1*^{L580P} missense variant rescues the molecular and cellular disease phenotype, providing proof of concept for CRISPR-based therapies.

INTRODUCTION

Noonan syndrome (NS) is a multi-systemic developmental disorder with a broad spectrum of symptoms and varying degrees of disease severity. Common clinical symptoms range from intellectual disability to facial dysmorphisms, webbed neck, skeletal deformities, short stature, and, in many cases, congenital heart disease.[1] With a prevalence of approximately 1 in 1,000–2,500

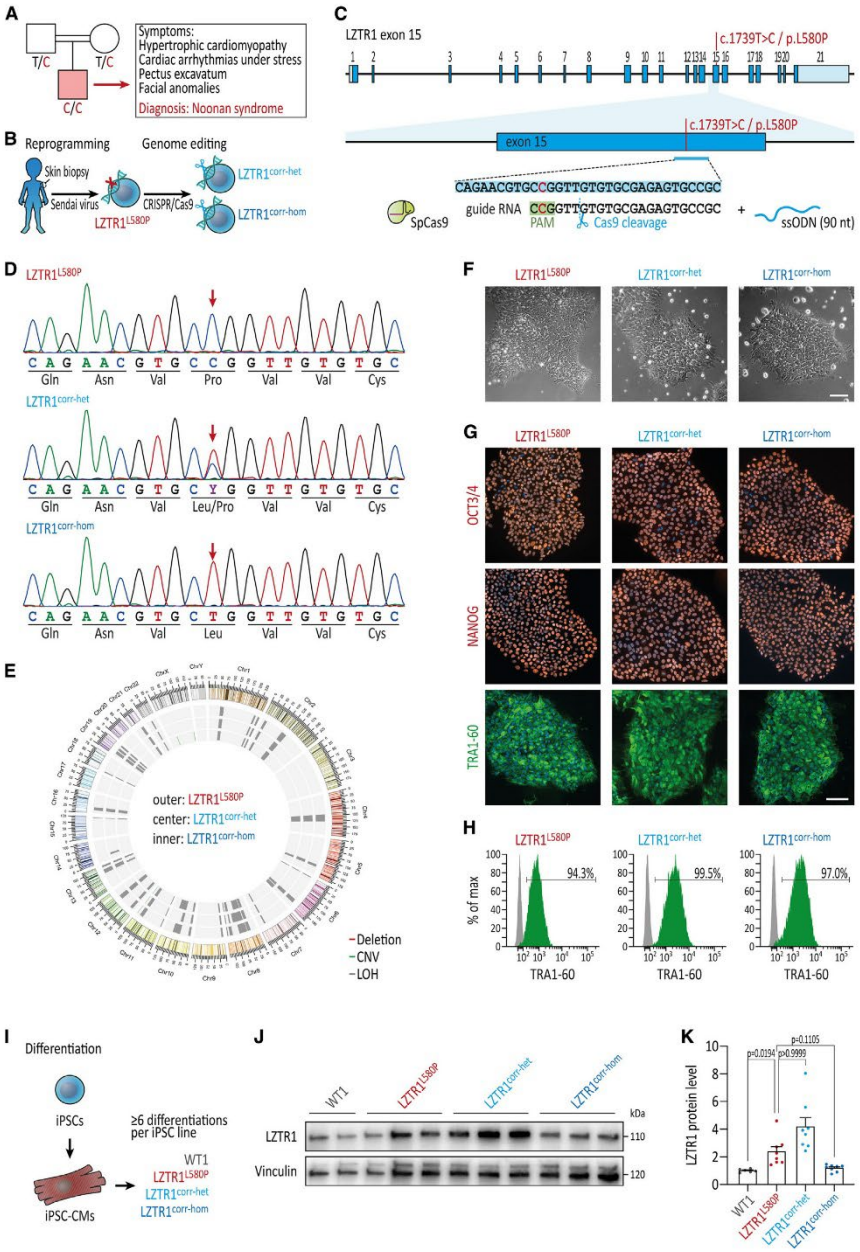

(legend on next page)

live births, NS is considered the most common monogenic disease associated with congenital heart defects and early-onset hypertrophic cardiomyopathy (HCM).[2] Young NS patients diagnosed with HCM are more prone to develop heart failure accompanied by a poor late survival.[3,4] Like other phenotypically overlapping syndromes classified as RASopathies, NS is caused by variants in RAS-mitogen-activated protein kinase (MAPK)-associated genes, all typically leading to an increase in signaling transduction.[5] Patients harboring causative gene variants in *RAF1*, *HRAS*, *RIT1*, and *LZTR1* are particularly at risk to develop severe and early-onset HCM.[6,7]

Recent studies by others and our group have identified the role of LZTR1 within the RAS-MAPK signaling cascade as a negative regulator of signaling activity. *LZTR1* encodes an adapter protein of the cullin 3 ubiquitin ligase complex by selectively targeting RAS proteins as substrates for degradation. *LZTR1* deficiency, caused by truncating or missense variants, results in an accumulation of the RAS protein pool and, as a consequence, in RAS-MAPK signaling hyperactivity.[8–10] Whereas dominant *LZTR1* variants generally cluster in the Kelch motif perturbing RAS binding to the ubiquitination complex,[11] the mechanistic consequences of recessive *LZTR1* missense variants, which are distributed over the entire protein, are not understood.

Human induced pluripotent stem cell-derived cardiomyocytes (iPSC-CMs) generated from patients with inherited forms of cardiomyopathies offer a platform to study the disease mechanisms in physiologically relevant cells and tissues.[12,13] A few RASopathy-linked iPSC-CM models have been described, including for variants in *PTPN11*, *RAF1*, *BRAF*, and *MRAS*.[14–17] With this in mind, we recently added additional information as to the role of *LZTR1*-truncating variants in NS pathophysiology.[10,18] In the present study, we investigated the functional consequences of a recessive missense variant *LZTR1*^{L580P} by utilizing patient-derived and CRISPR-corrected iPSC-CMs. We could show that *LZTR1*^{L580P} in homozygosity results in aberrant polymerization causing LZTR1 dysfunction, an increase in RAS guanosine triphosphatase (GTPase) levels, and cellular hypertrophy. Furthermore, genetic correction of the missense variant by CRISPR-Cas9 rescued the cellular phenotype, thereby providing proof of concept for future personalized CRISPR-based therapies.

RESULTS

LZTR1^{L580P} is causative for recessive NS

A 17-year-old male patient with HCM, stress-induced cardiac arrhythmias, pectus excavatum, and facial anomalies was referred to our clinic, and, based on the combination of symptoms, was diagnosed with NS (Figure 1A; Table S1). The patient was born to a consanguineous couple, and both parents showed neither apparent clinical symptoms nor distinctive NS-specific features. Whole-exome sequencing detected one highly suspicious homozygous variant in *LZTR1* (GenBank: NM_006767), c.1739T>C, leading to the substitution of an evolutionary conserved leucine at amino acid position 580 by proline (p.L580P). Both parents were heterozygous carriers, and the variant was not present in any current database of human genetic variations, including the >250,000 alleles of the Genome Aggregation Database (gnomAD).

To elucidate the molecular and functional consequences of the *LZTR1*^{L580P} missense variant, we generated iPSCs from the patient's skin fibroblasts using integration-free reprogramming methods and subsequently utilized CRISPR-Cas9 genome editing to engineer gene variant-corrected iPSC lines (Figure 1B). For genetic correction of the patient-specific iPSCs, the CRISPR guide RNA was designed to specifically target the mutated sequence in exon 15 of the *LZTR1* gene. Furthermore, the ribonucleoprotein-based CRISPR-Cas9 complex was combined with a single-stranded oligonucleotide serving as template for homology-directed repair (Figure 1C). Upon transfection, cells were singularized and individual clones were screened for successful editing to identify heterozygous corrected as well as homozygous corrected iPSC clones, LZTR1$^{corr\text{-}het}$ and LZTR1$^{corr\text{-}hom}$, respectively (Figure 1D). Molecular karyotyping of the edited iPSC clones confirmed chromosomal stability after genome editing and passaging (Figure 1E). As expected for individuals born from consanguineous parents, both patient-specific and CRISPR-corrected iPSCs demonstrated a noticeable reduction

Figure 1. Generation of patient-specific and CRISPR-corrected iPSCs

(A) Pedigree of the consanguineous family with healthy parents and the son affected by recessive NS harboring the *LZTR1* variant (c.1739T>C/p.L580P) in homozygosity.

(B) Generation of patient-specific iPSCs by reprogramming of patient's skin fibroblasts via integration-free Sendai virus and genetic correction of the missense variant by CRISPR-Cas9.

(C) Depiction of the genome editing approach for correction of the missense variant in *LZTR1* exon 15.

(D) Sanger sequencing of the patient-derived iPSCs (LZTR1^{L580P}) and the CRISPR-Cas9-edited heterozygous corrected (LZTR1$^{corr\text{-}het}$) and homozygous corrected (LZTR1$^{corr\text{-}hom}$) iPSCs.

(E) Molecular karyotyping demonstrated a high percentage of loss of heterozygosity (LOH) because of consanguinity as well as chromosomal stability of iPSCs after genome editing. CNV, copy number variation.

(F) Patient-specific and CRISPR-corrected iPSCs showed a typical human stem cell-like morphology; scale bar: 100 μm.

(G) Expression of key pluripotency markers OCT3/4, NANOG, and TRA-1-60 in the generated iPSC lines was assessed by immunocytochemistry; nuclei were counter-stained with Hoechst 33342 (blue); scale bar: 100 μm.

(H) Flow cytometry analysis of pluripotency marker TRA-1-60 detected homogeneous populations of pluripotent cells in generated iPSC lines. Gray peaks represent the negative controls.

(I) Differentiation of WT, patient-specific, and CRISPR-corrected iPSCs into iPSC-CMs.

(J) Representative blot of endogenous LZTR1 levels in iPSC-CMs at day 60 of differentiation, assessed by western blot; vinculin served as loading control; $n = 3$ individual differentiations per iPSC line.

(K) Quantitative analysis of western blots for LZTR1; data were normalized to total protein and to the corresponding WT samples on each membrane; $n = 6–8$ independent differentiations per iPSC line. Data were analyzed by non-parametric Kruskal-Wallis test with Dunn correction and are presented as mean ± SEM (K).

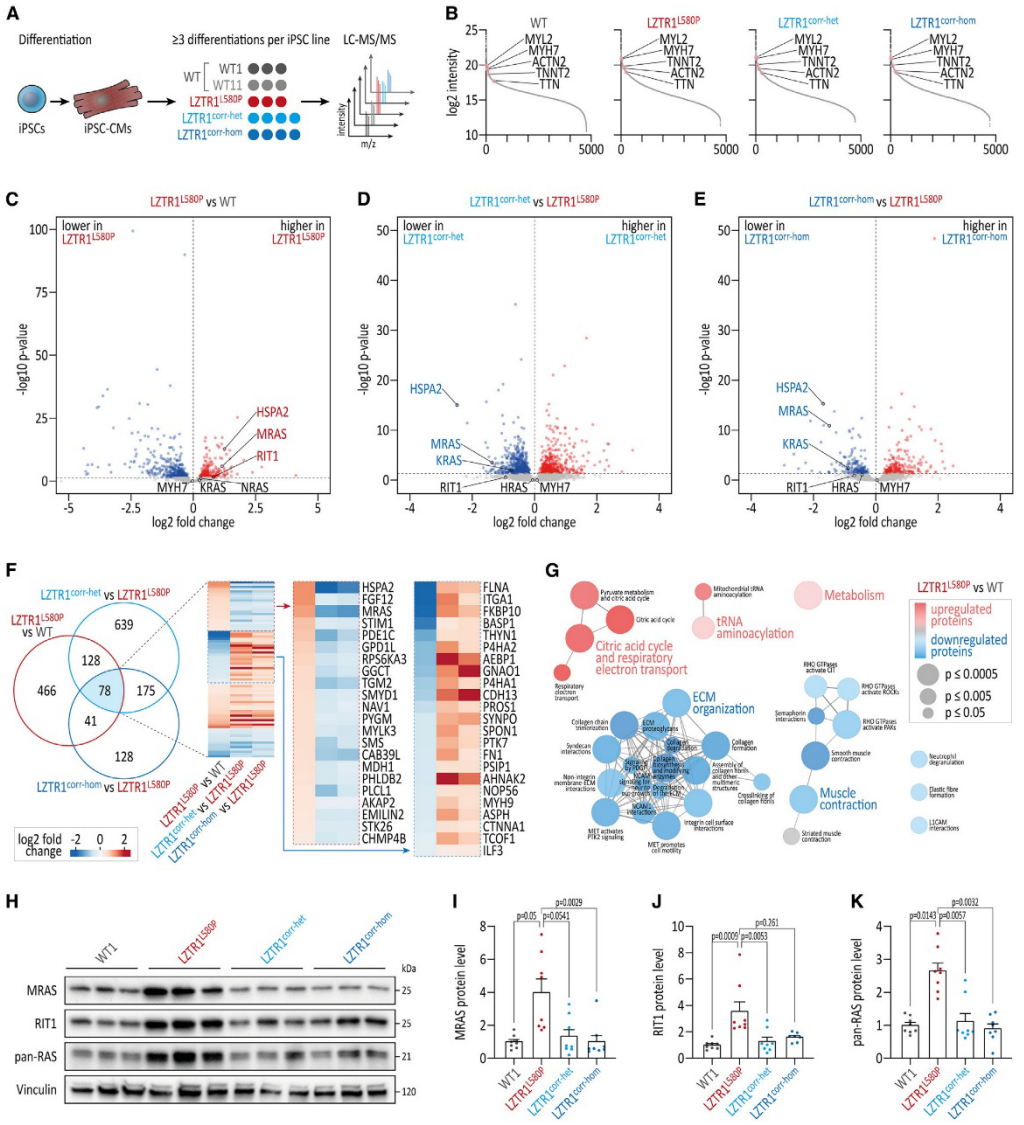

Figure 2. Homozygous *LZTR1*^{L580P} causes accumulation of RAS GTPases

(A) Two WT, the patient-specific, and the 2 CRISPR-corrected iPSC lines were differentiated into ventricular iPSC-CMs and analyzed by quantitative global proteomics via liquid chromatography-tandem mass spectrometry at day 60 of differentiation; $n = 3$–4 individual differentiations per iPSC line.

(B) Over 4,700 proteins were present in the individual proteomic samples, all showing comparable high abundance of cardiac markers myosin heavy-chain β (*MHY7*), cardiac troponin T (*TNNT2*), α-actinin (*ACTN2*), titin (*TTN*), and ventricular-specific MLC2V (*MYL2*).

(C–E) Volcano plots comparing patient's versus WT iPSC-CMs (C; LZTR1^{L580P} versus WT), heterozygous corrected versus non-corrected iPSC-CMs (D; LZTR1$^{corr\text{-}het}$ versus LZTR1^{L580P}), and homozygous corrected versus non-corrected iPSC-CMs (E; LZTR1$^{corr\text{-}hom}$ versus LZTR1^{L580P}) detected high abundance of RAS GTPases in patient samples.

(legend continued on next page)

of the overall heterozygosity. In addition, sequencing detected no obvious off-target modifications by genome editing (Figure S1). Subsequently, patient-derived and CRISPR-corrected iPSCs were verified for pluripotency (Figures 1F–1H). In addition to the patient-derived iPSC lines, iPSC lines from two unrelated healthy male donors, namely WT1 and WT11, were used as wild-type (WT) controls in this study.

At first, we aimed to determine whether the LZTR1^{L580P} protein remains stably expressed or is rapidly degraded after protein translation. LZTR1 proteins were robustly detected by western blot in differentiated iPSC-CMs (Figures 1I–1K). Interestingly, significantly higher LZTR1 protein levels were present in the patient-specific and the heterozygous corrected iPSC-CMs compared to WT and homozygous corrected cultures, suggesting an accumulation of the mutant LZTR1^{L580P} proteins.

Homozygous LZTR1^{L580P} causes accumulation of RAS GTPases

To investigate the impact of the identified homozygous *LZTR1*^{L580P} missense variant on the molecular mechanisms contributing to left ventricular hypertrophy, patient-specific, heterozygous and homozygous corrected, and two individual WT iPSC lines were differentiated into functional ventricular-like iPSC-CMs in feeder-free culture conditions,[19] and on day 60 of differentiation, subjected to unbiased proteome analyses (Figure 2A). We identified more than 4,700 proteins in the samples from the individual groups. All samples showed a comparably high abundance of prominent cardiac markers *MHY7*, *TNNT2*, *ACTN2*, and *TTN*, and ventricular-specific *MYL2*, indicating equal cardiomyocyte content in the different cultures (Figure 2B). By comparing the proteome profiles of LZTR1^{L580P} and WT iPSC-CMs, we identified enhanced abundance of the RAS family members muscle RAS oncogene homolog (MRAS) and RIT1 in the patient's iPSC-CMs (Figure 2C). This finding is in agreement with our previous observation in *LZTR1*-truncating variant carriers[10] and confirms the pivotal role of LZTR1 in targeting RAS GTPases for LZTR1-cullin 3 ubiquitin ligase complex-mediated ubiquitination and degradation.[8,9] Furthermore, it highlights that *LZTR1*^{L580P} results in protein loss of function, causing an accumulation of RAS proteins in the cells, which provides molecular evidence for the causative nature of the missense variant. Strikingly, protein levels of the RAS GTPases were normalized in both the heterozygous and the homozygous corrected iPSC-CMs, confirming that only one functional *LZTR1* allele is sufficient to regulate the protein pool of RAS GTPases in cardiomyocytes (Figures 2D and 2E). As anticipated, transcriptome analyses showed similar mRNA expression levels of RAS GTPases in the patient's and CRISPR-corrected iPSC lines, indicating a post-translational cause for the higher abundance of RAS proteins in LZTR1^{L580P} cultures (Figure S2). In contrast, the significantly elevated protein levels of the protein quality control-associated heat shock-related 70-kDa protein 2 (*HSPA2*) in the patient's cells in comparison to the WT and CRISPR-corrected cells were related to the upregulation of gene expression, suggesting that HSPA2 is not directly targeted by LZTR1 for degradation.

To assess the correlation of proteomic signatures with *LZTR1* deficiency, we performed a comparative analysis of (1) LZTR1^{L580P} versus WT, (2) LZTR1$^{corr\text{-}het}$ versus LZTR1^{L580P}, and (3) LZTR1$^{corr\text{-}hom}$ versus LZTR1^{L580P}. We found 78 proteins being differentially regulated in all 3 datasets (Figure 2F). Here, a profound subset of proteins that were significantly higher abundant in the patient's cells, such as the MAPK-activated protein kinase RPS6KA3, were normalized after heterozygous and homozygous CRISPR correction of the pathological *LZTR1* variant. Vice versa, numerous downregulated proteins in the patient samples were found to be elevated in the gene-edited iPSC-CMs. We performed a Reactome pathway enrichment analysis to detect dysregulated pathways and/or biological processes associated with *LZTR1*^{L580P}. Differentially abundant proteins in patient-derived samples were enriched in critical cardiac-related biological processes, such as muscle contraction and extracellular matrix organization, as well as in cellular routes associated with metabolism (Figure 2G). Consistent with the proteomic data, western blot analysis confirmed the strong accumulation of MRAS, RIT1, and the classical RAS GTPases (HRAS, KRAS, and NRAS; detected by pan-RAS) in the LZTR1^{L580P} cultures, and illustrated a normalization of RAS levels in the CRISPR-corrected isogenic iPSC-CMs to WT control levels (Figures 2H–2K).

Collectively, these data demonstrate that the missense variant *LZTR1*^{L580P} in homozygosity resulted in protein loss of function, causing an accumulation of RAS GTPases as the critical underlying disease mechanism in cardiomyocytes from the NS patient, and with this, correction of the homozygous missense variant on at least one allele normalized the molecular pathology.

Homozygous LZTR1^{L580P} does not induce strong ERK hyperactivity

To explore the impact of RAS GTPase accumulation on RAS-MAPK signaling activity, we used an ERK kinase translocation reporter (ERK-KTR) to measure ERK signaling dynamics in live cells.[20] Patient-specific, heterozygous and homozygous corrected, and WT iPSC-CMs were efficiently transduced with the ERK-KTR lentivirus, and the activity of ERK was analyzed at day 60 of differentiation by measuring the ratio of cytosolic (corresponding to active ERK) to nuclear (corresponding to inactive ERK) fluorescent signals (Figures 3A and 3B). The specificity of the ERK biosensor was confirmed by a selective response to MEK inhibition, whereas no change in ERK biosensor activity

(F) Comparison of differentially abundant proteins between the 3 datasets identified an overlap of 78 proteins, many of which showed opposite abundance in patient's versus CRISPR-corrected iPSC-CMs.
(G) Reactome pathway enrichment analysis of differentially abundant proteins in LZTR1^{L580P} versus WT displayed dysregulation of cardiac-related processes.
(H) Representative blots of RAS GTPase levels in iPSC-CMs at day 60 of differentiation, assessed by western blot; vinculin served as loading control; $n = 3$ individual differentiations per iPSC line.
(I–K) Quantitative analysis of western blots for MRAS (I), RIT1 (J), and pan-RAS recognizing HRAS, KRAS, and NRAS (K); data were normalized to total protein and to the corresponding WT samples on each membrane; $n = 8$ independent differentiations per iPSC line. Data were analyzed by non-parametric Kruskal-Wallis test with Dunn correction and are presented as mean ± SEM (I–K).

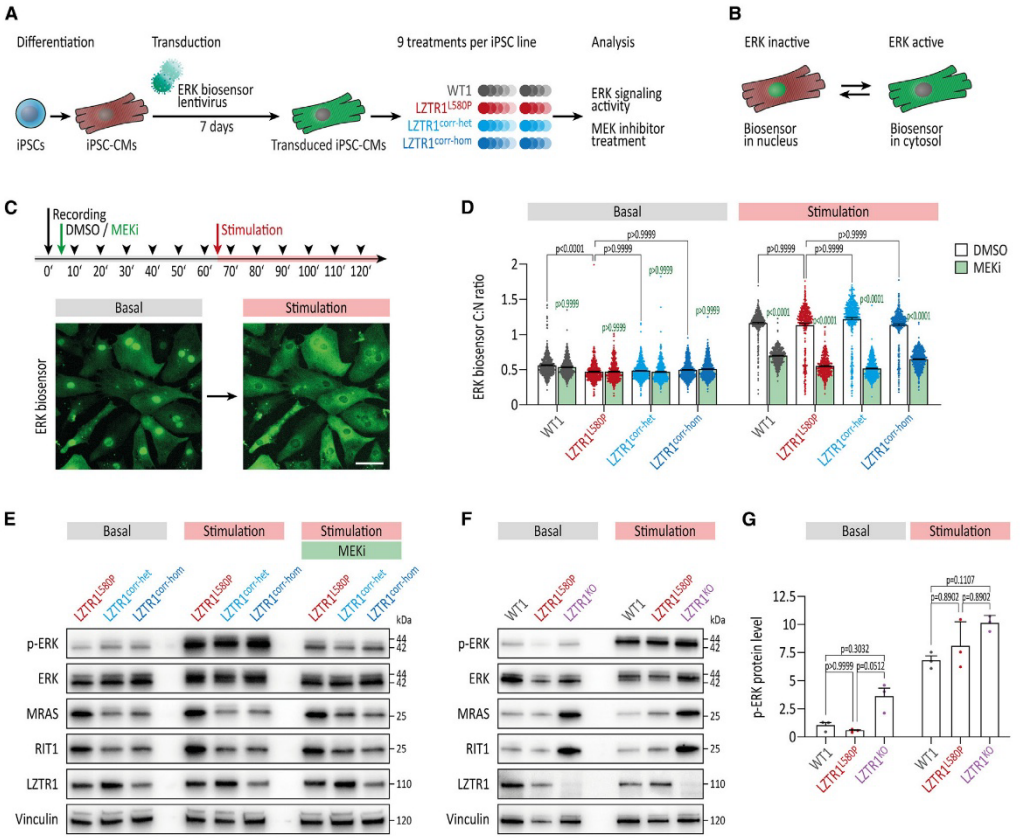

Figure 3. Homozygous *LZTR1*^{L580P} does not induce strong ERK hyperactivity

(A) WT, the patient-specific, and the 2 CRISPR-corrected iPSC lines were differentiated into ventricular iPSC-CMs and transduced around day 50 of differentiation with lentivirus containing an ERK kinase translocation reporter (ERK-KTR) to measure ERK signaling dynamics in real time.

(B) ERK activity was analyzed by measuring the ratio of cytosolic (corresponding to active ERK) to nuclear (corresponding to inactive ERK) fluorescent signals.

(C) Biosensor-transduced iPSC-CMs were treated with MEKi trametinib or with DMSO for 60 min, before stimulation with serum for another 60 min, and imaged every 10 min.

(D) Quantitative analysis of ERK biosensor cytosol:nucleus (C:N) ratio under basal conditions (60 min after MEKi/DMSO treatment) and 20 min after stimulation; $n = 2$ independent differentiations per iPSC line, with $n = 4–5$ individual wells per condition.

(E) Representative blots of p-ERK, ERK, MRAS, RIT1, and LZTR1 levels in iPSC-CMs at day 60 of differentiation under basal conditions and 30 min after stimulation with and without pre-treatment with MEKi, assessed by western blot; vinculin served as loading control.

(F) Representative blots of p-ERK, ERK, MRAS, RIT1, and LZTR1 levels in iPSC-CMs at day 60 of differentiation under basal conditions and 30 min after stimulation, assessed by western blot; vinculin served as loading control.

(G) Quantitative analysis of western blots for p-ERK protein levels; data were normalized to total protein and to the corresponding WT samples on each membrane; $n = 3$ independent differentiations per iPSC line.

Data were analyzed by non-parametric Kruskal-Wallis test with Dunn correction and are presented as mean ± SEM (D and G).

was observed when cells were treated with an inhibitor of the JNK pathway (Figure S3). Biosensor-transduced iPSC-CM cultures were treated with the MEK inhibitor (MEKi) trametinib or with DMSO for 60 min, before stimulation with fetal bovine serum for another 60 min, and imaged every 10 min (Figures 3C and S3). Under basal conditions, an equally low level of ERK activity was observed across all iPSC lines (Figure 3D). As expected, a strong increase in ERK activity was detected upon stimulation of the cells, while MEK inhibition was effective in normalizing ERK signaling activity (Figure 3D). The results of the imaging-based approach were confirmed by western blot analysis of uncorrected and CRISPR-corrected iPSC-CMs (Figure 3E).

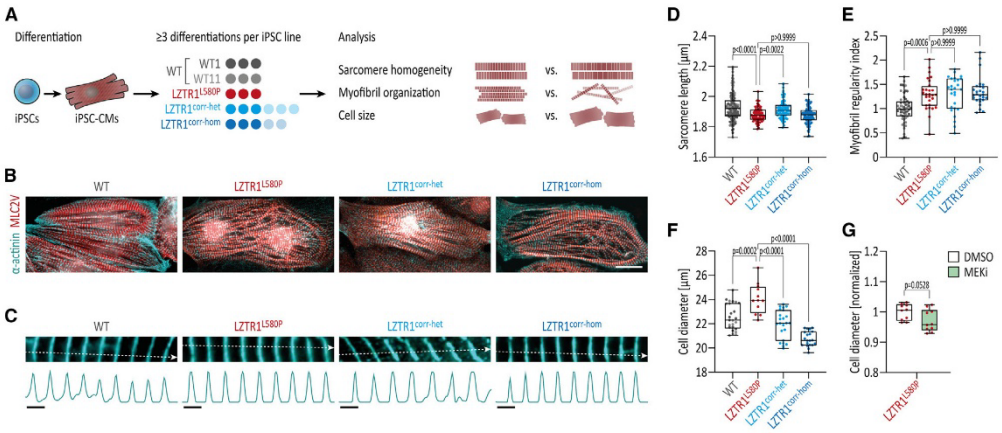

Figure 4. Homozygous *LZTR1*^{L580P} provokes cardiomyocyte hypertrophy

(A) Two WT, the patient-specific, and the 2 CRISPR-corrected iPSC lines were differentiated into ventricular iPSC-CMs and analyzed for sarcomere length, myofibril organization, and cell size at day 60 of differentiation.

(B) Representative images of iPSC-CMs stained for α-actinin and ventricular-specific MLC2V indicated a regular and well-organized sarcomeric assembly across all iPSC lines; scale bar: 20 μm.

(C) Analysis of the mean sarcomere length per cell was based on measurement of multiple α-actinin-stained individual myofibrils; representative myofibrils and corresponding intensity plots are shown; scale bar: 2 μm.

(D) Quantitative analysis displayed a typical sarcomere length in iPSC-CMs ranging from 1.7 to 2.2 μm across all iPSC lines; n = 75–135 cells from 3 individual differentiations per iPSC line.

(E) Quantitative analysis of the myofibril organization in iPSC-CMs, assessed by fast Fourier transform algorithm, demonstrated a high myofibril regularity across all iPSC lines; data were normalized to WT; n = 27–58 images from 3 individual differentiations per iPSC line.

(F) Quantitative analysis of the cell diameter in suspension in singularized iPSC-CMs, assessed by CASY cell counter, detected a hypertrophic cell diameter in the patient's cells, compared with WT and CRISPR-corrected iPSC-CMs; n = 12–25 samples from 3 to 6 individual differentiations per iPSC line.

(G) Quantitative analysis of the cell diameter in suspension in singularized patient-specific iPSC-CMs that were treated with MEKi trametinib or with DMSO for 5 days, assessed by CASY cell counter; n = 3 independent differentiations, with n = 3–4 individual wells per condition.

Data were analyzed by non-parametric Kruskal-Wallis test with Dunn correction (D–F) or unpaired t test (G) and are presented as mean ± SEM.

Since we did not observe increased ERK activity attributed to the homozygous *LZTR1*^{L580P} missense variant, we compared the patient-specific LZTR1^{L580P} cells with another patient line harboring biallelic truncating *LZTR1* variants (LZTR1^{KO}), which we reported in our previous study.[10] Here, higher levels of phosphorylated ERK were observed in the LZTR1^{KO} cultures under basal conditions and after stimulation (Figures 3F and 3G). Interestingly, LZTR1^{KO} iPSC-CMs exhibited a substantially higher accumulation of RAS GTPases compared to LZTR1^{L580P} cells, implying a partial residual function of LZTR1^{L580P} ubiquitin ligase complexes.

Homozygous LZTR1^{L580P} provokes cardiomyocyte hypertrophy

To elucidate the consequences of dysregulated RAS-MAPK signaling on the cellular characteristics of cardiomyocytes, we investigated sarcomere homogeneity, myofibril organization, and cell size of the patient-derived iPSC-CMs, the CRISPR-corrected cells, and WT controls at day 60 of differentiation (Figure 4A). All iPSC lines showed a well-organized sarcomeric organization with a pronounced striated expression of α-actinin and ventricular-specific MLC2V (Figure 4B). To analyze sarcomeric homogeneity, we measured the distances between the sarcomeric Z disks along individual myofibrils (Figure 4C). In agreement with the sarcomere length previously observed in neonatal and adult human hearts,[21] *LZTR1*-deficient as well as *LZTR1*-corrected and WT cells exhibited a typical sarcomere length ranging from 1.7 to 2.2 μm, with an average of approximately 1.9 μm across all iPSC lines (Figure 4D). As sarcomeric disarray has been frequently reported in other iPSC-CM models of both NS-associated and non-syndromic HCM,[15,22] we examined the myofibril organization in the individual iPSC-CMs. Quantitative analysis showed no decrease in sarcomere regularity or pathological myofibril organization in LZTR1^{L580P} cultures (Figure 4E). On the contrary, LZTR1^{L580P} and CRISPR-corrected iPSC-CMs even demonstrated a slightly higher myofibril regularity compared to unrelated controls, indicating that the pathological gene variant exerts no severe effect on sarcomere structures.

Since cardiomyocyte hypertrophy is a major hallmark of HCM, we further investigated the mean cell size of iPSC-CMs from all cell lines by utilizing our previously established assay to determine cell size in suspension.[10] Here, the patient's iPSC-CMs displayed a significant cellular enlargement compared to WT iPSC-CMs (Figure 4F). Strikingly, the hypertrophic phenotype was normalized in the CRISPR-corrected cells from both the

LZTR1$^{corr\text{-}het}$ and the LZTR1$^{corr\text{-}hom}$ isogenic cultures. Moreover, and in line with the molecular observations, heterozygous correction of the pathological variant was sufficient to significantly reduce cellular hypertrophy. Additionally, we assessed whether treatment with the MEK inhibitor trametinib for 5 days could reverse the cellular hypertrophy in the patient-specific iPSC-CMs (Figure 4G). No significant reduction in cell size was observed in MEKi-treated cells compared to DMSO-treated cells, suggesting that normalization of RAS-MAPK signaling activity is unable to alleviate the cellular pathology in the short term.

In summary, the patient's iPSC-CMs harboring the homozygous missense variant *LZTR1*^{L580P} recapitulated the cardiomyocyte hypertrophy *in vitro*. Importantly, CRISPR correction of the pathological variant was able to normalize the hypertrophic phenotype.

Homozygous LZTR1^{L580P} does not compromise contractile function

NS-associated and non-syndromic HCM are frequently associated with contractile dysfunction, and these patients are at risk of developing arrhythmias.[23,24] We generated engineered heart muscles (EHMs) from diseased, CRISPR-corrected, and WT iPSC-CMs enabling us to investigate the functional characteristics in a three-dimensional environment more closely resembling the native conditions of the human heart muscle (Figure S4A).[25,26] Microscopically, all iPSC lines formed homogeneous cardiac tissues without showing apparent cell line-dependent differences after 6 weeks of maturation (Figure S4B). Optical measurements were performed to study beating rate, force of contraction, and contraction kinetics in spontaneously contracting EHMs (Figures S4C–S4H). In comparison to WT EHMs, an increased spontaneous beat frequency was detected in the LZTR1^{L580P} EHMs. The beat rate acceleration was gradually normalized in the heterozygous and homozygous corrected variants. Low beat-to-beat variability indicated that the LZTR1 mutant tissues do not provoke arrhythmia. No significant differences in force of contraction were identified. In accordance with higher beat frequencies, an acceleration of contraction and relaxation kinetics were observed in LZTR1^{L580P}-, LZTR1$^{corr\text{-}het}$-, and the LZTR1$^{corr\text{-}hom}$-derived EHMs. However, since the altered kinetics were noticed in both diseased and CRISPR-corrected tissues, this rather suggested a mutation-independent effect. In addition, we examined the contractile properties of monolayer cultures by video analysis and did not observe any significant differences between WT, patient-specific, CRISPR-corrected, and LZTR1^{KO} iPSC-CMs (Figure S5).

Taken together, these functional data indicate that the missense variant *LZTR1*^{L580P} does not impact the contractile function and rhythmogenesis of cardiomyocytes.

Homozygous LZTR1^{L580P} induces polymerization of LZTR1 proteins

Considering the severe consequence of *LZTR1*^{L580P} on the molecular and cellular pathophysiology in cardiomyocytes, we aimed to determine the specific effect of this variant on protein structure, complex formation, as well as its subcellular localization. We were unable to visualize endogenous LZTR1 in our cell model by immunocytochemistry, by testing several commercial antibodies, or by N-terminal or C-terminal genetic tagging of the *LZTR1* gene locus. To circumvent these obstacles, we established ectopic expression of tagged *LZTR1* in WT iPSC-CMs at around day 60 of differentiation by lipofectamine-based plasmid transfection (Figure 5A). Besides *LZTR1*^{WT} and *LZTR1*^{L580P}, we screened the NS patient database (NSeuroNet)[27] for additional missense variants classified as likely pathogenic or variant of uncertain significance and located in close proximity to *LZTR1*^{L580P} (within the BACK1 domain), and included them in our screening panel (Figure 5B). Of note, except for *LZTR1*^{L580P} and *LZTR1*^{E563Q},[7] none of the other variants had been reported to be present in homozygosity in *LZTR1*-associated NS. In addition, we included a truncating variant *LZTR1*$^{\Delta BTB2\text{-}BACK2}$, which lacks the entire BTB2-BACK2 domain and mimics the genotype of the two siblings described in our previous study.[10]

As previously observed in other cell types (e.g., HeLa,[8] HEK293[28]), LZTR1^{WT} appeared as a dotted pattern evenly distributed throughout the cell (Figures 5C and S6A). A similar dotted appearance was observed for the variants LZTR1^{E563Q}, LZTR1^{I570T}, LZTR1^{V579M}, LZTR1^{E584K}, and LZTR1^{R619H}. As expected, the truncating variant LZTR1$^{\Delta BTB2\text{-}BACK2}$ showed a mislocalized homogeneous cytoplasmic distribution. Surprisingly, LZTR1^{L580P} formed large filaments in the cytoplasm (Figures 5C and S6A). To verify this initial finding, we co-expressed two differentially tagged *LZTR1* constructs and evaluated their overlap within the cells. Consistently, LZTR1^{L580P} appeared as large protein polymers, whereas LZTR1^{WT} remained speckle-like (Figure 5D). As *LZTR1*^{L580P} in the heterozygous state did not induce a disease phenotype based on clinical and experimental evidence, we hypothesized that the co-expression of LZTR1^{L580P} and LZTR1^{WT} might resolve the polymer chains. Strikingly, the LZTR1^{L580P}-induced filaments dispersed when co-expressed with the WT variant, implicating that the LZTR1 complexes exclusively assemble into protein polymers when the specific *LZTR1*^{L580P} missense variant is present on both alleles (Figure 5E). To quantitatively analyze these observations, we established an automated image-based speckle/filament recognition and computation (Figure S6B). While LZTR1^{WT} displayed a mean speckle size of 0.9 μm, the mean filament length per cell in LZTR1^{L580P} amounted to 7.9 μm (Figure 5F). Co-expression of mutant and WT constructs, and vice versa, normalized the speckle size to 1.2 μm and 1.3 μm, respectively.

These data provide evidence that the missense variant *LZTR1*^{L580P} induces polymerization of LZTR1 proteins, which may subsequently compromise the proper function of the ubiquitination machinery.

Homozygous LZTR1^{L580P} alters binding affinities of dimerization domains

Proteins from the BTB-BACK-Kelch domain family, including LZTR1, are predicted to assemble into homo-dimers.[9,28,29] However, our current knowledge regarding the exact domains responsible for LZTR1 dimerization is limited. To identify a plausible explanation for the *LZTR1*^{L580P}-induced polymerization, we utilized ColabFold, an AlphaFold-based platform for predicting protein structures and homo- and heteromer complexes.[30] We used a homo-trimer configuration of the experimentally

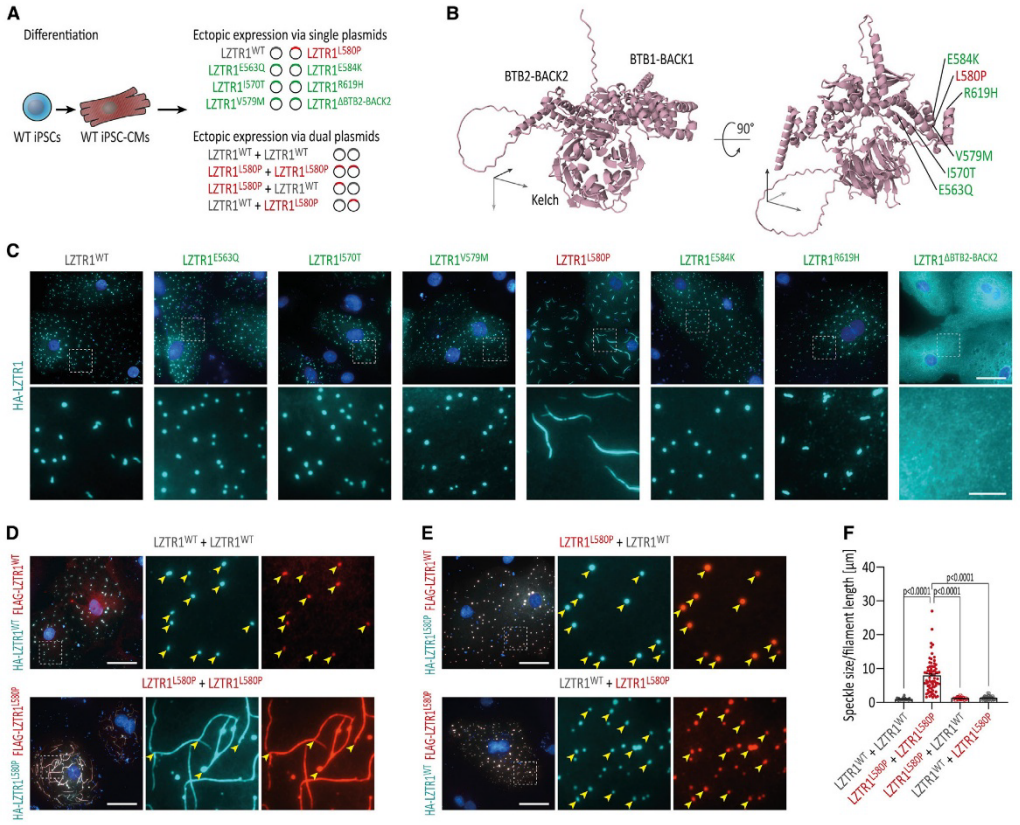

Figure 5. Homozygous *LZTR1*^{L580P} induces polymerization of LZTR1 proteins

(A) WT iPSCs were differentiated into ventricular iPSC-CMs, transfected at day 60 of differentiation with plasmids for ectopic expression of LZTR1 variants, and analyzed 24 h post-transfection for subcellular localization LZTR1 complexes.

(B) AlphaFold protein structure of monomeric LZTR1 highlighting the location of selected variants within the BACK1 domain.

(C) Representative images of iPSC-CMs after single plasmid transfection stained for hemagglutinin (HA)-tagged LZTR1 showed that LZTR1^{WT} and most other variants present a speckle-like pattern equally distributed throughout the cytoplasm, whereas missense variant LZTR1^{L580P} forms large filaments; nuclei were counter-stained with Hoechst 33342 (blue); scale bars: 20 µm (top), 5 µm (bottom).

(D and E) Representative images of iPSC-CMs after dual plasmid transfection stained for HA-tagged and FLAG-tagged LZTR1 confirmed the filament formation of LZTR1^{L580P} (D), whereas co-expression of LZTR1^{WT} and LZTR1^{L580P} in different combinations resolved the polymer chains (E); nuclei were counter-stained with Hoechst 33342 (blue); scale bar: 20 µm.

(F) Quantitative analysis of the mean speckle size and mean filament length per cell of HA-tagged LZTR1 in co-transfected iPSC-CMs, assessed by a customized CellProfiler pipeline, confirmed the formation of *LZTR1*^{L580P}-induced filaments; n = 34–74 cells per condition. Data were analyzed by non-parametric Kruskal-Wallis test with Dunn correction and are presented as mean ± SEM (F).

employed *LZTR1* variants (all within the BACK1 domain), and the AlphaFold-multimer predicted five high-quality models, each with an average predicted local distance difference test (a per-residue confidence metric) between 64.1 and 76.0. For all variants, we inspected the interaction between the chains through the predicted alignment error (PAE) generated by AlphaFold-multimer (Figure S7). A low PAE indicates that interfacing residues were correctly predicted across chains. Based on these predictions, we compared the top-ranked models of each variant according to the predicted template modeling score, which corresponded to overall topological accuracy (Figure 6A). The top-ranked model for LZTR1^{WT} showed interaction as a homo-dimer via the BACK2-BACK2 domain, while the third LZTR1 protein remained monomeric. We also observed the identical dimerization via the BACK2 domains for all other variants, except for LZTR1^{L580P} (Figure S7). In contrast, the top-ranked

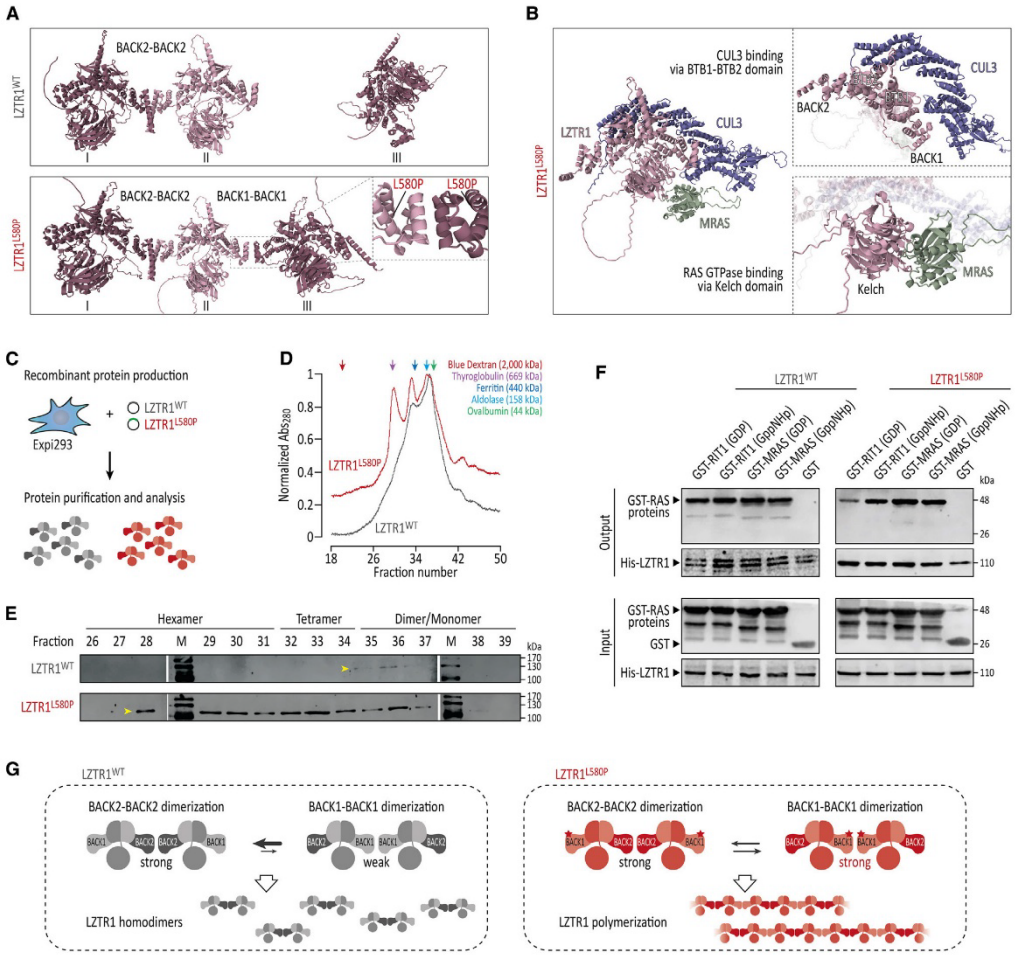

Figure 6. Homozygous *LZTR1*^{L580P} alters binding affinities of dimerization domains

(A) Computational modeling of the top-ranked LZTR1 homo-trimer interactions by ColabFold predicted a dimer plus monomer configuration via BACK2-BACK2 dimerization for LZTR1^{WT}, whereas LZTR1^{L580P} was predicted to form linear trimers via BACK2-BACK2 and BACK1-BACK1 dimerization.

(B) Computational modeling of the interaction between LZTR1^{L580P} and its binding partners predicted binding to cullin 3 (CUL3) via the BTB1-BTB2 domain and to MRAS via the Kelch domain.

(C) Production of LZTR1^{WT} and LZTR1^{L580P} recombinant proteins from Expi-293F cells for characterization of molecular masses of proteins and protein complexes.

(D) Analytical size-exclusion chromatography of soluble recombinant LZTR1 proteins detected a higher-order oligomerization profile for LZTR1^{L580P} compared to the less complex elution profile of LZTR1^{WT}.

(E) Immunoblotting of the fractions showed elution of LZTR1^{L580P} as hexamer, tetramer, and dimer/monomer, whereas LZTR1^{WT} eluted predominantly as dimer/monomer.

(F) Pull-down assay analysis showed comparable binding affinities of LZTR1^{WT} and LZTR1^{L580P} with MRAS and RIT1 proteins in both inactive (GDP-bound) and active (GppNHp-bound) states.

(G) Model for LZTR1 complex formation: whereas LZTR1^{WT} assembles in homo-dimers via the BACK2-BACK2 dimerization domain, LZTR1^{L580P} may alter the binding affinity of the BACK1 domain, causing the formation of linear LZTR1 polymer chains via dimerization of both BACK2 and BACK1 domains.

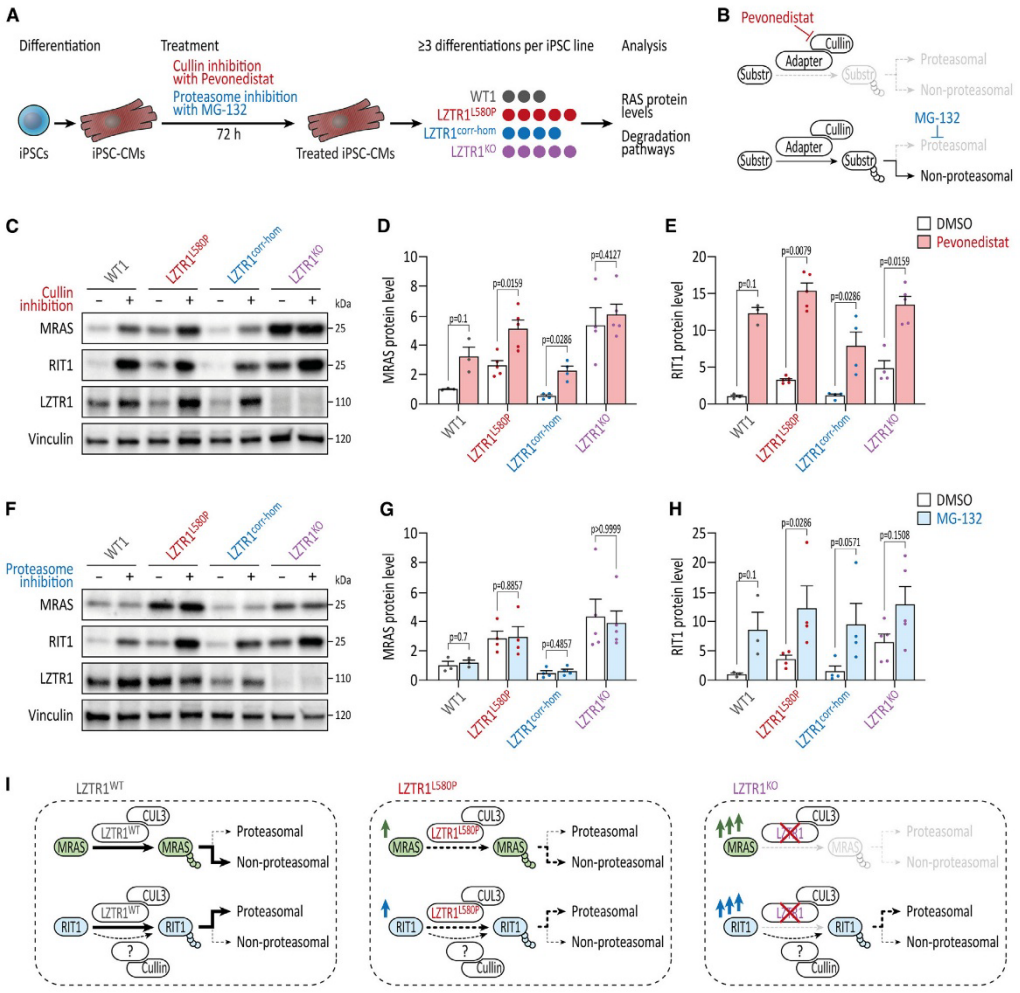

Figure 7. Homozygous *LZTR1*^{L580P} retains residual protein

(A) WT, the patient-specific, the homozygous CRISPR-corrected, and LZTR1^{KO} iPSC lines were differentiated into ventricular iPSC-CMs and treated with pevonedistat and MG-132 for 3 days to analyze the ubiquitin-mediated degradation of RAS GTPases; n = 3–5 individual differentiations/treatments per iPSC line.

(B) Mode of action of pevonedistat and MG-132 on degradation pathways: pevonedistat is a selective NEDD8-activating enzyme inhibitor, preventing neddylation of cullin RING ligases and blocking ubiquitin-mediated degradation via the proteasome and other degradation pathways, whereas MG-132 is a selective inhibitor specifically blocking the proteolytic activity of the 26S proteasome.

(C) Representative blots showing MRAS, RIT1, and LZTR1 levels in iPSC-CMs upon pevonedistat treatment for 3 days, assessed by western blot; vinculin served as loading control.

(D and E) Quantitative analysis of western blots for MRAS (D) and RIT1 (E) upon pevonedistat treatment; data were normalized to total protein and to the DMSO-treated WT samples on each membrane.

(F) Representative blots showing MRAS, RIT1, and LZTR1 levels in iPSC-CMs upon MG-132 treatment for 3 days, assessed by western blot; vinculin served as loading control.

(G and H) Quantitative analysis of western blots for MRAS (G) and RIT1 (H) upon MG-132 treatment; data were normalized to total protein and to the DMSO-treated WT samples on each membrane.

(legend continued on next page)

model for LZTR1^{L580P} predicted an interaction between all three chains, on the one hand via the BACK2-BACK2 domain and on the other hand via the BACK1-BACK1 domain (Figure 6A). In addition, we used AlphaFold-multimer to predict the interaction of LZTR1^{L580P} with the substrate MRAS and the ubiquitin ligase cullin 3 (Figure 6B). Within the multiprotein complex, MRAS was predicted to bind to the Kelch domain, whereas cullin 3 was predicted to interact with the BTB1-BTB2 domain of LZTR1.

To experimentally confirm the formation of LZTR1^{L580P} polymers, we produced soluble recombinant proteins of LZTR1^{WT} and LZTR1^{L580P} and analyzed the purified samples by analytical size-exclusion chromatography, allowing us to characterize the molecular masses of protein complexes (Figure 6C). A higher-order oligomerization profile was observed for LZTR1^{L580P}, whereas LZTR1^{WT} exhibited a less complex elution profile (Figure 6D). Immunoblotting of the fractions showed that LZTR1^{L580P} eluted as a hexamer with a molecular weight of approximately 700 kDa, as a tetramer corresponding to 450–550 kDa, and as a dimer/monomer with a molecular weight of 100–200 kDa (Figure 6E). In contrast, LZTR1^{WT} was characterized by a single peak, indicative of its predominantly dimeric/monomeric state. In addition, we examined the interaction of LZTR1^{WT} and LZTR1^{L580P} proteins with RIT1 and MRAS in their inactive (guanosine diphosphate [GDP]-bound) and active (GppNHp-bound; GppNHp is a non-hydrolyzable GTP analog) states. Both LZTR1^{WT} and mutant LZTR1^{L580P} were capable of binding their substrates in both nucleotide-bound states (Figure 6F).

Collectively, the *in silico* predictions and molecular analyses suggest that the missense variant *LZTR1^{L580P}* alters the binding affinities of the BACK1 domain, enabling the formation of linear LZTR1 polymer chains via both dimerization domains, thereby providing a rationale for the molecular and cellular impairments in NS (Figure 6G).

Homozygous LZTR1^{L580P} retains residual protein function

To investigate how severely the degradation of RAS GTPases is affected by the missense variant LZTR1^{L580P} (especially compared to the complete loss of LZTR1), we treated the patient-specific iPSC-CMs, the CRISPR-corrected cells, the LZTR1^{KO} cells, and the WT controls with the cullin RING ligase inhibitor pevonedistat (which blocks the ubiquitin-mediated degradation via the proteasome and other degradation pathways) or the proteasome inhibitor MG-132 and analyzed MRAS and RIT1 protein levels 3 days after treatment (Figures 7A and 7B). As expected, the inhibition of cullin-mediated ubiquitination by pevonedistat increased MRAS and RIT1 protein levels in WT and CRISPR-corrected iPSC-CMs (Figures 7C–7E). Treatment in patient-specific LZTR1^{L580P} cultures further increased the RAS GTPase levels, indicating residual function of the LZTR1^{L580P}-cullin 3 ubiquitin ligase complex. Interestingly, while MRAS accumulation in LZTR1^{KO} cultures could not be further increased by cullin inhibition, RIT1 protein levels were significantly higher after treatment in *LZTR1*-deficient cells. This suggests that MRAS is exclusively targeted for degradation by the LZTR1-cullin 3 ubiquitin ligase complex, whereas RIT1 can be additionally degraded in an *LZTR1*-independent manner. Furthermore, inhibition of the ubiquitin-proteasome system resulted in increased RIT1 levels, suggesting that RIT1 is predominantly degraded by the proteasomal pathway (Figures 7F–7H). In contrast, MRAS levels were not affected after treatment across all iPSC lines, indicating the degradation of MRAS by predominantly non-proteasomal pathways.

These data confirm that the missense variant *LZTR1^{L580P}* preserves some residual function compared to the complete loss of *LZTR1*. Furthermore, the results demonstrate that degradation of cardiomyocyte-specific MRAS is exclusively mediated by LZTR1 via non-proteasomal pathways, whereas degradation of RIT1 is mediated by both *LZTR1*-dependent and *LZTR1*-independent pathways.

DISCUSSION

Both autosomal dominant and autosomal recessive forms of *LZTR1*-associated NS have been described presenting with a broad clinical spectrum and various phenotypic expressions of symptoms. However, the mechanistic consequences of many of these mutations, mostly classified as variants of uncertain significance, are still under debate. In previous studies, we and others elucidated the role of LZTR1 as a critical negative regulator of the RAS-MAPK pathway by controlling the pool of RAS GTPases.[8–10,28,31] Using patient-derived iPSC-CMs from NS patients with biallelic truncating *LZTR1* variants, we have shown that *LZTR1* deficiency results in the accumulation of RAS levels, signaling hyperactivity and cardiomyocyte hypertrophy.[10] Furthermore, by genetically correcting one of the two affected alleles, we could show that one functional *LZTR1* allele is sufficient to maintain normal RAS-MAPK activity in cardiac cells. In contrast to the truncating variants, dominant *LZTR1* missense variants generally cluster in the Kelch motif. Based on heterologous expression systems, these dominant variants are considered to interfere with the recognition or binding of RAS substrates to the LZTR1 ubiquitination complex.[8,9,11,31] Much less is known about the functional relevance of recessive *LZTR1* missense variants, which are distributed throughout the entire protein. Detailed insights into specific structure-function relationships of LZTR1 are crucial to facilitate the development of patient-specific therapies.

In this study, we diagnosed a patient who presented with typical clinical features of NS, including an early-onset HCM, and confirmed this diagnosis on a genetic level by identifying the homozygous variant c.1739T>C/p.L580P in *LZTR1*. The variant has not been previously described in patients with NS,

(I) Model for LZTR1-mediated degradation of MRAS and RIT1 for LZTR1^{WT}, LZTR1^{L580P}, and LZTR1^{KO}: (left) MRAS is exclusively targeted by the LZTR1^{WT}-cullin 3 ubiquitin ligase complex for degradation, whereas RIT1 is additionally ubiquitinated by other cullin ubiquitin ligases and degraded predominantly by the proteasome; (center) the LZTR1^{L580P} decreases degradation of MRAS and RIT1; and (right) loss of LZTR1 completely prevents MRAS degradation, while RIT1 degradation remains functional to some extent in an LZTR1-independent manner.
Data were analyzed by non-parametric Kruskal-Wallis test with Dunn correction and are presented as mean ± SEM (D, E, G, and H).

and we classified *LZTR1*^{L580P} as likely causative based on its absence in gnomAD and our computational prediction. Apart from the *LZTR1* variant, no additional variants were detected in other NS-associated genes or RAS-associated candidates. By combining *in vitro* disease modeling using patient-specific and CRISPR-Cas9-corrected iPSC-CMs with molecular and cellular phenotyping and *in silico* structural modeling, we identified a *LZTR1*^{L580P}-specific disease mechanism provoking the cardiac pathology of NS. In detail, we found that (1) *LZTR1*^{L580P} is predicted to alter the binding affinity of the BACK1 dimerization domain that facilitates the formation of linear LZTR1 protein chains; (2) homozygous *LZTR1*^{L580P} fosters the assembly of large polymers of LZTR1 proteins causing LZTR1 complex dysfunction; (3) pathological LZTR1 complexes result in impaired degradation and accumulation of RAS GTPases and RAS-MAPK signaling hyperactivity; and (4) increased signaling activity induces global changes in the proteomic landscape, ultimately causing cellular hypertrophy. Importantly, correction of one allele—in line with the co-expression of WT and mutant *LZTR1* transcripts—is sufficient to normalize the cardiac disease phenotype at both molecular and cellular levels.

Based on recent publications, there is a broad consensus on the role of LZTR1 as an adaptor protein for the cullin 3 ubiquitin ligase complex targeting RAS proteins for ubiquitination and subsequent degradation.[8–11,28,31] In line with observations in other NS-associated genes and mutations, LZTR1 dysfunction and concomitant accumulation of RAS GTPases result in the hyperactivation of RAS-MAPK signaling. We confirmed robustly elevated RAS levels in patient-specific cells harboring the homozygous *LZTR1*^{L580P} missense variant. However, the accumulation of RAS GTPases and ERK hyperactivity was substantially higher in LZTR1^{KO} cells, supporting a partial residual function of LZTR1^{L580P} ubiquitin ligase complexes. Furthermore, it remains controversial whether LZTR1 is able to recognize all members of the RAS GTPase family for degradation or whether there is a selective affinity toward particular RAS members. Using heterologous expression systems, LZTR1 has been shown to interact with the highly conserved RAS proteins HRAS, KRAS, and NRAS.[8,28,31] However, Castel and colleagues observed a selective binding of LZTR1 to RIT1 and MRAS, but not to HRAS, KRAS, or NRAS.[9] Moreover, in homozygous *LZTR1* knockout mice, elevated RIT1 protein levels were detected in different organs, including brain, liver, and heart, while HRAS, KRAS, and NRAS levels remained unchanged.[32] Using global proteomics, we now provide further evidence that LZTR1 dysfunction in cardiomyocytes causes severe accumulation of MRAS and RIT1 and, to a lesser extent, elevation of the other RAS GTPases HRAS, KRAS, and NRAS, although all RAS proteins are robustly expressed in this cell type. We conclude that based on gene expression data and total protein levels, MRAS appears to be the most prominent RAS candidate in cardiomyocytes, driving the signaling hyperactivity in these cells. In addition, our inhibition experiments demonstrate that MRAS degradation is exclusively mediated by LZTR1 via proteasome-independent mechanisms, whereas RIT1 degradation is mediated by both LZTR1-dependent and LZTR1-independent pathways. These observations suggest that at endogenous expression levels, LZTR1 has a certain selectivity for MRAS and RIT1 and a lower affinity for the RAS GTPases HRAS, KRAS, and NRAS. However, we cannot exclude the possibility of cell-type-specific differences in LZTR1-RAS binding affinities.

Major hallmarks of pathological cardiac hypertrophy include impaired cardiac function, changes in extracellular matrix composition, fibrosis, and metabolic reprogramming and mitochondrial dysfunction.[33] In accordance, the proteomic disease signature of patient-derived iPSC-CM cultures detected impairments in muscle contraction, extracellular matrix organization, and metabolism—all crucial for proper cardiomyocyte function. Furthermore, *LZTR1*^{L580P}-derived iPSC-CMs recapitulated the patient's hypertrophic phenotype reflected by cellular enlargement. Strikingly, both the molecular profile and cellular hypertrophy were resolved upon CRISPR correction of the missense variant. Interestingly, no myofibrillar disarray was observed in our cell model. However, the presence of myofibril disarray in NS remains controversial: whereas structural defects were described in *RAF1*-associated iPSC models,[15,34] we and others did not observe any impact on sarcomere structures or myofibril organization in *LZTR1*-related, *PTPN11*-related, and *BRAF*-related iPSC-CMs,[10,14,16] implying potential genotype-dependent differences in the manifestation of myofibril disassembly in NS.

Missense variants in *LZTR1* located within the Kelch domain are predicted to affect substrate recognition, whereas missense variants in the BTB-BACK domain are assumed to impair either cullin 3 binding, proper homo-dimerization, or correct subcellular localization. Several studies have demonstrated that dominantly acting Kelch domain variants disrupt the recognition of RAS substrates but do not affect LZTR1 complex stability or subcellular localization.[8,9,11,31,35] In contrast, BTB-BACK missense variants showed no influence on RIT1 binding.[9,35] However, variants located in the BTB1 or the BTB2 domain, such as *LZTR1*^{V456G}, *LZTR1*^{R466Q}, *LZTR1*^{P520L}, and *LZTR1*^{R688C}, caused a subcellular mislocalization from defined speckles to a diffuse cytoplasmic distribution, similar to the findings obtained with truncating *LZTR1* variants.[8,31] In addition to these distinct pathological consequences of different variants analyzed so far, we now provide evidence for an alternative disease mechanism specific to the BACK1 domain-located *LZTR1*^{L580P}; ectopic expression of *LZTR1*^{L580P} in iPSC-CMs caused a pathological polymerization of LZTR1 ubiquitination complexes. This phenomenon was verified by *in silico* prediction and chromatography with purified recombinant LZTR1 proteins. In contrast, the binding probabilities of *LZTR1*^{L580P} to substrates and interaction partners were not significantly affected by the mutation. This remarkable phenotype was not observed for any other variant within the BACK1 domain. Notably, ectopic co-expression of *LZTR1*^{L580P} and *LZTR1*^{WT} alleviated polymerization, indicating that the assembly of LZTR1 polymer chains exclusively occurs when mutated proteins are present in the homozygous state. Oligomerization of another BTB-BACK family member had been reported previously: Marzahn and colleagues described that dimers from the cullin 3 ubiquitin ligase substrate adaptor SPOP (harboring only one BTB-BACK domain) self-associate into linear higher-order oligomers via BACK domain dimerization.[36] These SPOP oligomers assembled in membraneless cellular bodies, visualized as nuclear speckles, and it was proposed that the speckles may be important hotspots of ubiquitination. Based on these findings and our

data, we propose that LZTR1 complexes concentrate in cellular speckles (either as dimers or as oligomers) to form subcellular clusters for efficient ubiquitination and degradation of RAS proteins. However, *LZTR1*^{L580P}-induced polymerization of these complexes disrupts their proper function, leading to the accumulation of substrates. CRISPR-based correction was able to rescue the polymerization phenotype and may be a sustainable treatment option in the future. Alternatively, it may be possible to identify compounds that specifically prevent the interaction of LZTR1 complexes via BACK1-BACK1 dimerization.

Our knowledge of the specific domains responsible for LZTR1 homo-dimerization is still incomplete. While Castel and colleagues proposed that the BTB1 and the BACK1 domains are required for dimerization,[9] Steklov et al. observed impaired assembly in a BACK2 domain mutant *LZTR1* variant.[31] Based on *in silico* modeling, we now propose that LZTR1 can dimerize via either the BACK2-BACK2 domains or the BACK1-BACK1 domains. Although BACK2-BACK2 dimerization may be primarily utilized in LZTR1^{WT}, changes in the binding affinities of the BACK1 domain as a consequence of *LZTR1*^{L580P} facilitated tandem self-association of dimers to linear multimers.

Limitations of the study

So far, the relevance of certain *LZTR1* missense variants have been investigated in heterologous expression systems, failing to faithfully represent human cardiac physiology. Our study demonstrates the potential of patient-specific iPSCs to model human diseases and to detect variant-specific pathomechanisms. Despite the great advantages of this model system over other cellular models, iPSC-CMs possess certain limitations. As summarized by several reports, iPSC-CMs are considered to be developmentally immature characterized by molecular and functional properties similar to fetal CMs.[25,37,38] Although we complemented our study by utilizing three-dimensional EHMs, these *in vitro* models are currently not able to entirely resemble the disease phenotype at the organ level. EHM data showed altered kinetics between CRISPR-corrected and WT cells. Although these differences are likely consequences of different genetic backgrounds and potential disease-modifier variants, a manifested impairment in the patient fibroblasts (e.g., due to LZTR1 dysfunction) that persists after reprogramming and cardiac differentiation cannot be excluded. Due to unsuccessful genetic tagging of LZTR1 in iPSCs, the mutation-induced polymerization phenotype could only be observed by overexpression, which does not entirely reflect the endogenous condition. Furthermore, although different concentrations and time points were evaluated in iPSC-CMs prior to the inhibitor experiments, these experiments can only capture a snapshot of the degradation machinery, and additional experiments may be necessary to fully dissect the degradation pathway of RAS proteins. Although the *in silico* modeling by AlphaFold was consistent with the experimental data, this analysis must be undertaken with caution because the AlphaFold-multimer was not trained with single point variants in mind. In addition, due to technical prerequisites, we were unable to predict whether the trend would remain consistent for complexes with more than three chains.

Taken together, this study identified a specific mechanism causing recessive NS, which is initiated by *LZTR1*^{L580P}-induced polymerization of LZTR1 complexes, provoking molecular and cellular impairments associated with cardiac hypertrophy. Moreover, CRISPR correction of the missense variant on one allele was sufficient to rescue the phenotype, thereby providing proof of concept for a sustainable therapeutic approach.

STAR★METHODS

Detailed methods are provided in the online version of this paper and include the following:

- KEY RESOURCES TABLE
- RESOURCE AVAILABILITY
  - Lead contact
  - Materials availability
  - Data and code availability
- EXPERIMENTAL MODEL AND STUDY PARTICIPANT DETAILS
  - Human iPSC lines
  - Ethical approval
- METHOD DETAILS
  - Whole exome sequencing
  - Generation and culture of human iPSCs
  - Cardiomyocyte differentiation of iPSCs and generation of engineered heart muscle
  - Biosensor-based analysis of ERK signaling dynamics in iPSC-CMs
  - Proteomics and Western blot analysis of iPSC-CMs
  - Real-time PCR analysis of iPSC-CMs
  - Analysis of sarcomere length and myofibril organization of iPSC-CMs
  - Analysis of cell size of iPSC-CMs
  - Video-based contractility analysis of iPSC-CMs
  - Ectopic expression of LZTR1 variants in iPSC-CMs
  - Expression and purification of recombinant LZTR1 proteins
  - Analytical size exclusion chromatography (SEC) of soluble recombinant LZTR1 proteins
  - Pull-down assay for analysis of LZTR1-RAS interactions
  - In silico prediction of protein structures and multimer complexes
- QUANTIFICATION AND STATISTICAL ANALYSIS

SUPPLEMENTAL INFORMATION

Supplemental information can be found online at https://doi.org/10.1016/j.celrep.2024.114448.

ACKNOWLEDGMENTS

We thank Laura Cyganek, Yvonne Hintz, Nadine Gotzmann, Lisa Schreiber, and Yvonne Wedekind (Stem Cell Unit, University Medical Center Göttingen), Branimir Berečić, Tim Meyer, and Malte Tiburcy (Institute of Pharmacology and Toxicology, University Medical Center Göttingen), and Anja Wiechert and Manuela Gesell Salazar (Interfaculty Institute of Genetics and Functional Genomics, University Medicine Greifswald) for excellent technical assistance. This work was supported by the German Research Foundation (DFG) project nos. 417880571 and 501985000 to L.C., project no. 408077919 to I.C.C., project no. 193793266, Collaborative Research Center 1002, C04, D01, D02, and S01 to W.-H.Z., G.H., B.W., and L.C., and project no. 390729940, Germany's Excellence Strategy - EXC 2067/1 to A.V.B., G.H., W.-H.Z., B.W., and L.C.; the Else Kroner-Fresenius Foundation project no. 2019_A75 to L.C.; the German Federal Ministry of Education and Research (BMBF)/DZHK to E.H., G.H., W.-H.Z., B.W., and L.C.; the BMBF GeNeRARe project nos. 01GM1902F and 01GM1519D to I.C.C. and M.R.A.; and the Leducq Foundation project no. 20CVD04 to W.-H.Z.

AUTHOR CONTRIBUTIONS

Conceptualization, L.C. Investigation, A.V.B., O.G.-G., E.H., F.K., A.M., M.S., L.B., M.K., M.E., J.A., F.M., and L.C. Methodology, A.V.B., O.G.-G., and

L.C. Software, C.P. and H.S. Resources, I.C.C., L.G., D.W., and W.-H.Z. Supervision, G.H., W.-H.Z., M.R.A., and B.W. Visualization, L.C. Writing – original draft, L.C. Writing – review & editing, L.C., A.V.B., and O.G.-G. Funding acquisition, E.H., I.C.C., G.H., W.-H.Z., M.R.A., B.W., and L.C.

DECLARATION OF INTERESTS

The authors declare no competing interests.

Received: January 13, 2024
Revised: April 3, 2024
Accepted: June 20, 2024
Published: July 13, 2024

REFERENCES

1. Roberts, A.E., Allanson, J.E., Tartaglia, M., and Gelb, B.D. (2013). Noonan syndrome. Lancet *381*, 333–342. https://doi.org/10.1016/S0140-6736(12)61023-X.
2. Linglart, L., and Gelb, B.D. (2020). Congenital heart defects in Noonan syndrome: Diagnosis, management, and treatment. Am. J. Med. Genet. C Semin. Med. Genet. *184*, 73–80. https://doi.org/10.1002/ajmg.c.31765.
3. Hickey, E.J., Mehta, R., Elmi, M., Asoh, K., McCrindle, B.W., Williams, W.G., Manlhiot, C., and Benson, L. (2011). Survival implications: hypertrophic cardiomyopathy in Noonan syndrome. Congenit. Heart Dis. *6*, 41–47. https://doi.org/10.1111/j.1747-0803.2010.00465.x.
4. Wilkinson, J.D., Lowe, A.M., Salbert, B.A., Sleeper, L.A., Colan, S.D., Cox, G.F., Towbin, J.A., Connuck, D.M., Messere, J.E., and Lipshultz, S.E. (2012). Outcomes in children with Noonan syndrome and hypertrophic cardiomyopathy: a study from the Pediatric Cardiomyopathy Registry. Am. Heart J. *164*, 442–448. https://doi.org/10.1016/j.ahj.2012.04.018.
5. Aoki, Y., Niihori, T., Inoue, S.i., and Matsubara, Y. (2016). Recent advances in RASopathies. J. Hum. Genet. *61*, 33–39. https://doi.org/10.1038/jhg.2015.114.
6. Leoni, C., Blandino, R., Delogu, A.B., De Rosa, G., Onesimo, R., Verusio, V., Marino, M.V., Lanza, G.A., Rigante, D., Tartaglia, M., and Zampino, G. (2022). Genotype-cardiac phenotype correlations in a large single-center cohort of patients affected by RASopathies: Clinical implications and literature review. Am. J. Med. Genet. *188*, 431–445. https://doi.org/10.1002/ajmg.a.62529.
7. Johnston, J.J., van der Smagt, J.J., Rosenfeld, J.A., Pagnamenta, A.T., Alswaid, A., Baker, E.H., Blair, E., Borck, G., Brinkmann, J., Craigen, W., et al. (2018). Autosomal recessive Noonan syndrome associated with biallelic LZTR1 variants. Genet. Med. *20*, 1175–1185. https://doi.org/10.1038/gim.2017.249.
8. Bigenzahn, J.W., Collu, G.M., Kartnig, F., Pieraks, M., Vladimer, G.I., Heinz, L.X., Sedlyarov, V., Schischlik, F., Fauster, A., Rebsamen, M., et al. (2018). LZTR1 is a regulator of RAS ubiquitination and signaling. Science *362*, 1171–1177. https://doi.org/10.1126/science.aap8210.
9. Castel, P., Cheng, A., Cuevas-Navarro, A., Everman, D.B., Papageorge, A.G., Simanshu, D.K., Tankka, A., Galeas, J., Urisman, A., and McCormick, F. (2019). RIT1 oncoproteins escape LZTR1-mediated proteolysis. Science *363*, 1226–1230. https://doi.org/10.1126/science.aav1444.
10. Hanses, U., Kleinsorge, M., Roos, L., Yigit, G., Li, Y., Barbarics, B., El-Battrawy, I., Lan, H., Tiburcy, M., Hindmarsh, R., et al. (2020). Intronic CRISPR Repair in a Preclinical Model of Noonan Syndrome-Associated Cardiomyopathy. Circulation *142*, 1059–1076. https://doi.org/10.1161/CIRCULATIONAHA.119.044794.
11. Motta, M., Fidan, M., Bellacchio, E., Pantaleoni, F., Schneider-Heieck, K., Coppola, S., Borck, G., Salviati, L., Zenker, M., Cirstea, I.C., and Tartaglia, M. (2019). Dominant Noonan syndrome-causing LZTR1 mutations specifically affect the Kelch domain substrate-recognition surface and enhance RAS-MAPK signaling. Hum. Mol. Genet. *28*, 1007–1022. https://doi.org/10.1093/hmg/ddy412.
12. Sayed, N., Liu, C., and Wu, J.C. (2016). Translation of Human-Induced Pluripotent Stem Cells: From Clinical Trial in a Dish to Precision Medicine. J. Am. Coll. Cardiol. *67*, 2161–2176. https://doi.org/10.1016/j.jacc.2016.01.083.
13. van Mil, A., Balk, G.M., Neef, K., Buikema, J.W., Asselbergs, F.W., Wu, S.M., Doevendans, P.A., and Sluijter, J.P.G. (2018). Modelling inherited cardiac disease using human induced pluripotent stem cell-derived cardiomyocytes: progress, pitfalls, and potential. Cardiovasc. Res. *114*, 1828–1842. https://doi.org/10.1093/cvr/cvy208.
14. Meier, A.B., Raj Murthi, S., Rawat, H., Toepfer, C.N., Santamaria, G., Schmid, M., Mastantuono, E., Schwarzmayr, T., Berutti, R., Cleuziou, J., et al. (2022). Cell cycle defects underlie childhood-onset cardiomyopathy associated with Noonan syndrome. iScience *25*, 103596. https://doi.org/10.1016/j.isci.2021.103596.
15. Jaffré, F., Miller, C.L., Schänzer, A., Evans, T., Roberts, A.E., Hahn, A., and Kontaridis, M.I. (2019). Inducible Pluripotent Stem Cell-Derived Cardiomyocytes Reveal Aberrant Extracellular Regulated Kinase 5 and Mitogen-Activated Protein Kinase Kinase 1/2 Signaling Concomitantly Promote Hypertrophic Cardiomyopathy in RAF1-Associated Noonan Syndrome. Circulation *140*, 207–224. https://doi.org/10.1161/CIRCULATIONAHA.118.037227.
16. Josowitz, R., Mulero-Navarro, S., Rodriguez, N.A., Falce, C., Cohen, N., Ullian, E.M., Weiss, L.A., Rauen, K.A., Sobie, E.A., and Gelb, B.D. (2016). Autonomous and Non-autonomous Defects Underlie Hypertrophic Cardiomyopathy in BRAF-Mutant hiPSC-Derived Cardiomyocytes. Stem Cell Rep. *7*, 355–369. https://doi.org/10.1016/j.stemcr.2016.07.018.
17. Higgins, E.M., Bos, J.M., Dotzler, S.M., John Kim, C.S., and Ackerman, M.J. (2019). MRAS Variants Cause Cardiomyocyte Hypertrophy in Patient-Specific Induced Pluripotent Stem Cell-Derived Cardiomyocytes: Additional Evidence for MRAS as a Definitive Noonan Syndrome-Susceptibility Gene. Circ. Genom. Precis. Med. *12*, e002648. https://doi.org/10.1161/CIRCGEN.119.002648.
18. Knauer, C., Haltern, H., Schoger, E., Kügler, S., Roos, L., Zelarayán, L.C., Hasenfuss, G., Zimmermann, W.-H., Wollnik, B., and Cyganek, L. (2024). Preclinical evaluation of CRISPR-based therapies for Noonan syndrome caused by deep-intronic LZTR1 variants. Mol. Ther. Nucleic Acids *35*, 102123. https://doi.org/10.1016/j.omtn.2024.102123.
19. Kleinsorge, M., and Cyganek, L. (2020). Subtype-Directed Differentiation of Human iPSCs into Atrial and Ventricular Cardiomyocytes. STAR Protoc. *1*, 100026. https://doi.org/10.1016/j.xpro.2020.100026.
20. Kudo, T., Jeknić, S., Macklin, D.N., Akhter, S., Hughey, J.J., Regot, S., and Covert, M.W. (2018). Live-cell measurements of kinase activity in single cells using translocation reporters. Nat. Protoc. *13*, 155–169. https://doi.org/10.1038/nprot.2017.128.
21. Lemcke, H., Skorska, A., Lang, C.I., Johann, L., and David, R. (2020). Quantitative Evaluation of the Sarcomere Network of Human hiPSC-Derived Cardiomyocytes Using Single-Molecule Localization Microscopy. Int. J. Mol. Sci. *21*, 2819. https://doi.org/10.3390/ijms21082819.
22. Mosqueira, D., Mannhardt, I., Bhagwan, J.R., Lis-Slimak, K., Katili, P., Scott, E., Hassan, M., Prondzynski, M., Harmer, S.C., Tinker, A., et al. (2018). CRISPR/Cas9 editing in human pluripotent stem cell-cardiomyocytes highlights arrhythmias, hypocontractility, and energy depletion as potential therapeutic targets for hypertrophic cardiomyopathy. Eur. Heart J. *39*, 3879–3892. https://doi.org/10.1093/eurheartj/ehy249.
23. Levin, M.D., Saitta, S.C., Gripp, K.W., Wenger, T.L., Ganesh, J., Kalish, J.M., Epstein, M.R., Smith, R., Czosek, R.J., Ware, S.M., et al. (2018). Non-reentrant atrial tachycardia occurs independently of hypertrophic cardiomyopathy in RASopathy patients. Am. J. Med. Genet. *176*, 1711–1722. https://doi.org/10.1002/ajmg.a.38854.
24. Maron, B.J., Desai, M.Y., Nishimura, R.A., Spirito, P., Rakowski, H., Towbin, J.A., Rowin, E.J., Maron, M.S., and Sherrid, M.V. (2022). Diagnosis and Evaluation of Hypertrophic Cardiomyopathy: JACC State-of-the-Art Review. J. Am. Coll. Cardiol. *79*, 372–389. https://doi.org/10.1016/j.jacc.2021.12.002.

25. Cyganek, L., Tiburcy, M., Sekeres, K., Gerstenberg, K., Bohnenberger, H., Lenz, C., Henze, S., Stauske, M., Salinas, G., Zimmermann, W.-H., et al. (2018). Deep phenotyping of human induced pluripotent stem cell-derived atrial and ventricular cardiomyocytes. JCI Insight *3*, 99941. https://doi.org/10.1172/jci.insight.99941.

26. Tiburcy, M., Meyer, T., Liaw, N.Y., and Zimmermann, W.-H. (2020). Generation of Engineered Human Myocardium in a Multi-well Format. STAR Protoc. *1*, 100032. https://doi.org/10.1016/j.xpro.2020.100032.

27. NSEuroNet.com. https://nseuronet.com/php/. Accessed December 29, 2022.

28. Abe, T., Umeki, I., Kanno, S.-I., Inoue, S.I., Niihori, T., and Aoki, Y. (2020). LZTR1 facilitates polyubiquitination and degradation of RAS-GTPases. Cell Death Differ. *27*, 1023–1035. https://doi.org/10.1038/s41418-019-0395-5.

29. Canning, P., Cooper, C.D.O., Krojer, T., Murray, J.W., Pike, A.C.W., Chaikuad, A., Keates, T., Thangaratnarajah, C., Hojzan, V., Marsden, B.D., et al. (2013). Structural basis for Cul3 protein assembly with the BTB-Kelch family of E3 ubiquitin ligases. J. Biol. Chem. *288*, 7803–7814. https://doi.org/10.1074/jbc.M112.437996.

30. Mirdita, M., Schütze, K., Moriwaki, Y., Heo, L., Ovchinnikov, S., and Steinegger, M. (2022). ColabFold: making protein folding accessible to all. Nat. Methods *19*, 679–682. https://doi.org/10.1038/s41592-022-01488-1.

31. Steklov, M., Pandolfi, S., Baietti, M.F., Batiuk, A., Carai, P., Najm, P., Zhang, M., Jang, H., Renzi, F., Cai, Y., et al. (2018). Mutations in LZTR1 drive human disease by dysregulating RAS ubiquitination. Science *362*, 1177–1182. https://doi.org/10.1126/science.aap7607.

32. Cuevas-Navarro, A., Rodriguez-Muñoz, L., Grego-Bessa, J., Cheng, A., Rauen, K.A., Urisman, A., McCormick, F., Jimenez, G., and Castel, P. (2022). Cross-species analysis of LZTR1 loss-of-function mutants demonstrates dependency to RIT1 orthologs. Elife *11*, e76495. https://doi.org/10.7554/eLife.76495.

33. Nakamura, M., and Sadoshima, J. (2018). Mechanisms of physiological and pathological cardiac hypertrophy. Nat. Rev. Cardiol. *15*, 387–407. https://doi.org/10.1038/s41569-018-0007-y.

34. Nakhaei-Rad, S., Bazgir, F., Dahlmann, J., Busley, A.V., Buchholzer, M., Haghighi, F., Schänzer, A., Hahn, A., Kötter, S., Schanze, D., et al. (2022). Alteration of myocardial structure and function in RAF1-associated Noonan syndrome: Insights from cardiac disease modeling based on patient-derived iPSCs. Preprint at bioRxiv. https://doi.org/10.1101/2022.01.22.477319.

35. Wang, Y., Zhang, J., Zhang, P., Zhao, Z., Huang, Q., Yun, D., Chen, J., Chen, H., Wang, C., and Lu, D. (2020). LZTR1 inactivation promotes MAPK/ERK pathway activation in glioblastoma by stabilizing oncoprotein RIT1. Preprint at bioRxiv. https://doi.org/10.1101/2020.03.14.989954.

36. Marzahn, M.R., Marada, S., Lee, J., Nourse, A., Kenrick, S., Zhao, H., Ben-Nissan, G., Kolaitis, R.-M., Peters, J.L., Pounds, S., et al. (2016). Higher-order oligomerization promotes localization of SPOP to liquid nuclear speckles. EMBO J. *35*, 1254–1275. https://doi.org/10.15252/embj.201593169.

37. Karbassi, E., Fenix, A., Marchiano, S., Muraoka, N., Nakamura, K., Yang, X., and Murry, C.E. (2020). Cardiomyocyte maturation: advances in knowledge and implications for regenerative medicine. Nat. Rev. Cardiol. *17*, 341–359. https://doi.org/10.1038/s41569-019-0331-x.

38. Guo, Y., and Pu, W.T. (2020). Cardiomyocyte Maturation: New Phase in Development. Circ. Res. *126*, 1086–1106. https://doi.org/10.1161/CIRCRESAHA.119.315862.

39. Rössler, U., Hennig, A.F., Stelzer, N., Bose, S., Kopp, J., Søe, K., Cyganek, L., Zifarelli, G., Ali, S., von der Hagen, M., et al. (2021). Efficient generation of osteoclasts from human induced pluripotent stem cells and functional investigations of lethal CLCN7-related osteopetrosis. J. Bone Miner. Res. *36*, 1621–1635. https://doi.org/10.1002/jbmr.4322.

40. Yousefi, R., Fornasiero, E.F., Cyganek, L., Montoya, J., Jakobs, S., Rizzoli, S.O., Rehling, P., and Pacheu-Grau, D. (2021). Monitoring mitochondrial translation in living cells. EMBO Rep. *22*, e51635. https://doi.org/10.15252/embr.202051635.

41. Schmidt, U., Weigert, M., Broaddus, C., and Myers, G. (2018). Cell Detection with Star-Convex Polygons. In Cell Detection with Star-Convex Polygons, A.F. Frangi, J.A. Schnabel, C. Davatzikos, C. Alberola-López, and G. Fichtinger, eds. (Cham: Springer International Publishing), pp. 265–273.

42. Haeussler, M., Schönig, K., Eckert, H., Eschstruth, A., Mianné, J., Renaud, J.-B., Schneider-Maunoury, S., Shkumatava, A., Teboul, L., Kent, J., et al. (2016). Evaluation of off-target and on-target scoring algorithms and integration into the guide RNA selection tool CRISPOR. Genome Biol. *17*, 148. https://doi.org/10.1186/s13059-016-1012-2.

43. Ahlers, J., Althviz Moré, D., Amsalem, O., Anderson, A., Bokota, G., Boone, P., Bragantini, J., Buckley, G., Burt, A., Bussonnier, M., et al. (2023). Napari: A Multi-Dimensional Image Viewer for Python. Zenodo.

44. Zech, A.T.L., Prondzynski, M., Singh, S.R., Pietsch, N., Orthey, E., Alizoti, E., Busch, J., Madsen, A., Behrens, C.S., Meyer-Jens, M., et al. (2022). ACTN2 Mutant Causes Proteopathy in Human iPSC-Derived Cardiomyocytes. Cells *11*, 2745. https://doi.org/10.3390/cells11172745.

45. Suomi, T., and Elo, L.L. (2017). Enhanced differential expression statistics for data-independent acquisition proteomics. Sci. Rep. *7*, 5869. https://doi.org/10.1038/s41598-017-05949-y.

46. Seyednasrollah, F., Rantanen, K., Jaakkola, P., and Elo, L.L. (2016). ROTS: reproducible RNA-seq biomarker detector-prognostic markers for clear cell renal cell cancer. Nucleic Acids Res. *44*, e1. https://doi.org/10.1093/nar/gkv806.

47. Bindea, G., Mlecnik, B., Hackl, H., Charoentong, P., Tosolini, M., Kirilovsky, A., Fridman, W.-H., Pagès, F., Trajanoski, Z., and Galon, J. (2009). ClueGO: a Cytoscape plug-in to decipher functionally grouped gene ontology and pathway annotation networks. Bioinformatics *25*, 1091–1093. https://doi.org/10.1093/bioinformatics/btp101.

48. Pasqualin, C., Gannier, F., Yu, A., Malécot, C.O., Bredeloux, P., and Maupoil, V. (2016). SarcOptiM for ImageJ: high-frequency online sarcomere length computing on stimulated cardiomyocytes. Am. J. Physiol. Cell Physiol. *311*, C277–C283. https://doi.org/10.1152/ajpcell.00094.2016.

49. Nacak, T.G., Leptien, K., Fellner, D., Augustin, H.G., and Kroll, J. (2006). The BTB-kelch protein LZTR-1 is a novel Golgi protein that is degraded upon induction of apoptosis. J. Biol. Chem. *281*, 5065–5071. https://doi.org/10.1074/jbc.M509073200.

50. Eberth, A., and Ahmadian, M.R. (2009). In vitro GEF and GAP assays. Curr. Protoc. Cell Biol. *14*, Unit 14.9. https://doi.org/10.1002/0471143030.cb1409s43.

51. Evans, R., O'Neill, M., Pritzel, A., Antropova, N., Senior, A., Green, T., Žídek, A., Bates, R., Blackwell, S., Yim, J., et al. (2021). Protein Complex Prediction with AlphaFold-Multimer. Preprint at bioRxiv. https://doi.org/10.1101/2021.10.04.463034.

STAR★METHODS

KEY RESOURCES TABLE

REAGENT or RESOURCE	SOURCE	IDENTIFIER
Antibodies		
α-actinin monoclonal mouse	Sigma-Aldrich	RRID: AB_476766
Alexa 488 polyclonal goat anti-rabbit	Thermo Fisher Scientific	RRID: AB_143165
Alexa 555 polyclonal donkey anti-mouse	Thermo Fisher Scientific	RRID: AB_2536180
FLAG monoclonal mouse	Sigma-Aldrich	RRID: AB_262044
HA monoclonal rabbit	Cell Signaling	RRID: AB_1549585
His monoclonal rabbit	Thermo Fisher Scientific	RRID: AB_2810125
LZTR1 monoclonal rabbit	Abcam	RRID: AB_3076250
MLC2V polyclonal rabbit	Proteintech	RRID: AB_2147453
MRAS polyclonal rabbit	Proteintech	RRID: AB_10950895
MYC monoclonal mouse	Cell Signaling	RRID: AB_331783
NANOG monoclonal mouse	Thermo Fisher Scientific	RRID: AB_2536677
OCT3/4-PE monoclonal human	Miltenyi Biotec	RRID: AB_2784442
pan-RAS monoclonal mouse	Merck Millipore	RRID: AB_2121151
RIT1 polyclonal rabbit	Abcam	RRID: AB_882379
TRA-1-60 monoclonal mouse	Abcam	RRID: AB_778563
TRA-1-60-Alexa488 monoclonal mouse	BD Biosciences	RRID: AB_1645379
Vinculin monoclonal mouse	Sigma-Aldrich	RRID: AB_477629
HRP polyclonal donkey anti-rabbit	Sigma-Aldrich	RRID: AB_2722659
HRP polyclonal donkey anti-mouse	Sigma-Aldrich	RRID: AB_772210
Chemicals, peptides, and recombinant proteins		
Fetal bovine serum	Thermo Fisher Scientific	Cat# 10500-064
JNK-IN-8	Hycultec	Cat# HY-13319
MG-132	InvivoGen	Cat# tlrl-mg132-2
Pevonedistat (MLN49249)	Hycultec	Cat# HY-70062
Trametinib	Selleck Chemicals	Cat# S2673
Critical commercial assays		
BCA assay kit	Thermo Fisher Scientific	Cat# 23225
NucleoBond Xtra Midi Plus EF kit	Macherey-Nagel	Cat# 740410.50
ROX passive dye	Bio-Rad	Cat# 1725858
SureSelect Human All Exon V6 kit	Agilent	N/A
SYBR green PCR master mix	Bio-Rad	Cat# 1708880
Deposited data		
Mass spectrometry proteomics	This paper	ProteomeXchange: PXD038425 and PXD038417
Experimental models: Cell lines		
Human iPSC line: WT1	Rössler et al.[39]	UMGi014-C clone 14
Human iPSC line: WT11	Yousefi et al.[40]	UMGi130-A clone 8
Human iPSC line: LZTR1^{KO}	Hanses et al.[10]	UMGi030-A clone 14
Human iPSC line: LZTR1^{L580P}	This paper	UMGi137-A clone 2
Human iPSC line: L580P$^{corr-het}$	This paper	UMGi137-A-1 clone D8
Human iPSC line: L580P$^{corr-hom}$	This paper	UMGi137-A-1 clone D1
Human foreskin fibroblasts: HFF-1	ATCC	Cat# SCRC-1041
Expi-293F	Thermo Fisher Scientific	Cat# A14527

(*Continued on next page*)

Continued

REAGENT or RESOURCE	SOURCE	IDENTIFIER
HEK293T	ATCC	Cat# CRL-11268
Oligonucleotides		
Primers used in this study see Table S2	This paper	N/A
Recombinant DNA		
Plasmids used in this study see Table S3	This paper	N/A
Software and algorithms		
CellPathfinder	Yokogawa Electric Corporation	https://www.yokogawa.com/de/library/documents-downloads/software/lsc-cellpathfinder-software/
CellProfiler	BROAD institute	https://www.broadinstitute.org/publications/broad339241
ColabFold (version 02c53)	Mirdita et al.[30]	https://colab.research.google.com/github/sokrypton/ColabFold/blob/main/AlphaFold2.ipynb
CRISPOR	Tefor infrastructure	http://crispor.tefor.net/
CytoSolver	IonOptix	https://www.ionoptix.com/products/software/cytosolver-transient-analysis-tool/
GenomeStudio v2.0	Illumina	https://support.illumina.com/downloads/genomestudio-2-0.html
ImageJ	NIH	https://imagej.net/ij/
ImageLab	BioRad	https://www.bio-rad.com/de-de/product/image-lab-software?ID=KRE6P5E8Z
LabChart	ADInstruments	https://www.adinstruments.com/products/labchart
MATLAB	MathWorks	https://www.mathworks.com/
Prism 10	GraphPad	https://www.graphpad.com/scientific-software/prism
Spectronaut software	Biognosys	https://biognosys.com/software/spectrodive
StarDist	Schmidt et al.[41]	https://stardist.net/
Varbank 2.0	Cologne Center for Genomics (CCG)	https://varbank.ccg.uni-koeln.de/
Other		
Axio Imager M2 microscope	Carl Zeiss	N/A
CASY cell count system	OMNI Life Science	N/A
Cytomotion Lite system	IonOptix	N/A
CQ1 confocal image cytometer	Yokogawa Electric Corporation	N/A
MutationTaster		https://www.mutationtaster.org/
PolyPhen-2		http://genetics.bwh.harvard.edu/pph2/
SIFT		https://sift.bii.a-star.edu.sg/

RESOURCE AVAILABILITY

Lead contact

Further information and requests for resources and reagents should be directed to and will be fulfilled by the lead contact, Lukas Cyganek (lukas.cyganek@gwdg.de).

Materials availability

All human iPSC lines used in this study are deposited in the stem cell biobank of the University Medical Center Göttingen and are available for research use upon request. Requests of material, including iPSC lines and plasmids, can be directed to and will be fulfilled by the lead contact. Reagents and cell lines can be transferred after the completion of a materials transfer agreement.

Data and code availability

- The mass spectrometry proteomics datasets are available at the ProteomeXchange Consortium via the PRIDE partner repository (https://www.proteomexchange.org/) with the identifiers PXD038425 and PXD038417.
- This paper does not report original code.
- Any additional information required to reanalyze the data reported in this paper is available from the lead contact upon request.

EXPERIMENTAL MODEL AND STUDY PARTICIPANT DETAILS

Human iPSC lines

Human iPSC lines from two healthy donors (UMGi014-C clone 14 and UMGi130-A clone 8), from one NS patient with biallelic truncating variants in *LZTR1* (UMGi030-A clone 14), from one NS patient with a pathological missense variant in *LZTR1* (UMGi137-A clone 2), as well as heterozygous and homozygous CRISPR/Cas9-corrected iPSC lines (UMGi137-A-1 clone D8 and UMGi137-A-1 clone D1) were used in this study. Details on reprogramming and CRISPR/Cas9 editing are provided in the method details below.

Ethical approval

The study was approved by the Ethics Committee of the University Medical Center Göttingen (approval number: 10/9/15) and carried out in accordance with the approved guidelines. Written informed consent was obtained from all participants or their legal representatives prior to the participation in the study.

METHOD DETAILS

Whole exome sequencing

Whole exome sequencing on genomic DNA of the patient was performed using the SureSelect Human All Exon V6 kit (Agilent) on an Illumina HiSeq 4000 sequencer. The "Varbank 2.0" pipeline of the Cologne Center for Genomics (CCG) was used to analyze and interpret the exome data, as previously described.[10] Co-segregation analysis was performed in the family. Computational predictions for the pathogenicity of the variant were performed using MutationTaster (https://www.mutationtaster.org/), SIFT (https://sift.bii.a-star.edu.sg/), and PolyPhen-2 (http://genetics.bwh.harvard.edu/pph2/).

Generation and culture of human iPSCs

Human iPSC lines from two healthy donors, from one NS patient with biallelic truncating variants in *LZTR1* (NM_006767.4: c.27dupG/p.Q10Afs*24, c.1943-256C>T/p.T648fs*36), from one NS patient with a pathological missense variant in *LZTR1* (NM_006767.4: c.1739T>C/p.L580P; ClinVar: RCV000677201.1), as well as heterozygous and homozygous CRISPR/Cas9-corrected iPSC lines were used in this study. Wild type iPSC lines UMGi014-C clone 14 (isWT1.14, here abbreviated as WT1) and UMGi130-A clone 8 (isWT11.8, here abbreviated as WT11) were generated from dermal fibroblasts and peripheral blood mononuclear cells from two male donors, respectively, using the integration-free Sendai virus and described previously.[39,40] Patient-specific iPSC line UMGi030-A clone 14 (isHOCMx1.14, here abbreviated as LZTR1^{KO}) was generated from patient's dermal fibroblasts using the integration-free Sendai virus and described previously.[10] Patient-specific iPSC line UMGi137-A clone 2 (isNoonSf1.2, here abbreviated as LZTR1^{L580P}) was generated from patient's dermal fibroblasts using the integration-free Sendai virus according manufacturer's instructions with modifications, as previously described.[10] Genetic correction of the pathological gene variant in the patient-derived iPSC line UMGi137-A clone 2 was performed using ribonucleoprotein-based CRISPR/Cas9 using crRNA/tracrRNA and Hifi SpCas9 (IDT DNA technologies) by targeting exon 15 of the *LZTR1* gene, as previously described.[10] The guide RNA target sequence was (PAM in bold): 5'-GCGGCACTCTCGCACACAAC **CGG**-3'. For homology-directed repair, a single-stranded oligonucleotide with 45-bp homology arms was used. After automated clonal singularization using the single cell dispenser CellenOne (Cellenion/Scienion) in StemFlex medium (Thermo Fisher Scientific), successful genome editing was identified by Sanger sequencing and the CRISPR-corrected isogenic iPSC lines UMGi137-A-1 clone D8 (isNoonSf1-corr.D8, here abbreviated as L580P$^{corr\text{-}het}$) and UMGi137-A-1 clone D1 (isNoonSf1-corr.D1, here abbreviated as L580P$^{corr\text{-}hom}$) were established. Newly generated iPSC lines were maintained on Matrigel-coated (growth factor reduced, BD Biosciences) plates, passaged every 4–6 days with Versene solution (Thermo Fisher Scientific) and cultured in StemMACS iPS-Brew XF medium (Miltenyi Biotec) supplemented with 2 μM Thiazovivin (Merck Millipore) on the first day after passaging with daily medium change for at least ten passages before being used for molecular karyotyping, pluripotency characterization, and differentiation experiments. Pluripotency analysis via immunocytochemistry and flow cytometry was performed, as previously described.[10] For molecular karyotyping, genomic DNA of iPSC clones was sent for genome-wide analysis via Illumina BeadArray (Life&Brain, Germany). Digital karyotypes were analyzed in GenomeStudio v2.0 software (Illumina). For off-target screening, the top five predicted off-target regions for the respective guide RNA ranked by the CFD off-target score using CRISPOR[42] were analyzed by Sanger sequencing. Human iPSCs and iPSC-derivatives were cultured in feeder-free and serum-free culture conditions in a humidified incubator at 37°C and 5% CO_2.

Cardiomyocyte differentiation of iPSCs and generation of engineered heart muscle

Human iPSC lines were differentiated into ventricular iPSC-CMs via WNT signaling modulation and subsequent metabolic selection, as previously described,[19] and cultivated in feeder-free and serum-free culture conditions until day 60 post-differentiation before being used for molecular and cellular experiments. Defined, serum-free EHMs were generated from iPSC-CMs around day 30 of differentiation and human foreskin fibroblasts (ATCC) at a 70:30 ratio according to previously published protocols.[26] Optical analysis of contractility and rhythm of spontaneously beating EHMs in a 48 well plate (myrPlate TM5, myriamed GmbH) was performed between day 34 and day 42 of culture using a custom-built setup with a high-speed camera by recording the movement of the two UV light-absorbing flexible poles. Contractility parameters of EHM recordings of at least 1 min recording time were analyzed via a custom-build script in MATLAB (MathWorks). For each iPSC line, three individual differentiations were used for EHM casting.

Biosensor-based analysis of ERK signaling dynamics in iPSC-CMs

In brief, the ERK kinase translocation reporter (ERK-KTR) biosensor consists of an ERK-specific docking site, a nuclear localization signal (NLS), a nuclear export signal (NES), and mClover. Endogenous, phosphorylated ERK binds to the biosensor and phosphorylates its NLS and NES resulting in a nucleus-cytoplasm shuttling according to ERK activity.[20] ERK-KTR biosensor encoding lentiviral particles were produced in HEK293T cells transfected with transfer, envelope, and packaging plasmids using Lipofectamine 3000 (Thermo Fisher Scientific) according to manufacturer's instructions. pLentiPGK Puro DEST ERKKTRClover was a gift from Markus Covert (RRID:Addgene_90227), pMD2.G was a gift from Didier Trono (RRID:Addgene_12259), and psPAX2 was a gift from Didier Trono (RRID:Addgene_12260). Virus was harvested from day 2 to day 5 post-transfection by medium collection and centrifugation at 500×g at 4°C for 5 min. The harvested virus was filtered using a 0.45 μm filter and a syringe. For transduction, 15,000 iPSC-CMs were seeded per well of a 96-well plate and lentiviral transduction was performed 7 days after cell digestion. Lentivirus was diluted in culture medium supplemented with 100 U/ml penicillin, 100 μg/mL streptomycin (Thermo Fisher Scientific), and 10 μg/mL Polybrene Transfection Reagent (Merck). After 24 h of incubation, medium was replaced with cardio culture medium and cells were maintained for additional 7 days. For live-cell imaging, biosensor-transduced iPSC-CM cultures at day 60 of differentiation were treated with 100 nM MEK inhibitor trametinib (Selleck Chemicals), 100 nM JNK inhibitor JNK-IN-8 (Hycultec), or 1:1,000 DMSO (Sigma-Aldrich) for 60 min, before stimulation with 10% fetal bovine serum for another 60 min. Cells were imaged every 10 min for a total time of 120 min. Live cell imaging experiments were acquired using the CQ1 confocal image cytometer (Yokogawa Electric Corporation) and CellPathfinder software (Yokogawa Electric Corporation) under environmental control (37°C, 5% CO_2). Exported images were processed using the StarDist method for nucleus segmentation.[41] The StarDist network was retrained on 60 images from our dataset with annotations manually produced with napari.[43] For a new image, the nuclei were then segmented with StarDist, and a ring element around each nucleus was computed to approximate the cytosol. The mean fluorescence intensity of both compartments was measured for each cell individually.

Proteomics and Western blot analysis of iPSC-CMs

For proteomic analysis, iPSC-CMs were pelleted at day 60 of differentiation by scratching in RIPA buffer (Thermo Fisher Scientific) containing phosphatase and protease inhibitor (Thermo Fisher Scientific) and snap-frozen in liquid nitrogen. Cell pellets were reconstituted in 8 M urea/2 M thiourea solution (Sigma-Aldrich) and lysed by five freeze-thaw cycles at 30°C and 1.600 rpm. Protein containing supernatant was collected by centrifugation. Nucleic acid was degraded enzymatically with 0.125 U/μg benzonase (Sigma-Aldrich), and protein concentration was determined by Bradford assay (Bio-Rad). Five μg protein was processed for LC-MS/MS analysis, as previously described.[44] Briefly, protein was reduced (2.5 mM dithiothreitol, Sigma-Aldrich; 30 min at 37°C) and alkylated (10 mM iodacetamide, Sigma-Aldrich; 15 min at 37°C) before proteolytic digestion with LysC (enzyme to protein ratio 1:100, Promega) for 3 h and with trypsin (1:25, Promega) for 16 h both at 37°C. The reaction was stopped with 1% acetic acid (Sigma-Aldrich), and the peptide mixtures were desalted on C-18 reverse phase material (ZipTip μ-C18, Millipore). Eluted peptides were concentrated by evaporation under vacuum and subsequently resolved in 0.1% acetic acid/2% acetonitrile containing HRM/iRT peptides (Biognosys) according to manufacturer's recommendation. LC-MS/MS analysis was performed in data-independent acquisition (DIA) mode using an Ultimate 3000 UPLC system coupled to an Exploris 480 mass spectrometer (Thermo Scientific). Peptides were separated on a 25 cm Accucore column (75 μm inner diameter, 2.6 μm, 150 A, C18) at a flow rate of 300 nL/min in a linear gradient for 60 min. Spectronaut software (Biognosys) was used for the analysis of mass spectrometric raw data. For peptide and protein identification, the Direct DIA approach based on UniProt database limited to human entries was applied. Carbamidomethylation at cysteine was set as static modification, oxidation at methionine and protein N-terminal acetylation were defined as variable modifications, and up to two missed cleavages were allowed. Ion values were parsed when at least 20% of the samples contained high quality measured values. Peptides were assigned to protein groups and protein inference was resolved by the automatic workflow implemented in Spectronaut. Statistical data analysis was conducted using an in-house developed R tool and based on median-normalized ion peak area intensities. Methionine oxidized peptides were removed before quantification. Differential abundant proteins (p-value ≤ 0.05) were identified by the algorithm ROPECA[45] and application of the reproducibility-optimized peptide change averaging approach[46] applied on peptide level. Only proteins quantified by at least two peptides were considered for further analysis. Reactome pathway enrichment analysis was performed using the ClueGo plugin in Cytoscape.[47] For each iPSC line, at least three individual differentiations were analyzed. For Western blot analysis, protein containing supernatant was collected by centrifugation. Protein concentration was determined by BCA assay (Thermo Fisher Scientific). Samples were denatured at 95°C for 5 min 15 μg

protein were loaded onto a 4–15% Mini-PROTEAN TGX Stain-Free precast gel (Bio-Rad). The protein was separated by sodium dodecyl sulfate-polyacrylamide gel electrophoresis (SDS-PAGE) by applying 200 V for 30 min. Post-running, TGX gels were activated via UV light application using the Trans-Blot Turbo transfer system (Bio-Rad). While blotting, proteins were transferred to a nitrocellulose membrane (25 V constant, 1.3 A for 7 min). Total protein amount was detected via the ChemiDoc XRS+ (Bio-Rad) system and used for protein normalization. After 1 h in blocking solution (5% milk in TBS-T, Sigma-Aldrich), membranes were incubated in primary antibody solution (1% milk in TBS-T) overnight. Membrane was washed trice with TBS-T before applying the secondary antibody (1:10,000 in 1% milk in TBS-T) at RT for 1 h. After washing, signals were detected upon application of SuperSignal West Femto Maximum Sensitivity Substrat (Thermo Fisher Scientific). Image acquisition was performed with the ChemiDoc XRS+ (Bio-Rad) at the high-resolution mode. For protein quantification, ImageLab (Bio-Rad) was used and protein levels were first normalized to total protein and second to the corresponding WT samples on each blot. For ERK signaling analysis, iPSC-CMs at day 60 of differentiation were treated with 10 nM trametinib (Selleck Chemicals) for 30 min and stimulated with 10% fetal bovine serum (Thermo Fisher Scientific). For analysis of degradation pathways, iPSC-CMs at day 60 of differentiation were treated with 1–2 μM pevonedistat (Hycultec) or 750 nM MG-132 (InvivoGen) for three days. For each iPSC line, at least three individual differentiations/conditions were analyzed.

Real-time PCR analysis of iPSC-CMs

Pellets of iPSC-CMs at day 60 of differentiation were snap-frozen in liquid nitrogen and stored at −80°C. Total RNA was isolated using the NucleoSpin RNA Mini kit (Macherey-Nagel) according to manufacturer's instructions. 200 ng RNA was used for the first-strand cDNA synthesis by using the MULV Reverse Transcriptase and Oligo d(T)16 (Thermo Fisher Scientific). For real-time PCR, cDNA was diluted 1:1 with nuclease-free water (Promega). Quantitative real-time PCR reactions were carried out using the SYBR Green PCR master mix and ROX Passive Reference Dye (Bio-Rad) with Micro-Amp Optical 384-well plates, and the 7900HT fast real-time PCR system (Applied Biosystems) according to the manufacturer's instructions with the following parameters: 95°C for 10 min, followed by 40 cycles at 95°C for 15 s and 60°C for 1 min. Analysis was conducted using the ΔΔCT method and values were normalized to *GAPDH* gene expression and to WT controls. Primer sequences are listed in Table S2 in the supplement.

Analysis of sarcomere length and myofibril organization of iPSC-CMs

To analyze the sarcomere length and myofibril organization, iPSC-CMs were cultured on Matrigel-coated coverslips and fixed at day 60 of differentiation in 4% Roti-Histofix (Carl Roth) at RT for 10 min and blocked with 1% Bovine Serum Albumin (BSA; Sigma-Aldrich) in PBS (Thermo Fisher Scientific) overnight at 4°C. Primary antibodies were applied in 1% BSA and 0.1% Triton X-100 (Carl Roth) in PBS at 37°C for 1 h or at 4°C overnight. Secondary antibodies with minimal cross reactivity were administered in 1% BSA in PBS (Thermo Fisher Scientific) at RT for 1 h. Nuclei were stained with 8.1 μM Hoechst 33342 (Thermo Fisher Scientific) at RT for 10 min. Samples were mounted in Fluoromount-G (Thermo Fisher Scientific). Images were collected using the Axio Imager M2 microscopy system (Carl Zeiss) and Zen 2.3 software. For analysis of the sarcomere length, images with α-actinin staining of iPSC-CMs were evaluated using the SarcOptiM plugin in ImageJ (National Institutes of Health).[48] Here, three independent lines along different myofibrils within one cell were selected to calculate the mean sarcomere length per cell. For each iPSC line, three individual differentiations with 9–13 images per differentiation and two cells per image were analyzed. To analyze the myofibril organization, images with α-actinin staining of iPSC-CMs were processed using the Tubeness and Fast Fourier Transform plugins in ImageJ. Processed images were radially integrated using the Radial Profile Plot plugin in ImageJ and the relative amplitude of the first-order peak in the intensity profile as a measure of sarcomere and myofibril regularity was automatically analyzed using LabChart (ADInstruments). For each iPSC line, three individual differentiations with 7–11 images per differentiation were analyzed.

Analysis of cell size of iPSC-CMs

To study cellular hypertrophy, iPSC-CMs at day 60 of differentiation were analyzed for cell size in suspension, as previously described.[10] In brief, iPSC-CMs at day 50 of differentiation were plated at a density of 2.5×10^5 cells per well on Matrigel-coated 12-well plates. At day 60 of differentiation, cells were singularized with StemPro Accutase Cell Dissociation Reagent (Thermo Fisher Scientific) and measured for cell diameter using the CASY cell counter system (OMNI Life Science). Each value represents a mean of 5×10^2 to 1.5×10^4 cells per measurement. To exclude cell debris and cell clusters, only values within a diameter range of 15–40 μm were selected. For each iPSC line, at least three individual differentiations with 3–5 replicates per differentiation were analyzed. To study the effect of MEK inhibition on LZTR1^{L580P} iPSC-CMs, cultured at a density of 6×10^5 cells per well were treated with 10 nM trametinib for 5 days before being measured via the CASY cell counter.

Video-based contractility analysis of iPSC-CMs

To analyze contractile parameters in monolayer, iPSC-CMs were cultured on Matrigel-coated 6-well plates and measured using the Cytomotion imaging setup (IonOptix). Recordings (60–75 s in duration) were acquired at 250 frames per second. Contractile parameters (beat frequency, beat regularity, contraction and relaxation time) were analyzed using CytoSolver.

Ectopic expression of LZTR1 variants in iPSC-CMs

For ectopic expression studies, the human WT *LZTR1* coding sequence was synthesized (Genewiz/Azenta Life Sciences) and subcloned in *pcDNA3-HA-humanNEMO* (gift from Kunliang Guan, Addgene plasmid #13512) by exchanging the *NEMO* coding sequence. Additionally, the HA-tag was exchanged by an FLAG tag by synthesis of the fragment and subcloning in *pcDNA3-HA-LZTR1-WT* (Genewiz/Azenta Life Sciences). Patient-specific mutations were introduced into *pcDNA3-HA-LZTR1-WT* and *pcDNA3-FLAG-LZTR1-WT* using mutagenesis PCR. Plasmid DNA was isolated via the endotoxin-free NucleoBond Xtra Midi Plus EF kit (Macherey-Nagel). For transfection, WT1 iPSC-CMs cultured on Matrigel-coated 4-well chamber slides at a density of 7×10^4 cells per well were transfected at day 60 of differentiation with the respective plasmids using Lipofectamine Stem Transfection Reagent (Thermo Fisher Scientific) according to manufacturer's instructions with 700 ng per plasmid. After 24 h post-transfection, cells were fixed, stained, and imaged as described above.

To quantitatively analyze speckle size and filament length, a custom-build pipeline in CellProfiler (BROAD institute) was applied. For each *LZTR1* variant, plasmid transfections were performed in at least three replicates. All plasmids used are listed in Table S3 in the supplement.

Expression and purification of recombinant LZTR1 proteins

$LZTR1^{WT}$ and $LZTR1^{L580P}$ were expressed as C-terminal His-tagged proteins in Expi-293F cells (Thermo Fisher Scientific). pcDNA3.1-LZTR1-Myc-6xHis plasmid was a gift from Jens Kroll (Heidelberg University and German Cancer Research Center (DKFZ-ZMBH Alliance)).[49] The $LZTR1^{L580P}$ variant was introduced into the plasmid by site-directed mutagenesis as previously described.[11] Cells were transfected using ExpiFectamine 293 Reagent (Thermo Fisher Scientific) and cultured at a density of $3\text{-}5\times10^6$ cells/ml in a 37°C incubator with ≥80% relative humidity and 8% CO2 on an orbital shaker at 125×g for 3–4 days. Expression of the recombinant LZTR1 proteins was confirmed by Western blot analysis using an anti-His tag monoclonal rabbit antibody (Thermo Fisher Scientific). Following confirmation of expression, cells were harvested and lysed in a buffer containing 50 mM Tris/HCl (pH 7.4), 250 mM NaCl, 5 mM $MgCl_2$, 0.5 mM CHAPS, 0.5 mM sodium deoxycholate, 1 mM Na_3VO_4, 1 mM NaF, and 5% glycerol, and one complete EDTA-free protease inhibitor mixture tablet (Roche Diagnostics). The lysates were centrifuged at 20,000×g for 30 min at 4°C to obtain the soluble protein fraction containing the expressed LZTR1 proteins. Soluble fractions were applied to a Ni-NTA resin column and bound proteins, including LZTR1 proteins, were eluted with a buffer containing 50 mM Tris/HCl (pH 7.4), 250 mM NaCl, 5 mM $MgCl_2$, 5% glycerol, and 250 mM imidazole. Purified LZTR1 proteins were concentrated using a 30 kDa MWCO concentrator (Amicon), snap-frozen in liquid nitrogen, and stored at −80°C.

Analytical size exclusion chromatography (SEC) of soluble recombinant LZTR1 proteins

Purified LZTR1 proteins were centrifuged at 12,000×g for 10 min before being applied to an analytical Superose 6 10/300 SEC column (GE Healthcare Life Sciences) using a buffer containing 50 mM Tris/HCl (pH 7.4), 250 mM NaCl, 5 mM $MgCl_2$, 0.5 mM CHAPS, 0.5 mM sodium deoxycholate, and 5% glycerol at a flow rate of 0.5 mL/min. The column was calibrated using a kit (GE Healthcare Life Sciences) containing standards of known molecular weight, including blue dextran (2000 kDa), thyroglobulin (669 kDa), ferritin (440 kDa), aldolase (158 kDa), and ovalbumin (44 kDa) at their respective concentrations. The proteins were eluted with the equilibration buffer at a constant flow rate and the absorbance at 260 nm was monitored with a UV detector. The elution profiles were analyzed using OriginPro 2021 software (OriginLab) to determine the retention volume and molecular weight of the $LZTR1^{WT}$ and $LZTR1^{L580P}$ proteins. To ensure the accuracy of the SEC results, trichloroacetic acid precipitation of the SEC fractions was performed. The precipitated proteins were visualized by SDS-PAGE and Western blot analysis using an anti-His tag monoclonal rabbit antibody (Thermo Fisher Scientific) to determine the protein distribution in each fraction.

Pull-down assay for analysis of LZTR1-RAS interactions

Recombinant GST-fused RAS proteins in both inactive (GDP-bound) and active (GppNHp-bound) states were prepared according to established protocols.[50] In brief, nucleotide and protein concentrations were determined using HPLC and Bradford reagents, and aliquots were stored at −80°C. His Mag Sepharose Ni beads (GE Healthcare) were used for the protein-protein interaction assay. Recombinant $LZTR1^{WT}$ and $LZTR1^{L580P}$ proteins were each mixed with MRAS and RIT1 proteins in a buffer containing 50 mM Tris/HCl (pH 7.4), 250 mM NaCl, 10 mM $MgCl_2$, 20 mM imidazole, and 5% glycerol. Individual protein mixtures were prepared for each LZTR1 variant and RAS protein combination. Input samples were collected for analysis, representing the initial protein composition. The remaining volume of each sample was subjected to pull-down using His Mag Sepharose Ni beads. Mixtures were incubated for 1 h at 4°C to allow for specific protein-protein interactions. After incubation, beads were thoroughly washed with binding buffer to remove non-specific binding. Protein complexes were eluted from the beads using a buffer containing 250 mM imidazole. Eluted samples were analyzed by SDS-PAGE to visualize the separated proteins. To confirm the interactions, Western blotting was performed using an anti-His tag monoclonal rabbit antibody (Thermo Fisher Scientific) and GST monoclonal mouse antibody (own antibody). GST control samples were included in each pull-down experiment to serve as negative controls, assessing the specificity of observed protein-protein interactions.

In silico prediction of protein structures and multimer complexes

Homo-trimer configurations of the different *LZTR1* variants and configurations of LZTR1 with cullin 3 and MRAS were predicted using ColabFold (version 02c53)[30] and AlphaFold-multimer v2[51] with 6 recycles and no templates on an A5000 GPU with 24 GBs of RAM and repeated twice. The five predicted models for each variant were ranked according to the predicted template modeling score and interactions between the chains were inspected through the predicted alignment error generated by AlphaFold-multimer.

QUANTIFICATION AND STATISTICAL ANALYSIS

Data are presented as the mean ± standard error of the mean, unless otherwise specified. Statistical comparisons were performed using the D'Agostino-Pearson normality test and the nonparametric Kruskal-Wallis test followed by Dunn correction or the parametric t test in Prism 10 (GraphPad). Results were considered statistically significant when the p-value was ≤ 0.05.

Chapter IV. The *Chlamydia pneumoniae* effector SemD exploits its host's endocytic machinery by structural and functional mimicry

Authors: Fabienne Kocher, Violetta Applegate, Jens Reiners, Astrid Port, Dominik Spona, Sebastian Hänsch, Amin Mirzaiebadizi, Mohammad Reza Ahmadian, Sander HJ Smits, Johannes H Hegemann, Katja Mölleken

DOI: 10.1038/s41467-024-51681-3

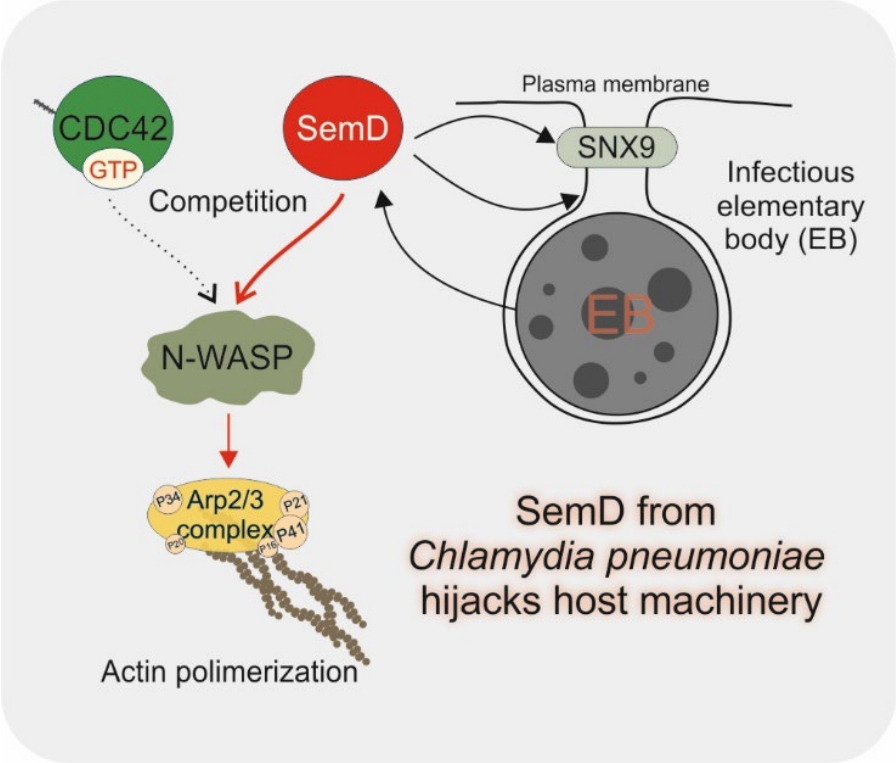

Status: Published

Journal: *Nature Communications*
JIF: 16.6
Contribution: ≈10–12%

A.M. suggested, designed, and performed a competition assay using stopped-flow fluorimetry to confirm host machinery exploitation by the *Chlamydia pneumoniae* effector SemD. He expressed and purified CDC42, and prepared both fluorescently labeled and GppNHp-bound forms. A.M. analyzed the resulting data, authored the corresponding *Materials and Methods* section, and contributed to the interpretation of results.

nature communications

Article

https://doi.org/10.1038/s41467-024-51681-3

The *Chlamydia pneumoniae* effector SemD exploits its host's endocytic machinery by structural and functional mimicry

Received: 12 February 2024

Accepted: 15 August 2024

Published online: 24 August 2024

Check for updates

Fabienne Kocher[1], Violetta Applegate[2], Jens Reiners[2], Astrid Port[2], Dominik Spona[1], Sebastian Hänsch[3], Amin Mirzaiebadizi[4], Mohammad Reza Ahmadian[4], Sander H. J. Smits[2,5], Johannes H. Hegemann[1,6] & Katja Mölleken[1,6]

To enter epithelial cells, the obligate intracellular pathogen *Chlamydia pneumoniae* secretes early effector proteins, which bind to and modulate the host-cell's plasma membrane and recruit several pivotal endocytic host proteins. Here, we present the high-resolution structure of an entry-related chlamydial effector protein, SemD. Co-crystallisation of SemD with its host binding partners demonstrates that SemD co-opts the Cdc42 binding site to activate the actin cytoskeleton regulator N-WASP, making active, GTP-bound Cdc42 superfluous. While SemD binds N-WASP much more strongly than Cdc42 does, it does not bind the Cdc42 effector protein FMNL2, indicating effector protein specificity. Furthermore, by identifying flexible and structured domains, we show that SemD can simultaneously interact with the membrane, the endocytic protein SNX9, and N-WASP. Here, we show at the structural level how a single effector protein can hijack central components of the host's endocytic system for efficient internalization.

The obligate intracellular bacterial pathogen *Chlamydia pneumoniae* (*Cpn*) causes infections of the upper and lower respiratory tract[1,2]. A certain proportion of these can result in severe respiratory illnesses, such as pneumonia, asthma and chronic bronchitis, as well as multiple sclerosis, inflammatory arthritis, lung cancer and Alzheimer's disease[2–6].

Cpn's developmental cycle begins with the adhesion of the infectious elementary body (EB) to the host-cell's plasma membrane (PM), and its internalisation into a membrane-enclosed "inclusion". The initial, transient contact between EB and host cell enables chlamydial surface proteins, such as Pmp proteins and LipP, to stably bind and activate host-cell receptors that trigger receptor-mediated internalisation[7–9]. However, engulfment of the EB requires a membrane vesicle that is three to four times larger in diameter than a classical endocytotic vesicle[10]. *Cpn* solves this problem by secreting several entry-related, early effector proteins directly into the host cell via its type-III-secretion system (T3SS). These include soluble factors, such as Cpn0572 (the homologue of *Chlamydia trachomatis (Ctr)* TarP), and proteins that bind to the host's PM, such as SemC and SemD[11–13]. By hijacking components of the host's endocytic machinery, early effectors trigger the formation of an intracellular membrane-enclosed vesicle that encompasses the EB[14–16]. The membrane-bound effectors SemC and SemD play a vital role in this process. Each possesses an amphipathic helix (APH) with high affinity for phosphatidylserine (PS),

[1]Heinrich Heine University Düsseldorf, Faculty of Mathematics and Natural Sciences, Institute for Functional Microbial Genomics, Düsseldorf, Germany. [2]Heinrich Heine University Düsseldorf, Faculty of Mathematics and Natural Sciences, Center for Structural Studies, Düsseldorf, Germany. [3]Heinrich Heine University Düsseldorf, Faculty of Mathematics and Natural Sciences, Center for Advanced Imaging, Düsseldorf, Germany. [4]Institute of Biochemistry and Molecular Biology II, Medical Faculty and University Hospital Düsseldorf, Heinrich Heine University Düsseldorf, Düsseldorf, Germany. [5]Heinrich Heine University Düsseldorf, Faculty of Mathematics and Natural Sciences, Institute of Biochemistry, Düsseldorf, Germany. [6]These authors jointly supervised this work: Johannes H. Hegemann, Katja Mölleken. e-mail: johannes.hegemann@hhu.de

a specific phospholipid found in the inner leaflet of the PM[12,13]. The binding of SemC to PS induces extensive membrane curvature while SemD (382 aa) recruits and activates central endocytic host proteins[12,13].

Downstream of its N-terminal APH, SemD harbours two proline-rich domains ($PRD1_{91\text{-}100}$ and $PRD2_{117\text{-}122}$, Fig. 1a), the first of which binds to the SH3 domain of SNX9[12]. During classical endocytosis, SNX9, a BAR domain (bin-amphiphysin-rvs) protein, binds to the PM, induces membrane curvature and promotes vesicle closure[17–19]. Similarly, by recruiting SNX9 via SemD, *Cpn* amplifies membrane deformation at the site of EB entry and ensures the closure and maturation of the endocytic vesicle.

SemD also possesses two centrally located WH2 domains, which are involved in G-actin binding[12]. Furthermore, the C-terminal 165 residues (aa 218-382) of SemD are required for recruitment of N-WASP, an endocytic host protein that re-organises the actin cytoskeleton by interacting with the actin-branching complex Arp2/3[12]. N-WASP is a ubiquitously expressed member of the WASP family[20]. Signal reception and transduction of N-WASP are mediated by its basic region (BR), its GTPase-binding domain (GBD) and its verprolin-central-acidic (VCA) domain, respectively. The GBD domain consists of the Cdc42/Rac interactive domain (CRIB) and a C-sub motif (Fig. 2a)[21,22]. In resting cells, N-WASP resides in an autoinhibited cytosolic state mediated by intramolecular interactions between the GBD and VCA domains[22,23]. During endocytosis, Cdc42, a small GTPase belonging to the Rho family, is activated by guanine nucleotide exchange factors (GEFs) that catalyse the replacement of bound GDP by GTP[24]. Active, GTP-bound Cdc42 ($Cdc42_{GTP}$) binds to the BR-GBD domain of N-WASP, and

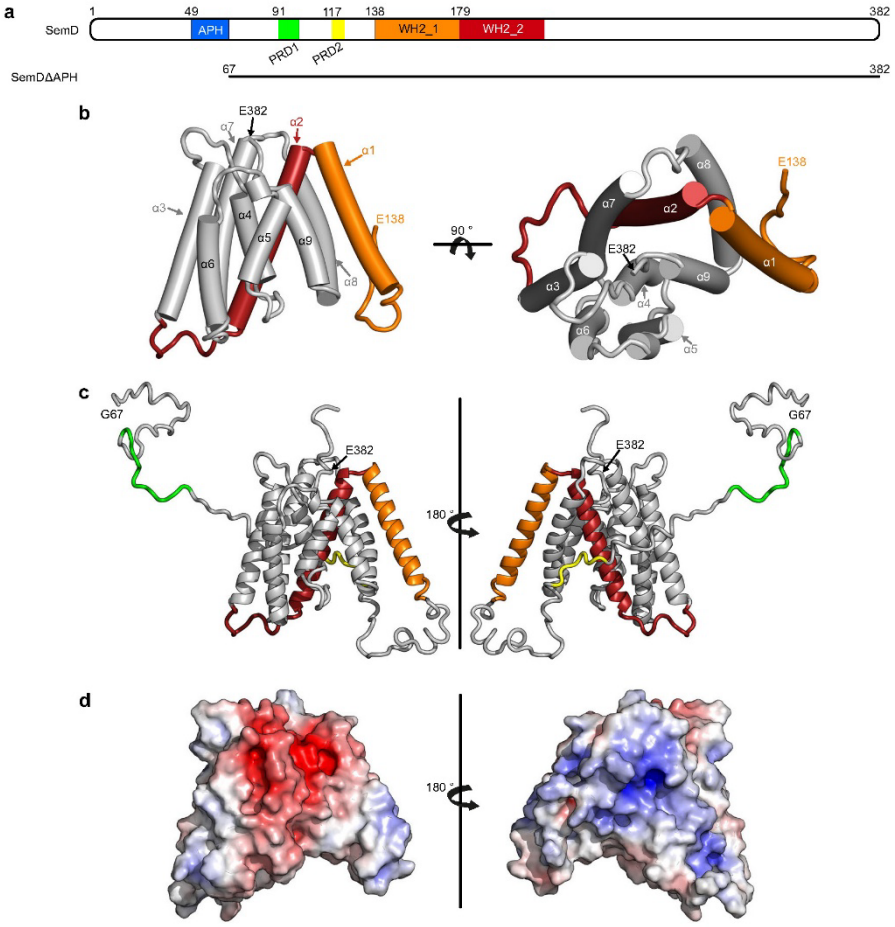

Fig. 1 | Crystal structure of SemDΔAPH. a Schematic representation of the primary structure of SemD, containing an $APH_{49\text{-}66}$, two proline-rich domains ($PRD_{191\text{-}100}$, $PRD2_{117\text{-}122}$) and two WH2 domains ($WH2\_1_{138\text{-}178}$, $WH2\_2_{179\text{-}216}$). $SemD\Delta APH_{67\text{-}382}$ is represented as a black bar. **b** The structure of SemDΔAPH as resolved by X-ray crystallography. The helices are depicted as cylinders and numbered from 1 to 9, starting at the N-terminus (α1- α9). In accordance with the colour code in **a**, the WH2_1 and WH2_2 are depicted in orange and red, respectively. The N-terminal E138 and the C-terminal E382 (both marked by black arrows) represent the first and last amino acids visible in the electron density. Right panel: 90° rotation. **c** SAXS best-fit CORAL model (χ^2 value of 1.197), based on the SemDΔAPH crystal structure, and including the added flexible tails (further models are shown in Supplementary Fig. 1h). PRD1 and PRD2 are coloured in green and yellow, respectively. Right panel: 180° rotation. G67 is the N-terminal amino acid, while E382, the last C-terminal residue of SemD, is followed by the C-terminal 10x-His-Tag. **d** Electrostatic surface representation of SemDΔAPH highlighting the negatively (red) and positively (blue) charged patches. Right panel: 180° rotation.

https://doi.org/10.1038/s41467-024-51681-3

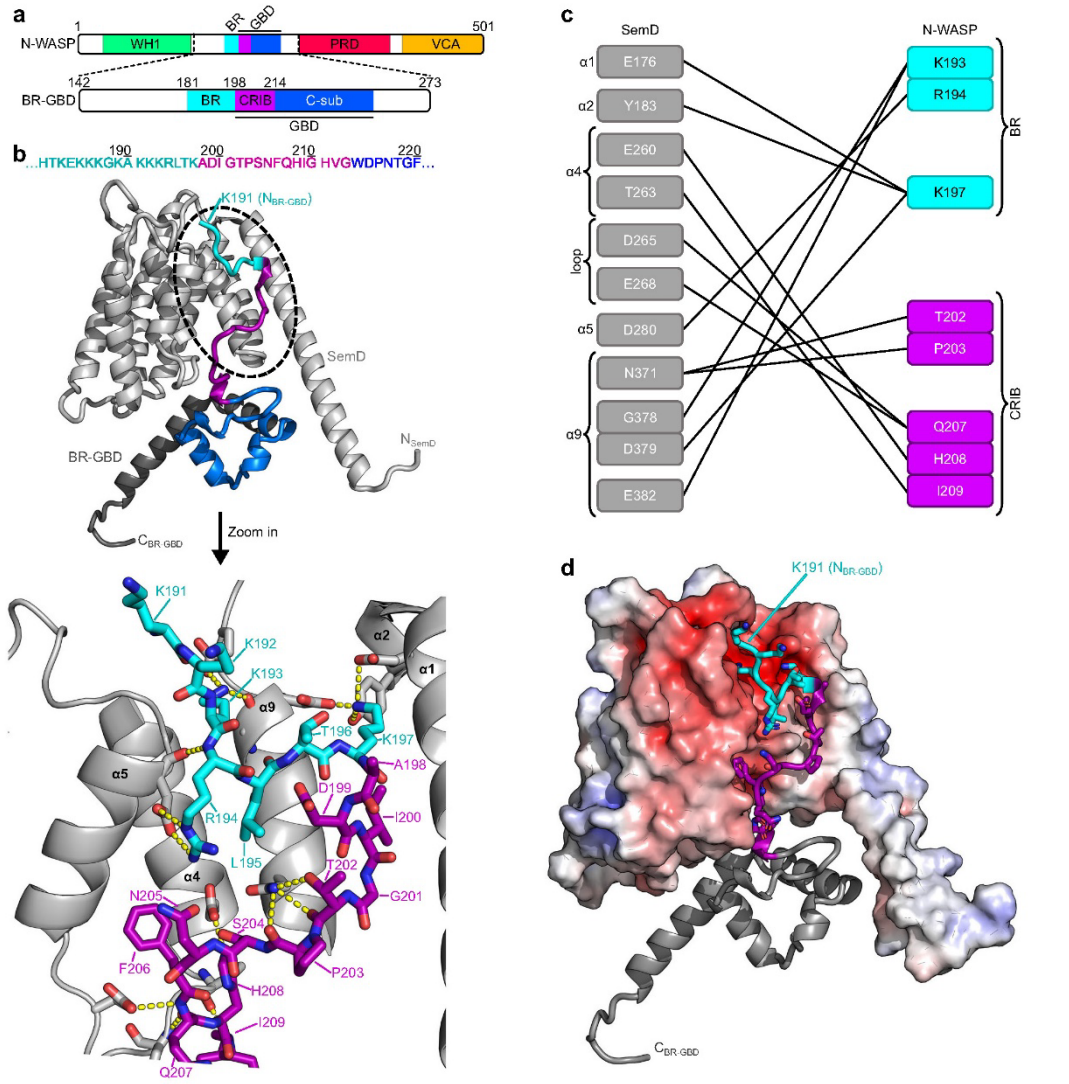

Fig. 2 | SemD engages with BR-GBD in a $Cdc42_{GTP}$-mimicking manner. **a** Schematic representation of the N-WASP primary sequence. $BR\text{-}GBD_{142\text{-}273}$ was used for complex formation with SemDΔAPH. It contains the $BR_{181\text{-}197}$ domain (basic region, cyan), the $CRIB_{198\text{-}213}$ domain (Cdc42/Rac interactive binding motif, magenta) and the $C\text{-}sub_{214\text{-}250}$ domain (blue). **b** The structure of SemDΔAPH in complex with BR-GBD as resolved by X-ray crystallography, shown in cartoon representation. SemDΔAPH is shown in light grey, BR-GBD is coloured in dark grey with the BR domain in cyan, the CRIB domain in magenta and C-sub domain in blue. The zoom in shows details of the binding of SemDΔAPH to BR-GBD. Important residues of SemDΔAPH and BR-GBD are shown in stick representation, while the rest of SemDΔAPH is shown as cartoon. Interactions (<3.5 Å) are shown by the yellow dashes. **c** Schematic representation of the detailed interactions between SemDΔAPH and BR-GBD. **d** Electrostatic representation of SemDΔAPH, highlighting the negatively charged patch in red and positively charged surface areas in blue. BR-GBD is coloured in dark grey (cartoon) with the BR domain in cyan and the CRIB domain in magenta, both depicted with stick residues.

triggers the release of the VCA domain, which in turn binds and actives the Arp2/3 complex (Supplementary Fig. 2b)[23,25]. Moreover, the BR binds to $PI(4,5)P_2$ in the inner leaflet of the PM, and recruits the actin polymerisation machinery to the site of endocytosis[26].

Cdc42 plays a central role in a large number of diverse biological processes such as the cell cycle, controlling gene transcription, regulating the cytoskeleton, cell movement and polarisation, hence being a target for many virulence factors secreted by bacterial pathogens[27–29]. These factors modulate the activity of Cdc42 by mimicking host regulators such as GEFs, GTPase activating proteins (GAPs) and guanine dissociation inhibitors (GDIs), or by covalently modifying Cdc42[30–34]. In addition, bacterial effector proteins can bind the autoinhibited Cdc42-binding domain of N-WASP, thereby initiating actin polymerisation[35].

During a *Cpn* infection, the C-terminus of the membrane-bound SemD interacts with the BR-GBD domain of N-WASP, thus triggering N-WASP activation and Arp2/3-mediated actin polymerisation via an unknown mechanism[12]. This ensures the provision of branched F-actin bundles required for extensive membrane deformation and maturation of the EB-containing vesicle.

In this work, we elucidate the mechanism involved by determining the three-dimensional structure of SemD, alone and in complex with its host interaction partners. We demonstrate that SemD, a protein of 382 aa, can interact simultaneously with the PM, SNX9 and N-WASP, thereby combining membrane association and deformation with modulation of the actin polymerisation machinery. Using small-angle X-ray scattering (SAXS), crystallography and mutational analysis, we show that SemD structurally and functionally mimics the activation of N-WASP by $Cdc42_{GTP}$, thus enabling *Cpn* to activate N-WASP in a $Cdc42_{GTP}$-independent manner. Further, by using pulldown assays and stopped-flow experiments, we show that SemD binds N-WASP more tightly than $Cdc42_{GTP}$, and that SemD is a specific N-WASP activator, not binding to formin like-protein L2 (FMNL2), another $Cdc42_{GTP}$-target protein. Our structural data also reveal that the N-WASP binding region of SemD is separated from its PRD1 – which is responsible for SNX9-SH3 binding – and from the membrane-binding APH domain via flexible linker regions. These features permit highly adaptable rearrangements of the individual binding sites, which reduce steric hindrance and facilitate simultaneous binding of the PM, SNX9 and N-WASP. These concurrent interactions enable *Cpn* to rapidly modulate the PM and the actin cytoskeleton, which ensures the successful formation of a large endocytic vesicle, and the rapid uptake of the EB within 15 minutes after its initial adhesion to a non-phagocytic host cell.

Results

SemD folds into a multipurpose interaction structure

To elucidate how SemD functions at the molecular level, we determined the 3D structure of the protein, N-terminally truncated up to and including the APH motif ($SemD\Delta APH_{67-382}$) at a resolution of 2.1 Å (Fig. 1a, b, Supplementary Fig. 1a, b and Supplementary Table 1). The resulting structure revealed that the C-terminal portion of SemDΔAPH (aa 138-382) folds into a rigid core, consisting of nine α-helices, which is N-terminally flanked by a long intrinsically disordered region (IDR, aa 67-137, Fig. 1b). Owing to its flexibility, the latter is not visible in the electron density. The proline-rich domains (PRD1 and PRD2) are within the IDR and provide a highly flexible interaction surface. The first and second α-helices harbour the WH2_1 and WH2_2 domains involved in G-actin binding[12] (Fig. 1b). Within the electron density, the amino acids are clearly visible, except for the connecting loop between helices 2 and 3, which is presumably flexible; here, the side-chains were not included in the final model. Although structural comparisons using EBI-fold revealed similar proteins (all with a root-mean-square deviation (RMSD) > 3.5 Å), no informative conclusions could be reached, since the only feature shared between them was a high helical content.

To clarify how SemDΔAPH behaves in solution, we performed SAXS analysis. We found that SemDΔAPH is a monomer in solution (Supplementary Table 2) and the *p(r)* function indicated a globular core – corresponding to the helical core domain revealed by the X-ray structure – and an elongated tail (Supplementary Fig. 1c–g). We calculated the theoretical scattering of the solved SemDΔAPH crystal structure and compared it with the experimental data for SemDΔAPH in solution. The resulting CRYSOL fit yielded a χ^2 value of 14.63 (an indicator on how well the model fits to the scattering curve in solution) and showed a high mismatch in the low s region (Supplementary Fig. 1c). This is not surprising, because the N-terminal residues (aa 67-137) are not solved in the crystal structure and the *p(r)* function showed an elongated tail, most probably the N-terminal region. Based on the information derived from SAXS data, we added the missing N-terminal residues (aa 67-137) to complete the SemDΔAPH structure (Fig. 1c). The resulting models showed that these N-terminal residues comprise the IDR tail (the best-fit model is shown in Fig. 1c, an overlay of independent models, showing the same tendency of the tail orientation, are shown in Supplementary Fig. 1h). This resulted in an improved χ^2 value of 1.20 (Supplementary Table 2). Furthermore, electrostatic analysis of the rigid core of SemD revealed a large, negatively charged patch on the front of the protein and a smaller positively charged patch on the back (Fig. 1d).

Taken together, the combined crystallographic and SAXS-based structure of SemDΔAPH reveals that its N-terminal segment, with which SH3 domain-containing proteins interact, is flexible. The nine α-helices that constitute the rigid core include the two WH2 domains, involved in G-actin binding, and the N-WASP interaction site[12]. Electrostatic analysis of the rigid core reveals two highly charged patches; a negative patch on the front and a positive patch on the back.

SemD structurally mimics $Cdc42_{GTP}$ for N-WASP activation

Generally, $Cdc42_{GTP}$ activates N-WASP by binding to its BR-GBD domain, which leads to the release of the VCA domain of N-WASP. The VCA domain then recruits the Arp2/3 complex, initiating actin branching and polymerisation (Supplementary Fig. 2b). However, during *Cpn* uptake, secreted SemD, whose APH domain interacts with the PM, binds to N-WASP and activates it in an as yet unknown fashion, thus initiating the formation of branched F-actin structures upon recruitment of the Arp2/3 complex[12]. Intriguingly, it has been shown that, when bound to synthetic membranes via its APH domain, SemD is capable of binding and activating N-WASP[12]. The interaction between the two proteins requires the C-terminal part of SemD (aa 218-382) and the BR-GBD segment of N-WASP (Fig. 2a)[12]. To understand the activation of N-WASP by SemD, we structurally analysed the complex formed by recombinant SemDΔAPH and the BR-GBD domain of N-WASP. To this end, we purified the recombinant proteins separately, allowed them to interact and isolated the resulting complex by size exclusion chromatography (SEC, Supplementary Fig. 2a). The elution fractions containing the complex were pooled and analysed by both crystallography and SAXS (Fig. 2b, d).

The co-crystal of SemDΔAPH in complex with BR-GBD yielded a structure with a medium resolution of 3.3 Å, which is attributable to the flexible termini of both proteins. Interestingly, the loop connecting helices 2 and 3 ($_{208}$GTSSTG$_{-213}$) of SemDΔAPH is stabilised in the complex and can now be modelled. Despite the moderate resolution of the crystals containing the SemDΔAPH – BR-GBD complex, the interaction surface between the two proteins is well resolved. Comparison of the structures of SemDΔAPH alone and in complex with BR-GBD revealed virtually identical conformations of the SemD core regions, as indicated by a low RMSD of 0.7 Å. Next, we identified intermolecular contact sites between SemDΔAPH and BR-GBD by identifying the amino acids that were closer than 3.5 Å to each other[36]. We found three positively charged residues within the BR domain of N-WASP (K193, R194 and K197) that interact directly with the negatively charged area found on the front of SemD, formed by helices α1, α2, α5 and α9 (Fig. 2b–d). Additionally, five residues of the N-WASP CRIB domain engage with residues in the SemD binding groove, mainly formed by helix α4, the adjacent loop and helix α9 (Fig. 2b, c). The N-WASP C-sub domain is located underneath the helical arrangement of SemDΔAPH, flanked by its extended helix α1 (Fig. 2b, d). Owing to the flexibility of the N-terminal domains of SemDΔAPH and BR-GBD, these regions are not resolved in the crystal structure of the complex.

Using SAXS, we validated the results obtained by crystallography. Analysis of BR-GBD alone showed that, in solution, it forms a monomer with a globular central region, flanked by a highly flexible N-terminal domain (Supplementary Fig. 3a–d, Supplementary Table 2). SAXS analysis of the SemDΔAPH – BR-GBD complex confirmed 1:1 stoichiometry in solution (Supplementary Table 2), in accordance with the

crystal structure. Analysis of the *p(r)* function and the dimensionless Kratky plot showed, that, upon formation of the complex, the unstructured segment of the BR-GBD does not adopt a specific secondary structure, but must take on a more constrained posture to bind to the core region of SemDΔAPH (Supplementary Fig. 3e–j), while the other domains retain their flexible characteristics. To confirm the position of the globular C-sub domain of N-WASP, we used the ensemble optimization method (EOM). Here, the interaction surface between SemDΔAPH and the N-WASP BR and CRIB segments found in the crystal structure is fixed, and the C-sub domain is allowed to vary freely in 3D space. Under these conditions, the conformation of the C-sub domain is the same as that seen in the crystal structure. Moreover, the final EOM models of the complex formed by SemDΔAPH and BR-GBD revealed, that an elongated complex conformation is preferred, which is attributable to the flexible N-termini of SemDΔAPH and BR-GBD (Supplementary Fig. 3k).

Taken together, our structural data show that the interaction of SemD with N-WASP requires the CRIB domain, together with the five C-terminal BR residues (aa 193-197) three of which are positively charged. Three of the five amino acids interact with the negatively charged patch on SemD, while the CRIB domain is embedded in the binding groove provided by SemD (Fig. 2).

SemD binds the N-WASP BR-GBD in a bipartite fashion

As described above, SemD binds to N-WASP by interacting with positively charged residues of the BR and with the CRIB domain. Moreover, structurally speaking, this mechanism is very similar to the interaction of WASP with $Cdc42_{GTP}$[37]. WASP and N-WASP belong to the same protein family, share 56% identity and 74% similarity, and have strikingly similar domain architectures and regulatory mechanisms[23]; however, the structure of the N-WASP – $Cdc42_{GTP}$ complex is not available thus far. Both proteins are crucial for transducing cell surface signals to the actin cytoskeleton, but while N-WASP is expressed ubiquitously, WASP is only present in non-erythroid hematopoietic cells[38]. To activate WASP (and N-WASP), $Cdc42_{GTP}$ interacts with the C-terminal residues of the BR domain – starting at the $KKK_{230\text{-}232}$ motif (corresponding to $KKR_{192\text{-}194}$ in N-WASP) – and with the CRIB domain (Fig. 3a)[23]. Mutational analysis indicated that the binding is strongly impeded when the $KKK_{230\text{-}232}$ motif in WASP is replaced by either uncharged or negatively charged amino acids[23,39]. Interestingly, with the C-terminal BR residues engaged in $Cdc42_{GTP}$ binding, the N-terminal BR residues can simultaneously bind to membranes containing $PI(4,5)P_2$, its preferred lipid[23].

Given the high structural similarity between the modes of interaction used by SemD and $Cdc42_{GTP}$ to bind and activate N-WASP, we tested for functional mimicry. To do so, we constructed deletion variants of the N-WASP BR-GBD domain lacking either the BR (BR-GBDΔ) or both the BR and the CRIB domain (BR-GBDΔΔ) (Fig. 3b). We also investigated whether or not the N-terminal BR residues mediate binding to $PI(4,5)P_2$ when SemD occupies the C-terminal BR residues. As an experimental setup, we chose to use giant unilamellar vesicles (GUVs) as a synthetic membrane model of the PM.

To test for recruitment of the individual BR-GBD variants by SemD, we used PS-containing GUVs, which mimic the lipid preferentially bound by SemD. For quantification, we calculated the fluorescence intensity ratio by measuring the maximal intensity at the perimeter of the GUV and setting it in relation to the average background intensity outside the GUV. In our control experiments, GFP alone showed no unspecific binding to GUV-bound SemD labelled with rhodamine ($SemD^{Rhod}$), and BR-GBD fused to GFP ($BR\text{-}GBD_{GFP}$) showed no binding to GUVs (Fig. 3c). Upon incubating $BR\text{-}GBD_{GFP}$ with $SemD^{Rhod}$ and GUVs, immediate colocalization of both proteins at the perimeter of the GUV was observed, indicating rapid and direct binding of $BR\text{-}GBD_{GFP}$ to GUV-bound $SemD^{Rhod}$ (Fig. 3c). Quantification revealed that binding persisted over a period of 20 min, and that fluorescence intensity at the GUV perimeter is 44.5 ± 15.3-fold higher than the average background fluorescence outside the GUV (Fig. 3d). Interestingly, upon incubation of $BR\text{-}GBD\Delta_{GFP}$ (lacking the BR domain) with $SemD^{Rhod}$ and GUVs, weak binding was visible after 5 min, which significantly increased over the next 15 min. However, even after 20 min, the fluorescence intensity ratio was more than 18-fold lower than the signal obtained for $BR\text{-}GBD_{GFP}$ (Fig. 3c, d). Finally, we also examined the binding of $BR\text{-}GBD\Delta\Delta_{GFP}$ (lacking both BR and CRIB) to $SemD^{Rhod}$. Quantification revealed a low fluorescence intensity ratio of 1.1 ± 0.2, which did not change over the next 20 min. Comparison of the data for $BR\text{-}GBD\Delta\Delta_{GFP}$ with the negative control GFP revealed no significant difference in fluorescence intensity ratio, at 1.1 ± 0.4. We therefore concluded that BR-GBDΔΔ, which lacks both BR and the CRIB domain, shows no recruitment to GUV-bound $SemD^{Rhod}$.

Next, we tested for simultaneous binding of $BR\text{-}GBD_{GFP}$ to $PI(4,5)P_2$ and $SemD^{Rhod}$ by using $PI(4,5)P_2$-containing GUVs. Indeed, $BR\text{-}GBD_{GFP}$ alone bound to $PI(4,5)P_2$-containing GUVs while $SemD^{Rhod}$ alone showed only a very weak colocalization to $PI(4,5)P_2$-containing GUVs (Supplementary Fig. 2c). When $SemD^{Rhod}$ was incubated with $PI(4,5)P_2$-bound $BR\text{-}GBD_{GFP}$, immediate colocalization of both proteins was observed at the perimeter of the GUV, suggesting that BR-GBD can indeed interact with both, lipids and SemD, simultaneously, in a manner similar to that of the N-WASP BR segment upon its interaction with $Cdc42_{GTP}$.

Taken together, these data imply that SemD not only structurally but also functionally mimics $Cdc42_{GTP}$ to recruit, bind and activate the central endocytic host protein N-WASP. Thereby, SemD binds to the BR-GBD via a bipartite interaction, which involves (i) the binding of positively charged amino acids located in the C-terminal BR domain to the negatively charged patch on SemD and (ii) the insertion of the CRIB domain into the binding groove provided by SemD. Thus, during *Cpn* uptake, the secreted and PM-bound SemD recruits N-WASP and abrogates its intramolecular autoinhibition by mimicking the $Cdc42_{GTP}$ activity in structure and function, leading to VCA release and finally to Arp2/3-mediated F-actin branching.

SemDΔAPH outcompetes $Cdc42_{GppNHp}$ for binding to N-WASP

So far, we have shown that SemD structurally and functionally mimics $Cdc42_{GTP}$ to bind and activate N-WASP. During a *Cpn* infection, PM-bound SemD redirects N-WASP function to the bacterial entry site thus mimicking $Cdc42_{GTP}$ for N-WASP binding. To compare N-WASP binding to SemD and $Cdc42_{GTP}$, respectively, we performed in vitro GFP-Trap® pulldown assays, using $BR\text{-}GBD_{GFP\text{-}His}$ as bait. $BR\text{-}GBD_{GFP\text{-}His}$ was incubated with $SemD\Delta APH_{His}$, or with Cdc42 bound to a non-hydrolysable GTP analogue ($Cdc42_{GppNHp}$)[23,40], or with equimolar amounts of $SemD\Delta APH_{His}$ and $Cdc42_{GppNHp}$. Following pulldown, we probed the composition of the flow through (FT) and elution fractions using immunodetection (Fig. 4a) and assessed the binding efficiency to $BR\text{-}GBD_{GFP\text{-}His}$, by correlating the band intensity of the elution to that of the FT (Elution:FT ratio, Fig. 4b). The negative control GFP indicated no unspecific binding to neither $SemD\Delta APH_{His}$ nor $Cdc42_{GppNHp}$ (Supplementary Fig. 4b). Conversely, the positive controls indicated evident binding of $SemD\Delta APH_{His}$ and $Cdc42_{GppNHp}$ respectively, to $BR\text{-}GBD_{GFP\text{-}His}$, with a quantified Elution:FT ratio of ~ 100% for each (Fig. 4a, b). Moreover, when equimolar ratios of $SemD\Delta APH_{His}$ and $Cdc42_{GppNHp}$ were added simultaneously to $BR\text{-}GBD_{GFP\text{-}His}$, $SemD\Delta APH_{His}$ showed an Elution:FT ratio of ~ 100 %, comparable to the positive control, while $Cdc42_{GppNHp}$ was now detected only in the FT (Fig. 4a, b). This experiment indicates that BR-GBD preferentially binds SemDΔAPH in the presence of active Cdc42. This result was confirmed and extended by stopped-flow measurements, in which addition of $SemD\Delta APH_{His}$ to a preformed $BR\text{-}GBD_{His}$ – $Cdc42_{GppNHp}$ complex led to dissociation of the latter (Fig. 4d), while $Cdc42_{GppNHp}$ in the absence of SemDΔAPH binds to $BR\text{-}GBD_{His}$ on a millisecond

https://doi.org/10.1038/s41467-024-51681-3

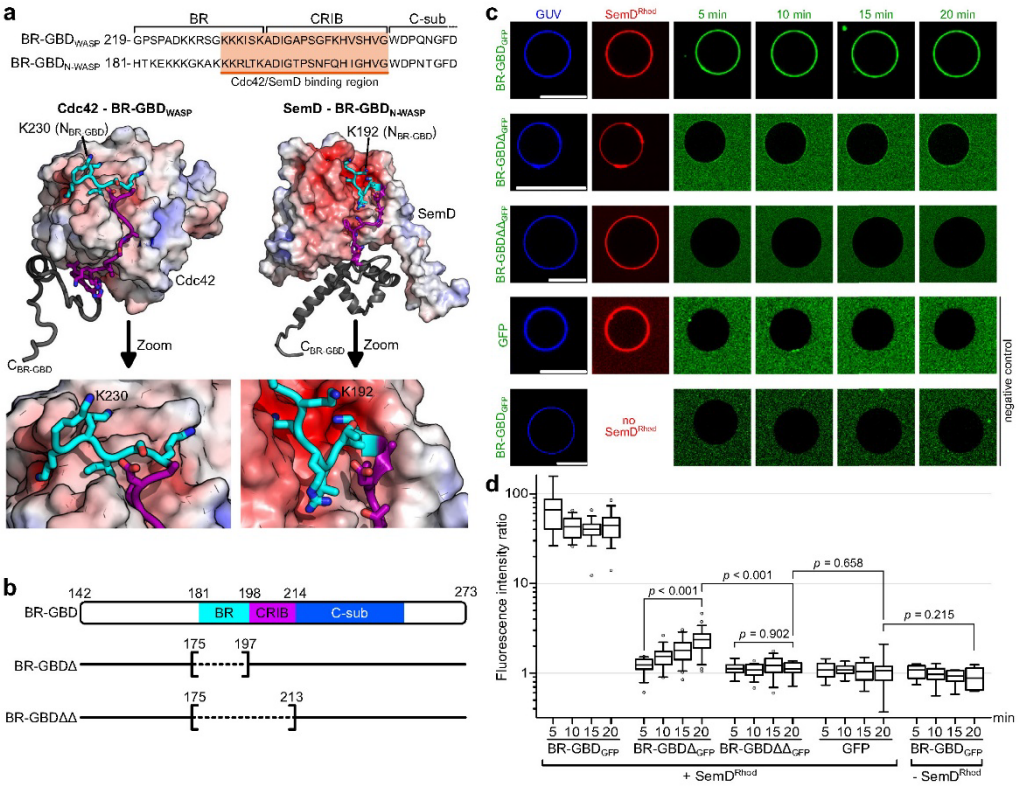

Fig. 3 | SemD recruits the BR-GBD region of N-WASP to membrane vesicles. **a** Amino acid sequence of WASP$_{219-259}$ (*human*) and N-WASP$_{181-221}$ (*Rattus norvegicus*) (of which the latter is identical to N-WASP$_{184-224}$ from *human*) (*top*). The orange box shows the sequence involved in binding to Cdc42$_{GTP}$ and SemD, respectively. The lower panel shows the structures of Cdc42$_{GTP}$ in complex with BR-GBD$_{WASP}$ (PDB: 1CEE[37]) and SemDΔAPH bound to BR-GBD$_{N-WASP}$. Cdc42$_{GTP}$ binds to the positively charged C-terminal KKK$_{230-232}$ motif of the BR from WASP and embeds the CRIB domain in the less charged binding groove. The same binding mechanism is observed for SemD, in which a negatively charged patch engages with the positively charged KKR$_{192-194}$ motif within the N-WASP BR domain and inserts the subsequent N-WASP CRIB domain into the SemD binding groove. **b** Schematic representation of BR-GBD and the deletion variants BR-GBDΔ (lacking the BR$_{175-197}$ domain) and BR-GBDΔΔ (lacking the BR$_{175-197}$ and the CRIB$_{198-213}$ domains). Dashed lines in square brackets mark the deleted protein regions. The first and last deleted amino acids are indicated. **c** Confocal images of PS-containing GUVs with rhodamine-labelled SemD (SemD^{Rhod}) and BR-GBD variants fused to GFP (BR-GBD$_{GFP}$). (scale bars 10 μm). **d** Quantification of bound protein to the GUV membrane based on the ratio of the maximal fluorescence at the perimeter of the GUV to the average background fluorescence outside the GUV. For each variant and time point, the fluorescence intensity ratio was calculated for up to 22 independent GUVs. The data are represented as boxplots with whiskers. The boxes are limited by the 25th and 75th percentile, including 50% of the data. The centre line shows the mean score. Whiskers denote 5–95% of all data and outliers are shown as grey dots. For comparing two groups, an unpaired, two-sided Student's *t* test was used. The data are representative for two independent data sets, both yielding similar results. Source data of both data sets are provided as Source Data file.

timescale (Fig. 4c). Collectively, these data show that SemD has a stronger binding capacity for N-WASP than active Cdc42$_{GTP}$, and is able to displace Cdc42$_{GTP}$ from the Cdc42$_{GTP}$ – N-WASP complex. Thus, during a *Cpn* infection, the locally secreted and PM-bound SemD underneath the invading EB most probably binds and activates cytosolic as well as Cdc42$_{GTP}$-bound N-WASP to initiate the branched F-actin mesh required for EB internalisation.

The preference of SemD for N-WASP over the physiological N-WASP activator Cdc42$_{GTP}$ raises the question of whether SemD is a specific activator of N-WASP or can also activate other Cdc42 target effectors. Cdc42 has been implicated as a key regulator of F-actin reorganisation, e.g. via activation of WASP/N-WASP to generate branched F-actin structures, as well as Formins, which play a critical role in nucleating actin filaments and promoting their elongation, thus influencing a large number of major cellular processes, involving actin dynamics such as cell motility, cell division and intracellular transport[41]. Formins are autoinhibited and require binding of active Cdc42$_{GTP}$ to the Formin GTPase binding domain for activation[42]. In in vitro pulldown assays, we tested whether SemD interacts with the mammalian FMNL2. We used recombinant FMNL2$_{GST}$ as bait and tested the binding of SemDΔAPH$_{His}$ and Cdc42$_{GppNHp}$ to it by analysing the FT and elution fractions (Fig. 4e). As expected, Cdc42$_{GppNHp}$ binds to FMNL2$_{GST}$, reaching an Elution:FT ratio significantly higher than the negative control with GST only (Fig. 4f). Interestingly, incubation of SemDΔAPH with GST or FMNL2$_{GST}$ showed no significant difference (Fig. 4e, f and Supplementary Fig. 4c, d). Thus, SemDΔAPH does not bind to FMNL2$_{GST}$, indicating that SemD specifically activates N-WASP and is not a general activator of Cdc42$_{GTP}$-dependent effector proteins, such as FMNL2.

Taken together, these data show that SemD copies Cdc42$_{GTP}$ at the EB entry side for N-WASP recruitment and activation.

https://doi.org/10.1038/s41467-024-51681-3

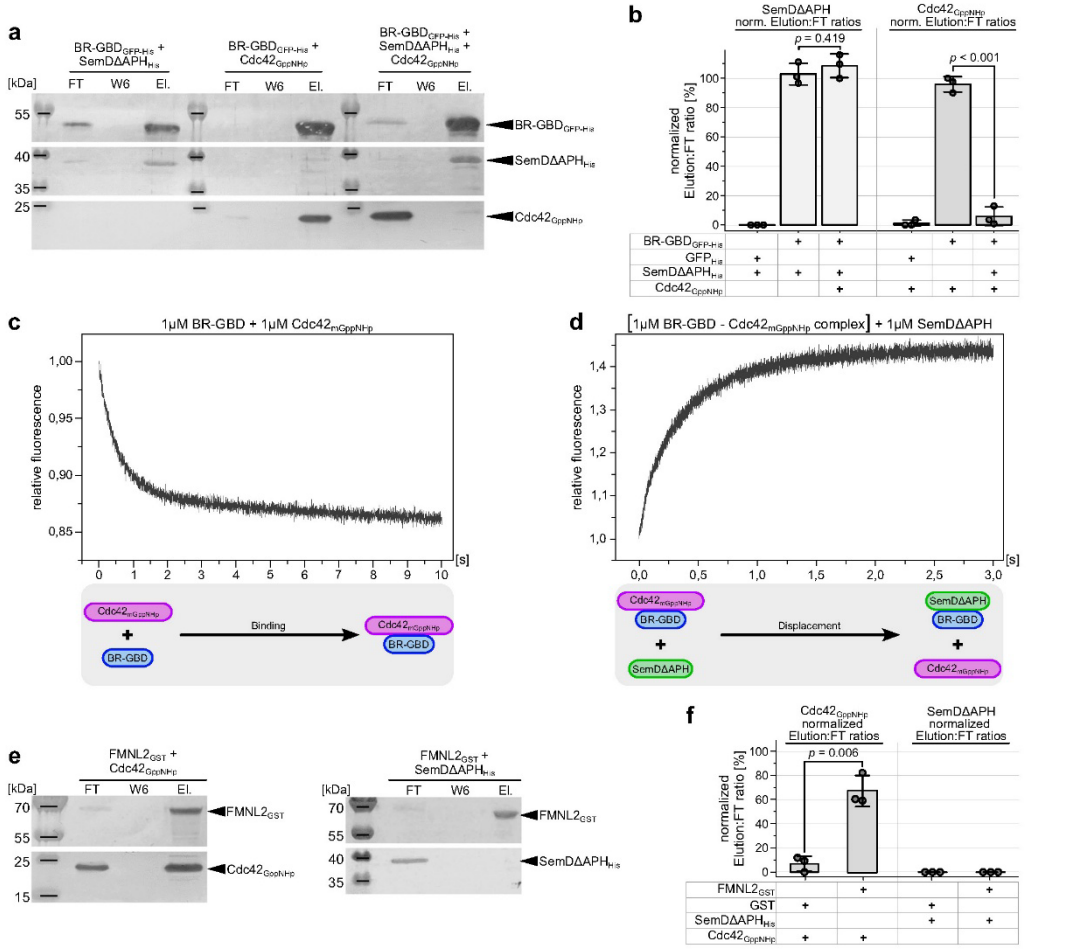

Fig. 4 | Relative to Cdc42$_{GppNHp}$, SemDΔAPH displays enhanced and specific binding to N-WASP. a GFP Trap® Pulldown experiments using equimolar ratios of purified recombinant SemDΔAPH$_{His}$, and active Cdc42 bound to the non-hydrolysable GTP analogue (Cdc42$_{GppNHp}$), were used to test their respective binding to BR-GBD$_{GFP-His}$. Complex formation between BR-GBD$_{GFP-His}$ and SemDΔAPH$_{His}$ or Cdc42$_{GppNHp}$ served as positive controls. Flow through (FT), wash 6 (W6) and elution (El.) fractions were analysed by SDS/PAGE and probed with anti-His (SemDΔAPH$_{His}$ and BR-GBD$_{GFP-His}$) and anti-Cdc42 (Cdc42) antibodies. Pull-down experiments were repeated three times with similar results. Replicates and negative controls are provided in Supplementary Fig. 4a and as Source Data to Fig. 4. **b** Quantification of western blotting in **a** is described in methods. Normalised (norm.) data are displayed as mean ± s.d. ($n = 3$ biologically independent experiments). Unpaired, two-sided Student's t-test was used to compare two groups. **c**, **d** Stopped-Flow experiments used to test the binding of equimolar ratios of BR-GBD$_{His}$ and Cdc42$_{mGppNHp}$ (**c**), as well as the displacement of Cdc42$_{mGppNHp}$ from BR-GBD$_{His}$ by the addition of an equimolar amount of SemDΔAPH$_{His}$ (**d**). The lower panels schematically indicate the relevant interactions. **e** GST-Agarose pulldown experiments used to probe the interactions of Formin L2$_{GST}$ (FMNL2$_{GST}$) with Cdc42$_{GppNHp}$ and SemDΔAPH$_{His}$ with Cdc42$_{GppNHp}$. Complex formation between Cdc42$_{GppNHp}$ and FMNL2$_{GST}$ served as a positive control. Flow through (FT), wash 6 (W6) and elution (El.) fractions were analysed by SDS/PAGE and probed with anti-His (SemDΔAPH$_{His}$), anti-GST (FMNL2$_{GST}$) and anti-Cdc42 (Cdc42) antibodies. Pulldown experiments were repeated three times with similar results. Replicates and negative controls are provided in Supplementary Fig. 4b, c and as Source Data to Fig. 4. **f** Quantification of western blotting in **e** is described in methods. Normalised (norm.) data are displayed as mean ± s.d. ($n = 3$ biologically independent experiments). Unpaired, two-sided Student's t test was used to compare two groups.

The SH3 domain of SNX9 stabilises the PRD1 in SemD

The SemD – N-WASP structure also revealed that the PRD1 and PRD2 domains of SemD, which are required for binding of the SH3 domain of Pacsin 2/3 or SNX9, are located on the flexible N-terminus of SemD, and not in its core region. To ascertain whether the interaction of SemD with SNX9 affects the structure of SemD and whether simultaneous binding of SNX9 and N-WASP to SemD is structurally feasible, we first examined the interaction between SemD and SNX9.

For this purpose, SemD, and a point mutated version ($_{mut}$SemD), in which the 12 proline and arginine residues in the PRD1 and PRD2 motifs were replaced by valine and alanine residues, respectively, were tested for interaction with the SH3 domain of SNX9 (Fig. 5a). Using PS-containing GUVs, that mimic the inner leaflet of the PM, we analysed

https://doi.org/10.1038/s41467-024-51681-3

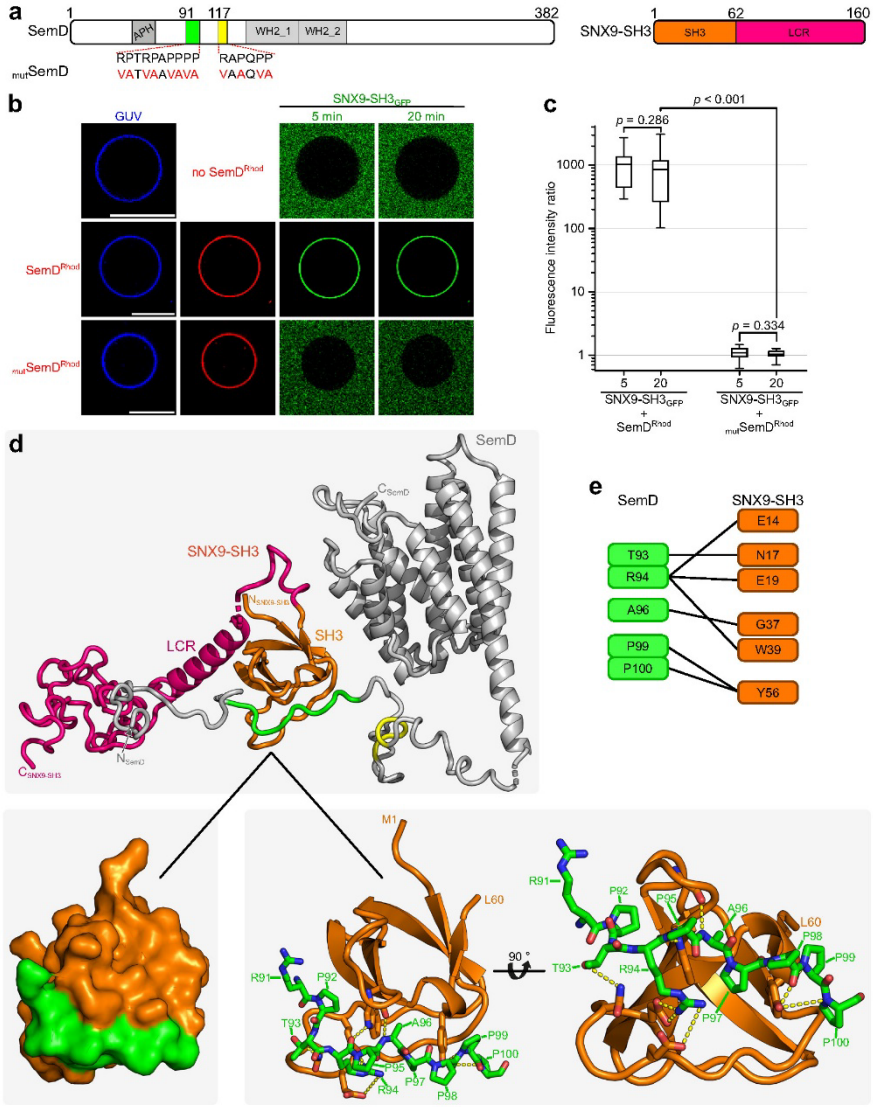

Fig. 5 | SemD binds to SNX9-SH3 PRD1. a (left) Schematic representation of SemD with PRD1 and PRD2 in green and yellow, respectively. Mutations for $SemD_{mut}$ are indicated by the amino acids in red. (right) Schematic representation of SNX9-SH3 with the SH3 in orange and the low complexity region (LCR) in pink. **b** Confocal images of PS-containing GUVs with labelled SemD or $SemD_{mut}$ and $SNX9\text{-}SH3_{GFP}$. (scale bars 10 μm). **c** Quantification of bound protein to the GUV membrane based on the ratio of the maximal fluorescence at the perimeter of the GUV to the average background fluorescence outside the GUV. For each variant and time point, the fluorescence intensity ratio was calculated for up to four independent GUVs. The data are represented as boxplots with whiskers. The boxes are limited by the 25th and 75th percentile, including 50 % of the data. The centre line shows the mean score. Whiskers denote 5–95% of all data and outliers are shown as grey dots. For comparing two groups, an unpaired, two-sided Student's *t* test was used. The data are representative for three independent data sets, all yielding similar results. Source data of all data sets are provided as Source Data file. **d** Cartoon model of SemDΔAPH (grey) with SNX9-SH3 (SH3 in orange) as determined by SAXS using the programme CORAL. SNX9-SH3 (orange) binds to PRD1 (green) of SemDΔAPH. (zoom in) The interactions between the two domains are displayed. **e** Proposed details of the interactions between the two domains, based on the model shown in **d**.

the ability of membrane-bound $SemD^{Rhod}$ and $_{mut}SemD^{Rhod}$ to recruit $SNX9\text{-}SH3_{GFP}$ (Fig. 5b). $SemD^{Rhod}$ immediately bound to PS-GUVs and rapidly recruited $SNX9\text{-}SH3_{GFP}$ (which does not bind to GUVs on its own), thus confirming published data[12] (Fig. 5b, c). Quantification revealed essentially immediate saturation of $SNX9\text{-}SH3_{GFP}$ binding to membrane-bound $SemD^{Rhod}$ with no further increase over the next 20 min. Strikingly, $_{mut}SemD^{Rhod}$ was unable to recruit $SNX9\text{-}SH3_{GFP}$ to GUVs at all (Fig. 5b, c). This complete loss of the ability of $_{mut}SemD^{Rhod}$

to recruit SNX9-SH3$_{GFP}$ clearly indicates that the PRD1 and/or PRD2 domain(s) are responsible for SNX9-SH3 binding. To analyse the effect of binding on the SemD structure, we set out to characterise the interaction on a structural level. Thus, we expressed and purified recombinant SemDΔAPH and SNX9-SH3, allowed for complex formation and purified the resulting complex via SEC (Supplementary Fig. 5). The isolated complex was then analysed by SAXS (Fig. 5d).

SAXS analysis of SNX9-SH3 apo indicated that the protein is found as a monomer in solution with a structured core, and a flexible region indicated via the Kratky plot (Supplementary Fig. 6 and Supplementary Table 2). We initially modelled the SemDΔAPH – SNX9-SH3 complex with AlphaFold2[43] to get information about the binding interface. It is predicted that the SH3 domain of SNX9 interacts with the PRD1 in SemD (Fig. 5d and Supplementary Fig. 7, Supplementary Table 2). The N-terminal part of the SemDΔAPH AlphaFold2 prediction showed very low values of the predicted local distance difference test (pLDDT <30), in line with our conclusion of the flexibility. The only exceptions are the amino acids responsible for the interaction with the SH3 domain from SNX9-SH3 (pLDDT values ~ 80). The SNX9-SH3 prediction showed only for the N-terminal part including the SH3 domain high pLDDT values (between 60–80) and the remaining C-terminal part remains unclear (pLDDT values < 30, Supplementary Fig. 7b). To prove the resulting AlphaFold2 complex model, we calculated the theoretical scattering pattern of this model and compared it with the experimental scattering data of the SemDΔAPH – SNX9-SH3 complex in solution. The resulting CRYSOL fit offered a χ^2 value of 8.49 and showed a high mismatch in the low s region (Supplementary Fig. 7c). This indicates that even the modelled complex contains all residues, and that the orientation of the domains/tails are not in line with the in-solution behaviour. The SAXS analysis of the SemDΔAPH – SNX9-SH3 complex confirmed a stoichiometry of 1:1, based on the molecular weight (Supplementary Table 2). We used the SemDΔAPH crystal structure and the binding interface of SH3 with PRD1 in SemD predicted by the AlphaFold2 model as a starting point for our modelling. The remaining flexible extensions were then remodelled with CORAL to better describe the in-solution behaviour of the SemDΔAPH – SNX9-SH3 complex (Supplementary Table 2). The resulting best-fit model of the remodelled SemDΔAPH – SNX9-SH3 complex is shown in Fig. 5d (an overlay of independent CORAL models is shown in Supplementary Fig. 7h). Based on our modelling, six residues of the SH3 domain bind to five specific residues of SemD PRD1 (Fig. 5d, e). Thus, PRD2 is not involved in direct contact with the SH3 of SNX9, in agreement with previous results obtained by Spona et al.[12], in which pulldown of SemD lacking the PRD1 showed no binding to SNX9.

Furthermore, structural analysis of the modelled complex showed that SH3 binding to PRD1 does not disrupt the conformation of the SemD core region, and therefore does not affect its ability to bind N-WASP. Indeed, the binding sites for host proteins on SemD are separated by flexible linkers, which minimise steric hindrance and allow the individual domains to be separately targeted in the 3D space.

SemD binds simultaneously to several host partners

Our findings thus far indicate that SemD contains spatially separated binding sites that are connected by highly flexible linker regions, which sterically allow simultaneous interactions with the PM, N-WASP and SNX9. To assess the potential concurrent binding of these interaction partners, we mixed and incubated recombinantly expressed SemDΔAPH, SNX9-SH3 and BR-GBD, and analysed the composition of the complex in the sample using SEC. Indeed, the resulting chromatogram showed one main peak, eluting at 9.9 ml, that contained all three proteins, as evidenced by SDS/PAGE analysis (Fig. 6a).

To set these findings in context with membrane-bound SemD, we used our GUV model system to ascertain whether such a complex is formed under these conditions. After allowing SemD^{Rhod} to bind to PS-containing GUVs, we added a three-fold molar excess (relative to SemD) of either DyLight 650 labelled SNX9-SH3 (SNX9-SH3$^{DyLight\,650}$) or BR-GBD$_{GFP}$, to fully saturate SemD^{Rhod}, which forms a 1:1 complex with SNX9-SH3 and with BR-GBD, respectively. We then added the second binding partner in an equimolar ratio to SemD^{Rhod}. As expected, even after the initial saturation of SemD^{Rhod} with one of the binding partners, the second partner was immediately recruited by SemD^{Rhod} (Fig. 6b). This effect does not depend on either the sequence of addition or the quantity of the introduced binding partner, indicating that a stable complex with both partners can be consistently assembled on the target membrane.

By combining our X-ray crystallographic and SAXS data for SemDΔAPH – BR-GBD and SemDΔAPH – SNX9-SH3, we were able to develop a potential 3D model for the complex that includes all three interaction partners (Fig. 6c), which confirmed that simultaneous interactions with SNX9-SH3 and BR-GBD are sterically possible. However, the exact arrangement of the individual binding sites remains elusive owing to the flexibility of the linker regions connecting the individual binding sites in SemD. Hence, our data indicate that PM-bound SemD can simultaneously recruit the host endocytic proteins SNX9 and N-WASP using spatially separated binding domains.

Discussion

As an obligate intracellular pathogen, *Chlamydia pneumoniae* interacts with host-cell proteins that ensure its survival and propagation. Perhaps the most critical stage in its replication cycle is its entry into a host cell.

For internalisation, the infectious EB (diameter 300-400 nm) requires co-option of the host's endocytic machinery to form a membrane-enclosed vesicle that is some 60 times larger in volume and 16 times larger in surface area than a classical endocytic vesicle (diameter 100 nm)[10]. This requires extensive remodelling of the PM and diversion of the host's actin cytoskeleton to enable growth, maturation and closure of the vesicle. Effector proteins translocated into the host cell play a vital role in these processes. The early secreted *Cpn* effector protein SemD binds to the inner leaflet of the PM below the invading EB and directly recruits G-actin and the essential endocytic proteins SNX9 and N-WASP[12].

Our structural study reveals that SemD interacts with host proteins via binding domains that are connected by intrinsically disordered linker sequences. This highly flexible arrangement facilitates simultaneous binding of several host endocytic proteins and modulation of the host's PM (Fig. 7). The precise contribution of these complexes to infection in vivo remains to be established, further complicated by the absence of a method for generating genetically manipulated *Cpn* strains.

We have shown in this study that SemD uses its C-terminal rigid core to bind and activate the actin nucleation- and branching-promoting factor N-WASP by structurally and functionally mimicking the normal role of the endogenous N-WASP activator Cdc42$_{GTP}$. Our structural and biochemical data further reveal that SemD provides the negatively charged patch and the binding groove required for selective binding of the positively charged C-terminal part of the BR and the CRIB domains of N-WASP, respectively, thus mimicking Cdc42$_{GTP}$-mediated N-WASP activation (Figs. 3a and 7). These interactions release the VCA domain of the autoinhibited N-WASP, which stimulates the Arp2/3 complex, thus promoting actin nucleation and branching. Intriguingly, the $K_{193}R_{194}K_{197}$ (KRK) motif in the C-terminal part of the BR region is responsible for both of these contacts with SemD (Fig. 2) and for binding to Cdc42$_{GTP}$, since a 9 aa deletion within the BR, that leaves the KRK motif intact, does not affect binding of the N-WASP mutant to Cdc42$_{GTP}$[25]. Mimicking of the endogenous Cdc42$_{GTP}$ protein, which is involved in many different cellular processes, requires specific activation of N-WASP by SemD. Based on our structural analysis, this occurs via the interaction of the KRK motif within the C-terminal BR region of N-WASP with a negatively charged patch on

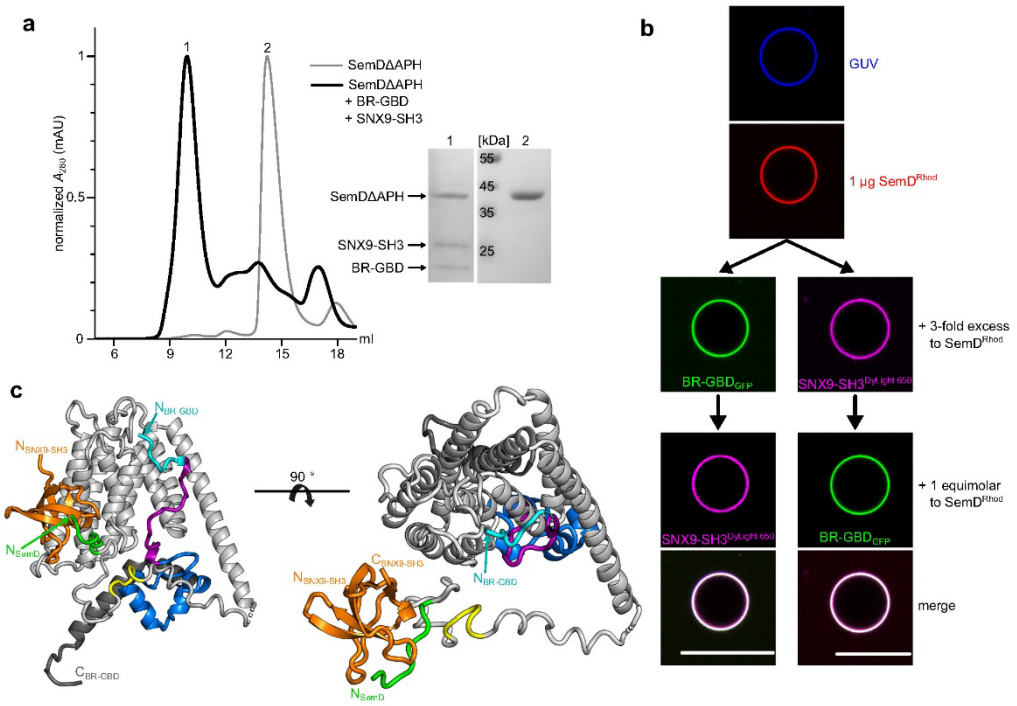

Fig. 6 | SemD simultaneously interacts with various binding partners. a SEC chromatograms of the complex composed of SemDΔAPH, BR-GBD and SNX9-SH3 (black), or SemDΔAPH alone (grey). The absorbance at 280 nm was normalised for the maximal absolute absorbance of the individual sample. The chromatogram of the complex revealed a major peak eluting at 9.9 ml (peak 1), while SemDΔAPH alone elutes at 14.2 ml (peak 2). The protein compositions of peaks 1 and 2 were analysed on an SDS gel (right) after staining with Coomassie brilliant blue. Lanes 1 and 2 were loaded with samples of the indicated peaks ($n = 1$). **b** Confocal images of PS-containing GUVs incubated with SemD^{Rhod}. A three-fold excess of either BR-GBD$_{GFP}$ ($n = 4$) or labelled SNX9-SH3 (SNX9-SH3$^{DyLight\ 650}$) ($n = 6$) was added, before the third binding partner was added in an equimolar ratio to SemD (scale bars 10 µm). **c** The structures of SNX9-SH3 and BR-GBD obtained by SAXS overlaid on SemDΔAPH. The nine core helices of SemDΔAPH are depicted in grey and the PRD1 and PRD2 in green and yellow, respectively. BR-GBD is depicted in cyan, magenta and blue, in accordance with the colour scheme in Fig. 2, and the depiction of the SNX9-SH3 domain in orange follows the colour scheme used in Fig. 5. Note that the three-dimensional orientation of the bound SH3 domain towards the nine-helix core might be different, owing to the presence of the flexible linker in between the two. Right panel: 90° rotation.

SemD, which is much larger than that found on Cdc42 (Fig. 3a) and involves negatively charged amino acids on four different helices (α1, α2, α5 and α9) of the SemD's rigid core (Fig. 2c). Indeed, membrane-bound SemD recruits the BR-GBD segment more than 18-fold more efficiently than the BR-GBDΔ mutant, which lacks residues 181 to 197 including the KRK motif (Fig. 3). Comparison of the rigid core structure of SemD alone and when bound to the BR-GBD fragment reveals almost identical conformations, suggesting that SemD serves as a stable platform for BR-GBD, thus maximising the chances for fast recruitment via electrostatic interactions. Our pulldown and stopped-flow experiments indicate that SemD binds N-WASP much more tightly than active Cdc42$_{GTP}$ does, and indeed SemD can displace Cdc42$_{GTP}$ from the Cdc42$_{GTP}$ – N-WASP complex (Fig. 4a–d). Thus, during a *Cpn* infection, SemD is secreted via the T3SS by the adhering EB, interacts with the cytosolic leaflet of the PM and recruits and activates cytosolic, autoinhibited N-WASP, but might also dislodge N-WASP from Cdc42$_{GTP}$ – N-WASP complexes. The strong binding of SemD to N-WASP probably accounts for the efficiency with which the locally PM-bound SemD recruits N-WASP to establish the branched F-actin mesh required for EB internalisation. Moreover, *Cpn* has maximised this actin-branching process by evolving a SemD protein, which according to our data does not bind to FMNL2, which is also activated by Cdc42$_{GTP}$ (Fig. 4e–f) and nucleates and elongates unbranched actin filaments at the barbed end[41]. Comparison of Cdc42$_{GTP}$ – N-WASP and SemD – N-WASP (Fig. 3a) with the Cdc42$_{GTP}$ – FMNL2 structure[44] reveals remarkable differences. N-WASP strongly interacts via its positively charged residues in the BR and the CRIB with the negatively charged patch on the front of Cdc42$_{GTP}$ and SemD, respectively. Conversely, FMNL2 interacts with Cdc42$_{GTP}$ via multiple hydrophobic and polar contacts formed between all five armadillo repeats of FMNL2 and the two switch regions of Cdc42. These differences probably account for the inability of SemD to bind FMNL2[44].

Thus, SemD is not only a very efficient activator of N-WASP, but is likely to be restricted in its activity to that protein. This would ensure that the limited numbers of SemD molecules secreted by the invading *Cpn* are fully available for this process. For actin nucleation and elongation of unbranched actin filaments *Cpn* secretes within the first 15 min of infection the soluble effector protein CPn0572, which belongs to the TarP protein family[45].

The SemD-mediated local reorganisation of the actin network is probably transient and short-lived, until bacterial entry has succeeded. In *Salmonella*, following host-cell entry, the architecture of the cytoskeleton is restored by, for example, the bacterial GTPase-activating protein SptP, which reverses the activation of Rac1

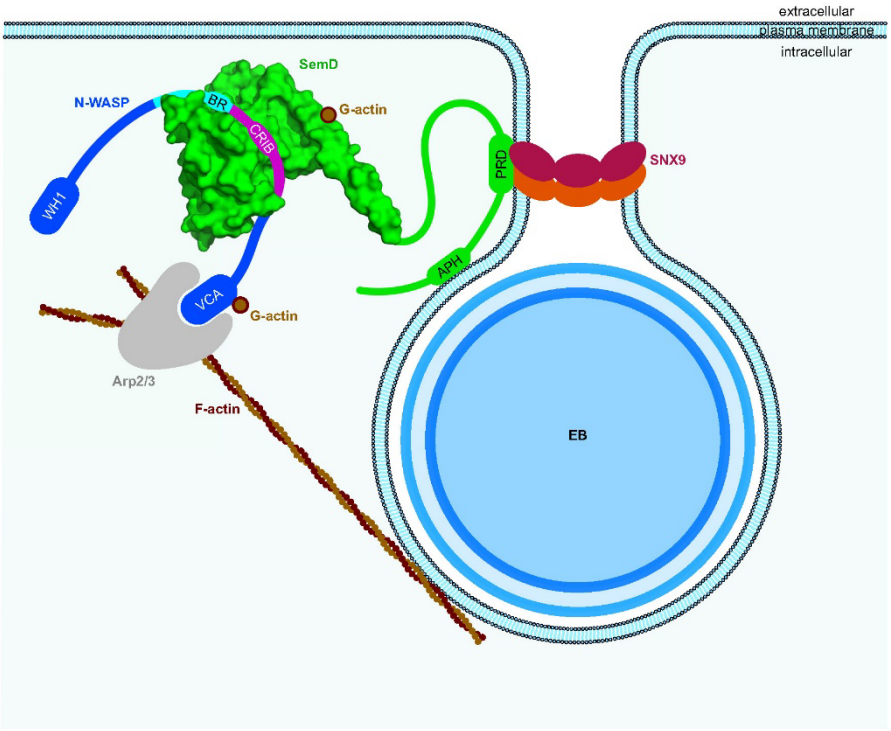

Fig. 7 | A chlamydial effector exploits structural and functional mimicry to manipulate the host endocytic machinery. The *Cpn* elementary body (EB) secrets SemD into the host cell, which binds to the inner leaflet of the plasma membrane. There, SemD recruits, binds and activates N-WASP by structurally and functionally mimicking the $Cdc42_{GTP}$ activation mechanism. SemD interacts with the C-terminal, positively charged amino acids of the N-WASP BR domain and further, the CRIB domain binds into the SemD binding groove. This then leads to the release of N-WASP from its auto-inhibited state. SemD also binds to the SNX9-SH3 domain, which brings the SNX9-BAR domain closer to the membrane. This in turn induces membrane deformation and eventually leads to closure of the matured endocytic vesicle. Due to the arrangement of the individual binding domains, which are connected by flexible linker regions, the binding sites can be freely oriented in 3D space, thus minimising steric hindrance. This can explain why SemD is postulated to be capable of binding simultaneously to the PM, SNX9 and N-WASP in vivo and hijacking their functions to promote the growth and maturation of the endocytic vesicle.

and Cdc42[46]. It will be interesting to ascertain how this is achieved by *Chlamydiae*.

The SemD-mediated activation of N-WASP differs fundamentally from that triggered by other pathogens, which evolved effector proteins mimicking modulators of Cdc42 activity, such as GAPs, GEFs and GDIs, or utilise covalent modification of the Rho GTPase (see introduction). The SemD activity is also completely different from the function of the effector $EspF_U$ secreted by enterohaemorrhagic *Escherichia coli* (EHEC). NMR data have revealed that $EspF_U$ binds the GBD domain via a C-like motif (similar to that found within the VCA domain) that releases the endogenous VCA domain in autoinhibited N-WASP[35,47]. Interestingly, initial data suggest that the *Ctr* effector TmeA might activate N-WASP like $EspF_U$ does which would imply that *Cpn* has evolved a completely different mechanism for F-actin polymerisation and branching, possibly as an adaptation to the different target tissues involved (*Cpn*: lung epithelia; *Ctr*: eye + urogenital tract epithelia)[48,49].

SemD also binds the BAR-containing protein SNX9, which is required for membrane deformation and recruitment of dynamin, and eventually leads to the scission of the matured vesicle[50]. Our model analysis suggests that, in the flexible N-terminal half of SemD, which is separated by a linker sequence from the rigid core that mediates N-WASP interaction, five residues in the PRD1 domain interact with six residues in the β-sheet structure of the SNX9-SH3 domain (Figs. 5 and 7). This binding mechanism is typical for proline-rich peptides that interact with SH3 domains, as has been shown for several other interaction partners (PDB: 1QWE, 2JMA, 2DRK, 2KXC). The predicted PRD2 domain is not involved in SH3 binding, as previously suggested by Spona et al.[12]. Thus, the amino acid sequences N- and C-terminal to PRD1 remain unstructured and may act as linkers that separate the PRD1 – SNX9-SH3 complex from the N-terminal membrane-binding domain APH and the C-terminal SemD core domain, which is involved in N-WASP binding (Figs. 6 and 7). Our structural model, based on the individual conformations of each protein pair (SemD + SNX9-SH3; SemD + $N\text{-}WASP_{BR\text{-}GBD}$), reveals that all protein interactions can occur simultaneously (Fig. 6c), and we have verified this by biochemical and membrane binding experiments that confirm concurrent recruitment of SNX9-SH3 and BR-GBD to GUV-bound SemD (Fig. 6b).

Helices α1 and α2 of SemD's rigid core carry the two predicted WH2 sequences essential for G-actin binding[12]. However, the stoichiometry of this interaction is not clear. Our SemD structure implies that WH2_1 on α-helix 1 is largely available for interaction with G-actin, while WH2_2 on α-helix 2 is not fully accessible (Fig. 1b, c), suggesting that WH2_1 might constitute the G-actin binding domain. Recruitment of G-actin by SemD increases the local G-actin concentration, which should promote formation of F-actin branches via the N-WASP-Arp2/3 pathway.

During evolution, *Cpn* has undergone a dramatic reduction in genome size to about 1 million bp in total. Consequently, many proteins must perform more than one task and our structural analysis reveals that this holds for SemD, an effector protein that is involved in the reshaping of membrane structure and actin cytoskeletal organisation during chlamydial endocytosis. Our data support a model in which a single PM-bound chlamydial effector protein, SemD, can simultaneously interact with several host proteins by separating the SemD binding domains with unstructured linker regions. Hence, the ability of SemD to mimic $Cdc42_{GTP}$ permits recruitment, binding and activation of the endocytic host protein N-WASP.

Methods

Antibodies and reagents

All lipids used in this study were obtained from Avanti Lipids and NHS-Rhodamine and DyLight650-NHS were sourced from Thermo Scientific. The primary antibody anti-penta-His (#34660, 1:2500) was purchased from Qiagen, anti-Cdc42 (#610929, 1:1000) was obtained from BD Transduction Laboratories and anti-GST (sc-374171, 1:500) was obtained from Santa Cruz Biotechnology. The secondary anti-mouse antibody coupled to alkaline phosphatase (#A3562, 1:30000) was purchased from Sigma-Aldrich.

Cloning, protein expression and purification

Cloning steps were carried out by in vivo homologous recombination in *Saccharomyces cerevisiae*. *semD* constructs used in this study were amplified from synthetic *semD* DNA purchased from GenScript, which was codon optimised for *Escherichia coli (E. coli)* expression. The *SNX9-SH3* sequence was amplified from a sequence encoding mCherry-SNX9[13], the *BR-GBD* fragments were amplified from a sequence encoding GFP-N-WASP (Addgene, #47406, *Rattus norvegicus*; The N-WASP BR-GBD protein fragment from *R. norvegicus* and *human* differ by 3 amino acids located N-terminal to the BR domain outside of our co-crystal structure). The fragments were integrated either into pSL4 (generating C-terminal 10xHis fusions) or into pDS94 (generating C-terminal GFP-10xHis fusions) (Plasmid list in Supplementary Table 4). The plasmid encoding FMNL2 (S171DD) fused to GST has been published previously[44]. Expression of the His-tagged proteins was carried out in *E. coli* BL21 (DE3, Invitrogen), and expression of GST-tagged FMNL2 was carried out in *E. coli* Rosetta. His-tagged proteins were purified using Ni-NTA Agarose (Cube Biotech) and dialysed in phosphate-buffered saline (PBS) (10 mM Na_2HPO_4, 1.8 mM KH_2PO_4, 137 mM NaCl, 2.7 mM KCl, pH 8.5), apart from SemDΔAPH for which a pH of 6.0 was used. GST-tagged FMNL2 was purified using Glutathione Agarose (Thermo Scientific) and dialysed in buffer containing 10 mM Tris-HCl, 150 mM NaCl, pH 8.5.

The preparation of Cdc42 in complex with guanosine 5′-(βγ-imino)-triphosphate (GppNHp) and N-methyl-anthraniloyl-labelled GppNHp (mGppNHp) was carried out as described by Eberth and Ahmadian[51]. In brief, human *CDC42* was integrated into pGEX-4T-1 (generating a GST-fusion)[23] and expressed in *E. coli* Rosetta. GDP-bound GST-Cdc42 was purified using a Glutathione sepharose column (Pharmacia, Uppsala, Sweden) and the GST-tags were cleaved with thrombin at 4 °C overnight. Proteins were reapplied to Glutathione Sepharose and cleaved Cdc42 was collected in the flow through. Protein quality and concentration were assessed by SDS-PAGE and high-performance liquid chromatography (HPLC), utilising a Beckman Gold HPLC system with a reversed-phase C18 column. GDP-bound Cdc42 proteins were incubated with a 1.5-fold excess of GppNHp/mGppNHp, non-hydrolysable GTP analogues, and agarose bead-coupled alkaline phosphatase (0.1–1 U per mg of Cdc42) to degrade GDP to GMP and Pi, thus facilitating the replacement of GDP with GppNHp/mGppNHp. The course of the reaction was monitored via HPLC using a buffer containing 100 mM potassium phosphate (pH 6.5), 10 mM tetrabutylammonium bromide, and 7.5–25% acetonitrile. Upon complete degradation of GDP, the samples were applied to prepacked NAP-5 columns to exchange the buffer for a fresh one devoid of free nucleotides. The concentration of nucleotide-bound Cdc42 was checked using the Bradford assay and HPLC to calculate the amount of active GppNHp-bound Cdc42. The proteins were then snap-frozen and stored at −80 °C for downstream analysis. Preparatory steps of $Cdc42_{GppNHp}$ are provided in Source Data.

Size exclusion chromatography

SEC was performed on an ÄKTA™ pure 25 L (Cytiva). For purified proteins, a pre-equilibrated HiLoad 16/600 Superdex 200 pg column was used with a flow-rate of 0.8 ml/min, for pre-formed complexes, a pre-equilibrated Superdex 200 increase 10/300 GL column (Cytiva) was used with a flow rate of 0.5 ml/min. All runs were performed at 4 °C.

Pulldown assays

Recombinant BR-GBD fused to GFP, or GFP alone, was mixed with an equimolar ratio of the test protein(s) and incubated for 5 min at RT. GFP Trap® agarose, preincubated in 3 % BSA, was added to the mixture, and binding was allowed to proceed for 30 min at 4 °C. After collection of the flow through, agarose was washed 6x with wash buffer (10 mM Tris-HCl, 200 mM NaCl, pH 8.5) and bound proteins were eluted by boiling the agarose in SDS sample buffer.

Recombinant FMNL2 fused to GST, or GST alone, was mixed with an equimolar ratio of the test protein(s) and incubated for 5 min at RT. Glutathione agarose was added to the mixture and binding was allowed for 30 min at 4 °C. After collecting the flow through, agarose was washed 6x with wash buffer (50 mM Tris-HCl, 150 mM NaCl, pH 8.5) and bound proteins were eluted by boiling the agarose in SDS sample buffer.

Individual steps were monitored by SDS/PAGE and immunoblot analysis, using specific primary and secondary antibodies.

Western blot quantification

Band intensities of the Flow Through (FT) and elution (El.) fractions were determined using the software GelAnalyzer 23.1.1. Bands were semi-automatically defined. The Elution:FT ratio [%] was calculated by dividing the intensity of the eluate by the total intensity, i.e. FT plus eluate. The ratio was normalised to the Elution:FT ratio [%] of the bait protein used. Individual band intensities and uncropped western blots are displayed in Source Data.

$$\text{Elution : FT ratio}[\%] = \frac{\text{Elution}}{\text{Elution} + \text{FT}} \tag{1}$$

$$\text{normalized elution : FT ratio}[\%] = \text{Elution : FT ratio} * \frac{1}{(\text{Elution : FT ratio})_{\text{bait}}} \tag{2}$$

Fluorescence stopped-flow spectrometry

Rapid fluorescence measurements were performed using a Hi-Tech Scientific stopped-flow spectrophotometer (Applied Photophysics SX20), as described by Hemsath et al.[23]. An excitation wavelength of 360 nm was used for N-methylanthraniloyl (m) derivatives of guanosine nucleotides in the stopped-flow analysis. Fluorescence detection was facilitated by a photomultiplier equipped with a cut-off filter to detect wavelengths above 408 nm. The association of N-WASP BR-GBD with mGppNHp-bound Cdc42 was measured using a buffer containing 30 mM Tris-HCl, 10 mM K_2HPO_4/KH_2PO_4 (pH 8.5), 5 mM $MgCl_2$ and 3 mM DTT at 25 °C. The experiment setup involved equimolar ratios of the proteins. The contents of one syringe containing 1 μM of mGppNHp-bound Cdc42 and a second syringe containing 1 μM N-WASP BR-GBD were rapidly mixed, and the change of relative

fluorescence was monitored in real-time. In a subsequent experiment, competition between SemDΔAPH and mGppNHp-bound Cdc42 was evaluated by rapidly mixing 1 μM of the pre-prepared complex of mGppNHp-bound Cdc42 and N-WASP BR-GBD with 1 μM of SemDΔAPH. The change in relative fluorescence was monitored in real-time.

Preparation of giant unilamellar vesicles

GUVs were prepared as described previously[52]. Briefly, PS-containing GUVs were prepared by mixing 9.75 mol% DOPC, 25 mol% cholesterol, 0.25 mol% Marina Blue™ DHPE and 25 mol% DOPS. Lipid mixtures were prepared and added to a chamber built of ITO-coated slides (Präzisions Glas & Optik) which were glued together with Vitrex (Vitrex Medical). The resulting cavity was filled with 10 % sucrose solution and sealed with Vitrex. The slides were connected via clamps to a frequency generator and an alternating voltage of 2.0 Vp-p was applied at a frequency of 11 Hz. The GUVs were grown in the dark at room temperature for 2–3 h.

Protein binding studies on giant unilamellar vesicles

For microscopic analyses, Angiogenesis μ-slides (Ibidi) were coated for 5–10 min at RT with 2 mg/ml β-casein (Merck) and washed three times with PBS. Then NHS-rhodamine-labelled recombinant SemD (1 μg) was mixed with 15 μl PBS and recombinant binding partner fused to GFP (1 μg) was added, together with 5 μl GUVs. For binding studies with three proteins, NHS-rhodamine-labelled recombinant SemD (1 μg) was mixed with recombinant BR-GBD fused to GFP (1-3 μg) and NHS-650–labelled recombinant SNX9-SH3 (1-3 μg) and 5 μl GUVs were added. The GUVs were allowed to settle down for 5 min at room temperature and then imaged for further 15 min at room temperature.

Microscopy

General imaging was performed using an inverse Nikon TiE Live Cell Confocal C2plus equipped with a 100x TIRF objective and a C2 SH C2 Scanner. All images were generated with Nikon NIS Elements software and quantified using ImageJ.

Fluorescence intensity ratio analysis

Acquired confocal GUV data were semi-automatically analysed using a self-written *fiji* macro to estimate signal accumulation at the perimeter of the GUV in relation to the surrounding medium. Multiple line selections were orthogonally placed at the GUV membrane, with the membrane placed in the middle. First, the macro plots a line-intensity profile for each selection with a given predefined linewidth (here: 5) in order to extract intensity data for the relevant signal channel and to store it in an array. The intensity of the signal surrounding the GUV is calculated as the mean intensity (I_{out}) of a predefined width (here: 1/5 of total profile length) at the front end of the line profile. Second, signal intensity peaks of the profile are identified by applying the built-in "array.findMaxima"-function with a given tolerance (here: 450), that returns peaks by default in descending significance order. The peak positions are checked, if they are located within a predefined width around the centre of the line profile (here: same as background width) and the intensity of the first, most significant peak (I_{peak}) within the limits, it is used for the following ratio calculation. Finally, the intensity ratio (r_{int}) is calculated as the quotient of signal intensity at the peak position (I_{peak}) divided by the mean signal intensity in the surrounding medium (I_{out}).

$$R_{int} = \frac{I_{peak}}{I_{out}} \quad (3)$$

Statistical analysis and data representation

Graphs were prepared using OriginPro v.2021b (OriginLab). For the comparison of two groups, an unpaired, two-sided Student's *t*-test was used. A *p*-value of less than 0.01 was considered as statistically significant. Images were prepared using the open-source software Inkscape (www.inkscape.org).

Structure determination via crystallisation

SemDΔAPH, either alone or in a complex with BR-GBD, was crystallised by sitting-drop vapour-diffusion in PBS at pH 6 (SemDΔAPH) or pH 8.5 (SemDΔAPH + BR-GBD) at 12 °C and at concentrations of 24 and 10 mg/ml, respectively. 0.1 μl were mixed with 0.1 μl of reservoir solution consisting of 0.1 M Citric acid (pH 2.5), 20% (w/v) PEG 6000 (pH 4) for SemDΔAPH and 0.1 M ammonium formate, 0.1 M MES (pH 6.2), 25% v/v PEG 400 for SemDΔAPH + BR-GBD. Crystals formed after 12-24 h (SemDΔAPH) or 5 d (SemDΔAPH + BR-GBD) were harvested and cryoprotected with mineral oil followed by flash-freezing in liquid nitrogen. Diffraction data were collected at −173 °C (100 K) at beamline P13 (DESY, Hamburg, Germany) using a 0.9763 Å wavelength for SemDΔAPH or at beamline ID30A-3 (ESRF, Grenoble, France) using a 0.9677 Å wavelength for SemDΔAPH + BR-GBD. Data reduction was performed using XDS[53] and Aimless[54] from the CCP4 Suite[55]. The structure was solved via molecular replacement with Phaser[56] using an AlphaFold[57] model (SemDΔAPH) or the apo structure (SemDΔAPH + BR-GBD) as search model. The initial model was refined alternating cycles of manual model building in COOT[58,59] and automatic refinement using Phenix[60] v.1.19.2. Data collection and refinement statistics are reported in Supplementary Table 1. In the SemDΔAPH + BR-GBD structure one amino acid, Glu207, was found not to obey the Ramachandran rule, and is positioned in the disallowed region. This residue is involved in a crystal contact.

SAXS measurement

SEC-SAXS data were collected on the P12 beamline (PETRA III, DESY Hamburg[61]). The sample-to-detector distance of the P12 beamline was 3.00 m, resulting in an achievable q-range of 0.03-0.07 nm-1. The measurements were performed at 20 °C with a protein concentration of 8 mg/ml for SemDΔAPH, 10 mg/ml for BR-GBD, 8 mg/ml for SemDΔAPH + BR-GBD and 3.3 mg/l for SemDΔAPH + SNX9-SH3. The SEC-SAXS runs were performed on a Superdex200 increase 10/300 GL column (100 μl injection volume, buffer: PBS pH 8.5 + 3 % glycerol) with a flow rate of 0.6 ml/min. 2400 frames were collected for each protein sample with an exposure time of 0.995 sec/frame. Data were collected on relative scale or absolute intensity against water.

All programmes used for data processing were part of the ATSAS Software package (Version 3.0.5)[62]. Primary data reduction was performed with the programmes CHROMIXS[63] and PRIMUS[64]. With the Guinier approximation[65], the forward scattering *I(0)* and the radius of gyration (R_g) were determined. The programme GNOM[66] was used to estimate the maximum particle dimension (D_{max}) with the pair-distribution function *p(r)*. The rigid body results from the crystal structure were used as a starting template to complete the structures of SemDΔAPH and BR-GBD (flexible N- and C-terminal parts were remodelled) with the programme CORAL[67]. The flexibility ensemble analysis of the SemDΔAPH + BR-GBD complex was done with EOM[68,69], based on the solved crystal structure and completed with the missing amino acids. The SemDΔAPH + SNX9-SH3 complex docking was done with CORAL[67], based on the solved SemDΔAPH structure and an AlphaFold2[43,57] prediction of the interaction site from the SH3 domain with the flexible SemDΔAPH tail.

Reporting summary

Further information on research design is available in the Nature Portfolio Reporting Summary linked to this article.

Data availability

We uploaded the SAXS data to the Small-Angle X-ray Scattering Biological Data Bank (SASBDB)[70], with the following accession codes: SASDTQ5 (SemDΔAPH), SASDTR5 (BR-GBD), SASDTS5 (SNX9-SH3),

SASDTT5 (SemDΔAPH + SNX9-SH3) and SASDTU5 (SemDΔAPH + BR-GBD). The crystal structures were deposited in the Protein Data Bank (PDB) with the accession codes 8S5R (SemDΔAPH) and 8S5T (SemDΔAPH+ BR-GBD). Further, the cited structures in this paper can be found with the following accession codes: 1QWE (C-SRC SH3 + APP12). 2JMA (R21A Spc-SH3:P41 complex). 2DRK (SH3 + Acan125). 2KXC (IRTKS-SH3 + ExpFu-R47). 1CEE (Cdc42 + WASP). The authors declare that the data supporting the findings of this study are available within the paper and its extended data files. Data underlying Figs. 3d, 4a, b, e, f, 5c and 6a and Supp. Figs. 2a, 4a, b, c, d and 5a are provided as Source Data files. All other data are available from the corresponding author upon request. Source data are provided with this paper.

Code availability

A custom code for Fiji 1.54 f used for the analysis of GUVs is available on https://github.com/SHaensch/2023_GUVQuant or https://doi.org/10.5281/zenodo.13165623.

References

1. Kuo, C. C. et al. Chlamydia pneumoniae (TWAR) in coronary arteries of young adults (15-34 years old). *Proc. Natl Acad. Sci. USA* **92**, 6911–6914 (1995).
2. Hahn, D. L. Chlamydia pneumoniae and chronic asthma: updated systematic review and meta-analysis of population attributable risk. *PLoS ONE* **16**, e0250034 (2021).
3. Balin, B. J. et al. Chlamydia pneumoniae: an etiologic agent for late-onset dementia. *Front. Aging Neurosci.* **10**, 302 (2018).
4. Beagley, K. W., Huston, W. M., Hansbro, P. M. & Timms, P. Chlamydial infection of immune cells: altered function and implications for disease. *Crit. Rev. Immunol.* **29**, 275–305 (2009).
5. Gerard, H. C. et al. Chlamydophila (Chlamydia) pneumoniae in the Alzheimer's brain. *FEMS Immunol. Med. Microbiol.* **48**, 355–366 (2006).
6. Porritt, R. A. & Crother, T. R. Chlamydia pneumoniae infection and inflammatory diseases. *Immunopathol. Dis. Ther.* **7**, 237–254 (2016).
7. Moelleken, K. & Hegemann, J. H. The Chlamydia outer membrane protein OmcB is required for adhesion and exhibits biovar-specific differences in glycosaminoglycan binding. *Mol. Microbiol.* **67**, 403–419 (2008).
8. Mölleken, K., Becker, E. & Hegemann, J. H. The Chlamydia pneumoniae invasin protein Pmp21 recruits the EGF receptor for host cell entry. *PLoS Pathog.* **9**, e1003325 (2013).
9. Galle, J. N., Fechtner, T., Eierhoff, T., Römer, W. & Hegemann, J. H. A Chlamydia pneumoniae adhesin induces phosphatidylserine exposure on host cells. *Nat. Commun.* **10**, 4644 (2019).
10. Rennick, J. J., Johnston, A. P. R. & Parton, R. G. Key principles and methods for studying the endocytosis of biological and nanoparticle therapeutics. *Nat. Nanotechnol.* **16**, 266–276 (2021).
11. Braun, C. et al. CPn0572, the C. pneumoniae ortholog of TarP, reorganizes the actin cytoskeleton via a newly identified F-actin binding domain and recruitment of vinculin. *PLoS ONE* **14**, e0210403 (2018).
12. Spona, D., Hanisch, P. T., Hegemann, J. H. & Mölleken, K. A single chlamydial protein reshapes the plasma membrane and serves as recruiting platform for central endocytic effector proteins. *Commun. Biol.* **6**, 520 (2023).
13. Hänsch, S. et al. Chlamydia-induced curvature of the host-cell plasma membrane is required for infection. *Proc. Natl Acad. Sci. USA* **117**, 2634–2644 (2020).
14. Cossart, P. & Sansonetti, P. J. Bacterial invasion: the paradigms of enteroinvasive pathogens. *Science* **304**, 242–248 (2004).
15. Cossart, P. & Helenius, A. Endocytosis of viruses and bacteria. *Cold Spring Harb Perspect Biol* **6**, a016972 (2014).
16. Colonne, P. M., Winchell, C. G. & Voth, D. E. Hijacking host cell highways: manipulation of the host actin cytoskeleton by obligate intracellular bacterial pathogens. *Front. Cell Infect. Microbiol.* **6**, 107 (2016).
17. Simunovic, M., Voth, G. A., Callan-Jones, A. & Bassereau, P. When physics takes over: BAR proteins and membrane curvature. *Trends Cell Biol.* **25**, 780–792 (2015).
18. Lundmark, R. & Carlsson, S. R. SNX9 - a prelude to vesicle release. *J. Cell Sci.* **122**, 5–11 (2009).
19. Lundmark, R. & Carlsson, S. R. Regulated membrane recruitment of dynamin-2 mediated by sorting nexin 9. *J. Biol. Chem.* **279**, 42694–42702 (2004).
20. Kramer, D. A., Piper, H. K. & Chen, B. WASP family proteins: Molecular mechanisms and implications in human disease. *Eur. J. Cell Biol.* **101**, 151244 (2022).
21. Machesky, L. M. & Insall, R. H. Scar1 and the related Wiskott-Aldrich syndrome protein, WASP, regulate the actin cytoskeleton through the Arp2/3 complex. *Curr. Biol.* **8**, 1347–1356 (1998).
22. Kim, A. S., Kakalis, L. T., Abdul-Manan, N., Liu, G. A. & Rosen, M. K. Autoinhibition and activation mechanisms of the Wiskott-Aldrich syndrome protein. *Nature* **404**, 151–158 (2000).
23. Hemsath, L., Dvorsky, R., Fiegen, D., Carlier, M. F. & Ahmadian, M. R. An electrostatic steering mechanism of Cdc42 recognition by Wiskott-Aldrich syndrome proteins. *Mol. Cell* **20**, 313–324 (2005).
24. Melendez, J., Grogg, M. & Zheng, Y. Signaling role of Cdc42 in regulating mammalian physiology. *J. Biol. Chem.* **286**, 2375–2381 (2011).
25. Rohatgi, R. et al. The interaction between N-WASP and the Arp2/3 complex links Cdc42-dependent signals to actin assembly. *Cell* **97**, 221–231 (1999).
26. Padrick, S. B. & Rosen, M. K. Physical mechanisms of signal integration by WASP family proteins. *Annu. Rev. Biochem.* **79**, 707–735 (2010).
27. Bustelo, X. R., Sauzeau, V. & Berenjeno, I. M. GTP-binding proteins of the Rho/Rac family: regulation, effectors and functions in vivo. *Bioessays* **29**, 356–370 (2007).
28. Fu, J. et al. The role of cell division control protein 42 in tumor and non-tumor diseases: a systematic review. *J. Cancer* **13**, 800–814 (2022).
29. Boquet, P. Small GTP binding proteins and bacterial virulence. *Microbes Infect.* **2**, 837–843 (2000).
30. Alto, N. M. et al. Identification of a bacterial type III effector family with G protein mimicry functions. *Cell* **124**, 133–145 (2006).
31. Huang, Z. et al. Structural insights into host GTPase isoform selection by a family of bacterial GEF mimics. *Nat. Struct. Mol. Biol.* **16**, 853–860 (2009).
32. Burkinshaw, B., Prehna, G., Worrall, L. & Strynadka, N. Structure of salmonella effector protein SopB N-terminal domain in complex with host Rho GTPase Cdc42. *J. Biol. Chem.* **287**, 13348–13355 (2012).
33. Schmidt, G. et al. Gln 63 of Rho is deamidated by Escherichia coli cytotoxic necrotizing factor-1. *Nature* **387**, 725–729 (1997).
34. Mosaddeghzadeh, N. & Ahmadian, M. R. The RHO family GTPases: mechanisms of regulation and signaling. *Cells* **10**, 1831 (2021).
35. Sallee, N. A. et al. The pathogen protein EspF(U) hijacks actin polymerization using mimicry and multivalency. *Nature* **454**, 1005–1008 (2008).
36. Tsai, C.-J., Lin, S. L., Wolfson, H. J. & Nussinov, R. Protein-protein interfaces: architectures and interactions in protein-protein interfaces and in protein cores. their similarities and differences. *Crit. Rev. Biochem. Mol. Biol.* **31**, 127–152 (1996).
37. Abdul-Manan, N. et al. Structure of Cdc42 in complex with the GTPase-binding domain of the 'Wiskott-Aldrich syndrome' protein. *Nature* **399**, 379–383 (1999).

38. Takenawa, T. & Suetsugu, S. The WASP-WAVE protein network: connecting the membrane to the cytoskeleton. *Nat. Rev. Mol. Cell Biol.* **8**, 37–48 (2007).
39. Wu, D. & Zhou, H. X. Designed mutations alter the binding pathways of an intrinsically disordered protein. *Sci. Rep.* **9**, 6172 (2019).
40. Ahmadian, M. R., Wittinghofer, A. & Herrmann, C. Fluorescence methods in the study of small GTP-binding proteins. *Methods Mol. Biol.* **189**, 45–63 (2002).
41. Schonichen, A. & Geyer, M. Fifteen formins for an actin filament: a molecular view on the regulation of human formins. *Biochim. Biophys. Acta* **1803**, 152–163 (2010).
42. Peng, J., Wallar, B. J., Flanders, A., Swiatek, P. J. & Alberts, A. S. Disruption of the Diaphanous-related formin Drf1 gene encoding mDia1 reveals a role for Drf3 as an effector for Cdc42. *Curr. Biol.* **13**, 534–545 (2003).
43. Mirdita, M. et al. ColabFold: making protein folding accessible to all. *Nat. Methods* **19**, 679–682 (2022).
44. Kuhn, S. et al. The structure of FMNL2-Cdc42 yields insights into the mechanism of lamellipodia and filopodia formation. *Nat. Commun.* **6**, 7088 (2015).
45. Zrieq, R., Braun, C. & Hegemann, J. H. The chlamydia pneumoniae tarp ortholog CPn0572 stabilizes host F-actin by displacement of cofilin. *Front. Cell Infect. Microbiol.* **7**, 511 (2017).
46. Fu, Y. & Galan, J. E. A salmonella protein antagonizes Rac-1 and Cdc42 to mediate host-cell recovery after bacterial invasion. *Nature* **401**, 293–297 (1999).
47. Cheng, H. C., Skehan, B. M., Campellone, K. G., Leong, J. M. & Rosen, M. K. Structural mechanism of WASP activation by the enterohaemorrhagic E. coli effector EspF(U). *Nature* **454**, 1009–1013 (2008).
48. Keb, G., Ferrell, J., Scanlon, K. R., Jewett, T. J. & Fields, K. A. Chlamydia trachomatis TmeA directly activates N-WASP to promote actin polymerization and functions synergistically with TarP during invasion. *mBio* **12**, e02861-20 (2021).
49. Faris, R., McCullough, A., Andersen, S. E., Moninger, T. O. & Weber, M. M. The Chlamydia trachomatis secreted effector TmeA hijacks the N-WASP-ARP2/3 actin remodeling axis to facilitate cellular invasion. *PLoS Pathog.* **16**, e1008878 (2020).
50. Carlton, J., Bujny, M., Rutherford, A. & Cullen, P. Sorting nexins-unifying trends and new perspectives. *Traffic* **6**, 75–82 (2005).
51. Eberth, A. & Ahmadian, M. R. In vitro GEF and GAP assays. *Curr. Protoc. Cell Biol.* **Chapter 14**, 19 (2009).
52. Mathivet, L., Cribier, S. & Devaux, P. F. Shape change and physical properties of giant phospholipid vesicles prepared in the presence of an AC electric field. *Biophys. J.* **70**, 1112–1121 (1996).
53. Kabsch, W. Xds. *Acta Crystallogr. D Biol. Crystallogr.* **66**, 125–132 (2010).
54. Evans, P. R. & Murshudov, G. N. How good are my data and what is the resolution? *Acta Crystallogr. D Biol. Crystallogr.* **69**, 1204–1214 (2013).
55. Winn, M. D. et al. Overview of the CCP4 suite and current developments. *Acta Crystallogr. D Biol. Crystallogr.* **67**, 235–242 (2011).
56. McCoy, A. J. et al. Phaser crystallographic software. *J. Appl. Crystallogr.* **40**, 658–674 (2007).
57. Jumper, J. et al. Highly accurate protein structure prediction with AlphaFold. *Nature* **596**, 583–589 (2021).
58. Emsley, P. & Cowtan, K. Coot: model-building tools for molecular graphics. *Acta Crystallogr. D Biol. Crystallogr.* **60**, 2126–2132 (2004).
59. Emsley, P., Lohkamp, B., Scott, W. G. & Cowtan, K. Features and development of Coot. *Acta Crystallogr. D Biol. Crystallogr.* **66**, 486–501 (2010).
60. Liebschner, D. et al. Macromolecular structure determination using X-rays, neutrons and electrons: recent developments in Phenix. *Acta Crystallogr. D Struct. Biol.* **75**, 861–877 (2019).
61. Blanchet, C. E. et al. Versatile sample environments and automation for biological solution X-ray scattering experiments at the P12 beamline (PETRA III, DESY). *J. Appl. Crystallogr* **48**, 431–443 (2015).
62. Manalastas-Cantos, K. et al. ATSAS 3.0: expanded functionality and new tools for small-angle scattering data analysis. *J. Appl. Crystallogr.* **54**, 343–355 (2021).
63. Panjkovich, A. & Svergun, D. I. CHROMIXS: automatic and interactive analysis of chromatography-coupled small-angle X-ray scattering data. *Bioinformatics* **34**, 1944–1946 (2018).
64. Konarev, P. V., Volkov, V. V., Sokolova, A. V., Koch, M. H. J. & Svergun, D. I. PRIMUS: a Windows PC-based system for small-angle scattering data analysis. *J. Appl. Crystallogr.* **36**, 1277–1282 (2003).
65. Guinier, A. Small-angle X-ray diffraction: application to the study of ultramicroscopic phenomena. *Ann. Phys.* **11**, 161–237 (1939).
66. Svergun, D. Determination of the regularization parameter in indirect-transform methods using perceptual criteria. *J. Appl. Crystallogr.* **25**, 495–503 (1992).
67. Petoukhov, M. V. et al. New developments in the ATSAS program package for small-angle scattering data analysis. *J. Appl. Crystallogr.* **45**, 342–350 (2012).
68. Bernado, P., Mylonas, E., Petoukhov, M. V., Blackledge, M. & Svergun, D. I. Structural characterization of flexible proteins using small-angle X-ray scattering. *J. Am. Chem. Soc.* **129**, 5656–5664 (2007).
69. Tria, G., Mertens, H. D., Kachala, M. & Svergun, D. I. Advanced ensemble modelling of flexible macromolecules using X-ray solution scattering. *IUCrJ* **2**, 207–217 (2015).
70. Kikhney, A. G., Borges, C. R., Molodenskiy, D. S., Jeffries, C. M. & Svergun, D. I. SASBDB: Towards an automatically curated and validated repository for biological scattering data. *Protein Sci.* **29**, 66–75 (2020).

Acknowledgements

We acknowledge DESY (Hamburg, Germany), a member of the Helmholtz Association HGF, for the provision of experimental facilities. Parts of this research were carried out at PETRA III and we would like to thank Haydyn Mertens and Dmytro Soloviov (EMBL Hamburg) for their assistance in using beamline P12. We also acknowledge the European Synchrotron Radiation Facility (ESRF) for the provision of synchrotron radiation facilities and we would like to thank Petra Pernot, for assistance in using beamline BM29. The crystal datasets were collected at the P13 beamline at DESY Hamburg and ID30A-3 at the ESRF Grenoble. Here, we would like to thank Selina Storm and Igor Melnikov for their excellent support during data collection. We thank our reviewers for the constructive comments. F.K. was a scholarship holder of the Graduate School "Molecules of Infection IV (MOI IV)" funded by the Jürgen Manchot Foundation. The Center for Structural Studies is funded by the DFG (Grant Nos. 417919780, INST 208/761-1 FUGG, INST 208/868-1 FUGG and INST 208/740-1 FUGG to S.H.J.S.). We acknowledge grant support from the DFG to A.M. and M.R.A. (grant number: AH 92/8-3) and to J.H.H. (Project-ID 267205415) of CRC 1208.

Author contributions

Conceptualisation: F.K., K.M. and J.H.H.; methodology F.K., K.M., M.R.A., A.M., S.H.J.S. and J.H.H.; investigation: F.K., V.A., J.R., A.P., D.S., S.H., A.M., M.R.A., S.H.J.S. and K.M., writing—original draft: F.K., K.M., S.H.J.S. and J.H.H.; writing—review & editing: F.K., K.M., S.H.J.S. and J.H.H; funding acquisition: J.H.H. and S.H.J.S.

Funding

Open Access funding enabled and organized by Projekt DEAL.

Competing interests

The authors declare no competing interests.

Additional information

Supplementary information The online version contains supplementary material available at https://doi.org/10.1038/s41467-024-51681-3.

Correspondence and requests for materials should be addressed to Johannes H. Hegemann.

Peer review information *Nature Communications* thanks Matthias Geyer, Laurent Terradot and the other, anonymous, reviewer for their contribution to the peer review of this work. A peer review file is available.

Chapter V. From Quiescence to Activation: The Reciprocal Regulation of Ras and Rho Signaling in Hepatic Stellate Cells

Authors: Saeideh Nakhaei-Rad*, Silke Pudewell*, Amin Mirzaiebadizi, Kazem Nouri, Doreen Reichert, Claus Kordes, Dieter Häussinger, Mohammad Reza Ahmadian

*These authors equally contributed to this study

DOI: 10.3390/cells14090674

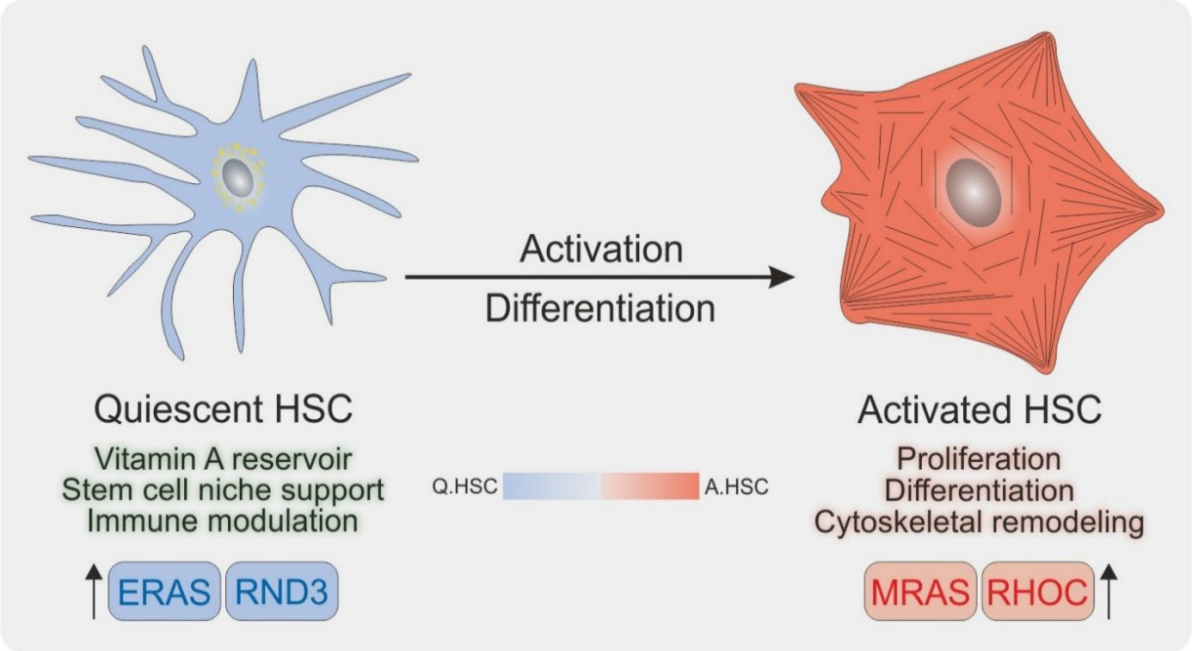

Status:	Published
Journal:	*Cells*
JIF:	5.1
Contribution:	≈15%

A.M. performed signaling analysis using Western blotting, including detection of GFAP, α-SMA, MRAS, phospho-ERK1/2, total ERK1/2, YAP, and γ-tubulin. A.M. contributed to data visualization, participated in writing, reviewing, and major editing the manuscript.

cells

MDPI

Communication

From Quiescence to Activation: The Reciprocal Regulation of Ras and Rho Signaling in Hepatic Stellate Cells

Saeideh Nakhaei-Rad [1,2,*,†], Silke Pudewell [1,†], Amin Mirzaiebadizi [1], Kazem Nouri [1,3], Doreen Reichert [4], Claus Kordes [5], Dieter Häussinger [6] and Mohammad Reza Ahmadian [1,*]

1 Institute of Biochemistry and Molecular Biology II, Medical Faculty and University Hospital Düsseldorf, Heinrich Heine University Düsseldorf, 40225 Düsseldorf, Germany; silke.pudewell@hhu.de (S.P.); amin.mirzaiebadizi@hhu.de (A.M.); kazem.nouri@vch.ca (K.N.)
2 Stem Cell Biology and Regenerative Medicine Research Group, Institute of Biotechnology, Ferdowsi University, Mashhad 9177948974, Iran
3 Department of Pathology and Laboratory Medicine, University of British Columbia, Vancouver, BC V6T 2B5, Canada
4 IUF—Leibniz Research Institute for Environmental Medicine, 40225 Düsseldorf, Germany; doreen.reichert@iuf-duesseldorf.de
5 Institute of Stem Cell Research and Regenerative Medicine, Medical Faculty, University Hospital Düsseldorf, Heinrich Heine University Düsseldorf, 40225 Düsseldorf, Germany; claus.kordes@hhu.de
6 Heinrich Heine University Düsseldorf, 40225 Düsseldorf, Germany; haeussin@uni-duesseldorf.de
* Correspondence: s.nakhaeirad@ferdowsi.um.ac.ir (S.N.-R.); reza.ahmadian@hhu.de (M.R.A.); Tel.: +98-51-38803798 (S.N.-R.); +49-211-8112384 (M.R.A.)
† These authors contributed equally to this work.

Abstract: Chronic liver diseases are marked by persistent inflammation and can evolve into liver fibrosis, cirrhosis, and hepatocellular carcinoma. In an affected liver, hepatic stellate cells (HSCs) transition from a quiescent to an activated state and adopt a myofibroblast-like cell phenotype. While these activated cells play a role in supporting liver regeneration, they can also have detrimental effects on liver function as the disease progresses to fibrosis and cirrhosis. These findings highlight the dynamic switching between different signaling pathways involving Ras, Rho GTPases, and Notch signaling. Notably, two specific members of the Ras and Rho GTPases, Eras and Rnd3, are predominantly expressed in quiescent HSCs, while Mras and Rhoc are more abundant in their activated forms. In addition, this study highlights the critical role of cytosolic Notch1 in quiescent HSCs and Rock in activated HSCs. We hypothesize that distinct yet interdependent intracellular signaling networks regulate HSC fate decisions in two key ways: by maintaining HSC quiescence and homeostasis and by facilitating HSC activation, thereby influencing processes such as proliferation, transdifferentiation, and mesenchymal transition. The proposed signaling model, combined with specific methodological tools for maintaining HSCs in a quiescent state, will deepen our understanding of the mechanisms underlying chronic liver disease and may also pave the way for innovative therapies. These therapies could include small molecule drugs targeting Ras- and Rho-dependent pathways.

Keywords: chronic liver disease; cirrhosis; hepatic stellate cells; liver fibrosis; quiescent state; Ras GTPases; Rho GTPases; small molecule inhibitors

Academic Editors: Pablo García De Frutos and Leo A. Van Grunsven

Received: 27 February 2025
Revised: 26 April 2025
Accepted: 1 May 2025
Published: 5 May 2025

Citation: Nakhaei-Rad, S.; Pudewell, S.; Mirzaiebadizi, A.; Nouri, K.; Reichert, D.; Kordes, C.; Häussinger, D.; Ahmadian, M.R. From Quiescence to Activation: The Reciprocal Regulation of Ras and Rho Signaling in Hepatic Stellate Cells. *Cells* **2025**, *14*, 674. https://doi.org/10.3390/cells14090674

1. Introduction

Chronic liver diseases have various underlying causes that lead to persistent liver inflammation, which can result in liver fibrosis, cirrhosis, and hepatocellular carcinoma. These are responsible for more than 1 million deaths worldwide each year [1]. At the onset

of fibrosis in liver disease, hepatic stellate cells (HSCs; also called Ito cells, lipocytes, fat-storing cells, or perisinusoidal cells) activate and transdifferentiate into contractile, matrix-producing myofibroblast-like cells, which are central events in hepatic fibrogenesis [2]. Myofibroblast-like cells produce the fibrous scar in hepatic fibrosis. HSCs contribute to 5–8% of total liver-resident cells and are located as pericytes of sinusoidal endothelial cells in the space of Disse bordered by hepatocytes [3]. HSCs play pivotal roles in liver development, immunomodulation, regeneration, and pathology [4]. They exhibit remarkable plasticity in their phenotype, gene expression profile, and cellular functions. In a healthy liver, HSCs remain quiescent and store vitamin A mainly as retinyl palmitate in cytoplasmic membrane-coated vesicles. Moreover, HSCs typically express ectodermal and mesodermal markers, i.e., glial fibrillary acidic protein (Gfap) and Desmin. They possess characteristics of stem cells, like the expression of *Wnt*, *Notch*, and *Eras* (embryonic stem cell-expressed Ras), which are required for developmental fate decisions [4,5]. HSCs have an expression profile that is highly reminiscent of mesenchymal stem cells. Because of their typical functions, such as differentiation into adipocytes and osteocytes and the support of hematopoietic stem cells, HSCs have been defined as liver-resident mesenchymal stem cells [6,7]. In recent years, it has become increasingly clear that pericytes support the vascular system by having a stem cell character [8], and they are also involved in developing chronic diseases such as fibrosis [9].

During activation, HSCs release vitamin A, upregulate various genes and differentiation markers, including α-smooth muscle actin (α-Sma) and collagen type I, and downregulate quiescence markers such as Gfap. Physiologically, HSCs represent pericytes and can produce an extracellular matrix (ECM). In pathophysiological conditions, the sustained activation of HSCs causes the accumulation of ECM in the liver. Fibrosis is a dynamic process involving cross-talk between HSCs, sinusoidal endothelial cells, liver-resident and -infiltrating immune cells, and hepatocytes [10]. Therefore, it is worthwhile to reconsider the impact of different signaling pathways on HSC fate decisions to modulate them. For example, quiescent HSCs might contribute to maintaining liver tissue but not fibrosis. Activated HSCs are multipotent cells, and studies have revealed a new aspect of HSC plasticity, i.e., their differentiation into liver progenitor cells during liver regeneration [11]. To date, several growth factors like platelet-derived growth factor (Pdgf), transforming growth factor-β (Tgfβ), and insulin-like growth factor 1 (IGF1), as well as different signaling pathways, have been described to control HSC activation through effector pathways, including canonical Wnt, Hedgehog, Notch, Ras-Mapk (mitogen-activated protein kinase), Pi3k (phosphoinositide 3-kinase)-Akt-Pkb (protein kinase B), Hippo-Yap (yes-associated protein), and Rho-Rock (Rho-kinase) [5,12–18]. However, it is necessary to identify the key players controlling HSC activation and to understand the mechanisms controlling HSC fate.

Altered Ras- and Rho-mediated signaling pathways represent some of the earliest events in HSC activation as identified by the present study and act as central hubs for intracellular signaling networks [5,19,20]. Ras and Rho proteins are small GTPases involved in diverse cellular processes, including intracellular metabolism, proliferation, morphogenesis, migration, and differentiation, and thus play critical roles in embryogenesis, development, and tissue remodeling [21]. In our molecular characterization of quiescent and activated HSCs, we identified the reciprocal and paralog-specific expression and activity of Ras- and Rho-related GTPases and associated signaling components such as Notch, Yap, and Erk [5,22]. Our data revealed a greater abundance of Eras, Rnd3, and Notch1 in the quiescent state, correlating with heightened activity in the Eras-Pi3k-Akt and Notch-Rnd3 pathways. Conversely, elevated levels of Mras and Rhoc were associated with activated HSCs, reflecting increased activities in the Ras-Mapk and Rhoc-Rock axes. These find-

ings provide new insights into the regulatory mechanisms distinguishing quiescent from activated HSCs and highlight the key molecular switches controlling this process.

2. Materials and Methods

The cell isolation procedure was approved by the local authority for animal protection (Landesamt für Natur, Umwelt und Verbraucherschutz Nordrhein-Westfalen, LANUV, Recklinghausen, Germany; reference number 84-02.04.2015.A287). Male Wistar rats (500–600 g) were obtained from the local animal facility of Heinrich Heine University (Düsseldorf, Germany) and used for the isolation of HSCs as described previously [5]. The number of animals used per experimental set was usually one, which resulted in a total number of animals of 3 to 5.

Cell isolation and culture, quantitative polymerase chain reaction (qPCR), immunoblotting, and confocal imaging were carried out according to previously described protocols [5]. Briefly, HSCs were seeded on stiff plastic shortly after their isolation and maintained as a monoculture in the presence of fetal calf serum (FCS). The combination of the rigid culture surface and the factors present in FCS, along with the conditions of monoculture, facilitates the activation of HSCs. Activation begins soon after cell isolation, with noticeable changes occurring between the 2nd and 3rd days of culture [1–3]. The qPCR primer sequences are listed in Supplementary Table S1. The antibodies used for immunoblotting and confocal imaging are listed in Supplementary Table S2. CRISPR/Cas9 genome editing was performed using four different guide RNAs (gRNA; Supplementary Table S3) for rat arginase 1 (Arg1; ID 29221) that were designed by using the Chopchop V3 online software tool [23]. The gRNAs were synthesized with the GeneArt Precision gRNA Synthesis Kit (Invitrogen, Carlsbad, CA, USA), pre-incubated with the TrueCut Cas9 Protein v2 (Invitrogen), and finally transferred into freshly isolated HSCs using the 4D-Nucleofector (program DS167; P3 Primary Cell 4D-Nucleofector X Kit L; Lonza, Basel, Switzerland). Control (mock) cells were treated similarly but without the gRNA. The HSCs were then cultured on plastic in DMEM with 10% FCS and 1% penicillin/streptomycin (37 °C, saturated humidity) for three days. The Arg1 KO efficacy was determined with Western blot.

3. Results and Discussion

3.1. Reciprocal, Paralog-Specific Ras and Rho GTPases in HSC Fate Determination

HSCs are the primary source of myofibroblast-like cells in liver fibrosis and primary liver cancer [24]. Freshly isolated quiescent Gfap-positive HSCs spontaneously undergo activation and transdifferentiation into myofibroblast-like cells when cultured on stiff plastic dishes, as indicated by the presence of α-Sma. We used the plasticity of freshly isolated HSCs as an in vitro cell model to investigate the control mechanisms that trigger their activation. In this regard, we focused on the molecular switches of Ras GTPases and their expression changes. The mRNA analysis revealed the remarkable changes in the family members of Ras between two states, quiescent vs. activated HSCs [5].

These data indicated the upregulation of a few genes related to the Ras GTPases, such as *Mras* (muscle Ras oncogene homolog), during the HSC activation phase. Eras, a unique member of the Ras family, was first identified in undifferentiated embryonic stem cells [25]. Unlike other members of the Ras family, Eras is not ubiquitously expressed, and its expression is cell-type and tissue-specific. We exclusively found Eras within quiescent but not activated HSCs (Figure 1A,B) [5]. In addition, Eras also regulates the Hippo pathway (Rassf-Mst-Lats), leading to the phosphorylation and subsequent degradation of Yap [5].

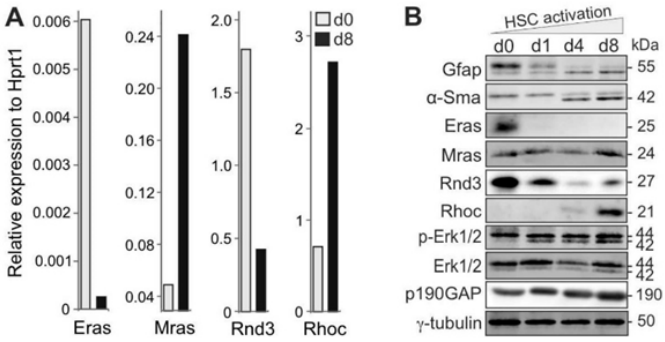

Figure 1. Reciprocal Ras signaling activities in quiescent and activated HSCs. (**A**) Differential *Eras*, *Mras*, *Rnd3*, and *Rhoc* expression in quiescent (d0) versus activated (d8) HSCs was analyzed with qPCR. Hypoxanthine-guanine phosphoribosyl transferase 1 (Hprt1) was used as a normalization control (n = 3). (**B**) Immunoblotting was performed to detect various signaling and marker proteins, as indicated, during HSC activation (n = 2). This analysis provides insight into the changes in protein expression associated with HSC activation. "d" stands for "day". Please check Supplementary Figure S1 for the original data of the Western blots.

Mapk and Pi3k-Akt are known as primary Ras-dependent signaling pathways. The activity of the Mapk signaling pathway is critical for cell proliferation and differentiation. It is significantly higher in activated than in quiescent HSCs, as evidenced by increased levels of phosphorylated Erk (p-Erk1/2) (Figure 1B). In contrast, the activation of Akt via the Pi3k and mTor complex 2 (mTorc2) pathways is particularly important in quiescent HSCs. Notably, Akt is more extensively phosphorylated at serine 473 by the rapamycin-insensitive mTorc2 complex compared with threonine 308 via the Pi3k-Pdk1 pathway, affecting various cellular processes in HSCs [5].

Remarkably, the downregulation of Eras was found to correlate with the upregulation of Mras (Figure 1B). We have previously demonstrated that Eras preferentially binds to the Pi3k effector protein and activates the Pi3k-Pdk1-Akt axis, not the Mapk pathway [5]. This suggests that Eras signaling through the Pi3k-Pdk1 and mTorc2 pathways fully activates Akt at both phosphorylation sites, thereby maintaining HSCs in their quiescent state. The increased activation of the Mapk pathway in activated HSCs is consistent with the increased expression of Mras, which has been shown to form a phosphatase holoenzyme complex with Shoc2 and PP1, controlling Raf1 dephosphorylation at S259 and initiating Mapk activation.

In addition to Ras family members, we observed the reciprocal expression of several Rho GTPases, including Rnd3 (Rho Family GTPase 3), and Rhoc (Ras Homolog Family Member C) (Figure 1A). Rho family proteins are key regulators of the actin cytoskeleton and influence various cellular processes, morphogenesis, proliferation, migration, and differentiation, which are fundamental for HSC activation [21]. Initial quantitative mRNA analyses of Rho family GTPases revealed the remarkable upregulation of Rnd3 in quiescent HSCs and Rhoc in activated HSCs (Figure 1A). Immunoblot analysis using validated antibodies against the Rho paralogs confirmed that Rnd3 and Rhoc are reciprocally expressed in quiescent and activated HSCs (Figure 1B). The high levels of Rhoc appear critical for HSC activation, but its activation might also be tightly regulated, most likely through its negative regulator p190RhoGAP (p190Rho guanosine triphosphatase-activating protein or p190GAP) [26]. Furthermore, it is striking that Rhoc and p190GAP are largely expressed in activated HSCs (Figure 1B). The regulation of p190GAP activity has been reported to control mechanical and Tgf-β signaling and, thus, the fibrotic phenotype of idiopathic

pulmonary fibroblasts [27]. Therefore, we propose that Rhoc and its inactivator p190GAP may be important components in the regulation of Rock (see below) during HSC activation and myofibroblast formation. Rnd3 has been reported to be a transcriptional target of activated Notch1 as it is more expressed in quiescent HCSs [28].

3.2. The Key Role of Cytosolic Notch1 and HSC Quiescence State

Notch proteins (Notch1–4) are conserved transmembrane receptors involved in numerous developmental processes, including stem cell self-renewal. Notch1 is expressed as a target gene of the canonical Wnt signaling pathway in quiescent HSCs [29]. Several studies suggest that Notch1 signaling regulates stem cell maintenance and counteracts their differentiation [30–32]. Quantitative mRNA analysis revealed the reciprocal expression of Notch1 and Notch2 during activation. In contrast to *Notch2*, *Notch1* and its target gene *Hes1* were found to be predominantly expressed in quiescent HSCs (Figure 2A).

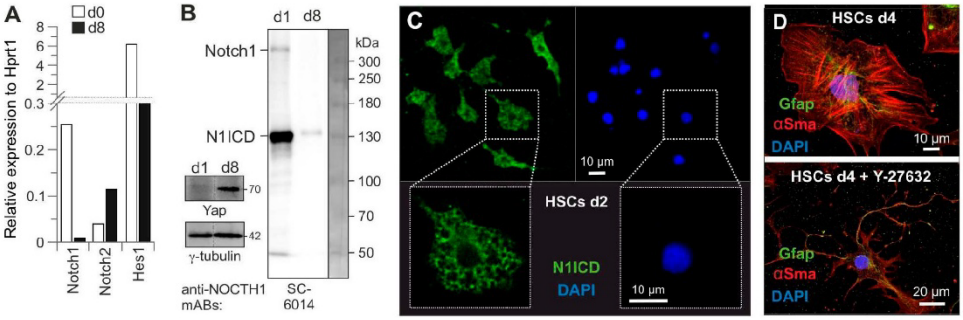

Figure 2. The significance of cytosolic Notch1 in quiescent HSCs and Rock in activated HSCs. (**A**) While *Notch1* and its target gene, *Hes1*, are downregulated during HSC activation, the expression of *Notch2*, a Yap target gene, is strongly upregulated. (**B**) In contrast to Yap, the Notch1 protein is predominantly present in HSCs (d1) as the Notch1 intracellular domain (N1ICD; Cell Signaling SC-6014). Full-length Notch1 was detected at 300 kDa. The Yap and γ-tubulin loading control blots have been trimmed to remove d1 and d4 (dashed line) (n = 2). (**C**) Full-length Notch1 and N1ICD are strikingly localized in the cytosol of HSCs (d2) using a cell signaling antibody (#4380). (**D**) Rock inhibition with 10 µM of Y-27632 (#S1049, Selleckchem) blocked culture-induced HSC activation, most likely by inhibiting the Rock-mediated morphological transition of HSCs. Untreated cells exhibit the cell shape of activated HSCs, which are much larger and contain more α-Sma, whereas Y-27632-treated cells are still stellate cells at d4 with Gfap-containing processes that more closely resemble quiescent HSCs. "d" stands for "day".

The canonical Notch1 signaling pathway involves the sequential proteolytic processing of Notch1 by Adam17 (a disintegrin and metalloprotease 17) and γ-secretase to release the intracellular domain of Notch1 (N1ICD), which, in turn, translocates to the nucleus and, as a multimeric protein complex, displaces transcriptional co-repressors by recruiting transcriptional co-activators. N1ICD has been shown to control transcription and maintain the undifferentiated status of stem cells [33,34]. As shown in Figure 2B, Notch1 is present in quiescent HSCs largely in a processed form as 120 kDa N1ICD, whereas Yap is exclusively present in activated HSCs [5], consistent with the expression of its target gene *Notch2* (Figure 2A). Subsequent confocal imaging revealed that Notch1 and/or N1ICD are largely present in the cytosol of quiescent HSCs (Figure 2C). Based on these data, we hypothesize that Notch1 activity appears to maintain HSC quiescence downstream of the Eras-Pi3k-Akt pathway; a direct role of Eras in this process remains to be investigated. Although Notch1 and N1ICD were mainly detected in cytosol, we could not rule out the transcriptional

activity of Notch1, while the expression of the Notch1 target gene, e.g., *Hes1* in quiescent HSCs (Figure 2A), indicates that N1ICD is still transcriptionally active. Interestingly, Hes1 has been shown to negatively regulate α-Sma and Col1α2 [35]. Thus, N1ICD-Hes1 activity may provide an anti-fibrotic strategy.

These results suggest that HSCs use different pathways downstream of Eras to determine their fate. In quiescent HSCs, the activation or differential regulation of the Pi3k-Pdk1 and *mTorc2* pathways by Eras appears essential for HSC quiescence [5]. In contrast, in activated HSCs, signaling transitions from Eras to Mras and from Rnd3 to Rhoc, activating the Raf-Mek-Erk and Rock pathways while inactivating the Hippo pathway. This shift facilitates cellular proliferation and mesenchymal transition, ultimately driving HSCs to transdifferentiate into myofibroblast-like cells, a critical event in liver fibrosis.

Therefore, we propose a hypothetical model in which Eras-Pi3k-mediated Akt activation counteracts the activation of the Mras-Raf1-Mek-Erk and Rhoc-Rock-Gfap axes (Figure 3) [36,37]. This can be achieved by expressing the Notch1 target gene Rnd3 (Figure 2A) [28], a Rhoc antagonist that directly binds and inhibits Rock [38].

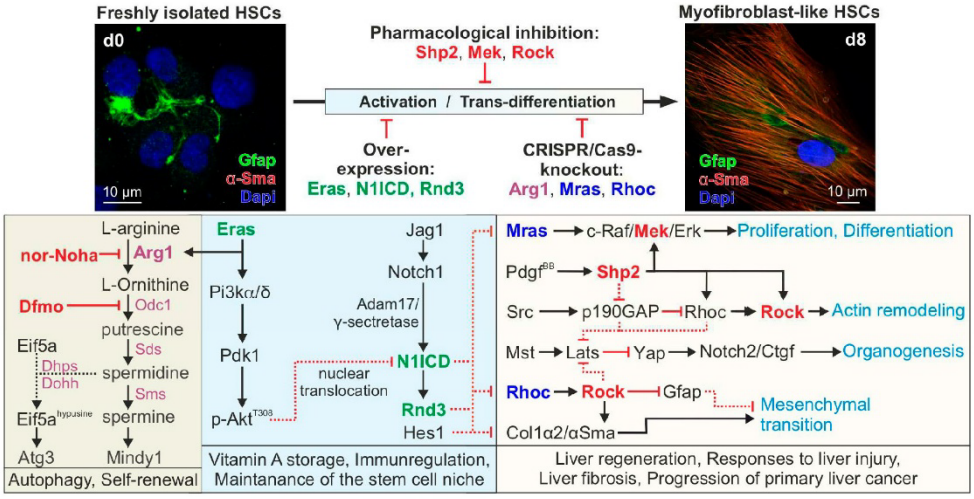

Figure 3. Proposed model of the reciprocal regulation of Ras and Rho GTPase-driven signaling pathways in quiescent vs. activated HSCs. Different signaling networks in quiescent and activated HSCs are subject to reciprocal, paralog-specific regulation by different signaling molecules that are critical for determining developmental fate decisions. L-arginine metabolism to polyamine derivatives, catalyzed by different enzymes, may control processes such as autophagy and self-renewal. The effects of Eras on the Pi3k/Akt axis may contribute to the maintenance of the quiescent state of HSCs by activating Notch1 signaling activity. This, in turn, leads to the inhibition of Mras/Raf1, Rhoc/Rock, and reduced levels of active Yap protein and Yap-mediated signaling, thereby inhibiting proliferation and mesenchymal transition, leading to HSC activation and myofibroblast formation. In addition, the reciprocal expression patterns of Notch1 and Gfap relative to Notch2, Collα2, and α-Sma that result from elevated Yap are another key to this regulatory process. We hypothesize that (i) the overexpression of Eras, N1ICD, or Rnd3 could either maintain HSC quiescence or significantly delay their activation; (ii) the CRISPR/Cas9 knockout of Arg1, Mras, or Rhoc could interfere with HSC activation; and (iii) the pharmacological inhibition of Shp2, Mek, or Rock could block HSC activation ex vivo and prevent the progression of liver fibrosis in vivo. See text for details. NOTE: The proposed model depicted here is hypothetical and based on the evaluated status of selected molecules. "d" stands for "day".

3.3. Rock a Key Determinant of HSC Activation

In liver fibrosis, the activation of HSCs involves phenotypic transformation into profibrotic and myofibroblastic cells with the increased contraction and secretion of ECM proteins [2,39]. In this context, the Rhoc-Rock signaling pathway may play a key role in orchestrating cytoskeletal reorganization and mobility via the non-receptor tyrosine kinase Src, thus playing a critical role in HSC activation and hepatic fibrogenesis [40]. To investigate this issue, we treated freshly isolated HSCs with the Rock inhibitor Y-27632 and analyzed HSC morphology using confocal imaging. Figure 2D clearly shows the delayed activation of HSCs in the presence of Y-27632; the cells were still Gfap-positive, and the stellate-like morphology at d4 of the culture was very similar to quiescent cells. The activation of the Rhoc-Rock pathway in HSCs can control the phosphorylation of Gfap filaments and their subsequent disassembly [41] and inhibit Hippo pathways leading to Yap activation [42]. This suggests that the activation of the Rhoc-Rock pathway is one of the early processes during HSC activation and, ultimately, pathogenesis, which is antagonized by the Notch1-induced expression of Rnd3 in quiescent HSCs (Figure 2A).

3.4. Role of Eras-Arg1-Polyamine Axis in HSC Homeostasis

Two important processes of HSCs—self-renewal and autophagy—are important prerequisites for the maintenance of liver homeostasis. These processes depend, among other things, on the availability of polyamines, such as spermidine and spermine which are natural molecules that have a variety of functions, including cell growth, cell differentiation, and cell survival. Studies have shown that spermidine exerts a protective effect on the liver, especially in the context of age-related changes [43]. Spermidine ingestion in mice leads to improvement in liver function by inhibiting HSC activation and liver fibrosis [44].

We recently identified and characterized the Eras-interacting proteins, including Arg1 (arginase 1) [22], a key enzyme of the urea cycle involved in de novo polyamine synthesis. Arg1, which is inversely regulated to iNos (inducible nitric-oxide synthase), is co-expressed and colocalized with Eras at the membrane of freshly isolated HSCs [22]. Arg1 catalyzes the hydrolysis of L-arginine to L-ornithine, which is further converted into polyamines such as putrescine, spermidine, and spermine by Odc1 (ornithine decarboxylase 1), Sds (spermidine synthase), and Sms (spermine synthase), respectively (Figure 3). Notably, polyamines are implicated in a broad range of cellular processes, including cell metabolism, transcription, translation, post-translational modifications (i.e., hypusination), and autophagy [44]. Using specific pharmacological inhibitors of L-arginine metabolism (Figure 3), we found that the inhibition of Arg1 or Odc1 accelerated HSC activation, as indicated by the loss of the stellate-like morphology and lipid droplet storage [22]. These data suggest that Arg1 catalytic activity may be a critical determinant of developmental fate decisions. This is accomplished by two possible polyamine effector pathways: autophagy and self-renewal (Figure 3).

Autophagy is achieved by the synthesis of hypusine from spermidine and the post-translational hypusination of Eif5a (eukaryotic translation initiation factor 5A) [45], which is, in turn, necessary for the translation of Atg3 (autophagy-related protein 3, which is part of the complex for Lc3 (microtubule-associated proteins 1A/1B light chain 3)) lipidation and converts Lc3-I to Lc3-II, therefore being central for autophagosome assembly [46]. Another effector of polyamines is Mindy1, a deubiquitinase that maintains stemness by sustaining Oct4 protein levels and inducing self-renewal in ESCs [47]. The stem cell marker Oct4 is expressed in quiescent HSCs [48]. HSCs are considered liver-resident mesenchymal stem cells, which can differentiate into diverse cell types in response to liver damage [49]. Moreover, the regulation of Mindy1 by the L-ornithine derivative spermine is, like Eras, anchored to the membrane by C-terminal isoprenylation [25,47] and appears to

be important for maintaining stem cell properties and controlling the quiescence of HSCs. However, Mindy1 may be one of the many polyamine effectors that participate in the maintenance of HSC quiescence. The role of polyamines in the modulation of autophagy and the quiescence of HSCs can be investigated through Arg1 knockout by pharmacological inhibitors of Arg1 and Odc1 (Figures 3 and 4).

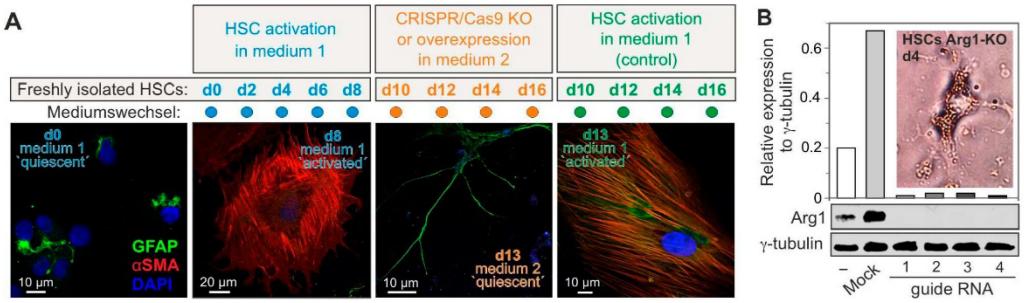

Figure 4. Culture conditions for the long-term maintenance of HSC quiescence. (**A**) Freshly isolated rat HSCs rapidly differentiate into myofibroblast-like cells (α-Sma^{high}) when cultured in the Dulbecco's modified Eagle's medium (DMEM) supplemented with 15% fetal calf serum and 50 units of penicillin/streptomycin (medium 1). When cultured for 8 days in medium 2, containing DMEM supplemented with 2% FBS, 50 ng/mL of insulin, 10 µM of retinol, 100 µM of oleic acid, 100 µM of palmitic acid, 20 ng/mL of Egf and 10 ng/mL of Fgf2, as shown in this example, they form their characteristic stellate-shaped morphology (Gfap^{high}). The replacement of medium 2 with medium 1 led to the activation of the HSCs and their transdifferentiation into the typical myofibroblast-like cells (α-Sma^{high}). Gfap is stained green, α-Sma is stained red, and DNA is stained blue with DAPI (n = 2). (**B**) Under the conditions used in (**A**), the Arg1 gene was successfully knocked out in HSCs on day 0 by CRISPR/Cas9 using four different gRNAs and Nucleofector technology (see Methods). Arg1 KO was also verified with Western blot analysis on day 3 of HSC culture in medium 2. cLSM showed a strikingly delayed activation of HSCs (they retained more and larger lipid droplets and appeared star-shaped) (n = 2). "d" stands for "day".

An essential aspect of studying primary HSCs as a model for liver fibrosis is to identify an optimal time window for manipulating freshly isolated cells through gene transfer or knockout while they remain in their quiescent state. Utilizing a recently published protocol, we have successfully established tools and approaches to maintain HSCs in their quiescent state (Figure 4). Cells are transfected on day 0, immediately after isolation, using medium 2. In this medium, HSCs remain undifferentiated for several days. These culture conditions allow for the genetic manipulation of quiescent HSCs, including gene knockouts, such as Arg1 (Figure 4), using CRISPR/Cas9 genome editing. Electroporation-based gene transfer has proven to be the most effective method for the efficient transfection of freshly isolated HSCs. Finally, the medium-preserving quiescence is replaced with medium 1 to facilitate HSC activation and transdifferentiation.

4. Conclusions and Future Directions

There is a long list of in vivo and clinical studies on the role of HSCs in the progression of liver diseases, including fibrosis, cirrhosis, and cancer. With the onset of fibrosis in liver disease, HSCs activate and transdifferentiate into myofibroblast-like cells that produce large amounts of collagen and other extracellular matrix components. However, ethical concerns, the use of animals in drug safety studies, the timing of experiments, and costs led to the consideration of replacing animal fibrosis models with in vitro HSC culture systems [50]. Furthermore, in vitro experiments allow us to study the complex mechanisms

involved in HSC activation and fibrosis development, to test cell-targeted stimulation or genetic manipulation (CRISPR/Cas9 knockout, overexpression, or treatment using specific pharmacological inhibitors), and to discover new anti-fibrogenic targets (Figure 3). As an in vitro model system for liver fibrosis, freshly isolated rat HSCs spontaneously activate into myofibroblast-like cells when cultured on stiff plastic dishes (Figure 4; see also [51,52]). Elevated mechanical stimuli are known to promote Yap transcriptional activity [53] and trigger liver fibrosis in vivo [54].

Since liver fibrosis begins as an intrinsic signaling process and, in its later stages, becomes dependent on microenvironmental factors—such as impaired blood flow due to inflammatory processes—it is evident that various stimuli induce selective signaling pathways involving Src, Rho, and Rock. This activation triggers the nuclear translocation of Yap, which increases the release of growth factors, such as Ctgf (connective tissue growth factor), by HSCs. In turn, this enhances the activation of the Mapk pathway (Figure 3). We therefore hypothesize that the various signaling proteins and their associated intracellular signaling pathways, on the one hand, maintain the quiescent state of HSCs and thus their homeostasis and, on the other hand, contribute to HSC activation and therefore control processes that are essential for the transition from a quiescent to a proliferative, migratory, and fibrogenic phenotype (i.e., myofibroblast-like cells) [17]. Therefore, targeting pathways involved in HSC activation represents a promising strategy to prevent the development and progression of liver fibrosis. The co-administration of sorafenib, an oral RAF kinase inhibitor, can prevent Erk activation in activated HSCs and has shown anti-fibrotic effects in a CCl_4-induced murine model [55]. In addition, blocking receptor tyrosine kinases such as Pdgfrβ by crenolanib via drinking water can improve thioacetamide-induced liver fibrosis in rats [56].

Supplementary Materials: The following supporting information can be downloaded at: https://www.mdpi.com/article/10.3390/cells14090674/s1, Figure S1: Original Western Blot Data; Table S1: The list of primers used in this study.; Table S2: Antibodies used in this study; Table S3: Guide RNAs used in this study.

Author Contributions: S.N.-R., S.P., A.M., K.N. and D.R.: Technical Support, Data Acquisition, Analysis, and Interpretation; C.K. and D.H.: Provide HSC primary cultures of rats, Data Analysis and Interpretation; D.H.: Project Initiation, Funding Acquisition, Resources and Fundraising; M.R.A.: Conception, Design, and Supervision. All authors coordinated, drafted, and approved the manuscript. All authors have read and agreed to the published version of the manuscript.

Funding: This study was supported by the Charlotte Ansmann Foundation for Aging Research of Heinrich Heine University (grant number 701.810.845), the German Research Foundation (DFG) through the Collaborative Research Center 974 (SFB 974, project number 190586431) "Communication and Systems Relevance during Liver Injury and Regeneration", the German Research Foundation (DFG; grant number: AH 92/8-1) and Ferdowsi University of Mashhad (grant number 49795).

Institutional Review Board Statement: The application for the animal experiment with file number 84-02.04.2015.A287 was approved by the LANUV on 21 September 2015. No animal experiment was performed in this study, as the liver was obtained from a dead animal.

Informed Consent Statement: Not applicable.

Data Availability Statement: It is affirmed that no new data were generated while compiling this manuscript. All referenced data sources are openly accessible and appropriately cited within the manuscript. Please do not hesitate to contact the corresponding author if any additional information or clarification is required.

Acknowledgments: We thank Doreen Floss, Jürgen Scheller, and Roland Piekorz for support.

Conflicts of Interest: The authors declare no conflicts of interest.

Abbreviations

Adam17, A disintegrin and metalloprotease 17; AKT (Pkb), Protein kinase B; Arg1, arginase 1; α-Sma, α-smooth muscle actin; Atg3, autophagy-related protein 3; Col1α2, Collagen type I alpha 2 chain; Raf1, rapidly accelerated fibrosarcoma 1; Ctgf, Connective tissue growth factor; DMEM, Dulbecco's modified Eagle's medium; ECM, extracellular matrix; DAPI, 4′,6-diamidino-2-phenylindole; Dhps, deoxyhypusine synthase; Dohh, deoxyhypusine hydroxylase; Eif5a, eukaryotic translation initiation factor 5A; Eras, embryonic stem cell-expressed Ras; Erk, extracellular-signal regulated kinase; Foxo1, Forkhead Box O1; Gfap, glial fibrillary acidic protein; Hes1, hairy and enhancer of split-1; Hprt11, Hypoxanthine-guanine phosphoribosyl transferase 1; HSC, hepatic stellate cell; iNos, inducible NO synthase; Igf1, insulin-like growth factor 1; Jag1, Jagged 1; Lats1/2, Large tumor suppressor kinase 1/2; Lc3, Microtubule-associated proteins 1A/1B light chain 3; Mapk, mitogen-activated protein kinase; Mindy1, MIU-containing novel deubiquitinaase 1; MIU, motif interacting with ubiquitin; Mras, muscle Ras oncogene homolog; Mst1/2, Macrophage stimulating 1/2; mTor, mechanistic target of rapamycin kinase; N1ICD, intracellular domain of Notch1; Odc1, ornithine decarboxylase 1; p190GAP, p190Rho guanosine triphosphatase-activating protein; Pdgf, platelet-derived growth factor; Pdk1, phosphoinositide-dependent kinase-1; Pi3k, Phosphoinositid-3-kinase; qPCR, quantitative polymerase chain reaction; Rhoc, Ras Homolog Family Member C; Rassf, Ras-Association Domain Family; Rnd3, Rho Family GTPase 3; Rock, Rho-associated coiled-coil kinase; Sds, spermidine synthase; Shp2 (Ptpn11), Src homology region 2 domain-containing phosphatase-2; Sms, spermine synthase; Tgfβ, transforming growth factor-β; Yap, yes-associated protein.

References

1. Cheemerla, S.; Balakrishnan, M. Global Epidemiology of Chronic Liver Disease. *Clin. Liver Dis.* **2021**, *17*, 365–370. [CrossRef] [PubMed]
2. Tsuchida, T.; Friedman, S.L. Mechanisms of hepatic stellate cell activation. *Nat. Rev. Gastroenterol. Hepatol.* **2017**, *14*, 397–411. [CrossRef]
3. Friedman, S.L. Hepatic stellate cells: Protean, multifunctional, and enigmatic cells of the liver. *Physiol. Rev.* **2008**, *88*, 125–172. [CrossRef]
4. Yin, C.; Evason, K.J.; Asahina, K.; Stainier, D.Y. Hepatic stellate cells in liver development, regeneration, and cancer. *J. Clin. Investig.* **2013**, *123*, 1902–1910. [CrossRef] [PubMed]
5. Nakhaei-Rad, S.; Nakhaeizadeh, H.; Götze, S.; Kordes, C.; Sawitza, I.; Hoffmann, M.J.; Franke, M.; Schulz, W.A.; Scheller, J.; Piekorz, R.P.; et al. The Role of Embryonic Stem Cell-expressed RAS (ERAS) in the Maintenance of Quiescent Hepatic Stellate Cells. *J. Biol. Chem.* **2016**, *291*, 8399–8413. [CrossRef]
6. Lee, Y.; Leslie, J.; Yang, Y.; Ding, L. Hepatic stellate and endothelial cells maintain hematopoietic stem cells in the developing liver. *J. Exp. Med.* **2021**, *218*, e20200882. [CrossRef] [PubMed]
7. Marycz, K.; Kornicka-Garbowska, K.; Galuppo, L.; Bourebaba, L. The Hepatic Stellate Cells (HSTCs) and Adipose-derived Mesenchymal Stem Cells (ASCs) Axis as a Potential Major Driver of Metabolic Syndrome—Novel Concept and Therapeutic Implications. *Stem Cell Rev. Rep.* **2022**, *18*, 1417–1422. [CrossRef]
8. Ahmed, T.A.; El-Badri, N. Pericytes: The Role of Multipotent Stem Cells in Vascular Maintenance and Regenerative Medicine. *Adv. Exp. Med. Biol.* **2018**, *1079*, 69–86. [CrossRef]
9. Dias, D.O.; Kalkitsas, J.; Kelahmetoglu, Y.; Estrada, C.P.; Tatarishvili, J.; Holl, D.; Jansson, L.; Banitalebi, S.; Amiry-Moghaddam, M.; Ernst, A.; et al. Pericyte-derived fibrotic scarring is conserved across diverse central nervous system lesions. *Nat. Commun.* **2021**, *12*, 5501. [CrossRef]
10. Dhar, D.; Baglieri, J.; Kisseleva, T.; Brenner, D.A. Mechanisms of liver fibrosis and its role in liver cancer. *Exp. Biol. Med.* **2020**, *245*, 96–108. [CrossRef]
11. Kordes, C.; Sawitza, I.; Götze, S.; Herebian, D.; Häussinger, D. Hepatic stellate cells contribute to progenitor cells and liver regeneration. *J. Clin. Investig.* **2014**, *124*, 5503–5515. [CrossRef] [PubMed]
12. Kordes, C.; Sawitza, I.; Häussinger, D. Canonical Wnt signaling maintains the quiescent stage of hepatic stellate cells. *Biochem. Biophys. Res. Commun.* **2008**, *367*, 116–123. [CrossRef]
13. Carloni, V.; Defranco, R.M.; Caligiuri, A.; Gentilini, A.; Sciammetta, S.C.; Baldi, E.; Lottini, B.; Gentilini, P.; Pinzani, M. Cell adhesion regulates platelet-derived growth factor-induced MAP kinase and PI-3 kinase activation in stellate cells. *Hepatology* **2002**, *36*, 582–591. [CrossRef] [PubMed]

14. Xie, G.; Karaca, G.; Swiderska-Syn, M.; Michelotti, G.A.; Krüger, L.; Chen, Y.; Premont, R.T.; Choi, S.S.; Diehl, A.M. Cross-talk between Notch and Hedgehog regulates hepatic stellate cell fate in mice. *Hepatology* **2013**, *58*, 1801–1813. [CrossRef]
15. Foglia, B.; Cannito, S.; Bocca, C.; Parola, M.; Novo, E. ERK Pathway in Activated, Myofibroblast-Like, Hepatic Stellate Cells: A Critical Signaling Crossroad Sustaining Liver Fibrosis. *Int. J. Mol. Sci.* **2019**, *20*, 2700. [CrossRef] [PubMed]
16. Huang, Z.; Khalifa, M.O.; Gu, W.; Li, T.S. Hydrostatic pressure induces profibrotic properties in hepatic stellate cells via the RhoA/ROCK signaling pathway. *FEBS Open Bio* **2022**, *12*, 1230–1240. [CrossRef] [PubMed]
17. Ye, B.; Yue, M.; Chen, H.; Sun, C.; Shao, Y.; Jin, Q.; Zhang, C.; Yu, G. YAP/TAZ as master regulators in liver regeneration and disease: Insights into mechanisms and therapeutic targets. *Mol. Biol. Rep.* **2024**, *52*, 78. [CrossRef]
18. Pibiri, M.; Simbula, G. Role of the Hippo pathway in liver regeneration and repair: Recent advances. *Inflamm. Regen.* **2022**, *42*, 59. [CrossRef]
19. Fukushima, M.; Nakamuta, M.; Kohjima, M.; Kotoh, K.; Enjoji, M.; Kobayashi, N.; Nawata, H. Fasudil hydrochloride hydrate, a Rho-kinase (ROCK) inhibitor, suppresses collagen production and enhances collagenase activity in hepatic stellate cells. *Liver Int.* **2005**, *25*, 829–838. [CrossRef]
20. Li, L.; Wang, J.Y.; Yang, C.Q.; Jiang, W. Effect of RhoA on transforming growth factor β1-induced rat hepatic stellate cell migration. *Liver Int.* **2012**, *32*, 1093–1102. [CrossRef]
21. Mosaddeghzadeh, N.; Ahmadian, M.R. The RHO Family GTPases: Mechanisms of Regulation and Signaling. *Cells* **2021**, *10*, 1831. [CrossRef] [PubMed]
22. Pudewell, S.; Lissy, J.; Nakhaeizadeh, H.; Taha, M.S.; Akbarzadeh, M.; Rezaei Adariani, S.; Nakhaei-Rad, S.; Li, J.; Kordes, C.; Häussinger, D.; et al. Physical Interaction between Embryonic Stem Cell-Expressed Ras (ERas) and Arginase-1 in Quiescent Hepatic Stellate Cells. *Cells* **2022**, *11*, 508. [CrossRef] [PubMed]
23. Labun, K.; Montague, T.G.; Krause, M.; Torres Cleuren, Y.N.; Tjeldnes, H.; Valen, E. CHOPCHOP v3: Expanding the CRISPR web toolbox beyond genome editing. *Nucleic Acids Res.* **2019**, *47*, W171–W174. [CrossRef] [PubMed]
24. Barry, A.E.; Baldeosingh, R.; Lamm, R.; Patel, K.; Zhang, K.; Dominguez, D.A.; Kirton, K.J.; Shah, A.P.; Dang, H. Hepatic Stellate Cells and Hepatocarcinogenesis. *Front. Cell Dev. Biol.* **2020**, *8*, 709. [CrossRef]
25. Takahashi, K.; Mitsui, K.; Yamanaka, S. Role of ERas in promoting tumour-like properties in mouse embryonic stem cells. *Nature* **2003**, *423*, 541–545. [CrossRef]
26. Bravo-Cordero, J.J.; Sharma, V.P.; Roh-Johnson, M.; Chen, X.; Eddy, R.; Condeelis, J.; Hodgson, L. Spatial regulation of RhoC activity defines protrusion formation in migrating cells. *J. Cell Sci.* **2013**, *126*, 3356–3369. [CrossRef]
27. Monaghan-Benson, E.; Wittchen, E.S.; Doerschuk, C.M.; Burridge, K. A Rnd3/p190RhoGAP pathway regulates RhoA activity in idiopathic pulmonary fibrosis fibroblasts. *Mol. Biol. Cell* **2018**, *29*, 2165–2175. [CrossRef]
28. Zhu, Z.; Todorova, K.; Lee, K.K.; Wang, J.; Kwon, E.; Kehayov, I.; Kim, H.G.; Kolev, V.; Dotto, G.P.; Lee, S.W.; et al. Small GTPase RhoE/Rnd3 is a critical regulator of Notch1 signaling. *Cancer Res.* **2014**, *74*, 2082–2093. [CrossRef]
29. Reister, S.; Kordes, C.; Sawitza, I.; Häussinger, D. The epigenetic regulation of stem cell factors in hepatic stellate cells. *Stem Cells Dev.* **2011**, *20*, 1687–1699. [CrossRef]
30. Duncan, A.W.; Rattis, F.M.; DiMascio, L.N.; Congdon, K.L.; Pazianos, G.; Zhao, C.; Yoon, K.; Cook, J.M.; Willert, K.; Gaiano, N.; et al. Integration of Notch and Wnt signaling in hematopoietic stem cell maintenance. *Nat. Immunol.* **2005**, *6*, 314–322. [CrossRef]
31. Ma, L.; Wang, Y.; Hui, Y.; Du, Y.; Chen, Z.; Feng, H.; Zhang, S.; Li, N.; Song, J.; Fang, Y.; et al. WNT/NOTCH Pathway Is Essential for the Maintenance and Expansion of Human MGE Progenitors. *Stem Cell Rep.* **2019**, *12*, 934–949. [CrossRef] [PubMed]
32. Liang, S.J.; Li, X.G.; Wang, X.Q. Notch Signaling in Mammalian Intestinal Stem Cells: Determining Cell Fate and Maintaining Homeostasis. *Curr. Stem Cell Res. Ther.* **2019**, *14*, 583–590. [CrossRef]
33. Moriyama, H.; Moriyama, M.; Isshi, H.; Ishihara, S.; Okura, H.; Ichinose, A.; Ozawa, T.; Matsuyama, A.; Hayakawa, T. Role of notch signaling in the maintenance of human mesenchymal stem cells under hypoxic conditions. *Stem Cells Dev.* **2014**, *23*, 2211–2224. [CrossRef]
34. Bigas, A.; Porcheri, C. Notch and Stem Cells. *Adv. Exp. Med. Biol.* **2018**, *1066*, 235–263. [CrossRef] [PubMed]
35. Zhang, K.; Zhang, Y.Q.; Ai, W.B.; Hu, Q.T.; Zhang, Q.J.; Wan, L.Y.; Wang, X.L.; Liu, C.B.; Wu, J.F. Hes1, an important gene for activation of hepatic stellate cells, is regulated by Notch1 and TGF-β/BMP signaling. *World J. Gastroenterol.* **2015**, *21*, 878–887. [CrossRef]
36. Young, L.C.; Hartig, N.; Muñoz-Alegre, M.; Oses-Prieto, J.A.; Durdu, S.; Bender, S.; Vijayakumar, V.; Vietri Rudan, M.; Gewinner, C.; Henderson, S.; et al. An MRAS, SHOC2, and SCRIB Complex Coordinates ERK Pathway Activation with Polarity and Tumorigenic Growth. *Mol. Cell* **2013**, *52*, 679–692. [CrossRef] [PubMed]
37. Reymond, N.; Im, J.H.; Garg, R.; Cox, S.; Soyer, M.; Riou, P.; Colomba, A.; Muschel, R.J.; Ridley, A.J. RhoC and ROCKs regulate cancer cell interactions with endothelial cells. *Mol. Oncol.* **2015**, *9*, 1043–1055. [CrossRef]
38. Komander, D.; Garg, R.; Wan, P.T.; Ridley, A.J.; Barford, D. Mechanism of multi-site phosphorylation from a ROCK-I:RhoE complex structure. *EMBO J.* **2008**, *27*, 3175–3185. [CrossRef]

39. Kisseleva, T.; Brenner, D. Molecular and cellular mechanisms of liver fibrosis and its regression. *Nat. Rev. Gastroenterol. Hepatol.* **2021**, *18*, 151–166. [CrossRef]
40. Görtzen, J.; Schierwagen, R.; Bierwolf, J.; Klein, S.; Uschner, F.E.; van der Ven, P.F.; Fürst, D.O.; Strassburg, C.P.; Laleman, W.; Pollok, J.M.; et al. Interplay of Matrix Stiffness and c-SRC in Hepatic Fibrosis. *Front. Physiol.* **2015**, *6*, 359. [CrossRef]
41. Yasui, Y.; Amano, M.; Nagata, K.; Inagaki, N.; Nakamura, H.; Saya, H.; Kaibuchi, K.; Inagaki, M. Roles of Rho-associated kinase in cytokinesis; mutations in Rho-associated kinase phosphorylation sites impair cytokinetic segregation of glial filaments. *J. Cell Biol.* **1998**, *143*, 1249–1258. [CrossRef] [PubMed]
42. Kono, K.; Tamashiro, D.A.; Alarcon, V.B. Inhibition of RHO-ROCK signaling enhances ICM and suppresses TE characteristics through activation of Hippo signaling in the mouse blastocyst. *Dev. Biol.* **2014**, *394*, 142–155. [CrossRef]
43. Shi, B.; Wang, W.; Ye, M.; Liang, M.; Yu, Z.; Zhang, Y.; Liu, Z.; Liang, X.; Ao, J.; Xu, F.; et al. Spermidine suppresses the activation of hepatic stellate cells to cure liver fibrosis through autophagy activator MAP1S. *Liver Int.* **2023**, *43*, 1307–1319. [CrossRef]
44. Sagar, N.A.; Tarafdar, S.; Agarwal, S.; Tarafdar, A.; Sharma, S. Polyamines: Functions, Metabolism, and Role in Human Disease Management. *Med. Sci.* **2021**, *9*, 44. [CrossRef] [PubMed]
45. Park, M.H.; Nishimura, K.; Zanelli, C.F.; Valentini, S.R. Functional significance of eIF5A and its hypusine modification in eukaryotes. *Amino Acids* **2010**, *38*, 491–500. [CrossRef] [PubMed]
46. Lubas, M.; Harder, L.M.; Kumsta, C.; Tiessen, I.; Hansen, M.; Andersen, J.S.; Lund, A.H.; Frankel, L.B. eIF5A is required for autophagy by mediating ATG3 translation. *EMBO Rep.* **2018**, *19*, e46072. [CrossRef]
47. James, C.; Zhao, T.Y.; Rahim, A.; Saxena, P.; Muthalif, N.A.; Uemura, T.; Tsuneyoshi, N.; Ong, S.; Igarashi, K.; Lim, C.Y.; et al. MINDY1 Is a Downstream Target of the Polyamines and Promotes Embryonic Stem Cell Self-Renewal. *Stem Cells* **2018**, *36*, 1170–1178. [CrossRef]
48. Kordes, C.; Sawitza, I.; Müller-Marbach, A.; Ale-Agha, N.; Keitel, V.; Klonowski-Stumpe, H.; Häussinger, D. CD133+ hepatic stellate cells are progenitor cells. *Biochem. Biophys. Res. Commun.* **2007**, *352*, 410–417. [CrossRef]
49. Kordes, C.; Sawitza, I.; Götze, S.; Häussinger, D. Hepatic stellate cells support hematopoiesis and are liver-resident mesenchymal stem cells. *Cell. Physiol. Biochem.* **2013**, *31*, 290–304. [CrossRef]
50. van Grunsven, L.A. 3D in vitro models of liver fibrosis. *Adv. Drug Deliv. Rev.* **2017**, *121*, 133–146. [CrossRef]
51. El Taghdouini, A.; Najimi, M.; Sancho-Bru, P.; Sokal, E.; van Grunsven, L.A. In vitro reversion of activated primary human hepatic stellate cells. *Fibrogenesis Tissue Repair* **2015**, *8*, 14. [CrossRef] [PubMed]
52. Yoneda, A.; Sakai-Sawada, K.; Niitsu, Y.; Tamura, Y. Vitamin A and insulin are required for the maintenance of hepatic stellate cell quiescence. *Exp. Cell Res.* **2016**, *341*, 8–17. [CrossRef] [PubMed]
53. Bertero, T.; Cottrill, K.A.; Annis, S.; Bhat, B.; Gochuico, B.R.; Osorio, J.C.; Rosas, I.; Haley, K.J.; Corey, K.E.; Chung, R.T.; et al. A YAP/TAZ-miR-130/301 molecular circuit exerts systems-level control of fibrosis in a network of human diseases and physiologic conditions. *Sci. Rep.* **2015**, *5*, 18277. [CrossRef] [PubMed]
54. Yanguas, S.C.; Cogliati, B.; Willebrords, J.; Maes, M.; Colle, I.; van den Bossche, B.; de Oliveira, C.; Andraus, W.; Alves, V.A.F.; Leclercq, I.; et al. Experimental models of liver fibrosis. *Arch. Toxicol.* **2016**, *90*, 1025–1048. [CrossRef]
55. Sung, Y.C.; Liu, Y.C.; Chao, P.H.; Chang, C.C.; Jin, P.R.; Lin, T.T.; Lin, J.A.; Cheng, H.T.; Wang, J.; Lai, C.P.; et al. Combined delivery of sorafenib and a MEK inhibitor using CXCR4-targeted nanoparticles reduces hepatic fibrosis and prevents tumor development. *Theranostics* **2018**, *8*, 894–905. [CrossRef]
56. Reichert, D.; Adolph, L.; Köhler, J.P.; Buschmann, T.; Luedde, T.; Häussinger, D.; Kordes, C. Improved Recovery from Liver Fibrosis by Crenolanib. *Cells* **2021**, *10*, 804. [CrossRef]

Chapter VI. KRAS-related long noncoding RNAs in human cancers

Authors: Mahsa Saliani, Amin Mirzaiebadizi, Ali Javadmanesh, Akram Siavoshi, Mohammad Reza Ahmadian

DOI: 10.1038/s41417-021-00381-x

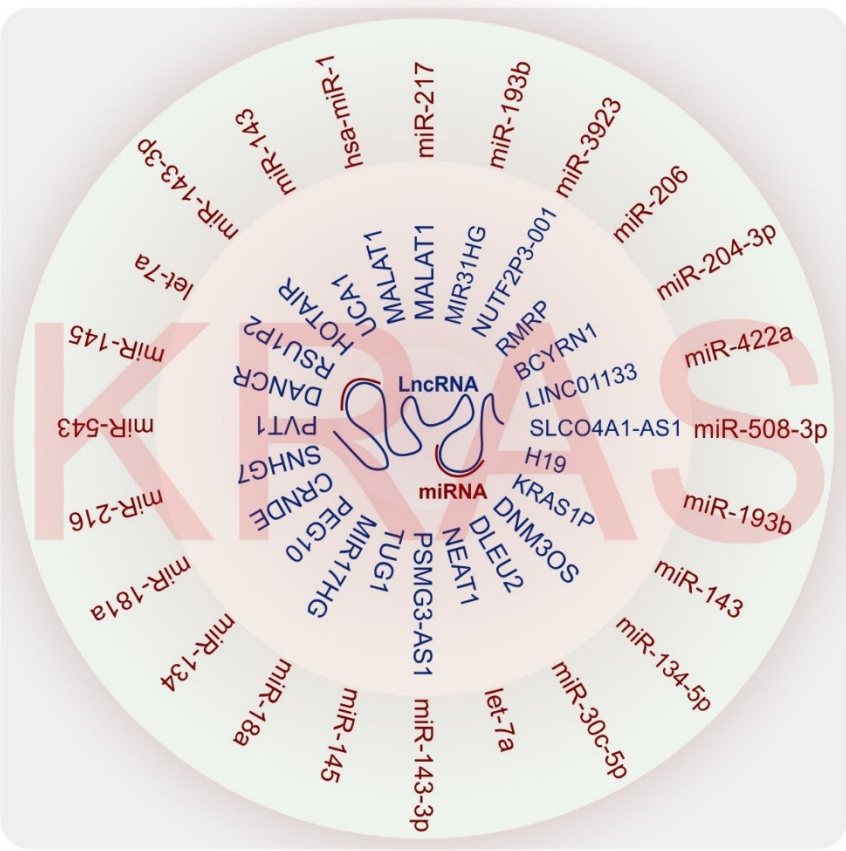

Status: Published

Journal: *Cancer gene therapy*
JIF: 4.8
Contribution: ≈30%

A.M. contributed to the literature review, manuscript writing, and in-depth reviewing, proofreading, and major editing.

REVIEW ARTICLE OPEN

Check for updates

KRAS-related long noncoding RNAs in human cancers

Mahsa Saliani[1,2], Amin Mirzaiebadizi[1], Ali Javadmanesh[3,4], Akram Siavoshi[5] and Mohammad Reza Ahmadian[1]✉

KRAS is one of the most widely prevalent proto-oncogenes in human cancers. The constitutively active KRAS oncoprotein contributes to both tumor onset and cancer development by promoting cell proliferation and anchorage-independent growth in a MAPK pathway-dependent manner. The expression of microRNAs (miRNAs) and the KRAS oncogene are known to be dysregulated in various cancers, while long noncoding RNAs (lncRNAs) can act as regulators of the miRNAs targeting *KRAS* oncogene in different cancers and have gradually become a focus of research in recent years. In this review article, we summarize recent advances in the research on lncRNAs that have sponging effects on KRAS-targeting miRNAs as crucial mediators of KRAS expression in different cell types and organs. A deeper understanding of lncRNA function in KRAS-driven cancers is of major fundamental importance and will provide a valuable clinical tool for the diagnosis, prognosis, and eventual treatment of cancers.

Cancer Gene Therapy (2022) 29:418–427; https://doi.org/10.1038/s41417-021-00381-x

INTRODUCTION

KRAS is a small GDP/GTP-binding protein that transduces extracellular signals and induces intracellular responses. KRAS cycles between an inactive, GDP-bound ("off") state, and an active, GTP-bound ("on") state. This off/on cycle is based on GDP/GTP exchange and GTP hydrolysis reactions stimulated by RAS-specific guanine nucleotide exchange factors (GEFs) and GTPase-activating proteins (GAPs), respectively [1]. GTP-bound KRAS transduces signals to its downstream effectors and thus activates multiple signaling pathways [2, 3]. Therefore, activated KRAS controls various cellular processes, including survival, growth, proliferation, differentiation, and apoptosis, all of which are known as hallmarks of cancer [4]. Somatic mutations in KRAS trigger the robust gain-of-function effects of oncogenic KRAS and neoplastic signal transduction owing to the reduction in GTP hydrolysis and resistance to GAP function [5, 6].

The *KRAS* oncogene has been extensively studied in human tumor malignancies [7, 8]. Intensive efforts to understand the mechanisms underlying the intracellular trafficking, regulation, and signaling pathways of KRAS have suggested several therapeutic strategies [9]. Despite its well-recognized importance in cancer promotion, only a few efforts in the past four decades have resulted in approved clinical therapeutic strategies for *KRAS*-mutant cancers [9–11]. Additionally, *KRAS* mutation is an important predictive marker in determining resistance to EGFR-targeted therapies [12]. Thus, further studies are needed to elucidate the mechanisms responsible for the modulation of *KRAS* to evaluate other potential therapeutic approaches.

Long noncoding RNAs (lncRNAs) are a class of noncoding RNAs (ncRNAs) with a minimum length of 200 nucleotides, which have been well studied in the context of RNA-based therapeutics [13, 14]. Although only a small fraction of known lncRNAs have been functionally characterized, there is growing evidence of their involvement in a variety of biological processes, human diseases, and malignancies [15]. These molecules, as the key regulators of gene expression, play essential roles in a wide variety of biological processes and signaling pathways involved in the progression of many human cancers [16–19]. Emerging evidence has suggested that various lncRNAs are likely to function as competing endogenous RNAs (ceRNAs). These lncRNAs act as oncogenes by sponging tumor suppressor microRNAs (miRNAs) [20, 21], thereby indirectly regulating the expression of the genes targeted by these miRNAs [22] (Fig. 1). Considering the wide diversity of miRNAs and their high capacity for regulating hundreds of genes, many driver oncogenes, such as *ERBB2*, *BRAF*, *EGFR*, *MYC*, *SRC*, and *BCL2*, are targeted by miRNAs [23–25]. In this regard, many tumor suppressor miRNAs have inhibitory effects on *KRAS*-associated tumrigenesis by downregulating *KRAS* expression [26, 27]. Therefore, oncogenic lncRNAs, as sponges of tumor suppressor miRNAs that target *KRAS*, promote cancer development via the upregulation of the *KRAS* oncogene [28–30].

It is evident that ceRNAs and miRNA response elements (MREs) are two essential components of the 'sponge effect' [31]. MREs are seed regions of 2-8 nucleotides in the 5' region of miRNA [32]. The ability of a miRNA to bind to its mRNA target and lncRNA via its MRE provides competition between mRNA and lncRNA for interaction with their target miRNA. The binding of lncRNA to miRNA as a ceRNA prevents the latter from recognizing mRNA and consequently results in its silencing. This interaction leads to the regulation of MREs on the targets, which plays an important role in posttranscriptional regulation and is known as the sponging effect [31] (Fig. 1).

Identification of mechanisms involved in *KRAS* regulation by lncRNAs is expected to greatly enhance our understanding of the

[1]Institute of Biochemistry and Molecular Biology II, Medical Faculty, Heinrich Heine University, Düsseldorf, Germany. [2]Department of Chemistry, Faculty of Science, Ferdowsi University of Mashhad, Mashhad, Iran. [3]Department of Animal Science, Faculty of Agriculture, Ferdowsi University of Mashhad, Mashhad, Iran. [4]Stem Cell Biology and Regenerative Medicine Research Group, Research Institute of Biotechnology, Ferdowsi University of Mashhad, Mashhad 9177948974, Iran. [5]Department of Biology, Sinabioelixir Group, Alborz Health Technology Development Center, Tehran, Iran. ✉email: reza.ahmadian@hhu.de

Received: 17 March 2021 Revised: 29 June 2021 Accepted: 11 August 2021
Published online: 6 September 2021

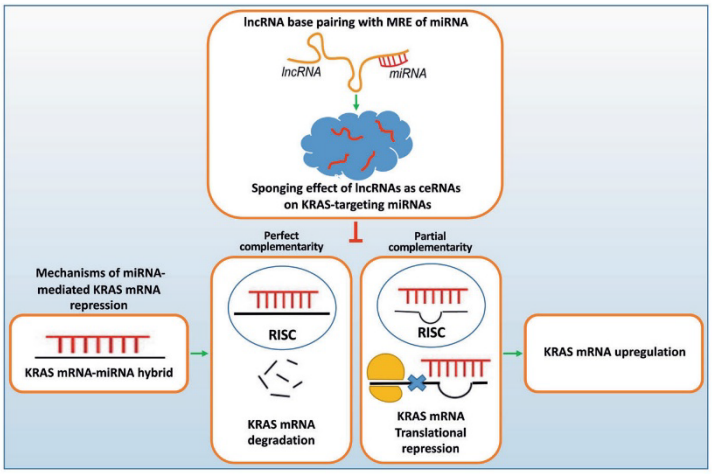

Fig. 1 Mechanism of KRAS gene regulation by oncogenic lncRNAs through sponging effects. As key gene regulators, tumor suppressor miRNAs bind to their targets and interfere with translation. The RNA-induced silencing complex (RISK) guides the antisense strand of the miRNA to bind to its target KRAS mRNA sequence in a complementary manner, forming a double-stranded helix. Perfect complementarity results in endonucleolytic cleavage, while partial complementarity subjects mRNA to translational repression. Oncogenic lncRNAs act as ceRNA decoys by presenting complementary sequences with MREs to sponge miRNAs from their target KRAS mRNAs. lncRNAs consequently promote KRAS mRNA stabilization and thus its upregulation.

mechanisms of tumorigenesis associated with *KRAS* regulation. While the sponging effect of lncRNAs on miRNAs that target *KRAS* seems to be one of the key mechanisms by which *KRAS* is regulated, details of other regulatory mechanisms remain to be elucidated. The association of lncRNAs with various regulatory apparatuses, such as chromatin remodeling factors, transcription factors, splicing machinery, nuclear trafficking modulators, and miRNAs, shows the complexity of their regulatory approaches [33, 34]. Therefore, to understand other regulatory effects of lncRNAs on *KRAS* expression, the role of all interactions between lncRNAs and other macromolecules, such as DNA, RNA, and proteins, in the regulation of gene expression should be considered. Based on the different methods of gene regulation by lncRNAs, lncRNAs are divided into guides, scaffolds, signaling molecules, decoys, and miRNA sponges, which affect the pretranscription, transcription, and posttranscriptional levels of gene expression [34, 35]. It is now evident that silencing G4 elements in the core promoter region of oncogenes such as *KRAS* is a highly valuable and new molecular target in the treatment of cancer [36]. Some innovative approaches have suggested that lncRNAs containing G4 structures as molecular decoys for G4-binding proteins prevent G4 formation in the promotor region of oncogenes, which leads to gene transcription [37]. Therefore, the determination of whether lncRNAs inhibit G4 element formation in the promotor region of *KRAS* reveals other mechanisms by which lncRNAs regulate *KRAS* expression at the pretranscription level. The results of another study demonstrated that KRASIM, a highly conserved microprotein encoded by the putative lncRNA NCBP2-AS2, plays a tumor-suppressive role by interacting with KRAS in HCC cells. KRASIM, as the first KRAS-binding protein encoded by a lncRNA, suppresses the protein level of KRAS and inhibits the ERK signaling pathway. Therefore, sequestration of the KRAS protein with peptides encoded by lncRNAs can be considered as an alternative lncRNA-associated posttranscriptional regulatory mechanism [38].

While lncRNAs have the capacity to regulate *KRAS* expression, abnormal levels of KRAS, one of the mediators of many cellular signaling pathways, reciprocally cause diverse molecular alterations, such as dysregulation of lncRNA expression. *KRAS* amplification has been shown to be a secondary means of KRAS activation, leading to its overexpression and neoplastic transformation. It was found that the levels of a KRAS-responsive lncRNA called KIMAT1 correlate with the KRAS levels and play a positive role in maintaining tumorigenesis [39]. Another study revealed that oncogenic RAS-induced lncRNA 1 (Orilnc1) can be regulated by the RAS-RAF-MEK-ERK pathway and is required for cell proliferation in RAS/BRAF-dependent human cancers [40].

The diversity of miRNAs with their various MREs provides a greater possibility for communication between different miRNAs and ceRNAs, two irreplaceable contributors to the sponging effect. This hypothesis suggests that the sponging effect is a key molecular mechanism underlying the networks corresponding to miRNAs, oncogenic lncRNAs, and many related oncogenic drivers that control various cancer-related biochemical processes. While *KRAS*-associated miRNAs have been widely studied in cancer, the role of *KRAS*-related lncRNAs in promoting cancer progression needs to be carefully examined. The ever-increasing number of *KRAS*-specific lncRNAs strongly indicates their potential contribution to and critical roles in the entire process of *KRAS*-driven carcinogenesis. This review compiles the current knowledge of *KRAS*-related oncogenic lncRNAs by considering their aberrant expression and their mechanism of action through sponging effects on *KRAS*-targeting miRNAs.

NONCODING RNAS IN KRAS-DRIVEN CANCERS

The noncoding transcriptome consists of a variety of different RNA types, such as transfer RNA (tRNAs), ribosomal RNAs (rRNAs), small nuclear RNAs (snRNAs), small nucleolar RNAs (snoRNAs), circular RNAs (circRNAs), miRNAs, and lncRNAs. Other than miRNAs and lncRNAs, as noncoding RNAs that play roles in tumorigenesis, accumulating evidence indicates that altered processing or activity of other RNA species can similarly contribute to cancer [13]. Intact tRNAs and tRNA fragments (tRFs) are correlated with tumorigenesis [41]. Upregulation of specific tRNA expression in breast cancers by the enhancement

of the translation of specific transcripts has been demonstrated in the progression of metastasis [42]. In particular, a proportion of tRFs that are of the same size as miRNAs and associated with Argonaute are able to function as miRNAs. To confirm the oncogenic activity of tRFs, altered levels have been indicated in leukemia and solid cancers [42–44]. It has been reported that some tRNA fragments, such as ts-47s and ts-46s, are upregulated by KRAS and PIK3CA mutations, respectively, leading to breast cancer chemoresistance [45, 46]. The results indicated that the expression of tRFs can be influenced by oncogenic mutations with a possible role in the promotion of carcinogenic processes. Other findings have demonstrated that the expression of different tRNAs corresponds to differences in KRAS protein levels. This proved that some translational programs, such as overexpression of proliferative tRNAs, have the ability to enhance the protein synthesis of oncogenes, including KRAS [47].

A wide range of data has indicated the fundamental importance of ribosomal biogenesis and its relationship with cell proliferation in many aspects of malignant transformations [48]. A series of rare inherited disorders leading to the production of altered ribosomes (so-called ribosomopathies) have even been characterized by a strong risk of cancer onset [49]. An imbalance in the ribosome biogenesis rate via an increase in ribosomal DNA transcription or an alteration in mature rRNA or ribosomal protein production may ultimately lead to the inactivation of p53 through different mechanisms [50]. As a consequence of *p53* repression, acquisition of cellular phenotypic changes characteristic of epithelial-mesenchymal transition (EMT) results in increased cell invasiveness. In addition, it has been reported that nuclear epithelial cell transforming sequence 2 (ECT2) with GEF activity is required for *KRAS-p53* lung tumorigenesis in vivo. ECT2-dependent ribosomal DNA transcription and activation of rRNA synthesis ultimately lead to neoplastic transformation [51]. In addition, nuclear and nucleolar superoxide dismutase are essential for lung cancer cell proliferation through interaction with the PeBoW complex and regulation of pre-rRNA maturation [52].

The RNA components of the spliceosome, uridine-rich (U) snRNAs, can regulate tissue-specific and cancer-specific alternative splicing [53]. Notably, recurrent mutations in U1 snRNA, as one of the most abundant noncoding RNAs, have been recently identified in multiple cancer types and play an important role in the splicing of pre-mRNAs [54]. Collectively, these studies indicate that abnormalities in U1 snRNA and alternative splicing of pre-mRNA are emerging as potentially important drivers of cancer [54, 55]. An alternative mechanism underlying changes in the U1 levels in alternations of cancer gene expression is changes in 3′-untranslated region (UTR) length, leading to the removal of miRNA binding sites. U1 overexpression lengthens the 3′UTR of KRAS to include a miRNA let-7 binding site with tumor-suppressive activity [56].

snoRNAs are conserved noncoding RNAs responsible for ribonucleoprotein guidance in cells for RNA posttranscriptional modification [57]. A study on the characterization of small snoRNAs in cancer identified an unexpected role for specific snoRNAs in the modulation of KRAS-driven carcinogenesis [58]. A human protein microarray screen discovered SNORD50A and SNORD50B as two snoRNAs that bind to KRAS. The results showed that loss of SNORD50A and SNORD50B expression enhances the amount of GTP-bound and active KRAS, leading to hyperactivated RAS-ERK1/ERK2 signaling [58]. The soluble NSF attachment protein receptor (SNARE) protein superfamily, which is critical for membrane fusion, is responsible for the vesicular transport that is essential for KRAS trafficking to the plasma membrane and active signaling [59]. In 2019, Che et al. found that the SNORD50A/B snoRNAs, as antagonists of SNAP23, SNAP29, and VAMP3 SNARE proteins, inhibit the process of KRAS localization to the membrane [59].

circRNAs constitute a distinct type of endogenous abundant noncoding RNA with a closed-loop structure and have been found to be overexpressed in cancers [60]. Strikingly, similar to lncRNAs, circRNAs have the potential to act as oncogenes or tumor suppressors, possibly by acting as sponges for miRNAs. Gorospe et al. found that circPVT1, as a circRNA, regulated the availability of let-7 miRNA, a well-characterized tumor suppressor with a target site on KRAS mRNA. This suggests that circPVT1, whose expression is elevated in dividing cells and down-regulated in senescent cells, can be considered a KRAS-related circRNA that acts by sponging let-7 [61]. Other results showed that a circRNA derived from Golgi glycoprotein 1 mRNA regulates *KRAS* expression and then promotes colorectal cancer development by targeting miR-622 [62].

Many studies have presented remarkable details of systematic alterations in the form of noncoding RNAs, such as miRNAs, lncRNAs, snRNAs, and circRNAs, with impacts on multiple facets of tumorigenesis.

KRAS-RELATED LNCRNAS IN SOLID TUMORS

Aberrant regulation of oncogenes, tumor suppressor genes, and miRNA genes are crucial in the pathogenesis of cancer. These alterations are sequential multistep processes that can ultimately contribute to malignant transformation [63]. The crucial roles of miRNAs in various biological processes, such as cell proliferation, tumor initiation, EMT, and tumor invasion, are directly related to malignancy [64]. Several studies have identified many tumor suppressor miRNAs targeting the *KRAS* oncogene in human cancers, which affect cancer-associated cellular and molecular mechanisms [65, 66]. Notably, research progress on the interactions between lncRNAs and miRNAs in human cancer has introduced an extra layer of complexity in the miRNA-target interaction network [31]. With the development of the analysis of regulatory networks, differential expression, and signaling pathways, lncRNAs have emerged as crucial regulators in various biological processes [67, 68].

In this review, we mainly focus on confirmed *KRAS*-related lncRNAs whose oncogenic roles as suppressors of *KRAS*-targeting miRNAs have been verified (Fig. 2). These lncRNAs act as molecular sponges of *KRAS*-targeting miRNAs, most likely contributing to *KRAS* upregulation. We also summarize a large number of lncRNAs potentially capable of regulating KRAS, possibly through sponging of previously recognized *KRAS*-targeting miRNAs (Fig. 2) [31].

CONFIRMED KRAS-RELATED LNCRNAS

MALAT1

MALAT1, which was first identified in lung cancer, plays an important role in the pathogenesis of various human diseases, such as cancer [69–71] and autoimmune and inflammatory diseases [72]. MALAT1 behaves as an oncogene in the initiation and progression of many cancers [73, 74]. MALAT1, as a molecular sponge of miR-217, an inhibitor of *KRAS* [75], promotes *KRAS* signaling in pancreatic ductal adenocarcinoma (PDAC) [76]. In this regard, knockdown of MALAT1 results in a significant reduction in MEK and ERK1/2 phosphorylation by attenuating KRAS protein expression, emphasizing the role of MALAT1 in protecting *KRAS* mRNA from repression by miR-217 [76]. Moreover, miR-1 has been shown to suppress breast cancer development by downregulating *KRAS* and MALAT1 transcription, which emphasizes the potential role of miR-1 as a tumor-suppressive miRNA and MALAT1 as an oncogenic lncRNA via the regulation of *KRAS* [66].

MIR31HG

MIR31HG is a lncRNA with 2166 nucleotides that originates from the intronic region of the Harbi1 gene and is responsible for coding miR-31. MIR31HG is markedly upregulated in cancer tissues, with potential roles in cancer initiation, progression, and metastasis. It was confirmed that MIR31HG facilitates esophageal squamous cell carcinoma cell proliferation and functions as a

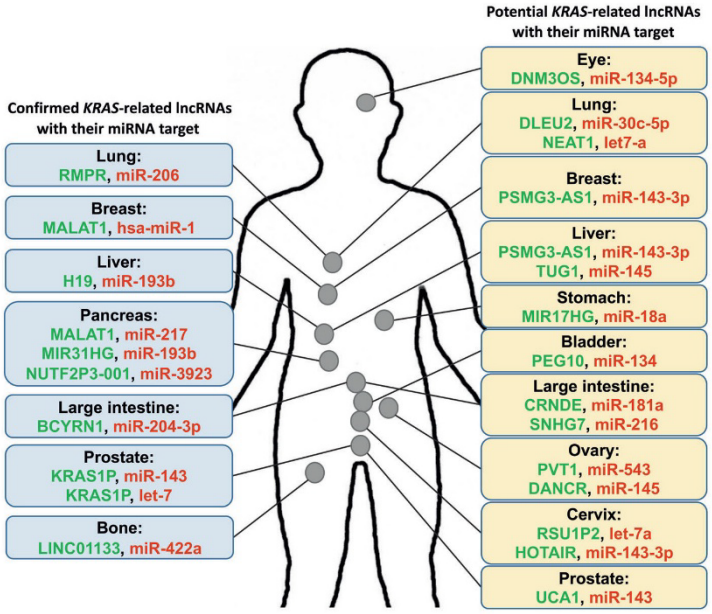

Fig. 2 Lists of the confirmed (left) and potential (right) KRAS-related lncRNAs in different tissues. lncRNAs are presented in green, indicating their upregulation as oncogenic regulators in carcinogenesis. miRNAs with tumor suppressor activity are presented in red, indicating their repression due to the sponging effect of lncRNAs in malignancies. The left and right panels illustrate the confirmed and potential KRAS-related lncRNAs as well as their miRNAs, respectively (Supplementary Table S1).

ceRNA by sponging miR-34a, allowing upregulation of *c-Met* [77]. MIR31HG inhibits oncogene-induced cell senescence by regulating transcription of the tumor suppressor p16 (*INK4A*) [78]. The interaction of the MIR31HG transcript with the genomic regions of *INK4A* and MIR31HG contributes to the recruitment of polycomb-group protein complexes and then the repression of *INK4A*. In addition, *SP1*-induced MIR31HG was found to be significantly upregulated in NSCLC tissues and cell lines, which promotes cell migration and invasion by sponging miR-214 [79]. It has been reported that miR-193b is able to directly target MIR31HG, resulting in cancer progression by counteracting miR-193b in pancreatic cancer [80]. Based on the significant role of the *KRAS* mutation in pancreatic cancer, these results confirm the potential role of MIR31HG in the malignant transformation of different tumors, including *KRAS*-driven pancreatic cancer.

KRAS1P

KRAS1P is considered as a pseudogene of *KRAS*. Its expression is amplified in most cancers with mutated *KRAS*, which indicates a positive correlation between these genes. The transcript levels of *KRAS* and KRAS1P correlate directly in prostate cancer, neuroblastoma, retinoblastoma, and hepatocellular carcinoma (HCC), which illustrates a proto-oncogenic role of KRAS1P in cancer [81–83]. While the detailed mechanism by which KRAS1P regulates *KRAS* as a pseudogene-derived noncoding RNA has not been well recognized, its activity as a sponge for miRNAs that bind to the 3′UTR of *KRAS* has been proposed [84]. Two studies have reported the possible role of KRAS1P as a ceRNA with binding sites for some *KRAS*-targeting miRNAs, such as miR-143 and the let-7 miRNA family [85, 86]. Thus, KRAS1P can potentially act as an oncogenic lncRNA to inhibit degradation of the *KRAS* transcript [84].

BCYRN1

BCYRN1 is a newly identified brain cytoplasmic lncRNA of 200 nucleotides, which is transcribed from human chromosome 2p21. The high expression of BCYRN1 in various tumor cell lines suggests the role of BCYRN1 as an oncogenic lncRNA [87, 88]. In gastric cancer tissues, it is associated with tumor depth, lymph node metastasis, cell proliferation, cell cycle progression, migration, and invasion [89]. BCYRN1 is upregulated in colorectal cancer (CRC) tissues, which is related to tumor growth and advanced pathological stages via *NPR3* overexpression [90]. Moreover, the promotion of glycolysis and tumor progression in non-small cell lung cancer (NSCLC) are observed as the result of BCYRN1 overexpression [91]. High BCYRN1 expression induces glycolysis through the repression of miR-149 and upregulation of *PKM2* as the target of miR-149. Strikingly, as a ceRNA, BCYRN1 affects the development of CRC via regulation of the miR-204-3p/*KRAS* axis [92]. Therefore, negative regulation of *KRAS* by miR-204-3p suggests BCYRN1 as another confirmed *KRAS*-related lncRNA.

NUTF2P3-001

Overexpression of NUTF2P3-001 in pancreatic cancer and chronic pancreatitis tissues is positively correlated with cancer cell characteristics, such as tumor size and distant metastasis [93]. It was reported that NUTF2P3-001, as an oncogenic lncRNA, competes with the 3′UTR of *KRAS* mRNA for binding to miR-3923. In addition, downregulation of NUTF2P3-001 inhibits the viability, proliferation, and invasion of pancreatic cancer cells and contributes to a decrease in *KRAS* expression [93]. Hence, these data provide an alternative lncRNA-mediated regulatory mechanism for the tumor oncogene *KRAS*.

RMRP

RMRP lncRNA is widely expressed in different human and mouse tissues [94]. Previous studies have indicated that the expression of RMRP is dysregulated in gastric cancer [95]. Suppression of miR-206 by RMRP positively modulates Cyclin D2 expression and cell cycle progression, which provides us with a better understanding of the mechanism underlying RMPR carcinogenesis [96]. Furthermore, ectopic expression of RMRP was observed to promote cell proliferation, colony formation, and invasion in lung adenocarcinoma [97]. It was indicated that miR-206 acts as a tumor suppressor miRNA in oral squamous cell carcinoma by directly targeting *KRAS* [98]. Inhibition of miR-206 by RMRP was demonstrated to result in overexpression of *KRAS*, *FMNL2*, and *SOX9* in lung adenocarcinoma [99], confirming RMPR as one of the *KRAS*-related lncRNAs.

H19

H19, with both oncogenic and tumor suppressor activities, acts as a double-edged sword via mechanisms such as miRNA sponging [100]. The let-7 family miRNAs that control human RAS oncogene expression are often downregulated in human cancers [86, 101, 102]. H19 possesses both canonical and noncanonical binding sites for the let-7 family of miRNAs, which plays predominant roles not only in cancer but also in development and metabolism [103]. H19 promotes pancreatic cancer metastasis by inhibiting let-7 suppression on its target *HMGA2*-mediated EMT in PDACs [100, 104]. Considering the role of let-7 in targeting *KRAS*, H19 may influence *KRAS* expression levels in PDAC. To confirm other sponging effects of H19, H19 overexpression exerted proangiogenic effects, possibly by downregulating miR-181a and inducing the JNK and AMPK signaling pathways to facilitate angiogenesis [30]. Considering the tumor-suppressive effect of miR-181a via downregulation of *KRAS* and the role of the *KRAS* mutation in vascular malformations, it is assumed that H19 has an indirect effect on *KRAS* upregulation [105, 106]. This can also be mediated by miR-193b, another *KRAS*-regulating miRNA [107]. Overexpression of H19 has been shown to attenuate miR-193b-mediated inhibition of multiple driver oncogenes, including *EGFR*, *KRAS*, *PTEN*, *IGF1R*, and *MAPK1*, suggesting that lncRNA H19 serves as a *KRAS* regulator through miR-193b sponging [108].

LINC01133

LINC01133, with a length of 1154 nucleotides, is located on chromosome 1q23.2 and was first reported to be involved in CRC and NSCLC [109, 110]. A positive correlation has been found between high LINC01133 expression and poor prognosis in patients. LINC01133 downregulation leads to the repression of proliferation and invasion of lung cancer cells [111]. Nevertheless, other studies have shown low LINC01133 expression in CRC and breast cancer tissues [112, 113]. Therefore, it can be concluded that the expression levels of LINC01133 vary among various types of cancer, suggesting that there is a tissue-specific regulation of its expression that may be directly related to its function. Other results showed that LINC01133 aggravates the proliferation, migration, and invasion of osteosarcoma by sponging miR-422a, which targets *KRAS*, exerting antitumor effects [114, 115].

SLCO4A1-AS1

The role of SLCO4A1-AS1 in the tumorigenesis of CRC has been demonstrated in several studies, confirming its upregulation in CRC tissues and its relation with poor prognosis and tumor metastasis [116, 117]. SLCO4A1-AS1 has been reported to serve as an oncogenic lncRNA in CRC by activating the WNT/β-catenin signaling pathway [117]. The oncogenic role of SLCO4A1-AS1 in CRC promotion has been attributed to the stabilization of SLCO4A1, a transmembrane protein with sodium-independent organic anion transporter activity. In addition, the axis of the SLCO4A1-AS1/miR-508-3p/PARD3 autophagy pathway has been proposed as another carcinogenic mechanism of SLCO4A1-AS1 in the development of CRC through a sponging effect [116]. SLCO4A1-AS1 knockdown in HCT116 and SW480 cells led to the downregulation of *EGFR*, *KRAS*, *BRAF*, and *MAP3K1* expression [118]. Therefore, SLCO4A1-AS1 can be considered as a *KRAS*-related lncRNA. However, the corresponding miRNA has not yet been identified.

POTENTIAL KRAS-RELATED LNCRNAS

On the basis of the significant role of *KRAS* oncogenic mutations, many miRNAs that target *KRAS* have been discovered in many human cancer tissues [119, 120]. The inhibitory effect of miRNAs on *KRAS* expression led us to search for miRNAs that are sponged by oncogenic lncRNAs to find potential *KRAS*-related lncRNAs. Therefore, a review of the previously recognized KRAS-targeting miRNAs helps us to predict some oncogenic lncRNAs with sponging effects, which may participate in the regulation of *KRAS*. To identify potential *KRAS*-related lncRNAs, two steps were taken. In the first step, a collection of miRNAs that target *KRAS* were identified. Second, an extensive literature study was performed to determine lncRNAs with sponging effects on the miRNAs (Fig. 2). For example, a significant role of miR-143 in the inhibition of *KRAS* translation was confirmed to contribute to the suppression of cell growth [85]. In this regard, other supporting documents showed the interaction of PSMG3-AS1 lncRNA as a sponge with miR-143-3p in HCC and breast cancer tissues [16, 121]. According to the targeting of *KRAS* by miR-143 and the sponging effect of PSMG3-AS1 on this miRNA, it can be assumed that PSMG3-AS1 can be a potential *KRAS*-associated lncRNA. Similarly, miR-181a is a known miRNA with the ability to target *KRAS* mRNA. With this information, lncRNA CRNDE, whose sponging effect on miR-181a was previously confirmed, can be considered one of the other potential *KRAS*-related lncRNAs [122]. Therefore, a thorough understanding of the plethora of tumor suppressor miRNAs contributing to *KRAS*-targeting and its downregulation provides mechanistic insight into discovering potential *KRAS*-related oncogenic lncRNAs that act as molecular sponges. Accordingly, there is a large number of potential *KRAS*-related lncRNAs sponging the *KRAS*-targeting miRNAs (Fig. 2; Supplementary Table S1).

RAS-RELATED LNCRNAS ASSOCIATED WITH LEUKEMIA

Leukemia, as a heterogeneous group of malignant neoplasms in the hematopoietic system, is classified on the basis of its clinical behavior and histological origin. Although leukemia is a common malignant cancer of the hematopoietic system, its mechanism of pathogenesis has not been fully elucidated [123]. One of the main causes of this malignancy is related to acquired and infrequently inherited genetic alterations [124]. Moreover, epigenetic alterations, such as heritable and reversible changes, can also lead to some malignant behaviors, such as cancer relapse. For instance, as well-studied leukemia, acute myeloid leukemia (AML) is a typical consequence of these abnormalities and gene mutations [125]. In addition to these valuable efforts, an urgent need to elucidate the mechanism of cancer malignancy triggered the researchers to search for new molecular systems, including regulatory transcripts such as miRNAs and lncRNAs.

Oncogenic RAS mutations are highly prevalent in hematopoietic malignancies and are associated with poor survival [126]. While somatic mutations, such as KRAS mutations, cause a series of downstream secondary alterations in the transcriptome of cancer cells, evidence showing the role of lncRNAs in the pathophysiology of hematological malignancies has drastically increased in the last decade [127]. Therefore, understanding the role of KRAS mutations in large-scale alterations in the transcriptional profiles of leukemia cells, including the dysregulation of lncRNA

expression, provides more details on the pathogenic mechanisms. In this regard, the results of a pairwise analysis study comparing patients with KRAS mutations showed 26 differentially expressed lncRNAs (17 upregulated and 9 downregulated) compared to juvenile myelomonocytic leukemia (JMML) patients without this mutation [128]. Other differentially expressed RNAs between JMML patients and normal bone marrow controls revealed that the expression of 29 (19 up- and 10 downregulated) lncRNAs was dysregulated in the subgroup of KRAS-mutant patients with overexpressed lnc-ACOT9-1 [129]. lncRNA MORRBID regulates the lifespan of short-lived myeloid cells in response to extracellular pro-survival signals through the suppression of the pro-apoptotic gene BCL2L11 (also known as BIM) [130]. The high expression of MORRBID accompanied by *KRAS* and *NRAS* mutations is associated with poor overall survival of JMML patients [131].

Although the exact mechanism by which KRAS-related lncRNAs function in leukemia has not been elucidated, the sponging effect on miRNAs can be considered one of the regulatory procedures. Wang and colleagues demonstrated the role of MALAT1 in sponging miR-101 to inhibit its interaction with the 3′UTR of its target mRNA, myeloid cell leukemia 1 (MCL1). This competition between MALAT1 and MCL1 causes a decrease in MCL1 expression and a consequent increase in drug resistance in lung cancer [132]. In addition to the contribution of lncRNAs in leukemogenesis, recent studies on the role of lncRNAs as biomarkers in the diagnosis, prognosis, and therapeutic response have emphasized lncRNAs as essential regulatory factors in leukemia patients [133–135].

lncRNAs as therapeutic targets

lncRNAs are key regulators of gene expression and act through different mechanisms, including genomic imprinting, epigenetic regulation, mRNA and protein stability regulation, protein sequestration, miRNA sponging, protein translation regulation, and alternative splicing. Therefore, not only sponging effects but also other mechanisms are involved in gene regulation by lncRNAs, which provides the possible application of extensive therapeutic strategies [136].

With rapid developments in high-throughput screening methods and bioinformatics, large numbers of cancer-related genes and their associated regulatory lncRNAs will be discovered in the near future [137–139]. Considering the critical roles of lncRNAs in malignancies, lncRNA-based therapeutics may represent promising approaches in cancer treatment through novel technologies [140, 141]. Antisense oligonucleotides (ASOs), which may form a DNA-RNA structure with their target RNA through base pairing rules, could be exploited as promising tools for targeting oncogenic lncRNAs [142]. Aptamers are specific structures in the form of oligonucleotides or peptide molecules that possess the ability to bind specifically and structurally to the desired target, such as lncRNA, and prevent the interactions of the lncRNA with its corresponding targets [136]. The CRISPR/Cas9 genome editing technique, a technology for the specific DNA modification of targeted genes, has been found to be a successful approach to silence the transcription of many carcinogenic lncRNAs [143]. Although the rapid development of a new generation of gene-editing tools, such as ASOs or CRISPR/Cas9-based therapy, has already shown the feasibility of gene-editing for cancer treatment, their off-target events or unstable efficiency originating from the spatiotemporal specificity of lncRNAs should also be evaluated for further clinical applications [14]. Neutralizing targeted lncRNAs by exogenous double-stranded RNA via RNA interference (RNAi) transfection is an alternative strategy that has shown some significant results due to its specificity [144]. Despite its specificity, the RNAi method efficiency is transient due to the natural instability of RNA molecules, which necessitates solid experimental analysis to confirm the practicability of this technology [145]. In contrast to oncogenic lncRNAs, some lncRNAs with tumor suppressor activity, such as CR749391 and LET, are known to be expressed at low levels in tumors [146, 147]. Thus, induction of these lncRNAs could be a possible therapeutic approach for cancer treatment. For example, viral transfection, as the main method for plasmid transmission to the target site, could be applied to transfect exogenously synthesized tumor suppressor lncRNA plasmids into cancer cells to upregulate the expression of corresponding lncRNAs. This lncRNA-based strategy could be investigated for cancer treatment; however, solid experimental analysis is required to validate the feasibility and practicability of this strategy [14]. Aside from the fact that lncRNAs themselves could serve as possible therapeutic targets, recent documents have proven the utility of peptides/proteins encoded by lncRNAs as other potential targets [148]. lncRNAs are known as RNA molecules that do not encode proteins, but recent findings have shown that peptides/proteins encoded by lncRNAs do indeed exist and surprisingly have tumorigenic effects [148]. Therefore, peptides/proteins encoded by lncRNAs might be hidden oncopeptides/oncoproteins representing promising drug targets for treating tumor growth [148]. On the other hand, some proteins encoded by lncRNAs have tumor-suppressive effects that inhibit the carcinogenesis of oncoproteins such as KRAS [38]. Taken together, these findings suggest that lncRNAs could serve as novel therapeutic targets for cancer therapy.

CONCLUSION AND PERSPECTIVE

Approximately 25% of all human cancers have oncogenic mutations in the *RAS* family of oncogenes, most frequently the *KRAS* gene, resulting in the aberrant activation of RAS proteins and consequently their downstream pathways and leading to malignant transformation. To date, diverse therapeutic approaches have been used to interfere with mutant *KRAS*-mediated signaling. Although KRAS proto-oncogene mutations are responsible for the conversion of *KRAS* to its oncoprotein form with increased activity, suppression of mutant *KRAS* gene expression could be an approach to inhibit oncoprotein production. In this review, we focused on the sponging effect as a strategy for KRAS downregulation, considering the established roles of both miRNAs and lncRNAs. The fact that the majority of lncRNAs are expressed in a highly cell- or tissue-specific manner makes them effective therapeutic targets for cancer treatment. However, many questions remain to be addressed. How many lncRNAs are functionally and clinically relevant for KRAS-driven cancers? How can we develop systematic genomic and functional approaches to understand the role of lncRNAs in the initiation, progression, and alternative metastasis of KRAS-mutant cancers? How can we integrate patient genomic and transcriptomic data with KRAS mutations to establish a lncRNA discovery pipeline to drive preclinical studies? Finally, how does a tissue-specific expression of lncRNAs provide therapeutic candidates for tissues with a higher frequency of KRAS mutation? In addition to the questions above, the authors of this review present some suggestions for future studies concerning lncRNAs as therapeutic targets. More oncogenic lncRNAs with sponging effects on other tumor-suppressive miRNAs that target KRAS or its downstream effectors should be discovered. Proteins/peptides encoded by lncRNAs and their oncogenic or tumor-suppressing effects should be investigated. The ability to target KRAS-related oncogenic lncRNAs through various methods, such as nucleic acid-based drugs, gene-editing methods, small molecule inhibitors, miRNA mimics, catalytic degradation of lncRNAs by ribozymes, targeting lncRNA secondary and tertiary structures, and synthetic lncRNA mimics, must be studied. More importantly, further characterization of interactions between oncogenic lncRNAs and associating proteins, which form ribonucleoprotein complexes and could be involved in KRAS signaling, may lead to the identification of novel

therapeutic targets and the development of new anti-KRAS drugs. Hopefully, the increased success rate of nucleic acid therapeutics provides an outstanding opportunity to discover lncRNAs as viable candidates for therapeutic targets in KRAS-dependent malignant transformation.

REFERENCES

1. Simanshu DK, Nissley DV, McCormick F. RAS proteins and their regulators in human disease. Cell. 2017;170:17–33.
2. Fruman DA, Chiu H, Hopkins BD, Bagrodia S, Cantley LC, Abraham RT. The PI3K pathway in human disease. Cell. 2017;170:605–35.
3. Yuan TL, Amzallag A, Bagni R, Yi M, Afghani S, Burgan W, et al. Differential effector engagement by oncogenic KRAS. Cell Rep. 2018;22:1889–902.
4. Hanahan D, Weinberg RA. Hallmarks of cancer: the next generation. Cell. 2011;144:646–74.
5. Scheffzek K, Ahmadian MR, Kabsch W, Wiesmüller L, Lautwein A, Schmitz F, et al. The Ras-RasGAP complex: structural basis for GTPase activation and its loss in oncogenic Ras mutants. Science. 1997;277:333–9.
6. Scheffzek K, Ahmadian MR, Wittinghofer A. GTPase-activating proteins: helping hands to complement an active site. Trends Biochem Sci. 1998;23:257–62.
7. McCormick F. K-Ras protein as a drug target. J Mol Med (Berl). 2016;94:253–8. https://doi.org/10.1158/1078-0432.
8. Ryan MB, Corcoran RB. Therapeutic strategies to target RAS-mutant cancers. Nat Rev Clin Oncol. 2018;15:709–20.
9. Saliani M, Jalal R, Ahmadian MR. From basic researches to new achievements in therapeutic strategies of KRAS-driven cancers. Cancer Biol Med. 2019;16:435–61.
10. Moore AR, Rosenberg SC, McCormick F, Malek S. RAS-targeted therapies: is the undruggable drugged? Nat Rev Drug Discov. 2020;19:533–52.
11. Stalnecker CA, Der CJ. RAS, wanted dead or alive: advances in targeting RAS mutant cancers. Sci Signal. 2020;13:eaay6013.
12. Misale S, Yaeger R, Hobor S, Scala E, Janakiraman M, Liska D, et al. Emergence of KRAS mutations and acquired resistance to anti-EGFR therapy in colorectal cancer. Nature. 2012;486:532–6.
13. Goodall GJ, Wickramasinghe VO. RNA in cancer. Nat Rev Cancer. 2021;21:22–36.
14. Jiang M-C, Ni J-J, Cui W-Y, Wang B-Y, Zhuo W. Emerging roles of lncRNA in cancer and therapeutic opportunities. Am J Cancer Res. 2019;9:1354–66.
15. Bhan A, Soleimani M, Mandal SS. Long noncoding RNA and cancer: a new paradigm. Cancer Res. 2017;77:3965–81.
16. Cui Y, Fan Y, Zhao G, Zhang Q, Bao Y, Cui Y, et al. Novel lncRNA PSMG3-AS1 functions as a miR-143-3p sponge to increase the proliferation and migration of breast cancer cells. Oncol Rep. 2020;43:229–39.
17. Dai Q, Deng J, Zhou J, Wang Z, Yuan X-F, Pan S, et al. Long non-coding RNA TUG1 promotes cell progression in hepatocellular carcinoma via regulating miR-216b-5p/DLX2 axis. Cancer Cell Int. 2020;20:8.
18. Domvri K, Petanidis S, Anestakis D, Porpodis K, Bai C, Zarogoulidis P, et al. Exosomal lncRNA PCAT-1 promotes Kras-associated chemoresistance via immunosuppressive miR-182/miR-217 signaling and p27/CDK6 regulation. Oncotarget. 2020;11:2847–62.
19. Fernandes JCR, Acuña SM, Aoki JI, Floeter-Winter LM, Muxel SM. Long non-coding RNAs in the regulation of gene expression: physiology and disease. Non-Coding RNA. 2019;5:17.
20. Lin X, Yang F, Qi X, Li Q, Wang D, Yi T, et al. LncRNA DANCR promotes tumor growth and angiogenesis in ovarian cancer through direct targeting of miR-145. Mol Carcinog. 2019;58:2286–96.
21. Liu C, Hou J, Shan F, Wang L, Lu H, Ren T. Long non-coding RNA CRNDE promotes colorectal carcinoma cell progression and paclitaxel resistance by regulating miR-126-5p/ATAD2 axis. Onco Targets Ther. 2020;13:4931–42.
22. López-Urrutia E, Bustamante Montes LP, Ladrón de Guevara Cervantes D, Pérez-Plasencia C, Campos-Parra AD. Crosstalk between long non-coding RNAs, Micro-RNAs and mRNAs: deciphering molecular mechanisms of master regulators in cancer. Front oncol. 2019;9:669.
23. Wu H, Wei M, Jiang X, Tan J, Xu W, Fan X, et al. lncRNA PVT1 promotes tumorigenesis of colorectal cancer by stabilizing miR-16-5p and interacting with the VEGFA/VEGFR1/AKT axis. Mol Ther - Nucleic Acids. 2020;20:438–50.
24. Zhu K, Ding H, Yu A, Liao Z, Fu Z, Hong Y, et al. Co-targeting of EGFR by co-expressed miRNA-193a-3p/−5p in lung cancer. ExRNA. 2019;1:29.
25. Motti ML, Minopoli M, Carluccio GD, Ascierto PA, Carriero MV. MicroRNAs as key players in melanoma cell resistance to MAPK and immune checkpoint inhibitors. Int J Mol Sci. 2020;21:4544.
26. Kolenda T, Guglas K, Kopczyńska M, Sobocińska J, Teresiak A, Bliźniak R, et al. Good or not good: role of miR-18a in cancer biology. Rep Pract Oncol Radiother. 2020;25:808–19.
27. Kolenda T, Przybyła W, Teresiak A, Mackiewicz A, Lamperska KM. The mystery of let-7d–a small RNA with great power. Contemp Oncol. 2014;18:293.
28. Yuan J, Tan L, Yin Z, Zhu W, Tao K, Wang G, et al. MIR17HG-miR-18a/19a axis, regulated by interferon regulatory factor-1, promotes gastric cancer metastasis via Wnt/β-catenin signalling. Cell Death Dis. 2019;10:454.
29. Zhang J, Huang J, Chen W, Hu Z, Wang X. miR-143-3p targets lncRNA PSMG3-AS1 to inhibit the proliferation of hepatocellular carcinoma cells. Cancer Manag Res. 2020;12:6303.
30. Zhu A, Chu L, Ma Q, Li Y. Long non-coding RNA H19 down-regulates miR-181a to facilitate endothelial angiogenic function. Artif Cells Nanomed Biotechnol. 2019;47:2698–705.
31. Sun B, Liu C, Li H, Zhang L, Luo G, Liang S, et al. Research progress on the interactions between long non-coding RNAs and microRNAs in human cancer (Review). Oncol Lett. 2020;19:595–605.
32. Lewis BP, Burge CB, Bartel DP. Conserved seed pairing, often flanked by adenosines, indicates that thousands of human genes are microRNA targets. Cell. 2005;120:15–20.
33. Li Z, Zhao W, Wang M, Zhou X. The role of long noncoding RNAs in gene expression regulation. Gene Expression Profiling in Cancer. 2019. https://www.intechopen.com/chapters/64307.
34. He R-Z, Luo D-X, Mo Y-Y. Emerging roles of lncRNAs in the post-transcriptional regulation in cancer. Genes Dis. 2019;6:6–15.
35. Kansara S, Pandey V, Lobie PE, Sethi G, Garg M, Pandey AK. Mechanistic involvement of Long non-coding RNAs in Oncotherapeutics resistance in triple-negative breast cancer. Cells. 2020;9:1511.
36. Morgan RK, Batra H, Gaerig VC, Hockings J, Brooks TA. Identification and characterization of a new G-quadruplex forming region within the kRAS promoter as a transcriptional regulator. Biochim Biophys Acta. 2016;1859:235–45.
37. Wu R, Li L, Bai Y, Yu B, Xie C, Wu H, et al. The long noncoding RNA LUCAT1 promotes colorectal cancer cell proliferation by antagonizing Nucleolin to regulate MYC expression. Cell Death Dis. 2020;11:908.
38. Xu W, Deng B, Lin P, Liu C, Li B, Huang Q, et al. Ribosome profiling analysis identified a KRAS-interacting microprotein that represses oncogenic signaling in hepatocellular carcinoma cells. Sci China Life Sci. 2020;63:529–42.
39. Shi L, Magee P, Fassan M, Sahoo S, Leong HS, Lee D, et al. A KRAS-responsive long non-coding RNA controls microRNA processing. Nat Commun. 2021;12:1–19.
40. Zhang D, Zhang G, Hu X, Wu L, Feng Y, He S, et al. Oncogenic RAS regulates long noncoding RNA Orilnc1 in human cancer. Cancer Res. 2017;77:3745–57.
41. Balatti V, Pekarsky Y, Croce CM. Role of the tRNA-derived small RNAs in cancer: new potential biomarkers and target for therapy. Adv Cancer Res. 2017;135:173–87.
42. Goodarzi H, Nguyen HC, Zhang S, Dill BD, Molina H, Tavazoie SF. Modulated expression of specific tRNAs drives gene expression and cancer progression. Cell. 2016;165:1416–27.
43. Pekarsky Y, Balatti V, Palamarchuk A, Rizzotto L, Veneziano D, Nigita G, et al. Dysregulation of a family of short noncoding RNAs, tsRNAs, in human cancer. Proc Natl Acad Sci. 2016;113:5071–6.
44. Zhang Y, Qian H, He J, Gao W. Mechanisms of tRNA-derived fragments and tRNA halves in cancer treatment resistance. Biomark Res. 2020;8:52.
45. Balatti V, Nigita G, Veneziano D, Drusco A, Stein GS, Messier TL, et al. tsRNA signatures in cancer. Proc Natl Acad Sci. 2017;114:8071–6.
46. Rimawi MF, De Angelis C, Contreras A, Pareja F, Geyer FC, Burke KA, et al. Low PTEN levels and PIK3CA mutations predict resistance to neoadjuvant lapatinib and trastuzumab without chemotherapy in patients with HER2 over-expressing breast cancer. Breast Cancer Res Treat. 2018;167:731–40.
47. Benisty H, Weber M, Hernandez-Alias X, Schaefer MH, Serrano L. Proliferation specific codon usage facilitates oncogene translation. Proc Natl Acad Sci U S A. 2020;117:30848–56.
48. Penzo M, Montanaro L, Treré D, Derenzini M. The ribosome biogenesis-cancer connection. Cells. 2019;8:55.
49. Narla A, Ebert BL. Ribosomopathies: human disorders of ribosome dysfunction. Blood, J Am Soc Hematol. 2010;115:3196–205.
50. Donati G, Bertoni S, Brighenti E, Vici M, Trere D, Volarevic S, et al. The balance between rRNA and ribosomal protein synthesis up-and down-regulates the tumour suppressor p53 in mammalian cells. Oncogene. 2011;30:3274–88.
51. Justilien V, Ali SA, Jamieson L, Yin N, Cox AD, Der CJ, et al. Ect2-dependent rRNA synthesis is required for KRAS-TRP53-driven lung adenocarcinoma. Cancer Cell. 2017;31:256–69.
52. Wang X, Zhang H, Sapio R, Yang J, Wong J, Zhang X, et al. SOD1 regulates ribosome biogenesis in KRAS mutant non-small cell lung cancer. Nat Commun. 2021;12:2259.
53. Dvinge H, Guenthoer J, Porter PL, Bradley RK. RNA components of the spliceosome regulate tissue-and cancer-specific alternative splicing. Genome Res. 2019;29:1591–604.

54. Shuai S, Suzuki H, Diaz-Navarro A, Nadeu F, Kumar SA, Gutierrez-Fernandez A, et al. The U1 spliceosomal RNA is recurrently mutated in multiple cancers. Nature. 2019;574:712–6.
55. Dvinge H, Kim E, Abdel-Wahab O, Bradley RK. RNA splicing factors as oncoproteins and tumour suppressors. Nat Rev Cancer. 2016;16:413.
56. Oh J-M, Venters CC, Di C, Pinto AM, Wan L, Younis I, et al. U1 snRNP regulates cancer cell migration and invasion in vitro. Nat Commun. 2020;11:1.
57. Liang J, Wen J, Huang Z, Chen X-P, Zhang B-X, Chu L. Small nucleolar RNAs: insight into their function in cancer. Front Oncol. 2019;9:587.
58. Siprashvili Z, Webster DE, Johnston D, Shenoy RM, Ungewickell AJ, Bhaduri A, et al. The noncoding RNAs SNORD50A and SNORD50B bind K-Ras and are recurrently deleted in human cancer. Nat Genet. 2016;48:53–8.
59. Che Y, Siprashvili Z, Kovalski JR, Jiang T, Wozniak G, Elcavage L, et al. KRAS regulation by small non-coding RNAs and SNARE proteins. Nat Commun. 2019;10:5118.
60. Vo JN, Cieslik M, Zhang Y, Shukla S, Xiao L, Zhang Y, et al. The landscape of circular RNA in cancer. Cell. 2019;176:869–81.e13.
61. Panda AC, Grammatikakis I, Kim KM, De S, Martindale JL, Munk R, et al. Identification of senescence-associated circular RNAs (SAC-RNAs) reveals senescence suppressor CircPVT1. Nucleic Acids Res. 2017;45:4021–35.
62. Hao S, Qu R, Hu C, Wang M, Li Y. A circular RNA derived from golgi glycoprotein 1 mRNA regulates KRAS expression and promotes colorectal cancer progression by targeting microRNA-622. Onco Targets Ther. 2020;13:12637.
63. Jansson MD, Lund AH. MicroRNA and cancer. Mol Oncol. 2012;6:590–610.
64. Macfarlane L-A, Murphy PR. MicroRNA: biogenesis, function and role in cancer. Curr Genomics. 2010;11:537–61.
65. Kazmi HR, Chandra A, Kumar S, Satyam LK, Gupta A, Nigam J, et al. A let-7 microRNA binding site polymorphism in the KRAS 3′ UTR is associated with increased risk and reduced survival for gallbladder cancer in North Indian population. J Cancer Res Clin Oncol. 2016;142:2577–83.
66. Liu R, Li J, Lai Y, Liao Y, Liu R, Qiu W. Hsa-miR-1 suppresses breast cancer development by down-regulating K-ras and long non-coding RNA MALAT1. Int J Biol Macromolecules. 2015;81:491–7.
67. Huang Q, Yan J, Agami R. Long non-coding RNAs in metastasis. Cancer Metastasis Rev. 2018;37:75–81.
68. Rossi MN, Antonangeli F. LncRNAs: new players in apoptosis control. Int J Cell Biol. 2014;2014:473857.
69. Jiao F, Hu H, Han T, Yuan C, Wang L, Jin Z, et al. Long noncoding RNA MALAT-1 enhances stem cell-like phenotypes in pancreatic cancer cells. Int J Mol Sci. 2015;16:6677–93.
70. Li L, Chen H, Gao Y, Wang YW, Zhang GQ, Pan SH, et al. Long Noncoding RNA MALAT1 promotes aggressive pancreatic cancer proliferation and metastasis via the stimulation of autophagy. Mol Cancer Therapeutics. 2016;15:2232–43.
71. Tang R, Jiang M, Liang L, Xiong D, Dang Y, Chen G. Long noncoding RNA MALAT-1 can predict poor prognosis: a meta-analysis. Med Sci Monit. 2016;22:302–9.
72. Yang H, Liang N, Wang M, Fei Y, Sun J, Li Z, et al. Long noncoding RNA MALAT-1 is a novel inflammatory regulator in human systemic lupus erythematosus. Oncotarget. 2017;8:77400–6.
73. Gutschner T, Hämmerle M, Eissmann M, Hsu J, Kim Y, Hung G, et al. The noncoding RNA MALAT1 is a critical regulator of the metastasis phenotype of lung cancer cells. Cancer Res. 2013;73:1180–9.
74. Wei Y, Niu B. Role of MALAT1 as a prognostic factor for survival in various cancers: a systematic review of the literature with meta-analysis. Dis Markers. 2015;2015:164635.
75. Zhao WG, Yu SN, Lu ZH, Ma YH, Gu YM, Chen J. The miR-217 microRNA functions as a potential tumor suppressor in pancreatic ductal adenocarcinoma by targeting KRAS. Carcinogenesis. 2010;31:1726–33.
76. Liu P, Yang H, Zhang J, Peng X, Lu Z, Tong W, et al. The lncRNA MALAT1 acts as a competing endogenous RNA to regulate KRAS expression by sponging miR-217 in pancreatic ductal adenocarcinoma. Sci Rep. 2017;7:5186.
77. Chu J, Jia J, Yang L, Qu Y, Yin H, Wan J, et al. LncRNA MIR31HG functions as a ceRNA to regulate c-Met function by sponging miR-34a in esophageal squamous cell carcinoma. Biomedicine Pharmacother. 2020;128:110313.
78. Montes M, Nielsen MM, Maglieri G, Jacobsen A, Højfeldt J, Agrawal-Singh S, et al. The lncRNA MIR31HG regulates p16 INK4A expression to modulate senescence. Nat Commun. 2015;6:1–15.
79. Dandan W, Jianliang C, Haiyan H, Hang M, Xuedong L. Long noncoding RNA MIR31HG is activated by SP1 and promotes cell migration and invasion by sponging miR-214 in NSCLC. Gene. 2019;692:223–30.
80. Yang H, Liu P, Zhang J, Peng X, Lu Z, Yu S, et al. Long noncoding RNA MIR31HG exhibits oncogenic property in pancreatic ductal adenocarcinoma and is negatively regulated by miR-193b. Oncogene. 2016;35:3647–57.
81. Plantaz D, Mohapatra G, Matthay KK, Pellarin M, Seeger RC, Feuerstein BG. Gain of chromosome 17 is the most frequent abnormality detected in neuroblastoma by comparative genomic hybridization. Am J Pathol. 1997;150:81–9.
82. van der Wal JE, Hermsen MAJA, Gille HJP, Schouten-Van Meeteren NYN, Moll AC, Imhof SM, et al. Comparative genomic hybridisation divides retinoblastomas into a high and a low level chromosomal instability group. J Clin Pathol. 2003;56:26–30.
83. Zimonjic DB, Keck CL, Thorgeirsson SS, Popescu NC. Novel recurrent genetic imbalances in human hepatocellular carcinoma cell lines identified by comparative genomic hybridization. Hepatol. 1999;29:1208–14.
84. Poliseno L, Salmena L, Zhang J, Carver B, Haveman WJ, Pandolfi PP. A coding-independent function of gene and pseudogene mRNAs regulates tumour biology. Nature. 2010;465:1033–8.
85. Chen X, Guo X, Zhang H, Xiang Y, Chen J, Yin Y, et al. Role of miR-143 targeting KRAS in colorectal tumorigenesis. Oncogene. 2009;28:1385–92.
86. Long XB, Sun GB, Hu S, Liang GT, Wang N, Zhang XH, et al. Let-7a microRNA functions as a potential tumor suppressor in human laryngeal cancer. Oncol Rep. 2009;22:1189–95.
87. Booy EP, McRae EKS, Koul A, Lin F, McKenna SA. The long non-coding RNA BC200 (BCYRN1) is critical for cancer cell survival and proliferation. Mol Cancer. 2017;16:109.
88. Yu JH, Chen Y. Clinical significance of lncRNA BCYRN1 in colorectal cancer and its role in cell metastasis. Eur Rev Med Pharmacol Sci. 2019;23:9371–8.
89. Zhai H, Li Y. BCYRN1 is correlated with progression and prognosis in gastric cancer. Biosci Rep. 2019;39:BSR20190505.
90. Gu L, Lu L, Zhou D, Liu Z. Long Noncoding RNA BCYRN1 promotes the proliferation of colorectal cancer cells via up-regulating NPR3 expression. Cell Physiol Biochem. 2018;48:2337–49.
91. Lang N, Wang C, Zhao J, Shi F, Wu T, Cao H. Long non-coding RNA BCYRN1 promotes glycolysis and tumor progression by regulating the miR-149/PKM2 axis in non-small-cell lung cancer. Mol Med Rep. 2020;21:1509–16.
92. Yang L, Zhang Y, Bao J, Feng J-F. Long non-coding RNA BCYRN1 exerts an oncogenic role in colorectal cancer by regulating the miR-204-3p/KRAS axis. Cancer Cell Int. 2020;20:453.
93. Li X, Deng S-J, Zhu S, Jin Y, Cui S-P, Chen J-Y, et al. Hypoxia-induced lncRNA-NUTF2P3-001 contributes to tumorigenesis of pancreatic cancer by derepressing the miR-3923/KRAS pathway. Oncotarget 2016;7:6000–14.
94. Rosenbluh J, Nijhawan D, Chen Z, Wong K-K, Masutomi K, Hahn WC. RMRP is a non-coding RNA essential for early murine development. PloS ONE. 2011;6:e26270.
95. Song H, Sun W, Ye G, Ding X, Liu Z, Zhang S, et al. Long non-coding RNA expression profile in human gastric cancer and its clinical significances. J Transl Med. 2013;11:225.
96. Shao Y, Ye M, Li Q, Sun W, Ye G, Zhang X, et al. LncRNA-RMRP promotes carcinogenesis by acting as a miR-206 sponge and is used as a novel biomarker for gastric cancer. Oncotarget. 2016;7:37812–24.
97. Wang Y, Luo X, Liu Y, Han G, Sun D. Long noncoding RNA RMRP promotes proliferation and invasion via targeting miR-1-3p in non-small-cell lung cancer. J Cell Biochem. 2019;120:15170–81.
98. Lin F, Yao L, Xiao J, Liu D, Ni Z. MiR-206 functions as a tumor suppressor and directly targets K-Ras in human oral squamous cell carcinoma. Onco Targets Ther. 2014;7:1583–91.
99. Meng Q, Ren M, Li Y, Song X. LncRNA-RMRP acts as an oncogene in lung cancer. PLoS One. 2016;11:e0164845.
100. Lim YWS, Xiang X, Garg M, Le MT, Wong AL-A, Wang L, et al. The double-edged sword of H19 lncRNA: Insights into cancer therapy. Cancer Lett. 2020;500:253–62.
101. Akao Y, Nakagawa Y, Naoe T. let-7 microRNA functions as a potential growth suppressor in human colon cancer cells. Biol Pharm Bull. 2006;29:903–6.
102. Luu C, Heinrich EL, Duldulao M, Arrington AK, Fakih M, Garcia-Aguilar J, et al. TP53 and let-7a micro-RNA regulate K-Ras activity in HCT116 colorectal cancer cells. PloS ONE. 2013;8:e70604–e.
103. Kallen AN, Zhou XB, Xu J, Qiao C, Ma J, Yan L, et al. The imprinted H19 lncRNA antagonizes let-7 microRNAs. Mol Cell. 2013;52:101–12.
104. Ma C, Nong K, Zhu H, Wang W, Huang X, Yuan Z, et al. H19 promotes pancreatic cancer metastasis by derepressing let-7's suppression on its target HMGA2-mediated EMT. Tumour Biol: J Int Soc Oncodev Biol Med. 2014;35:9163–9.
105. Fish JE, Flores Suarez CP, Boudreau E, Herman AM, Gutierrez MC, Gustafson D, et al. Somatic gain of KRAS function in the endothelium is sufficient to cause vascular malformations that require MEK but Not PI3K signaling. Circ Res. 2020;127:727–43.
106. Shin KH, Bae SD, Hong HS, Kim RH, Kang MK, Park NH. miR-181a shows tumor suppressive effect against oral squamous cell carcinoma cells by down-regulating K-ras. Biochemical biophysical Res Commun. 2011;404:896–902.

107. Gastaldi C, Bertero T, Xu N, Bourget-Ponzio I, Lebrigand K, Fourre S, et al. miR-193b/365a cluster controls progression of epidermal squamous cell carcinoma. Carcinogenesis. 2014;35:1110–20.
108. Ye Y, Guo J, Xiao P, Ning J, Zhang R, Liu P, et al. Macrophages-induced long noncoding RNA H19 up-regulation triggers and activates the miR-193b/MAPK1 axis and promotes cell aggressiveness in hepatocellular carcinoma. Cancer Lett. 2020;469:310–22.
109. Zhang W, Du M, Wang T, Chen W, Wu J, Li Q, et al. Long non-coding RNA LINC01133 mediates nasopharyngeal carcinoma tumorigenesis by binding to YBX1. Am J Cancer Res. 2019;9:779–90.
110. Zang C, Nie F-Q, Wang Q, Sun M, Li W, He J, et al. Long non-coding RNA LINC01133 represses KLF2, P21 and E-cadherin transcription through binding with EZH2, LSD1 in non small cell lung cancer. Oncotarget. 2016;7:11696–707.
111. Zhang J, Zhu N, Chen X. A novel long noncoding RNA LINC01133 is upregulated in lung squamous cell cancer and predicts survival. Tumour Biol: J Int Soc Oncodev Biol Med. 2015;36:7465–71.
112. Song Z, Zhang X, Lin Y, Wei Y, Liang S, Dong C. LINC01133 inhibits breast cancer invasion and metastasis by negatively regulating SOX4 expression through EZH2. J Cell Mol Med. 2019;23:7554–65.
113. Zhang JH, Li AY, Wei N. Downregulation of long non-coding RNA LINC01133 is predictive of poor prognosis in colorectal cancer patients. Eur Rev Med Pharmacol Sci. 2017;21:2103–7.
114. Zhang H, He Q-Y, Wang G-C, Tong D-K, Wang R-K, Ding W-B, et al. miR-422a inhibits osteosarcoma proliferation by targeting BCL2L2 and KRAS. Biosci Rep. 2018;38:BSR20170339.
115. Zeng HF, Qiu HY, Feng FB. Long noncoding RNA LINC01133 functions as an miR-422a sponge to aggravate the tumorigenesis of human osteosarcoma. Oncol Res. 2018;26:335–43.
116. Wang Z, Jin J. LncRNA SLCO4A1-AS1 promotes colorectal cancer cell proliferation by enhancing autophagy via miR-508-3p/PARD3 axis. Aging. 2019;11:4876–89.
117. Yu J, Han Z, Sun Z, Wang Y, Zheng M, Song C. LncRNA SLCO4A1-AS1 facilitates growth and metastasis of colorectal cancer through β-catenin-dependent Wnt pathway. J Exp Clin Cancer Res. 2018;37:222.
118. Tang R, Chen J, Tang M, Liao Z, Zhou L, Jiang J, et al. LncRNA SLCO4A1-AS1 predicts poor prognosis and promotes proliferation and metastasis via the EGFR/MAPK pathway in colorectal cancer. Int J Biol Sci. 2019;15:2885–96.
119. Fan C, Lin Y, Mao Y, Huang Z, Liu AY, Ma H, et al. MicroRNA-543 suppresses colorectal cancer growth and metastasis by targeting KRAS, MTA1 and HMGA2. Oncotarget. 2016;7:21825–39.
120. Graziano F, Canestrari E, Loupakis F, Ruzzo A, Galluccio N, Santini D, et al. Genetic modulation of the Let-7 microRNA binding to KRAS 3′-untranslated region and survival of metastatic colorectal cancer patients treated with salvage cetuximab–irinotecan. Pharmacogenomics J. 2010;10:458–64.
121. Zhang J, Huang J, Chen W, Hu Z, Wang X. miR-143-3p targets lncRNA PSMG3-AS1 to inhibit the proliferation of hepatocellular carcinoma cells. Cancer Manag Res. 2020;12:6303–9.
122. Han P, Li J-W, Zhang B-M, Lv J-C, Li Y-M, Gu X-Y, et al. The lncRNA CRNDE promotes colorectal cancer cell proliferation and chemoresistance via miR-181a-5p-mediated regulation of Wnt/β-catenin signaling. Mol Cancer. 2017;16:9.
123. Wu J, Fantasia JE, Kaplan R. Oral manifestations of acute myelomonocytic leukemia: a case report and review of the classification of leukemias. J Periodontol. 2002;73:664–8.
124. Garg M, Nagata Y, Kanojia D, Mayakonda A, Yoshida K, Haridas Keloth S, et al. Profiling of somatic mutations in acute myeloid leukemia with FLT3-ITD at diagnosis and relapse. Blood. J Am Soc Hematol. 2015;126:2491–501.
125. Kirtonia A, Pandya G, Sethi G, Pandey AK, Das BC, Garg M. A comprehensive review of genetic alterations and molecular targeted therapies for the implementation of personalized medicine in acute myeloid leukemia. J Mol Med. 2020;98:1069–91.
126. Ward AF, Braun BS, Shannon KM. Targeting oncogenic Ras signaling in hematologic malignancies. Blood. 2012;120:3397–406.
127. Bhat AA, Younes SN, Raza SS, Zarif L, Nisar S, Ahmed I, et al. Role of non-coding RNA networks in leukemia progression, metastasis and drug resistance. Mol Cancer. 2020;19:1–21.
128. Hofmans M, Lammens T, Helsmoortel HH, Bresolin S, Cavé H, Flotho C, et al. The long non-coding RNA landscape in juvenile myelomonocytic leukemia. Haematologica. 2018;103:e501.
129. Mattias H, Lammens T, Depreter B, Wu Y, Erlacher M, Aurélie C, et al. Long non-coding RNAs as novel therapeutic targets in juvenile myelomonocytic leukemia. Sci Rep. 2021;11:2801.
130. Kotzin JJ, Spencer SP, McCright SJ, Kumar DBU, Collet MA, Mowel WK, et al. The long non-coding RNA Morrbid regulates Bim and short-lived myeloid cell lifespan. Nature 2016;537:239–43.
131. Cai Z, Zhang C, Kotzin JJ, Williams A, Henao-Mejia J, Kapur R. Role of lncRNA Morrbid in PTPN11 (Shp2) E76K-driven juvenile myelomonocytic leukemia. Blood Adv. 2020;4:3246–51.
132. Wang H, Wang L, Zhang G, Lu C, Chu H, Yang R, et al. MALAT1/miR-101-3p/MCL1 axis mediates cisplatin resistance in lung cancer. Oncotarget. 2018;9:7501.
133. Cruz-Miranda GM, Hidalgo-Miranda A, Bárcenas-López DA, Núñez-Enríquez JC, Ramírez-Bello J, Mejía-Aranguré JM, et al. Long non-coding RNA and acute leukemia. Int J Mol Sci. 2019;20:735.
134. Dieter C, Lourenco ED, Lemos NE. Association of long non-coding RNA and leukemia: a systematic review. Gene. 2020;735:144405.
135. Gao J, Wang F, Wu P, Chen Y, Jia Y. Aberrant LncRNA expression in leukemia. J Cancer. 2020;11:4284.
136. Pandya G, Kirtonia A, Sethi G, Pandey AK, Garg M. The implication of long non-coding RNAs in the diagnosis, pathogenesis and drug resistance of pancreatic ductal adenocarcinoma and their possible therapeutic potential. Biochim Biophys Acta Rev Cancer. 2020;1874:188423.
137. Siavoshi A, Taghizadeh M, Dookhe E, Piran M, Saliani M, Mohammad Ganji S. Network analysis of differential gene expression to identify hub genes in ovarian cancer. J Cell Mol Res. 2020;12:1–9.
138. Huang R, Zhou L, Chi Y, Wu H, Shi L. LncRNA profile study reveals a seven-lncRNA signature predicts the prognosis of patients with colorectal cancer. Biomark Res. 2020;8:1–16.
139. Leon LM, Gautier M, Allan R, Ilié M, Nottet N, Pons N, et al. Correction: The nuclear hypoxia-regulated NLUCAT1 long non-coding RNA contributes to an aggressive phenotype in lung adenocarcinoma through regulation of oxidative stress. Oncogene. 2019;38:7146–65.
140. Jiang M-C, Ni J-J, Cui W-Y, Wang B-Y, Zhuo W. Emerging roles of lncRNA in cancer and therapeutic opportunities. Am J Cancer Res. 2019;9:1354.
141. Jariwala N, Sarkar D. Emerging role of lncRNA in cancer: a potential avenue in molecular medicine. Ann Transl Med. 2016;4:286.
142. Bennett CF, Baker BF, Pham N, Swayze E, Geary RS. Pharmacology of antisense drugs. Annu Rev Pharmacol Toxicol. 2017;57:81–105.
143. Gilbert LA, Horlbeck MA, Adamson B, Villalta JE, Chen Y, Whitehead EH, et al. Genome-scale CRISPR-mediated control of gene repression and activation. Cell. 2014;159:647–61.
144. Elbashir SM, Harborth J, Lendeckel W, Yalcin A, Weber K, Tuschl T. Duplexes of 21-nucleotide RNAs mediate RNA interference in cultured mammalian cells. Nature. 2001;411:494–8.
145. Watanabe C, Cuellar TL, Haley B. Quantitative evaluation of first, second, and third generation hairpin systems reveals the limit of mammalian vector-based RNAi. RNA Biol. 2016;13:25–33.
146. Shi S, Li D, Li Y, Feng Z, Du Y, Nie Y. LncRNA CR749391 acts as a tumor suppressor to upregulate KLF6 expression via interacting with miR-181a in gastric cancer. Exp Therapeutic Med. 2020;19:569–78.
147. Zhou C, Wang X, Yang N, Xue S, Li W, Xie P. LncRNA LET function as a tumor suppressor in breast cancer development. Eur Rev Med Pharmacol Sci. 2018;22:6002–7.
148. Zhu S, Wang J, He Y, Meng N, Yan G-R. Peptides/proteins encoded by non-coding RNA: a novel resource bank for drug targets and biomarkers. Front Pharmacol. 2018;9:1295.

ACKNOWLEDGEMENTS

We are grateful to group members Niloufar Mosaddeghzedeh, Neda Sadat Kazemein Jasemi, Silke Pudewell, Mehrnaz Mehrabipour, and Farhad Bazgir from the Institute of Biochemistry and Molecular Biology II of the Heinrich Heine University for the critical reading of the manuscript.

AUTHOR CONTRIBUTIONS

M.S. and M.R.A. contributed to the conception, design of the article, and supervision, prepared the figures and the supplementary Table S1. A.M.B. contributed in paper writing and provided critical revision of the article. All authors gave final approval of the accepted version for publication.

FUNDING

This study was supported by the European Network on Noonan Syndrome and Related Disorders (NSEuroNet, grant number: 01GM1621B), and the German Federal Ministry of Education and Research (BMBF) – German Network of RASopathy Research (GeNeRARe, grant numbers: 01GM1902C). Open Access funding enabled and organized by Projekt DEAL.

COMPETING INTERESTS

The authors declare no competing interests.

ADDITIONAL INFORMATION

Supplementary information The online version contains supplementary material available at https://doi.org/10.1038/s41417-021-00381-x.

Correspondence and requests for materials should be addressed to M.R.A.

Reprints and permission information is available at http://www.nature.com/reprints

Publisher's note Springer Nature remains neutral with regard to jurisdictional claims in published maps and institutional affiliations.

Chapter VII. RHO GTPase-related long noncoding RNAs in human cancers

Authors: Mahsa Saliani*, Amin Mirzaiebadizi*, Niloufar Mosaddeghzadeh, Mohammad Reza Ahmadian

*These authors equally contributed to this study

DOI: 10.3390/cancers13215386

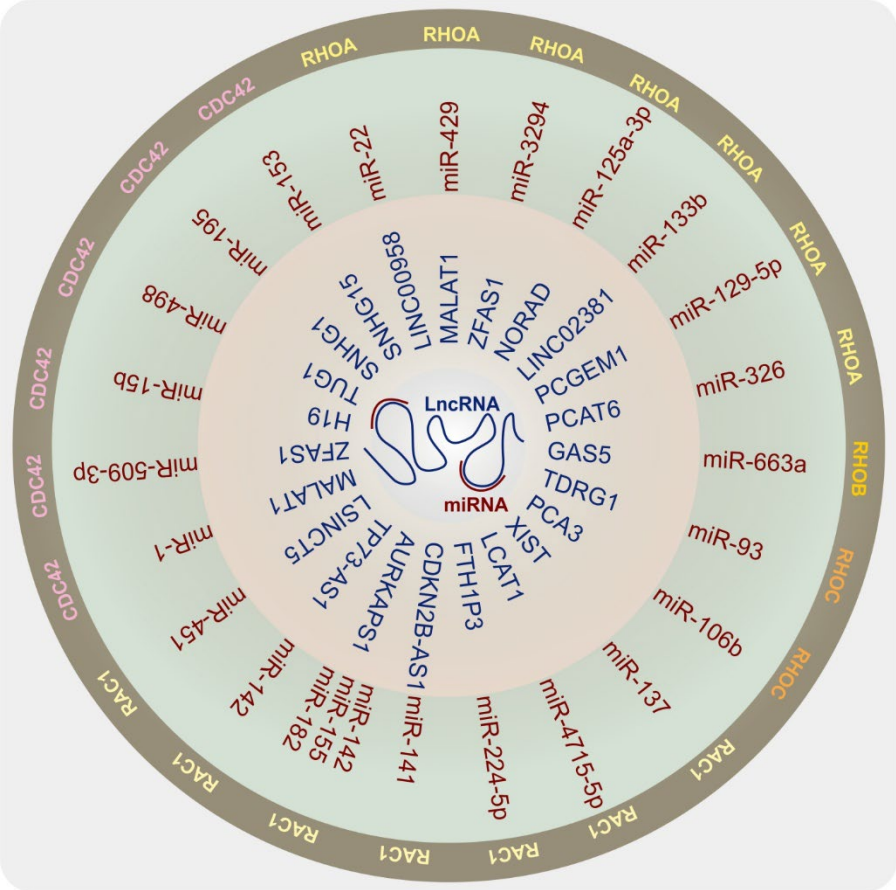

Status:	Published
Journal:	*Cancers*
JIF:	4.5
Contribution:	≈40%

A.M. contributed to the design and conception of the study, conducted an in-depth literature review, participated in manuscript writing, and performed comprehensive proofreading and critical editing of the final version.

cancers

MDPI

Review

RHO GTPase-Related Long Noncoding RNAs in Human Cancers

Mahsa Saliani [1,2,†], Amin Mirzaiebadizi [1,†], Niloufar Mosaddeghzadeh [1] and Mohammad Reza Ahmadian [1,*]

[1] Institute of Biochemistry and Molecular Biology II, Medical Faculty and University Hospital Düsseldorf, Heinrich-Heine University, 40225 Düsseldorf, Germany; mahsa.saliani@hhu.de (M.S.); aminmirzaie1992@gmail.com (A.M.); mosaddeg@uni-duesseldorf.de (N.M.)
[2] Department of Chemistry, Faculty of Science, Ferdowsi University of Mashhad, Mashhad 9177948974, Iran
* Correspondence: Reza.ahmadian@hhu.de; Tel.: +49-211-811-2384
† These authors equally contributed to this work.

Simple Summary: Whilst mutations in genes encoding RHO GTPase proteins are rare in different type of cancers, altered expression of several RHO GTPases has been reported in a variety of human malignancies. As key regulators of gene expression, lncRNAs coordinate a wide range of molecular processes, including post-translational regulation through miRNA sponging. The purpose of the present study was to address the current state of knowledge about the lncRNAs involved in the regulation of the expression of the RHO GTPases including RHOA, RHOB, RHOC, RAC1, and CDC42, with a specific focus on the regulatory mechanism of lncRNAs as the molecular sponges of miRNAs. Considering the critical roles of lncRNAs in malignancies, lncRNA-based therapeutics are representing promising approaches in cancer treatment through novel technologies. In this regard, well-characterized examples of lncRNAs associated with tumorigenicity present experimental frameworks for future studies in this rapidly evolving field.

Abstract: RHO GTPases are critical signal transducers that regulate cell adhesion, polarity, and migration through multiple signaling pathways. While all these cellular processes are crucial for the maintenance of normal cell homeostasis, disturbances in RHO GTPase-associated signaling pathways contribute to different human diseases, including many malignancies. Several members of the RHO GTPase family are frequently upregulated in human tumors. Abnormal gene regulation confirms the pivotal role of lncRNAs as critical gene regulators, and thus, they could potentially act as oncogenes or tumor suppressors. lncRNAs most likely act as sponges for miRNAs, which are known to be dysregulated in various cancers. In this regard, the significant role of miRNAs targeting RHO GTPases supports the view that the aberrant expression of lncRNAs may reciprocally change the intensity of RHO GTPase-associated signaling pathways. In this review article, we summarize recent advances in lncRNA research, with a specific focus on their sponge effects on RHO GTPase-targeting miRNAs to crucially mediate gene expression in different cancer cell types and tissues. We will focus in particular on five members of the RHO GTPase family, including RHOA, RHOB, RHOC, RAC1, and CDC42, to illustrate the role of lncRNAs in cancer progression. A deeper understanding of the widespread dysregulation of lncRNAs is of fundamental importance for confirmation of their contribution to RHO GTPase-dependent carcinogenesis.

Keywords: carcinogenesis; lncRNAs; miRNAs; RHO GTPases; signal transduction; sponge effect

Citation: Saliani, M.; Mirzaiebadizi, A.; Mosaddeghzadeh, N.; Ahmadian, M.R. RHO GTPase-Related Long Noncoding RNAs in Human Cancers. *Cancers* **2021**, *13*, 5386. https://doi.org/10.3390/cancers13215386

Academic Editor: Paulo Matos

Received: 8 September 2021
Accepted: 22 October 2021
Published: 27 October 2021

1. Introduction

RHO family proteins are GDP/GTP-binding proteins of the RAS superfamily that transduce extracellular signals into intracellular responses. They cycle, with some exceptions, between an inactive GDP-bound ("off") state and an active GTP-bound ("on") state (Figure 1) [1,2]. Fully processed GTPases remain locked in an inactive GDP-bound form in the cytosol via the formation of stoichiometric complexes with RHO GDP dissociation

inhibitors (GDIs) [3]. During the signal transduction to its downstream effectors to activate multiple signaling pathways, most RHO GTPases acquire their active state with the exchange of GDP for GTP as a consequence of two continuous steps. The first step involves their release from GDI complexes, followed by rapid GDP/GTP exchange, a process catalyzed by RHO-specific guanine nucleotide exchange factors (GEFs) [1,2,4–6]. In the active state, conformational changes of two flexible regions, called switch I and switch II, provide a functional platform for the interaction of RHO GTPases with their regulators and effectors [7,8]. At the end of the GTPase cycle, hydrolysis of the bound GTP is stimulated by GTPase-activating proteins (GAPs) and converts RHO GTPases to the GDP-bound inactive state [2,9,10]. RhoGDI can extract both inactive and active RhoGTPases, and found that extraction of active RhoGTPase contributes to their spatial regulation around cell wounds [9].

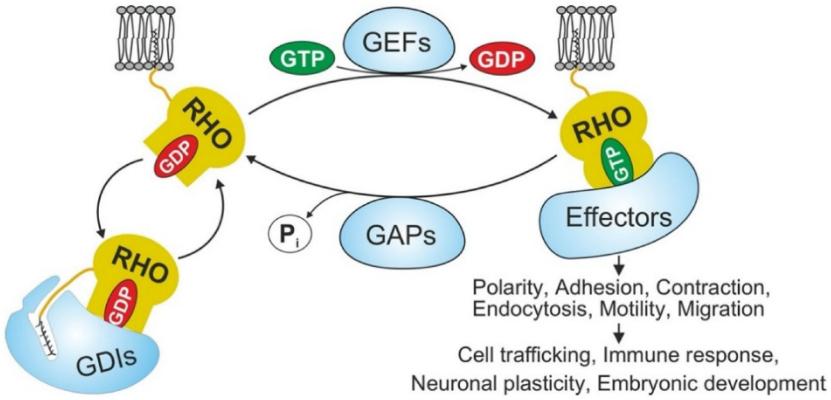

Figure 1. Molecular mechanisms of RHO GTPase regulation and signaling. Most of RHO GTPases (20 canonical members) act as molecular switches, in order to transduce signals from receptors to downstream pathways. This switch mechanism is tightly regulated through three classes of particular proteins: Guanine nucleotide exchange factors (GEFs: 74 DBL and 11 DOCK family members) catalyze the exchange of GDP for GTP, thereby turning on the signal transduction. GTPase-activating proteins (GAPs; 66 ARHGAP family members) bind to GTP-bound RHO GTPases and accelerate their very slow intrinsic GTP hydrolysis, leading to signaling the switch off. Guanine nucleotide dissociation inhibitor (GDIs: three known members) bind to isoprenylated, GDP-bound RHO GTPases and displace them from the membrane. GTP-bound, active RHO GTPases associate with and activate different downstream effectors (more than 70 known members), and thus accomplish various biochemical processes and cellular functions.

As with most RAS superfamily proteins, the maturation of the newly translated RHO GTPases requires a stepwise posttranslational modification. This modification includes the incorporation of a geranylgeranyl moiety (in some cases, farnesyl or palmitate groups) onto the CAAX box (C is cysteine, A is any aliphatic amino acid, and X is any amino acid) on the endoplasmic reticulum [10,11], the subsequent cleavage of the AAX tripeptide, and the methylation of the newly exposed C-terminal isoprenylcysteine residue [12]. In stimulated cells, isoprenylated RHO GTPases are specifically associated with the cellular membrane, which is essential for their biological activity (Figure 1). In resting cells, however, GDIs extract them from the membrane and create a cytosolic pool of inactivated RHO GTPases [13].

To date, 20 canonical members of the RHO family have been identified in humans and can be categorized into distinct subfamilies based on their sequence homology [2,14]: RHO (RHOA, RHOB, and RHOC); RAC (RAC1, RAC1B, RAC2, RAC3, and RHOG); CDC42 (CDC42, G25K, TC10/RHOQ, TCL/RHOJ, WRCH1/RHOU, and WRCH2/RHOV); RHOD (RHOD and RIF/RHOF); RND (RND1/RHO6, RND2/RHO7, and RND3/RHO8/RHOE); and TTF/RHOH [15]. Some studies also include the members of the RHOBTB and Miro

families among those proteins; however, these 'atypical' GTPases are highly divergent from the rest of the RHO GTPases in terms of structure, overall amino acid homology, subcellular localization, and biological functions [16].

Activated RHO GTPases bind to their downstream effectors and thereby regulate diverse cellular processes (Figure 1), including the reorganization of the actin cytoskeleton and thereby cell adhesion, polarity, and migration [17,18]. Thus, they are associated with the control of various biological processes, such as cell trafficking, wound healing, immune response, embryonal development, and neuronal plasticity [19,20]. Given the critical roles of RHO GTPases in cell signaling, the deregulation of their downstream pathways is known to contribute to the development of diverse diseases [21–23]. Abnormal expression of different RHO GTPases has been reported in many human tumors [24]. While most studies on RHO GTPase-associated tumorigenesis have narrowly focused on cytoskeletal-related biological processes and canonical pathways, the contribution of noncanonical mechanisms has also been observed [16]. These mechanisms include the regulation of autocrine and paracrine loops critical for remodeling of the tumor microenvironment and tumor growth [25], nucleolar functions connected with either efficient ribogenesis or the suppression of nucleolar stress in cancer cells [26–28], the regulation of both the centrosome and chromosome stability [27,29], the regulation of the YAP/TAZ pathway [30], and the recruitment of pathways to avoid antitumoral immune responses [31]. These observations highlight the key role of RHO GTPases in tumorigenesis but, at the same time, challenge the widely established functional archetypes in the field and the therapeutic feasibility of these pathways.

Contrary to recent studies that report the identification of new driver mutations in some RHO GTPases members, such as RAC1, RHOA, and CDC42 [32], analysis of cancer genomes has demonstrated that mutations affecting RHO signaling pathways are found at low frequency in a limited spectrum of tumor types [18,21,33]. While mutations in genes encoding RHO GTPases are rare in cancer, alternative mechanisms lead to the spurious activation of RHO pathways, which could add multiple regulatory layers controlling the steady-state levels and activation dynamics of RHO signaling elements. Consistent with this view, RHO GTPases can be further regulated by several approaches, including transcriptional regulation [34], alternative splicing [33,35,36], microRNA (miRNA)-mediated transcript stability [37], protein steady-state levels, posttranslational modifications [38], sequestration in endosomes [12], time of residence in membranes [39], intracellular trafficking [40], and F-actin-dependent cytoskeletal events [41]. In particular, miRNAs, as negative regulators of gene expression, repress RHO GTPases through degradation or translational blockade of their associated mRNAs [42,43]. While the processing of mRNA by miRNAs is essential for gene expression, the established role of long noncoding RNAs (lncRNAs) in the regulation of miRNAs highlights the potential mechanisms by which these RNA subtypes contribute to neoplastic transformations [44,45].

The involvement of lncRNAs in tumorigenesis and cancer progression may result from their roles in cell division, migration, differentiation, and apoptosis [46,47]. As critical gene regulators, lncRNAs interact with DNA, RNA, and proteins to modulate gene expression at the pretranscriptional, transcriptional, and posttranscriptional levels [48–51]. In this regard, the associations between lncRNA and the regulatory machinery of chromatin remodeling, transcription, splicing, and nuclear trafficking clarify the details of the regulatory aspects of these RNA species [52–54]. lncRNAs act as competing endogenous RNAs (ceRNAs) to regulate other RNA transcripts by competing for shared miRNAs [52,55]. According to the dysregulation of many miRNAs in RHO GTPase-dependent malignancies, lncRNAs are, as negative regulators of miRNAs, likely to become a focus in the future development of new RHO GTPase-based therapies [56]. Significantly, recent studies have reported that lncRNAs and members of RHO GTPase signaling cascades are dysregulated in various human cancers (Figure 2) [53,54].

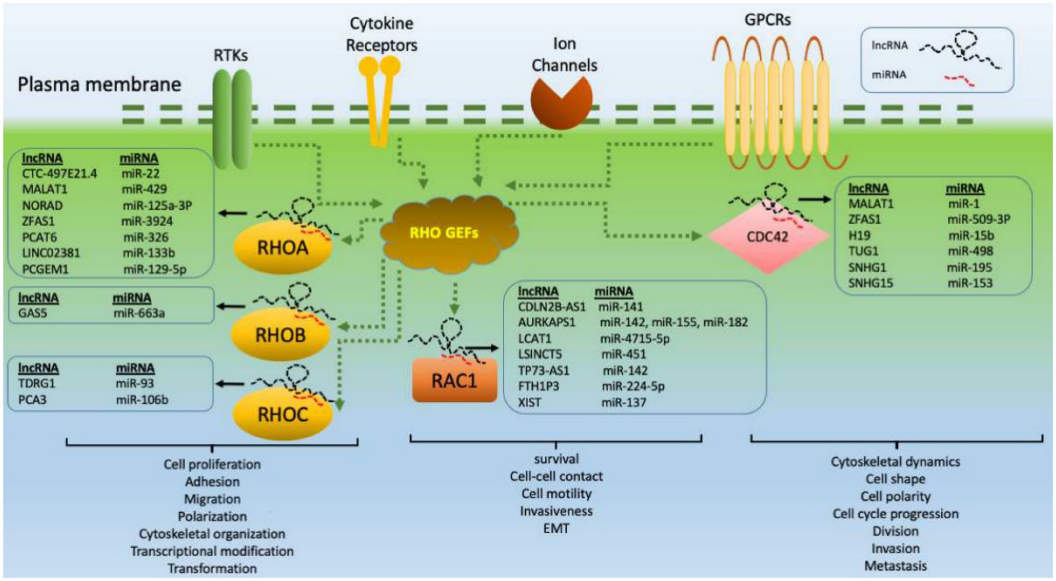

Figure 2. RHO GTPase-related lncRNAs. RHO GTPases are activated by RHO GEFs via different receptors, including GPCRs (G-protein coupled receptors with various ligands, such as Angiotensin II, Endothelin, LPA, S1P1, Thrombin, and Thromboxane A2), RTKs (receptor tyrosine kinases with ligands, such as EGF, Ephrins, NGF, PDGF, and VEGF), ion channels (with ligands, including nicotinic acetylcholine or glutamate), and cytokine receptors (with ligands, including Interferons, Interleukins, and Tumor necrosis factors). Members of the RHO GTPase family, such as RHOA, RHOB, RHOC, RAC1, and CDC42, are modulated by lncRNAs, which are the key regulators of gene expression. They play essential roles in a wide variety of signaling pathways, and thus processes involved in tumor progression. lncRNAs act as ceRNAs by sponging tumor suppressor miRNAs, thereby indirectly regulating the expression of genes related to RHO GTPases.

miRNAs are noncoding RNA molecules that can control the expression of their target mRNAs [57]. These short sequences suppress target genes by either inhibiting translation or initiating degradation of mRNA based on complementarity [58]. The expression of several RHO GTPases can be regulated by miRNAs [59]. Notably, most of the studies on miRNAs have been performed in cancer models, and demonstrated that the modulation of RHO GTPase expression with miRNAs can affect cancer development. For instance, it has been reported that RHOA is downregulated by miR-340-5p and mir-200 to inhibit cancer progression [60,61]. RHOB is the target of miR-21, and RHOBTB1 is suppressed by miR-31 [62,63]. Also, CDC42 is a target of miR-29 and miR-137 [64,65]. Given the significance of miRNAs in the direct regulation of members of the RHO GTPase family, emerging evidence has revealed that numerous lncRNAs that modify RHO GTPases are likely to act as ceRNAs. These lncRNAs function as oncogenes by sponging tumor suppressor RHO GTPase-related miRNAs (Figure 2) [66,67], thereby indirectly contributing to the regulation of the expression of the RHO GTPase genes targeted by these miRNAs. Thus, the current knowledge of RHO GTPase-related oncogenic lncRNAs in relation to their aberrant expression and their mechanism of action through sponging effects on RHO GTPase-targeting miRNAs are discussed.

Up to now, a number of lncRNAs related to a few RHO GTPase members, such as RHOA, RHOB, RHOC, RAC1, and CDC42, have been identified. Therefore, this article addresses the current state of knowledge about the regulatory mechanisms of lncRNAs in the expression of genes related to RHOA, RHOB, RHOC, RAC1, and CDC42 with a specific focus on lncRNAs as molecular sponges of miRNAs.

1.1. RHOA-Related lncRNAs

Metastasis-associated lung adenocarcinoma transcript 1 (MALAT1) is a well-studied lncRNA. It is extremely abundant in nuclear speckles and was originally discovered in a study of metastasis in patients with early-stage NSCLC [68,69]. MALAT1 is located at chr11q13 and is approximately 8500 nucleotides in length. It is conserved throughout mammalian species, and plays important roles in development and evolution [70]. Although MALAT1 is abundant in normal cells, many studies have shown that this lncRNA promotes cell proliferation, migration, and metastasis in cancer tissues by affecting several signaling pathways, such as Wnt/β-catenin [71] and PI3K/AKT [71]. MALAT1 has molecular functions in the alternative splicing of pre-mRNA and in transcriptional and posttranscriptional regulation [72]. One of the main mechanisms of MALAT1 in post-translational regulation is its function as a ceRNA that leads to the progression of various cancers [73]. Tumor-suppressor activity of miR-429 in breast cancer [74], CRC [75], and nasopharyngeal cancer [76] has been approved by different studies. Xiao et al. reported that lncRNA MALAT1 had high expression in human lung adenocarcinoma tissues (vs. paracancerous normal tissues, $t = 16.387$, $p < 0.001$), and its expression was associated with tumor size, lymph node metastasis, and TNM staging in patients. In this study, thirty-nine cases of lung adenocarcinoma tumor tissues and normal tissues from 22 males and 17 females, aged 45–78 years, were collected and the two-year survival of patients with low expression of MALAT1 was significantly higher than that of MALAT1 high expression in lung adenocarcinoma patients (Long rank = 4.773, $p = 0.0289$) [77]. MALAT1 acts as a ceRNA for miR-429 to regulate RHOA expression in lung adenocarcinoma cells. The upregulation of MALAT1 promoted cell proliferation, invasion, and migration of lung cancer cells by sponging miR-429 and consequently inducing RHOA expression [77].

Noncoding RNA activated by DNA damage (NORAD; also referred to as LINC00657) is a cytoplasmic lncRNA transcribed from the exon of chr20q11.23 [78]. This highly conserved lncRNA is upregulated in response to DNA damage, and it is required for genome stability as well as proper mitotic divisions through sequestration and negative regulation of PUMILIO (PUM) proteins, which are among deeply conserved RBPs negatively regulating gene expression [79,80]. NORAD has a crucial function in carcinogenesis, and its dysregulation has been implicated in various types of cancers [81–83]. Several studies demonstrated that NORAD could act as a ceRNA to sponge miRNAs and ultimately regulate the expression of several factors that play vital roles in cancer progression [84–87]. The ability of miR-125a-3p to increase the chemosensitivity of pancreatic cancer cells by inhibition of epithelial-to-mesenchymal transition (EMT) was reported [88]. Li et al. have shown that NORAD promoted the migration and invasion of pancreatic cancer cells through competitive binding to miR-125a-3p, causing RHOA deregulation [89]. In this study, analysis of microarray expression profiles between 55 pancreatic ductal adenocarcinoma cells (PDAC) and normal pancreas tissues, showed the significant upregulation of NORAD in cancer patients ($p < 0.001$). They also suggested that the upregulation of NORAD could occur through hypoxia, which thereby stimulates hypoxia-induced EMT [89].

The role of lncRNA zinc finger antisense 1 (ZFAS1) in breast cancer was originally exhibited by Askarian-Amiri et al. [90]. ZFAS1, a 17,561 bp transcript from the 5′ end of the ZNFX1 gene, is located on chr20q13.13. The expression of ZFAS1 is low in breast cancer cells, and it has antitumor activity [90,91]. Numerous studies have revealed its overexpression and roles in tumor growth and metastasis in various cancers, including bladder cancer [92], hepatocellular carcinoma (HCC) [93], colorectal cancer (CRC) [94], prostate cancer [95], and NSCLC [96]. In fact, being a molecular sponge for miRNAs is one of the regulatory mechanisms whereby ZFAS1 serves to adjust the proliferation, invasion, and metastasis of cancer cells [97]. Liu et al. investigated the differential expression of ZFAS1 using nine GEO datasets (252 tumor samples and 56 normal samples), and identified that ZFAS1 had upregulated expression in PDAC (adjusted p. value (3.79E−10) [44]. ZFAS1 expression level in PDAC were further validated by data from the ONCOMINE, UALCAN, and GEPIA databases; all of them supported the GEO results, and it was also

recognized to act as a miR-3924 sponge [44]. It was claimed that ROCK2 can be considered as the target of ZFAS1/miR-3924, and its level of expression was decreased upon ZFAS1 knockdown. Therefore, the contribution of ZFAS1/miR-3924 in tumor metastasis via the RHOA/ROCK2 pathway was reported, confirming its potential regulatory effect on RHO GTPase members [44].

Prostate cancer-associated transcript 6 (PCAT6) is a member of a group of 121 lncRNAs associated with prostate cancer [98]. PCAT6 is an intergenic lncRNA that is located at chr1q32.1, and it is reported to have an oncogenic role in various human cancers [99]. Several studies demonstrated that PCAT6 was overexpressed in several tumor tissues, such as GC [100], HCC [101], cervical cancer [102], NSCLC [103], lung cancer [104], and CRC [105], and this overexpression could facilitate the proliferation and metastasis of those cancers. It was indicated that PCAT6 may act as a ceRNA to suppress miRNAs and regulate the expression of their targets [99]. Tu et al. reported that the relative PCAT6 expression levels in CCA specimens were obtained compared with non-tumor tissues (n = 20 pairs). This was owing to the study of the relationship between PCAT6 expression and the development of CCA. High expression of PCAT6 was observed in CCA tissues compared to the non-tumorous tissues ($p < 0.001$). It was also found that PCAT6 induced M2 polarization of macrophages in cholangiocarcinoma via competitive binding to miR-326, and modulated the RHOA signaling pathway [45]. Low expression of miR-326 in many tumors was dramatically related with unfavorable prognosis, tumor development, metastasis, and progression [106]. Thus, PCAT6 may be a potential target of immunotherapy in cholangiocarcinoma treatment [45].

As a type of new intergenic lncRNA, LINC02381 is located at chr12q13.13 [107]. LINC02381 has been reported to be involved in many cancers, including CRC [107] and GC [108], as well as autoimmune diseases, such as rheumatoid arthritis [109]. LINC02381 can regulate the PI3K-AKT, MAP2K3/p38, and WNT signaling pathways via competitive binding to miRNAs, such as miR-96, miR-18, miR-21, miR-27a, and miR-590p [107–109]. The important role of miR-133b in the inhibition of tumorigenesis suggested its potential application as tumor-suppressor miRNA [110,111]. In the study by Chen et al., thirty groups of cervical tumor tissues and normal tissues were taken to illustrate that the expression of LINC02381 was remarkably upregulated in cervical cancer tissues ($p < 0.05$). In addition, patients with higher expression levels of LINC02381 had advanced tumor stage and lymph nodes metastasis [112]. Data showed that LINC02381 promoted cell viability and migration in cervical cancer cells through endogenous competition with miR-133b, which led to the overexpression of its downstream protein, RHOA. Therefore, LINC02381 is considered a novel target for the treatment of cervical cancer [112].

Prostate cancer gene expression marker 1 (PCGEM1) is a prominent lncRNA that has critical roles in the development and carcinogenesis of prostate cells [113]. PCGEM1 is mapped to chr2q32, and plays an important role in the apoptotic response, proliferation, colony formation, and progression of several types of cancers [114]. PCGEM1 acts as an oncogenic factor in cervical carcinoma [115], NSCLC [116], prostate cancer [113], and glioma [117] by acting as a ceRNA for miRNAs, such as miR-642a-5p, miR-433-3p, miR148a, and miR-539-5p. Results of the study showed that the expression level of PCGEM1 was significantly higher in ovarian cancer tissues than in normal ovarian tissues (14 normal ovarian tissue and 50 epithelial ovarian cancer tissue specimens; $p < 0.05$) [118]. Furthermore, PCGEM1 induced cell proliferation, migration, and invasion by targeting miR-129-5p and modulating the expression of RHOA and its downstream effectors [118]. Alternatively, the ability of miR-129-5p in the inhibition of ovarian cancer cell proliferation and survival was defined previously, which highlighted the role of the PCGEM1 and miR-129-5p as the treatment options in epithelial ovarian cancer [119].

Taken together, a list of the currently validated lncRNAs which are responsible for sponging RHOA-targeting miRNAs could act as a reference resource. This represents an extra layer of the complexity of the underlying mechanisms involved in RHO-driven cancers, and provides a promising avenue for therapeutic intervention.

1.2. RHOB-Related lncRNAs

Several studies have shown that RHOA and RHOC positively contribute to tumor promotion, but the distinct role of RHOB as a tumor suppressor or an oncogene in cancer remains elusive [120]. Additionally, in contrast to RHOA and RHOC, RHOB localizes not only at the plasma membrane but also on endosomes, multivesicular bodies, and in the nucleus, which could contribute to its contrasting behaviors in cancer biology [120]. Some studies have indicated that the oncogenic role of RHOB in tumor formation acts by inducing proliferation, angiogenesis, invasion, and migration [121–123]. On the other hand, more recent investigations have confirmed the downregulation of RHOB in some tumors, suggesting it has tumor suppressor activity [124,125]. lncRNA growth arrest specific 5 (GAS5), located at chr1q25.1, has been reported to have tumor suppressive activity in multiple human cancers by modulating several cellular processes [126]. GAS5 can act as a ceRNA to modulate the expression of many genes and their associated signaling pathways. Bioinformatics analysis of complementary regions of GAS5 to miRNAs determined 690 candidates, among which 234 miRNAs presented statistically significant binding [127]. GAS5 suppresses miR-21, an oncogene in numerous solid tumors and lymphoma, and FGF1, a regulator of proliferation and apoptosis, so it can be considered as a mediator of the GAS5/miR-21 axis [128]. In NSCLC, inhibition of GAS5 expression resulted in chemoresistance due to the competition between GAS5 and PTEN for miR-21 binding, regarding the tumor-suppressor activity of PTEN as a negative regulator of the AKT/PKB signaling pathway [129]. Furthermore, the capacity of GAS5 to bind to other oncogenic miRNAs confirms the pivotal role of this lncRNA in the modulation of different cancer-related genes [130–132]. Strikingly, regulation of RHOB by GAS5 illustrates the ability of this RNA molecule to be a modulator of the RHO GTPase family [53]. It was discovered that miR-663a expression was remarkably elevated in both tissues and plasmas of osteosarcoma patients [133]. In this regard, the GAS5 expression level was significantly reduced ($p < 0.001$) in osteosarcoma tissues ($n = 20$) compared with normal tissues ($n = 20$), and was negatively correlated with miR-663a expression. Moreover, it was found that RHOB expression can be negatively modulated by miR-663a. Therefore, upregulation of GAS5 and RHOB inhibited osteosarcoma cell proliferation, migration, and invasion in vitro, while overexpression of miR-663a induced malignancy in these cells [53].

Overall, the wide range of potential interactions between miRNAs and RHO GTPases, and lncRNAs such as GAS5 in various malignancies, provides new challenges and opportunities for the development of new treatment options (Figure 2).

1.3. RHOC-Related lncRNAs

RHOC has been widely reported to act as a master regulator of actin organization [134]. It has been shown to impact the motility of cancer cells, is essentially involved in invasion and metastasis, and contributes to carcinoma promotion in the breasts, pancreas, lungs, ovaries, and cervix, among several others [135,136]. The most interesting discovery has been its significant role in metastasis [137]. In addition, it has the ability to regulate various other features, such as cell migration, adhesion, cell polarity, angiogenesis, motility, invasion, metastasis, and anoikis resistance [138,139]. These findings suggest that RHOC contributes to the plasticity required for cancer cells to display diverse functions based on microenvironmental cues. Taken together, studies have also suggested that the inhibition of RHOC through gene regulators such as lncRNAs may be a new therapeutic target to abolish advanced tumor phenotypes.

Testis developmental related gene 1 (TDRG1) was first identified as a human testicular-specific gene, and proved to be a key regulator in reproductive organ-related cancers [140]. This lncRNA is a 1.1 kb transcript located at chr6p212.1-p21.2 and spans 1.18 kb with two exons and one intron. It encodes a 100 amino acid protein with unknown function [140,141]. TDRG1 was initially considered a key modulator in spermatogenesis and sperm motility [142]. Additionally, it may be involved in the promotion of testicular germ cell tumors [143]. Furthermore, as a modulator in reproductive organ-related tumors,

TDRG1 was indicated to play a role in cell proliferation, migration, and invasion in endometrial carcinoma [141,144] and epithelial ovarian carcinoma. It was recently reported that TDRG1 is significantly overexpressed in bone marrow mesenchymal stem cells [145]. TDRG1 was found to be more highly expressed in (EOC) tissues than in normal ovarian tissues ($p < 0.05$), and its downregulation inhibited EOC cell division, migration, and division [146]. Studies have indicated that TDRG1 is a potential binding site for miR-93, and upregulation of TDRG1 represses miR-93 expression [146]. Moreover, downregulation of TDRG1 decreased the expression of RHOC, p70S6K, BCL-XL, and MMP2, which are targets of miR-93. Other data indicated that serum levels of miR-93 ($p = 0.0001$) was downregulated in EOC patients compared with healthy women [147]. Taken together, these results demonstrate that TDRG1 could be an alternative therapeutic target in EOC or other cancers through the inhibition of RHOC [146].

Among the characterized biomarkers, prostate cancer gene 3 (PCA3) is considered one of the most promising for its diagnostic potential for the prediction of prostate biopsy results and therapeutic outcomes [148]. PCA3 (also known as DD3 or DD3PCA3) is located on chr9, and is transcribed into a noncoding prostate-specific RNA that is upregulated 60 to 100 times in tumor cells compared to normal prostate tissue [149]. The results of another study showed that the expression level of lncRNA PCA3 in epithelial ovarian cancer cell lines including BeWo cells, JEG-3 cells, and JAR cells was higher than that in normal ovarian HTR-8 cells ($p < 0.001$) [150]. It was discovered that suppression of PCA3 expression in EOC cells by siRNA transfection remarkably impeded cell division, migration, and invasion [150]. While extensive exploration of miR-106b-5p has determined opposite functions involved in different cancer cell biological behaviors, its tumor-suppressor activity in epithelial ovarian cancer tissues was observed [151]. Bioinformatics analysis and dual-luciferase reporter assays reported that PCA3 had potential binding sites for miR-106b-5p. Thus, PCA3 could function as a molecular sponge and prevent miR-106b-5p from binding to its targets. Knockdown of lncRNA PCA3 by siRNA resulted in overexpression of miR-106b and downregulation of RAS, RHOC, BCL/XL, p70S6K, and MMP2, which are targets of miR-106b [150].

Recognition of TDRG1 and PCA3 as the two positive regulators of RHOC with the ever-increasing number of other RHO GTPase-specific lncRNAs strongly indicates their potential contribution with the entire process of *RHO GTPase*-driven carcinogenesis (Figure 2).

1.4. RAC1-Related lncRNAs

RAC1 plays diverse roles in dynamic cell biological processes, including cell survival, cell-cell contacts, cell motility, EMT, and cell invasiveness [152]. Proper function of RAC1 is provided through precise regulation by regulators and downstream effectors and their modifications to its specific accumulation and subcellular localization [2,24]. Hence, any disturbances in each step of regulation produce critical changes to the expression and activity of RAC1, which in many cases can lead to cancer progression and metastasis. To date, overexpression of RAC1 has been observed in breast cancer [153], while its mutations have been identified in prostate [154], testicular [155], melanoma [156], and NSCLC cancers [157]. Hence, it is obvious that the number of RAC1 mutations and the mechanism of perturbations in RAC1 expression should be clearly studied to design new drugs for cancer patients. One of the regulatory mechanisms involved in the regulation of RAC1 expression is the sponging effect of lncRNAs, including CDKN2B-AS1, AURKAPS1, LCAT1, LSINCT5, TP73-AS1, FTH1P3, and XIST (Figure 2).

Cyclin-dependent kinase inhibitor 2B antisense RNA 1 (CDKN2B-AS1), also known as ANRIL, is located at the INK4 locus in the antisense direction of the CDKN2A and CDKN2B genes, and has epigenetic regulation of these nearby genes by recruiting the polycomb repressor complex 1 and 2 [158,159]. CDKN2B-AS1 is an oncogenic lncRNA that is upregulated in many cancerous tissues, such as ovarian cancer [160], bladder cancer [161], laryngeal squamous cell cancer [162], HCC [163], cervical cancer [164], and NSCLC [165]. The overexpression of CDKN2B-AS1 correlated with cell invasion, proliferation, tumor

metastasis, and inhibition of apoptosis and senescence [166]. Various articles have shown that CDKN2B-AS1 could interact with miRNAs, such as miR-181a-5p [166], let-7c-5p [167], miR-143-3p [160], miR-122 [168], and miR-378b [169], to regulate cancer progression. Dasgupta et al. found that CDKN2B-AS1 expression as an oncogenic lncRNA increased from lower grade and stage to higher grade and stage in renal cell carcinoma based on the TCGA-KIRC (normal = 72, tumor = 518), TCGA-KICH (normal = 25, tumor = 66), and TCGA-KIRP (normal = 30, tumor = 197; $p < 0.05$) databases. Moreover, higher expression was significantly ($p < 0.0001$) correlated to overall survival. CDKN2B-AS1 targeted miR-141 to induce tumor progression and metastasis in renal cell carcinoma via the cyclin D/RAC1/paxillin network. Strikingly, cyclin D1 and D2 were direct targets of miR-141, which could regulate RAC1 and phospho-paxillin expression and contribute to EMT [170].

AURKAPS1 is the pseudogene of AURKA (Aurora Kinase A), and it is a protein-coding gene located on chr1 in the intron of the RAB3GAP2 gene. Compared with the AURKA gene, AURKAPS1 has the absence of a 359–560 coding sequence region, and differences in the 3′-terminal nucleotide sequence and nucleotide mutations. To date, the function and abnormal expression of AURKAPS1 in cancerous tissues have been reported in few articles [171]. Li et al. reported that AURKAPS1 expression in 124 cases of HCC tissues was significantly higher than in adjacent normal liver tissues. Additionally, the expression level of AURKAPS1 was positively correlated with tumor size ($p < 0.006$) and TNM stage ($p < 0.046$), confirming its carcinogenic role [171]. AURKAPS1 increased HCC cell migration and invasion through competitive binding to miR-142, miR-155, and miR-182, promoting the expression of their target RAC1. Although the high expression of miR-182-5p and miR-155 correlated with poor prognosis and acceleration of liver cancer cell growth, the inhibition of metastasis for miR-142 has been reported in HCC [171–173]. Hence, AURKAPS1 and its corresponding miRNAs could be considered appropriate cancer biomarkers to provide a promising therapeutic strategy for human liver cancer [171].

For the first time, Yang et al. introduced lung cancer-associated transcript 1 (LCAT1) as a novel lncRNA that does not have protein-coding capacity [174,175]. LCAT1, located at chr2q31.1, is 896 bp in length and contains one transcript with three exons. Analysis of RNA-seq data of 485 lung adenocarcinoma tissues and 56 adjacent normal tissues from TCGA, and qPCR results of 25 paired lung adenocarcinoma tissues and corresponding adjacent normal tissues was performed. Data revealed that LCAT1 expression was elevated in lung cancer tissues in comparison to normal tissues ($p < 0.001$), so it could promote cell proliferation, migration, and invasion [175]. In these cells, LCAT1 indirectly upregulated RAC1 and its downstream effector, PAK1, through competitive binding to miR-4715-5p [175]. Similarly, it was found that HOTAIR as a ceRNA for miR-4715-5p promoted the cell growth, migration, and invasion [176]. Accordingly, the LCAT1-miR-4715-5p-RAC1/PAK1 axis could be a specific target for the treatment of lung cancer patients with LCAT1 overexpression in their cancer cells [174].

LSINCT5 (long stress-induced noncoding transcript) is an intergenic lncRNA located at chr5:2,765,705–2,768,351 between the IRX4 and IRX2 genes. LSINCT5 is a 2.6-kb polyadenylated transcript, and is transcribed from the negative strand by RNA Polymerase III [177]. Numerous studies have shown that LSINCT5 could be implicated in cancer development and has critical roles in metastasis, proliferation, and apoptosis of cancerous cells. Bladder cancer [178], osteosarcoma [179], endometrial carcinoma [180], gastrointestinal cancer [181], and breast and ovarian cancers [177] are among the cancers in which LSINCT5 plays significant roles in their progression. Liu et al. demonstrated that LSINCT5 expression in 56 glioma tissues was remarkably higher than that in 16 normal samples ($p < 0.001$) [182]. Knockdown of lncRNA LSINCT5 in human glioma cells triggered cell apoptosis and suppressed cell viability, migration, and invasion. LSINCT5 knockdown led to miR-451 overexpression and RAC1 downregulation, inhibiting the PI3K/AKT, WNT/β-catenin, and NFκB pathways [182]. Strikingly, downregulation of miR-451 in gliomas has been suggested by several different research groups with the role in suppression of cell growth, proliferation, and induction of cell apoptosis [183].

p73 antisense RNA 1 (TP73-AS1), also known as KIAA0495 or PDAM, is transcribed from chr1p36, and has an approximately 216 bp overlap with the TP71 gene located on the opposite strand [184]. Many studies have revealed that TP73-AS1 has a critical role in the development of different cancers [185]. Tumor-node-metastasis stage, tumor size, lymph node metastasis, and prognosis are among the clinicopathological characteristics associated with abnormal TP73-AS1 expression. Moreover, TP73-AS1 could participate in the promotion of cancer cell proliferation, invasion, and metastasis as well as the inhibition of apoptosis [184]. In some cancers, this lncRNA could act as a ceRNA to prevent the degradation of mRNA [186–190]. For example, Yang et al. reported the significant higher expression of TP73-AS1 in 46 primary osteosarcoma tissues in comparison with their matched adjacent normal bone ($p < 0.05$). In this study, the overexpression of TP73-AS1 could facilitate osteosarcoma cell proliferation and invasion in vitro, as well as tumor growth in vivo through competitive binding to miR-142, which could thereby positively regulate RAC1 protein [191]. Moreover, the significant effect of miR-142 on suppression of proliferation and induction of apoptosis for osteosarcoma cells has been recognized [192].

FTH1P3 (ferritin heavy chain 1 pseudogene 3, NR_002201) is considered a member of the FHC gene family. It is approximately 954 nucleotides in length, and located on chr2p23.3 [193]. FTH1P3 is a newly identified lncRNA in cancer cells, and its overexpression in cancer cell lines and tissues has been demonstrated by several studies. FTH1P3 can promote cell proliferation, migration, invasion, and tumor progression in uveal melanoma [194], oral squamous cell carcinoma [193], laryngeal squamous cell carcinoma [195], cervical cancer [196], and NSCLC. Zheng et al. reported that the expression level of FTH1P3 was upregulated in uveal melanoma cell lines (C918, MUM-2B, OCM-1A, and MUM-2C) compared to that melanocyte cell line (D78). Similarly, in 25 uveal melanoma patient samples, a higher expression of FTH1P3 was observed than in the 25 normal samples ($p < 0.01$) [194]. In addition, it was indicated that the upregulation of FTH1P3 targeted miR-224-5p in uveal melanoma, and caused an increase in the expression of RAC1 and Fizzled 5, which are direct target genes of miR-224-5p. Particularly, other studies proved that miR-224-5 contributed to the proliferation, invasion, and migration of uveal melanoma cells by regulating the expression of PIK3R3 and AKT3 [197]. As a result, FTH1P3 has a critical role in uveal melanoma progression, and could be a potential therapeutic target for uveal melanoma [194].

One of the first lncRNAs identified to be involved in the epigenetic processes was X-inactive–specific transcript (XIST). The XIST gene is located in the X chromosome inactivation center of chrXq13.2, and was discovered in early 1990 [198]. XIST has an indispensable role in the X-chromosome inactivation (XCI) process for dosage compensation of sex chromosomes between males (XY) and females (XX) [199]. Despite its original role in XCI, XIST also participates in the regulation of cell growth and development as well as the progression of tumors and other human diseases, such as Alzheimer's [200], acute myocardial infarction [201], cardiac morbidities [202], myocardial infarction [203], and acute kidney injury [204]. Many studies have demonstrated the aberrant expression of XIST in cancer cells and tissues, and revealed the association of XIST with tumorigenesis, metastasis, and cell apoptosis. Bladder [205], breast [206], colorectal [207], lung [208], melanoma [209], gastric [210], and ovarian cancers [211] as well as osteosarcoma [212] and glioma [213] are all among these cancers with aberrant expression of XIST. Data revealed that XIST expression was dramatically upregulated in 30 glioma tissues compared with 18 normal brain tissues, and was positively correlated with tumor grade ($p < 0.05$) [214]. Its function as a ceRNA is one of the most common mechanisms by which XIST contributes to cancer promotion [215]. For instance, in glioma, lncRNA XIST modulated RAC1 expression by functioning as a ceRNA of miR-137, which led to cell proliferation. While in glioma, the antiapoptotic capability of tumor cells has been associated with disease progression and therapy resistance, and it has been shown that miR-137 could induce apoptosis in cancer cells [216]. Thus, it was revealed that the XIST-miR-137-RAC1 pathway regulatory axis could be a therapeutic target in the treatment of glioma [214].

Collectively, these data suggest that dysregulation of network corresponding RAC1, miRNAs, and oncogenic lncRNAs needs to be carefully examined to increase our understanding about potential oncogenic drivers associated with the RHOC-related tumorigenesis (Figure 2).

1.5. CDC42-Related lncRNAs

CDC42, a prominent member of the RHO subfamily, is connected with cytoskeletal dynamics, cell shape, cell polarity, cell cycle progression, division, invasion, migration, and metastasis [19]. Its significant role as a regulator of numerous cellular processes indicates its involvement in the promotion of many human cancers [217,218]. CDC42 is connected with the tumorigenesis and promotion of esophageal squamous cell carcinoma (ESCC) [219,220]. Upregulation of CDC42 may induce HCC proliferation and metastasis, while miR-195 was shown to inhibit metastasis of HCC by suppressing CDC42 expression [221]. Moreover, it was reported that miR-29, as an invasion suppressor, downregulates CDC42 in gliomas [222]. It was also found that CDC42 could promote cellular invasion and metastasis in breast and colon cancers [223]. The ability of several lncRNAs to regulate RHO GTPases through their sponging activity has been reported. In this regard, MALAT1 is recognized as one of these lncRNAs because it increased the expression of CDC42 via miR-1 sponging [224]. ZFAS1 is another lncRNA considered to be a molecular sponge for miR-509-3p with a regulatory effect on CDC42 [225]. There are also other types of CDC42-related lncRNAs that are explained in the following sections (Figure 2). On the basis of the remarkable role of CDC42 in the processes underlying tumor formation, newly recognized regulatory mechanisms for CDC42 and CDC42-related signaling pathways, such as lncRNAs, may inhibit the process of neoplastic transformation by impeding the abnormal overexpression of CDC42.

H19 is an imprinted gene in the 11p15.5 region, and is expressed exclusively from the maternal allele. Overexpression of H19 in cancer cell lines and sample patients and its oncogenic activities have been demonstrated by several studies [226]. Functionally, H19 mainly acts as a molecular sponge or ceRNA of its diverse miRNA targets, such as miR-874, miR-675, miR-200, miR-107, miR194, miR-130a, miR196b, miR-193b, and let-7b, and it modulates the expression of many genes, resulting in multiple functions in the regulation of different cellular processes [227–234]. Thus, its role as the critical regulator of many targeted genes indicates its definite association with the development and progression of many human tumors [235,236]. For instance, overexpression of H19 in samples of primary HCCs ($n = 46$) and in comparison with the adjacent normal liver tissues ($n = 46$) was observed [237]. Strikingly, while H19 and CDC42 were overexpressed, miR-15b was downregulated in HCC cells and tissues [237]. The high expression of miR-15b-5p has been revealed to play an essential part in hepato-carcinogenesis through diverse regulation approaches [238]. H19 knockdown suppressed proliferation, migration, and invasion and increased apoptosis, which was rescued by a miR-15b inhibitor. In addition, H19 knockdown inhibited the CDC42/PAK1 pathway and EMT progression, providing a deeper understanding of the miR-15b/CDC42/PAK1 axis and the regulatory effects of H19 in HCC carcinogenesis [237].

Taurine upregulated 1 (TUG1) is a novel lncRNA with 7598 nucleotides. It is localized to chr22q12.2, and it is associated with tumorigenesis [239]. In recent years, TUG1 has been shown to be abnormally expressed in multiple types of cancers and plays crucial regulatory roles in various cancer-associated biological processes, such as the regulation of cell proliferation, apoptosis, differentiation, angiogenesis, invasion, metastasis, and drug resistance [239,240]. A recent publication showed that in 27 paired ESCC tissues and adjoining normal esophageal tissues, TUG1 was conspicuously upregulated in cancer samples ($p < 0.0001$), and high TUG1 expression was correlated with tumor size ($p = 0.032$), TNM stage ($p < 0.001$), and lymph node status ($p < 0.001$) [241]. Therefore, enhanced TUG1 expression might be related to the development of ESCC. This lncRNA exerts its function via several molecular mechanisms mainly by acting as a ceRNA to sponge various miRNAs.

An increasing number of studies have demonstrated that the sponging activity of TUG1 as an oncogenic lncRNA has been implicated in many human malignancies [242–244]. Whereas overexpression of miR-498 in ESCC cell lines induced remarkable reductions of cell proliferation, the decrease in TUG1 reduced CDC42 expression by binding to miR-498, resulting in silencing of the proliferation and invasion of ESCC [245]. Importantly, the increase in proliferation and invasion induced by miR-498 reduction was improved by CDC42 overexpression, indicating that TUG1 could be a potential therapeutic target for ESCC [241].

The lncRNA small nucleolar RNA host gene 1 (SNHG1) is reported to increase cell proliferation, migration, and invasion in different cancers, including HCC [246,247], cervical cancer [248], prostate cancer [249], and non-small cell lung cancer [250]. Determination of the expression level in 36 esophageal cancer (EC) tissue samples and paracancerous tissues were obtained, revealing that SNHG1 was significantly upregulated in EC ($p < 0.01$) [251]. However, few studies have evaluated the role of SNHG1 in cell migration and invasion in EC. It was reported that decreased expression of miR-195 played a regulatory role in promoting the pathogenesis of the EC [252]. While SNHG1 and CDC42 were significantly upregulated, miR-195 was remarkably repressed in both EC tissues and cell lines. Additionally, the suppression of either SNHG1 or CDC42 led to inhibition of cell proliferation, migration, and invasion. However, the inhibition of miR-195 resulted in the promotion of cell proliferation, migration, and invasion, and reversed the effects of si-SNHG1 [251].

Small nucleolar RNA host gene 15 (SNHG15) is a typical lncRNA that has been revealed to be upregulated as a tumor facilitator in NSCLC [253], CRC [254,255], breast cancer [256], pancreatic cancer [257], and GC [258]. Mechanistic investigation found that SNHG15, as the molecular sponge of miR-200a-3P, upregulated YAP1 as an oncogene and led to induction of the Hippo signaling pathway [259]. The results of another study indicated that SNHG15 is highly expressed in glioma vascular endothelial cells ($p < 0.05$), while its knockdown suppressed cell proliferation, migration, and tube formation in vitro [260]. Moreover, knockdown of SNHG15 reduced the expression of VEGFA and CDC42, which are promoters of angiogenesis. Additional analysis confirmed that SNHG15 affected endothelial cell function by targeting miR-153 as a negative regulator of CDC42 and VEGFA. The tumor-suppressor activity of miR-153 was determined in another study through the reduction of stem cell-like phenotype and tumor growth of lung adenocarcinoma cells [261]. Therefore, SNHG15 and its target miR-153 could serve as new potential therapeutic targets for the antiangiogenic treatment of glioma through the downregulation of CDC42 [260].

Data summarized here demonstrate a strong rationale for targeting CDC42-related regulator lncRNAs as a potential therapeutic approach to control various cancer-related biochemical processes (Figure 2).

2. Indirect Regulatory Effects of lncRNAs on RHO GTPases

The on and off states of the RHO GTPases is directly regulated by three specific classes of regulator families, consisting of multiple different members (Figure 1) [2]. Furthermore, the capacity of RHO GTPases to mediate a wide range of intracellular signaling pathways is attributed to their connection with their diverse downstream targets, called effector proteins [2]. To date, more than 70 potential effectors as the kinases or scaffolding proteins have been identified for RHO GTPases [262,263]. Kinases are recognized as an important class of RHO effectors, and result in downstream phosphorylation signal transductions [264]. The second group of effectors comprise of scaffolding proteins, which probably form a framework contributed in signaling cascades, particularly through reorganization of filamentous actin dynamics [265,266].

In addition to direct regulation of Rho GTPases themselves, lncRNAs as ceRNAs are also indirectly involved in modulation of RHO GTPases by targeting their regulators (GAPs, GEFs, and GDIs) and effectors. Upregulation of CTC-497E21.4 (also known as LINC00958) in GC tissue promoted cell proliferation, invasion, and metastasis by sponging miR-22, and subsequently induced the expression of NET1 [41]. Interestingly, NET1 activates as a

RHOA-specific GEF RHOA signaling pathway. Thus, CTC-497E21.4/miR-22/NET1 can be referred to as an indirect modulatory axis of RHOA-mediated signaling [41]. Rho-associated coiled-coil containing kinases (ROCKI and ROCKII) act as RHOA effectors in the regulation of cellular contraction, motility, morphology, polarity, gene expression, and cell division [267]. An elevated expression of MALAT1 was observed in osteosarcoma patients, and correlated with poor prognosis. Downregulation of MALAT1 as a ceRNA for miR-144-3p inhibited tumor cell invasion by reducing the expression of ROCKI/ROCKII in osteosarcoma cells [268]. The modulatory effects of lncRNAs on RHO GTPase regulation and signaling adds another level of complexity and stringency to existing regulatory frameworks and control mechanisms that require further investigation.

3. Epigenetic Regulation of RHO GTPases by lncRNAs

It is now clear that perturbations of epigenetic regulation are a key feature of many neoplastic transformations [269]. In the nucleus, different lncRNAs play a vital role as the key regulators of the epigenetic status of protein-coding genes. In fact, of the diverse array of functions assigned to lncRNAs, one attractive perspective is the direct interaction between lncRNAs and epigenetic modifiers to modulate chromatin conformation [270]. Recruitment histone-modifying machineries, such as writers, readers, and erasers of histones to the specific subnuclear domains and genetic loci, result in the fine-tuning of chromatin structure [271]. Many researches have established that EZH2 functions as an inhibitor of RNA transcription by histone modification; namely, H3K27me3. It was found that TUG1 represses the expression of *RND3*, one atypical member of the RHO family [14,36], through recruitment of EZH2 protein to the *RND3* promoter regions and modification of H3K27me3 [239]. Based on another paradigm, lncRNAs could be involved in modification of nuclear architecture and the three-dimensional genome structure. Therefore, orchestrating chromatin folding and compartmentalization to direct enhancer-promoter communication shapes the outcomes of gene transcription [272]. Another mechanistic layer of lncRNAs-mediated epigenetic alternations is associated with alternative splicing. Interaction between lncRNAs and splice-regulatory factors may influence the processing of pre-mRNA, and thus of selecting the alternative transcript isoforms [273]. Interestingly, lncRNAs are not only recognized as the master regulators of the genome epigenetics, but also as the targets of epigenetic modifiers [274]. It has been demonstrated that modified transcripts of lncRNAs, such as their N6-Methyladenosine (m6A) residues, are associated with cancer progression [275]. For instance, m6A-modified transcripts of GAS5, as one of the regulators of RHOB, induced phosphorylation and subsequently ubiquitin-mediated degradation of YAP, leading to the inhibition of malignant transformation [276]. m6A reader YTHDF3 facilitates the degradation of m6A-modified lncRNA GAS5 and thus contributes to cancer development. In conclusion, lncRNAs act as regulators and targets of epigenetic factors, which establishes a cross-regulating network in tumors and unveils a novel dimension of cancer biology.

4. lncRNAs as Novel Therapeutic Targets

The well-established role of the lncRNAs in different diseases provides a theoretical basis to utilize lncRNAs as pharmacological targets. Recent progress in the generation, purification, and cellular delivery of RNAs have enabled the development of RNA-based therapeutics, including small interfering RNAs (siRNAs), antisense oligonucleotides (ASO), aptamers, microRNAs, and messenger RNAs. SiRNAs complementary to the target lncRNAs recruit the RNA-induced silencing complex (RISC) and induce lncRNA degradation [277–280]. Antisense oligonucleotides, which are chemically synthesized short single-stranded DNA sequences with 15–20 nucleotides, can bind to complementary RNA and provoking RNA degradation or inhibit translation [281]. Application of specific ASO technology, including peptide nucleic acids (PNAs), phosphorodiamidate morpholino oligomers, and locked nucleic acids (LNA) for lncRNA-targeted therapy has grown rapidly, indicating their clinical prospects [282,283]. Particularly, the most recent third

generation ASOs, including PNAs with modified nucleotides, are often used for targeting lncRNAs [284,285]. According to specific cellular localization of lncRNAs in the nucleus or the cytoplasm, some therapeutic strategies could be applied for more effective lncRNAs targeting. In this regard, ASOs and siRNAs can more effectively inhibit nuclear and cytoplasmic lncRNAs, respectively. More efficiently, for lncRNAs with dual cellular or uncertain localization, a combination targeting strategy using both ASO and siRNA has been shown to be successful [286,287]. The CRISPR/Cas9 system as an alternative RNA-based therapy with successful results has stimulated research into lncRNA-targeting [288,289]. In addition to nucleic acid-based therapeutic technologies, small-molecule compounds have been proven to be effective entities to disrupt lncRNA spatial secondary and tertiary structures or lncRNA-protein interactions [290,291]. Recently, a number of studies have demonstrated that plant-derived natural compounds have a credible regulatory effect on lncRNAs; however, the lack of accurate targets and mechanisms is a limitation of phytochemicals [292]. In the past few years, approval of ASO and siRNA-based therapies by the FDA have led to clinical breakthroughs [293]. Primary results are conceivable that targeting lncRNAs provides a plethora of opportunities in the near future for precision medicine. For instance, studies into mitochondrial lncRNAs (mtlncRNAs) have progressed rapidly, and to this end, the FDA has approved a clinical trial of Andes-1537, a short single-stranded phosphorothioate ASO. This type of ASO binds to the antisense non-coding mitochondrial RNA (ASncmtRNA), and it is under clinical investigation for the targeted therapy of solid tumors, including a phase I clinical trial of the patients with advanced metastatic cancer (NCT02508441). The clinical results of phase I confirmed that Andes-1537 was well-tolerated. In addition, another clinical trial of Andes-1537 for different solid tumors (NCT03985072) was started last year [294]. Taken together, the application of lncRNAs as pharmacological targets has reviewed the transition of lncRNAs from the role of disease coding to acting as drug candidates, providing new insights into the treatment of diseases. Another therapeutic strategy is based on enzymatic DNA (DNAzymes), which exploits the catalytic capabilities of DNAzymes to cleave target RNAs, such as mRNAs and lncRNAs, with exceptional selectivity [295]. In contrast to gene-editing approaches, such as CRISPR/Cas9, DNAzymes do not permanently modify the genome, and enable a transient and dose-dependent reduction of the target-RNA levels. In contrast to miRNA, siRNA, or ASO, DNAzymes are self-sufficient catalysts that do not depend on cellular proteins. This strategy might provide eminent advantages over existing approaches, including effective responses to emerging drug resistances and the fast development of personalized drugs.

5. Conclusions and Future Directions

The RHO family GTPases, as signal transduction elements, plays vital roles in several central biological processes that are remarkably essential for the maintenance of cellular homeostasis, and any perturbation of their signaling function causes diverse human diseases, especially cancer progression and metastasis [17–20]. Hence, comprehensive studies on different aspects of RHO GTPase structures, functions, and interactions as well as their mechanisms of regulation could help us to find new selective therapeutic strategies for cancer treatment. Among the various regulatory actions in live cells, lncRNAs orchestrate diverse fundamental processes, such as gene expression, epigenetic regulation, genomic imprinting, chromosome organization, allosteric regulation of enzyme activity, and miRNA sponging [296]. Determination of the modulatory mechanisms of lncRNAs concerning the RHO GTPase signaling pathways is anticipated to substantially expand our knowledge about the mechanisms of cancer progression. The role of lncRNAs as molecular sponges of miRNAs that target RHO GTPases should be further studied. It is worth mentioning that merely a limited assortment of well-known lncRNAs have been functionally characterized. However, growing evidence of their engagement in diverse human diseases and malignancies makes these transcripts versatile therapeutic targets for RNA-based therapeutic strategies [297]. In this review, we concentrated on the sponging effect as an approach for RHO GTPase downregulation. Since the majority of lncRNAs

are expressed in a highly cell- or tissue-specific pattern, they may be efficient therapeutic targets for cancer therapy. Nevertheless, several questions remain to be addressed: (i) How many lncRNAs are functionally and clinically related to RHO GTPase-driven cancers? (ii) How can systematic genomic and functional approaches be developed to discover the roles of lncRNAs in the initiation and progression of RHO GTPase-mutant cancers? (iii) How can we incorporate genomic and transcriptomic data from cancer patients with RHO GTPase mutations to establish a lncRNA discovery pipeline to progress preclinical studies to clinical practice? (iv) How can we confirm that the tissue-specific expression of lncRNAs represent therapeutic candidates for tissues with a higher rate of RHO GTPase mutations?

Furthermore, various studies should be carried out to increase our understanding of the intricacies of RHO GTPase regulation with regard to lncRNAs that would be considered therapeutic targets: (i) A small number of RHO family small GTPases, such as RHOA, RAC1, and CDC42, have been well studied thus far, but there is a crucial demand to investigate the functions of other less-characterized members as well as their mechanisms of regulation. (ii) Apart from discovering more lncRNAs with sponging effects on miRNAs targeting RHO GTPases, a comprehensive study should be performed on the regulatory lncRNAs of RHO GTPase regulators, such as GDIs, GEFs, and GAPs (Figure 1). (iii) In addition to the investigation of the mechanisms of regulation of lncRNAs, the oncogenic or tumor-suppressing effects of proteins/peptides encoded by these noncoding RNAs should be clarified. (iv) The ability to target RHO GTPase-related oncogenic lncRNAs via diverse strategies, including gene-editing methods—e.g., CRISPR–Cas9 technology, nucleic acid-based drugs, catalytic degradation by ribozymes or DNAzymes, small molecule inhibitors, synthetic lncRNA and miRNA mimics, and targeting the secondary and tertiary structures of lncRNAs—should be investigated. (v) To find new drugs for abnormal RHO GTPase activity, the possible interactions of lncRNAs with their associated proteins, which could form ribonucleoprotein complexes, should be studied.

lncRNAs as the pharmaceutical targets provide a plethora of opportunities in the future. In fact, therapeutic approaches which are on the basis of the gene therapy to treat disease by artificially regulating gene expression are called "third generation" of clinical drugs. This kind of treatment is promising for controlling diseases at the genetic level, and is able to overcome the drawbacks of biological incompatible proteins. From the outlook of the clinical breakthrough in targeted mRNA drugs and the progressive recruitment for clinical trials of miRNAs, it is now conceivable that targeting lncRNAs will probably play a critical role in gene therapy in the near future. Although the significant role of the lncRNAs in the tumorigenesis and its potential clinical application in future is bright, some concerns and questions remain. The fundamental researches on the function of druggable lncRNAs and the potential downstream responses are insufficient currently; therefore, unexpected outcomes and inappropriate pathological effects may occur when lncRNA-targeted drugs are used clinically. Moreover, highly specific targeting methods and delivery systems development are required to guarantee that only the selected lncRNA is affected. Due to the insufficient data on clinical trials, the efficacy and safety of lncRNA drugs in humans remain undetermined. Therefore, further advances in lncRNA-targeted drugs are distinctly dependent on the in-depth basic research into the function and mechanisms of lncRNAs. In this regard, the diverse mode of the action repertoire of lncRNAs reveals various opportunities for their targeting. Importantly, there has been an identification of plenty of modified residues in lncRNA transcripts, indicating the epigenetic regulation of lncRNAs and its potential effects on cancer progression. For instance, m6A-modified transcripts of GAS5, as one of the regulators of RHOB, induced phosphorylation and subsequently ubiquitin-mediated degradation of YAP, leading to the inhibition of malignant transformation [276]. Exploitation of high-throughput methods—such as chromatin RNA in situ reverse transcription sequencing (CRIST-seq) for identification of lncRNAs within the regulatory elements of genes, and RNA immunoprecipitation, crosslinking, and immunoprecipitation (CLIP), as well as RNA pull-down techniques for discovering the interaction between proteomes and lncRNAs—will uncover more important roles and new

mechanistic insights. An interesting progression is the detection of natural antisense transcripts (NATs): lncRNAs that are transcribed in the antisense direction to coding genes, and negatively regulate them in cis. ASOs that target NATs, called 'antagoNATs', have indicated very encouraging preclinical results for gene reactivation in the central nervous system. Such brilliant developments confirmed that the establishment of lncRNA-based therapeutics into clinical testing is imminent. In the case of the RHO GTPase-related lncRNAs, results showed that the subcutaneous delivery of MALAT1 phosphorothioate-modified ASO successfully suppressed primary tumor differentiation. From the perspective of the clinical benefits in RHO GTPase-related anti-lncRNA plant-derived natural compounds, credible anti-cancer activity of curcumin was reported through its downregulatory effect on H19. Tissue specific expression of several lncRNAs have also created remarkable treatment opportunities, including therapeutic manipulation of lncRNA promoters. Administration of a plasmid (BC-819) carrying the gene for diphtheria toxin under the regulation of the H19 gene promoter was utilized to investigate its anti-tumor responses in various solid tumors. A phase I/II clinical trial of intravesical BC-819 in patients with invasive bladder cancer has revealed mild and local toxicity along with complete and partial response rates of 22% and 44%, respectively. Therefore, the highly selective expression of various lncRNAs prompts the assessment of using tissue or cell-type specific lncRNA promoters to induce cytotoxic effects in disease-related cells.

Finally, a significant challenge that has not been well explored is the illumination of the gap in knowledge of spatiotemporal regulation of signal transduction and RHO GTPase activity to specifically explain the interaction of RHO GTPases with their distinct effectors and regulators. Among these regulatory mechanisms, the roles of accessory proteins and noncoding RNAs, particularly lncRNAs, in the spatiotemporal regulation of cell signaling should be fully investigated. The clarification of these important issues not only leads to the explanation of many aspects of RHO GTPase activity and their signaling pathways, but also prompts the discovery and development of novel drugs against various diseases, specifically cancer.

Author Contributions: M.S., A.M. and N.M. designed and wrote the article. M.R.A. contributed to the conception and provided critical revision of the article. All authors gave final approval of the accepted version for publication. All authors have read and agreed to the published version of the manuscript.

Funding: This research was funded by the German Federal Ministry of Education and Research (BMBF)—German Network of RASopathy Research (GeNeRARe, grant number: 01GM1902C), and the European Network on Noonan Syndrome and Related Disorders (NSEuroNet, grant number: 01GM1621B).

Acknowledgments: The authors are grateful to Mohammad Taheri for helpful discussions.

Conflicts of Interest: The authors declare no conflict of interest.

Abbreviations

GDIs	GDP dissociation inhibitors
GEFs	guanine nucleotide exchange factors
GAPs	GTPase-activating proteins
microRNA	miRNA
lncRNAs	long non-coding RNAs
CeRNAs	competing endogenous RNAs
NSCLC	non-small cell lung cancer
GC	gastric cancer
MALAT1	metastasis associated in lung adenocarcinoma transcript 1
PDAC	pancreatic ductal adenocarcinoma cells

NORAD	non-coding RNA activated by DNA damage
RBPs	RNA-binding proteins
EMT	epithelial-to-mesenchymal transition
ZFAS1	zinc finger antisense 1
HCC	hepatocellular carcinoma
CRC	colorectal cancer
PCAT6	prostate cancer-associated transcript 6
PCGEM1	prostate cancer gene expression marker 1
GAS5	growth arrest specific 5
TDRG1	testis developmental-related gene 1
EOC	epithelial ovarian cancer
PCA3	prostate cancer gene 3
CDKN2B-AS1	cyclin-dependent kinase inhibitor 2B antisense RNA 1
AURKAPS1	pseudogene of aurora kinase A
LCAT1	lung cancer associated transcript 1
LSINCT5	long stress-induced noncoding transcripts
TP73-AS1	P73 antisense RNA 1
FTH1P3	ferritin heavy chain 1 pseudogene 3
XCI	X-chromosome inactivation
ESCC	esophageal squamous cell carcinoma
TUG1	taurine upregulated 1
SNHG1	small nucleolar RNA host gene 1
EC	esophageal cancer
SNHG15	small nucleolar RNA host gene 15
M6A	N6-Methyladenosine (m6A).

References

1. Dvorsky, R.; Ahmadian, M.R. Always look on the bright site of Rho: Structural implications for a conserved intermolecular interface. *EMBO Rep.* **2004**, *5*, 1130–1136. [CrossRef]
2. Mosaddeghzadeh, N.; Ahmadian, M.R. The RHO family GTPases: Mechanisms of regulation and signaling. *Cells* **2021**, *10*, 1831. [CrossRef] [PubMed]
3. Garcia-Mata, R.; Boulter, E.; Burridge, K. The'invisible hand': Regulation of RHO GTPases by RHOGDIs. *Nat. Rev. Mol. Cell Biol.* **2011**, *12*, 493–504. [CrossRef] [PubMed]
4. Rossman, K.L.; Der, C.J.; Sondek, J. GEF means go: Turning on RHO GTPases with guanine nucleotide-exchange factors. *Nat. Rev. Mol. Cell Biol.* **2005**, *6*, 167–180. [CrossRef] [PubMed]
5. Zhang, S.-C.; Gremer, L.; Heise, H.; Janning, P.; Shymanets, A.; Cirstea, I.C.; Krause, E.; Nürnberg, B.; Ahmadian, M.R. Liposome reconstitution and modulation of recombinant prenylated human Rac1 by GEFs, GDI1 and Pak1. *PLoS ONE* **2014**, *9*, e102425. [CrossRef]
6. Jaiswal, M.; Dvorsky, R.; Ahmadian, M.R. Deciphering the molecular and functional basis of Dbl family proteins: A novel systematic approach toward classification of selective activation of the Rho family proteins. *J. Biol. Chem.* **2013**, *288*, 4486–4500. [CrossRef] [PubMed]
7. Nakhaei-Rad, S.; Haghighi, F.; Nouri, P.; Rezaei Adariani, S.; Lissy, J.; Kazemein Jasemi, N.S.; Dvorsky, R.; Ahmadian, M.R. Structural fingerprints, interactions, and signaling networks of RAS family proteins beyond RAS isoforms. *Crit. Rev. Biochem. Mol. Biol.* **2018**, *53*, 130–156. [CrossRef]
8. Nakhaeizadeh, H.; Amin, E.; Nakhaei-Rad, S.; Dvorsky, R.; Ahmadian, M.R. The RAS-Effector Interface: Isoform-Specific Differences in the Effector Binding Regions. *PLoS ONE* **2016**, *11*, e0167145. [CrossRef]
9. Golding, A.E.; Visco, I.; Bieling, P.; Bement, W.M. Extraction of active RhoGTPases by RhoGDI regulates spatiotemporal patterning of RhoGTPases. *Elife* **2019**, *8*, e50471. [CrossRef]
10. Roberts, P.J.; Mitin, N.; Keller, P.J.; Chenette, E.J.; Madigan, J.P.; Currin, R.O.; Cox, A.D.; Wilson, O.; Kirschmeier, P.; Der, C.J. Rho Family GTPase modification and dependence on CAAX motif-signaled posttranslational modification. *J. Biol. Chem.* **2008**, *283*, 25150–25163. [CrossRef]
11. Mitin, N.; Roberts, P.J.; Chenette, E.J.; Der, C.J. Posttranslational lipid modification of Rho family small GTPases. In *Rho GTPases*; Springer: Berlin/Heidelberg, Germany, 2012; pp. 87–95.
12. Phuyal, S.; Farhan, H. Multifaceted Rho GTPase Signaling at the Endomembranes. *Front. Cell Dev. Biol.* **2019**, *7*, 127. [CrossRef] [PubMed]
13. Cherfils, J.; Zeghouf, M. Regulation of small gtpases by gefs, gaps, and gdis. *Physiol. Rev.* **2013**, *93*, 269–309. [CrossRef]

14. Jaiswal, M.; Communication, S.; Jaiswal, M.; Fansa, E.K.; Dvorsky, R.; Ahmadian, M.R. New insight into the molecular switch mechanism of human Rho family proteins: Shifting a paradigm. *Biol. Chem* **2012**, *394*, 89–95. [CrossRef]
15. Hodge, R.G.; Ridley, A.J. Regulation and functions of RhoU and RhoV. *Small GTPases* **2020**, *11*, 8–15. [CrossRef]
16. Bustelo, X.R. RHO GTPases in cancer: Known facts, open questions, and therapeutic challenges. *Biochem. Soc. Trans.* **2018**, *46*, 741–760. [CrossRef]
17. Haga, R.B.; Ridley, A.J. Rho GTPases: Regulation and roles in cancer cell biology. *Small GTPases* **2016**, *7*, 207–221. [CrossRef]
18. Hall, A.; Nobes, C.D. Rho GTPases: Molecular switches that control the organization and dynamics of the actin cytoskeleton. *Philos. Trans. R. Soc. London. Ser. B Biol. Sci.* **2000**, *355*, 965–970. [CrossRef]
19. Clayton, N.S.; Ridley, A.J. Targeting Rho GTPase Signaling Networks in Cancer. *Front. Cell Dev. Biol.* **2020**, *8*, 222. [CrossRef]
20. Etienne-Manneville, S.; Hall, A. Rho GTPases in cell biology. *Nature* **2002**, *420*, 629–635. [CrossRef]
21. Luo, L. RHO GTPASES in neuronal morphogenesis. *Nat. Rev. Neurosci.* **2000**, *1*, 173–180. [CrossRef] [PubMed]
22. Mulloy, J.C.; Cancelas, J.A.; Filippi, M.-D.; Kalfa, T.A.; Guo, F.; Zheng, Y. Rho GTPases in hematopoiesis and hemopathies. *Blood J. Am. Soc. Hematol.* **2010**, *115*, 936–947. [CrossRef] [PubMed]
23. Luo, T.; Ou, J.N.; Cao, L.F.; Peng, X.Q.; Li, Y.M.; Tian, Y.Q. The Autism-Related lncRNA MSNP1AS Regulates Moesin Protein to Influence the RhoA, Rac1, and PI3K/Akt Pathways and Regulate the Structure and Survival of Neurons. *Autism Res.* **2020**, *13*, 2073–2082. [CrossRef] [PubMed]
24. Svensmark, J.H.; Brakebusch, C. Rho GTPases in cancer: Friend or foe? *Oncogene* **2019**, *38*, 7447–7456. [CrossRef] [PubMed]
25. Menacho-Marquez, M.; García-Escudero, R.; Ojeda, V.; Abad, A.; Delgado, P.; Costa, C.; Ruiz, S.; Alarcón, B.; Paramio, J.M.; Bustelo, X.R. The Rho exchange factors Vav2 and Vav3 favor skin tumor initiation and promotion by engaging extracellular signaling loops. *PLoS Biol.* **2013**, *11*, e1001615. [CrossRef] [PubMed]
26. Justilien, V.; Ali, S.A.; Jamieson, L.; Yin, N.; Cox, A.D.; Der, C.J.; Murray, N.R.; Fields, A.P. Ect2-dependent rRNA synthesis is required for KRAS-TRP53-driven lung adenocarcinoma. *Cancer Cell* **2017**, *31*, 256–269. [CrossRef]
27. Gonyo, P.; Bergom, C.; Brandt, A.C.; Tsaih, S.-W.; Sun, Y.; Bigley, T.M.; Lorimer, E.L.; Terhune, S.S.; Rui, H.; Flister, M.J. SmgGDS is a transient nucleolar protein that protects cells from nucleolar stress and promotes the cell cycle by regulating DREAM complex gene expression. *Oncogene* **2017**, *36*, 6873–6883. [CrossRef] [PubMed]
28. Justilien, V.; Lewis, K.C.; Murray, N.R.; Fields, A.P. Oncogenic Ect2 signaling regulates rRNA synthesis in NSCLC. *Small GTPases* **2019**, *10*, 388–394. [CrossRef] [PubMed]
29. Pancione, M.; Cerulo, L.; Remo, A.; Giordano, G.; Gutierrez-Uzquiza, Á.; Bragado, P.; Porras, A. Centrosome Dynamics and Its Role in Inflammatory Response and Metastatic Process. *Biomolecules* **2021**, *11*, 629. [CrossRef] [PubMed]
30. Diamantopoulou, Z.; White, G.; Fadlullah, M.Z.; Dreger, M.; Pickering, K.; Maltas, J.; Ashton, G.; MacLeod, R.; Baillie, G.S.; Kouskoff, V. TIAM1 antagonizes TAZ/YAP both in the destruction complex in the cytoplasm and in the nucleus to inhibit invasion of intestinal epithelial cells. *Cancer Cell* **2017**, *31*, 621–634.e626. [CrossRef] [PubMed]
31. Vu, H.L.; Rosenbaum, S.; Purwin, T.J.; Davies, M.A.; Aplin, A.E. RAC1 P29S regulates PD-L1 expression in melanoma. *Pigment. Cell Melanoma Res.* **2015**, *28*, 590–598. [CrossRef] [PubMed]
32. Aspenström, P. Activated Rho GTPases in Cancer-The Beginning of a New Paradigm. *Int. J. Mol. Sci.* **2018**, *19*, 3949. [CrossRef] [PubMed]
33. Dai, Y.; Luo, W.; Yue, X.; Ma, W.; Wang, J.; Chang, J. Identification and characterization of a new isoform of small GTPase RhoE. *Commun. Biol.* **2020**, *3*, 572. [CrossRef] [PubMed]
34. Croft, D.R.; Olson, M.F. Transcriptional regulation of Rho GTPase signaling. *Transcription* **2011**, *2*, 211–215. [CrossRef]
35. Lee, J.; Villarreal, O.D.; Chen, X.; Zandee, S.; Young, Y.K.; Torok, C.; Lamarche-Vane, N.; Prat, A.; Rivest, S.; Gosselin, D.; et al. QUAKING Regulates Microexon Alternative Splicing of the Rho GTPase Pathway and Controls Microglia Homeostasis. *Cell Rep.* **2020**, *33*, 108560. [CrossRef]
36. Fiegen, D.; Haeusler, L.-C.; Blumenstein, L.; Herbrand, U.; Dvorsky, R.; Vetter, I.R.; Ahmadian, M.R. Alternative splicing of Rac1 generates Rac1b, a self-activating GTPase. *J. Biol. Chem.* **2004**, *279*, 4743–4749. [CrossRef] [PubMed]
37. Liu, M.; Bi, F.; Zhou, X.; Zheng, Y. Rho GTPase regulation by miRNAs and covalent modifications. *Trends Cell Biol.* **2012**, *22*, 365–373. [CrossRef]
38. Olson, M.F. Rho GTPases, their post-translational modifications, disease-associated mutations and pharmacological inhibitors. *Small GTPases* **2018**, *9*, 203–215. [CrossRef]
39. Hynds, D.L. Subcellular localization of Rho GTPases: Implications for axon regeneration. *Neural Regen. Res.* **2015**, *10*, 1032–1033. [CrossRef] [PubMed]
40. Olayioye, M.A.; Noll, B.; Hausser, A. Spatiotemporal Control of Intracellular Membrane Trafficking by Rho GTPases. *Cells* **2019**, *8*, 1478. [CrossRef]
41. Spiering, D.; Hodgson, L. Dynamics of the Rho-family small GTPases in actin regulation and motility. *Cell Adhes. Migr.* **2011**, *5*, 170–180. [CrossRef]
42. Zong, W.; Feng, W.; Jiang, Y.; Cao, Y.; Ke, Y.; Shi, X.; Ju, S.; Cong, H.; Wang, X.; Cui, M. LncRNA CTC-497E21. 4 promotes the progression of gastric cancer via modulating miR-22/NET1 axis through RhoA signaling pathway. *Gastric Cancer* **2020**, *23*, 228–240. [CrossRef]

43. Feng, M.; Li, G.; Dou, F. Long-chain non-coding RNA LOC554202 promotes proliferation, migration, and invasion of nasopharyngeal carcinoma cells by binding to microRNA-31 expression and regulating RhoA expression. *Eur. Rev. Med. Pharmacol. Sci.* **2020**, *24*, 10550–10556. [PubMed]
44. Liu, J.; Zhu, Y.; Ge, C. LncRNA ZFAS1 promotes pancreatic adenocarcinoma metastasis via the RHOA/ROCK2 pathway by sponging miR-3924. *Cancer Cell Int.* **2020**, *20*, 249. [CrossRef] [PubMed]
45. Tu, J.; Wu, F.; Chen, L.; Zheng, L.; Yang, Y.; Ying, X.; Song, J.; Chen, C.; Hu, X.; Zhao, Z. Long Non-Coding RNA PCAT6 Induces M2 Polarization of Macrophages in Cholangiocarcinoma via Modulating miR-326 and RhoA-ROCK Signaling Pathway. *Front. Oncol.* **2020**, *10*, 605877. [CrossRef]
46. Jiang, M.-C.; Ni, J.-J.; Cui, W.-Y.; Wang, B.-Y.; Zhuo, W. Emerging roles of lncRNA in cancer and therapeutic opportunities. *Am. J. Cancer Res.* **2019**, *9*, 1354–1366.
47. Carlevaro-Fita, J.; Lanzós, A.; Feuerbach, L.; Hong, C.; Mas-Ponte, D.; Pedersen, J.S.; Abascal, F.; Amin, S.B.; Bader, G.D.; Barenboim, J.; et al. Cancer LncRNA Census reveals evidence for deep functional conservation of long noncoding RNAs in tumorigenesis. *Commun. Biol.* **2020**, *3*, 56. [CrossRef]
48. He, R.-Z.; Luo, D.-X.; Mo, Y.-Y. Emerging roles of lncRNAs in the post-transcriptional regulation in cancer. *Genes Dis.* **2019**, *6*, 6–15. [CrossRef]
49. Goodall, G.J.; Wickramasinghe, V.O. RNA in cancer. *Nat. Rev. Cancer* **2021**, *21*, 22–36. [CrossRef] [PubMed]
50. McHugh, C.A.; Chen, C.K.; Chow, A.; Surka, C.F.; Tran, C.; McDonel, P.; Pandya-Jones, A.; Blanco, M.; Burghard, C.; Moradian, A.; et al. The Xist lncRNA interacts directly with SHARP to silence transcription through HDAC3. *Nature* **2015**, *521*, 232–236. [CrossRef]
51. Kim, J.; Piao, H.-L.; Kim, B.-J.; Yao, F.; Han, Z.; Wang, Y.; Xiao, Z.; Siverly, A.N.; Lawhon, S.E.; Ton, B.N.; et al. Long noncoding RNA MALAT1 suppresses breast cancer metastasis. *Nat. Genet.* **2018**, *50*, 1705–1715. [CrossRef] [PubMed]
52. López-Urrutia, E.; Bustamante Montes, L.P.; Ladrón de Guevara Cervantes, D.; Pérez-Plasencia, C.; Campos-Parra, A.D. Crosstalk Between Long Non-coding RNAs, Micro-RNAs and mRNAs: Deciphering Molecular Mechanisms of Master Regulators in Cancer. *Front. Oncol.* **2019**, *9*, 669. [CrossRef]
53. Yao, X.; Li, X.; Luo, Y.; Xu, X.; Liu, J.; Bu, J. LncRNA GAS5 Regulates Osteosarcoma Cell Proliferation, Migration, and Invasion by Regulating RHOB via Sponging miR-663a. *Cancer Manag. Res.* **2020**, *12*, 8253. [CrossRef]
54. Chen, L.; Zhang, D.; Ding, T.; Liu, F.; Xu, X.; Tian, Y.; Xiao, J.; Shen, H. LncRNA NR2F2-AS1 Upregulates Rac1 to Increase Cancer Stemness in Clear Cell Renal Cell Carcinoma. *Cancer Biother. Radiopharm.* **2020**, *35*, 301–306. [CrossRef] [PubMed]
55. Leon, L.M.; Gautier, M.; Allan, R.; Ilié, M.; Nottet, N.; Pons, N.; Paquet, A.; Lebrigand, K.; Truchi, M.; Fassy, J.; et al. Correction: The nuclear hypoxia-regulated NLUCAT1 long non-coding RNA contributes to an aggressive phenotype in lung adenocarcinoma through regulation of oxidative stress. *Oncogene* **2021**, *40*, 2621. [CrossRef] [PubMed]
56. Ghafouri-Fard, S.; Noroozi, R.; Abak, A.; Taheri, M.; Salimi, A. Emerging role of lncRNAs in the regulation of Rho GTPase pathway. *Biomed. Pharmacother.* **2021**, *140*, 111731. [CrossRef] [PubMed]
57. Kehl, T.; Backes, C.; Kern, F.; Fehlmann, T.; Ludwig, N.; Meese, E.; Lenhof, H.-P.; Keller, A. About miRNAs, miRNA seeds, target genes and target pathways. *Oncotarget* **2017**, *8*, 107167–107175. [CrossRef]
58. O'Brien, J.; Hayder, H.; Zayed, Y.; Peng, C. Overview of MicroRNA Biogenesis, Mechanisms of Actions, and Circulation. *Front. Endocrinol.* **2018**, *9*, 402. [CrossRef] [PubMed]
59. Humphries, B.A.; Wang, Z.; Yang, C. MicroRNA regulation of the small rho gtpase regulators—Complexities and opportunities in targeting cancer metastasis. *Cancers* **2020**, *12*, 1092. [CrossRef]
60. Algaber, A.; Al-Haidari, A.; Madhi, R.; Rahman, M.; Syk, I.; Thorlacius, H. MicroRNA-340-5p inhibits colon cancer cell migration via targeting of RhoA. *Sci. Rep.* **2020**, *10*, 16934. [CrossRef]
61. He, L.; Wang, J.; Chang, D.; Lv, D.; Li, H.; Feng, H. Effect of miRNA-200b on the proliferation and apoptosis of cervical cancer cells by targeting RhoA. *Open Med.* **2020**, *15*, 1019–1027. [CrossRef]
62. Liu, M.; Tang, Q.; Qiu, M.; Lang, N.; Li, M.; Zheng, Y.; Bi, F. miR-21 targets the tumor suppressor RhoB and regulates proliferation, invasion and apoptosis in colorectal cancer cells. *FEBS Lett.* **2011**, *585*, 2998–3005. [CrossRef] [PubMed]
63. Xu, R.S.; Wu, X.D.; Zhang, S.Q.; Li, C.F.; Yang, L.; Li, D.D.; Zhang, B.G.; Zhang, Y.; Jin, J.P.; Zhang, B. The tumor suppressor gene RhoBTB1 is a novel target of miR-31 in human colon cancer. *Int. J. Oncol.* **2013**, *42*, 676–682. [CrossRef]
64. Park, S.-Y.; Lee, J.H.; Ha, M.; Nam, J.-W.; Kim, V.N. miR-29 miRNAs activate p53 by targeting p85α and CDC42. *Nat. Struct. Mol. Biol.* **2009**, *16*, 23–29. [CrossRef] [PubMed]
65. Liu, M.; Lang, N.; Qiu, M.; Xu, F.; Li, Q.; Tang, Q.; Chen, J.; Chen, X.; Zhang, S.; Liu, Z.; et al. miR-137 targets Cdc42 expression, induces cell cycle G1 arrest and inhibits invasion in colorectal cancer cells. *Int. J. Cancer* **2011**, *128*, 1269–1279. [CrossRef] [PubMed]
66. Lin, X.; Yang, F.; Qi, X.; Li, Q.; Wang, D.; Yi, T.; Yin, R.; Zhao, X.; Zhong, X.; Bian, C. LncRNA DANCR promotes tumor growth and angiogenesis in ovarian cancer through direct targeting of miR-145. *Mol. Carcinog.* **2019**, *58*, 2286–2296. [CrossRef]
67. Liu, C.; Hou, J.; Shan, F.; Wang, L.; Lu, H.; Ren, T. Long Non-Coding RNA CRNDE Promotes Colorectal Carcinoma Cell Progression and Paclitaxel Resistance by Regulating miR-126-5p/ATAD2 Axis. *OncoTargets Ther.* **2020**, *13*, 4931. [CrossRef] [PubMed]
68. Eißmann, M.; Gutschner, T.; Hämmerle, M.; Günther, S.; Caudron-Herger, M.; Groß, M.; Schirmacher, P.; Rippe, K.; Braun, T.; Zörnig, M.; et al. Loss of the abundant nuclear non-coding RNA MALAT1 is compatible with life and development. *RNA Biol.* **2012**, *9*, 1076–1087. [CrossRef] [PubMed]

69. Ji, P.; Diederichs, S.; Wang, W.; Böing, S.; Metzger, R.; Schneider, P.M.; Tidow, N.; Brandt, B.; Buerger, H.; Bulk, E. MALAT-1, a novel noncoding RNA, and thymosin β 4 predict metastasis and survival in early-stage non-small cell lung cancer. *Oncogene* **2003**, *22*, 8031–8041. [CrossRef] [PubMed]
70. Li, Q.; Shen, F.; Zhao, L. The relationship between lncRNA PCGEM1 and STAT3 during the occurrence and development of endometrial carcinoma. *Biomed. Pharmacother.* **2018**, *107*, 918–928. [CrossRef]
71. Dong, Y.; Liang, G.; Yuan, B.; Yang, C.; Gao, R.; Zhou, X. MALAT1 promotes the proliferation and metastasis of osteosarcoma cells by activating the PI3K/Akt pathway. *Tumor Biol.* **2015**, *36*, 1477–1486. [CrossRef] [PubMed]
72. Zhang, X.; Hamblin, M.H.; Yin, K.-J. The long noncoding RNA Malat1: Its physiological and pathophysiological functions. *RNA Biol.* **2017**, *14*, 1705–1714. [CrossRef]
73. Shi, X.; Sun, M.; Wu, Y.; Yao, Y.; Liu, H.; Wu, G.; Yuan, D.; Song, Y. Post-transcriptional regulation of long noncoding RNAs in cancer. *Tumor Biol.* **2015**, *36*, 503–513. [CrossRef]
74. Ye, Z.-B.; Ma, G.; Zhao, Y.-H.; Xiao, Y.; Zhan, Y.; Jing, C.; Gao, K.; Liu, Z.-H.; Yu, S.-J. miR-429 inhibits migration and invasion of breast cancer cells in vitro. *Int. J. Oncol.* **2015**, *46*, 531–538. [CrossRef] [PubMed]
75. Cristóbal, I.; Rincón, R.; Manso, R.; Caramés, C.; Aguilera, O.; Madoz-Gurpide, J.; Rojo, F.; García-Foncillas, J. Deregulation of miR-200b, miR-200c and miR-429 indicates its potential relevant role in patients with colorectal cancer liver metastasis. *J. Surg. Oncol.* **2014**, *110*, 484–485. [CrossRef]
76. Wang, Z.; Zhu, Z.; Lin, Z.; Luo, Y.; Liang, Z.; Zhang, C.; Chen, J.; Peng, P. miR-429 suppresses cell proliferation, migration and invasion in nasopharyngeal carcinoma by downregulation of TLN1. *Cancer Cell Int.* **2019**, *19*, 115. [CrossRef]
77. Xiao, H.; Zhu, Q.; Zhou, J. Long non-coding RNA MALAT1 interaction with miR-429 regulates the proliferation and EMT of lung adenocarcinoma cells through RhoA. *Int. J. Clin. Exp. Pathol.* **2019**, *12*, 419–430. [PubMed]
78. Yang, Z.; Zhao, Y.; Lin, G.; Zhou, X.; Jiang, X.; Zhao, H. Noncoding RNA activated by DNA damage (NORAD): Biologic function and mechanisms in human cancers. *Clin. Chim. Acta* **2019**, *489*, 5–9. [CrossRef] [PubMed]
79. Lee, S.; Kopp, F.; Chang, T.-C.; Sataluri, A.; Chen, B.; Sivakumar, S.; Yu, H.; Xie, Y.; Mendell, J.T. Noncoding RNA NORAD regulates genomic stability by sequestering PUMILIO proteins. *Cell* **2016**, *164*, 69–80. [CrossRef]
80. Munschauer, M.; Nguyen, C.T.; Sirokman, K.; Hartigan, C.R.; Hogstrom, L.; Engreitz, J.M.; Ulirsch, J.C.; Fulco, C.P.; Subramanian, V.; Chen, J. The NORAD lncRNA assembles a topoisomerase complex critical for genome stability. *Nature* **2018**, *561*, 132–136. [CrossRef] [PubMed]
81. Zhang, J.; Li, X.-Y.; Hu, P.; Ding, Y.-S. LncRNA NORAD contributes to colorectal cancer progression by inhibition of miR-202-5p. *Oncol. Res.* **2018**, *26*, 1411. [CrossRef] [PubMed]
82. Huo, H.; Tian, J.; Wang, R.; Li, Y.; Qu, C.; Wang, N. Long non-coding RNA NORAD upregulate SIP1 expression to promote cell proliferation and invasion in cervical cancer. *Biomed. Pharmacother.* **2018**, *106*, 1454–1460. [CrossRef] [PubMed]
83. Zhou, K.; Ou, Q.; Wang, G.; Zhang, W.; Hao, Y.; Li, W. High long non-coding RNA NORAD expression predicts poor prognosis and promotes breast cancer progression by regulating TGF-β pathway. *Cancer Cell Int.* **2019**, *19*, 63. [CrossRef] [PubMed]
84. Miao, Z.; Guo, X.; Tian, L. The long noncoding RNA NORAD promotes the growth of gastric cancer cells by sponging miR-608. *Gene* **2019**, *687*, 116–124. [CrossRef]
85. Geng, Q.; Li, Z.; Li, X.; Wu, Y.; Chen, N. LncRNA NORAD, sponging miR-363-3p, promotes invasion and EMT by upregulating PEAK1 and activating the ERK signaling pathway in NSCLC cells. *J. Bioenerg. Biomembr.* **2021**, *53*, 321–332. [CrossRef]
86. Wang, B.; Xu, L.; Zhang, J.; Cheng, X.; Xu, Q.; Wang, J.; Mao, F. LncRNA NORAD accelerates the progression and doxorubicin resistance of neuroblastoma through up-regulating HDAC8 via sponging miR-144-3p. *Biomed. Pharmacother.* **2020**, *129*, 110268. [CrossRef]
87. Wang, X.; Zou, J.; Chen, H.; Zhang, P.; Lu, Z.; You, Z.; Sun, J. Long noncoding RNA NORAD regulates cancer cell proliferation and migration in human osteosarcoma by endogenously competing with miR-199a-3p. *IUBMB Life* **2019**, *71*, 1482–1491. [CrossRef] [PubMed]
88. Liu, G.; Ji, L.; Ke, M.; Ou, Z.; Tang, N.; Li, Y. miR-125a-3p is responsible for chemosensitivity in PDAC by inhibiting epithelial-mesenchymal transition via Fyn. *Biomed. Pharmacother.* **2018**, *106*, 523–531. [CrossRef]
89. Li, H.; Wang, X.; Wen, C.; Huo, Z.; Wang, W.; Zhan, Q.; Cheng, D.; Chen, H.; Deng, X.; Peng, C. Long noncoding RNA NORAD, a novel competing endogenous RNA, enhances the hypoxia-induced epithelial-mesenchymal transition to promote metastasis in pancreatic cancer. *Mol. Cancer* **2017**, *16*, 169. [CrossRef]
90. Askarian-Amiri, M.E.; Crawford, J.; French, J.D.; Smart, C.E.; Smith, M.A.; Clark, M.B.; Ru, K.; Mercer, T.R.; Thompson, E.R.; Lakhani, S.R. SNORD-host RNA Zfas1 is a regulator of mammary development and a potential marker for breast cancer. *Rna* **2011**, *17*, 878–891. [CrossRef]
91. Fan, S.; Fan, C.; Liu, N.; Huang, K.; Fang, X.; Wang, K. Downregulation of the long non-coding RNA ZFAS1 is associated with cell proliferation, migration and invasion in breast cancer. *Mol. Med. Rep.* **2018**, *17*, 6405–6412. [CrossRef]
92. Yang, H.; Li, G.; Cheng, B.; Jiang, R. ZFAS1 functions as an oncogenic long non-coding RNA in bladder cancer. *Biosci. Rep.* **2018**, *38*. [CrossRef]
93. Li, T.; Xie, J.; Shen, C.; Cheng, D.; Shi, Y.; Wu, Z.; Deng, X.; Chen, H.; Shen, B.; Peng, C. Amplification of long noncoding RNA ZFAS1 promotes metastasis in hepatocellular carcinoma. *Cancer Res.* **2015**, *75*, 3181–3191. [CrossRef]
94. Deng, H.; Wang, M.; Xu, Q.; Yao, H. ZFAS1 Promotes Colorectal Cancer Metastasis Through Modulating miR-34b/SOX4 Targeting. *Cell Biochem. Biophys.* **2021**, *79*, 387–396. [CrossRef]

95. Pan, J.; Xu, X.; Wang, G. lncRNA ZFAS1 is involved in the proliferation, invasion and metastasis of prostate cancer cells through competitively binding to miR-135a-5p. *Cancer Manag. Res.* **2020**, *12*, 1135. [CrossRef]
96. Tian, F.; Meng, F.; Wang, X. Overexpression of long-noncoding RNA ZFAS1 decreases survival in human NSCLC patients. *Eur. Rev. Med. Pharm. Sci.* **2016**, *20*, 5126–5131.
97. Dong, D.; Mu, Z.; Zhao, C.; Sun, M. ZFAS1: A novel tumor-related long non-coding RNA. *Cancer Cell Int.* **2018**, *18*, 125. [CrossRef]
98. Prensner, J.R.; Iyer, M.K.; Balbin, O.A.; Dhanasekaran, S.M.; Cao, Q.; Brenner, J.C.; Laxman, B.; Asangani, I.A.; Grasso, C.S.; Kominsky, H.D. Transcriptome sequencing across a prostate cancer cohort identifies PCAT-1, an unannotated lincRNA implicated in disease progression. *Nat. Biotechnol.* **2011**, *29*, 742–749. [CrossRef]
99. Li, M.; Yu, X.; Zheng, Q.; Zhang, Q.; He, Y.; Guo, W. Promising role of long non-coding RNA PCAT6 in malignancies. *Biomed. Pharmacother.* **2021**, *137*, 111402. [CrossRef]
100. Dong, D.; Lun, Y.; Sun, B.; Sun, H.; Wang, Q.; Yuan, G.; Quan, J. Silencing of long non-coding RNA PCAT6 restrains gastric cancer cell proliferation and epithelial-mesenchymal transition by targeting microRNA-15a. *Gen. Physiol. Biophys.* **2020**, *39*, 1–12. [CrossRef]
101. Luo, Y.; Lin, J.; Zhang, Y.; Dai, G.; Li, A.; Liu, X. LncRNA PCAT6 predicts poor prognosis in hepatocellular carcinoma and promotes proliferation through the regulation of cell cycle arrest and apoptosis. *Cell Biochem. Funct.* **2020**, *38*, 895–904. [CrossRef]
102. Ma, Z.; Gu, G.; Pan, W.; Chen, X. LncRNA PCAT6 accelerates the progression and chemoresistance of cervical cancer through up-regulating ZEB1 by sponging miR-543. *OncoTargets Ther.* **2020**, *13*, 1159. [CrossRef] [PubMed]
103. Shi, X.; Liu, Z.; Liu, Z.; Feng, X.; Hua, F.; Hu, X.; Wang, B.; Lu, K.; Nie, F. Long noncoding RNA PCAT6 functions as an oncogene by binding to EZH2 and suppressing LATS2 in non-small-cell lung cancer. *EBioMedicine* **2018**, *37*, 177–187. [CrossRef]
104. Wan, L.; Zhang, L.; Fan, K.; Cheng, Z.-X.; Sun, Q.-C.; Wang, J.-J. Knockdown of long noncoding RNA PCAT6 inhibits proliferation and invasion in lung cancer cells. *Oncol. Res. Featur. Preclin. Clin. Cancer Ther.* **2016**, *24*, 161–170. [CrossRef]
105. Wu, H.; Zou, Q.; He, H.; Liang, Y.; Lei, M.; Zhou, Q.; Fan, D.; Shen, L. Long non-coding RNA PCAT6 targets miR-204 to modulate the chemoresistance of colorectal cancer cells to 5-fluorouracil-based treatment through HMGA2 signaling. *Cancer Med.* **2019**, *8*, 2484–2495. [CrossRef]
106. Pan, Y.-J.; Wan, J.; Wang, C.-B. MiR-326: Promising biomarker for cancer. *Cancer Manag. Res.* **2019**, *11*, 10411. [CrossRef] [PubMed]
107. Jafarzadeh, M.; Soltani, B.M.; Soleimani, M.; Hosseinkhani, S. Epigenetically silenced LINC02381 functions as a tumor suppressor by regulating PI3K-Akt signaling pathway. *Biochimie* **2020**, *171*, 63–71. [CrossRef]
108. Jafarzadeh, M.; Soltani, B.M. Long noncoding RNA LOC400043 (LINC02381) inhibits gastric cancer progression through regulating Wnt signaling pathway. *Front. Oncol.* **2020**, *10*, 2189. [CrossRef] [PubMed]
109. Wang, J.; Zhao, Q. Linc02381 Exacerbates rheumatoid arthritis through adsorbing miR-590-5p and activating the mitogen-activated protein kinase signaling pathway in rheumatoid arthritis-fibroblast-like synoviocytes. *Cell Transplant.* **2020**, *29*, 0963689720938023. [CrossRef]
110. Patron, J.P.; Fendler, A.; Bild, M.; Jung, U.; Müller, H.; Arntzen, M.Ø.; Piso, C.; Stephan, C.; Thiede, B.; Mollenkopf, H.-J.; et al. MiR-133b targets antiapoptotic genes and enhances death receptor-induced apoptosis. *PLoS ONE* **2012**, *7*, e35345. [CrossRef] [PubMed]
111. Wang, Q.-Y.; Zhou, C.-X.; Zhan, M.-N.; Tang, J.; Wang, C.-L.; Ma, C.-N.; He, M.; Chen, G.-Q.; He, J.-R.; Zhao, Q. MiR-133b targets Sox9 to control pathogenesis and metastasis of breast cancer. *Cell Death Dis.* **2018**, *9*, 752. [CrossRef]
112. Chen, X.; Zhang, Z.; Ma, Y.; Su, H.; Xie, P.; Ran, J. LINC02381 Promoted Cell Viability and Migration via Targeting miR-133b in Cervical Cancer Cells. *Cancer Manag. Res.* **2020**, *12*, 3971–3979. [CrossRef] [PubMed]
113. Srikantan, V.; Zou, Z.; Petrovics, G.; Xu, L.; Augustus, M.; Davis, L.; Livezey, J.R.; Connell, T.; Sesterhenn, I.A.; Yoshino, K.; et al. PCGEM1, a prostate-specific gene, is overexpressed in prostate cancer. *Proc. Natl. Acad. Sci. USA* **2000**, *97*, 12216–12221. [CrossRef]
114. Petrovics, G.; Zhang, W.; Makarem, M.; Street, J.P.; Connelly, R.; Sun, L.; Sesterhenn, I.A.; Srikantan, V.; Moul, J.W.; Srivastava, S. Elevated expression of PCGEM1, a prostate-specific gene with cell growth-promoting function, is associated with high-risk prostate cancer patients. *Oncogene* **2004**, *23*, 605–611. [CrossRef] [PubMed]
115. Liu, Y.; Wang, Y.; Shen, X.; Chen, C.; Ni, H.; Sheng, N.; Hua, M.; Wu, Y. Down-regulation of lncRNA PCGEM1 inhibits cervical carcinoma by modulating the miR-642a-5p/LGMN axis. *Exp. Mol. Pathol.* **2020**, *117*, 104561. [CrossRef] [PubMed]
116. Weng, L.; Qiu, K.; Gao, W.; Shi, C.; Shu, F. LncRNA PCGEM1 accelerates non-small cell lung cancer progression via sponging miR-433-3p to upregulate WTAP. *BMC Pulm. Med.* **2020**, *20*, 213. [CrossRef] [PubMed]
117. Liu, S.-L.; Chen, M.-H.; Wang, X.-B.; You, R.-K.; An, X.-W.; Zhao, Q.; Wang, R.-S. LncRNA PCGEM1 contributes to malignant behaviors of glioma by regulating miR-539-5p/CDK6 axis. *Aging (Albany NY)* **2021**, *13*, 5475. [CrossRef] [PubMed]
118. Chen, S.; Wang, L.L.; Sun, K.X.; Liu, Y.; Guan, X.; Zong, Z.H.; Zhao, Y. LncRNA PCGEM1 Induces Ovarian Carcinoma Tumorigenesis and Progression Through RhoA Pathway. *Cell. Physiol. Biochem.* **2018**, *47*, 1578–1588. [CrossRef] [PubMed]
119. Tan, G.; Cao, X.; Dai, Q.; Zhang, B.; Huang, J.; Xiong, S.; yu Zhang, Y.; Chen, W.; Yang, J.; Li, H. A novel role for microRNA-129-5p in inhibiting ovarian cancer cell proliferation and survival via direct suppression of transcriptional co-activators YAP and TAZ. *Oncotarget* **2015**, *6*, 8676. [CrossRef] [PubMed]
120. Ju, J.A.; Gilkes, D.M. RhoB: Team Oncogene or Team Tumor Suppressor? *Genes* **2018**, *9*, 67. [CrossRef]

121. Calvayrac, O.; Mazières, J.; Figarol, S.; Marty-Detraves, C.; Raymond-Letron, I.; Bousquet, E.; Farella, M.; Clermont-Taranchon, E.; Milia, J.; Rouquette, I. The RAS-related GTP ase RHOB confers resistance to EGFR-tyrosine kinase inhibitors in non-small-cell lung cancer via an AKT-dependent mechanism. *EMBO Mol. Med.* **2017**, *9*, 238–250. [CrossRef]
122. Jin, L.; Liu, W.-R.; Tian, M.-X.; Jiang, X.-F.; Wang, H.; Zhou, P.-Y.; Ding, Z.-B.; Peng, Y.-F.; Dai, Z.; Qiu, S.-J. CCL24 contributes to HCC malignancy via RhoB-VEGFA-VEGFR2 angiogenesis pathway and indicates poor prognosis. *Oncotarget* **2017**, *8*, 5135. [CrossRef]
123. Privat, M.; Cavard, A.; Zekri, Y.; Ponelle-Chachuat, F.; Molnar, I.; Sonnier, N.; Bignon, Y.-J. A high expression ratio of RhoA/RhoB is associated with the migratory and invasive properties of basal-like Breast Tumors. *Int. J. Med. Sci.* **2020**, *17*, 2799. [CrossRef]
124. Ju, J.A.; Godet, I.; DiGiacomo, J.W.; Gilkes, D.M. RhoB is regulated by hypoxia and modulates metastasis in breast cancer. *Cancer Rep.* **2020**, 3, e1164. [CrossRef] [PubMed]
125. Chen, W.; Niu, S.; Ma, X.; Zhang, P.; Gao, Y.; Fan, Y.; Pang, H.; Gong, H.; Shen, D.; Gu, L. RhoB acts as a tumor suppressor that inhibits malignancy of clear cell renal cell carcinoma. *PLoS ONE* **2016**, *11*, e0157599. [CrossRef] [PubMed]
126. Ji, J.; Dai, X.; Yeung, S.-C.J.; He, X. The role of long non-coding RNA GAS5 in cancers. *Cancer Manag. Res.* **2019**, *11*, 2729. [CrossRef]
127. Toraih, E.A.; Alghamdi, S.A.; El-Wazir, A.; Hosny, M.M.; Hussein, M.H.; Khashana, M.S.; Fawzy, M.S. Dual biomarkers long non-coding RNA GAS5 and microRNA-34a co-expression signature in common solid tumors. *PLoS ONE* **2018**, *13*, e0198231. [CrossRef] [PubMed]
128. Hu, L.; Ye, H.; Huang, G.; Luo, F.; Liu, Y.; Liu, Y.; Yang, X.; Shen, J.; Liu, Q.; Zhang, J. Long noncoding RNA GAS5 suppresses the migration and invasion of hepatocellular carcinoma cells via miR-21. *Tumor Biol.* **2016**, *37*, 2691–2702. [CrossRef]
129. Cao, L.; Chen, J.; Ou, B.; Liu, C.; Zou, Y. GAS5 knockdown reduces the chemo-sensitivity of non-small cell lung cancer (NSCLC) cell to cisplatin (DDP) through regulating miR-21/PTEN axis. *Biomed. Pharmacother.* **2017**, *93*, 570–579. [CrossRef]
130. Gao, Z.-Q.; Wang, J.-f.; Chen, D.-H.; Ma, X.-S.; Yang, W.; Zhe, T.; Dang, X.-W. Long non-coding RNA GAS5 antagonizes the chemoresistance of pancreatic cancer cells through down-regulation of miR-181c-5p. *Biomed. Pharmacother.* **2018**, *97*, 809–817. [CrossRef] [PubMed]
131. Yang, W.; Hong, L.; Xu, X.; Wang, Q.; Huang, J.; Jiang, L. LncRNA GAS5 suppresses the tumorigenesis of cervical cancer by downregulating miR-196a and miR-205. *Tumor Biol.* **2017**, *39*, 1010428317711315. [CrossRef]
132. Zhang, X.-F.; Ye, Y.; Zhao, S.-J. LncRNA Gas5 acts as a ceRNA to regulate PTEN expression by sponging miR-222-3p in papillary thyroid carcinoma. *Oncotarget* **2018**, *9*, 3519. [CrossRef] [PubMed]
133. Huang, C.; Sun, Y.; Ma, S.; Vadamootoo, A.S.; Wang, L.; Jin, C. Identification of circulating miR-663a as a potential biomarker for diagnosing osteosarcoma. *Pathol.-Res. Pract.* **2019**, *215*, 152411. [CrossRef] [PubMed]
134. Thomas, P.; Pranatharthi, A.; Ross, C.; Srivastava, S. RhoC: A fascinating journey from a cytoskeletal organizer to a Cancer stem cell therapeutic target. *J. Exp. Clin. Cancer Res.* **2019**, *38*, 328. [CrossRef] [PubMed]
135. Gou, W.-F.; Zhao, Y.; Lu, H.; Yang, X.-F.; Xiu, Y.-L.; Zhao, S.; Liu, J.-M.; Zhu, Z.-T.; Sun, H.-Z.; Liu, Y.-P. The role of RhoC in epithelial-to-mesenchymal transition of ovarian carcinoma cells. *BMC Cancer* **2014**, *14*, 477. [CrossRef]
136. Kleer, C.G.; Griffith, K.A.; Sabel, M.S.; Gallagher, G.; van Golen, K.L.; Wu, Z.-F.; Merajver, S.D. RhoC-GTPase is a novel tissue biomarker associated with biologically aggressive carcinomas of the breast. *Breast Cancer Res. Treat.* **2005**, *93*, 101–110. [CrossRef]
137. Lang, S.; Busch, H.; Boerries, M.; Brummer, T.; Timme, S.; Lassmann, S.; Aktories, K.; Schmidt, G. Specific role of RhoC in tumor invasion and metastasis. *Oncotarget* **2017**, *8*, 87364–87378. [CrossRef] [PubMed]
138. Yilmaz, M.; Christofori, G. EMT, the cytoskeleton, and cancer cell invasion. *Cancer Metastasis Rev.* **2009**, *28*, 15–33. [CrossRef] [PubMed]
139. Lin, M.; DiVito, M.M.; Merajver, S.D.; Boyanapalli, M.; Van Golen, K.L. Regulation of pancreatic cancer cell migration and invasion by RhoC GTPase and caveolin-1. *Mol. Cancer* **2005**, *4*, 21. [CrossRef]
140. Jiang, X.; Li, D.; Yang, J.; Wen, J.; Chen, H.; Xiao, X.; Dai, Y.; Yang, J.; Tang, Y. Characterization of a novel human testis-specific gene: Testis developmental related gene 1 (TDRG1). *Tohoku J. Exp. Med.* **2011**, *225*, 311–318. [CrossRef]
141. Jiang, H.; Liang, M.; Jiang, Y.; Zhang, T.; Mo, K.; Su, S.; Wang, A.; Zhu, Y.; Huang, G.; Zhou, R. The lncRNA TDRG1 promotes cell proliferation, migration and invasion by targeting miR-326 to regulate MAPK1 expression in cervical cancer. *Cancer Cell Int.* **2019**, *19*, 152. [CrossRef]
142. Chen, H.; Sun, J.; He, Y.; Zou, Q.; Wu, Q.; Tang, Y. Expression and localization of testis developmental related gene 1 (TDRG1) in human spermatozoa. *Tohoku J. Exp. Med.* **2015**, *235*, 103–109. [CrossRef] [PubMed]
143. Gan, Y.; Yang, J.; Wang, Y.; Tan, Z.; Jiang, X.; Tang, Y. In vitro study on shRNA-mediated reduction of testis developmental related gene 1 expression and its effects on the proliferation, invasion and apoptosis of NTERA-2 cells. *Oncol. Lett.* **2015**, *10*, 61–66. [CrossRef]
144. Chen, S.; Wang, L.-l.; Sun, K.-x.; Liu, Y.; Guan, X.; Zong, Z.-h.; Zhao, Y. LncRNA TDRG1 enhances tumorigenicity in endometrial carcinoma by binding and targeting VEGF-A protein. *Biochim. Biophys. Acta (BBA)-Mol. Basis Dis.* **2018**, *1864*, 3013–3021. [CrossRef] [PubMed]
145. Jiang, S.; Xia, M.; Yang, J.; Shao, J.; Liao, X.; Zhu, J.; Jiang, H. Novel insights into a treatment for aplastic anemia based on the advanced proliferation of bone marrow-derived mesenchymal stem cells induced by fibroblast growth factor 1. *Mol. Med. Rep.* **2015**, *12*, 7877–7882. [CrossRef]

146. Chen, S.; Wang, L.L.; Sun, K.X.; Xiu, Y.L.; Zong, Z.H.; Chen, X.; Zhao, Y. The role of the long non-coding RNA TDRG1 in epithelial ovarian carcinoma tumorigenesis and progression through miR-93/RhoC pathway. *Mol. Carcinog.* **2018**, *57*, 225–234. [CrossRef]
147. Meng, X.; Joosse, S.A.; Müller, V.; Trillsch, F.; Milde-Langosch, K.; Mahner, S.; Geffken, M.; Pantel, K.; Schwarzenbach, H. Diagnostic and prognostic potential of serum miR-7, miR-16, miR-25, miR-93, miR-182, miR-376a and miR-429 in ovarian cancer patients. *Br. J. Cancer* **2015**, *113*, 1358–1366. [CrossRef]
148. Merola, R.; Tomao, L.; Antenucci, A.; Sperduti, I.; Sentinelli, S.; Masi, S.; Mandoj, C.; Orlandi, G.; Papalia, R.; Guaglianone, S.; et al. PCA3 in prostate cancer and tumor aggressiveness detection on 407 high-risk patients: A National Cancer Institute experience. *J. Exp. Clin. Cancer Res.* **2015**, *34*, 15. [CrossRef] [PubMed]
149. Loeb, S.; Partin, A.W. Review of the literature: PCA3 for prostate cancer risk assessment and prognostication. *Rev. Urol.* **2011**, *13*, e191. [PubMed]
150. Wang, Y.-N.; Liu, S.-Y.; Wang, L.; Han, L.-Y. Long noncoding RNA PCA3 contributes to the progression of choriocarcinoma by acting as a ceRNA against miR-106b. *Int. J. Clin. Exp. Pathol.* **2019**, *12*, 1609–1617.
151. Yang, C.; Dou, R.; Yin, T.; Ding, J. MiRNA-106b-5p in human cancers: Diverse functions and promising biomarker. *Biomed. Pharmacother.* **2020**, *127*, 110211. [CrossRef] [PubMed]
152. Kotelevets, L.; Chastre, E. Rac1 signaling: From intestinal homeostasis to colorectal cancer metastasis. *Cancers* **2020**, *12*, 665. [CrossRef] [PubMed]
153. Fritz, G.; Just, I.; Kaina, B. Rho GTPases are over-expressed in human tumors. *Int. J. Cancer* **1999**, *81*, 682–687. [CrossRef]
154. Chang, M.T.; Asthana, S.; Gao, S.P.; Lee, B.H.; Chapman, J.S.; Kandoth, C.; Gao, J.; Socci, N.D.; Solit, D.B.; Olshen, A.B. Identifying recurrent mutations in cancer reveals widespread lineage diversity and mutational specificity. *Nat. Biotechnol.* **2016**, *34*, 155–163. [CrossRef] [PubMed]
155. Bagrodia, A.; Lee, B.H.; Lee, W.; Cha, E.K.; Sfakianos, J.P.; Iyer, G.; Pietzak, E.J.; Gao, S.P.; Zabor, E.C.; Ostrovnaya, I. Genetic determinants of cisplatin resistance in patients with advanced germ cell tumors. *J. Clin. Oncol.* **2016**, *34*, 4000. [CrossRef] [PubMed]
156. Hodis, E.; Watson, I.R.; Kryukov, G.V.; Arold, S.T.; Imielinski, M.; Theurillat, J.-P.; Nickerson, E.; Auclair, D.; Li, L.; Place, C. A landscape of driver mutations in melanoma. *Cell* **2012**, *150*, 251–263. [CrossRef]
157. Stallings-Mann, M.L.; Waldmann, J.; Zhang, Y.; Miller, E.; Gauthier, M.L.; Visscher, D.W.; Downey, G.P.; Radisky, E.S.; Fields, A.P.; Radisky, D.C. Matrix metalloproteinase induction of Rac1b, a key effector of lung cancer progression. *Sci. Transl. Med.* **2012**, *4*, 142ra95. [CrossRef] [PubMed]
158. Thakur, N.; Kupani, M.; Mannan, R.; Pruthi, A.; Mehrotra, S. Genetic association between CDKN2B/CDKN2B-AS1 gene polymorphisms with primary glaucoma in a North Indian cohort: An original study and an updated meta-analysis. *BMC Med Genom.* **2021**, *14*, 1. [CrossRef] [PubMed]
159. Bayoglu, B.; Yuksel, H.; Cakmak, H.A.; Dirican, A.; Cengiz, M. Polymorphisms in the long non-coding RNA CDKN2B-AS1 may contribute to higher systolic blood pressure levels in hypertensive patients. *Clin. Biochem.* **2016**, *49*, 821–827. [CrossRef]
160. Xu, C.; Zhai, J.; Fu, Y. LncRNA CDKN2B-AS1 promotes the progression of ovarian cancer by miR-143-3p/SMAD3 axis and predicts a poor prognosis. *Neoplasma* **2020**, *67*, 782–793. [CrossRef]
161. Zhu, H.; Li, X.; Song, Y.; Zhang, P.; Xiao, Y.; Xing, Y. Long non-coding RNA ANRIL is up-regulated in bladder cancer and regulates bladder cancer cell proliferation and apoptosis through the intrinsic pathway. *Biochem. Biophys. Res. Commun.* **2015**, *467*, 223–228. [CrossRef] [PubMed]
162. Cui, X.; Yu, T.; Shang, J.; Xiao, D.; Wang, X. Long non-coding RNA CDKN2B-AS1 facilitates laryngeal squamous cell cancer through regulating miR-497/CDK6 pathway. *OncoTargets Ther.* **2019**, *12*, 8853. [CrossRef] [PubMed]
163. Shen, X.; Li, Y.; He, F.; Kong, J. LncRNA CDKN2B-AS1 Promotes Cell Viability, Migration, and Invasion of Hepatocellular Carcinoma via Sponging miR-424-5p. *Cancer Manag. Res.* **2020**, *12*, 6807. [CrossRef] [PubMed]
164. Zhang, J.-J.; Wang, D.-D.; Du, C.-X.; Wang, Y. Long noncoding RNA ANRIL promotes cervical cancer development by acting as a sponge of miR-186. *Oncol. Res.* **2018**, *26*, 345. [CrossRef] [PubMed]
165. Naemura, M.; Murasaki, C.; Inoue, Y.; Okamoto, H.; Kotake, Y. Long Noncoding RNA ANRIL Regulates Proliferation of Non-small Cell Lung Cancer and Cervical Cancer Cells. *Anticancer Res.* **2015**, *35*, 5377–5382.
166. Zhu, L.; Zhang, Q.; Li, S.; Jiang, S.; Cui, J.; Dang, G. Interference of the long noncoding RNA CDKN2B-AS1 upregulates miR-181a-5p/TGFβI axis to restrain the metastasis and promote apoptosis and senescence of cervical cancer cells. *Cancer Med.* **2019**, *8*, 1721–1730. [CrossRef]
167. Huang, Y.; Xiang, B.; Liu, Y.; Wang, Y.; Kan, H. LncRNA CDKN2B-AS1 promotes tumor growth and metastasis of human hepatocellular carcinoma by targeting let-7c-5p/NAP1L1 axis. *Cancer Lett.* **2018**, *437*, 56–66. [CrossRef]
168. Abula, A.; Saimaiti, G.; Maimaiti, X.; Wuqikun, W.; Abulaiti, A.; Ren, P.; Yusufu, A. The stimulative function of long noncoding RNA CDKN2B-AS1 in osteosarcoma by targeting the microRNA-122/CCNG1 axis. *J. Recept. Signal Transduct.* **2020**, 1–9. [CrossRef]
169. Wang, G.; Xu, G.; Wang, W. Long noncoding RNA CDKN2B-AS1 facilitates lung cancer development through regulating miR-378b/NR2C2. *OncoTargets Ther.* **2020**, *13*, 10641. [CrossRef]
170. Dasgupta, P.; Kulkarni, P.; Majid, S.; Hashimoto, Y.; Shiina, M.; Shahryari, V.; Bhat, N.S.; Tabatabai, L.; Yamamura, S.; Saini, S. LncRNA CDKN2B-AS1/miR-141/cyclin D network regulates tumor progression and metastasis of renal cell carcinoma. *Cell Death Dis.* **2020**, *11*, 660. [CrossRef]

171. Li, J.; Guo, W.; Xue, W.; Xu, P.; Deng, Z.; Zhang, D.; Zheng, S.; Qiu, X. Long noncoding RNA AURKAPS1 potentiates malignant hepatocellular carcinoma progression by regulating miR-142, miR-155 and miR-182. *Sci. Rep.* **2019**, *9*, 19645. [CrossRef]
172. Cao, M.-Q.; You, A.B.; Zhu, X.-D.; Zhang, W.; Zhang, Y.-Y.; Zhang, S.-Z.; Zhang, K.-W.; Cai, H.; Shi, W.-K.; Li, X.-L.; et al. miR-182-5p promotes hepatocellular carcinoma progression by repressing FOXO3a. *J. Hematol. Oncol.* **2018**, *11*, 12. [CrossRef]
173. Fu, Y.; Sun, L.Q.; Huang, Y.; Quan, J.; Hu, X.; Tang, D.; Kang, R.; Li, N.; Fan, X.G. miR-142-3p Inhibits the Metastasis of Hepatocellular Carcinoma Cells by Regulating HMGB1 Gene Expression. *Curr. Mol. Med.* **2018**, *18*, 135–141. [CrossRef] [PubMed]
174. Cheng, L.; Wang, P.; Tian, R.; Wang, S.; Guo, Q.; Luo, M.; Zhou, W.; Liu, G.; Jiang, H.; Jiang, Q. LncRNA2Target v2.0: A comprehensive database for target genes of lncRNAs in human and mouse. *Nucleic Acids Res.* **2019**, *47*, D140–D144. [CrossRef] [PubMed]
175. Yang, J.; Qiu, Q.; Qian, X.; Yi, J.; Jiao, Y.; Yu, M.; Li, X.; Li, J.; Mi, C.; Zhang, J.; et al. Long noncoding RNA LCAT1 functions as a ceRNA to regulate RAC1 function by sponging miR-4715-5p in lung cancer. *Mol. Cancer* **2019**, *18*, 171. [CrossRef] [PubMed]
176. Li, H.; Cui, Z.; Lv, X.; Li, J.; Gao, M.; Yang, Z.; Bi, Y.; Zhang, Z.; Wang, S.; Li, S.; et al. Long Non-coding RNA HOTAIR Function as a Competing Endogenous RNA for miR-149-5p to Promote the Cell Growth, Migration, and Invasion in Non-small Cell Lung Cancer. *Front. Oncol.* **2020**, *10*, 528520. [CrossRef]
177. Silva, J.M.; Boczek, N.J.; Berres, M.W.; Ma, X.; Smith, D.I. LSINCT5 is over expressed in breast and ovarian cancer and affects cellular proliferation. *RNA Biol.* **2011**, *8*, 496–505. [CrossRef] [PubMed]
178. Zhu, X.; Li, Y.; Zhao, S.; Zhao, S. LSINCT5 activates Wnt/β-catenin signaling by interacting with NCYM to promote bladder cancer progression. *Biochem. Biophys. Res. Commun.* **2018**, *502*, 299–306. [CrossRef]
179. He, W.; Lu, M.; Xiao, D. LSINCT5 predicts unfavorable prognosis and exerts oncogenic function in osteosarcoma. *Biosci. Rep.* **2019**, *39*, BSR20190612. [CrossRef]
180. Jiang, H.; Li, Y.; Li, J.; Zhang, X.; Niu, G.; Chen, S.; Yao, S. Long noncoding RNA LSINCT5 promotes endometrial carcinoma cell proliferation, cycle, and invasion by promoting the Wnt/β-catenin signaling pathway via HMGA2. *Ther. Adv. Med Oncol.* **2019**, *11*, 1758835919874649. [CrossRef] [PubMed]
181. Xu, M.-D.; Qi, P.; Weng, W.-W.; Shen, X.-H.; Ni, S.-J.; Dong, L.; Huang, D.; Tan, C.; Sheng, W.-Q.; Zhou, X.-Y. Long non-coding RNA LSINCT5 predicts negative prognosis and exhibits oncogenic activity in gastric cancer. *Medicine* **2014**, *93*, e303. [CrossRef]
182. Liu, B.; Cao, W.; Ma, H. Knockdown of lncRNA LSINCT5 suppresses growth and metastasis of human glioma cells via up-regulating miR-451. *Artif. Cells Nanomed. Biotechnol.* **2019**, *47*, 2507–2515. [CrossRef] [PubMed]
183. Tian, Y.; Nan, Y.; Han, L.; Zhang, A.; Wang, G.; Jia, Z.; Hao, J.; Pu, P.; Zhong, Y.; Kang, C. MicroRNA miR-451 downregulates the PI3K/AKT pathway through CAB39 in human glioma. *Int. J. Oncol.* **2012**, *40*, 1105–1112. [CrossRef]
184. Chen, C.; Shu, L.; Zou, W. Role of long non-coding RNA TP73-AS1 in cancer. *Biosci Rep* **2019**, *39*, BSR20192274. [CrossRef] [PubMed]
185. Liu, C.; Ren, L.; Deng, J.; Wang, S. LncRNA TP73-AS1 promoted the progression of lung adenocarcinoma via PI3K/AKT pathway. *Biosci. Rep.* **2019**, *39*, BSR20180999. [CrossRef]
186. Cai, Y.; Yan, P.; Zhang, G.; Yang, W.; Wang, H.; Cheng, X. Long non-coding RNA TP73-AS1 sponges miR-194 to promote colorectal cancer cell proliferation, migration and invasion via up-regulating TGFα. *Cancer Biomark.* **2018**, *23*, 145–156. [CrossRef] [PubMed]
187. Xiao, S.; Wang, R.; Wu, X.; Liu, W.; Ma, S. The long noncoding RNA TP73-AS1 interacted with miR-124 to modulate glioma growth by targeting inhibitor of apoptosis-stimulating protein of p53. *DNA Cell Biol.* **2018**, *37*, 117–125. [CrossRef] [PubMed]
188. Miao, H.; Lu, J.; Guo, Y.; Qiu, H.; Zhang, Y.; Yao, X.; Li, X.; Lu, Y. LncRNA TP73-AS1 enhances the malignant properties of pancreatic ductal adenocarcinoma by increasing MMP14 expression through miRNA-200a sponging. *J. Cell. Mol. Med.* **2021**, *25*, 3654–3664. [CrossRef] [PubMed]
189. Wang, B.; Sun, X.; Huang, K.-J.; Zhou, L.-S.; Qiu, Z.-J. Long non-coding RNA TP73-AS1 promotes pancreatic cancer growth and metastasis through miRNA-128-3p/GOLM1 axis. *World J. Gastroenterol.* **2021**, *27*, 1993. [CrossRef]
190. Xu, J.; Zhang, J. LncRNA TP73-AS1 is a novel regulator in cervical cancer via miR-329-3p/ARF1 axis. *J. Cell. Biochem.* **2020**, *121*, 344–352. [CrossRef]
191. Yang, G.; Song, R.; Wang, L.; Wu, X. Knockdown of long non-coding RNA TP73-AS1 inhibits osteosarcoma cell proliferation and invasion through sponging miR-142. *Biomed. Pharmacother.* **2018**, *103*, 1238–1245. [CrossRef]
192. Gao, Y.-F.; Zhang, Q.-J.; Yu, Z.; Liu, S.-H.; Liang, J. miR-142 suppresses proliferation and induces apoptosis of osteosarcoma cells by upregulating Rb. *Oncol. Lett.* **2018**, *16*, 733–740. [CrossRef]
193. Zhang, C.-Z. Long non-coding RNA FTH1P3 facilitates oral squamous cell carcinoma progression by acting as a molecular sponge of miR-224-5p to modulate fizzled 5 expression. *Gene* **2017**, *607*, 47–55. [CrossRef] [PubMed]
194. Zheng, X.; Tang, H.; Zhao, X.; Sun, Y.; Jiang, Y.; Liu, Y. Long non-coding RNA FTH1P3 facilitates uveal melanoma cell growth and invasion through miR-224-5p. *PLoS ONE* **2017**, *12*, e0184746. [CrossRef] [PubMed]
195. Yuan, H.; Jiang, H.; Wang, Y.; Dong, Y. Increased expression of lncRNA FTH1P3 predicts a poor prognosis and promotes aggressive phenotypes of laryngeal squamous cell carcinoma. *Biosci Rep* **2019**, *39*, BSR20181644. [CrossRef] [PubMed]
196. Lv, R.; Zhang, Q.W. The long noncoding RNA FTH1P3 promotes the proliferation and metastasis of cervical cancer through microRNA-145. *Oncol. Rep.* **2020**, *43*, 31–40. [CrossRef] [PubMed]
197. Li, J.; Liu, X.; Li, C.; Wang, W. miR-224-5p inhibits proliferation, migration, and invasion by targeting PIK3R3/AKT3 in uveal melanoma. *J. Cell. Biochem.* **2019**, *120*, 12412–12421. [CrossRef] [PubMed]

198. Brown, C.J.; Hendrich, B.D.; Rupert, J.L.; Lafreniere, R.G.; Xing, Y.; Lawrence, J.; Willard, H.F. The human XIST gene: Analysis of a 17 kb inactive X-specific RNA that contains conserved repeats and is highly localized within the nucleus. *Cell* **1992**, *71*, 527–542. [CrossRef]
199. Brockdorff, N.; Ashworth, A.; Kay, G.F.; Cooper, P.; Smith, S.; McCabe, V.M.; Norris, D.P.; Penny, G.D.; Patel, D.; Rastan, S. Conservation of position and exclusive expression of mouse Xist from the inactive X chromosome. *Nature* **1991**, *351*, 329–331. [CrossRef] [PubMed]
200. Yue, D.; Guanqun, G.; Jingxin, L.; Sen, S.; Shuang, L.; Yan, S.; Minxue, Z.; Ping, Y.; Chong, L.; Zhuobo, Z. Silencing of long noncoding RNA XIST attenuated Alzheimer's disease-related BACE1 alteration through miR-124. *Cell Biol. Int.* **2020**, *44*, 630–636. [CrossRef] [PubMed]
201. Peng, H.; Luo, Y.; Ying, Y. lncRNA XIST attenuates hypoxia-induced H9c2 cardiomyocyte injury by targeting the miR-122-5p/FOXP2 axis. *Mol. Cell. Probes* **2020**, *50*, 101500. [CrossRef]
202. Xiao, L.; Gu, Y.; Sun, Y.; Chen, J.; Wang, X.; Zhang, Y.; Gao, L.; Li, L. The long noncoding RNA XIST regulates cardiac hypertrophy by targeting miR-101. *J. Cell. Physiol.* **2019**, *234*, 13680–13692. [CrossRef] [PubMed]
203. Lin, B.; Xu, J.; Wang, F.; Wang, J.; Zhao, H.; Feng, D. LncRNA XIST promotes myocardial infarction by regulating FOS through targeting miR-101a-3p. *Aging (Albany NY)* **2020**, *12*, 7232. [CrossRef] [PubMed]
204. Tang, B.; Li, W.; Ji, T.; Li, X.; Qu, X.; Feng, L.; Zhu, Y.; Qi, Y.; Zhu, C.; Bai, S. Downregulation of XIST ameliorates acute kidney injury by sponging miR-142-5p and targeting PDCD4. *J. Cell. Physiol.* **2020**, *235*, 8852–8863. [CrossRef]
205. Chen, D.; Chen, T.; Guo, Y.; Wang, C.; Dong, L.; Lu, C. Platycodin D (PD) regulates LncRNA-XIST/miR-335 axis to slow down bladder cancer progression in vitro and in vivo. *Exp. Cell Res.* **2020**, *396*, 112281. [CrossRef] [PubMed]
206. Zhang, M.; Wang, F.; Xiang, Z.; Huang, T.; Zhou, W.B. LncRNA XIST promotes chemoresistance of breast cancer cells to doxorubicin by sponging miR-200c-3p to upregulate ANLN. *Clin. Exp. Pharmacol. Physiol.* **2020**, *47*, 1464–1472. [CrossRef]
207. Yang, L.g.; Cao, M.z.; Zhang, J.; Li, X.y.; Sun, Q.l. LncRNA XIST modulates HIF-1A/AXL signaling pathway by inhibiting miR-93-5p in colorectal cancer. *Mol. Genet. Genom. Med.* **2020**, *8*, e1112. [CrossRef]
208. Rong, H.; Chen, B.; Wei, X.; Peng, J.; Ma, K.; Duan, S.; He, J. Long non-coding RNA XIST expedites lung adenocarcinoma progression through upregulating MDM2 expression via binding to miR-363-3p. *Thorac. Cancer* **2020**, *11*, 659–671. [CrossRef]
209. Tian, K.; Sun, D.; Chen, M.; Yang, Y.; Wang, F.; Guo, T.; Shi, Z. Long noncoding RNA X-inactive specific transcript facilitates cellular functions in melanoma via miR-139-5p/ROCK1 pathway. *OncoTargets Ther.* **2020**, *13*, 1277. [CrossRef]
210. Zheng, W.; Li, J.; Zhou, X.; Cui, L.; Wang, Y. The lncRNA XIST promotes proliferation, migration and invasion of gastric cancer cells by targeting miR-337. *Arab J. Gastroenterol.* **2020**, *21*, 199–206. [CrossRef] [PubMed]
211. Zuo, K.; Zhao, Y.; Zheng, Y.; Chen, D.; Liu, X.; Du, S.; Liu, Q. Long non-coding RNA XIST promotes malignant behavior of epithelial ovarian cancer. *OncoTargets Ther.* **2019**, *12*, 7261. [CrossRef] [PubMed]
212. Sun, X.; Wei, B.; Peng, Z.-H.; Fu, Q.-L.; Wang, C.-J.; Zheng, J.-C.; Sun, J.-C. Knockdown of lncRNA XIST suppresses osteosarcoma progression by inactivating AKT/mTOR signaling pathway by sponging miR-375-3p. *Int. J. Clin. Exp. Pathol.* **2019**, *12*, 1507. [PubMed]
213. Shen, J.; Xiong, J.; Shao, X.; Cheng, H.; Fang, X.; Sun, Y.; Di, G.; Mao, J.; Jiang, X. Knockdown of the long noncoding RNA XIST suppresses glioma progression by upregulating miR-204-5p. *J. Cancer* **2020**, *11*, 4550. [CrossRef]
214. Wang, Z.; Yuan, J.; Li, L.; Yang, Y.; Xu, X.; Wang, Y. Long non-coding RNA XIST exerts oncogenic functions in human glioma by targeting miR-137. *Am. J. Transl. Res.* **2017**, *9*, 1845–1855. [PubMed]
215. Wang, W.; Min, L.; Qiu, X.; Wu, X.; Liu, C.; Ma, J.; Zhang, D.; Zhu, L. Biological Function of Long Non-coding RNA (LncRNA) Xist. *Front. Cell Dev. Biol.* **2021**, *9*, 1447.
216. Wang, Y.; Chen, R.; Zhou, X.; Guo, R.; Yin, J.; Li, Y.; Ma, G. miR-137: A Novel Therapeutic Target for Human Glioma. *Mol. Ther. Nucleic Acids* **2020**, *21*, 614–622. [CrossRef] [PubMed]
217. Xiao, X.-H.; Lv, L.-C.; Duan, J.; Wu, Y.-M.; He, S.-J.; Hu, Z.-Z.; Xiong, L.-X. Regulating Cdc42 and its signaling pathways in cancer: Small molecules and MicroRNA as new treatment candidates. *Molecules* **2018**, *23*, 787. [CrossRef]
218. Maldonado, M.d.M.; Medina, J.I.; Velazquez, L.; Dharmawardhane, S. Targeting Rac and Cdc42 GEFs in metastatic cancer. *Front. Cell Dev. Biol.* **2020**, *8*, 201. [CrossRef]
219. Sharma, P.; Saini, N.; Sharma, R. miR-107 functions as a tumor suppressor in human esophageal squamous cell carcinoma and targets Cdc42. *Oncol. Rep.* **2017**, *37*, 3116–3127. [CrossRef]
220. Fu, M.-G.; Li, S.; Yu, T.-T.; Qian, L.-J.; Cao, R.-S.; Zhu, H.; Xiao, B.; Jiao, C.-H.; Tang, N.-N.; Ma, J.-J. Differential expression of miR-195 in esophageal squamous cell carcinoma and miR-195 expression inhibits tumor cell proliferation and invasion by targeting of Cdc42. *FEBS Lett.* **2013**, *587*, 3471–3479. [CrossRef] [PubMed]
221. Sun, N.; Ye, L.; Chang, T.; Li, X.; Li, X. microRNA-195-Cdc42 axis acts as a prognostic factor of esophageal squamous cell carcinoma. *Int. J. Clin. Exp. Pathol.* **2014**, *7*, 6871. [PubMed]
222. Shi, C.; Ren, L.; Sun, C.; Yu, L.; Bian, X.; Zhou, X.; Wen, Y.; Hua, D.; Zhao, S.; Luo, W. miR-29a/b/c function as invasion suppressors for gliomas by targeting CDC42 and predict the prognosis of patients. *Br. J. Cancer* **2017**, *117*, 1036–1047. [CrossRef] [PubMed]
223. Lee, S.; Craig, B.T.; Romain, C.V.; Qiao, J.; Chung, D.H. Silencing of CDC42 inhibits neuroblastoma cell proliferation and transformation. *Cancer Lett.* **2014**, *355*, 210–216. [CrossRef] [PubMed]

224. Chou, J.; Wang, B.; Zheng, T.; Li, X.; Zheng, L.; Hu, J.; Zhang, Y.; Xing, Y.; Xi, T. MALAT1 induced migration and invasion of human breast cancer cells by competitively binding miR-1 with cdc42. *Biochem. Biophys. Res. Commun.* **2016**, *472*, 262–269. [CrossRef] [PubMed]
225. Zhou, Y.; Si, L.; Liu, Z.; Shi, Y.; Agula, B. Long Noncoding RNA ZFAS1 Promotes Progression of NSCLC via Regulating of miR-590-3p. *Cell Transpl.* **2020**, *29*, 963689720919435. [CrossRef] [PubMed]
226. Wang, J.; Zhao, L.; Shang, K.; Liu, F.; Che, J.; Li, H.; Cao, B. Long non-coding RNA H19, a novel therapeutic target for pancreatic cancer. *Mol. Med.* **2020**, *26*, 30. [CrossRef]
227. Zhang, L.; Yang, F.; Yuan, J.-H.; Yuan, S.-X.; Zhou, W.-P.; Huo, X.-S.; Xu, D.; Bi, H.-S.; Wang, F.; Sun, S.-H. Epigenetic activation of the MiR-200 family contributes to H19-mediated metastasis suppression in hepatocellular carcinoma. *Carcinogenesis* **2013**, *34*, 577–586. [CrossRef]
228. Fang, Y.; Hu, J.; Wang, Z.; Zong, H.; Zhang, L.; Zhang, R.; Sun, L. LncRNA H19 functions as an Aquaporin 1 competitive endogenous RNA to regulate microRNA-874 expression in LPS sepsis. *Biomed. Pharmacother.* **2018**, *105*, 1183–1191. [CrossRef]
229. Luo, H.; Wang, J.; Liu, D.; Zang, S.; Ma, N.; Zhao, L.; Zhang, L.; Zhang, X.; Qiao, C. The lncRNA H19/miR-675 axis regulates myocardial ischemic and reperfusion injury by targeting PPARα. *Mol. Immunol.* **2019**, *105*, 46–54. [CrossRef] [PubMed]
230. Cui, J.; Mo, J.; Luo, M.; Yu, Q.; Zhou, S.; Li, T.; Zhang, Y.; Luo, W. c-Myc-activated long non-coding RNA H19 downregulates miR-107 and promotes cell cycle progression of non-small cell lung cancer. *Int. J. Clin. Exp. Pathol.* **2015**, *8*, 12400.
231. Sun, Y.; Zhu, Q.; Yang, W.; Shan, Y.; Yu, Z.; Zhang, Q.; Wu, H. LncRNA H19/miR-194/PFTK1 axis modulates the cell proliferation and migration of pancreatic cancer. *J. Cell. Biochem.* **2019**, *120*, 3874–3886. [CrossRef] [PubMed]
232. Hu, Q.; Yin, J.; Zeng, A.; Jin, X.; Zhang, Z.; Yan, W.; You, Y. H19 functions as a competing endogenous RNA to regulate EMT by sponging miR-130a-3p in glioma. *Cell. Physiol. Biochem.* **2018**, *50*, 233–245. [CrossRef] [PubMed]
233. Ren, J.; Fu, J.; Ma, T.; Yan, B.; Gao, R.; An, Z.; Wang, D. LncRNA H19-elevated LIN28B promotes lung cancer progression through sequestering miR-196b. *Cell Cycle* **2018**, *17*, 1372–1380. [CrossRef] [PubMed]
234. Ye, Y.; Guo, J.; Xiao, P.; Ning, J.; Zhang, R.; Liu, P.; Yu, W.; Xu, L.; Zhao, Y.; Yu, J. Macrophages-induced long noncoding RNA H19 up-regulation triggers and activates the miR-193b/MAPK1 axis and promotes cell aggressiveness in hepatocellular carcinoma. *Cancer Lett.* **2020**, *469*, 310–322. [CrossRef] [PubMed]
235. Lim, Y.W.S.; Xiang, X.; Garg, M.; Le, M.T.; Wong, A.L.-A.; Wang, L.; Goh, B.-C. The double-edged sword of H19 lncRNA: Insights into cancer therapy. *Cancer Lett.* **2020**, *500*, 253–262.
236. Ghafouri-Fard, S.; Esmaeili, M.; Taheri, M. H19 lncRNA: Roles in tumorigenesis. *Biomed. Pharmacother.* **2020**, *123*, 109774. [CrossRef] [PubMed]
237. Zhou, Y.; Fan, R.-G.; Qin, C.-L.; Jia, J.; Wu, X.-D.; Zha, W.-Z. LncRNA-H19 activates CDC42/PAK1 pathway to promote cell proliferation, migration and invasion by targeting miR-15b in hepatocellular carcinoma. *Genomics* **2019**, *111*, 1862–1872. [CrossRef]
238. Pan, W.Y.; Zeng, J.H.; Wen, D.Y.; Wang, J.Y.; Wang, P.P.; Chen, G.; Feng, Z.B. Oncogenic value of microRNA-15b-5p in hepatocellular carcinoma and a bioinformatics investigation. *Oncol Lett* **2019**, *17*, 1695–1713. [CrossRef]
239. Zhou, H.; Sun, L.; Wan, F. Molecular mechanisms of TUG1 in the proliferation, apoptosis, migration and invasion of cancer cells. *Oncol. Lett.* **2019**, *18*, 4393–4402. [CrossRef] [PubMed]
240. Shen, X.; Hu, X.; Mao, J.; Wu, Y.; Liu, H.; Shen, J.; Yu, J.; Chen, W. The long noncoding RNA TUG1 is required for TGF-β/TWIST1/EMT-mediated metastasis in colorectal cancer cells. *Cell Death Dis.* **2020**, *11*, 65. [CrossRef]
241. Wang, Z.; Liu, J.; Wang, R.; Wang, Q.; Liang, R.; Tang, J. Long Non-Coding RNA Taurine Upregulated Gene 1 (TUG1) Downregulation Constrains Cell Proliferation and Invasion through Regulating Cell Division Cycle 42 (CDC42) Expression Via MiR-498 in Esophageal Squamous Cell Carcinoma Cells. *Med Sci. Monit. Int. Med J. Exp. Clin. Res.* **2020**, *26*, e919714. [CrossRef]
242. Dai, Q.; Deng, J.; Zhou, J.; Wang, Z.; Yuan, X.-f.; Pan, S.; Zhang, H.-b. Long non-coding RNA TUG1 promotes cell progression in hepatocellular carcinoma via regulating miR-216b-5p/DLX2 axis. *Cancer Cell Int.* **2020**, *20*, 8. [CrossRef] [PubMed]
243. Zhu, J.; Shi, H.; Liu, H.; Wang, X.; Li, F. Long non-coding RNA TUG1 promotes cervical cancer progression by regulating the miR-138-5p-SIRT1 axis. *Oncotarget* **2017**, *8*, 65253. [CrossRef]
244. Yang, B.; Tang, X.; Wang, Z.; Sun, D.; Wei, X.; Ding, Y. TUG1 promotes prostate cancer progression by acting as a ceRNA of miR-26a. *Biosci. Rep.* **2018**, *38*, BSR20180677. [CrossRef]
245. Islam, F.; Gopalan, V.; Law, S.; Tang, J.C.-O.; Kwok-Wah, C.; Alfred King-Yin, L. MiR-498 in esophageal squamous cell carcinoma: Clinicopathological impacts and functional interactions. *Hum. Pathol.* **2017**, *62*, 141–151. [CrossRef] [PubMed]
246. Zheng, C.; Yu, S. Expression and gene regulatory network of SNHG1 in hepatocellular carcinoma. *BMC Med. Genom.* **2021**, *14*, 28. [CrossRef] [PubMed]
247. Huang, D.; Wei, Y.; Zhu, J.; Wang, F. Long non-coding RNA SNHG1 functions as a competitive endogenous RNA to regulate PDCD4 expression by sponging miR-195-5p in hepatocellular carcinoma. *Gene* **2019**, *714*, 143994. [CrossRef]
248. Liu, Y.; Yang, Y.; Li, L.; Liu, Y.; Geng, P.; Li, G.; Song, H. LncRNA SNHG1 enhances cell proliferation, migration, and invasion in cervical cancer. *Biochem. Cell Biol.* **2018**, *96*, 38–43. [CrossRef]
249. Li, J.; Zhang, Z.; Xiong, L.; Guo, C.; Jiang, T.; Zeng, L.; Li, G.; Wang, J. SNHG1 lncRNA negatively regulates miR-199a-3p to enhance CDK7 expression and promote cell proliferation in prostate cancer. *Biochem. Biophys. Res. Commun.* **2017**, *487*, 146–152. [CrossRef]

250. Cui, Y.; Zhang, F.; Zhu, C.; Geng, L.; Tian, T.; Liu, H. Upregulated lncRNA SNHG1 contributes to progression of non-small cell lung cancer through inhibition of miR-101-3p and activation of Wnt/β-catenin signaling pathway. *Oncotarget* **2017**, *8*, 17785. [CrossRef]
251. Chen, Y.; Sheng, H.G.; Deng, F.M.; Cai, L.L. Downregulation of the long noncoding RNA SNHG1 inhibits tumor cell migration and invasion by sponging miR-195 through targeting Cdc42 in oesophageal cancer. *Kaohsiung J. Med. Sci.* **2021**, *37*, 181–191. [CrossRef]
252. Gao, X.; Lu, M.; Xu, W.; Liu, C.; Wu, J. miR-195 inhibits esophageal cancer cell proliferation and promotes apoptosis by downregulating YAP1. *Int. J. Clin. Exp. Pathol.* **2019**, *12*, 275–281.
253. Jin, B.; Jin, H.; Wu, H.B.; Xu, J.J.; Li, B. Long non-coding RNA SNHG15 promotes CDK14 expression via miR-486 to accelerate non-small cell lung cancer cells progression and metastasis. *J. Cell. Physiol.* **2018**, *233*, 7164–7172. [CrossRef]
254. Jiang, H.; Li, T.; Qu, Y.; Wang, X.; Li, B.; Song, J.; Sun, X.; Tang, Y.; Wan, J.; Yu, Y. Long non-coding RNA SNHG15 interacts with and stabilizes transcription factor Slug and promotes colon cancer progression. *Cancer Lett.* **2018**, *425*, 78–87. [CrossRef] [PubMed]
255. Sun, X.; Bai, Y.; Yang, C.; Hu, S.; Hou, Z.; Wang, G. Long noncoding RNA SNHG15 enhances the development of colorectal carcinoma via functioning as a ceRNA through miR-141/SIRT1/Wnt/beta-catenin axis. *Artif Cells Nanomed Biotechnol.* **2019**, *47*, 2536–2544. [CrossRef]
256. Kong, Q.; Qiu, M. Long noncoding RNA SNHG15 promotes human breast cancer proliferation, migration and invasion by sponging miR-211-3p. *Biochem. Biophys. Res. Commun.* **2018**, *495*, 1594–1600. [CrossRef] [PubMed]
257. Ma, Z.; Huang, H.; Wang, J.; Zhou, Y.; Pu, F.; Zhao, Q.; Peng, P.; Hui, B.; Ji, H.; Wang, K. Long non-coding RNA SNHG15 inhibits P15 and KLF2 expression to promote pancreatic cancer proliferation through EZH2-mediated H3K27me3. *Oncotarget* **2017**, *8*, 84153. [CrossRef] [PubMed]
258. Chen, S.-x.; Yin, J.-f.; Lin, B.-c.; Su, H.-f.; Zheng, Z.; Xie, C.-y.; Fei, Z.-h. Upregulated expression of long noncoding RNA SNHG15 promotes cell proliferation and invasion through regulates MMP2/MMP9 in patients with GC. *Tumor Biol.* **2016**, *37*, 6801–6812. [CrossRef]
259. Wu, D.-M.; Wang, S.; Wen, X.; Han, X.-R.; Wang, Y.-J.; Shen, M.; Fan, S.-H.; Zhang, Z.-F.; Shan, Q.; Li, M.-Q.; et al. LncRNA SNHG15 acts as a ceRNA to regulate YAP1-Hippo signaling pathway by sponging miR-200a-3p in papillary thyroid carcinoma. *Cell Death Dis.* **2018**, *9*, 947. [CrossRef]
260. Ma, Y.; Xue, Y.; Liu, X.; Qu, C.; Cai, H.; Wang, P.; Li, Z.; Li, Z.; Liu, Y. SNHG15 affects the growth of glioma microvascular endothelial cells by negatively regulating miR-153. *Oncol. Rep.* **2017**, *38*, 3265–3277. [CrossRef]
261. Zhao, G.; Zhang, Y.; Zhao, Z.; Cai, H.; Zhao, X.; Yang, T.; Chen, W.; Yao, C.; Wang, Z.; Wang, Z.; et al. MiR-153 reduces stem cell-like phenotype and tumor growth of lung adenocarcinoma by targeting Jagged1. *Stem Cell Res. Ther.* **2020**, *11*, 170. [CrossRef]
262. Bishop, A.L.; Hall, A. Rho GTPases and their effector proteins. *Biochem. J.* **2000**, *348 Pt 2*, 241–255. [CrossRef] [PubMed]
263. Prudnikova, T.Y.; Rawat, S.J.; Chernoff, J. Molecular Pathways: Targeting the Kinase Effectors of RHO-Family GTPases. *Clin. Cancer Res.* **2015**, *21*, 24–29. [CrossRef] [PubMed]
264. Tang, Y.; He, Y.; Zhang, P.; Wang, J.; Fan, C.; Yang, L.; Xiong, F.; Zhang, S.; Gong, Z.; Nie, S.; et al. LncRNAs regulate the cytoskeleton and related Rho/ROCK signaling in cancer metastasis. *Mol. Cancer* **2018**, *17*, 77. [CrossRef] [PubMed]
265. Hedman, A.C.; Smith, J.M.; Sacks, D.B. The biology of IQGAP proteins: Beyond the cytoskeleton. *EMBO Rep.* **2015**, *16*, 427–446. [CrossRef] [PubMed]
266. Liu, C.-A.; Wang, M.-J.; Chi, C.-W.; Wu, C.-W.; Chen, J.-Y. Rho/Rhotekin-mediated NF-κB activation confers resistance to apoptosis. *Oncogene* **2004**, *23*, 8731–8742. [CrossRef] [PubMed]
267. Amin, E.; Dubey, B.N.; Zhang, S.C.; Gremer, L.; Dvorsky, R.; Moll, J.M.; Taha, M.S.; Nagel-Steger, L.; Piekorz, R.P.; Somlyo, A.V.; et al. Rho-kinase: Regulation, (dys)function, and inhibition. *Biol. Chem.* **2013**, *394*, 1399–1410. [CrossRef] [PubMed]
268. Wang, Y.; Zhang, Y.; Yang, T.; Zhao, W.; Wang, N.; Li, P.; Zeng, X.; Zhang, W. Long non-coding RNA MALAT1 for promoting metastasis and proliferation by acting as a ceRNA of miR-144-3p in osteosarcoma cells. *Oncotarget* **2017**, *8*, 59417–59434. [CrossRef]
269. Morlando, M.; Fatica, A. Alteration of Epigenetic Regulation by Long Noncoding RNAs in Cancer. *Int. J. Mol. Sci.* **2018**, *19*, 570. [CrossRef]
270. Chen, J.; Wang, Y.; Wang, C.; Hu, J.-F.; Li, W. LncRNA Functions as a New Emerging Epigenetic Factor in Determining the Fate of Stem Cells. *Front. Genet.* **2020**, *11*, 277. [CrossRef]
271. Hanly, D.J.; Esteller, M.; Berdasco, M. Interplay between long non-coding RNAs and epigenetic machinery: Emerging targets in cancer? *Philos. Trans. R. Soc. B Biol. Sci.* **2018**, *373*, 20170074. [CrossRef] [PubMed]
272. Engreitz, J.M.; Pandya-Jones, A.; McDonel, P.; Shishkin, A.; Sirokman, K.; Surka, C.; Kadri, S.; Xing, J.; Goren, A.; Lander, E.S.; et al. The Xist lncRNA exploits three-dimensional genome architecture to spread across the X chromosome. *Science* **2013**, *341*, 1237973. [CrossRef]
273. Tripathi, V.; Ellis, J.D.; Shen, Z.; Song, D.Y.; Pan, Q.; Watt, A.T.; Freier, S.M.; Bennett, C.F.; Sharma, A.; Bubulya, P.A.; et al. The nuclear-retained noncoding RNA MALAT1 regulates alternative splicing by modulating SR splicing factor phosphorylation. *Mol. Cell* **2010**, *39*, 925–938. [CrossRef] [PubMed]
274. Yang, X.; Liu, M.; Li, M.; Zhang, S.; Hiju, H.; Sun, J.; Mao, Z.; Zheng, M.; Feng, B. Epigenetic modulations of noncoding RNA: A novel dimension of Cancer biology. *Mol. Cancer* **2020**, *19*, 64. [CrossRef] [PubMed]
275. Li, Z.; Weng, H.; Su, R.; Weng, X.; Zuo, Z.; Li, C.; Huang, H.; Nachtergaele, S.; Dong, L.; Hu, C.; et al. FTO Plays an Oncogenic Role in Acute Myeloid Leukemia as a N(6)-Methyladenosine RNA Demethylase. *Cancer Cell* **2017**, *31*, 127–141. [CrossRef] [PubMed]

276. Ni, W.; Yao, S.; Zhou, Y.; Liu, Y.; Huang, P.; Zhou, A.; Liu, J.; Che, L.; Li, J. Long noncoding RNA GAS5 inhibits progression of colorectal cancer by interacting with and triggering YAP phosphorylation and degradation and is negatively regulated by the m(6)A reader YTHDF3. *Mol. Cancer* **2019**, *18*, 143. [CrossRef] [PubMed]
277. Khorkova, O.; Wahlestedt, C. Oligonucleotide therapies for disorders of the nervous system. *Nat. Biotechnol.* **2017**, *35*, 249–263. [CrossRef] [PubMed]
278. Liang, Y.; Chen, X.; Wu, Y.; Li, J.; Zhang, S.; Wang, K.; Guan, X.; Yang, K.; Bai, Y. LncRNA CASC9 promotes esophageal squamous cell carcinoma metastasis through upregulating LAMC2 expression by interacting with the CREB-binding protein. *Cell Death Differ.* **2018**, *25*, 1980–1995. [CrossRef] [PubMed]
279. Vaidya, A.M.; Sun, Z.; Ayat, N.; Schilb, A.; Liu, X.; Jiang, H.; Sun, D.; Scheidt, J.; Qian, V.; He, S.; et al. Systemic Delivery of Tumor-Targeting siRNA Nanoparticles against an Oncogenic LncRNA Facilitates Effective Triple-Negative Breast Cancer Therapy. *Bioconj. Chem.* **2019**, *30*, 907–919. [CrossRef] [PubMed]
280. Pang, H.; Ren, Y.; Li, H.; Chen, C.; Zheng, X. LncRNAs linc00311 and AK141205 are identified as new regulators in STAT3-mediated neuropathic pain in bCCI rats. *Eur. J. Pharmacol.* **2020**, *868*, 172880. [CrossRef]
281. Crooke, S.T. Molecular mechanisms of antisense oligonucleotides. *Nucleic Acid Ther.* **2017**, *27*, 70–77. [CrossRef]
282. Arun, G.; Diermeier, S.; Akerman, M.; Chang, K.-C.; Wilkinson, J.E.; Hearn, S.; Kim, Y.; MacLeod, A.R.; Krainer, A.R.; Norton, L. Differentiation of mammary tumors and reduction in metastasis upon Malat1 lncRNA loss. *Genes Dev.* **2016**, *30*, 34–51. [CrossRef]
283. Özeş, A.R.; Wang, Y.; Zong, X.; Fang, F.; Pilrose, J.; Nephew, K.P. Therapeutic targeting using tumor specific peptides inhibits long non-coding RNA HOTAIR activity in ovarian and breast cancer. *Sci. Rep.* **2017**, *7*, 894. [CrossRef] [PubMed]
284. Taiana, E.; Favasuli, V.; Ronchetti, D.; Todoerti, K.; Pelizzoni, F.; Manzoni, M.; Barbieri, M.; Fabris, S.; Silvestris, I.; Cantafio, M.E.G. Long non-coding RNA NEAT1 targeting impairs the DNA repair machinery and triggers anti-tumor activity in multiple myeloma. *Leukemia* **2020**, *34*, 234–244. [CrossRef] [PubMed]
285. Amodio, N.; Stamato, M.A.; Juli, G.; Morelli, E.; Fulciniti, M.; Manzoni, M.; Taiana, E.; Agnelli, L.; Cantafio, M.E.G.; Romeo, E. Drugging the lncRNA MALAT1 via LNA gapmeR ASO inhibits gene expression of proteasome subunits and triggers anti-multiple myeloma activity. *Leukemia* **2018**, *32*, 1948–1957. [CrossRef] [PubMed]
286. Li, W.; Guo, B.; Li, X.; Zhou, Y.; Huang, S.; Rouskas, G.N. A large-scale nesting ring multi-chip architecture for manycore processor systems. *Opt. Switch. Netw.* **2019**, *31*, 183–192. [CrossRef]
287. Liu, B.; Xu, G.; Rong, S.; Santillan, D.A.; Santillan, M.K.; Snetselaar, L.G.; Bao, W. National Estimates of e-Cigarette Use Among Pregnant and Nonpregnant Women of Reproductive Age in the United States, 2014–2017. *JAMA Pediatrics* **2019**, *173*, 600–602. [CrossRef]
288. Yao, Y.E.; Li, Q.C. Research progress of relationship between notch signaling pathway and asthma. *J Pr. Med* **2019**, *35*, 315–317.
289. Chen, Q.; Cai, J.; Wang, Q.; Wang, Y.; Liu, M.; Yang, J.; Zhou, J.; Kang, C.; Li, M.; Jiang, C. Long noncoding RNA NEAT1, regulated by the EGFR pathway, contributes to glioblastoma progression through the WNT/β-catenin pathway by scaffolding EZH2. *Clin. Cancer. Res.* **2018**, *24*, 684–695. [CrossRef]
290. Pedram Fatemi, R.; Salah-Uddin, S.; Modarresi, F.; Khoury, N.; Wahlestedt, C.; Faghihi, M.A. Screening for small-molecule modulators of long noncoding RNA-protein interactions using AlphaScreen. *J. Biomol. Screen.* **2015**, *20*, 1132–1141. [CrossRef]
291. Abulwerdi, F.A.; Xu, W.; Ageeli, A.A.; Yonkunas, M.J.; Arun, G.; Nam, H.; Schneekloth, J.S.; Dayie, T.K.; Spector, D.; Baird, N.; et al. Selective Small-Molecule Targeting of a Triple Helix Encoded by the Long Noncoding RNA, MALAT1. *ACS Chem. Biol.* **2019**, *14*, 223–235. [CrossRef]
292. Geng, W.; Guo, X.; Zhang, L.; Ma, Y.; Wang, L.; Liu, Z.; Ji, H.; Xiong, Y. Resveratrol inhibits proliferation, migration and invasion of multiple myeloma cells via NEAT1-mediated Wnt/β-catenin signaling pathway. *Biomed. Pharmacother.* **2018**, *107*, 484–494. [CrossRef] [PubMed]
293. Damase, T.R.; Sukhovershin, R.; Boada, C.; Taraballi, F.; Pettigrew, R.I.; Cooke, J.P. The Limitless Future of RNA Therapeutics. *Front. Bioeng. Biotechnol.* **2021**, *9*, 628137. [CrossRef] [PubMed]
294. Dhawan, M.S.; Aggarwal, R.R.; Boyd, E.; Comerford, K.; Zhang, J.; Méndez, B.; Valenzuela, P.; Grabowsky, J.; Thomas, S.; Munster, P.N. Phase 1 study of ANDES-1537: A novel antisense oligonucleotide against non-coding mitochondrial DNA in advanced solid tumors. *J. Clin. Oncol.* **2018**, *36*, 2557. [CrossRef]
295. Chan, C.W.; Khachigian, L.M. DNAzymes and their therapeutic possibilities. *Intern. Med. J.* **2009**, *39*, 249–251. [CrossRef]
296. Quinn, J.J.; Chang, H.Y. Unique features of long non-coding RNA biogenesis and function. *Nat. Rev. Genet.* **2016**, *17*, 47–62. [CrossRef] [PubMed]
297. Bhan, A.; Soleimani, M.; Mandal, S.S. Long Noncoding RNA and Cancer: A New Paradigm. *Cancer Res.* **2017**, *77*, 3965–3981. [CrossRef] [PubMed]

Chapter VIII. Modulating PAK1: Accessory Proteins as Promising Therapeutic Targets

Authors: Amin Mirzaiebadizi, Rana Shafabakhsh, Mohammad Reza Ahmadian

DOI: 10.3390/biom15020242

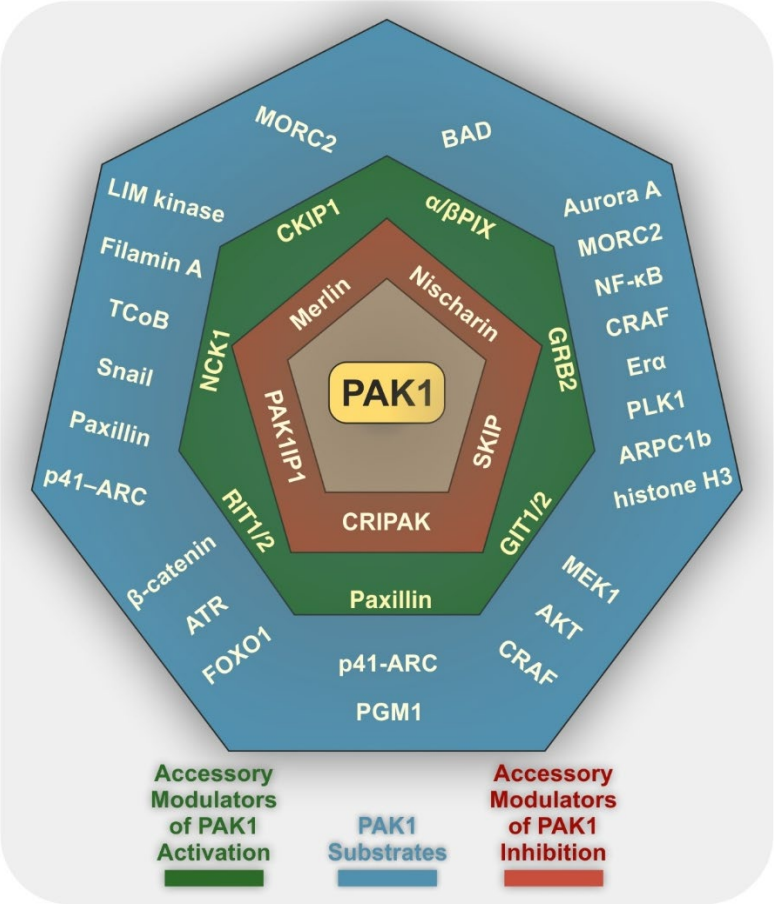

Status: Published

Journal: *Biomolecules*
JIF: 4.8
Contribution: ≈70%

A.M. Coordinated and drafted the manuscript. He designed and prepared all graphical schematics. A.M. performed in-depth proofreading and carried out the final review and editing of the manuscript.

biomolecules

MDPI

Review

Modulating PAK1: Accessory Proteins as Promising Therapeutic Targets

Amin Mirzaiebadizi [1], Rana Shafabakhsh [2] and Mohammad Reza Ahmadian [1,*]

[1] Institute of Biochemistry and Molecular Biology II, Medical Faculty, Heinrich Heine University Düsseldorf, 40225 Düsseldorf, Germany; amin.mirzaiebadizi@hhu.de
[2] Institute for Experimental Molecular Imaging, RWTH Aachen University Hospital, 52074 Aachen, Germany; rshafabakhsh@ukaachen.de
* Correspondence: reza.ahmadian@hhu.de

Abstract: The p21-activated kinase (PAK1), a serine/threonine protein kinase, is critical in regulating various cellular processes, including muscle contraction, neutrophil chemotaxis, neuronal polarization, and endothelial barrier function. Aberrant PAK1 activity has been implicated in the progression of several human diseases, including cancer, heart disease, and neurological disorders. Increased PAK1 expression is often associated with poor clinical prognosis, invasive tumor characteristics, and therapeutic resistance. Despite its importance, the cellular mechanisms that modulate PAK1 function remain poorly understood. Accessory proteins, essential for the precise assembly and temporal regulation of signaling pathways, offer unique advantages as therapeutic targets. Unlike core signaling components, these modulators can attenuate aberrant signaling without completely abolishing it, potentially restoring signaling to physiological levels. This review highlights PAK1 accessory proteins as promising and novel therapeutic targets, opening new horizons for disease treatment.

Keywords: PAK1; p21-activated kinase; accessory proteins; scaffold proteins; adaptor proteins; α/βPIX; CKIP1; GIT1; GRB2; NCK1; paxillin; RIT1; accessory inhibitors; merlin; nischarin; PAK1P1

Academic Editors: Avisek Majumder, Shabana Bano and Kasturi Nayak

Received: 16 January 2025
Revised: 3 February 2025
Accepted: 5 February 2025
Published: 7 February 2025

Citation: Mirzaiebadizi, A.; Shafabakhsh, R.; Ahmadian, M.R. Modulating PAK1: Accessory Proteins as Promising Therapeutic Targets. *Biomolecules* **2025**, *15*, 242. https://doi.org/10.3390/biom15020242

1. General Introduction

PAK1 is a key member of the PAK family of serine/threonine protein kinases, which consists of type I (PAK1–3) and type II (PAK4–6) PAKs, each with distinct regulatory mechanisms. As an effector of the RHO GTPases RAC1 and CDC42 [1], PAK1 plays a pivotal role in cellular processes related to cytoskeletal remodeling, including cell contraction, adhesion, motility, and polarity [2–6]. Once activated, PAK1 controls multiple proliferation and survival pathways, including MAPK, AKT, Wnt/β-catenin, and NF-κB [4]. Importantly, the PAK1 function is tightly regulated by its precise spatiotemporal localization at the plasma membrane, which depends on its recruitment and activation [7].

Amplification of the PAK1 gene and high levels of PAK1 protein are often associated with poor clinical prognosis, invasive tumor characteristics, and resistance to therapy [4,8,9]. Mutations in upstream GTPases, such as RAC1 [10], RAC2 [11], and RAS [12], can lead to the hyperactivation of PAK1, linking oncogenic signaling to phenotypic changes in cancer cells. In addition to cancer progression, PAK1 functions have been implicated in aging, neurodevelopmental disorders, liver disease, immune system abnormalities, and cardioprotection [13–18]. Given these diverse roles, exploring novel strategies to inhibit PAK1 is critical, particularly in light of the genetic evidence and the observed acute toxicities

associated with various types of PAK1 inhibitors. The next sections will discuss several aspects of PAK1 regulation, modulation, and functions.

2. Mechanism of PAK1 Activation

PAK1 is activated by the CDC42 and RAC groups of small GTPases through several upstream signals, including estrogen, insulin, EGF, PDGF, IGF-1, and thrombin [19–21]. PAK1 (60.6 kDa; 545 amino acids or aa) consists of two distinct regions (Figure 1A) [22]. The conserved N-terminal non-catalytic region contains two overlapping domains, namely the p21-binding domain (PBD; aa 67–113) and the autoinhibitory domain (AID; aa 83–149). It also contains three conserved proline-rich regions (aa 12–18, 40–45, and 186–203) that serve as binding sites for several accessory proteins. An integral part of the PBD is the CDC42/RAC interactive binding (CRIB; aa 75–90) motif, where the binding of CDC42 or RAC1 initiates PAK1 activation [23,24]. This activation likely requires the association of PAK1 with the acidic phospholipid of the plasma membrane via a basic region (BR; aa 48–72) [25]. The C-terminal region of PAK1 contains a conserved Ser/Thr kinase domain (aa 250–520) with a single phosphorylation site (Thr-423) that is phosphorylated upon PAK1 activation [26].

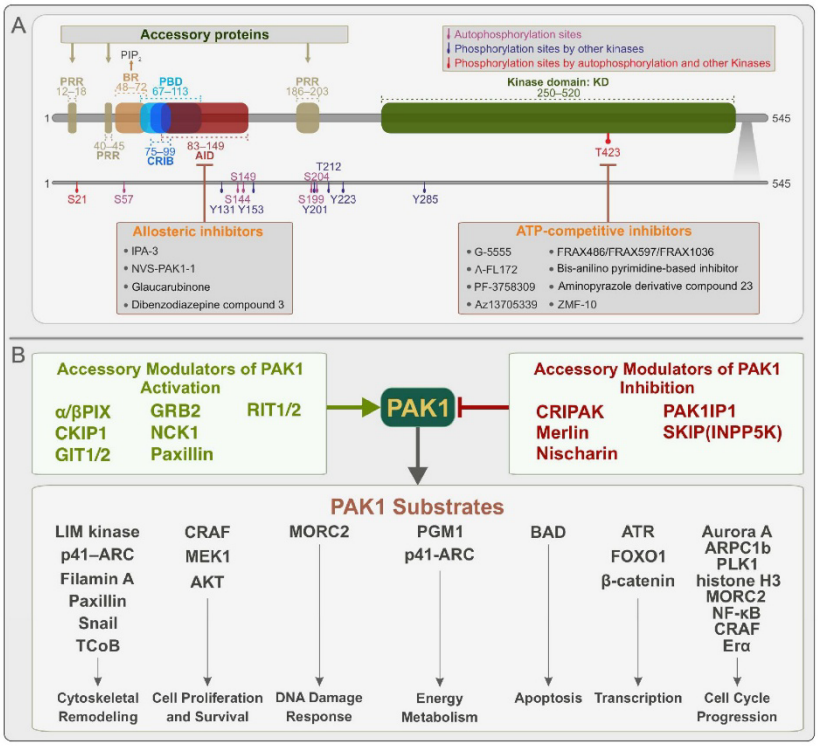

Figure 1. Overview of PAK1 domain organization, activation, inhibition, and interaction sites and key modulators and substrates. (**A**) Schematic representation of the domain organization of PAK1 (60.6 kDa; 545 amino acids), highlighting modulation and inhibition sites. See the text for further details. (**B**) Summary of accessory proteins that act as modulators of PAK1 activity and a diverse set of PAK1 substrates involved in maintaining cellular homeostasis.

Inactive PAK1 has been proposed to exist in an asymmetric trans-autoinhibited dimeric form [27–29], in which the AID of one PAK1 molecule contacts the kinase domain of

the other, stabilizing the catalytic site in an autoinhibited state. The recruitment and activation of PAK1 at the plasma membrane require interactions at two sites, namely PBD binding with membrane-associated CDC42 or RAC1 and the BR binding with acidic phospholipids, particularly phosphatidylinositol-4,5-bisphosphate [25]. These events lead to the release of AID from the kinase domain, dimer/monomer equilibrium, and subsequent phosphorylation at Thr423 [30]. Once activated, PAK1 phosphorylates its substrates in a context-dependent manner that is tightly modulated by accessory proteins (Figure 1B).

Phosphorylation plays a critical role in stabilizing the active conformation of PAK1 and modulating its downstream signaling functions. In addition to phosphorylation sites within its activation loop, multiple phosphorylation events occur in the N-terminal non-catalytic region, affecting PAK1 activity and protein interactions [31]. PAK1 phosphorylation sites can be divided into three groups, namely (i) autophosphorylation sites, where PAK1 phosphorylates itself to regulate activation and substrate interactions (Ser21, Ser57, Ser144, Ser149, Ser199, and Ser204); (ii) phosphorylation sites modified by other kinases, including Tyr131, phosphorylated by SRC family kinases; Tyr153, Tyr201, and Tyr285, phosphorylated by JAK2; Tyr223, phosphorylated by CK2; and Thr212, phosphorylated by p35/Cdk5, Cdc2, and Erk1/2; and (iii) sites phosphorylated by both PAK1 and external kinases, such as Ser21, which is phosphorylated by AKT, PKG, PAK1, and Thr423, which is phosphorylated by PDK1 and PAK1 [31–36]. The activation state of PAK1 is further regulated by protein phosphatases, such as PP2A, which counteract phosphorylation events and fine-tune its activity [37]. These regulatory mechanisms provide the spatiotemporal control of PAK1 signaling, allowing for the precise modulation of cellular processes (Figure 1A).

PAK1 is susceptible to inhibition by a number of ATP-competitive and allosteric inhibitors that have been developed to counteract its dysregulated activity in diseases such as cancer [38–40]. ATP-competitive inhibitors occupy the ATP-binding pocket within the kinase domain, thereby preventing ATP access and blocking its catalytic activity. However, the development of highly selective inhibitors for PAK1 remains challenging due to the flexibility of its ATP-binding cleft and the significant sequence similarity it shares with other PAK family members [38]. Despite these challenges, several ATP-competitive inhibitors have been developed to target PAK1 activity, including G-5555, FL172, PF-3758309, AZ13705339, FRAX compounds, bis-anilinopyrimidine-based inhibitors, the aminopyrazole derivative compound 23, and ZMF-10 [38–40]. Allosteric inhibitors, on the other hand, bind to regulatory regions outside the ATP-binding pocket and induce conformational changes that interfere with PAK1 activation. These inhibitors often achieve greater specificity within the kinome by targeting regions that are less conserved among kinases. However, their potency is generally lower than that of ATP-competitive inhibitors because these binding sites are shallower and contain fewer key residues that contribute to strong inhibitor interactions [38]. Among the known allosteric inhibitors, IPA-3, NVS-PAK1-1, glaucarubinone, and the dibenzodiazepine compound 3 prevent PAK1 activation by interfering with its autoregulatory mechanism and upstream interactions [38–40]. The development of these inhibitors highlights the therapeutic potential of targeting PAK1 in diseases where its dysregulation plays a key role [40]. The classification of PAK1 inhibitors and their binding sites on PAK1 are shown in Figure 1A.

3. PAK1 Substrates

PAK1 exerts its activity primarily by phosphorylating a broad spectrum of substrates typically involved in maintaining cellular homeostasis. These substrates regulate processes such as energy production and consumption, the maintenance of genetic integrity, gene expression, the organization of cellular structures, movement, growth, programmed cell death, and differentiation (Figure 1) [4,41].

Energy metabolism: PAK1 phosphorylates and enhances the enzymatic activity of phosphoglucomutase 1 (PGM1), an important regulatory enzyme in cellular glucose utilization and energy homeostasis [42]. PGM1 catalyzes the reversible conversion between glucose-1-phosphate and glucose-6-phosphate. The actin polymerizing ARP2/3 subunit p41ARC is another PAK1 substrate in skeletal muscle cells [43]. It has been suggested that p41ARC links NWASP-cortactin-mediated actin polymerization and GLUT4 translocation to the plasma membrane by vesicle exocytosis.

DNA damage response: Microrchidia CW-type zinc finger 2 (MORC2) associates with chromatin and is phosphorylated by PAK1 at serine 739, promoting the PAK1 phosphorylation-dependent induction of gamma-H2AX, a critical step in the cellular response to DNA damage [44]. PAK1 is activated in response to UV-B radiation and then translocates to the nucleus to bind C-FOS, which acts as a transcriptional regulator of the ataxia-telangiectasia and RAD3-related protein (ATR) gene [45]. It has been reported that TCL/RHOJ-mediated activation of PAK1 in response to drug-induced DNA damage can suppress ATR [46].

Transcription: Nuclear PAK1 binds to the promoter region of the DNA repair kinase ATR through C-Fos, thereby regulating its transcription [45]. Nuclear PAK1 has also been shown to drive the transcription of fibronectin, which is critical for promoting the growth and migration of pancreatic cancer cells [47]. PAK1 phosphorylates FOXO1 to prevent its nuclear translocation and transcriptional activity [48]. PAK1-mediated phosphorylation stabilizes β-catenin and promotes TCF/LEF-dependent transcriptional activity [49,50].

Cell cycle progression: PAK1 contributes significantly to cell cycle progression by phosphorylating several proteins, including Aurora A, ARPC1b, PLK1, histone H3, MORC2, NFκB, and CRAF [40]. Increased expression of PAK1 in breast cancer cells increases cyclin D1 mRNA and protein levels and its nuclear accumulation [51]. Activated PAK1 phosphorylates and activates estrogen receptor-α (ERα), upregulates cyclin D1 expression through the NFκB pathway, and controls cell cycle progression [51]. In addition, CDK4 forms a complex with PAK1 in response to monocyte chemotactic protein 1 [52], activating the cyclin D1-CDK6-CDK4-PAK1 axis, which controls smooth muscle cell migration and proliferation. Silencing of PAK1 has been shown to reduce cyclin E and CDK2 expression, leading to cell cycle arrest at the G1 and S phases in hepatocellular carcinoma [53]. PAK1 also appears to be involved in the phosphorylation of retinoblastoma (Rb) and the activation of E2F transcription factors [54].

Cytoskeletal remodeling: PAK1 phosphorylates several key factors involved in cytoskeletal remodeling, including LIM kinase, p41–ARC, Filamin A, Paxillin, snail, and tubulin cofactor B (TCoB), thereby controlling various cellular processes. LIM kinase phosphorylates cofilin to prevent actin depolymerization [55,56]. The p41–ARC subunit of the Arp2/3 complex promotes actin nucleation and cell motility [57,58]. Filamin A, a filamentous actin cross-linking protein, anchors various cytoskeletal proteins and regulates cell adhesion and migration [59–62]. Paxillin phosphorylation triggers the formation of adhesion junctions and focal adhesions, thereby controlling cell contractility and motility [63–65]. PAK1 negatively modulates myosin light-chain phosphorylation by inhibiting myosin phosphatase target subunit 1 (MYPT1), increasing muscle contraction [66–68]. Snail phosphorylation by PAK1 controls epithelial cell permeability [69] and contributes to epithelial–mesenchymal transition (EMT) [70]. Phosphorylated by cyclin B1/CDK2, PAK1 controls microtubule reorganization by activating TCoB, a protein responsible for tubulin heterodimer assembly [71] and by inactivating stathmin, a microtubule destabilizing factor [72–74]. PAK1 regulates microtubule organization and spindle positioning during the metaphase-to-anaphase transition in conjunction with its activity against Aurora A, TACC3, and LIMK1 [66].

Cell proliferation and survival: PAK1 promotes cross-talk with RAF and PI3K signaling networks and contributes to cell proliferation and survival [41]. It phosphorylates CRAF and MEK1 and enhances ERK activity [75–78]. As a scaffolding protein, PAK1 modulates the PI3K-PDK1-AKT-mTOR pathway by facilitating the recruitment of AKT to the plasma membrane via PDK1, leading to AKT activation [79].

Apoptosis: PAK1 can interfere with the interaction of the BCL-2-associated agonist of cell death (BAD) with BCL2 and the induction of apoptosis in two ways [80]. PAK1 phosphorylates BAD directly [81] or indirectly through the phosphorylation of CRAF and its translocation to the mitochondria [80]. The shorter isoform of the PITSLRE protein kinase family, p110C, has been shown to bind to PAK1 and prevent BAD phosphorylation [82].

4. Accessory Proteins for PAK1

Accessory proteins are modulatory proteins that facilitate the spatiotemporal organization of signaling complexes during processing but are not directly involved in signal transduction [83]. They possess a variety of protein–protein interaction domains, motifs, and inherently disordered regions (IDRs) that allow them to interact with and link different signaling molecules. Thus, accessory proteins regulate and enhance signaling by directing the local assembly of protein complexes through multiple interactions. This is achieved either by reducing the dimensionality of the interactions or by increasing the local levels of interacting proteins [84]. Scaffolding, adaptor, anchoring, and docking proteins are the four major groups that can be categorized according to their structure and how they perform their functions [85].

In addition, accessory proteins can control interference between different signaling pathways, increase the residence time of proteins on the membrane, stimulate nanocluster formation, sequester effectors to inhibit their activation, and determine cell type specificity and subcellular localization of signaling cassettes. Because of their modulatory properties, accessory proteins can play critical roles in various situations. The expression of accessory proteins is tightly regulated but is often aberrant in malignant tumors (see below). Targeting accessory modulators rather than the core components of disease-relevant pathways has several advantages. Most importantly, this approach reduces abnormal signaling to physiological levels through strong suppression without eliminating them. This shifts the focus from the "inhibition" to "attenuation" of signaling [86].

The regulation of the subcellular localization of PAK1 is important in controlling its functions. For example, various stimuli localize and activate PAK1 at focal adhesion complexes and leading-edge membrane ruffles [87,88]. Below, we highlight the accessory proteins involved in PAK1 modulation and their roles in various types of cancers and developmental disorders, opening new avenues for therapeutic intervention, with these candidates emerging as promising targets. Based on their roles, accessory proteins for PAK1 can be classified into two groups, comprising modulators of PAK1 activation and modulators of PAK1 inhibition (Figure 1).

4.1. Modulators of PAK1 Activation

Many signaling molecules, including αPIX, βPIX, CKIP1, GIT1, GIT2, GRB2, NCK1, Paxillin, RIT1, and RIT2, positively modulate PAK1 activity (Figure 2).

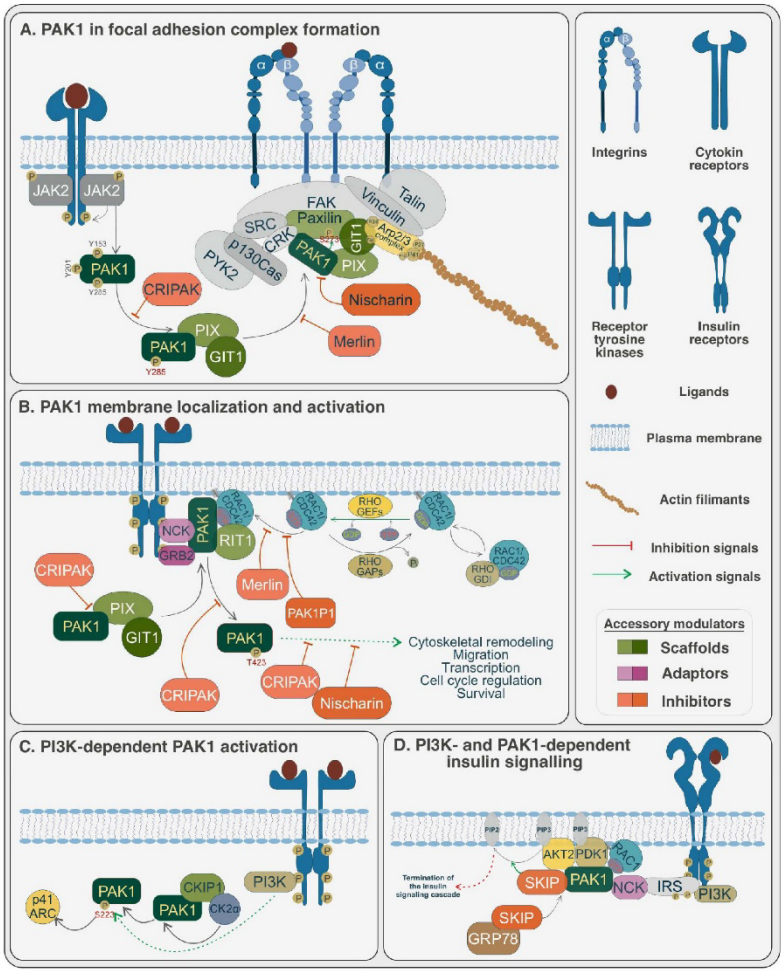

Figure 2. Schematic illustration of PAK1 modulation by accessory proteins. (**A**) PAK1 and focal adhesion complex formation: PAK1 interacts with scaffolding proteins such as αPIX and GIT and focal adhesion components like Paxillin to regulate adhesion assembly and cytoskeletal remodeling. Negative regulators, including Nischarin, CRIPAK, and Merlin, interfere with PAK1 binding, thereby inhibiting focal adhesion stability and PAK1 activity. (**B**) PAK1 membrane localization, activation, and function: PAK1 is recruited to the plasma membrane via adaptor proteins such as NCK and GRB2 and becomes activated through its interaction with GTP-bound RAC1. Once activated, PAK1 participates in various downstream pathways. Additional regulatory proteins, including CRIPAK, Nischarin, Merlin, and PAK1IP1, limit PAK1 activation or its kinase activity to maintain balanced signaling. (**C**) PI3K-dependent activation of PAK1: PAK1 is phosphorylated by the CK2α-CKIP-1 complex in a PI3K-dependent manner, which promotes its activity at membrane ruffles and enables the phosphorylation of substrates such as p41-Arc, driving cell signaling. (**D**) PI3K- and PAK1-dependent insulin signaling: Insulin receptor activation leads to IRS1 phosphorylation and PAK1 membrane recruitment, mediated by NCK. Active PAK1 interacts with PDK1 and AKT2 at the membrane, while the SKIP-GRP78 complex translocates from the ER to the membrane. SKIP binds PAK1, converting PIP3 to PIP2 and terminating the insulin signaling cascade.

α/βPIX: αPIX (also called COOL2 or ARHGEF6; 87.5 kDa; 776 amino acids) and βPIX (also called COOL1 or ARHGEF7; 90.0 kDa; 803 amino acids) are members of the DBL family RHOGEFs [19]. Each consists of a calponin homology (CH), an SH3 domain, a DBL homology (DH), a pleckstrin homology (PH), a proline-rich domain (PRD), a CAT/GIT binding domain (CBD), and a coiled-coil (CC) region. α/βPIX are generally accepted as GEFs for RAC1 and CDC42. Extensive biochemical analysis revealed that some DBL family proteins, including α/βPIX DH-PH tandems, lack GEF activity, suggesting that these proteins act as scaffolding proteins [89]. Accordingly, αPIX and βPIX interact with several proteins, including PAK1 [90], PAK4 [91], GIT1 [92], integrin-linked kinase (ILK), focal adhesion-associated β-Parvin [93], dynamin-2 [94], and BIN2/BRAP1 [95]. They are involved in integrin-dependent neurite outgrowth, the regulation of podosome size and number in macrophages, and podosome formation, motility, and phagocytosis in leukocytes. The loss of αPIX causes X-chromosomal nonspecific cognitive impairment [96].

The high-affinity interaction between the proline-rich region (amino acids 186–203) of PAK1 and the SH3 domain of αPIX controls PAK1 recruitment to focal complexes [90,97]. TCR-induced PAK1 activation in Jurkat cells depends on PAK1 complexing with PIX and GIT2 [98]. Accordingly, PAK1 can control cytoskeletal reorganization and transcriptional regulation in T cells. One key regulator of this process is CBL-B, an E3 ubiquitin ligase that competitively blocks the receptor-mediated PIX-PAK interaction [99]. In addition, CBL-B catalyzes the receptor ubiquitination, thereby exerting a dual regulatory effect, interfering with βPIX-modulated PAK1 activation and promoting receptor ubiquitination to modulate receptor signaling [99]. In addition, αPIX has been shown to modulate EGFR trafficking by controlling receptor recycling and degradation [100].

CKIP1: CKIP1 (also called PLEKHO1 or OC120; 46.2 kDa; 409 amino acids) is a casein kinase-2 α-subunit (CK2α)-interacting protein, consisting of an N-terminal PH domain and a C-terminal autoinhibitory leucine zipper with basic and acidic motifs and five proline-rich motifs distributed throughout the protein [101]. Due to its scaffolding properties, CKIP1 rapidly translocates to the plasma membrane in response to various signals, such as insulin, by binding to PIP3 [102]. This process recruits several signaling molecules, including CK2 [103], actin capping proteins [104], AP1 [105], IFP35 [106], ATM [107], and AKT [108], to modulate their activities. During apoptosis, CKIP1 is cleaved by caspase-3 and translocates to the nucleus, where its C-terminal cleavage product represses AP-1 activity [105]. Thus, CKIP1 controls several cellular processes, including morphogenesis, migration, and differentiation [109].

The ternary complex consisting of CK2α, CKIP-1, and PAK1, translocates to membrane ruffles in response to EGF, where CKIP-1 mediates the interaction between CK2α and PAK1 in a PI3K-dependent manner 1 [110]. This process results in the CK2-mediated phosphorylation of PAK1 at Ser223, leading to full PAK1 activation, as observed in prostate cancer cells. The inhibition of CKIP1 prevents PAK1-mediated actin cytoskeleton dynamics and cell migration without altering PAK1 expression and other PAK1 activities in these cells [110].

GIT1/2: GIT1 (also called CAT1, APP1; 84.3 kDa; 761 amino acids) and GIT2 (also called CAT2, or p95APP2, or PKL; 84.5 kDa; 759 amino acids) belong to the ARFGAP protein family and consist of an N-terminal ARFGAP domain, ankyrin repeats, SPA homology domain (SHD), synaptic localization domain (SLD), and Paxillin binding site (PBS).

GIT1 is detected in the vasculature and bronchial epithelia of the lung and in the vasculature and bile ducts of the liver, whereas GIT2 is ubiquitously expressed [111]. GIT1/2 regulates various cellular processes, including membrane trafficking, focal adhesion assembly and disassembly, migration, and chemotaxis, through the spatial localization of various signaling molecules, including GRKs, PLCγ, NOTCH1, mTOR, MEK1, ERK1, FAK, Paxillin, and α/βPIX via the activation of integrins, RTKs, and GPCRs [84,92,111–115].

GIT2 has also been reported to function as an integrator protein in aging processes [116]; GIT2 knockout mice age faster than age-matched WT controls [117].

GIT1/2 interact with α/βPIX to recruit PAK1, linking PAK1 activity to multiple signaling pathways in different cell types [118–120]. Increasing the local concentration of PAK1 can stimulate its kinase activity [121]. Recruiting PAK1 to the membrane at the T cell–APC junction increases its local concentrations, thereby promoting its activation [122]. GIT1/2 and α/βPIX form large complexes inside the cell [112,113], and this oligomerization is essential for adhesion site localization. Mutations that disrupt the GIT-PIX interaction or PIX homodimerization cause both proteins to disperse throughout the cytoplasm [121,123]. Thus, GIT1/2 promote the integration of multiple signaling pathways and regulate cell migration and protrusion.

GRB2: GRB2 (25.2 kDa; 217 amino acids) is a ubiquitously expressed adaptor protein consisting of three domains, namely a central SH2 domain flanked by two terminal SH3 domains. GRB2 binds to various signaling molecules and modulatory proteins and plays both positive and negative roles in controlling transmembrane receptor signaling [124]. Its best-studied function is to recruit the RAS activator SOS1 and link it to growth factor receptors [125,126].

GRB2 binds to PAK1 in response to EGF receptor activation via its second proline-rich motif (amino acids 40–45), an interaction that controls actin remodeling [127]. The transcriptional activity of the ERK1/2-KLF2 axis fine-tunes GRB2-modulated PAK1 activation, thereby influencing endothelial cell proliferation, migration, and angiogenesis [128]. The molecular nature of the GRB2-PAK1 complex formation in a cellular context is still unclear. A complex consisting of PAK1, SOS1, and KRAS has been detected in sensitized bone marrow mast cells [129]. Whether GRB2 is part of this complex is uncertain. However, a stoichiometric complex between GRB2, PAK1, and SOS1 seems unlikely because both SH3 domains of GRB2 are required to recruit and activate SOS1 at the plasma membrane [125]. Thrombin has been shown to trigger PAK1 activation in vascular smooth muscle cells via an EGFR-GAB1-SHP2-RAC1/CDC42-dependent mechanism [130]. GRB2 may be an important adaptor protein in this context, as it is directly associated with activated EGFR and GAB1 [84]. GAB1 acts as a docking platform for several signaling molecules, including SHP2, PLCγ, and PI3K, and it cross-links different signaling pathways [84].

NCK1: NCK1 (42.9 kDa; 377 amino acids) is a ubiquitously expressed adaptor protein consisting of three tandem SRC homology 3 (SH3) domains followed by a C-terminal SRC homology 2 (SH2) domain. The SH2 domain binds to specific phosphotyrosine residues of numerous transmembrane proteins, including growth factor receptors, ephrin receptors, cell adhesion molecules, T cell antigen receptors, and nephrin. NCK1 links extracellular signals to intracellular events by selectively targeting a large number of proline-rich region-containing signaling molecules with its three SH3 domains, thereby driving pathways related to cytoskeletal reorganization [131–133].

The direct association of the second SH3 domain of NCK1 with the very N-terminal proline-rich region (amino acids 12–18) of PAK1 is critical for the recruitment of PAK1 to activated transmembrane proteins at the plasma membrane [134,135]. NCK1 links various upstream signals to PAK1 and thereby determines the specificity of PAK1-controlled biological processes in a cell type-dependent manner. These processes include the promotion of endothelial paracellular pore formation and permeability [136], blastomere adhesion regulated by EPHA4 receptor tyrosine kinase [137], inflammation induced by oxidative stress [138], cell migration stimulated by AKT [139], and focal adhesion formation and cell migration induced by VEGF [140]. Interestingly, NCK1 is a substrate of EPHA4, which phosphorylates conserved tyrosines in the SH3 domains, thereby blocking SH3 interactions as a negative feedback mechanism [141].

Diseases associated with the NCK1-PAK1 interaction are diverse. NCK1 promotes angiogenesis in cervical squamous cell carcinoma and ovarian cancer via the RAC1/PAK1/MMP2 axis [142,143] and in colorectal cancer via the NCK1/STAT3/PAK1/ERK axis [144]. Similarly, the endothelial PDGF-B/NCK1/Pak1 axis promotes angiogenic sprouting and pathological neovascular tufting in ischemic retinopathy [145]. In contrast, NCK1 can interfere with the prolactin-activated JAK2/PAK1 axis, which plays a role in breast cancer promotion [146]. Targeting the NCK-PAK1 interaction could block the angiogenesis and neovascularization of tumor cells, providing a potential new approach to prevent ocular neovascular disease and improve retinal wound healing [145]. The small-molecule inhibitor AX-024 has been reported to bind to the SH3 domains of NCK1, interfere with its binding to the T cell receptor (TCR) subunit CD3ε, and block T cell activation [147,148]

Paxillin: The scaffold protein Paxillin (64.5 kDa; 591 amino acids) plays a key role in the assembly of focal adhesions and thus in cell migration [149]. It consists of an N-terminal region with five leucine–aspartate-rich (LD) motifs and a C-terminal region with four tandem LIN11-ISL1-MEC-3 (LIM) domains. These domains allow Paxillin to interact with a variety of proteins, including CRK, CSK, FAK, FRNK, GIT1, Merlin, p130Cas, PYK2, Talin, Vinculin, and SRC.

The association of GIT1, an ARFGAP-like protein, with Paxillin recruits PIX and PAK1 to the focal complex [115]. PAK1 activity has been shown to couple focal adhesion (FA) dynamics to leading-edge actin dynamics [150,151]. However, local regulation is not only triggered solely by mechanosensitive proteins. Signaling pathways, often triggered by protein phosphorylation, can occur at adhesions independently of tension [152,153]. For example, the PAK1-mediated phosphorylation of Paxillin at Ser-273 enhances adhesion dynamics and promotes the formation of the trimeric protein complex GIT1/PIX/PAK1, which associates with Paxillin after its phosphorylation [64,118].

RIT1/2: RIT1 (25.1 kDa; 219 amino acids) and RIT2 (24.7 kDa; 217 amino acids) belong to the RAS family of small GTPases, consisting of a central GDP/GTP-binding (G) domain flanked by variable amino acid extensions. They act as molecular switches in the cell, cycling between a GTP-bound active form and a GDP-bound inactive form [154,155]. RIT1/2 are classified as RAS-like without CAAX (C is cysteine, A is any aliphatic amino acid, and X is any amino acid), meaning they are not post-translationally isoprenylated like classical RAS proteins [156]. The ubiquitously expressed RIT1 and its neuron-specific paralog RIT2 were identified in 1996 as a novel subfamily of RAS-related proteins in the mouse retina [157]. Several studies using transgenic and knockout animal models have elucidated the emerging roles of RIT1/2 in regulating cell survival, proliferation, differentiation, and morphogenesis [155]. Genetic studies have implicated RIT1 and RIT2 signaling in both malignancies and developmental disorders, including Parkinson's disease, autism, schizophrenia, and Noonan syndrome [158–162].

RIT1 has been reported to control actin dynamics and cell motility by forming a complex with PAK1, which also contains RAC1 or CDC42 [65]. The CRIB domain of PAK1 interacts directly with RIT1 in a nucleotide-independent manner. The ectopic expression of RIT1 leads to the disassembly of stress fiber and focal adhesions. The coexpression of dominant negative CDC42 or RAC1 and kinase-dead PAK1 prevents this effect [65].

4.2. Modulators of PAK1 Inhibition

Various proteins, including CRIPAK, Merlin, Nischarin, PAK1IP, and SKIP, negatively modulate PAK1 activity (Figure 2).

CRIPAK: CRIPAK (49 kDa; 446 amino acids) consists of an N-terminal C4 zinc finger domain followed by 12 C3H1 zinc finger domains. CRIPAK binds to ERα in a ligand-sensitive manner and also to PAK1 [163].

The binding site of CRIPAK in PAK1 has been localized to amino acids 132–270, which partially overlap with the Pak1 inhibitory domain (amino acids 83–149). The binding of CRIPAK may enhance the function of the autoinhibitory domain, thereby reducing PAK1 activation. Alternatively, because the CRIPAK's binding site overlaps with the PIX binding region in Pak1, CRIPAK-mediated inhibition could result from its potential interference with the binding of other regulatory proteins, such as PIX [98,164].

The literature on the negative regulation of PAK1 by cysteine-rich inhibitors of PAK1 (CRIPAK) is limited. Talukder et al. [163] were the first to report CRIPAK as a PAK inhibitor, showing that it is widely expressed in various human cells and tissues. They identified CRIPAK as a novel PAK1-interacting protein. In addition, their data showed that CRIPAK binds to PAK1 through its N-terminal regulatory domain and blocks PAK1 kinase activity both in vitro and in vivo. CRIPAK prevents PAK1-mediated LIMK activation and contributes to estrogen receptor (ER) transactivation in breast cancer cells. On the other hand, the selective inhibition of endogenous CRIPAK resulted in increased PAK1 activity, thereby promoting cytoskeletal remodeling. Hormonal induction increased CRIPAK expression and enhanced its colocalization with the ER in the nucleus.

CRIPAK exerts a potent inhibitory effect on PAK1 activity through multiple mechanisms. First, the CRIPAK interaction region in PAK1 overlaps with the PAK1 autoinhibitory domain, implying that the CRIPAK-PAK1 interaction may enhance the function of the autoinhibitory domain, thereby reducing PAK1 activation. Second, since the CRIPAK binding site also overlaps with the PIX interaction region in PAK1, this interference may strongly disrupt the interaction of other regulatory partners. Physiologically, the loss of PAK1 inhibitors could lead to dysregulated PAK1 activation. Interestingly, the CRIPAK gene is located on chromosome 4p16.3, a region that is frequently deleted in breast tumors. This suggests that loss of CRIPAK in breast cancer cells could lead to persistent PAK1 activation, potentially contributing to breast carcinogenesis. Conversely, their data indicated that CRIPAK inhibits PAK1-mediated ER transactivation. In addition, 17-β-estradiol stimulates CRIPAK expression, while ER signaling enhances the nuclear localization of CRIPAK, where CRIPAK and ER colocalize in the presence of estrogen. These findings suggest that the loss of CRIPAK in breast tumors may enhance hormone independence via PAK1 regulation.

Merlin: Merlin (also called neurofibromin-2 or schwannomin; 69.7 kDa; 595 amino acids) is a member of the ezrin, radixin, and moesin (ERM) protein family, which is involved in signal transduction pathways by linking membrane proteins to the actin cytoskeleton. It consists of an N-terminal FERM domain, followed by an α-helical domain and a C-terminal domain. The latter physically binds to the FERM domain, forming a head-to-tail autoinhibited conformation that is released upon interaction with angiomotin [165]. Merlin binds phosphoinositides, including PIP2 [166], and binds PIKE-L, a brain-specific nuclear GTPase, to suppress PI3K activity [166]. Merlin also binds directly to ERBB2 [167], βII-spectrin [168], LATS1/2 [165], the VEGFR2–VE-cadherin complex at cell–cell junctions [169], the E3 ubiquitin ligase DCAF1 [170], the neurofibromin/Spred1 complex [171], the RAS/p120RASGAP complex [172], and β-catenin [173]. Consequently, the loss of Merlin activates RAC1 and RAS, leading to the hyperactivation of the PAK1, mTORC1, EGFR-RAS-ERK, PI3K-AKT, WNT, and LATS1/2 pathways [174,175].

Merlin binds directly to the PBD of PAK1, interfering with the binding of RAC1 and Paxillin. It also inhibits the recruitment of PAK1 to the focal adhesion complexes, thereby preventing its activation [176]. In addition, Merlin interacts with the tight junction protein angiomotin, which inhibits RAC1 activity [170]. Accordingly, Merlin deficiency in neurofibromatosis type 2 patients is associated with increased levels of GTP-bound RAC1 [177] and the hyperactivation of PAK1 [178]. Interestingly, constitutively active

variants of RAC1 and PAK1 prevent Merlin from inhibiting RAS-induced activation of the MAPK pathway [179].

Nischarin: Nischarin (IRAS; 166.6 kDa; 1504 amino acids) consists of an N-terminal phosphoinositide-binding PHOX homology (PX) domain followed by leucine-rich repeats, a coiled-coil glutamine-rich region, an integrin-binding domain, and an alanine–proline-rich region. Nischarin interacts with several transmembrane proteins, including the integrin alpha5 subunit [180], the opioid receptor [181], the glutamate transporter GLT-1 [182], the adaptor protein IRS4 [183], the small GTPases RAB 4, 9, 14, and 38, and RAC1 [184], and kinases such as STK11/LKB1 [185], LIMK1 [186], and PAK1 [187,188]. It modulates various processes, including transcription, cytoskeletal reorganization, proliferation, survival, and differentiation [189–191]. Nischarin is expressed in various cell types and organs [189] and acts as a tumor suppressor gene when upregulated in cancer cells [192], inhibiting EMT and migration [191,193]. It is also associated with cardiac remodeling and dysfunction [194].

The upregulation of Nischarin in breast and colon epithelial cell lines has been shown to selectively inhibit RAC1/PAK1-induced migration and invasion [195]. Interestingly, Nischarin binds directly to the kinase domain of RAC1-activated PAK1 at the leading edge of a migrating cell, thereby inhibiting PAK kinase activity [187]. Endogenous Nischarin has also been shown to inhibit neurite outgrowth by blocking PAK1 activity at the neuronal membrane [196]. Nischarin's inhibition of PAK1 prevents downstream effects such as the PAK1-mediated phosphorylation of LIMK, which would normally inhibit cofilin, an actin-severing protein, leading to actin filament assembly. By binding to the kinase domain of active LIMK, Nischarin deactivates it and prevents actin assembly during cytoskeletal reorganization [186].

PAK1IP1: PAK1IP1 (also known as hPIP1 or WDR84; 44 kDa; 392 amino acids) binds to the N-terminus of PAK1 and inhibits its activation by CDC42 [197]. PAK1IP1 is a human Gβ-like WD repeat protein, and its overexpression inhibits PAK-mediated c-JNK and NFκB signaling pathways [197]. Homozygous variants of PAK1IP1 have been shown to cause severe developmental defects of the brain and craniofacial skeleton, including a median orofacial cleft [198]. This may be related to the nuclear role of PAK1IP1 in ribosome biogenesis [199] or its interaction with MDM2 to upregulate p53 [198,200]. It remains unclear whether PAK1 is involved in this context. In addition, PAK1 translocates to the nucleus, where it may play a role in DNA repair and transcription [45,47].

SKIP: SKIP (also called INPP5K; 51.1 kDa; 448 amino acids) is a member of the phosphoinositide 5-phosphatase family. It consists of a 5-phosphatase domain followed by a C-terminal SKICH (SKIP carboxy homology) domain, essential for protein–protein interaction and subcellular localization [201]. SKIP binds several proteins, including MAD2L1BP, SODD, GRP78, and PAK1, and is involved in cell cycle control, adhesion, and migration processes.

SKIP's interaction with glucose-regulated protein 78 (GPR78), an endoplasmic reticulum (ER) chaperone involved in the ER stress response and the unfolded protein response (UPR), is required for its localization to the ER. Ijuin and coworkers proposed a model in which cytosolic SKIP interacts directly with GRP78 via its SKICH domain under basal unstimulated conditions [202–206]. However, this model raises the unresolved question of how cytosolic SKIP interacts with GRP78, which is located on the luminal side of the ER [206].

Upon insulin stimulation, the SKIP-GRP78 complex translocates from the ER to the plasma membrane, where activated PAK1 displaces GRP78 and binds to SKIP via an 11-amino acid region within the kinase domain of PAK. This interaction links SKIP to the insulin receptor complex, resulting in PtdIns(3,4,5)P3 dephosphorylation, de-

creased AKT2 phosphorylation, and the subsequent inactivation of insulin signaling. Co-immunoprecipitation experiments confirmed the association of SKIP with GRP78 [207].

Reduced SKIP expression in cells or in SKIP-modified (PpsBrdm1/+) heterozygous mice increases insulin signaling sensitivity in muscle cells and reduces diet-induced obesity in these mice [208–210]. In addition, SKIP expression is increased in skeletal muscle tissue from high-fat-fed and diabetic/obese mice compared to wild-type mice, linking SKIP to these metabolic conditions [203]. Supplementation of the culture medium with a synthetic peptide that matches the sequence of the PAK1 kinase domain that interacts with SKIP increases insulin signaling in muscle cell lines, likely by disrupting the formation of the SKIP-PAK1 complex [204].

As a mechanistic insight, Ijuin et al. [211] identified how SKIP-PAK1 interactions affect insulin signaling and glucose uptake. Upon insulin stimulation, SKIP translocates to membrane ruffles and binds activated PAK1 from a complex with PIP3 effectors such as AKT2, PDK1, and Rac1, leading to the inactivation of certain signaling proteins. SKIP can inhibit both the Rac1-dependent kinase activity and the scaffolding functions of PAK1. This inhibition limits Rac1 activity, which subsequently inactivates PAK1 and dissociates the AKT2-PDK1-PAK1 complex, allowing for rapid termination of the insulin signaling cascade.

These findings suggest that targeting the SKIP-PAK1 interaction may be a promising therapeutic strategy to improve systemic insulin-dependent glucose uptake and treat hyperglycemia. Notably, recent studies have identified an 11-amino acid peptide within the kinase domain of PAK1 that is essential for its interaction with SKIP. Expression of this peptide sequence in skeletal muscle cells enhances insulin signaling, and supplementation with a synthetic peptide of this sequence can improve insulin signaling and glucose uptake in skeletal muscle cell lines [204].

4.3. PAK1 and Focal Adhesion Complex Formation

Focal adhesions are dynamic multi-protein assemblies that mediate interactions between the extracellular matrix and the actin cytoskeleton, playing a pivotal role in cell migration and mechanosensing [212]. PAK1 is tightly regulated within focal adhesions by its interactions with scaffolding proteins such as αPIX, GIT1, and Paxillin (Figure 2) [97–99,115,118–120]. These accessory proteins coordinate the spatial localization and activity of PAK1, ensuring precise signal transduction within the adhesion complex. A key mechanism for the spatial regulation of PAK1 involves its association with the PAK1-PIX-GIT complex. This interaction is stabilized by the SH3 domain of αPIX, which binds to the proline-rich region of PAK1. Phosphorylation at Y285, downstream of cytokine receptor activation (including JAK2-mediated pathways), further promotes the assembly of the PAK1-PIX-GIT complex [31]. Once recruited to focal adhesions, αPIX and GIT stabilize PAK1 at these sites, facilitating its interactions with other adhesion components. Paxillin, an adaptor protein, links the PAK1-PIX-GIT complex to core focal adhesion components, such as focal adhesion kinase (FAK), by directly binding to GIT1. This connection promotes the assembly and maturation of focal adhesions and integrates PAK1 into signaling pathways that regulate cytoskeletal remodeling and focal adhesion dynamics. The PAK1-mediated phosphorylation of Paxillin at S273 further enhances these processes, highlighting its role in modulating cell migration [31]. Negative regulators also play a critical role in modulating PAK1 activity at focal adhesions. CRIPAK binds to a site on PAK1 overlapping the PIX interaction region, disrupting interactions with other regulatory partners [163]. Nischarin negatively regulates PAK1 by directly binding to its kinase domain, inhibiting its activity and destabilizing the PAK1-PIX-GIT-Paxillin complex [187,195]. Merlin, another regulatory protein, binds to the PBD of PAK1, interfering with RAC1 and Paxillin binding [176]. This prevents PAK1 recruitment to focal adhesion complexes and inhibits its activation. Collectively, these regu-

latory interactions ensure that PAK1 activity is tightly controlled within focal adhesions, maintaining cellular homeostasis and preventing aberrant signaling (Figure 2) [213].

4.4. PAK1 Membrane Localization, Activation, and Function

The recruitment of PAK1 to the plasma membrane is a critical step for its activation and subsequent signaling [214]. Accessory proteins such as GIT1, PIX, NCK1, and GRB2 play essential roles in mediating this localization and activation, ensuring precise spatiotemporal regulation of PAK1 activity. Upon receptor tyrosine kinase (RTK) activation by growth factors, RTKs undergo dimerization and phosphorylation, creating docking sites for adaptor proteins like NCK1 and GRB2 [127,128,215]. These adaptors recruit PAK1 to the plasma membrane, where it interacts with active GTP-bound RAC1 or CDC42 via its CRIB motif. In resting cells, RhoGDI sequesters RAC1 in the cytoplasm by interacting with its lipid anchor. Upon stimulation, RhoGEFs facilitate the exchange of GDP for GTP on RAC1, promoting its translocation to the plasma membrane. RhoGAPs deactivate RAC1 by accelerating GTP hydrolysis. Once localized to the membrane, PAK1 undergoes a conformational change upon binding to GTP-bound RAC1/CDC42, relieving its autoinhibition [19,65]. This leads to phosphorylation at Thr-423 within its kinase domain, a critical step for its activation. RIT1 stabilizes the interaction of PAK1 with RAC1 and CDC42, further enhancing its activation and downstream signaling [65]. Active PAK1 initiates diverse signaling pathways, including those involved in cytoskeletal remodeling, transcriptional regulation, cell cycle progression, survival, and migration. Several accessory proteins serve as negative regulators of PAK1 at the membrane [19]. CRIPAK exerts its inhibitory effects through multiple mechanisms: it overlaps with the PIX interaction region, disrupts regulatory interactions, and enhances PAK1 autoinhibition [163]. PAK1IP1 binds to the N-terminus of PAK1, blocking its activation. Nischarin inhibits PAK1 by binding directly to its kinase domain, suppressing its ability to phosphorylate substrates [187,195]. Merlin interferes with RAC1 binding by targeting the PBD of PAK1, thereby preventing its activation and membrane localization [176]. These finely tuned regulatory mechanisms highlight the importance of accessory proteins in controlling PAK1 membrane localization and activity, ensuring balanced signaling outcomes. Such a regulation is critical for maintaining cellular processes and preventing pathological conditions driven by aberrant PAK1 activation (Figure 2) [40,216].

5. PAK1 in Cancer Therapy and Resistance

Recent advances highlight the therapeutic potential of targeting PAK1 as a strategy to address cancer progression and therapy resistance [40]. In melanoma, PAK1 hyperactivation promotes cell survival, proliferation, and immune evasion, contributing to resistance against BRAF and MEK inhibitors. Studies demonstrate that PAK1 inhibition enhances the efficacy of these therapies by modulating the MAPK and PI3K/AKT pathways. A novel PAK1-selective degrader, BJG-05-039, combines targeted degradation with kinase inhibition, providing a dual mechanism to suppress both the enzymatic and scaffolding functions of PAK1. Synergistic approaches, such as combining PAK1 inhibitors with immune checkpoint therapies, are also being explored to boost anti-tumor immunity. While promising, challenges related to drug specificity, bioavailability, and toxicity remain key barriers to clinical translation [217].

In various cancers, PAK1 activation is closely linked to resistance mechanisms against standard therapies. For instance, in non-small cell lung cancer (NSCLC), PAK1 enhances β-catenin-mediated cancer stemness, stabilizing markers such as OCT4 and SOX2 and driving tumor aggressiveness and chemoresistance. Clinical evidence indicates that high PAK1 expression correlates with poor responses to cisplatin therapy. Combining MEK/ERK

inhibitors like AZD6244 or targeting β-catenin-driven stemness with agents such as BBI-608 restores cisplatin sensitivity, offering a promising avenue for overcoming resistance. Similarly, in BRAF-mutant melanomas, PAK1 activation drives resistance by engaging the AKT signaling pathway. Targeting PAK1-regulated Wnt/β-catenin signaling has shown potential to improve drug sensitivity across multiple cancers [218].

In estrogen receptor-positive (ER+) breast cancer, PAK1 hyperactivation mediates resistance to endocrine therapy (ET) and CDK4/6 inhibitors by driving epithelial-to-mesenchymal transition (EMT) and MAPK pathway activation. Pharmacological inhibitors like PF-3758309 and NVS-PAK1-1 restore drug sensitivity by suppressing tumor invasion and growth. Combining PAK1 inhibitors with ET and CDK4/6 inhibitors represents a promising strategy to address resistance and improve patient outcomes in this aggressive breast cancer subtype [219].

The concept of modulating PAK1 rather than completely inhibiting it is emerging as a refined therapeutic approach to attenuate aberrant cancer signaling. By targeting accessory proteins involved in PAK1 regulation and modulation, it may be possible to fine-tune PAK1 activity, reducing cancer invasion and drug resistance without fully blocking essential cellular processes. This paradigm shift opens the door to innovative therapies that focus on balancing signaling dynamics, offering patients more effective and sustainable treatment options.

6. Conclusions and Perspective

Over the past three decades, novel pathway components, structural insights, biophysical principles, biomimetic strategies, and clinical drug candidates have emerged in the field of receptor-driven PAK1 signaling. As outlined, several accessory proteins, each with different sizes and domain architectures, regulate the binding and function of molecular components within the PAK1 pathways. These proteins orchestrate PAK1 assembly and activation in a context-dependent manner. The specificity, efficacy, and fidelity of signaling are largely determined by the spatial localization and temporal dynamics of these interactions, protecting against potential deleterious effects.

PAK1 serves as a key player in various pathological conditions, particularly cancer, making it a promising target for therapeutic agents or blockers. However, the direct inhibition of core signaling components, such as PAK1, often results in the complete shutdown of signaling. This blockade can lead to the emergence of multi-characteristics in cancer cells, including new features that allow them to evade therapy and develop drug resistance [219,220]. Such effects can contribute to increased off-target effects and enhanced aggressiveness of the tumor. Therefore, the traditional "inhibitor" concept, which focuses on completely blocking core pathway components, may need to be reassessed. Therapeutic strategies could benefit from exploring more refined approaches that modulate signaling, potentially minimizing these unintended consequences.

In this context, accessory proteins play a crucial role in modulating signaling pathways. These proteins ensure the strength, efficiency, and specificity of signal transduction by regulating the compartmentalization and site-specific localization of signaling molecules [84]. This regulation ensures that signaling events occur accurately and within the correct cellular context. Accessory proteins also offer dynamic control over core signaling components, such as PAK1, influencing critical cellular processes like migration, cytoskeletal remodeling, and survival. As such, they represent promising therapeutic targets because they allow for a more precise modulation of signaling without the need for the complete inhibition of core pathway components.

Among the various accessory proteins that modulate signaling pathways, several are key in regulating PAK1 activation and inhibition. For example, targeting PIX, a scaffolding

protein that modulates PAK1 localization, and Paxillin, which plays a central role in the assembly of focal adhesions and cell migration, could potentially reduce PAK1 signaling and focal adhesion complex formation. Furthermore, targeting adaptor proteins like NCK and GRB2, as well as RIT1, may decrease PAK1 membrane localization and activation by RAC1/CDC42, thereby downregulating PAK1 signaling. Another promising approach is to explore strategies that stabilize the interaction of modulators of PAK1 inhibition, thereby extending the residence time required for PAK1 activation, which could provide a novel method for fine-tuning PAK1 signaling.

The inhibition of CKIP1 has been shown to prevent PAK1-driven actin cytoskeleton remodeling and cell migration without affecting PAK1 expression or other activities [110]. The small-molecule inhibitor AX-024 binds to the SH3 domains of NCK1, disrupting its interaction with the TCR subunit CD3ε and inhibiting T cell activation [148]. These findings highlight the potential of targeting accessory proteins to achieve a more targeted and controlled modulation of PAK1 activity. However, the discovery of inhibitors targeting accessory proteins remains limited, and this represents a major gap in the development of more effective therapies.

Alternative strategies to direct PAK1 inhibition, such as targeting accessory proteins, have been explored and show great promise for fine-tuning PAK1 signaling. For example, Chow et al. introduced a PAK1-selective degrader, which may offer more potent pharmacological effects than traditional catalytic inhibition [221]. Another approach focuses on targeting long noncoding RNAs (lncRNAs) associated with the PAK1 pathways. LncRNAs regulate gene expression through various mechanisms, including genomic imprinting, epigenetic regulation, and miRNA sponging, which could open up new therapeutic avenues [222]. Zhou et al. demonstrated that lncRNA-H19 activates the CDC42/PAK1 pathway to promote proliferation and invasion in hepatocellular carcinoma [223]. Similarly, Luo et al. showed that lncRNA MALAT1 facilitates BM-MSC differentiation into endothelial cells and improves erectile dysfunction via the miR-206/CDC42/PAK1/Paxillin axis [224]. These findings suggest that targeting lncRNAs in RAC1/CDC42 and PAK1 pathways could offer promising therapeutic outcomes.

Although the current literature is somewhat limited, existing data highlight the importance of a precisely controlled spatiotemporal organization of PAK1 by accessory proteins. Future research should explore these modulators to develop novel therapeutic strategies. Harnessing this level of control over PAK1 activity holds great promise for advancing disease treatment, offering a more refined approach to combatting diseases like cancer with limited undesirable side effects of direct pathway inhibition.

Author Contributions: All authors coordinated, drafted, and approved the manuscript. All authors have read and agreed to the published version of the manuscript.

Funding: This study was supported by the German Research Foundation (DFG; grant number: AH 92/8-3).

Institutional Review Board Statement: Not applicable.

Informed Consent Statement: Not applicable.

Data Availability Statement: It is affirmed that no new data were generated while compiling this review manuscript. All referenced data sources are openly accessible and appropriately cited within the manuscript. Please do not hesitate to contact the corresponding author if any additional information or clarification is required.

Acknowledgments: The authors thank Arezoo Shahba and Roland Piekorz for reading and editing the manuscript.

Conflicts of Interest: The authors declare no conflicts of interest.

Abbreviations

AID: autoinhibitory domain; AKT: protein kinase B; ARHGEF: Rho guanine nucleotide exchange factor; ARP2/3: actin-related protein 2/3; ATR: ataxia-telangiectasia and RAD3-related protein; BAD: BCL-2-associated agonist of cell death; BCL-2: B-cell lymphoma 2; BR: basic region; CBD: CAT/GIT binding domain; CC: coiled coil; CDK: cyclin-dependent kinase; CH: calponin homology; CK2α: casein kinase 2 alpha; CKIP1: casein kinase 2 interacting protein-1; CRAF: RAF proto-oncogene serine/threonine-protein kinase; CRIB: CDC42/RAC interactive binding; DH: DBL homology; EGF: epidermal growth factor; EMT: epithelial–mesenchymal transition; ER: endoplasmic reticulum; ERα: estrogen receptor alpha; FOXO1: Forkhead box O1; GEF: guanine nucleotide exchange factor; GIT: G protein-coupled receptor kinase interacting ArfGAP; GLUT4: glucose transporter type 4; GRB2: growth factor receptor-bound protein 2; GRP78: glucose-regulated protein 78; IDRs: inherently disordered regions; IGF-1: insulin-like growth factor 1; IRS1: insulin receptor substrate 1; MORC2: microrchidia CW-type zinc finger 2; mTOR: mechanistic target of rapamycin; MYPT1: myosin phosphatase target subunit 1; NCK1: non-catalytic region of tyrosine kinase adaptor protein 1; NFκB: nuclear factor kappa B; PAK1: p21-activated kinase 1; PBD: p21-binding domain; PDGF: platelet-derived growth factor; PDK1: 3-phosphoinositide-dependent protein kinase 1; PGM1: phosphoglucomutase 1; PH: pleckstrin homology; PI3K: phosphatidylinositol 3-kinase; PIP2: phosphatidylinositol (4,5)-bisphosphate; PIP3: phosphatidylinositol (3,4,5)-trisphosphate; PIX: PAK-interacting exchange factor; PLK1: polo-like kinase 1; PRD: proline-rich domain; Rb: retinoblastoma protein; SH3: SRC homology 3; SKIP: skeletal muscle and kidney enriched inositol phosphatase; TCF/LEF: T cell factor/lymphoid enhancer factor; TCoB: tubulin cofactor B.

References

1. Manser, E.; Leung, T.; Salihuddin, H.; Zhao, Z.S.; Lim, L. A brain serine/threonine protein kinase activated by Cdc42 and Rac1. *Nature* **1994**, *367*, 40–46. [CrossRef]
2. Ha, B.H.; Morse, E.M.; Turk, B.E.; Boggon, T.J. Signaling, regulation, and specificity of the type II p21-activated kinases. *J. Biol. Chem.* **2015**, *290*, 12975–12983. [CrossRef] [PubMed]
3. Rane, C.K.; Minden, A. P21 activated kinases: Structure, regulation, and functions. *Small GTPases* **2014**, *5*, e28003. [CrossRef]
4. Radu, M.; Semenova, G.; Kosoff, R.; Chernoff, J. PAK signalling during the development and progression of cancer. *Nat. Rev. Cancer* **2014**, *14*, 13–25. [CrossRef]
5. Kichina, J.V.; Goc, A.; Al-Husein, B.; Somanath, P.R.; Kandel, E.S. PAK1 as a therapeutic target. *Expert Opin. Ther. Targets* **2010**, *14*, 703–725. [CrossRef]
6. Ong, C.C.; Jubb, A.M.; Zhou, W.; Haverty, P.M.; Harris, A.L.; Belvin, M.; Friedman, L.S.; Koeppen, H.; Hoeflich, K.P. p21-activated kinase 1: PAK'ed with potential. *Oncotarget* **2011**, *2*, 491. [CrossRef] [PubMed]
7. Manser, E.; Lim, L. Roles of PAK family kinases. *Prog. Mol. Subcell. Biol.* **1999**, *22*, 115–133. [CrossRef] [PubMed]
8. Holm, C.; Rayala, S.; Jirström, K.; Stål, O.; Kumar, R.; Landberg, G. Association between Pak1 expression and subcellular localization and tamoxifen resistance in breast cancer patients. *J. Natl. Cancer Inst.* **2006**, *98*, 671–680. [CrossRef]
9. Kamai, T.; Shirataki, H.; Nakanishi, K.; Furuya, N.; Kambara, T.; Abe, H.; Oyama, T.; Yoshida, K.-I. Increased Rac1 activity and Pak1 overexpression are associated with lymphovascular invasion and lymph node metastasis of upper urinary tract cancer. *BMC Cancer* **2010**, *10*, 164. [CrossRef] [PubMed]
10. Ong, C.C.; Jubb, A.M.; Jakubiak, D.; Zhou, W.; Rudolph, J.; Haverty, P.M.; Kowanetz, M.; Yan, Y.; Tremayne, J.; Lisle, R. P21-activated kinase 1 (PAK1) as a therapeutic target in BRAF wild-type melanoma. *J. Natl. Cancer Inst.* **2013**, *105*, 606–607. [CrossRef] [PubMed]
11. Caye, A.; Strullu, M.; Guidez, F.; Cassinat, B.; Gazal, S.; Fenneteau, O.; Lainey, E.; Nouri, K.; Nakhaei-Rad, S.; Dvorsky, R. Juvenile myelomonocytic leukemia displays mutations in components of the RAS pathway and the PRC2 network. *Nat. Genet.* **2015**, *47*, 1334–1340. [CrossRef] [PubMed]
12. Balbin, O.A.; Prensner, J.R.; Sahu, A.; Yocum, A.; Shankar, S.; Malik, R.; Fermin, D.; Dhanasekaran, S.M.; Chandler, B.; Thomas, D. Reconstructing targetable pathways in lung cancer by integrating diverse omics data. *Nat. Commun.* **2013**, *4*, 2617. [CrossRef] [PubMed]
13. Kelly, M.L.; Chernoff, J. Mouse models of PAK function. *Cell. Logist.* **2012**, *2*, 84–88. [CrossRef]

14. Amirthalingam, M.; Palanisamy, S.; Tawata, S. p21-Activated kinase 1 (PAK1) in aging and longevity: An overview. *Ageing Res. Rev.* **2021**, *71*, 101443. [CrossRef] [PubMed]
15. Nussinov, R.; Yavuz, B.R.; Arici, M.K.; Demirel, H.C.; Zhang, M.; Liu, Y.; Tsai, C.-J.; Jang, H.; Tuncbag, N. Neurodevelopmental disorders, like cancer, are connected to impaired chromatin remodelers, PI3K/mTOR, and PAK1-regulated MAPK. *Biophys. Rev.* **2023**, *15*, 163–181. [CrossRef]
16. Qiu, X.; Xu, H.; Wang, K.; Gao, F.; Xu, X.; He, H. P-21 activated kinases in liver disorders. *Cancers* **2023**, *15*, 551. [CrossRef]
17. Wang, Y.; Wang, S.; Lei, M.; Boyett, M.; Tsui, H.; Liu, W.; Wang, X. The p21-activated kinase 1 (Pak1) signalling pathway in cardiac disease: From mechanistic study to therapeutic exploration. *Br. J. Pharmacol.* **2018**, *175*, 1362–1374. [CrossRef] [PubMed]
18. Naïja, A.; Merhi, M.; Inchakalody, V.; Fernandes, Q.; Mestiri, S.; Prabhu, K.S.; Uddin, S.; Dermime, S. The role of PAK4 in the immune system and its potential implication in cancer immunotherapy. *Cell. Immunol.* **2021**, *367*, 104408. [CrossRef]
19. Mosaddeghzadeh, N.; Ahmadian, M.R. The RHO family GTPases: Mechanisms of regulation and signaling. *Cells* **2021**, *10*, 1831. [CrossRef] [PubMed]
20. Chetty, A.K.; Ha, B.H.; Boggon, T.J. Rho family GTPase signaling through type II p21-activated kinases. *Cell. Mol. Life Sci.* **2022**, *79*, 598. [CrossRef] [PubMed]
21. Kanumuri, R.; Saravanan, R.; Pavithra, V.; Sundaram, S.; Rayala, S.K.; Venkatraman, G. Current trends and opportunities in targeting p21 activated kinase-1 (PAK1) for therapeutic management of breast cancers. *Gene* **2020**, *760*, 144991. [CrossRef]
22. Zhao, Z.-s.; Manser, E. PAK family kinases: Physiological roles and regulation. *Cell. Logist.* **2012**, *2*, 59–68. [CrossRef] [PubMed]
23. Hemsath, L.; Dvorsky, R.; Fiegen, D.; Carlier, M.-F.; Ahmadian, M.R. An electrostatic steering mechanism of Cdc42 recognition by Wiskott-Aldrich syndrome proteins. *Mol. Cell* **2005**, *20*, 313–324. [CrossRef] [PubMed]
24. Bagrodia, S.; Cerione, R.A. Pak to the future. *Trends Cell Biol.* **1999**, *9*, 350–355. [CrossRef]
25. Strochlic, T.I.; Viaud, J.; Rennefahrt, U.E.; Anastassiadis, T.; Peterson, J.R. Phosphoinositides are essential coactivators for p21-activated kinase 1. *Mol. Cell* **2010**, *40*, 493–500. [CrossRef]
26. Zenke, F.T.; King, C.C.; Bohl, B.P.; Bokoch, G.M. Identification of a central phosphorylation site in p21-activated kinase regulating autoinhibition and kinase activity. *J. Biol. Chem.* **1999**, *274*, 32565–32573. [CrossRef] [PubMed]
27. Wang, J.; Wu, J.W.; Wang, Z.X. Structural insights into the autoactivation mechanism of p21-activated protein kinase. *Structure* **2011**, *19*, 1752–1761. [CrossRef]
28. Lei, M.; Lu, W.; Meng, W.; Parrini, M.-C.; Eck, M.J.; Mayer, B.J.; Harrison, S.C. Structure of PAK1 in an autoinhibited conformation reveals a multistage activation switch. *Cell* **2000**, *102*, 387–397. [CrossRef]
29. Pirruccello, M.; Sondermann, H.; Pelton, J.G.; Pellicena, P.; Hoelz, A.; Chernoff, J.; Wemmer, D.E.; Kuriyan, J. A dimeric kinase assembly underlying autophosphorylation in the p21 activated kinases. *J. Mol. Biol.* **2006**, *361*, 312–326. [CrossRef]
30. Buchwald, G.; Hostinova, E.; Rudolph, M.G.; Kraemer, A.; Sickmann, A.; Meyer, H.E.; Scheffzek, K.; Wittinghofer, A. Conformational switch and role of phosphorylation in PAK activation. *Mol. Cell. Biol.* **2001**, *21*, 5179–5189. [CrossRef]
31. Hammer, A.; Diakonova, M. Tyrosyl phosphorylated serine-threonine kinase PAK1 is a novel regulator of prolactin-dependent breast cancer cell motility and invasion. *Recent Adv. Prolactin Res.* **2015**, *846*, 97–137.
32. Rashid, T.; Banerjee, M.; Nikolic, M. Phosphorylation of Pak1 by the p35/Cdk5 kinase affects neuronal morphology. *J. Biol. Chem.* **2001**, *276*, 49043–49052. [CrossRef]
33. Zhong, J.L.; Banerjee, M.D.; Nikolic, M. Pak1 and its T212 phosphorylated form accumulate in neurones and epithelial cells of the developing rodent. *Dev. Dyn. Off. Publ. Am. Assoc. Anat.* **2003**, *228*, 121–127. [CrossRef]
34. Shin, Y.J.; Kim, Y.-B.; Kim, J.-H. Protein kinase CK2 phosphorylates and activates p21-activated kinase 1. *Mol. Biol. Cell* **2013**, *24*, 2990–2999. [CrossRef] [PubMed]
35. Mayhew, M.W.; Jeffery, E.D.; Sherman, N.E.; Nelson, K.; Polefrone, J.M.; Pratt, S.J.; Shabanowitz, J.; Parsons, J.T.; Fox, J.W.; Hunt, D.F. Identification of phosphorylation sites in βPIX and PAK1. *J. Cell Sci.* **2007**, *120*, 3911–3918. [CrossRef] [PubMed]
36. Grebeňová, D.; Holoubek, A.; Röselová, P.; Obr, A.; Brodská, B.; Kuželová, K. PAK1, PAK1Δ15, and PAK2: Similarities, differences and mutual interactions. *Sci. Rep.* **2019**, *9*, 17171. [CrossRef]
37. Staser, K.; Shew, M.A.; Michels, E.G.; Mwanthi, M.M.; Yang, F.-C.; Clapp, D.W.; Park, S.-J. A Pak1-PP2A-ERM signaling axis mediates F-actin rearrangement and degranulation in mast cells. *Exp. Hematol.* **2013**, *41*, 56–66.e2. [CrossRef]
38. Semenova, G.; Chernoff, J. Targeting pak1. *Biochem. Soc. Trans.* **2017**, *45*, 79–88. [CrossRef] [PubMed]
39. Sampat, N.; Minden, A. Inhibitors of the p21 activated kinases. *Curr. Pharmacol. Rep.* **2018**, *4*, 238–249. [CrossRef]
40. Yao, D.; Li, C.; Rajoka, M.S.R.; He, Z.; Huang, J.; Wang, J.; Zhang, J. P21-Activated Kinase 1: Emerging biological functions and potential therapeutic targets in Cancer. *Theranostics* **2020**, *10*, 9741. [CrossRef] [PubMed]
41. Baker, N.M.; Yee Chow, H.; Chernoff, J.; Der, C.J. Molecular Pathways: Targeting RAC–p21-Activated Serine–Threonine Kinase Signaling in RAS-Driven Cancers. *Clin. Cancer Res.* **2014**, *20*, 4740–4746. [CrossRef]
42. Gururaj, A.; Barnes, C.J.; Vadlamudi, R.K.; Kumar, R. Regulation of phosphoglucomutase 1 phosphorylation and activity by a signaling kinase. *Oncogene* **2004**, *23*, 8118–8127. [CrossRef] [PubMed]

43. Tunduguru, R.; Zhang, J.; Aslamy, A.; Salunkhe, V.A.; Brozinick, J.T.; Elmendorf, J.S.; Thurmond, D.C. The actin-related p41ARC subunit contributes to p21-activated kinase-1 (PAK1)–mediated glucose uptake into skeletal muscle cells. *J. Biol. Chem.* **2017**, *292*, 19034–19043. [CrossRef]
44. Li, D.-Q.; Nair, S.S.; Ohshiro, K.; Kumar, A.; Nair, V.S.; Pakala, S.B.; Reddy, S.D.N.; Gajula, R.P.; Eswaran, J.; Aravind, L. MORC2 signaling integrates phosphorylation-dependent, ATPase-coupled chromatin remodeling during the DNA damage response. *Cell Rep.* **2012**, *2*, 1657–1669. [CrossRef]
45. Beesetti, S.; Mavuluri, J.; Surabhi, R.; Oberyszyn, T.; Tober, K.; Pitani, R.; Joseph, L.; Venkatraman, G.; Rayala, S. Transcriptional regulation of ataxia–telangiectasia and Rad3-related protein by activated p21-activated kinase-1 protects keratinocytes in UV-B-induced premalignant skin lesions. *Oncogene* **2017**, *36*, 6154–6163. [CrossRef]
46. Ho, H.; Aruri, J.; Kapadia, R.; Mehr, H.; White, M.A.; Ganesan, A.K. RhoJ regulates melanoma chemoresistance by suppressing pathways that sense DNA damage. *Cancer Res.* **2012**, *72*, 5516–5528. [CrossRef]
47. Jagadeeshan, S.; Krishnamoorthy, Y.; Singhal, M.; Subramanian, A.; Mavuluri, J.; Lakshmi, A.; Roshini, A.; Baskar, G.; Ravi, M.; Joseph, L. Transcriptional regulation of fibronectin by p21-activated kinase-1 modulates pancreatic tumorigenesis. *Oncogene* **2015**, *34*, 455–464. [CrossRef] [PubMed]
48. Jiramongkol, Y.; Lam, E.W.-F. FOXO transcription factor family in cancer and metastasis. *Cancer Metastasis Rev.* **2020**, *39*, 681–709. [CrossRef]
49. Zhu, G.; Wang, Y.; Huang, B.; Liang, J.; Ding, Y.; Xu, A.; Wu, W. A Rac1/PAK1 cascade controls β-catenin activation in colon cancer cells. *Oncogene* **2012**, *31*, 1001–1012. [CrossRef] [PubMed]
50. Arias-Romero, L.E.; Villamar-Cruz, O.; Huang, M.; Hoeflich, K.P.; Chernoff, J. Pak1 kinase links ErbB2 to β-catenin in transformation of breast epithelial cells. *Cancer Res.* **2013**, *73*, 3671–3682. [CrossRef]
51. Balasenthil, S.; Sahin, A.A.; Barnes, C.J.; Wang, R.-A.; Pestell, R.G.; Vadlamudi, R.K.; Kumar, R. p21-activated kinase-1 signaling mediates cyclin D1 expression in mammary epithelial and cancer cells. *J. Biol. Chem.* **2004**, *279*, 1422–1428. [CrossRef] [PubMed]
52. Kundumani-Sridharan, V.; Singh, N.K.; Kumar, S.; Gadepalli, R.; Rao, G.N. Nuclear factor of activated T cells c1 mediates p21-activated kinase 1 activation in the modulation of chemokine-induced human aortic smooth muscle cell F-actin stress fiber formation, migration, and proliferation and injury-induced vascular wall remodeling. *J. Biol. Chem.* **2013**, *288*, 22150–22162. [PubMed]
53. Zhang, Z.-L.; Liu, G.-c.; Peng, L.; Zhang, C.; Jia, Y.-M.; Yang, W.-H.; Mao, L. Effect of PAK1 gene silencing on proliferation and apoptosis in hepatocellular carcinoma cell lines MHCC97-H and HepG2 and cells in xenograft tumor. *Gene Ther.* **2018**, *25*, 284–296. [CrossRef] [PubMed]
54. Zaldua, N.; Llavero, F.; Artaso, A.; Gálvez, P.; Lacerda, H.M.; Parada, L.A.; Zugaza, J.L. Rac1/p21-activated kinase pathway controls retinoblastoma protein phosphorylation and E2F transcription factor activation in B lymphocytes. *FEBS J.* **2016**, *283*, 647–661. [CrossRef]
55. Misra, U.K.; Deedwania, R.; Pizzo, S.V. Binding of activated α2-macroglobulin to its cell surface receptor GRP78 in 1-LN prostate cancer cells regulates PAK-2-dependent activation of LIMK. *J. Biol. Chem.* **2005**, *280*, 26278–26286. [CrossRef]
56. Bagheri-Yarmand, R.; Mazumdar, A.; Sahin, A.A.; Kumar, R. LIM kinase 1 increases tumor metastasis of human breast cancer cells via regulation of the urokinase-type plasminogen activator system. *Int. J. Cancer* **2006**, *118*, 2703–2710. [CrossRef]
57. Vadlamudi, R.K.; Li, F.; Barnes, C.J.; Bagheri-Yarmand, R.; Kumar, R. p41-Arc subunit of human Arp2/3 complex is a p21-activated kinase-1-interacting substrate. *EMBO Rep.* **2004**, *5*, 154–160. [CrossRef] [PubMed]
58. Webb, B.A.; Eves, R.; Crawley, S.W.; Zhou, S.; Côté, G.P.; Mak, A.S. PAK1 induces podosome formation in A7r5 vascular smooth muscle cells in a PAK-interacting exchange factor-dependent manner. *Am. J. Physiol.-Cell Physiol.* **2005**, *289*, C898–C907. [CrossRef]
59. Vadlamudi, R.K.; Li, F.; Adam, L.; Nguyen, D.; Ohta, Y.; Stossel, T.P.; Kumar, R. Filamin is essential in actin cytoskeletal assembly mediated by p21-activated kinase 1. *Nat. Cell Biol.* **2002**, *4*, 681–690. [CrossRef] [PubMed]
60. Hammer, A.; Rider, L.; Oladimeji, P.; Cook, L.; Li, Q.; Mattingly, R.R.; Diakonova, M. Tyrosyl phosphorylated PAK1 regulates breast cancer cell motility in response to prolactin through filamin A. *Mol. Endocrinol.* **2013**, *27*, 455–465. [CrossRef]
61. Ding, I.; Ostrowska-Podhorodecka, Z.; Lee, W.; Liu, R.S.; Carneiro, K.; Janmey, P.A.; McCulloch, C.A. Cooperative roles of PAK1 and filamin A in regulation of vimentin assembly and cell extension formation. *Biochim. Biophys. Acta BBA-Mol. Cell Res.* **2020**, *1867*, 118739. [CrossRef]
62. Misra, S.; Ghatak, S.; Moreno-Rodriguez, R.A.; Norris, R.A.; Hascall, V.C.; Markwald, R.R. Periostin/filamin-A: A candidate central regulatory axis for valve fibrogenesis and matrix compaction. *Front. Cell Dev. Biol.* **2021**, *9*, 649862. [CrossRef] [PubMed]
63. Zhang, W.; Huang, Y.; Gunst, S.J. p21-Activated kinase (Pak) regulates airway smooth muscle contraction by regulating paxillin complexes that mediate actin polymerization. *J. Physiol.* **2016**, *594*, 4879–4900. [CrossRef]
64. Rajah, A.; Boudreau, C.G.; Ilie, A.; Wee, T.-L.; Tang, K.; Borisov, A.Z.; Orlowski, J.; Brown, C.M. Paxillin S273 phosphorylation regulates adhesion dynamics and cell migration through a common protein complex with PAK1 and βPIX. *Sci. Rep.* **2019**, *9*, 11430. [CrossRef]

65. Meyer zum Büschenfelde, U.; Brandenstein, L.I.; von Elsner, L.; Flato, K.; Holling, T.; Zenker, M.; Rosenberger, G.; Kutsche, K. RIT1 controls actin dynamics via complex formation with RAC1/CDC42 and PAK1. *PLoS Genet.* **2018**, *14*, e1007370. [CrossRef] [PubMed]
66. Peng, L.; He, Y.; Wang, W.; Dai, J.; Li, Q.; Ju, S. PAK1-Dependent Regulation of Microtubule Organization and Spindle Migration Is Essential for the Metaphase I–Metaphase II Transition in Porcine Oocytes. *Biomolecules* **2024**, *14*, 237. [CrossRef]
67. Monasky, M.M.; Taglieri, D.M.; Patel, B.G.; Chernoff, J.; Wolska, B.M.; Ke, Y.; Solaro, R.J. p21-activated kinase improves cardiac contractility during ischemia-reperfusion concomitant with changes in troponin-T and myosin light chain 2 phosphorylation. *Am. J. Physiol.-Heart Circ. Physiol.* **2012**, *302*, H1224–H1230. [CrossRef] [PubMed]
68. Chu, J.; Pham, N.T.; Olate, N.; Kislitsyna, K.; Day, M.-C.; LeTourneau, P.A.; Kots, A.; Stewart, R.H.; Laine, G.A.; Cox, C.S. Biphasic regulation of myosin light chain phosphorylation by p21-activated kinase modulates intestinal smooth muscle contractility. *J. Biol. Chem.* **2013**, *288*, 1200–1213. [CrossRef]
69. Forsyth, C.B.; Tang, Y.; Shaikh, M.; Zhang, L.; Keshavarzian, A. Role of snail activation in alcohol-induced iNOS-mediated disruption of intestinal epithelial cell permeability. *Alcohol. Clin. Exp. Res.* **2011**, *35*, 1635–1643. [CrossRef] [PubMed]
70. Cao, F.; Yin, L.-X. PAK1 promotes proliferation, migration and invasion of hepatocellular carcinoma by facilitating EMT via directly up-regulating Snail. *Genomics* **2020**, *112*, 694–702. [CrossRef] [PubMed]
71. Vadlamudi, R.K.; Barnes, C.J.; Rayala, S.; Li, F.; Balasenthil, S.; Marcus, S.; Goodson, H.V.; Sahin, A.A.; Kumar, R. p21-activated kinase 1 regulates microtubule dynamics by phosphorylating tubulin cofactor B. *Mol. Cell. Biol.* **2005**, *25*, 3726–3736. [CrossRef] [PubMed]
72. Banerjee, M.; Worth, D.; Prowse, D.M.; Nikolic, M. Pak1 phosphorylation on t212 affects microtubules in cells undergoing mitosis. *Curr. Biol.* **2002**, *12*, 1233–1239. [CrossRef] [PubMed]
73. Takahashi, K.; Suzuki, K. Membrane transport of WAVE2 and lamellipodia formation require Pak1 that mediates phosphorylation and recruitment of stathmin/Op18 to Pak1–WAVE2–kinesin complex. *Cell Signal* **2009**, *21*, 695–703. [CrossRef] [PubMed]
74. Morimura, S.; Takahashi, K. Rac1 and Stathmin but Not EB1 Are Required for Invasion of Breast Cancer Cells in Response to IGF-I. *Int. J. Cell Biol.* **2011**, *2011*, 615912. [CrossRef] [PubMed]
75. Chaudhary, A.; King, W.; Mattaliano, M.; Frost, J.; Diaz, B.; Morrison, D.; Cobb, M.; Marshall, M.; Brugge, J. Phosphatidylinositol 3-kinase regulates Raf1 through Pak phosphorylation of serine 338. *Curr. Biol.* **2000**, *10*, 551–554. [CrossRef]
76. Coles, L.C.; Shaw, P.E. PAK1 primes MEK1 for phosphorylation by Raf-1 kinase during cross-cascade activation of the ERK pathway. *Oncogene* **2002**, *21*, 2236–2244. [CrossRef] [PubMed]
77. Sun, H.; King, A.J.; Diaz, H.B.; Marshall, M.S. Regulation of the protein kinase Raf-1 by oncogenic Ras through phosphatidylinositol 3-kinase, Cdc42/Rac and Pak. *Curr. Biol.* **2000**, *10*, 281–284. [CrossRef] [PubMed]
78. Eblen, S.T.; Slack, J.K.; Weber, M.J.; Catling, A.D. Rac-PAK signaling stimulates extracellular signal-regulated kinase (ERK) activation by regulating formation of MEK1-ERK complexes. *Mol. Cell. Biol.* **2002**, *22*, 6023–6033. [CrossRef] [PubMed]
79. Higuchi, M.; Onishi, K.; Kikuchi, C.; Gotoh, Y. Scaffolding function of PAK in the PDK1–Akt pathway. *Nat. Cell Biol.* **2008**, *10*, 1356–1364. [CrossRef]
80. Ye, D.Z.; Jin, S.; Zhuo, Y.; Field, J. p21-Activated kinase 1 (Pak1) phosphorylates BAD directly at serine 111 in vitro and indirectly through Raf-1 at serine 112. *PLoS ONE* **2011**, *6*, e27637. [CrossRef]
81. Schürmann, A.; Mooney, A.; Sanders, L.; Sells, M.; Wang, H.; Reed, J.; Bokoch, G. p21-activated kinase 1 phosphorylates the death agonist bad and protects cells from apoptosis. *Mol. Cell. Biol.* **2000**, *20*, 453–461. [CrossRef] [PubMed]
82. Chen, C.; Yan, J.; Sun, Q.; Yao, L.; Jian, Y.; Lu, J.; Gu, J. Induction of apoptosis by p110C requires mitochondrial translocation of the proapoptotic BCL-2 family member BAD. *FEBS Lett.* **2006**, *580*, 813–821. [CrossRef]
83. Mosaddeghzadeh, N.; Pudewell, S.; Bazgir, F.; Kazemein Jasemi, N.S.; Krumbach, O.H.; Gremer, L.; Willbold, D.; Dvorsky, R.; Ahmadian, M.R. CDC42-IQGAP Interactions Scrutinized: New Insights into the Binding Properties of the GAP-Related Domain. *Int. J. Mol. Sci.* **2022**, *23*, 8842. [CrossRef] [PubMed]
84. Pudewell, S.; Wittich, C.; Kazemein Jasemi, N.S.; Bazgir, F.; Ahmadian, M.R. Accessory proteins of the RAS-MAPK pathway: Moving from the side line to the front line. *Commun. Biol.* **2021**, *4*, 696. [CrossRef]
85. Buday, L.; Tompa, P. Functional classification of scaffold proteins and related molecules. *FEBS J.* **2010**, *277*, 4348–4355. [CrossRef] [PubMed]
86. Pudewell, S.; Ahmadian, M.R. Spotlight on Accessory Proteins: RTK-RAS-MAPK Modulators as New Therapeutic Targets. *Biomolecules* **2021**, *11*, 895. [CrossRef] [PubMed]
87. Dharmawardhane, S.; Schurmann, A.; Sells, M.A.; Chernoff, J.; Schmid, S.L.; Bokoch, G.M. Regulation of macropinocytosis by p21-activated kinase-1. *Mol. Biol. Cell* **2000**, *11*, 3341–3352. [CrossRef]
88. Sells, M.A.; Pfaff, A.; Chernoff, J. Temporal and spatial distribution of activated Pak1 in fibroblasts. *J. Cell Biol.* **2000**, *151*, 1449–1458. [CrossRef]

89. Jaiswal, M.; Dvorsky, R.; Ahmadian, M.R. Deciphering the Molecular and Functional Basis of Dbl Family Proteins: A NOVEL SYSTEMATIC APPROACH TOWARD CLASSIFICATION OF SELECTIVE ACTIVATION OF THE Rho FAMILY PROTEINS*♦. *J. Biol. Chem.* **2013**, *288*, 4486–4500. [CrossRef] [PubMed]
90. Manser, E.; Loo, T.-H.; Koh, C.-G.; Zhao, Z.-S.; Chen, X.-Q.; Tan, L.; Tan, I.; Leung, T.; Lim, L. PAK kinases are directly coupled to the PIX family of nucleotide exchange factors. *Mol. Cell* **1998**, *1*, 183–192. [CrossRef] [PubMed]
91. Gringel, A.; Walz, D.; Rosenberger, G.; Minden, A.; Kutsche, K.; Kopp, P.; Linder, S. PAK4 and αPIX determine podosome size and number in macrophages through localized actin regulation. *J. Cell. Physiol.* **2006**, *209*, 568–579. [CrossRef] [PubMed]
92. Zhao, Z.-S.; Manser, E.; Loo, T.-H.; Lim, L. Coupling of PAK-interacting exchange factor PIX to GIT1 promotes focal complex disassembly. *Mol. Cell. Biol.* **2000**, *20*, 6354–6363. [CrossRef]
93. Rosenberger, G.; Jantke, I.; Gal, A.; Kutsche, K. Interaction of αPIX (ARHGEF6) with β-parvin (PARVB) suggests an involvement of αPIX in integrin-mediated signaling. *Hum. Mol. Genet.* **2003**, *12*, 155–167. [CrossRef]
94. Keum, S.; Yang, S.J.; Park, E.; Kang, T.; Choi, J.-H.; Jeong, J.; Hwang, Y.E.; Kim, J.-W.; Park, D.; Rhee, S. Beta-Pix-dynamin 2 complex promotes colorectal cancer progression by facilitating membrane dynamics. *Cell. Oncol.* **2021**, *44*, 1287–1305. [CrossRef] [PubMed]
95. Sánchez-Barrena, M.J.; Vallis, Y.; Clatworthy, M.R.; Doherty, G.J.; Veprintsev, D.B.; Evans, P.R.; McMahon, H.T. Bin2 is a membrane sculpting N-BAR protein that influences leucocyte podosomes, motility and phagocytosis. *PLoS ONE* **2012**, *7*, e52401. [CrossRef] [PubMed]
96. Kutsche, K.; Yntema, H.; Brandt, A.; Jantke, I.; Gerd Nothwang, H.; Orth, U.; Boavida, M.G.; David, D.; Chelly, J.; Fryns, J.-P. Mutations in ARHGEF6, encoding a guanine nucleotide exchange factor for Rho GTPases, in patients with X-linked mental retardation. *Nat. Genet.* **2000**, *26*, 247–250. [CrossRef] [PubMed]
97. Mott, H.R.; Nietlispach, D.; Evetts, K.A.; Owen, D. Structural analysis of the SH3 domain of β-PIX and its interaction with α-p21 activated kinase (PAK). *Biochemistry* **2005**, *44*, 10977–10983. [CrossRef] [PubMed]
98. Ku, G.M.; Yablonski, D.; Manser, E.; Lim, L.; Weiss, A. A PAK1–PIX–PKL complex is activated by the T-cell receptor independent of Nck, Slp-76 and LAT. *EMBO J.* **2001**, *20*, 457–465. [CrossRef]
99. Flanders, J.A.; Feng, Q.; Bagrodia, S.; Laux, M.T.; Singavarapu, A.; Cerione, R.A. The Cbl proteins are binding partners for the Cool/Pix family of p21-activated kinase-binding proteins. *FEBS Lett.* **2003**, *550*, 119–123. [CrossRef]
100. Kortüm, F.; Harms, F.L.; Hennighausen, N.; Rosenberger, G. αPIX is a trafficking regulator that balances recycling and degradation of the epidermal growth factor receptor. *PLoS ONE* **2015**, *10*, e0132737. [CrossRef] [PubMed]
101. Xi, S.; Tie, Y.; Lu, K.; Zhang, M.; Yin, X.; Chen, J.; Xing, G.; Tian, C.; Zheng, X.; He, F. N-terminal PH domain and C-terminal auto-inhibitory region of CKIP-1 coordinate to determine its nucleus-plasma membrane shuttling. *FEBS Lett.* **2010**, *584*, 1223–1230. [CrossRef]
102. Safi, A.; Vandromme, M.; Caussanel, S.; Valdacci, L.; Baas, D.; Vidal, M.; Brun, G.; Schaeffer, L.; Goillot, E. Role for the pleckstrin homology domain-containing protein CKIP-1 in phosphatidylinositol 3-kinase-regulated muscle differentiation. *Mol. Cell. Biol.* **2004**, *24*, 1245–1255. [CrossRef]
103. Bosc, D.G.; Graham, K.C.; Saulnier, R.B.; Zhang, C.; Prober, D.; Gietz, R.D.; Litchfield, D.W. Identification and characterization of CKIP-1, a novel pleckstrin homology domain-containing protein that interacts with protein kinase CK2. *J. Biol. Chem.* **2000**, *275*, 14295–14306. [CrossRef]
104. Canton, D.A.; Olsten, M.E.K.; Kim, K.; Doherty-Kirby, A.; Lajoie, G.; Cooper, J.A.; Litchfield, D.W. The pleckstrin homology domain-containing protein CKIP-1 is involved in regulation of cell morphology and the actin cytoskeleton and interaction with actin capping protein. *Mol. Cell. Biol.* **2005**, *25*, 3519–3534. [CrossRef]
105. Zhang, L.; Xing, G.; Tie, Y.; Tang, Y.; Tian, C.; Li, L.; Sun, L.; Wei, H.; Zhu, Y.; He, F. Role for the pleckstrin homology domain-containing protein CKIP-1 in AP-1 regulation and apoptosis. *EMBO J.* **2005**, *24*, 766–778. [CrossRef] [PubMed]
106. Zhang, L.; Tang, Y.; Tie, Y.; Tian, C.; Wang, J.; Dong, Y.; Sun, Z.; He, F. The PH domain containing protein CKIP-1 binds to IFP35 and Nmi and is involved in cytokine signaling. *Cell Signal* **2007**, *19*, 932–944. [CrossRef] [PubMed]
107. Zhang, L.; Tie, Y.; Tian, C.; Xing, G.; Song, Y.; Zhu, Y.; Sun, Z.; He, F. CKIP-1 recruits nuclear ATM partially to the plasma membrane through interaction with ATM. *Cell Signal* **2006**, *18*, 1386–1395. [CrossRef]
108. Tokuda, E.; Fujita, N.; Oh-hara, T.; Sato, S.; Kurata, A.; Katayama, R.; Itoh, T.; Takenawa, T.; Miyazono, K.; Tsuruo, T. Casein kinase 2–interacting protein-1, a novel Akt pleckstrin homology domain-interacting protein, down-regulates PI3K/Akt signaling and suppresses tumor growth in vivo. *Cancer Res.* **2007**, *67*, 9666–9676. [CrossRef]
109. Fu, L.; Zhang, L. Physiological functions of CKIP-1: From molecular mechanisms to therapy implications. *Ageing Res. Rev.* **2019**, *53*, 100908. [CrossRef] [PubMed]
110. Kim, Y.B.; Shin, Y.J.; Roy, A.; Kim, J.H. The Role of the Pleckstrin Homology Domain-containing Protein CKIP-1 in Activation of p21-activated Kinase 1 (PAK1). *J. Biol. Chem.* **2015**, *290*, 21076–21085. [CrossRef] [PubMed]
111. Frank, S.R.; Hansen, S.H. The PIX–GIT complex: AG protein signaling cassette in control of cell shape. In *Seminars in Cell & Developmental Biology*; Academic Press: Cambridge, MA, USA, 2008; Volume 19, pp. 234–244.

112. Premont, R.T.; Perry, S.J.; Schmalzigaug, R.; Roseman, J.T.; Xing, Y.; Claing, A. The GIT/PIX complex: An oligomeric assembly of GIT family ARF GTPase-activating proteins and PIX family Rac1/Cdc42 guanine nucleotide exchange factors. *Cell Signal* **2004**, *16*, 1001–1011. [CrossRef] [PubMed]
113. Paris, S.; Longhi, R.; Santambrogio, P.; de Curtis, I. Leucine-zipper-mediated homo- and hetero-dimerization of GIT family p95-ARF GTPase-activating protein, PIX-, paxillin-interacting proteins 1 and 2. *Biochem. J.* **2003**, *372*, 391–398. [CrossRef] [PubMed]
114. Hoefen, R.J.; Berk, B.C. The multifunctional GIT family of proteins. *J. Cell Sci.* **2006**, *119*, 1469–1475. [CrossRef] [PubMed]
115. Turner, C.E.; Brown, M.C.; Perrotta, J.A.; Riedy, M.; Nikolopoulos, S.N.; McDonald, A.R.; Bagrodia, S.; Thomas, S.; Leventhal, P.S. Paxillin LD4 motif binds PAK and PIX through a novel 95-kD ankyrin repeat, ARF–GAP protein: A role in cytoskeletal remodeling. *J. Cell Biol.* **1999**, *145*, 851–863. [CrossRef]
116. van Gastel, J.; Boddaert, J.; Jushaj, A.; Premont, R.T.; Luttrell, L.M.; Janssens, J.; Martin, B.; Maudsley, S. GIT2—A keystone in ageing and age-related disease. *Ageing Res. Rev.* **2018**, *43*, 46–63. [CrossRef]
117. Martin, B.; Chadwick, W.; Janssens, J.; Premont, R.T.; Schmalzigaug, R.; Becker, K.G.; Lehrmann, E.; Wood, W.H.; Zhang, Y.; Siddiqui, S. GIT2 acts as a systems-level coordinator of neurometabolic activity and pathophysiological aging. *Front. Endocrinol.* **2016**, *6*, 191. [CrossRef] [PubMed]
118. Nayal, A.; Webb, D.J.; Brown, C.M.; Schaefer, E.M.; Vicente-Manzanares, M.; Horwitz, A.R. Paxillin phosphorylation at Ser273 localizes a GIT1–PIX–PAK complex and regulates adhesion and protrusion dynamics. *J. Cell Biol.* **2006**, *173*, 587–589. [CrossRef] [PubMed]
119. Zhou, W.; Li, X.; Premont, R.T. Expanding functions of GIT Arf GTPase-activating proteins, PIX Rho guanine nucleotide exchange factors and GIT–PIX complexes. *J. Cell Sci.* **2016**, *129*, 1963–1974. [CrossRef] [PubMed]
120. Santiago-Medina, M.; Gregus, K.A.; Gomez, T.M. PAK–PIX interactions regulate adhesion dynamics and membrane protrusion to control neurite outgrowth. *J. Cell Sci.* **2013**, *126*, 1122–1133. [CrossRef]
121. Loo, T.H.; Ng, Y.W.; Lim, L.; Manser, E. GIT1 activates p21-activated kinase through a mechanism independent of p21 binding. *Mol. Cell. Biol.* **2004**, *24*, 3849–3859. [CrossRef]
122. Phee, H.; Abraham, R.T.; Weiss, A. Dynamic recruitment of PAK1 to the immunological synapse is mediated by PIX independently of SLP-76 and Vav1. *Nat. Immunol.* **2005**, *6*, 608–617. [CrossRef] [PubMed]
123. Kim, S.; Lee, S.H.; Park, D. Leucine zipper-mediated homodimerization of the p21-activated kinase-interacting factor, beta Pix. Implication for a role in cytoskeletal reorganization. *J. Biol. Chem.* **2001**, *276*, 10581–10584. [CrossRef] [PubMed]
124. Neumann, K.; Oellerich, T.; Urlaub, H.; Wienands, J. The B-lymphoid Grb2 interaction code. *Immunol. Rev.* **2009**, *232*, 135–149. [CrossRef] [PubMed]
125. Jasemi NS, K.; Ahmadian, M.R. Allosteric regulation of GRB2 modulates RAS activation. *Small GTPases* **2022**, *13*, 282–286. [CrossRef] [PubMed]
126. Kazemein Jasemi, N.S.; Herrmann, C.; Magdalena Estirado, E.; Gremer, L.; Willbold, D.; Brunsveld, L.; Dvorsky, R.; Ahmadian, M.R. The intramolecular allostery of GRB2 governing its interaction with SOS1 is modulated by phosphotyrosine ligands. *Biochem. J.* **2021**, *478*, 2793–2809. [CrossRef] [PubMed]
127. Puto, L.A.; Pestonjamasp, K.; King, C.C.; Bokoch, G.M. p21-activated kinase 1 (PAK1) interacts with the Grb2 adapter protein to couple to growth factor signaling. *J. Biol. Chem.* **2003**, *278*, 9388–9393. [CrossRef]
128. Pi, J.; Liu, J.; Zhuang, T.; Zhang, L.; Sun, H.; Chen, X.; Zhao, Q.; Kuang, Y.; Peng, S.; Zhou, X. Elevated expression of miR302-367 in endothelial cells inhibits developmental angiogenesis via CDC42/CCND1 mediated signaling pathways. *Theranostics* **2018**, *8*, 1511. [CrossRef] [PubMed]
129. Huang, H.; Liu, Y.; Wang, Y.; Liu, H.; Xie, B.; Zheng, M.B.; Yang, L.; Huang, Q.; Wu, Y.; Wu, G. Semaphorin-3 Promotes Specific Immunotherapy Effects on Experimental Food Allergy. *J. Immunol. Res.* **2022**, *2022*, 5414993. [CrossRef] [PubMed]
130. Wang, D.; Paria, B.C.; Zhang, Q.; Karpurapu, M.; Li, Q.; Gerthoffer, W.T.; Nakaoka, Y.; Rao, G.N. A role for Gab1/SHP2 in thrombin activation of PAK1: Gene transfer of kinase-dead PAK1 inhibits injury-induced restenosis. *Circ. Res.* **2009**, *104*, 1066–1075. [CrossRef]
131. Alfaidi, M.; Scott, M.L.; Orr, A.W. Sinner or saint?: Nck adaptor proteins in vascular biology. *Front. Cell Dev. Biol.* **2021**, *9*, 688388. [CrossRef]
132. Bywaters, B.C.; Rivera, G.M. Nck adaptors at a glance. *J. Cell Sci.* **2021**, *134*, jcs258965. [CrossRef]
133. Buday, L.; Wunderlich, L.; Tamás, P. The Nck family of adapter proteins: Regulators of actin cytoskeleton. *Cell Signal* **2002**, *14*, 723–731. [CrossRef] [PubMed]
134. Galisteo, M.L.; Chernoff, J.; Su, Y.-C.; Skolnik, E.Y.; Schlessinger, J. The adaptor protein Nck links receptor tyrosine kinases with the serine-threonine kinase Pak1. *J. Biol. Chem.* **1996**, *271*, 20997–21000. [CrossRef] [PubMed]
135. Bokoch, G.M.; Wang, Y.; Bohl, B.P.; Sells, M.A.; Quilliam, L.A.; Knaus, U.G. Interaction of the Nck adapter protein with p21-activated kinase (PAK1). *J. Biol. Chem.* **1996**, *271*, 25746–25749. [CrossRef]

136. Alfaidi, M.; Bhattarai, U.; Orr, A.W. Nck1, But Not Nck2, Mediates Disturbed Flow-Induced p21-Activated Kinase Activation and Endothelial Permeability. *J. Am. Heart Assoc.* **2020**, *9*, e016099. [CrossRef] [PubMed]
137. Bisson, N.; Poitras, L.; Mikryukov, A.; Tremblay, M.; Moss, T. EphA4 signaling regulates blastomere adhesion in the Xenopus embryo by recruiting Pak1 to suppress Cdc42 function. *Mol. Biol. Cell* **2007**, *18*, 1030–1043. [CrossRef] [PubMed]
138. Chen, J.; Leskov, I.L.; Yurdagul Jr, A.; Thiel, B.; Kevil, C.G.; Stokes, K.Y.; Orr, A.W. Recruitment of the adaptor protein Nck to PECAM-1 couples oxidative stress to canonical NF-κB signaling and inflammation. *Sci. Signal.* **2015**, *8*, ra20. [CrossRef]
139. Zhou, G.-L.; Zhuo, Y.; King, C.C.; Fryer, B.H.; Bokoch, G.M.; Field, J. Akt phosphorylation of serine 21 on Pak1 modulates Nck binding and cell migration. *Mol. Cell. Biol.* **2003**, *23*, 8058–8069. [CrossRef]
140. Stoletov, K.V.; Ratcliffe, K.E.; Spring, S.C.; Terman, B.I. NCK and PAK participate in the signaling pathway by which vascular endothelial growth factor stimulates the assembly of focal adhesions. *J. Biol. Chem.* **2001**, *276*, 22748–22755. [CrossRef]
141. Dionne, U.; Chartier, F.J.; de Los Santos, Y.L.; Lavoie, N.; Bernard, D.N.; Banerjee, S.L.; Otis, F.; Jacquet, K.; Tremblay, M.G.; Jain, M. Direct phosphorylation of SRC homology 3 domains by tyrosine kinase receptors disassembles ligand-induced signaling networks. *Mol. Cell* **2018**, *70*, 995–1007.e11. [CrossRef]
142. Xia, P.; Huang, M.; Zhang, Y.; Xiong, X.; Yan, M.; Xiong, X.; Yu, W.; Song, E. NCK1 promotes the angiogenesis of cervical squamous carcinoma via Rac1/PAK1/MMP2 signal pathway. *Gynecol. Oncol.* **2019**, *152*, 387–395. [CrossRef] [PubMed]
143. Gonzalez-Villasana, V.; Fuentes-Mattei, E.; Ivan, C.; Dalton, H.J.; Rodriguez-Aguayo, C.; Fernandez-de Thomas, R.J.; Aslan, B.; Del, C.M.P.; Velazquez-Torres, G.; Previs, R.A.; et al. Rac1/Pak1/p38/MMP-2 Axis Regulates Angiogenesis in Ovarian Cancer. *Clin. Cancer Res. Off. J. Am. Assoc. Cancer Res.* **2015**, *21*, 2127–2137. [CrossRef]
144. Zhang, F.; Lu, Y.-X.; Chen, Q.; Zou, H.-M.; Zhang, J.-M.; Hu, Y.-H.; Li, X.-M.; Zhang, W.-J.; Zhang, W.; Lin, C.; et al. Identification of NCK1 as a novel downstream effector of STAT3 in colorectal cancer metastasis and angiogenesis. *Cell Signal* **2017**, *36*, 67–78. [CrossRef] [PubMed]
145. Dubrac, A.; Künzel, S.E.; Künzel, S.H.; Li, J.; Chandran, R.R.; Martin, K.; Greif, D.M.; Adams, R.H.; Eichmann, A. NCK-dependent pericyte migration promotes pathological neovascularization in ischemic retinopathy. *Nat. Commun.* **2018**, *9*, 3463. [CrossRef]
146. Tao, J.; Oladimeji, P.; Rider, L.; Diakonova, M. PAK1-Nck regulates cyclin D1 promoter activity in response to prolactin. *Mol. Endocrinol.* **2011**, *25*, 1565–1578. [CrossRef] [PubMed]
147. Borroto, A.; Reyes-Garau, D.; Jiménez, M.A.; Carrasco, E.; Moreno, B.; Martínez-Pasamar, S.; Cortés, J.R.; Perona, A.; Abia, D.; Blanco, S. First-in-class inhibitor of the T cell receptor for the treatment of autoimmune diseases. *Sci. Transl. Med.* **2016**, *8*, 370ra184. [CrossRef] [PubMed]
148. Alarcon, B.; Borroto, A. Small molecule AX-024 targets T cell receptor signaling by disrupting CD3ε-Nck interaction. *J. Biol. Chem.* **2020**, *295*, 10076. [CrossRef] [PubMed]
149. Brown, M.C.; Turner, C.E. Paxillin: Adapting to change. *Physiol. Rev.* **2004**, *84*, 1315–1339. [CrossRef]
150. Brown, M.C.; West, K.A.; Turner, C.E. Paxillin-dependent paxillin kinase linker and p21-activated kinase localization to focal adhesions involves a multistep activation pathway. *Mol. Biol. Cell* **2002**, *13*, 1550–1565. [CrossRef]
151. Zhao, Z.S.; Manser, E. PAK and other Rho-associated kinases–effectors with surprisingly diverse mechanisms of regulation. *Biochem. J.* **2005**, *386*, 201–214. [CrossRef]
152. Meenderink, L.M.; Ryzhova, L.M.; Donato, D.M.; Gochberg, D.F.; Kaverina, I.; Hanks, S.K. P130Cas Src-binding and substrate domains have distinct roles in sustaining focal adhesion disassembly and promoting cell migration. *PLoS ONE* **2010**, *5*, e13412. [CrossRef]
153. Lawson, C.; Lim, S.T.; Uryu, S.; Chen, X.L.; Calderwood, D.A.; Schlaepfer, D.D. FAK promotes recruitment of talin to nascent adhesions to control cell motility. *J. Cell Biol.* **2012**, *196*, 223–232. [CrossRef] [PubMed]
154. Colicelli, J. Human RAS superfamily proteins and related GTPases. *Sci. STKE Signal Transduct. Knowl. Environ.* **2004**, *2004*, Re13. [CrossRef]
155. Shi, G.X.; Cai, W.; Andres, D.A. Rit subfamily small GTPases: Regulators in neuronal differentiation and survival. *Cell Signal* **2013**, *25*, 2060–2068. [CrossRef] [PubMed]
156. Nakhaei-Rad, S.; Haghighi, F.; Nouri, P.; Rezaei Adariani, S.; Lissy, J.; Kazemein Jasemi, N.S.; Dvorsky, R.; Ahmadian, M.R. Structural fingerprints, interactions, and signaling networks of RAS family proteins beyond RAS isoforms. *Crit. Rev. Biochem. Mol. Biol.* **2018**, *53*, 130–156. [CrossRef]
157. Lee, C.H.; Della, N.G.; Chew, C.E.; Zack, D.J. Rin, a neuron-specific and calmodulin-binding small G-protein, and Rit define a novel subfamily of ras proteins. *J. Neurosci. Off. J. Soc. Neurosci.* **1996**, *16*, 6784–6794. [CrossRef]
158. Van, R.; Cuevas-Navarro, A.; Castel, P.; McCormick, F. The molecular functions of RIT1 and its contribution to human disease. *Biochem. J.* **2020**, *477*, 2755–2770. [CrossRef] [PubMed]
159. Cavé, H.; Caye, A.; Ghedira, N.; Capri, Y.; Pouvreau, N.; Fillot, N.; Trimouille, A.; Vignal, C.; Fenneteau, O.; Alembik, Y. Mutations in RIT1 cause Noonan syndrome with possible juvenile myelomonocytic leukemia but are not involved in acute lymphoblastic leukemia. *Eur. J. Hum. Genet.* **2016**, *24*, 1124–1131. [CrossRef] [PubMed]

160. Yaoita, M.; Niihori, T.; Mizuno, S.; Okamoto, N.; Hayashi, S.; Watanabe, A.; Yokozawa, M.; Suzumura, H.; Nakahara, A.; Nakano, Y. Spectrum of mutations and genotype–phenotype analysis in Noonan syndrome patients with RIT1 mutations. *Human Genet.* **2016**, *135*, 209–222. [CrossRef] [PubMed]
161. Che, M.; Lan, Q. RIT1 Promotes Glioma Proliferation and Invasion via the AKT/ERK/NF-κB Signaling Pathway. *J. Mol. Neurosci.* **2022**, *72*, 1547–1556. [CrossRef] [PubMed]
162. Berger, A.; Imielinski, M.; Duke, F.; Wala, J.; Kaplan, N.; Shi, G.; Andres, D.; Meyerson, M. Oncogenic RIT1 mutations in lung adenocarcinoma. *Oncogene* **2014**, *33*, 4418–4423. [CrossRef] [PubMed]
163. Talukder, A.H.; Meng, Q.; Kumar, R. CRIPak, a novel endogenous Pak1 inhibitor. *Oncogene* **2006**, *25*, 1311–1319. [CrossRef]
164. Daniels, R.H.; Zenke, F.T.; Bokoch, G.M. αPix stimulates p21-activated kinase activity through exchange factor-dependent and-independent mechanisms. *J. Biol. Chem.* **1999**, *274*, 6047–6050. [CrossRef] [PubMed]
165. Li, Y.; Zhou, H.; Li, F.; Chan, S.W.; Lin, Z.; Wei, Z.; Yang, Z.; Guo, F.; Lim, C.J.; Xing, W. Angiomotin binding-induced activation of Merlin/NF2 in the Hippo pathway. *Cell Res.* **2015**, *25*, 801–817. [CrossRef] [PubMed]
166. Mani, T.; Hennigan, R.F.; Foster, L.A.; Conrady, D.G.; Herr, A.B.; Ip, W. FERM domain phosphoinositide binding targets merlin to the membrane and is essential for its growth-suppressive function. *Mol. Cell. Biol.* **2011**, *31*, 1983–1996. [CrossRef]
167. Houshmandi, S.S.; Emnett, R.J.; Giovannini, M.; Gutmann, D.H. The neurofibromatosis 2 protein, merlin, regulates glial cell growth in an ErbB2-and Src-dependent manner. *Mol. Cell. Biol.* **2009**, *29*, 1472–1486. [CrossRef]
168. Scoles, D.R.; Huynh, D.P.; Morcos, P.A.; Coulsell, E.R.; Robinson, N.G.; Tamanoi, F.; Pulst, S.M. Neurofibromatosis 2 tumour suppressor schwannomin interacts with βII-spectrin. *Nat. Genet.* **1998**, *18*, 354–359. [CrossRef]
169. Bae, J.H.; Yang, M.J.; Jeong, S.-h.; Kim, J.; Hong, S.P.; Kim, J.W.; Kim, Y.H.; Koh, G.Y. Gatekeeping role of Nf2/Merlin in vascular tip EC induction through suppression of VEGFR2 internalization. *Sci. Adv.* **2022**, *8*, eabn2611. [CrossRef] [PubMed]
170. Yi, C.; Troutman, S.; Fera, D.; Stemmer-Rachamimov, A.; Avila, J.L.; Christian, N.; Persson, N.L.; Shimono, A.; Speicher, D.W.; Marmorstein, R. A tight junction-associated Merlin-angiomotin complex mediates Merlin's regulation of mitogenic signaling and tumor suppressive functions. *Cancer Cell* **2011**, *19*, 527–540. [CrossRef] [PubMed]
171. Cui, Y.; Ma, L.; Schacke, S.; Yin, J.C.; Hsueh, Y.-P.; Jin, H.; Morrison, H. Merlin cooperates with neurofibromin and Spred1 to suppress the Ras–Erk pathway. *Human Mol. Genet.* **2020**, *29*, 3793–3806. [CrossRef]
172. Cui, Y.; Groth, S.; Troutman, S.; Carlstedt, A.; Sperka, T.; Riecken, L.B.; Kissil, J.L.; Jin, H.; Morrison, H. The NF2 tumor suppressor merlin interacts with Ras and RasGAP, which may modulate Ras signaling. *Oncogene* **2019**, *38*, 6370–6381. [CrossRef]
173. Kim, M.; Kim, S.; Lee, S.; Kim, W.; Sohn, M.; Kim, H.; Kim, J.; Jho, E. Merlin inhibits Wnt/β-catenin signaling by blocking LRP6 phosphorylation. *Cell Death Differ.* **2016**, *23*, 1638–1647. [CrossRef] [PubMed]
174. Zhou, L.; Hanemann, C.O. Merlin, a multi-suppressor from cell membrane to the nucleus. *FEBS Lett.* **2012**, *586*, 1403–1408. [CrossRef] [PubMed]
175. Schulz, A.; Zoch, A.; Morrison, H. A neuronal function of the tumor suppressor protein merlin. *Acta Neuropathol. Commun.* **2014**, *2*, 82. [CrossRef] [PubMed]
176. Kissil, J.L.; Wilker, E.W.; Johnson, K.C.; Eckman, M.S.; Yaffe, M.B.; Jacks, T. Merlin, the product of the Nf2 tumor suppressor gene, is an inhibitor of the p21-activated kinase, Pak1. *Mol. Cell* **2003**, *12*, 841–849. [CrossRef]
177. Kaempchen, K.; Mielke, K.; Utermark, T.; Langmesser, S.; Hanemann, C.O. Upregulation of the Rac1/JNK signaling pathway in primary human schwannoma cells. *Hum. Mol. Genet.* **2003**, *12*, 1211–1221. [CrossRef]
178. Gehlhausen, J.R.; Park, S.J.; Hickox, A.E.; Shew, M.; Staser, K.; Rhodes, S.D.; Menon, K.; Lajiness, J.D.; Mwanthi, M.; Yang, X.; et al. A murine model of neurofibromatosis type 2 that accurately phenocopies human schwannoma formation. *Human Mol. Genet.* **2015**, *24*, 1–8. [CrossRef]
179. Morrison, H.; Sperka, T.; Manent, J.; Giovannini, M.; Ponta, H.; Herrlich, P. Merlin/neurofibromatosis type 2 suppresses growth by inhibiting the activation of Ras and Rac. *Cancer Res.* **2007**, *67*, 520–527. [CrossRef] [PubMed]
180. Alahari, S.K.; Lee, J.W.; Juliano, R.L. Nischarin, a novel protein that interacts with the integrin α5 subunit and inhibits cell migration. *J. Cell Biol.* **2000**, *151*, 1141–1154. [CrossRef]
181. Li, S.; Zhang, X.-q.; Liu, C.-c.; Wang, Z.-y.; Lu, G.-y.; Shen, H.-w.; Wu, N.; Li, J.; Li, F. IRAS/Nischarin modulates morphine reward by glutamate receptor activation in the nucleus accumbens of mouse brain. *Biomed. Pharmacother.* **2022**, *153*, 113346. [CrossRef] [PubMed]
182. Gupta, S.; Bazargani, N.; Drew, J.; Howden, J.H.; Modi, S.; Al Awabdh, S.; Marie, H.; Attwell, D.; Kittler, J.T. The non-adrenergic imidazoline-1 receptor protein nischarin is a key regulator of astrocyte glutamate uptake. *iScience* **2022**, *25*, 104127. [CrossRef] [PubMed]
183. Sano, H.; Liu, S.C.; Lane, W.S.; Piletz, J.E.; Lienhard, G.E. Insulin receptor substrate 4 associates with the protein IRAS. *J. Biol. Chem.* **2002**, *277*, 19439–19447. [CrossRef]
184. Kuijl, C.; Pilli, M.; Alahari, S.K.; Janssen, H.; Khoo, P.S.; Ervin, K.E.; Calero, M.; Jonnalagadda, S.; Scheller, R.H.; Neefjes, J. Rac and Rab GTPases dual effector Nischarin regulates vesicle maturation to facilitate survival of intracellular bacteria. *EMBO J.* **2013**, *32*, 713–727. [CrossRef]

185. Jain, P.; Baranwal, S.; Dong, S.; Struckhoff, A.P.; Worthylake, R.A.; Alahari, S.K. Integrin-binding protein nischarin interacts with tumor suppressor liver kinase B1 (LKB1) to regulate cell migration of breast epithelial cells. *J. Biol. Chem.* **2013**, *288*, 15495–15509. [CrossRef]
186. Ding, Y.; Milosavljevic, T.; Alahari, S.K. Nischarin inhibits LIM kinase to regulate cofilin phosphorylation and cell invasion. *Mol. Cell. Biol.* **2008**, *28*, 3742–3756. [CrossRef]
187. Alahari, S.K.; Reddig, P.J.; Juliano, R.L. The integrin-binding protein Nischarin regulates cell migration by inhibiting PAK. *EMBO J.* **2004**, *23*, 2777–2788. [CrossRef] [PubMed]
188. Reddig, P.J.; Xu, D.; Juliano, R.L. Regulation of p21-activated kinase-independent Rac1 signal transduction by nischarin. *J. Biol. Chem.* **2005**, *280*, 30994–31002. [CrossRef] [PubMed]
189. Maziveyi, M.; Alahari, S.K. Breast cancer tumor suppressors: A special emphasis on novel protein nischarin. *Cancer Res.* **2015**, *75*, 4252–4259. [CrossRef]
190. Zheng, P.; Pan, C.; Zhou, C.; Liu, B.; Wang, L.; Duan, S.; Ding, Y. Contribution of Nischarin/IRAS in CNS development, injury and diseases. *J. Adv. Res.* **2023**, *54*, 43–57. [CrossRef]
191. Okpechi, S.C.; Yousefi, H.; Nguyen, K.; Cheng, T.; Alahari, N.V.; Collins-Burow, B.; Burow, M.E.; Alahari, S.K. Role of Nischarin in the pathology of diseases: A special emphasis on breast cancer. *Oncogene* **2022**, *41*, 1079–1086. [CrossRef] [PubMed]
192. Baranwal, S.; Wang, Y.; Rathinam, R.; Lee, J.; Jin, L.; McGoey, R.; Pylayeva, Y.; Giancotti, F.; Blobe, G.C.; Alahari, S.K. Molecular characterization of the tumor-suppressive function of nischarin in breast cancer. *J. Natl. Cancer Inst.* **2011**, *103*, 1513–1528. [CrossRef]
193. Alahari, S.K.; Nasrallah, H. A membrane proximal region of the integrin alpha5 subunit is important for its interaction with nischarin. *Biochem. J.* **2004**, *377*, 449–457. [CrossRef] [PubMed]
194. Mukaddam-Daher, S. An "I" on cardiac hypertrophic remodelling: Imidazoline receptors and heart disease. *Can. J. Cardiol.* **2012**, *28*, 590–598. [CrossRef] [PubMed]
195. Alahari, S.K. Nischarin inhibits Rac induced migration and invasion of epithelial cells by affecting signaling cascades involving PAK. *Exp. Cell Res.* **2003**, *288*, 415–424. [CrossRef] [PubMed]
196. Ding, Y.; Li, Y.; Lu, L.; Zhang, R.; Zeng, L.; Wang, L.; Zhang, X. Inhibition of Nischarin Expression Promotes Neurite Outgrowth through Regulation of PAK Activity. *PLoS ONE* **2015**, *10*, e0144948. [CrossRef] [PubMed]
197. Xia, C.; Ma, W.; Stafford, L.J.; Marcus, S.; Xiong, W.-C.; Liu, M. Regulation of the p21-activated kinase (PAK) by a human Gβ-like WD-repeat protein, hPIP1. *Proc. Natl. Acad. Sci. USA* **2001**, *98*, 6174–6179. [CrossRef]
198. Ross, A.P.; Mansilla, M.A.; Choe, Y.; Helminski, S.; Sturm, R.; Maute, R.L.; May, S.R.; Hozyasz, K.K.; Wojcicki, P.; Mostowska, A. A mutation in mouse Pak1ip1 causes orofacial clefting while human PAK1IP1 maps to 6p24 translocation breaking points associated with orofacial clefting. *PLoS ONE* **2013**, *8*, e69333. [CrossRef]
199. Saveanu, C.; Rousselle, J.-C.; Lenormand, P.; Namane, A.; Jacquier, A.; Fromont-Racine, M. The p21-activated protein kinase inhibitor Skb15 and its budding yeast homologue are 60S ribosome assembly factors. *Mol. Cell. Biol.* **2007**, *27*, 2897–2909. [CrossRef] [PubMed]
200. Yu, W.; Qiu, Z.; Gao, N.; Wang, L.; Cui, H.; Qian, Y.; Jiang, L.; Luo, J.; Yi, Z.; Lu, H. PAK1IP1, a ribosomal stress-induced nucleolar protein, regulates cell proliferation via the p53–MDM2 loop. *Nucleic Acids Res.* **2011**, *39*, 2234–2248. [CrossRef] [PubMed]
201. Schurmans, S.; Catsyne, C.-A.V.; Desmet, C.; Moës, B. The phosphoinositide 5-phosphatase INPP5K: From gene structure to in vivo functions. *Adv. Biol. Regul.* **2021**, *79*, 100760. [CrossRef]
202. Ijuin, T.; Takenawa, T. Regulation of insulin signaling and glucose transporter 4 (GLUT4) exocytosis by phosphatidylinositol 3, 4, 5-trisphosphate (PIP3) phosphatase, skeletal muscle, and kidney enriched inositol polyphosphate phosphatase (SKIP). *J. Biol. Chem.* **2012**, *287*, 6991–6999. [CrossRef] [PubMed]
203. Ijuin, T.; Hosooka, T.; Takenawa, T. Phosphatidylinositol 3, 4, 5-trisphosphate phosphatase SKIP links endoplasmic reticulum stress in skeletal muscle to insulin resistance. *Mol. Cell. Biol.* **2016**, *36*, 108–118. [CrossRef] [PubMed]
204. Ijuin, T.; Takenawa, T. Improvement of insulin signaling in myoblast cells by an addition of SKIP-binding peptide within Pak1 kinase domain. *Biochem. Biophys. Res. Commun.* **2015**, *456*, 41–46. [CrossRef] [PubMed]
205. Ijuin, T.; Hatano, N.; Hosooka, T.; Takenawa, T. Regulation of insulin signaling in skeletal muscle by PIP3 phosphatase, SKIP, and endoplasmic reticulum molecular chaperone glucose-regulated protein 78. *Biochim. Biophys. Acta BBA-Mol. Cell Res.* **2015**, *1853*, 3192–3201. [CrossRef] [PubMed]
206. Ijuin, T.; Hatano, N.; Takenawa, T. Glucose-regulated protein 78 (GRP 78) binds directly to PIP 3 phosphatase SKIP and determines its localization. *Genes Cells* **2016**, *21*, 457–465. [CrossRef]
207. Wiessner, M.; Roos, A.; Munn, C.J.; Viswanathan, R.; Whyte, T.; Cox, D.; Schoser, B.; Sewry, C.; Roper, H.; Phadke, R. Mutations in INPP5K, encoding a phosphoinositide 5-phosphatase, cause congenital muscular dystrophy with cataracts and mild cognitive impairment. *Am. J. Hum. Genet.* **2017**, *100*, 523–536. [CrossRef]
208. Ijuin, T.; Takenawa, T. SKIP negatively regulates insulin-induced GLUT4 translocation and membrane ruffle formation. *Mol. Cell. Biol.* **2003**, *23*, 1209–1220. [CrossRef]

209. Ijuin, T.; Yu, Y.E.; Mizutani, K.; Pao, A.; Tateya, S.; Tamori, Y.; Bradley, A.; Takenawa, T. Increased insulin action in SKIP heterozygous knockout mice. *Mol. Cell. Biol.* **2008**, *28*, 5184–5195. [CrossRef] [PubMed]
210. Xiong, Q.; Deng, C.-Y.; Chai, J.; Jiang, S.-W.; Xiong, Y.-Z.; Li, F.-E.; Zheng, R. Knockdown of endogenous SKIP gene enhanced insulin-induced glycogen synthesis signaling in differentiating C2C12 myoblasts. *BMB Rep.* **2009**, *42*, 119–124. [CrossRef]
211. Ijuin, T.; Takenawa, T. Regulation of insulin signaling by the phosphatidylinositol 3,4,5-triphosphate phosphatase SKIP through the scaffolding function of Pak1. *Mol. Cell. Biol.* **2012**, *32*, 3570–3584. [CrossRef] [PubMed]
212. Nagano, M.; Hoshino, D.; Koshikawa, N.; Akizawa, T.; Seiki, M. Turnover of focal adhesions and cancer cell migration. *Int. J. Cell Biol.* **2012**, *2012*, 310616. [CrossRef]
213. Wozniak, M.A.; Modzelewska, K.; Kwong, L.; Keely, P.J. Focal adhesion regulation of cell behavior. *Biochim. Biophys. Acta BBA-Mol. Cell Res.* **2004**, *1692*, 103–119. [CrossRef] [PubMed]
214. Lu, W.; Mayer, B.J. Mechanism of activation of Pak1 kinase by membrane localization. *Oncogene* **1999**, *18*, 797–806. [CrossRef]
215. Lu, W.; Katz, S.; Gupta, R.; Mayer, B.J. Activation of Pak by membrane localization mediated by an SH3 domain from the adaptor protein Nck. *Curr. Biol.* **1997**, *7*, 85–94. [CrossRef] [PubMed]
216. Ong, C.C.; Jubb, A.M.; Haverty, P.M.; Zhou, W.; Tran, V.; Truong, T.; Turley, H.; O'Brien, T.; Vucic, D.; Harris, A.L. Targeting p21-activated kinase 1 (PAK1) to induce apoptosis of tumor cells. *Proc. Natl. Acad. Sci. USA* **2011**, *108*, 7177–7182. [CrossRef] [PubMed]
217. Kichina, J.V.; Maslov, A.; Kandel, E.S. PAK1 and therapy resistance in melanoma. *Cells* **2023**, *12*, 2373. [CrossRef] [PubMed]
218. Chen, M.-J.; Wu, D.-W.; Wang, Y.-C.; Chen, C.-Y.; Lee, H. PAK1 confers chemoresistance and poor outcome in non-small cell lung cancer via β-catenin-mediated stemness. *Sci. Rep.* **2016**, *6*, 34933.
219. Belli, S.; Esposito, D.; Allotta, A.; Servetto, A.; Ciciola, P.; Pesapane, A.; Ascione, C.M.; Napolitano, F.; Di Mauro, C.; Vigliar, E. Pak1 pathway hyper-activation mediates resistance to endocrine therapy and CDK4/6 inhibitors in ER+ breast cancer. *npj Breast Cancer* **2023**, *9*, 48. [CrossRef] [PubMed]
220. Li, B.; Jia, R.; Li, W.; Zhou, Y.; Guo, D.; Teng, Q.; Du, S.; Li, M.; Li, W.; Sun, T. PAK1 mediates bone marrow stromal cell-induced drug resistance in acute myeloid leukemia via ERK1/2 signaling pathway. *Front. Cell Dev. Biol.* **2021**, *9*, 686695. [CrossRef] [PubMed]
221. Chow, H.-Y.; Karchugina, S.; Groendyke, B.J.; Toenjes, S.; Hatcher, J.; Donovan, K.A.; Fischer, E.S.; Abalakov, G.; Faezov, B.; Dunbrack, R. Development and utility of a PAK1-selective degrader. *J. Med. Chem.* **2022**, *65*, 15627–15641. [CrossRef] [PubMed]
222. Saliani, M.; Mirzaiebadizi, A.; Mosaddeghzadeh, N.; Ahmadian, M.R. RHO GTPase-related long noncoding RNAs in human cancers. *Cancers* **2021**, *13*, 5386. [CrossRef] [PubMed]
223. Zhou, Y.; Fan, R.-G.; Qin, C.-L.; Jia, J.; Wu, X.-D.; Zha, W.-Z. LncRNA-H19 activates CDC42/PAK1 pathway to promote cell proliferation, migration and invasion by targeting miR-15b in hepatocellular carcinoma. *Genomics* **2019**, *111*, 1862–1872. [CrossRef] [PubMed]
224. Sun, X.; Luo, L.; Li, J. LncRNA MALAT1 facilitates BM-MSCs differentiation into endothelial cells via targeting miR-206/VEGFA axis. *Cell Cycle* **2020**, *19*, 3018–3028. [CrossRef]

Chapter IX. Unraveling the Impact of KRAS Accessory Proteins on Oncogenic Signaling Pathways

Authors: Vanshika Garg*, Raphael N. H. M. Hofmann*, Moazzam Saleem*, Amin Mirzaiebadizi, Ghazaleh Sadat Hashemi, Tooba Hameed, Bahareh Jooyeh, Silke Pudewell, Mehrnaz Mehrabipour, Niloufar Mosaddeghzadeh, Roland P. Piekorz, Mohammad Reza Ahmadian

*These authors equally contributed to this study

DOI: -

Status: To be submitted

Journal: …
JIF: …
Contribution: ≈10%

A.M. performed expression testing for KRAS(G12V), Galectin-3, IQGAP1, SHOC2, and NPM1, and established a protocol for the expression and purification of Galectin-3, and addressing its protein instability. He purified and prepared KRAS in GDP- and GppNHp-bound forms and performed a pull-down assay. He Provided technical support and contributed to scientific discussions. A.M. conducted in-depth proofreading and carried out the final review and major editing of the manuscript.

Unraveling the Impact of KRAS Accessory Proteins on Oncogenic Signaling Pathways

Vanshika Garg[1#], Raphael N. H. M. Hofmann[1#], Moazzam Saleem[1#§], Amin Mirzaiebadizi[1], Ghazaleh Sadat Hashemi[1], Tooba Hameed[1], Bahareh Jooyeh[1§], Silke Pudewell[1], Mehrnaz Mehrabipour[1§], Niloufar Mosaddeghzadeh[1§], Roland P. Piekorz[1], Mohammad Reza Ahmadian[1*]

[1] Institute of Biochemistry and Molecular Biology II, Medical Faculty, Heinrich Heine University Düsseldorf, Düsseldorf, Germany

[#] These authors contributed equally to this work.

[§] Current Addresses: Moazzam Saleem, Department of Biology, Institute of Genetics, The Faculty of Mathematics and Natural Sciences, Heinrich Heine University Düsseldorf, Düsseldorf, Germany; Bahareh Jooyeh, Signal Transduction of Cellular Motility, Internal Medicine IV, Science Unit for Basic and Clinical Medicine, Justus Liebig University Giessen, 35392, Giessen, Germany; Mehrnaz Mehrabipour, Vascular Biology Program, Department of Surgery, Boston Children's Hospital, Harvard Medical School, Boston, MA, United States; Niloufar Mosaddeghzadeh, Department of Translational Genomics, Faculty of Medicine and University Hospital Cologne, University of Cologne, 50923 Cologne, Germany.

*Corresponding authors: reza.ahmadian@hhu.de

Running title: Impact of Accessory Proteins on KRAS Signaling

Abstract

KRAS is a well-characterized oncogene that continuously activates multiple signaling pathways to drive tumorigenesis. While various strategies have been developed to directly inhibit key components of the KRAS signaling cascade, leading to the FDA approval of selective small-molecule inhibitors, these approaches face significant limitations due to therapeutic resistance and toxicity. In this study, we investigated the CRISPR-Cas9-mediated knockout (KO) of genes encoding KRAS accessory proteins: galectin-3 (GAL3), phosphodiesterase delta (PDEδ), nucleophosmin (NPM1), IQ motif-containing GTPase-activating protein 1 (IQGAP1), and the scaffold protein SHOC2, using several adenocarcinoma cell lines harboring the KRAS(G12V) mutation and the HEK-293 cell line. We assessed the activation of ERK and AKT kinases downstream of KRAS and evaluated cell proliferation. GAL3 and PDEδ KO significantly reduced MAPK and PI3K–AKT pathway activity and impaired cell proliferation. In contrast, NPM1 KO led to reciprocal modulation of the MAPK and PI3K–AKT pathways, while IQGAP1 KO enhanced PI3K–AKT and mTORC2–AKT signaling without affecting the MAPK pathway. SHOC2 KO selectively disrupted MAPK activation. These findings provide new insights into KRAS-associated accessory proteins as potential combinatorial drug targets, offering an alternative strategy to complement direct KRAS inhibition.

Keywords: Accessory proteins, KRAS, adenocarcinoma, cancer scaffold proteins, Galectin-3, PDE-delta, Nucleophosmin, IQGAP1, SHOC2, oncogene, MAPK, AKT, signal transduction

Introduction

KRAS4B (hereafter referred to as KRAS) plays a central role in the transduction of signals from receptor tyrosine kinases to intracellular effectors involved in several signaling pathways, particularly those regulating cell survival and proliferation. KRAS functions as a molecular switch by cycling between an inactive GDP-bound (`off´) state and an active GTP-bound (`on´) state [1]. This cycling is regulated by GDP/GTP exchange and GTP hydrolysis reactions, which are promoted by RAS-specific guanine nucleotide exchange factors (GEFs, such as son of

sevenless, SOS) and GTPase-activating proteins (GAPs, such as neurofibromin, NF1) [2]. In its active, GTP-bound form, KRAS transduces signals to its downstream effectors, including RAF and PI3K kinases, leading to the activation of key downstream pathways such as the mitogen-activated protein kinase (MAPK) and PI3K–AKT–mTOR [1]. The regulation and function output of KRAS is critically dependent on localization to the plasma membrane, which is mediated by posttranslational modification of a critical C-terminal cysteine residue and a cluster of six positively charged lysine residues. Phosphodiesterase δ (PDEδ) plays a key role in this process by binding farnesylated KRAS from the intracellular membranes and facilitating its delivery to the plasma membrane [1].

More than 25% of all solid tumors harbor mutations in the *KRAS* gene [3]. Gain-of-function mutations in *KRAS* are particularly associated with lethal forms of cancer, especially in adenocarcinoma cells of the pancreas, colon, and lung [4, 5]. These mutations most frequently affect glycine 12 (G12) and glutamine 61 (Q61). Q61 is a catalytic residue essential for GTP hydrolysis; its mutation to any other amino acid effectively abolishes KRAS-mediated GTP hydrolysis [5, 6]. In contrast, G12 is located in the active site between the β-/γ-phosphates of GTP, adjacent to both catalytic Q61 and the GAP arginine finger [6-8]. Substitution of G12, even with alanine, results in severe steric hindrance, interfering with GAP binding and impairing KRAS GTPase activity. This resistance to GAP-mediated hydrolysis [6, 9] leads to the accumulation of KRAS in its active, GTP-bound state, thereby promoting persistent signaling pathways and uncontrolled tumor cell proliferation [10].

Intensive efforts to elucidate the mechanisms of intracellular trafficking, regulation, and downstream signaling of KRAS have led to the development of several therapeutic strategies [11]. The challenges of directly targeting the KRAS oncogene, along with the identification of upstream kinases such as receptor tyrosine kinases (RTKs) and downstream effectors including components of the MAPK, PI3K–AKT–mTORC1, and mTORC2–AKT pathways, have led to the development of several kinase inhibitors for targeted cancer therapy. Although KRAS is the most frequently altered oncogenic protein in solid tumors, it has long been considered 'undruggable' [4, 12, 13]. However, advances in structure-based drug design have led to the development of inhibitors selective for GDP- or GTP-bound KRAS G12 mutants [4, 12, 13]. Clinical trials of covalent KRAS(G12C)-specific inhibitors such as adagrasib (MRTX849) and sotorasib (AMG510) have shown promising therapeutic activity in cancers harboring this mutation. Additionally, a novel approach involves designing small molecules that `glue´ GTP-bound KRAS G12D mutants to their regulatory GAP proteins, thereby restoring GTPase activity and inhibiting oncogenic signaling [14]. This method has led to the identification of two new compounds that specifically inhibit the growth of PANC-1 cells harboring the KRAS G12D mutation, demonstrating significantly lower IC_{50} values and higher specificity compared to existing inhibitors like MRTX1133. However, various genomic and histologic mechanisms contribute to acquired resistance and on-target toxicities associated with small-molecule inhibitors targeting components of the RTK–KRAS–MAPK axis [13, 15-17]. A recent study demonstrated that both on-target and off-target mechanisms confer resistance to adagrasib [17], including secondary KRAS mutations (e.g., G12D/R/V/W, G13D, Q61H, R68S, H95D/Q/R, Y96C) and high-level amplification of the KRAS(G12C) allele. In addition, bypass resistance mechanisms, such as MET amplification, activating mutations in NRAS, BRAF, MAP2K1, and RET, oncogenic fusions involving ALK, RET, BRAF, RAF1, and FGFR3, as well as loss-of-function mutations in tumor suppressors such as NF1 and PTEN have been identified [17]. These findings underscore the urgent need for new combinatorial therapeutic strategies to prevent or overcome resistance in KRAS-mutant cancers.

Emerging evidence suggests that core or constituent signaling components assemble into macromolecular complexes and cooperate in spatially defined clusters within the cell [18]. It is therefore important to note that the stoichiometric imbalance within such complexes, whether due to gene overexpression, depletion, knockout, or targeted protein degradation, can disrupt their equilibrium and impair protein function or the activity of the entire protein complex [19]. The strength, efficiency, specificity, and fidelity of signal transduction are governed by

mechanisms that enhance molecular connectivity, increase local concentration, and reduce dimensionality. One such mechanism is liquid-liquid phase separation (LLPS), in which two liquid phases with distinct protein compositions emerge from a single homogeneous solution [20]. A large number of proteins, collectively referred to as accessory proteins (Box 1), meet the criteria to promote LLPS and have been reported to act as adaptor, anchoring, docking, or scaffold proteins across diverse signaling networks [14, 18, 21, 22]. Many of these accessory proteins orchestrate the assembly and spatiotemporal localization of key components of the RTK–KRAS–MAPK pathway [18]. Accessory proteins can be categorized into four distinct functional groups: (1) anchoring proteins, which bind to the membrane and other effectors (mostly kinases); (2) docking proteins, which interact with receptors such as RTKs or GPCRs and multiple effectors; (3) adaptor proteins, which link two signaling components (e.g., RTKs and SOS1/2); and (4) scaffold proteins, which simultaneously bind multiple partners and serve as organizing platforms for signaling complexes[18].

Although dysregulated core components of the RTK–RAS–MAPK pathway are among the most intensively studied targets for disease treatment, accessory proteins deserve greater attention. Despite substantial advances in our understanding of this signaling network, the functional significance of accessory modulators in both normal physiology and human disease, particularly cancer, remains incompletely understood. In particular, selective inhibition of CNK1, IQGAP1, KSR1, and SHP2 has been shown to disrupt hyperactive RAS–MAPK signaling in cancer cells. Given the critical contribution of accessory proteins to signaling fidelity and network assembly, and their operation largely from the periphery of canonical pathways, we propose that functional perturbation at specific sites within accessory proteins may `attenuate´ rather than completely `inhibit´ signaling through the hyperactivated RTK–RAS–MAPK axis [18].

Direct targeting of constituent members of the RTK–RAS–MAPK axis for disease treatment, such as in cancer, remains a major challenge. Therapies for KRAS-mutant cancers are still a significant unmet clinical need, despite the development of allele-specific inhibitors that trap and inactivate KRAS(G12C) [23, 24]. Three decades of research have led to significant advances in tumor treatment [25]. However, adverse side effects remain substantial, and more specific therapies could significantly reduce patient burden. Unfortunately, many of the expectations for RAS pathway-targeted drugs have not been fulfilled. High toxicity and rapid resistance acquisition have limited the success of many of the drugs developed to date [25, 26]. Selective inhibition of certain accessory proteins, including CNK1, IQGAP1, KSR, and SHP2, has recently been shown to attenuate hyperactive RTK–RAS–MAPK signaling pathways in cancer cells and reduce tumor growth (Box 2) [27-30]. For example, combining SHP2 inhibitors with MEK inhibitors has been shown to interfere with feedback reactivation by SHP2 and block the onset of resistance in KRAS-driven cancers [30-33]. Although accessory proteins are increasingly recognized as therapeutic targets in RTK–RAS–MAPK-related diseases, only a small number of accessory protein inhibitors have been identified to date [18, 34].

In the present study, the effects of ablation of key accessory proteins on downstream signaling pathways, including ERK and AKT, were systematically investigated. To this end, we performed CRISPR-Cas9 knockout (KO) of galectin-3, PDEδ, NPM1, IQGAP1, and SHOC2 (Box 1), in KRAS(G12V)-mutant adenocarcinoma cell lines. The results highlight the essential role of these accessory proteins in modulating KRAS-dependent signaling and identify them as promising candidates for combinatorial or alternative therapeutic targeting.

Materials and methods

Cell lines

The cell lines used in this study are summarized in Supplementary Table S1. Cells were cultured in Dulbecco's modified eagle medium (DMEM) supplemented with 10% fetal bovine serum (FBS) and 1% penicillin/streptomycin, except for Capan-1 and SHP-77, which were cultured in Iscove's modified Dulbecco's medium (IMDM) and Gibco Roswell Park Memorial

Institute (RPMI) 1640 medium, respectively. Cells were grown in an exponential growth phase at 37°C, 5% CO_2, and 95% humidity.

CRISPR-Cas9-mediated gene editing
The CRISPR-Cas9 KO was performed as previously described [35]. Briefly, purified TrueCut™ Cas9 protein v2 (Thermo Fisher Scientific) was incubated with TrueGuide™ synthetic single guide RNA (sgRNAs) targeting the genes of the respective accessory proteins (see Supplementary Table S2) in nucleofection solution (LONZA) for 30 minutes at room temperature. One million cells were resuspended in the mixture and nucleofected using the 4D Nucleofector X-Unit (LONZA) with pulse code DN-100 for SW-480 and SHP-77, CM-130 for HEK-293, and CA-163 for CAPAN1. Cells were expanded for one week, and gene knockouts were verified by immunoblotting.

Immunoblotting and antibodies
Immunoblotting was performed as previously described [36]. The antibodies used are listed in Supplementary Table S3. Cell lysates were prepared in lysis buffer containing 50 mM Tris-HCl, pH 7.5, 100 mM NaCl, 2 mM $MgCl_2$, 1% Igepal CA-630, 10% glycerol, 20 mM beta- beta-glycerophosphate, 1 mM sodium orthovanadate, and EDTA-free protease inhibitor cocktail (Roche). Protein concentrations were determined by the Bradford assay (Bio-Rad).

Cell proliferation and viability assays
Proliferation of KO and wild-type (WT) cells was assessed using different protocols depending on the accessory protein and cell type. For GAL3, 1×10^5 SW480 cells, and for PDEδ, 1×10^4 cells were seeded per well in a 12-well plate. Proliferation was monitored for eight days. Cell numbers were estimated using both an automated counter and a Neubauer chamber. Trypan blue staining (1:1 ratio with the cell suspension) was used to distinguish between viable and non-viable cells. For NPM1, proliferation was analyzed in HEK-293, SHP-77, and Capan-1 cells by seeding 1×10^5 cells per well in 12-well plates. Cell counts were performed on days 0, 1, 3, and 5 using a Neubauer chamber after staining with trypan blue (1:1). For IQGAP1, 5,000 Capan-1 cells were seeded per well in a 96-well plate. After 6 hours, 20 µL of CellTiter-Blue reagent (Promega) was added. Fluorescence intensity at 590 nm was measured using a Tecan Infinite M200 PRO reader at 0 hours and again after 2 hours of incubation. This procedure was repeated on days 1, 2, 3, 4, and 7. The change in fluorescence was used as a measure of cell viability. All experiments were performed in three independent biological replicates (N = 3).

Cell migration (wound healing or scratch assay)
To assess migration, 1.5×10^5 cells were seeded in 12-well plates and grown to confluence. A standardized cross-shaped scratch was made using a 200 µL pipette tip. Images were captured at 0, 3, 6, 9, and 24 hours using a light microscope. The width of the scratch was measured and normalized to the initial time point. Closure rates were analyzed to quantify the migration rate.

Statistical analysis
All statistical analyses were conducted using standard methods appropriate for the experimental design. Graphs for the NPM1 and IQGAP1 immunoblots were generated using Microsoft Excel. An unpaired, two-sided Student's t-test was performed for comparisons between two groups, e.g., wildtype (WT) vs. knockout (KO). Statistical significance was indicated as follows: $P \leq 0.05$ (*), $P \leq 0.01$ (**), $P \leq 0.001$ (***), and $P \leq 0.0001$ (****). Proliferation graphs for NPM1, GAL3, and PDEδ were created using OriginPro v.2025b (OriginLab). A two-way repeated measures ANOVA followed by a Tukey's post hoc test was conducted [37], with significance levels denoted as above. Immunoblot graphs for GAL3, PDEδ, and SHOC2 were prepared in OriginPro v.2025b as well. One-way ANOVA was used for group comparisons, and significance was indicated using the same star notation. For IQGAP1, in addition to immunoblots, cell viability and migration data were plotted in Microsoft

Excel. We assessed statistical significance for these assays using GraphPad Prism 10. All final figures in this paper were compiled and edited using CorelDRAW.

Results and Discussion

Rationale for selecting human KRAS(G12V)-mutant cancer cell lines

KRAS mutations are among the most common genetic alterations found in cancer, particularly in pancreatic (86%), colorectal (41%), and lung (32%) adenocarcinomas. Most of these mutations affect codon 12, including G12D (45%) and G12V (35%) in pancreatic and colorectal cancer, and G12C (46%) and G12V (23%) in lung cancer [23]. Our study initially started with the pancreatic adenocarcinoma cell line PANC-1, which harbors a homozygous KRAV(G12D) mutation and is widely used as a well-characterized *in vitro* model for investigating cancer mechanisms and potential therapeutic strategies (Supplementary Table S1).

Before knocking out the accessory proteins in PANC-1 cells, we visualized the endogenous KRAS protein. To this end, we tested the specificity of several polyclonal and monoclonal anti-RAS antibodies, including those previously evaluated by Der and coworkers [38]. These antibodies were tested using purified RAS family proteins expressed in *Escherichia coli*, overexpressed proteins in HEK-293 cells, and PANC-1 cell lysates (Supplementary Table S1). Two antibodies (#23-4.2 from Millipore and #C-19 from Santa Cruz), reported to be KRAS-specific [38], showed no reactivity with lysates from PANC-1 or other KRAS-mutant cell lines. To resolve this issue, we screened additional antibodies and identified one (#D2H12, Cell Signaling) that revealed high selectivity for KRAS(G12V), but not for other variants such as G12D and G12C or wild-type KRAS in HEK-293 cells (Fig. 1).

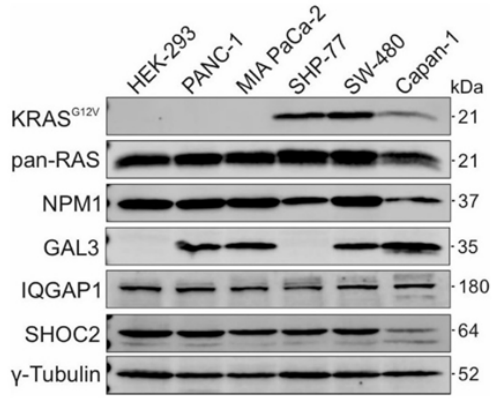

Figure 1. Relative expression of KRAS and KRAS-related accessory proteins in cancer cell lines. Immunoblotting was performed with a KRAS(G12V)-specific antibody (#D2H12, Cell Signaling), a pan-RAS antibody (#05-516, Millipore), and a γ-tubulin antibody (#T5326, Sigma) as a loading control. Antibodies used to detect accessory proteins detection included GAL3 (#ab2785), NPM1 (#ab10530), IQGAP1 (#ab56529), and SHOC2 (#HPA009164). Total cell lysates were adjusted to a 50 mg/ml protein concentration. Original blots are shown in Supplementary Figure S1.

Based on these findings, we selected three KRAS(G12V)-mutant adenocarcinoma cell lines: Capan-1 (pancreatic), SW-480 (colorectal), and SHP-77 (lung) to knock out the KRAS-associated accessory proteins GAL3, PDEδ, NPM1, IQGAP1, and SHOC2, which are differentially expressed (Fig. 1). Using this model, we examined cell proliferation, migration, and downstream signaling via the MAPK, PI3K–PDK1–AKT, and mTORC2–AKT signaling pathways.

Galectin-3 KO disrupt MAPK and PI3K–AKT signaling

Galectin-3 (GAL3; also known as lectin L-29 or MAC-2) is a 35 kDa protein consisting of 250 amino acids that has been implicated in tumor progression and metastasis through its role in cell-cell adhesion, cell-matrix interactions, growth regulation, apoptosis, angiogenesis, and mRNA splicing [39]. Structurally, GAL3 contains an intrinsically disordered N-terminal domain and a canonical carbohydrate recognition domain (CRD) at the C-terminus, which distinguishes it from other galectin family members. The CRD forms a hydrophobic pocket proposed to accommodate the farnesyl group of KRAS [40]. Phosphorylation by casein kinase-1 (CK1) promotes GAL3 translocation from the nucleus to the plasma membrane, where it stabilizes KRAS•GTP nanoclustering (Fig. 2A) [41]. While the GAL3–KRAS complex is primarily associated with PI3K–AKT signaling, its contribution to the MAPK pathway is less well characterized [42].

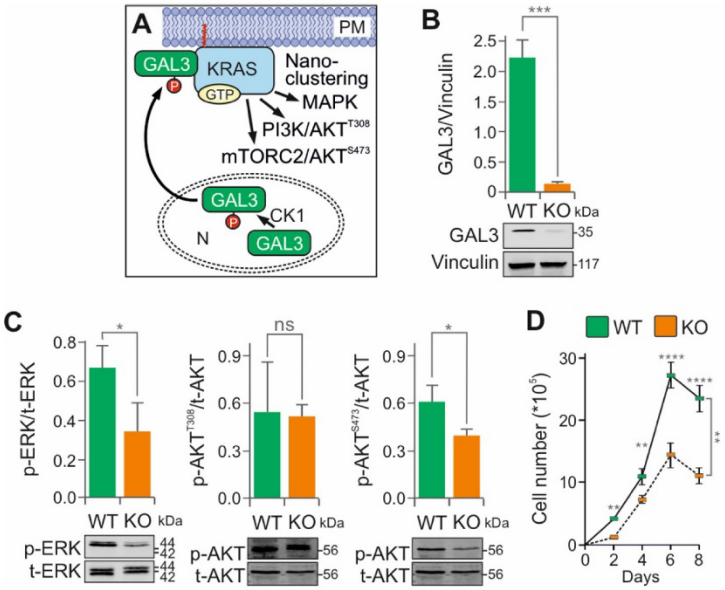

Figure 2. The essential modulatory function of galectin-3 in KRAS signaling in cancer cells. (**A**) Phosphorylation of GAL3 by casein kinase-1 (CK1) in the nucleus (N) induces its translocation to the plasma membrane (PM), where it is recruited into KRAS nanoclusters. (**B**) The *LGALS3* gene, encoding GAL3, was efficiently knocked out (KO) in KRAS(G12V) SW-480 cells using the CRISPR-Cas9 method. (**C**) Representative immunoblots of phosphorylated ERK (p-ERK) versus total ERK (t-ERK), and phosphorylated AKT (p-AKT) versus total AKT (t-AKT), using lysates from SW-480 WT and *GAL3* KO cells. Bar graphs represent the mean of three independent experiments (N = 3), normalized to the loading control vinculin. Statistical significance was determined by an unpaired two-tailed t-test (*P < 0.05, **P < 0.01, ***P < 0.001; ns, not significant). (**D**) Growth curves showing the mean values of daily cell counts (N = 3; Neubauer chamber) for SW-480 WT and GAL3 KO cells. Statistical analysis was performed by one-way ANOVA followed by Tukey's post-hoc test (*P < 0.05, **P < 0.01, ***P < 0.001, ****P < 0.0001). Original blots are shown in Supplementary Figure S2.

We investigated the modulatory function of GAL3 in SW-480 cells by CRISPR-Cas9-mediated KO (Fig. 2B). As shown in Figure 2C, *GAL3* KO significantly impaired both the MAPK and mTORC2–AKT pathways, while the PI3K–AKT pathway remained largely unaffected. Reduced proliferation of *GAL3* KO cells (Fig. 2D) correlated with decreased p-ERK1/2 levels, supporting the role of GAL3 in stabilizing KRAS membrane association and downstream

signaling [43]. These findings are consistent with previous studies in *Gal3* KO mouse embryonic fibroblasts, which also showed reduced p-ERK1/2 signaling [41].

Several proteins, including PDEδ, prenylin, and calmodulin, have been proposed to affect the membrane localization and intracellular trafficking of farnesylated KRAS [44]. In contrast to these factors, which enhance KRAS dissociation from the plasma membrane, GAL3 specifically reduces the dissociation rate of activated KRAS. A dominant negative mutant of GAL3 GAL3(V125A) has been shown to bind GTP-bound KRAS, impair nanocluster formation and MAPK activity, and suppress cell growth [40]. However, in our study, GST pulldown assays using bacterially expressed and purified GAL3 and KRAS proteins failed to demonstrate a direct interaction with either GDP- or GTP-bound KRAS (data not shown), possibly due to the absence of post-translational modifications.

KRAS nanoclusters refer to nanoscale aggregates of KRAS on the plasma membrane that facilitate the assembly of signaling complexes [45]. Several studies have implicated GAL3 in the stabilization of these nanoclusters (Fig. 2A). It is proposed that GTP-bound KRAS recruits GAL3 from the cytosol to the membrane, where GAL3 becomes a component of the nanocluster, thereby modulating the magnitude of KRAS•GTP signaling output in a concentration-dependent manner [40, 46, 47]. Our data are consistent with this proposed scaffolding role, although the precise molecular mechanisms underlying GAL3-mediated nanocluster formation remain to be elucidated.

PDE6D (PDEδ) KO impairs MAPK and PI3K–AKT signaling

Phosphodiesterases (PDEs) comprise a large family of enzymes with 11 isoenzyme classes and over 50 subunits that play essential roles in various signaling pathways [48]. Among them, PDEδ (also known as PDE6D or PrBP) is particularly important for the spatial organization of prenylated KRAS by facilitating its cytoplasmic diffusion and regulating its dynamic association with cellular membranes (Fig. 5A) [49].

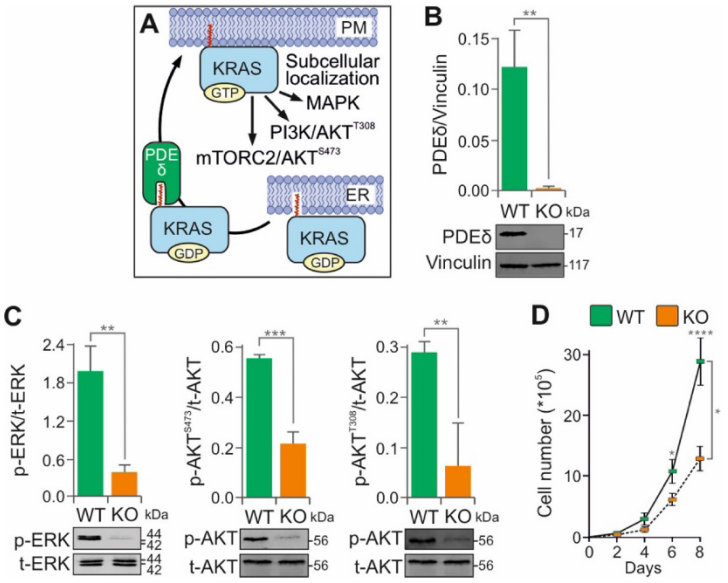

Figure 3. PDEδ is essential for KRAS(G12V) signaling in SW-480 cancer cells. (**A**) Schematic illustrating the proposed role of PDEδ in regulating KRAS spatial dynamics and membrane association. (**B**) The *PDE6D* gene, encoding PDEδ, was efficiently knocked out (KO) in KRAS(G12V) SW-480 cells using CRISPR-Cas9. (**C**) Bar graphs represent the mean

of three independent experiments (N = 3), normalized to the loading control vinculin. Statistical significance was assessed by unpaired two-tailed t-test (*P < 0.05, **P < 0.01, ***P < 0.001). (**D**) Growth curves show the mean daily cell counts (N = 3; Neubauer chamber) for SW-480 WT and *PDEδ* KO cells. Statistical analysis was performed by one-way ANOVA followed by Tukey's post-hoc test (*P < 0.05, **P < 0.01, ***P < 0.001, ****P < 0.0001). Original blots are shown in Supplementary Figure S3.

To investigate the role of PDEδ in KRAS-driven signaling, we generated PDE6D KO cells using CRISPR-Cas9 technology in the KRAS(G12V)-mutant SW-480 colorectal adenocarcinoma cell line (Fig. 3B). Immunoblotting revealed a significant reduction in phosphorylated ERK and AKT levels upon PDE6D knockout, indicating impaired MAPK and PI3K–AKT signaling (Fig. 3C). This signaling impairment correlated with a substantial decrease in cell proliferation (Fig. 3D), suggesting a critical role for PDEδ in maintaining KRAS effector pathways.

Our results are consistent with previous studies showing that impairment of the PDE6D–KRAS interaction attenuates KRAS-driven signaling [49]. However, they contrast with recent siRNA-mediated knockdown experiments that showed minimal effects on ERK activity [50]. This discrepancy may be due to the incomplete suppression achieved by transient knockdown, leaving residual PDEδ activity sufficient to support partial KRAS membrane localization. In addition, variation in dependence on PDE□ between different KRAS-mutant cell types may also contribute to these divergent observations.

The coordinated reduction in p-AKT(Ser473) and p-AKT(Thr308) suggests that PDEδ regulates AKT signaling at multiple levels, including upstream PI3K–PDK1 and mTORC2 inputs. Given that small-molecule inhibitors of PDEδ have been shown to impair KRAS membrane localization and reduce tumor growth in xenograft models [49], our data support PDEδ as a promising therapeutic target in KRAS-mutant cancers, particularly colorectal adenocarcinoma.

Nucleophosmin KO affects RAS signaling in HEK-293 cells, but not in KRAS-mutant cancer cells

Nucleophosmin (NPM1; also known as B23, numatrin, or NO38) is a 37-kDa multifunctional phosphoprotein of 294 amino acids. It is predominantly localized to the nucleolus and plays critical roles in RNA processing events, including transcription, ribosome biogenesis, mRNA stability, translation, and miRNA regulation [51]. Notably, the KRAS-responsive lncRNA KIMAT1, a MYC target, promotes lung tumorigenesis by enhancing the processing of oncogenic miRNAs through the stabilization of NPM1 [52, 53]. Although NPM1 functions primarily in the nucleus, it shuttles between the nuclear and cytoplasmic compartments and can translocate to the plasma membrane. Mutant forms of NPM1 have been shown to enhance RAS–MAPK signaling, thereby promoting adhesion, migration, and invasion in acute myeloid leukemia (AML) cells [54]. Furthermore, genetic ablation of *NPM1* reduces tumor progression in non-small cell lung cancer (NSCLC), validating NPM1 as a therapeutic target in KRAS-driven tumors [55]. Interestingly, NPM1 has been reported to stabilize KRAS association with the cytoplasmic leaflet of the plasma membrane, thereby modulating MAPK signaling (Fig. 4A) [47].

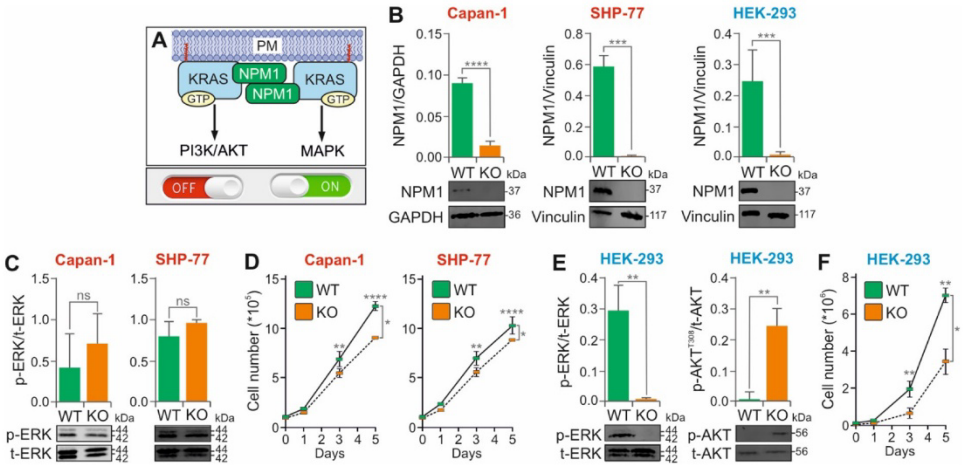

Figure 4. Reciprocal modulation of MAPK and PI3K-AKT signaling pathways by NPM1 in HEK-293 cells. (**A**) Schematic representation of the proposed role of NPM1 in stabilizing KRAS at the plasma membrane (PM), promoting activation of the MAPK pathway while inhibiting PI3K–AKT signaling. (**B**) Confirmation of *NPM1* KO in KRAS(G12V)-mutant cell lines (Capan-1 and SHP-77) and KRAS wild-type HEK-293 cells using CRISPR-Cas9 technology. NPM1 KO was verified by immunoblotting. (**C**) Representative immunoblots of phosphorylated ERK (p-ERK) versus total ERK (t-ERK), using lysates from Capan-1 and SHP-77 WT and NPM1 KO cells. (**D**) Growth curves showing the mean values of daily cell counts (N = 3; Neubauer chamber) for Capan-1 and SHP-77 WT and NPM1 KO cells. (**E**) Representative immunoblots of p-ERK versus t-ERK and phosphorylated AKT (p-AKT) versus total AKT (t-AKT), using lysates from HEK-293 WT and NPM1 KO cells. (**F**) Growth curves showing the mean values of daily cell counts (N = 3; Neubauer chamber) for HEK-293 WT and NPM1 KO cells. Bar graphs represent the mean of three independent experiments (N = 3), normalized to the loading control GAPDH or vinculin. Statistical significance was assessed by unpaired two-tailed t-test (*P < 0.05, **P < 0.01, ***P < 0.001; ns, not significant). For growth curves, statistical analysis was performed using one-way ANOVA followed by Tukey's post hoc test (*P < 0.05, **P < 0.01, ***P < 0.001, ****P < 0.0001). Original blots are shown in Supplementary Figure S4.

To investigate the functional role of NPM1 in KRAS signaling, we knocked out NPM1 in Capan-1, SHP-77, and HEK-293 cell lines using CRISPR-Cas9 (Fig. 4B). The KO efficiency was confirmed by immunoblotting. In the KRAS(G12V)-mutant adenocarcinoma cell lines Capan-1 and SHP-77, NPM1 KO had no significant effect on MAPK signaling as measured by p-ERK1/2 levels (Figure 4C), although a modest but reproducible reduction in proliferation was observed (Fig. 4D). In contrast, *NPM1* KO in the KRAS wild-type HEK-293 cell line resulted in a significant reduction in p-ERK1/2 and a striking increase in p-AKT (Fig. 4E), accompanied by a substantial decline in proliferation (Fig. 4F). These results suggest that *NPM1* KO does not reverse the strong activation of signaling in KRAS-mutant cancer cells but instead alters the downstream signaling in KRAS wild-type HEK-293 cells. In this context, NPM1 appers to promote the RAS–MAPK pathway while suppressing the RAS–PI3K–AKT pathway (Fig. 4A).

The role of NPM1 in cancer, particularly its mutations and interactions with KRAS, has received considerable attention due to its impact on signaling pathways involved in cell proliferation and differentiation. In this study, no significant changes in ERK phosphorylation were observed upon *NPM1* KO in the KRAS(G12V)-mutant adenocarcinoma cell lines. Previous studies have reported NPM1 overexpression in various malignancies [56] and identified frameshift mutations in approximately 35% of adult AML cases [57, 58]. These mutations often co-occur with activating KRAS mutations [59, 60], suggesting a potential cooperative role in

leukemogenesis. Genetic ablation of *NPM1* in a mouse model of KRAS-mutant adenocarcinoma has been shown to shift cancer cell metabolism from aerobic glycolysis to oxidative phosphorylation and reduce tumor proliferation [55], supporting its candidacy as a potential therapeutic target in KRAS-driven cancers. Although ectopic NPM1 expression has been reported to increase p-ERK levels (Inder et al., 2009), we did not observe changes in ERK phosphorylation in the KRAS(G12V) background, suggesting that constitutively active KRAS maintains MAPK pathway activation independent of NPM1 status.

In contrast, *NPM1* KO in the KRAS wild-type HEK-293 cell line significantly altered downstream signaling, with decreased ERK phosphorylation and increased AKT phosphorylation. This finding supports the idea that NPM1 is required to stabilize KRAS at the plasma membrane [61]. Immunoprecipitation studies have shown that an AML-associated NPM1 mutant (a four-nucleotide insertion in exon 11) interacts with KRAS [62, 63]. Overexpression of this mutant increases p-ERK levels [54], which is consistent with our findings. It has also been suggested that this mutant promotes AML cell invasiveness by upregulating matrix metalloproteinases (MMPs) through activation of the RAS–MAPK pathway, further highlighting its role in leukemogenesis. However, our GST pulldown assays with purified proteins did not confirm a direct interaction between wild-type NPM1 and KRAS (data not shown).

Notably, *NPM1* KO in HEK-293 cells also resulted in increased AKT phosphorylation, likely due to the destabilization of PTEN, a key negative regulator of the PI3K pathway. NPM1 has been reported to interact with PTEN and regulate its stability via ubiquitination [64]. In the absence of NPM1, PTEN degradation may result in enhanced PI3K–AKT signaling.

In conclusion, NPM1 appears to modulate both the MAPK and PI3K-AKT pathways in a KRAS context-dependent manner. In KRAS(G12V)-mutant cell lines, its KO has minimal effect due to constitutive downstream, whereas in KRAS wild-type cells, NPM1 promotes MAPK activation and restrains AKT signaling. These findings support a broader role for NPM1 in KRAS signaling modulation and warrant further investigation of its mechanism and therapeutic potential.

***IQGAP1* KO does not alter MAPK signaling, but positively affects PI3K-PDK1-AKT activation**

Activation of RAF kinase at the plasma membrane through direct interaction with KRAS•GTP is a well-established mechanism [65]. Upon activation, BRAF/RAF1 heterodimers phosphorylate MEK1/2, which then phosphorylate ERK1/2 at the TEY motif. Activated ERK1/2 are then distributed to various subcellular compartments, where they phosphorylate downstream substrates. The assembly of macromolecular complexes involving MAPK components and their interaction with RAS nanoclusters at the membrane define the RAS–MAPK signaling axis. This process is supported by homo- and heterodimerization of the signaling proteins and orchestrated by accessory proteins that provide spatial and temporal precision, as well as signal fidelity and amplification [18]. One of the most prominent scaffold proteins involved in this regulation is IQ Motif Containing GTPase Activating Protein 1 (IQGAP1), also known as p195 or SAR1, a multidomain protein composed of 1657 amino acids with a molecular weight of approximately 180 kDa [18, 66, 67].

IQGAP1 has been reported to scaffold and facilitate the RAF–MEK–ERK signaling by interacting with the epidermal growth factor receptor (EGFR) [68, 69] and to coordinate PI3K signaling by assembling a multienzyme complex that promotes PIP_3 generation and subsequent AKT activation (Fig. 5A) [70]. With over one hundred documented binding partners [71], IQGAP1 is involved in cytoskeletal remodeling, cell proliferation, differentiation, and other regulatory functions that vary depending on the cell type and physiological context. Because of its central role in tumorigenesis, IQGAP1 and its associated pathways are being evaluated as potential targets for cancer therapy [72].

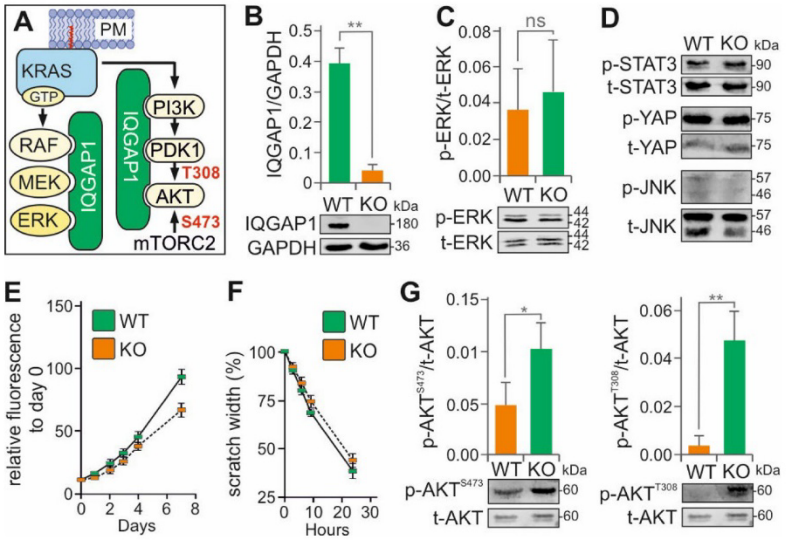

Figure 5. The regulatory role of IQGAP1 in PI3K–AKT signaling in KRAS(G12V)-mutant Capan-1 cells. (**A**) IQGAP1 is proposed to function as a scaffold protein for components of both the MAPK (RAF, MEK, ERK) and PI3K–AKT (PI3K, PDK1, AKT) pathways. (**B**) The *IQGAP1* gene was efficiently knocked out (KO) in KRAS(G12V) Capan-1 cells using the CRISPR-Cas9 method. (**C**) Representative immunoblots of phosphorylated ERK (p-ERK) versus total ERK (t-ERK), using lysates from Capan-1 WT and *IQGAP1* KO cells. (**D**) Representative immunoblots phosphorylated STAT3 (p-STAT3), YAP (p-YAP), and JNK (p-JNK) versus total STAT3 (t-STAT3), YAP (t-YAP), and JNK (t-JNK), using lysates from Capan-1 WT and *IQGAP1* KO cells. (**E**) Growth curves show the mean daily cell count values (N = 3; Neubauer chamber) for Capan-1 WT and *IQGAP1* KO cells. (**F**) Cell migration was assessed using a scratch assay. The plots show the mean values of wound closure (N = 3) over time for Capan-1 WT and *IQGAP1* KO cells. (**G**) Representative immunoblots of phosphorylated AKT (p-AKT) versus total AKT (t-AKT), using lysates from Capan-1 WT and *IQGAP1* KO cells. Bar graphs represent the mean of three independent experiments (N = 3), normalized to the loading control GAPDH. Statistical significance was assessed using an unpaired two-tailed t-test (*P < 0.05, **P < 0.01, ***P < 0.001, ****P < 0.0001; ns, not significant). Original blots are shown in Supplementary Figure S5.

In this study, we generated *IQGAP1* KO in the Capan-1 cell line using CRISPR-Cas9 (Fig. 5B). Immunoblot analysis revealed that *IQGAP1* KO did not affect ERK phosphorylation (Fig. 5C). Similarly, the phosphorylation status of other signaling proteins, including JNK, YAP, and STAT3, remained unchanged (Fig. 5D). Cell proliferation and migration also showed no significant difference between *IQGAP1* KO and wild-type cells (Fig. 5E, F). In contrast, we observed a significant increase in AKT phosphorylation at threonine 308, the PDK1 target site within the PI3K pathway, in *IQGAP1* KO cells compared to wild-type controls (Fig. 5G). This suggests that IQGAP1 acts as a negative modulator of the KRAS–PI3K–PDK1–AKT signaling axis in the KRAS(G12V)-mutant Capan-1 cells.

IQGAP1 is frequently overexpressed in various cancers, including pancreatic adenocarcinoma [73, 74], colorectal cancer [75], hepatocellular carcinoma [76], ovarian cancer [77] , and glioma [78]. As a scaffold protein for MAPK components [79, 80], it was initially thought to interact with ERK via the WW domain, although recent evidence suggests that the IQ domain is both necessary and sufficient for high-affinity binding [68, 80, 81]. IQGAP1 also facilitates crosstalk

between mTOR and AKT [82] and directly promotes PIP_3 generation by binding to PI3K [70, 83, 84].

Interestingly, despite the proposed scaffolding functions of IQGAP1, we did not observe changes in ERK phosphorylation following *IQGAP1* knockout. Instead, levels of phosphorylated AKT at threonine 308 (p-AKT^{T308}) were significantly increased, with a modest increase also observed at serine 473 (p-AKT^{S473}). These results differ from previous reports characterizing IQGAP1 as a positive regulator of AKT signaling. For example, siRNA-mediated knockdown of IQGAP1 in Capan-1 cells was reported to leave p-AKT levels unaffected while reducing p-ERK levels [85]. In KRAS wild-type cells, high levels of IQGAP1 may favor the PI3K–AKT signaling by interacting with FOXO1, a downstream target of AKT, while interfering with the scaffolding of the MAPK pathway [86]. In KRAS-mutant cells, IQGAP1 may instead promote ERK signaling while limiting AKT activation. Thus, loss of IQGAP1 could remove this bias and shift the balance in favor of PI3K–AKT pathway activation. An additional explanation may involve a feedback mechanism regulated by p70S6K. IQGAP1 has been proposed to affect p70S6K, and its loss may relieve a negative feedback loop, thereby increasing AKT activity [87].

SHOC2 KO selectively disrupts KRAS(G12V)-driven MAPK signaling

SHOC2 (also known as SUR-8 or SOC2) is a scaffold protein that facilitates activation of the RAS–MAPK pathway by coordinating the assembly of signaling complexes. It forms a ternary complex with protein phosphatase 1 (PP1C) and GTP-bound MRAS, a member of the RAS family. This SHOC2–MRAS–PP1C complex specifically dephosphorylates inhibitory serine residues on RAF kinases, such as p-CRAF(S259) and p-BRAF(S365) (Fig. 6A) [88-90]. This dephosphorylation step relieves autoinhibition, thereby enabling RAF activation and subsequent MEK1/2 phosphorylation. The functional importance of this complex is underscored by gain-of-function mutations in all three components in Noonan syndrome, which enhance complex formation and MAPK signaling [91, 92].

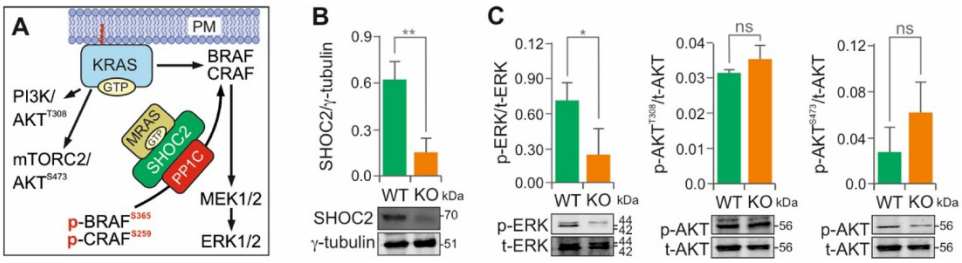

Figure 6. SHOC2 selectively modulates MAPK signaling in KRAS(G12V) SHP-77 cells. (**A**) Schematic representation of SHOC2-mediated RAF activation via dephosphorylation by the SHOC2–MRAS–PP1C complex. (**B**) The *SHOC2* gene was knocked out (KO) in KRAS(G12V) adenocarcinoma SHP-77 cells using the CRISPR-Cas9 method. (**C**) Representative immunoblots of phosphorylated ERK (p-ERK) versus total ERK (t-ERK), and phosphorylated AKT (p-AKT) versus total AKT (t-AKT), using lysates from SHP-77 WT and *SHOC2* KO cells. Bar graphs represent the mean of three independent experiments (N = 3), normalized to the loading control γ-tubulin. Statistical significance was assessed using an unpaired two-tailed t-test (*P < 0.05, **P < 0.01, ***P < 0.001; ns, not significant). Original blots are shown in Supplementary Figure S6.

After confirming SHOC2 expression in various cell lines (Fig. 1), we generated *SHOC2* KO in the KRAS(G12V) adenocarcinoma cell line SHP-77 using CRISPR-Cas9 (Fig. 6B). As shown in Figure 6C, *SHOC2* KO resulted in a marked reduction in ERK phosphorylation, whereas

AKT phosphorylation at both T308 and S473 remained unchanged. These results demonstrate that SHOC2 specifically modulates the MAPK axis downstream of KRAS, without affecting the AKT pathways.

Our results are consistent with previous studies demonstrating the essential role of SHOC2 in the activation of the MAPK pathway [93]. SHOC2 facilitates the recruitment of PP1C to inactive BRAF and CRAF, thereby promoting the dephosphorylation and activation of RAF kinases (Fig. 1A). SHOC2 expression and mutation status vary among tumor types, and alterations in the axis are implicated in multiple cancer subtypes [94, 95]. SHOC2 overexpression has been associated with increased ERK phosphorylation in several cancers, including colorectal, lung, and breast tumors [89, 93, 96-98]. Beyond cancer, SHOC2 deregulation has been implicated in developmental disorders. Germline gain-of-function mutations in *SHOC2* cause Noonan-like syndrome with loose anagen hair, a distinct RASopathy characterized by aberrant MAPK signaling [99-101].

Conclusions

In this study, we highlight a class of modulatory proteins, termed `accessory proteins´, that are increasingly recognized as promising therapeutic targets in RAS–MAPK-driven diseases. These proteins do not function as direct components of canonical signaling cascades, but instead coordinate the assembly and spatiotemporal localization of key signaling molecules, thereby shaping overall signaling output [18]. Accessory proteins can be classified into four functional subtypes, as outlined in Box 1.

Our results demonstrate that the loss of specific KRAS-associated accessory proteins significantly alters KRAS signaling outputs in both KRAS(G12V)-mutant adenocarcinoma cells and KRAS wild-type HEK-293 cells. In particular, we identified GAL3, PDEδ, SHOC2, and IQGAP1 as key modulators of KRAS-centric interaction networks, positioning them as strong candidates for therapeutic intervention (Box 2).

These proteins also offer opportunities to refine combination therapeutic strategies aimed at overcoming resistance to KRAS-targeted therapies. Notably, previous studies have shown that depletion of accessory proteins such as SHOC2 can reduce the likelihood of acquired drug resistance [90, 102-104]. In addition, our findings, including the reciprocal modulation of MAPK and AKT signaling upon *NPM1* KO in KRAS wild-type cells, and the unexpected increase in p-AKT upon *IQGAP1* KO, provide novel insights. These results support the concept that certain accessory proteins may function as molecular switches that selectively activate or repress specific signaling pathways depending on the cellular context.

Although the last three decades of research have led to major advances in cancer treatment, more effective therapeutic strategies are still needed, particularly for cancers harboring KRAS mutations. Several accessory proteins have been suggested as promising targets in RAS-mutant cancers, but only a small number of inhibitors have been discovered.

A key advantage of targeting modulatory proteins rather than core or constituent pathway components is that hyperactive signaling can be attenuated to physiological levels rather than blocked completely. This strategy may reduce toxicity and limit the compensatory feedback reactivation often observed with direct kinase inhibition. For example, *Ksr* KO in mice does not eliminate ERK phosphorylation but reduces RAS-driven tumorigenesis and is well tolerated during development [25, 105].

One illustrative example is the scaffolding protein SHOC2. Its depletion enhances the therapeutic effect of MEK inhibitor treatment by interfering with feedback reactivation through the RAF pathway [106]. SHOC2 forms a holoenzyme complex with PP1C and MRAS that enables RAF dimerization by dephosphorylating inhibitory serine residues. While *SHOC2* KO is embryonic lethal in mice, it is tolerated in adult animals and human cell lines, and its loss

inhibits the growth of RAS mutant cancer cells [106]. In addition to its role in cancer, SHOC2 mutations have been implicated in developmental disorders such as Mazzanti syndrome and prenatal-onset hypertrophic cardiomyopathy [99, 101]. These mutations cause persistent membrane localization or enhanced binding of MRAS and PPP1CB, highlighting the finely tuned regulatory role of SHOC2 in RAS-MAPK signaling.

Another example is the anchoring protein CNK1, which localizes to the membrane via its pleckstrin homology (PH) domain and promotes RAF activation by binding to both RAS and RAF via its N- and C-terminal domains [107]. The PH domain inhibitor PHT-7.3 prevents CNK1 from colocalizing with membrane-localized RAS and selectively inhibits the proliferation of KRAS mutant, but not wild-type, cancer cell lines [108].

A further example is the tyrosine phosphatase SHP2, which plays a key role in integrating RTK signals and is essential for cell growth and proliferation. Blocking SHP2 in cancers driven by RTK activation has been shown to attenuate tumor growth. Allosteric inhibitors of SHP2 suppress signaling through the MAPK pathway and inhibit the proliferation of RTK-activated tumors. This offers a strategy to overcome resistance in cancer treatments [109]. It also has potential for combination therapies. SHP2 inhibition could enhance the efficacy of other treatments, such as MEK inhibitors, by reducing MAPK and mTOR signaling activities [110].

As shown in our study, PDEδ can significantly affect both pathways and could be used in cancer therapy. Moreover, the combination of inhibition of PDEδ function, when combined with sildenafil, which activates PKG2, synergistically suppresses KRAS-driven tumor growth in preclinical models [111].

Collectively, the results of this study provide a comprehensive functional map of KRAS-associated accessory proteins and their influence on MAPK and AKT signaling. By uncovering their distinct and context-dependent regulatory roles, we highlight these modulators as attractive but underexplored therapeutic targets. Future efforts to develop selective inhibitors of accessory proteins may pave the way for more effective and durable treatment strategies in KRAS-driven cancers.

Author Contributions Statement

Funding
This study was supported by the German Research Foundation (DFG; AH 92/8-3), the European Network on Noonan Syndrome and Related Disorders (NSEuroNet, 01GM1602B)

Acknowledgments
We would like to thank our colleague Axel Gödecke for providing reagents and Soheila Rezaei Aradiani, Saeideh Nakhaei-Rad, and Radovan Dvrosky for their support and discussions.

Conflict of Interest
The authors declare no conflict of interest.

Abbreviations
AKT, Protein kinase B
ALK, Anaplastic lymphoma kinase
AML, Acute myeloid leukemia
BRAF, B-Rapidly accelerated fibrosarcoma Serine/threonine-protein kinase
Cas9, CRISPR-associated protein 9
cGMP, Cyclic guanosine monophosphate
CK1, Casein Kinase 1
CNK1, Connector enhancer of kinase suppressor of RAS 1
CO_2, Carbon dioxide
CRAF, C-Rapidly accelerated fibrosarcoma Serine/threonine-protein kinase
CRD, Carbohydrate recognition domain
CRISPR, Clustered regularly interspaced short palindromic repeat
DMEM, Dulbecco's Modified Eagle Medium
EGF, Epidermal growth factor
EGFR, Epidermal growth factor receptor
ERK, Extracellular signal regulated kinase
FBS, Fetal bovine serum
FDA, Food and Drug Administration
FGFR3, Fibroblast growth factor receptor 3
FOXO1, Forkhead box protein O1
GAL3, Galectin-3
GAP, GTPase activating protein
GAPDH, Glyceraldehyde 3-phosphate dehydrogenase
GDP, Guanine diphosphate
GEF, Guanine nucleotide exchange factor
GPCR, G protein-coupled receptor
GRB2, Growth factor receptor-binding protein 2
GST, Glutathione S-transferase
GTP, Guanine triphosphate
HEK-293, Human embryonic kidney 293
lncRNA, long non-coding RNA
IQGAP1, IQ Motif-containing GTPase-Activating Protein 1
JNK, c-Jun N-terminal kinase
kDa, Kilodalton
KIMAT1, KRAS-induced MYC-activated Transcript 1
KO, Knockout
KRAS, Kirsten rat sarcoma
KSR1, Kinase suppressor of RAS-1
LLPS, Liquid-Liquid phase separation
MAP2K1, Mitogen-activated protein kinase kinase 1
MAPK, Mitogen-activated protein kinase
MEK, Dual specificity mitogen-activated protein kinase kinase
MET, Mesenchymal-Epithelial Transition factor
MMPs, Matrix metalloproteinases
MRAS, Muscle RAS oncogene homolog
mRNA, Messenger Ribonucleic Acid
mTOR, Mammalian target of rapamycin
mTORC2, Mammalian target of rapamycin complex
MYC, Avian Myelocytomatosis Viral Oncogene Homolog
NF1, Neurofibromatosis type 1
NPM1, Nucleophosmin 1
NRAS, Neuroblastoma RAS viral oncogene homolog
NSCLC, Non-small cell lung cancer
PDE, Phosphodiesterase
PDE6δ, Delta subunit of phosphodiesterase 6
PDK1, 3-phosphoinositide-dependent protein kinase 1
PH, Pleckstrin homology
PI3K, Phosphatidylinositol 3-kinase
PIP_3, Phosphatidylinositol (3,4,5)-triphosphate
PP1C, Protein phosphatase 1
PP1CB, protein phosphatase 1 catalytic subunit beta
PTEN, Phosphatase and tensin homolog
RAF, Rapidly accelerated fibrosarcoma
RAS, Rat sarcoma
RET, Rearranged during transfection (proto-oncogene tyrosine-protein kinase receptor)
RNA, Ribonucleic Acid
RTK, Receptor tyrosine kinase
sgRNA, Single-guide RNA
SHP-77, Shadyside Hospital, Pittsburgh 77
SHP2, SH2 domain-containing tyrosine phosphatase 2
siRNA, Small Interfering RNA
SOS, Son of sevenless
SOS1/2, Son of sevenless homolog 1/2
STAT3, Signal Transducer and Activator of Transcription 3
WT, Wild-Type
YAP, Yes1-associated transcriptional regulator

References

1. Nakhaei-Rad, S., et al., *Structural fingerprints, interactions, and signaling networks of RAS family proteins beyond RAS isoforms.* Critical reviews in biochemistry and molecular biology, 2018. **53**(2): p. 130-156.
2. Hennig, A., et al., *Ras activation revisited: role of GEF and GAP systems.* Biological chemistry, 2015. **396**(8): p. 831-848.
3. Sanclemente, M., et al., *c-RAF ablation induces regression of advanced Kras/Trp53 mutant lung adenocarcinomas by a mechanism independent of MAPK signaling.* Cancer cell, 2018. **33**(2): p. 217-228. e4.
4. Moore, A.R., et al., *RAS-targeted therapies: is the undruggable drugged?* Nature Reviews Drug Discovery, 2020. **19**(8): p. 533-552.
5. Zhu, C., et al., *Targeting KRAS mutant cancers: from druggable therapy to drug resistance.* Molecular Cancer, 2022. **21**(1): p. 1-19.
6. Scheffzek, K., et al., *The Ras-RasGAP complex: structural basis for GTPase activation and its loss in oncogenic Ras mutants.* Science, 1997. **277**(5324): p. 333-339.
7. Mittal, R., et al., *Formation of a transition-state analog of the Ras GTPase reaction by Ras· GDP, tetrafluoroaluminate, and GTPase-activating proteins.* Science, 1996. **273**(5271): p. 115-117.
8. Ahmadian, M.R., et al., *Confirmation of the arginine-finger hypothesis for the GAP-stimulated GTP-hydrolysis reaction of Ras.* Nature structural biology, 1997. **4**(9): p. 686-689.
9. Ahmadian, M.R., et al., *Guanosine triphosphatase stimulation of oncogenic Ras mutants.* Proceedings of the National Academy of Sciences, 1999. **96**(12): p. 7065-7070.
10. Zhu, G., et al., *Role of oncogenic KRAS in the prognosis, diagnosis and treatment of colorectal cancer.* Molecular cancer, 2021. **20**(1): p. 1-17.
11. Saliani, M., R. Jalal, and M.R. Ahmadian, *From basic researches to new achievements in therapeutic strategies of KRAS-driven cancers.* Cancer Biology & Medicine, 2019. **16**(3): p. 435.
12. Stalnecker, C.A. and C.J. Der, *RAS, wanted dead or alive: Advances in targeting RAS mutant cancers.* Science signaling, 2020. **13**(624): p. eaay6013.
13. Punekar, S.R., et al., *The current state of the art and future trends in RAS-targeted cancer therapies.* Nature Reviews Clinical Oncology, 2022. **19**(10): p. 637-655.
14. Randelovic, I., et al., *Gluing GAP to RAS Mutants: A New Approach to an Old Problem in Cancer Drug Development.* Int J Mol Sci, 2024. **25**(5).
15. Cooper, A.J., L.V. Sequist, and J.J. Lin, *Third-generation EGFR and ALK inhibitors: mechanisms of resistance and management.* Nature Reviews Clinical Oncology, 2022: p. 1-16.
16. Cohen, P., D. Cross, and P.A. Jänne, *Kinase drug discovery 20 years after imatinib: Progress and future directions.* Nature reviews drug discovery, 2021. **20**(7): p. 551-569.
17. Awad, M.M., et al., *Acquired resistance to KRASG12C inhibition in cancer.* New England Journal of Medicine, 2021. **384**(25): p. 2382-2393.
18. Pudewell, S., et al., *Accessory proteins of the RAS-MAPK pathway: moving from the side line to the front line.* Commun Biol, 2021. **4**(1): p. 696.
19. Prelich, G., *Gene overexpression: uses, mechanisms, and interpretation.* Genetics, 2012. **190**(3): p. 841-854.
20. Lyon, A.S., W.B. Peeples, and M.K. Rosen, *A framework for understanding the functions of biomolecular condensates across scales.* Nature Reviews Molecular Cell Biology, 2021. **22**(3): p. 215-235.
21. Sato, M., et al., *Accessory proteins for G proteins: partners in signaling.* Annu Rev Pharmacol Toxicol, 2006. **46**: p. 151-87.
22. Mirzaiebadizi, A., R. Shafabakhsh, and M.R. Ahmadian, *Modulating PAK1: Accessory Proteins as Promising Therapeutic Targets.* Biomolecules, 2025. **15**(2).
23. Moore, A.R., et al., *RAS-targeted therapies: is the undruggable drugged?* Nat Rev Drug Discov, 2020. **19**(8): p. 533-552.
24. Ostrem, J.M., et al., *K-Ras(G12C) inhibitors allosterically control GTP affinity and effector interactions.* Nature, 2013. **503**(7477): p. 548-51.
25. Matallanas, D. and P. Crespo, *New druggable targets in the Ras pathway?* Curr Opin Mol Ther, 2010. **12**(6): p. 674-83.
26. Vasan, N., J. Baselga, and D.M. Hyman, *A view on drug resistance in cancer.* Nature, 2019. **575**(7782): p. 299-309.
27. Indarte, M., et al., *Correction: An Inhibitor of the Pleckstrin Homology Domain of CNK1 Selectively Blocks the Growth of Mutant KRAS Cells and Tumors.* Cancer Res, 2019. **79**(20): p. 5457.

28. Tari, A.M., et al., *Liposome-incorporated Grb2 antisense oligodeoxynucleotide increases the survival of mice bearing bcr-abl-positive leukemia xenografts.* Int J Oncol, 2007. **31**(5): p. 1243-50.
29. Dhawan, N.S., A.P. Scopton, and A.C. Dar, *Small molecule stabilization of the KSR inactive state antagonizes oncogenic Ras signalling.* Nature, 2016. **537**(7618): p. 112-116.
30. Xie, J., et al., *Allosteric Inhibitors of SHP2 with Therapeutic Potential for Cancer Treatment.* J Med Chem, 2017. **60**(24): p. 10205-10219.
31. Mainardi, S., et al., *SHP2 is required for growth of KRAS-mutant non-small-cell lung cancer in vivo.* Nat Med, 2018. **24**(7): p. 961-967.
32. Ruess, D.A., et al., *Mutant KRAS-driven cancers depend on PTPN11/SHP2 phosphatase.* Nat Med, 2018. **24**(7): p. 954-960.
33. Fu, N.J., et al., *Hexachlorophene, a selective SHP2 inhibitor, suppresses proliferation and metastasis of KRAS-mutant NSCLC cells by inhibiting RAS/MEK/ERK and PI3K/AKT signaling pathways.* Toxicol Appl Pharmacol, 2022. **441**: p. 115988.
34. Pudewell, S. and M.R. Ahmadian, *Spotlight on Accessory Proteins: RTK-RAS-MAPK Modulators as New Therapeutic Targets.* Biomolecules, 2021. **11**(6).
35. Pudewell, S., et al., *New mechanistic insights into the RAS-SIN1 interaction at the membrane.* Front Cell Dev Biol, 2022. **10**: p. 987754.
36. Nakhaei-Rad, S., et al., *The Role of Embryonic Stem Cell-expressed RAS (ERAS) in the Maintenance of Quiescent Hepatic Stellate Cells.* J Biol Chem, 2016. **291**(16): p. 8399-413.
37. Golestan, A.M., et al., *The Effects of NDRG2 Overexpression on Cell Proliferation and Invasiveness of SW48 Colorectal Cancer Cell Line.* Iran J Med Sci, 2015. **40**(5): p. 430-9.
38. Waters, A.M., et al., *Evaluation of the selectivity and sensitivity of isoform- and mutation-specific RAS antibodies.* Sci Signal, 2017. **10**(498).
39. Califice, S., V. Castronovo, and F. Van Den Brûle, *Galectin-3 and cancer (Review).* Int J Oncol, 2004. **25**(4): p. 983-92.
40. Shalom-Feuerstein, R., et al., *K-ras nanoclustering is subverted by overexpression of the scaffold protein galectin-3.* Cancer Res, 2008. **68**(16): p. 6608-16.
41. Levy, R., et al., *Galectin-3 mediates cross-talk between K-Ras and Let-7c tumor suppressor microRNA.* PLoS One, 2011. **6**(11): p. e27490.
42. Elad-Sfadia, G., et al., *Galectin-3 augments K-Ras activation and triggers a Ras signal that attenuates ERK but not phosphoinositide 3-kinase activity.* J Biol Chem, 2004. **279**(33): p. 34922-30.
43. Siddiqui, F.A., et al., *Novel Small Molecule Hsp90/Cdc37 Interface Inhibitors Indirectly Target K-Ras-Signaling.* Cancers (Basel), 2021. **13**(4).
44. Bhagatji, P., et al., *Multiple cellular proteins modulate the dynamics of K-ras association with the plasma membrane.* Biophys J, 2010. **99**(10): p. 3327-35.
45. Plowman, S.J., et al., *H-ras, K-ras, and inner plasma membrane raft proteins operate in nanoclusters with differential dependence on the actin cytoskeleton.* Proc Natl Acad Sci U S A, 2005. **102**(43): p. 15500-5.
46. Tian, T., et al., *Mathematical modeling of K-Ras nanocluster formation on the plasma membrane.* Biophys J, 2010. **99**(2): p. 534-43.
47. Inder, K.L., et al., *Nucleophosmin and nucleolin regulate K-Ras plasma membrane interactions and MAPK signal transduction.* J Biol Chem, 2009. **284**(41): p. 28410-28419.
48. Maurice, D.H., et al., *Cyclic nucleotide phosphodiesterases (PDEs): coincidence detectors acting to spatially and temporally integrate cyclic nucleotide and non-cyclic nucleotide signals.* Biochem Soc Trans, 2014. **42**(2): p. 250-6.
49. Zimmermann, G., et al., *Small molecule inhibition of the KRAS-PDEdelta interaction impairs oncogenic KRAS signalling.* Nature, 2013. **497**(7451): p. 638-42.
50. Chen, Y.H., et al., *EPHA2 feedback activation limits the response to PDEdelta inhibition in KRAS-dependent cancer cells.* Acta Pharmacol Sin, 2020. **41**(2): p. 270-277.
51. Nouri, K., et al., *Biophysical Characterization of Nucleophosmin Interactions with Human Immunodeficiency Virus Rev and Herpes Simplex Virus US11.* PLoS One, 2015. **10**(12): p. e0143634.
52. Saliani, M., et al., *KRAS-related long noncoding RNAs in human cancers.* Cancer Gene Ther, 2022. **29**(5): p. 418-427.
53. Shi, L., et al., *A KRAS-responsive long non-coding RNA controls microRNA processing.* Nat Commun, 2021. **12**(1): p. 2038.
54. Xian, J., et al., *Nucleophosmin Mutants Promote Adhesion, Migration and Invasion of Human Leukemia THP-1 Cells through MMPs Up-regulation via Ras/ERK MAPK Signaling.* Int J Biol Sci, 2016. **12**(2): p. 144-55.

55. Li, F., et al., *Epigenetic CRISPR Screens Identify Npm1 as a Therapeutic Vulnerability in Non-Small Cell Lung Cancer.* Cancer Res, 2020. **80**(17): p. 3556-3567.
56. Lim, M.J. and X.W. Wang, *Nucleophosmin and human cancer.* Cancer Detect Prev, 2006. **30**(6): p. 481-90.
57. Falini, B., et al., *Both carboxy-terminus NES motif and mutated tryptophan(s) are crucial for aberrant nuclear export of nucleophosmin leukemic mutants in NPMc+ AML.* Blood, 2006. **107**(11): p. 4514-23.
58. Falini, B., et al., *Cytoplasmic nucleophosmin in acute myelogenous leukemia with a normal karyotype.* N Engl J Med, 2005. **352**(3): p. 254-66.
59. Reuter, C.W., et al., *Lack of noncanonical RAS mutations in cytogenetically normal acute myeloid leukemia.* Ann Hematol, 2014. **93**(6): p. 977-82.
60. Verhaak, R.G., et al., *Mutations in nucleophosmin (NPM1) in acute myeloid leukemia (AML): association with other gene abnormalities and previously established gene expression signatures and their favorable prognostic significance.* Blood, 2005. **106**(12): p. 3747-54.
61. Inder, K.L., M.M. Hill, and J.F. Hancock, *Nucleophosmin and nucleolin regulate K-Ras signaling.* Commun Integr Biol, 2010. **3**(2): p. 188-90.
62. Meloni, G., et al., *Late relapse of acute myeloid leukemia with mutated NPM1 after eight years: evidence of NPM1 mutation stability.* Haematologica, 2009. **94**(2): p. 298-300.
63. Meloni, G., et al., *Late relapse of acute myeloid leukemia with mutated NPM1 after eight years: evidence of NPM1 mutation stability.* Haematologica, 2008. **94**(2): p. 298-300.
64. Noguera, N.I., et al., *Nucleophosmin/B26 regulates PTEN through interaction with HAUSP in acute myeloid leukemia.* Leukemia, 2013. **27**(5): p. 1037-43.
65. Rezaei Adariani, S., et al., *Structural snapshots of RAF kinase interactions.* Biochem Soc Trans, 2018. **46**(6): p. 1393-1406.
66. Weissbach, L., et al., *Identification of a human rasGAP-related protein containing calmodulin-binding motifs.* J Biol Chem, 1994. **269**(32): p. 20517-21.
67. Weissbach, L., A. Bernards, and D.W. Herion, *Binding of myosin essential light chain to the cytoskeleton-associated protein IQGAP1.* Biochem Biophys Res Commun, 1998. **251**(1): p. 269-76.
68. Bardwell, A.J., et al., *The WW domain of the scaffolding protein IQGAP1 is neither necessary nor sufficient for binding to the MAPKs ERK1 and ERK2.* J Biol Chem, 2017. **292**(21): p. 8750-8761.
69. McNulty, D.E., et al., *MAPK scaffold IQGAP1 binds the EGF receptor and modulates its activation.* J Biol Chem, 2011. **286**(17): p. 15010-21.
70. Choi, S., et al., *Agonist-stimulated phosphatidylinositol-3,4,5-trisphosphate generation by scaffolded phosphoinositide kinases.* Nat Cell Biol, 2016. **18**(12): p. 1324-1335.
71. Smith, J.M., A.C. Hedman, and D.B. Sacks, *IQGAPs choreograph cellular signaling from the membrane to the nucleus.* Trends Cell Biol, 2015. **25**(3): p. 171-84.
72. Wei, T. and P.F. Lambert, *Role of IQGAP1 in Carcinogenesis.* Cancers (Basel), 2021. **13**(16).
73. Lu, Z., et al., *Differential expression profiling of human pancreatic adenocarcinoma and healthy pancreatic tissue.* Proteomics, 2004. **4**(12): p. 3975-88.
74. Wang, X.X., et al., *Overexpression of IQGAP1 in human pancreatic cancer.* Hepatobiliary Pancreat Dis Int, 2013. **12**(5): p. 540-5.
75. Hayashi, H., et al., *Overexpression of IQGAP1 in advanced colorectal cancer correlates with poor prognosis-critical role in tumor invasion.* Int J Cancer, 2010. **126**(11): p. 2563-74.
76. White, C.D., et al., *IQGAP1 and IQGAP2 are reciprocally altered in hepatocellular carcinoma.* BMC Gastroenterol, 2010. **10**: p. 125.
77. Dong, P., et al., *Overexpression and diffuse expression pattern of IQGAP1 at invasion fronts are independent prognostic parameters in ovarian carcinomas.* Cancer Lett, 2006. **243**(1): p. 120-7.
78. McDonald, K.L., et al., *IQGAP1 and IGFBP2: valuable biomarkers for determining prognosis in glioma patients.* J Neuropathol Exp Neurol, 2007. **66**(5): p. 405-17.
79. Ren, J.-G., Z. Li, and D.B. Sacks, *IQGAP1 modulates activation of B-Raf.* Proceedings of the National Academy of Sciences, 2007. **104**(25): p. 10465-10469.
80. Roy, M., Z.G. Li, and D.B. Sacks, *IQGAP1 is a scaffold for mitogen-activated protein kinase signaling.* Molecular and Cellular Biology, 2005. **25**(18): p. 7940-7952.
81. Jameson, K.L., et al., *IQGAP1 scaffold-kinase interaction blockade selectively targets RAS-MAP kinase-driven tumors.* Nat Med, 2013. **19**(5): p. 626-630.
82. Chen, F., et al., *IQGAP1 is overexpressed in hepatocellular carcinoma and promotes cell proliferation by Akt activation.* Exp Mol Med, 2010. **42**(7): p. 477-83.
83. Chen, M., et al., *The Specificity of EGF-Stimulated IQGAP1 Scaffold Towards the PI3K-Akt Pathway is Defined by the IQ3 motif.* Scientific Reports, 2019. **9**(1): p. 9126.

84. Rameh, L.E. and A.M. Mackey, *IQGAP1 makes PI(3)K signalling as easy as PIP, PIP(2), PIP(3).* Nat Cell Biol, 2016. **18**(12): p. 1263-1265.
85. Li, J.H., et al., *IQGAP1 Maintains Pancreatic Ductal Adenocarcinoma Clonogenic Growth and Metastasis.* Pancreas, 2019. **48**(1): p. 94-98.
86. Choi, S. and R.A. Anderson, *And Akt-ion! IQGAP1 in control of signaling pathways.* EMBO J, 2017. **36**(8): p. 967-969.
87. Tekletsadik, Y.K., R. Sonn, and M.A. Osman, *A conserved role of IQGAP1 in regulating TOR complex 1.* J Cell Sci, 2012. **125**(Pt 8): p. 2041-52.
88. Young, L.C., et al., *An MRAS, SHOC2, and SCRIB complex coordinates ERK pathway activation with polarity and tumorigenic growth.* Mol Cell, 2013. **52**(5): p. 679-92.
89. Rodriguez-Viciana, P., et al., *A phosphatase holoenzyme comprised of Shoc2/Sur8 and the catalytic subunit of PP1 functions as an M-Ras effector to modulate Raf activity.* Mol Cell, 2006. **22**(2): p. 217-30.
90. Boned Del Rio, I., et al., *SHOC2 complex-driven RAF dimerization selectively contributes to ERK pathway dynamics.* Proc Natl Acad Sci U S A, 2019. **116**(27): p. 13330-13339.
91. Zambrano, R.M., et al., *Further evidence that variants in PPP1CB cause a rasopathy similar to Noonan syndrome with loose anagen hair.* Am J Med Genet A, 2017. **173**(2): p. 565-567.
92. Young, L.C., et al., *SHOC2-MRAS-PP1 complex positively regulates RAF activity and contributes to Noonan syndrome pathogenesis.* Proc Natl Acad Sci U S A, 2018. **115**(45): p. E10576-E10585.
93. You, X., et al., *SHOC2 plays an oncogenic or tumor-suppressive role by differentially targeting the MAPK and mTORC1 signals in liver cancer.* Life Med, 2024. **3**(3): p. lnae023.
94. Xie, C.M., et al., *The FBXW7-SHOC2-Raptor Axis Controls the Cross-Talks between the RAS-ERK and mTORC1 Signaling Pathways.* Cell Rep, 2019. **26**(11): p. 3037-3050 e4.
95. Jang, H., et al., *The leucine-rich repeat signaling scaffolds Shoc2 and Erbin: cellular mechanism and role in disease.* FEBS J, 2021. **288**(3): p. 721-739.
96. Kaduwal, S., et al., *Sur8/Shoc2 promotes cell motility and metastasis through activation of Ras-PI3K signaling.* Oncotarget, 2015. **6**(32): p. 33091-105.
97. Jeoung, M., et al., *Shoc2-tranduced ERK1/2 motility signals--Novel insights from functional genomics.* Cell Signal, 2016. **28**(5): p. 448-459.
98. Gu, A.Y., et al., *Whole-genome CRISPR-Cas9 knockout screens identify SHOC2 as a genetic dependency in NRAS-mutant melanoma.* Cancer Commun (Lond), 2025.
99. Cordeddu, V., et al., *Mutation of SHOC2 promotes aberrant protein N-myristoylation and causes Noonan-like syndrome with loose anagen hair.* Nat Genet, 2009. **41**(9): p. 1022-6.
100. Hannig, V., et al., *A Novel SHOC2 Variant in Rasopathy.* Hum Mutat, 2014. **35**(11): p. 1290-4.
101. Motta, M., et al., *Clinical and functional characterization of a novel RASopathy-causing SHOC2 mutation associated with prenatal-onset hypertrophic cardiomyopathy.* Hum Mutat, 2019. **40**(8): p. 1046-1056.
102. Kaplan, F.M., et al., *SHOC2 and CRAF mediate ERK1/2 reactivation in mutant NRAS-mediated resistance to RAF inhibitor.* J Biol Chem, 2012. **287**(50): p. 41797-807.
103. Sulahian, R., et al., *Synthetic Lethal Interaction of SHOC2 Depletion with MEK Inhibition in RAS-Driven Cancers.* Cell Rep, 2019. **29**(1): p. 118-134 e8.
104. Geng, W., et al., *SHOC2 mediates the drug-resistance of triple-negative breast cancer cells to everolimus.* Cancer Biol Ther, 2023. **24**(1): p. 2206362.
105. Nguyen, A., et al., *Kinase suppressor of Ras (KSR) is a scaffold which facilitates mitogen-activated protein kinase activation in vivo.* Mol Cell Biol, 2002. **22**(9): p. 3035-45.
106. Jones, G.G., et al., *SHOC2 phosphatase-dependent RAF dimerization mediates resistance to MEK inhibition in RAS-mutant cancers.* Nat Commun, 2019. **10**(1): p. 2532.
107. Therrien, M., et al., *Functional analysis of CNK in RAS signaling.* Proc Natl Acad Sci U S A, 1999. **96**(23): p. 13259-63.
108. Indarte, M., et al., *An Inhibitor of the Pleckstrin Homology Domain of CNK1 Selectively Blocks the Growth of Mutant KRAS Cells and Tumors.* Cancer Res, 2019. **79**(12): p. 3100-3111.
109. Sun, Y., et al., *Allosteric SHP2 Inhibitor, IACS-13909, Overcomes EGFR-Dependent and EGFR-Independent Resistance Mechanisms toward Osimertinib.* Cancer Res, 2020. **80**(21): p. 4840-4853.
110. Valencia-Sama, I., et al., *SHP2 Inhibition with TNO155 Increases Efficacy and Overcomes Resistance of ALK Inhibitors in Neuroblastoma.* Cancer Res Commun, 2023. **3**(12): p. 2608-2622.
111. Kaya, P., et al., *An Improved PDE6D Inhibitor Combines with Sildenafil To Inhibit KRAS Mutant Cancer Cell Growth.* J Med Chem, 2024. **67**(11): p. 8569-8584.

112. Xiao-Pei, H., et al., *Systematic identification of Celastrol-binding proteins reveals that Shoc2 is inhibited by Celastrol.* Biosci Rep, 2018. **38**(6).
113. Hauseman, Z.J., et al., *Targeting the SHOC2-RAS interaction in RAS-mutant cancers.* Nature, 2025.
114. Schneeweis, C., et al., *AP1/Fra1 confers resistance to MAPK cascade inhibition in pancreatic cancer.* Cell Mol Life Sci, 2022. **80**(1): p. 12.
115. Sodir, N.M., et al., *SHP2: A Pleiotropic Target at the Interface of Cancer and Its Microenvironment.* Cancer Discov, 2023. **13**(11): p. 2339-2355.
116. Yuan, X., et al., *Recent Advances of SHP2 Inhibitors in Cancer Therapy: Current Development and Clinical Application.* J Med Chem, 2020. **63**(20): p. 11368-11396.
117. Chen, Y.N., et al., *Allosteric inhibition of SHP2 phosphatase inhibits cancers driven by receptor tyrosine kinases.* Nature, 2016. **535**(7610): p. 148-52.
118. Zhang, Y., et al., *Identification of linderalactone as a natural inhibitor of SHP2 to ameliorate CCl(4)-induced liver fibrosis.* Front Pharmacol, 2023. **14**: p. 1098463.
119. Ahmed, R., K. Anam, and H. Ahmed, *Development of Galectin-3 Targeting Drugs for Therapeutic Applications in Various Diseases.* Int J Mol Sci, 2023. **24**(9).
120. Ruvolo, P.P., *Galectin 3 as a guardian of the tumor microenvironment.* Biochim Biophys Acta, 2016. **1863**(3): p. 427-437.
121. Sigamani, A., et al., *An Oral Galectin Inhibitor in COVID-19-A Phase II Randomized Controlled Trial.* Vaccines (Basel), 2023. **11**(4).
122. Michael, J.V. and L.E. Goldfinger, *Concepts and advances in cancer therapeutic vulnerabilities in RAS membrane targeting.* Semin Cancer Biol, 2019. **54**: p. 121-130.
123. Stasenko, M., et al., *Targeting galectin-3 with a high-affinity antibody for inhibition of high-grade serous ovarian cancer and other MUC16/CA-125-expressing malignancies.* Sci Rep, 2021. **11**(1): p. 3718.
124. Vuong, L., et al., *An Orally Active Galectin-3 Antagonist Inhibits Lung Adenocarcinoma Growth and Augments Response to PD-L1 Blockade.* Cancer Res, 2019. **79**(7): p. 1480-1492.
125. Siddiqui, F.A., et al., *PDE6D Inhibitors with a New Design Principle Selectively Block K-Ras Activity.* ACS Omega, 2020. **5**(1): p. 832-842.
126. Papke, B., et al., *Identification of pyrazolopyridazinones as PDEdelta inhibitors.* Nat Commun, 2016. **7**: p. 11360.
127. Martin-Gago, P., et al., *A PDE6delta-KRas Inhibitor Chemotype with up to Seven H-Bonds and Picomolar Affinity that Prevents Efficient Inhibitor Release by Arl2.* Angew Chem Int Ed Engl, 2017. **56**(9): p. 2423-2428.
128. Canovas Nunes, S., et al., *Validation of a small molecule inhibitor of PDE6D-RAS interaction with favorable anti-leukemic effects.* Blood Cancer J, 2022. **12**(4): p. 64.
129. Issa, G.C., et al., *The menin inhibitor revumenib in KMT2A-rearranged or NPM1-mutant leukaemia.* Nature, 2023. **615**(7954): p. 920-924.
130. Ranieri, R., et al., *Current status and future perspectives in targeted therapy of NPM1-mutated AML.* Leukemia, 2022. **36**(10): p. 2351-2367.

Box 1
Accessory proteins related to the RTK-RAS-MAPK signaling cascade can be divided into at least four subgroups (see for more details [18].

- Anchoring proteins bind to the membrane and other effectors (mostly kinases): CNK1, FLOT1, FLOT2, GAB1, GAB2, LAT, NTAL, PAQR10, PAQR11, PDEδ, SEF1

- Docking proteins that bind to receptors (*e.g.*, RTKs and GPCRs) and more than one effector: ß-Arrestin 1, ß-Arrestin 2, DOK1, DOK2, FRS2, IRS2

- Adaptor proteins that link two signaling components (*e.g.*, receptor and GEF): CRKL, CBL, GRB2, SHC, SHP2

- Scaffold proteins that bind two or more partners and provide a signaling platform: ASPP1, ASPP2, Calmodulin, Erbin, FHL1, FHL2, Galectin 1, Galectin 3, GIT1, IQGAP1, KSR1, Merlin, MORG1, MP1, Nucleolin, Nucleophosmin, Paxillin, PEA15, RGS14, RKIP, SHOC2, SPRED1, SPRED2, SPRED3, SPRY1, SPRY2

Box 2

Primary targets	Inhibitors or Compounds	Approval status	Comment	References
KSR	APS-2-79	Not FDA-approved; currently used only as an experimental drug	APS-2-79 antagonizes heterodimerization of RAF and prevents conformational changes necessary for phosphorylation of KSR-bound MEK. Increased potency of MEK-inhibitors in RAS-mutant cell lines	[29]
SHOC2	Celasterol	Not approved by the FDA due to low bioavailability and physiological instability.	Celasterol decreased ERK1/2 phosphorylation and proliferation in SW480 colorectal cancer cellline	[112]
	Compound 6	Preclinical (in vitro and in vivo studies)	Compound 6 decreases MAPK-signaling and proliferation in NRAS(Q61L) mutated cells	[113]
	dTAG-13	Preclinical (cell-based models)	dTAG-13 is an inhibitor of FRA1. Inhibition of FRA1 increases the sensitivity of KRAS-mutated pancreas adenocarcinomas to RAF-, MEK- and ERK-inhibition	[114]
CNK1	PHT-7.0 PHT-7.3 PHT-7.10	Not FDA-approved; currently used only as an experimental drug in laboratory research	Binding of the pleckstrin homology (PH-) domain of CNK1 inhibits proliferation, as well as RAS/RAF/MEK/ERK-, RHO- and RAL A/B- signaling in KRAS mutated lung und colon cancer cells, but show less effect on KRAS-wildtype cells.	[108]
SHP2	JAB-3068 TNO155 RMC-4630 RLY-1971 BBP-398 BR790 BPI-442096 BR790 ET0038 GDC-1971 GH21 HBI-2376 HS-10381 ICP-189 JAB-3312 PF-07284892 SH3809 ERAS-601	Currently in clinical trials; not yet approved by the FDA	SHP2 Inhibition disrupts SOS1´s GEF function. A wide variety of SHP2-inhibitors are being tested, especially in combination with other known inhibitory cancer drugs, as SHP2 is known to be a link between several oncogenic signaling pathways	[115, 116]
	SHP099	Still in clinical trials and not FDA-approved, but widely used in preclinical research as an SHP2 inhibitor	An allosteric SHP2 inhibitor that stabilizes the auto-inhibited conformation, thereby suppressing RAS–ERK signaling and inhibiting proliferation of RTK-driven cancer cells.	[117]
	Linderal-actone (LIN)	Preclinical research	An orthosteric SHP2 inhibitor that blocks the substrate-binding site, effective against gain-of-function mutants and reduces liver fibrosis in vivo.	[118]
GAL3	MCP	Currently in clinical trials; not yet approved by the FDA	Modified citrus pectin (MCP) inhibits GAL3 by blocking its carbohydrate-binding domain, reducing tumor cell adhesion, aggregation, and metastasis. It has demonstrated anti-metastatic effects in vitro and in vivo, particularly in breast and prostate cancer models.	[119]
	GCS-100	Currently in clinical trials; not yet approved by the FDA	A modified pectin GAL3 inhibitor that restores T cell activity and induces IFN-γ production, enhancing anti-tumor immune responses in vitro and in vivo.	[120]
	GM-CT-01	Currently in clinical trials; not yet approved by the FDA	A galactomannan polysaccharide that binds to GAL3, disrupting its interaction with glycoproteins on tumor and immune cells. It has been studied for its potential to enhance immune responses and inhibit tumor growth.	[120]

	GR-MD-02 (Belapectin)	Currently in clinical trials; not yet approved by the FDA	It is a complex carbohydrate drug that targets GAL3, a protein implicated in various fibrotic and inflammatory diseases. By binding to GAL-3, GR-MD-02 disrupts its function, thereby modulating the tumor microenvironment and enhancing anti-tumor immune responses.	[119]
	ProLectin-M (PL-M)	Currently in clinical trials; not yet approved by the FDA	It is an orally administered galectin-3 antagonist that binds to the N-terminal domain of Gal-3, thereby inhibiting SARS-CoV-2 from entering host cells.	[121]
	TD139	Currently in clinical trials; not yet approved by the FDA	A potent inhaled GAL3 inhibitor that demonstrated safety, target engagement, and reduced plasma biomarkers linked to IPF progression in a Phase 1/2a study	[122]
	14D11	Preclinical research	A high-affinity monoclonal antibody that inhibits GAL3 by blocking its carbohydrate-binding domain, reducing AKT/ERK signaling and tumor invasion. Effective against MUC16/CA-125-expressing cancers, including high-grade serous ovarian cancer.	[123]
	GB1107	Preclinical research	GB1107 is an orally active small-molecule GAL3 inhibitor that suppresses lung adenocarcinoma growth and metastasis. It enhances anti-tumor immunity by promoting M1 macrophage polarization and increasing $CD8^+$ T-cell infiltration. When combined with PD-L1 blockade, GB1107 amplifies cytotoxic and apoptotic responses.	[124]
PDE6D (PDEδ)	Deltaflexin1,2	Still under clinical trials, not FDA approved	These are selective PDE6D inhibitors that disrupts the interaction between PDE6D and oncogenic K-Ras, impairing K-Ras membrane localization and nanoclustering. This leads to reduced proliferation in K-Ras-mutant cancer cells and inhibition of tumor sphere formation, while sparing H-Ras signaling pathways.	[125]
	Deltaflexin 3	Still under clinical trials, not FDA approved	It is an improved PDE6D inhibitor that blocks KRAS membrane localization by disrupting its interaction with the chaperone PDE6D. It selectively impairs the growth of KRAS-mutant cancer cells and shows enhanced anti-tumor efficacy when combined with Sildenafil.	[111]
	Deltarasin	Still under clinical trials, not FDA approved	Deltarasin is a small-molecule inhibitor that disrupts the interaction between KRAS and the prenyl-binding protein PDE6δ, thereby preventing KRAS membrane localization. This inhibition impairs KRAS signaling pathways, such as MAPK and mTOR, leading to reduced proliferation and increased apoptosis in KRAS-dependent cancer cells.	[126]
	Deltazinone-1	Still under clinical trials, not FDA approved	It is a selective pyrazolopyridazinone inhibitor of PDEδ, exhibiting a high binding affinity. It impedes the PDEδ-Ras interaction, leading to the delocalization of prenylated Ras proteins and a dose-dependent reduction in proliferation of KRas-dependent cancer cell lines.	[126]
	Deltason-amide-1,2	Still under clinical trials, not FDA approved	These are advanced PDEδ–KRas inhibitors with picomolar affinity and up to seven hydrogen bonds, designed to resist Arl2-mediated release. They effectively disrupt KRas localization and signaling, showing strong anti-proliferative effects in KRas-driven cancer cells.	[127]
	DW0254	Preclinical research	DW0254 is a potent small-molecule inhibitor of the PDEδ–RAS interaction that disrupts RAS membrane localization by binding PDEδ's hydrophobic pocket. It inhibits RAC activation and MAPK/ERK and PI3K/AKT pathways, reducing proliferation and inducing apoptosis in RAS-mutant leukemia cells, with notable tumor suppression in vivo.	[128]
NPM1	Revumenib	FDA-approved inhibitor	Revumenib is a selective menin inhibitor that targets the menin-KMT2A interaction, showing promising efficacy in KMT2A-rearranged and NPM1-mutant acute leukaemias by restoring myeloid differentiation.	[129]
	NSC348884	Still under clinical trials, not FDA approved	Disrupts NPM1 oligomerization, inducing apoptosis in leukemic cells.	[130]

	Avrainvill-amide	Still under clinical trials, not FDA approved	Binds to the C-terminal domain of NPM1, promoting its relocalization to the nucleolus.	[130]
	Leptomycin B,	Still under clinical trials, not FDA approved	An irreversible XPO1 inhibitor that blocks nuclear export but is limited by toxicity.	[130]
	SINE compounds: KPT-185 KPT-249 KPT-251 KPT-276 KPT-335 Selinexor)	Still under clinical trials, not FDA approved	Reversible XPO1 inhibitors that impede nuclear export; selinexor showed limited efficacy due to dosing constraints.	[130]
	Eltanexor (KPT-8602)	Still under clinical trials, not FDA approved	A second-generation XPO1 inhibitor with improved tolerability and efficacy, especially when administered frequently.	[130]
	Ziftomenib (KO539)	Still under clinical trials, not FDA approved	A menin inhibitor that downregulates HOX/MEIS1 expression, showing promise in NPM1-mutated AML.	[130]
	Dactinomycin (Actinomycin D)	Still under clinical trials, not FDA approved	Induces nucleolar stress, leading to NPM1 degradation.	[130]
	ATRA/ATO	Still under clinical trials, not FDA approved	Promote selective degradation of mutant NPM1, sparing the wild-type protein.	[130]
	Deguelin (-)-Epigallo-catechin-3-gallate Imidazo-quinoxaline Derivatives:	Still under clinical trials, not FDA approved	Natural compounds that induce degradation of mutant NPM1 protein.	[130]
	CBS9106	Still under clinical trials, not FDA approved	Reversible inhibitor of exportin-1 (XPO1). It blocks nuclear export of proteins such as mutant NPM1, leading to their nuclear retention and promoting apoptosis in leukemic cells	[130]

Supplementary Information

Table S1. Human cell lines used in this study.

Cell line[a]	Accession number	Origin/Tissue	KRAS mutation[b]	Other mutations[b]
HEK-293	CVCL_0063	Kidney	WT	SV40 large T antigen
PANC-1	CVCL_0480	Pancreas	G12D (1)	CDKN2a (2), TP53 (2)
MIA PaCa-2	CVCL_0428	Pancreas	G12C (2)	CDKN2a (2), TP53 (2)
SHP-77	CVCL_1693	Lung	G12V (2)	ABL1 (2), RAC1 Y32C (2), TP53 (2)
SW480	CVCL_0546	Colon	G12V (2)	APC (1), TP53 (2)
Capan-1	CVCL_0237	Pancreas	G12V (2)	BRCA2 (2), SMAD4 (2), TP53 (2)

[a] Resource: Cellosaurus. [b] Numbers in brackets represent the number of mutant alleles (1, heterozygous; 2, homozygous); amp., amplification; HEK, Human embryonic kidney 293T.

Table S2. Guide-RNAs[a] used in this study.

PDEδ (PDE6D)	ACCTTCGGGATGCTGAGACA
GAL3 (LGALS3)	CATGATGCGTTATCTGGGTC
IQGAP1	GGGGTCTACCTTGCCAAACT
NPM1	TGCAGAGTCAGAGATGAAG
SHOC2	GGAAGAGAATTCAATGCGTT

[a] Guide RNAs have been ordered from Thermofisher Scientific. (https://www.thermofisher.com/de/de/home/life-science/genome-editing/crispr-libraries/trueguide-grnas.html)

Table S3. Antibodies used in this study.

Antibody[a]	Species	Supplier	Reference
AKT	Mouse	Cell Signaling	2920S
pAKT (T308)	Rabbit	Cell Signaling	2965S
pAKT (S473)	Rabbit	Cell Signaling	9271, 4060S
ERK1/2	Rabbit	Cell Signaling	9102
pERK1/2	Mouse	Cell Signaling	9106S
Galectin-3	Mouse	Abcam	ab2785
GAPDH	Rabbit	Cell Signaling	2118S
GAPDH	Mouse	Thermo Fisher Scientific	39-8600
IQGAP1	Mouse	Abcam	ab56529
JNK	Rabbit	Cell Signaling	9252S
pJNK (T183/Y185)	Rabbit	Cell Signaling	9251
$KRAS^{G12V}$	Rabbit	Cell Signaling	D2H12
NPM1	Mouse	Abcam	ab10530
Pan-RAS	Mouse	Millipore	05-516
Paxillin	Mouse	Sigma-Aldrich	MAB3060
PDEδ	Rabbit	Abcam	ab5665
SHOC2	Rabbit	Sigma-Aldrich	HPA009164
STAT3	Mouse	Cell Signaling	9139
pSTAT3	Rabbit	Cell Signaling	4324
α-tubulin	Rabbit	Abcam	ab52866
γ-tubulin	Mouse	Sigma-Aldrich	T5326
Vinculin	Mouse	Sigma-Aldrich	V9131
YAP	Rabbit	Cell Signaling	4912
pYAP (S127)	Rabbit	Cell Signaling	4911
IR©Dye 680RD anti-mouse	Donkey	Licor	926-68072
IR©Dye 800CW anti-rabbit	Donkey	Licor	926-32213

[a] The anbibody diultions were 1:1000, except for IR©Dye 680RD anti-mouse and IR©Dye 800CW anti-rabbit, which were 1:10.000.

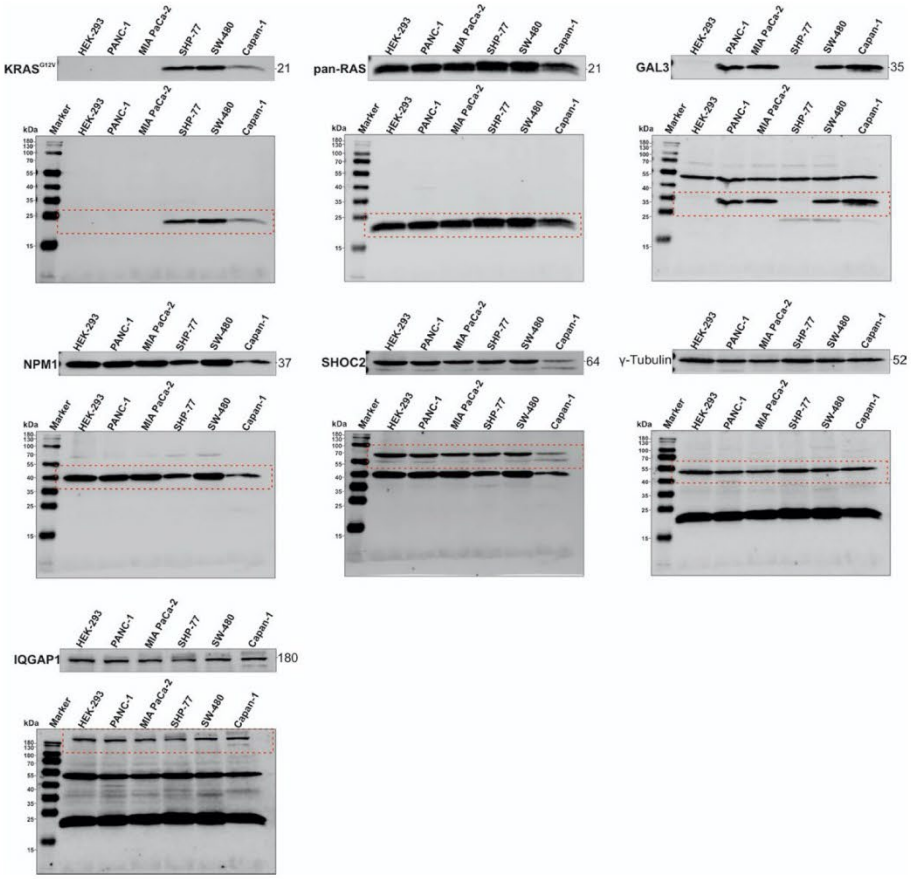

Figure S1. Original blots of KRAS and KRAS-related accessory proteins in cancer cell lines. See Figure 1 for more details.

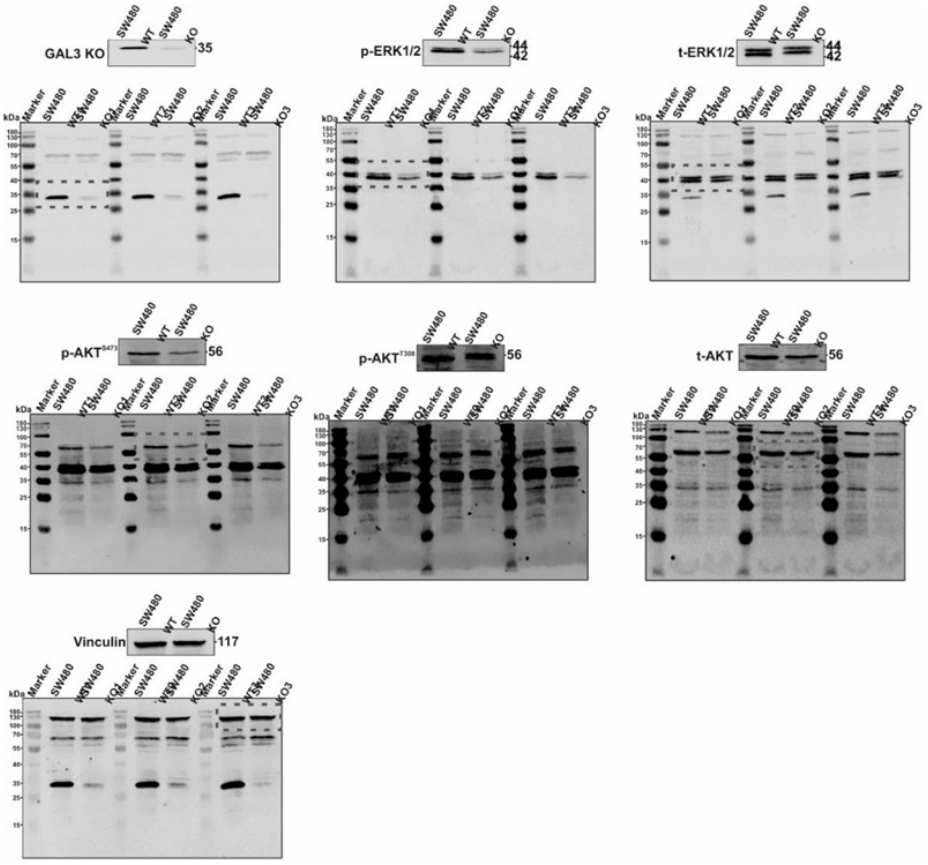

Figure S2. Original blots of *GAL3* WT and KO SW-480 cells. See Figure 2 for more details.

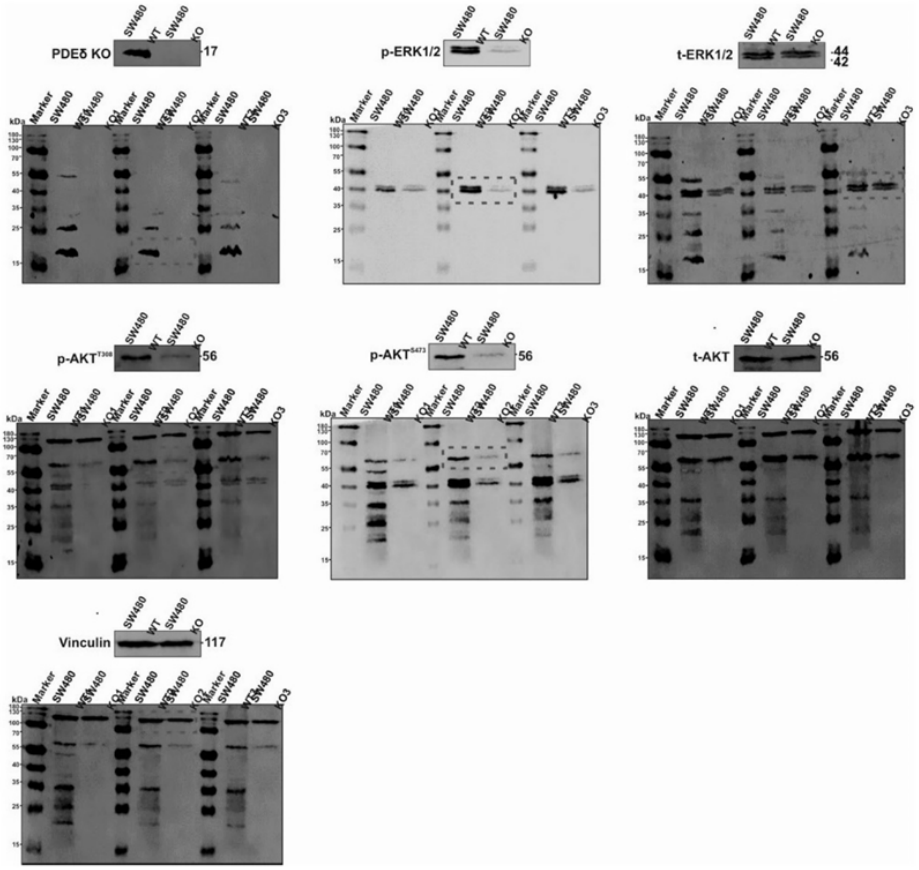

Figure S3. Original blots of *PDE6D* WT and KO SW-480 cells. See Figure 3 for more details.

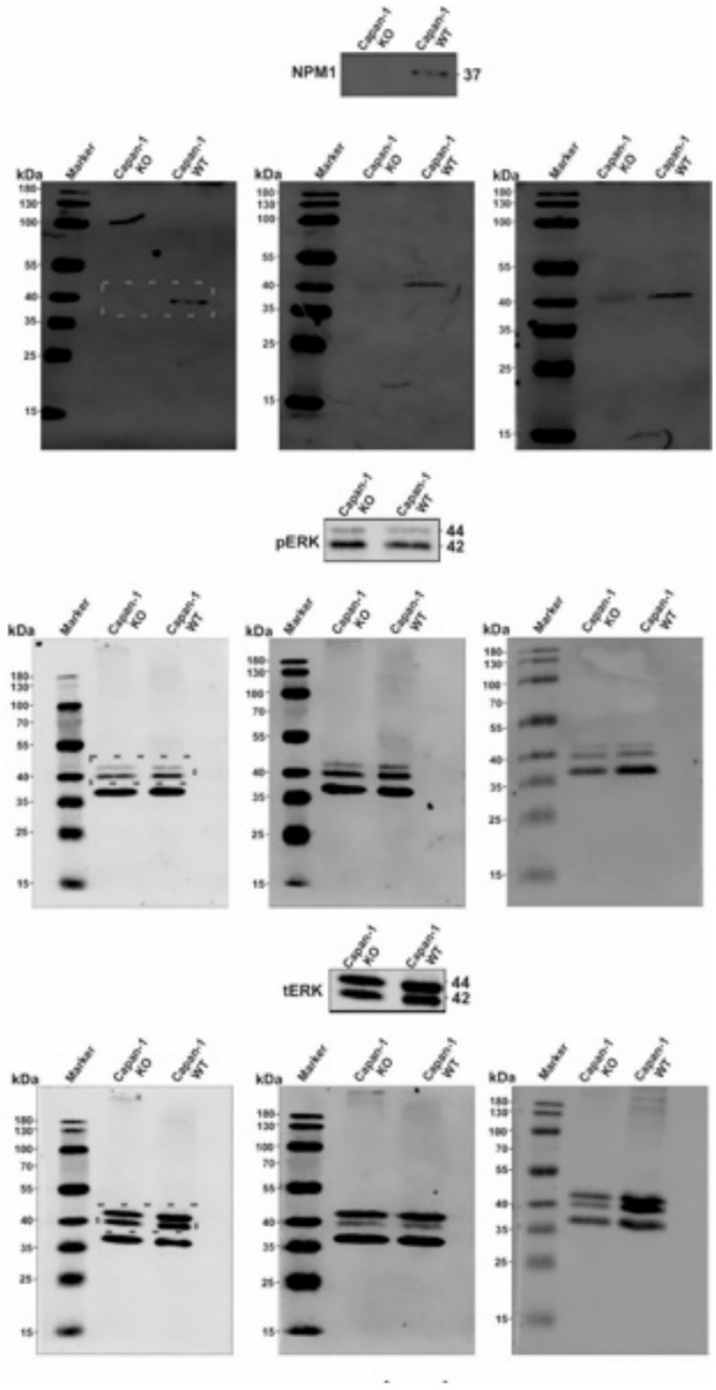
Caspin-1 KO
Caspin-1 WT
NPM1
37
kDa
Marker
180
130
100
55
40
35
25
15
pERK
44
42
70
tERK

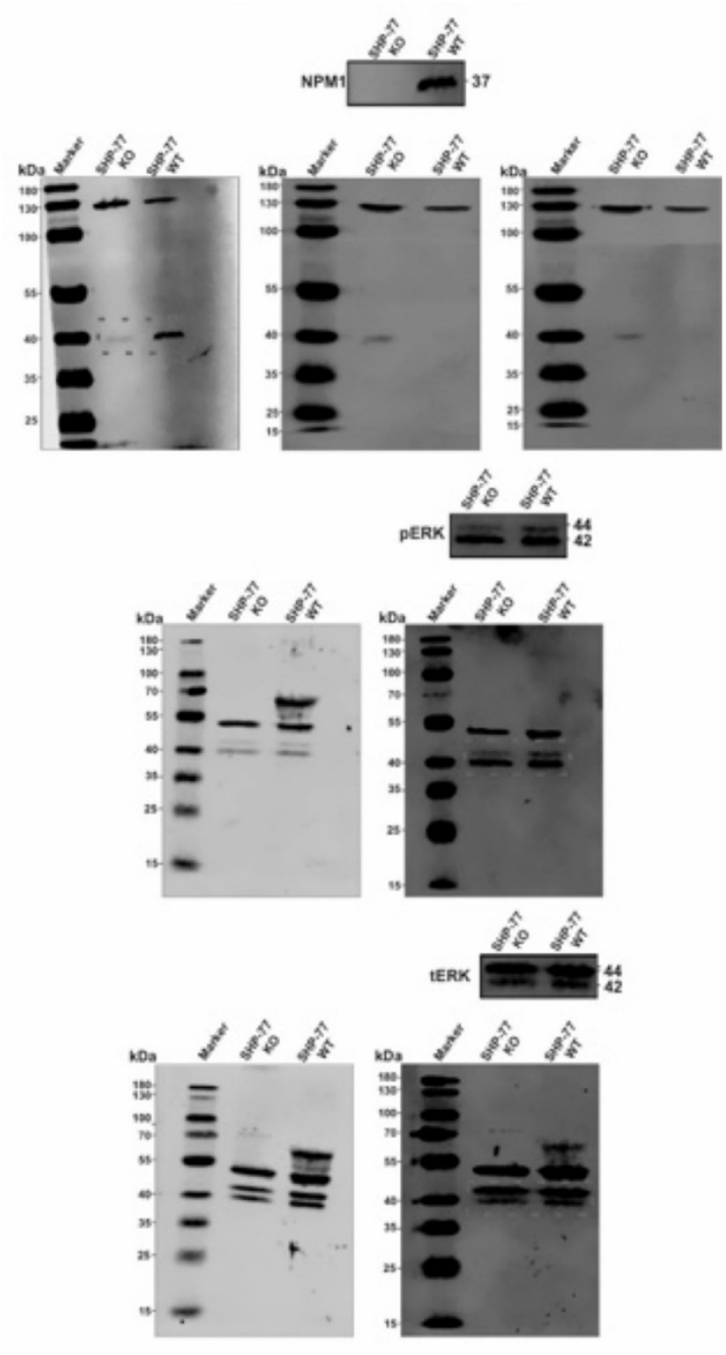
SHP-7T KO
SHP-7T WT
NPM1
37
kDa
Marker
180
130
100
70
55
40
35
25
15
pERK
44
42
tERK

30

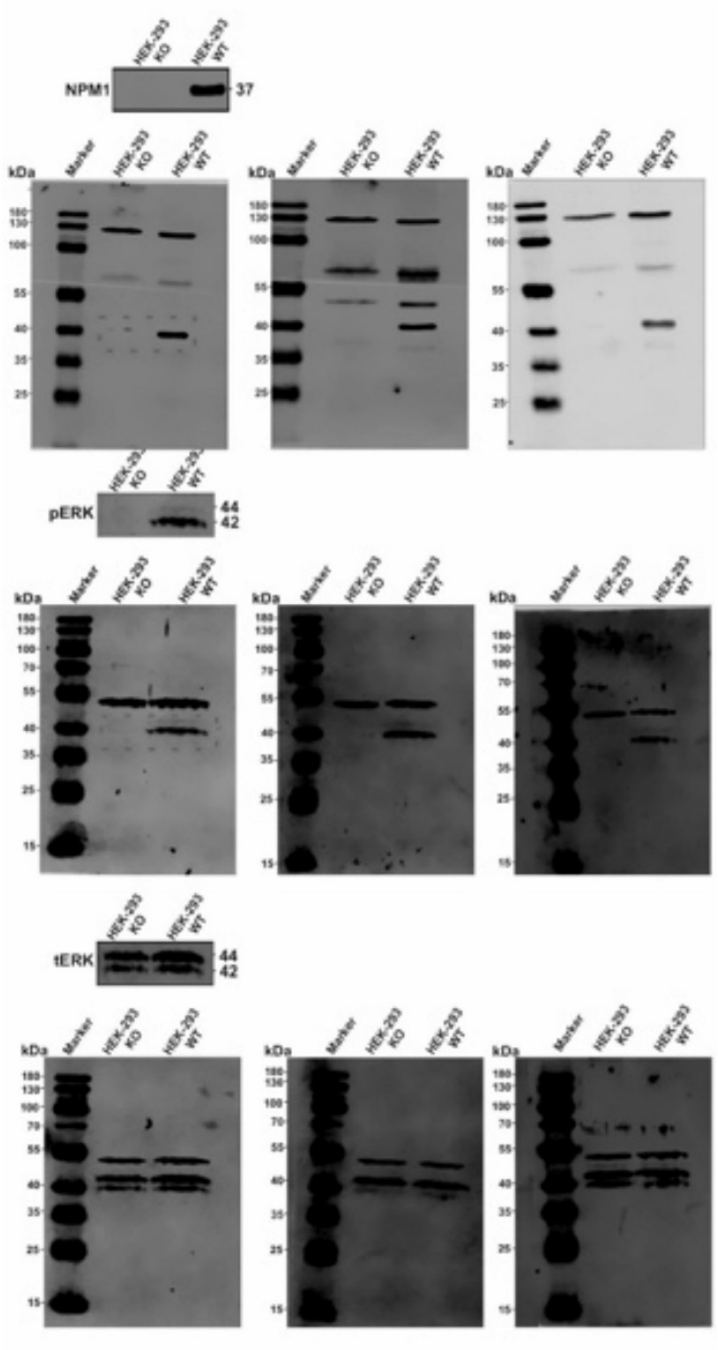
HEK-293 KO
HEK-293 WT
NPM1
37
kDa
Marker
180
130
100
55
40
35
25
pERK
44
42
70
15
tERK

31

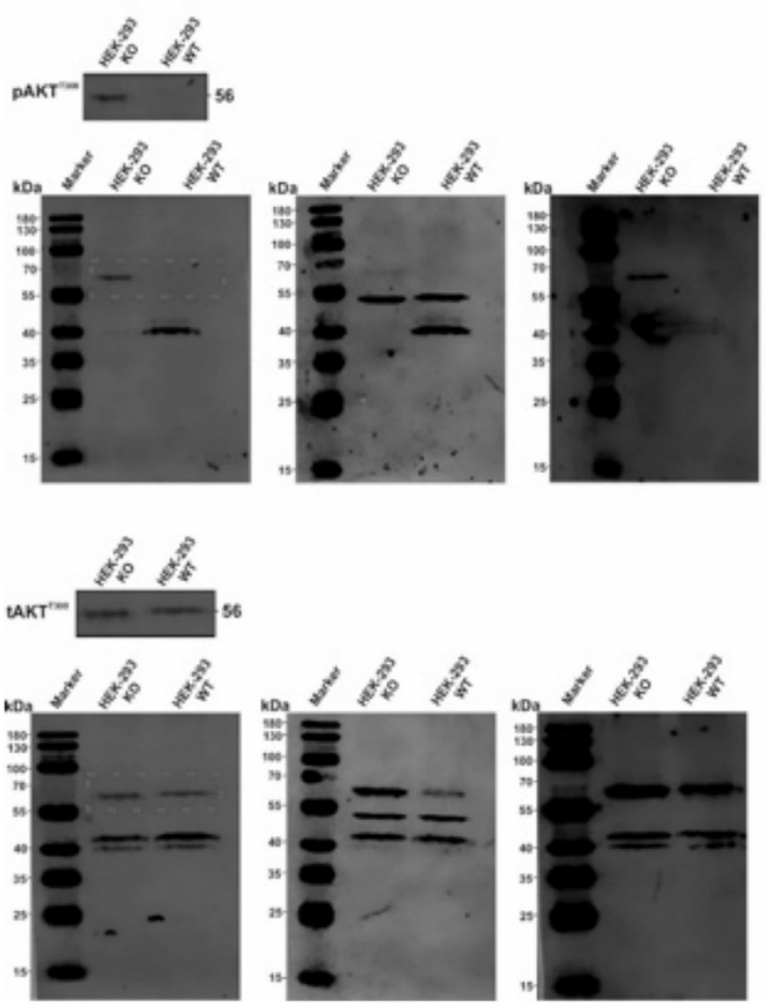

Figure S4. Original blots of *NPM1* WT and KO Capan-1, SHP-77 and HEK-293 cells. See Figure 4 for more details.

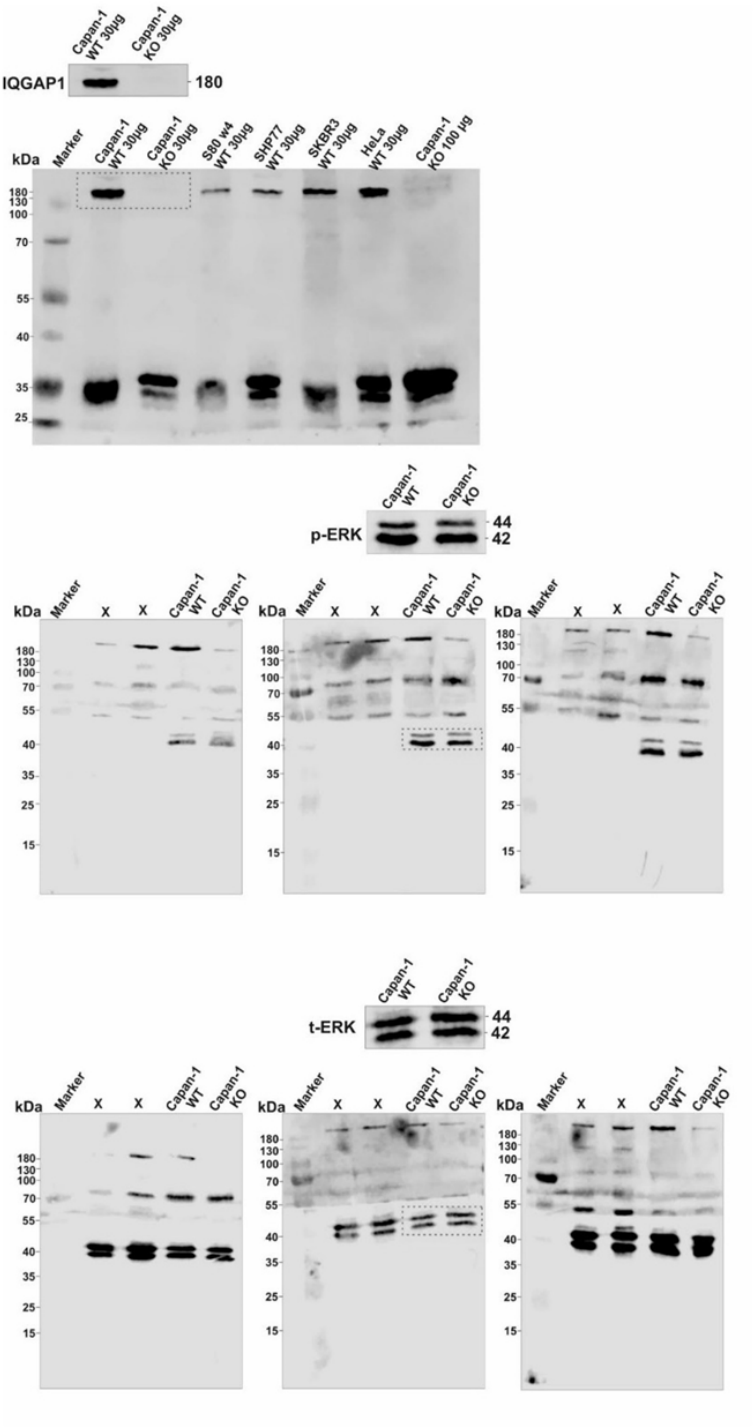
Capan-1 WT 30µg
Capan-1 KO 30µg
IQGAP1
180
kDa
Marker
Capan-1 WT 30µg
Capan-1 KO 30µg
S80 w4 WT 30µg
SHP77 WT 30µg
SKBR3 WT 30µg
HeLa WT 30µg
Capan-1 KO 100 µg
180
130
100
70
55
40
35
25
Capan-1 WT
Capan-1 KO
p-ERK
44
42
kDa
Marker
X
X
Capan-1 WT
Capan-1 KO
180
130
100
70
55
40
35
25
15
Capan-1 WT
Capan-1 KO
t-ERK
44
42
kDa
Marker
X
X
Capan-1 WT
Capan-1 KO
180
130
100
70
55
40
35
25
15

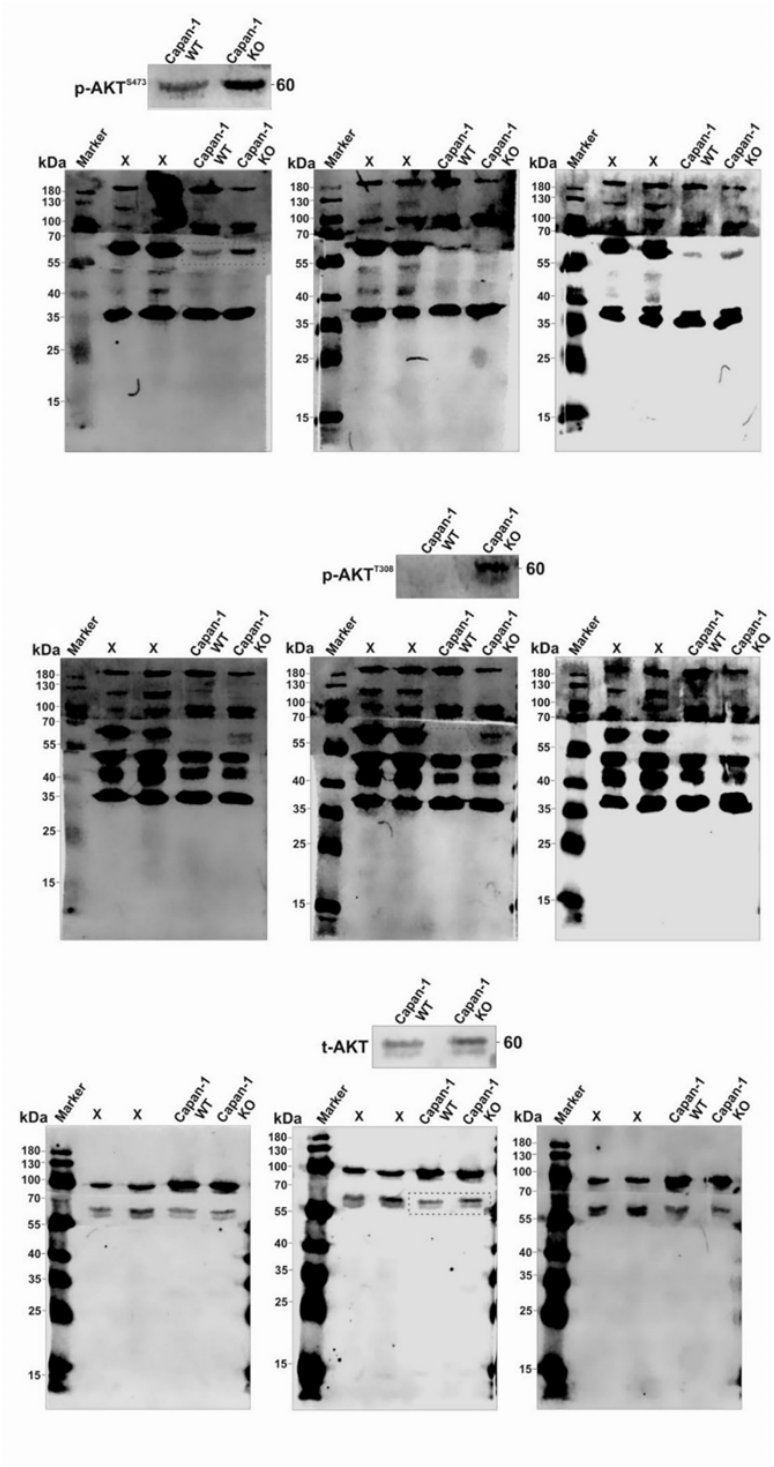
Capan-1 WT
Capan-1 KO
p-AKT S473
60
kDa
Marker
x
x
Capan-1 WT
Capan-1 KO
180
130
100
70
55
40
35
25
15
p-AKT T308
t-AKT

34

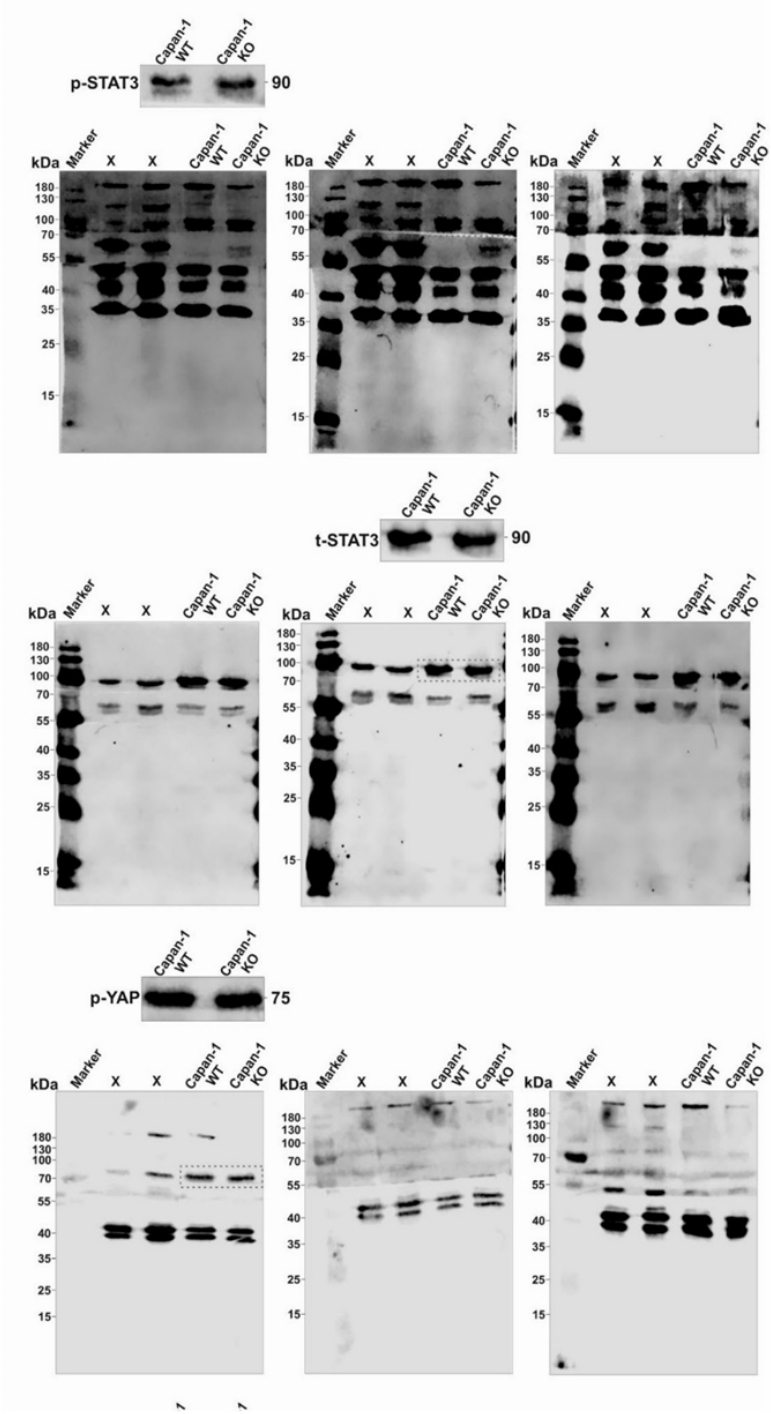
Capan-1 WT
Capan-1 KO
p-STAT3
90
kDa
Marker
X
X
Capan-1 WT
Capan-1 KO
180
130
100
70
55
40
35
25
15
t-STAT3
90
p-YAP
75

35

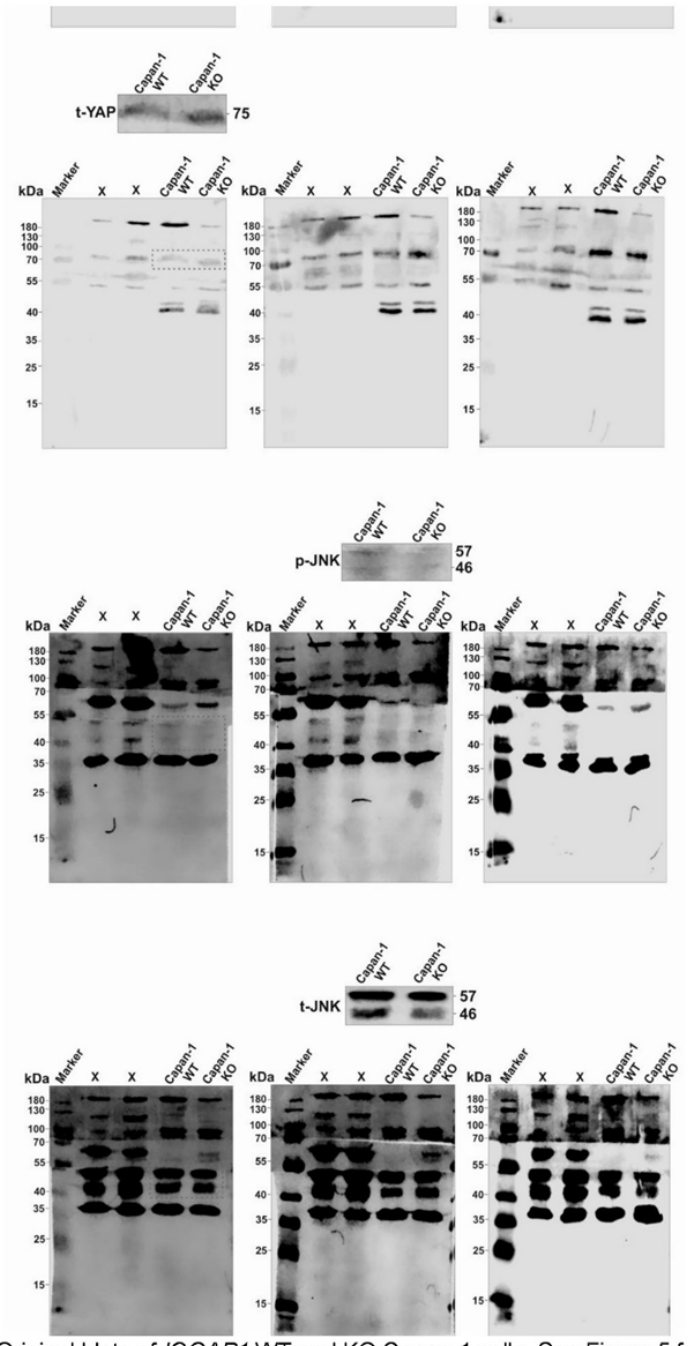

Figure S5. Original blots of *IQGAP1* WT and KO Capan-1 cells. See Figure 5 for more details.

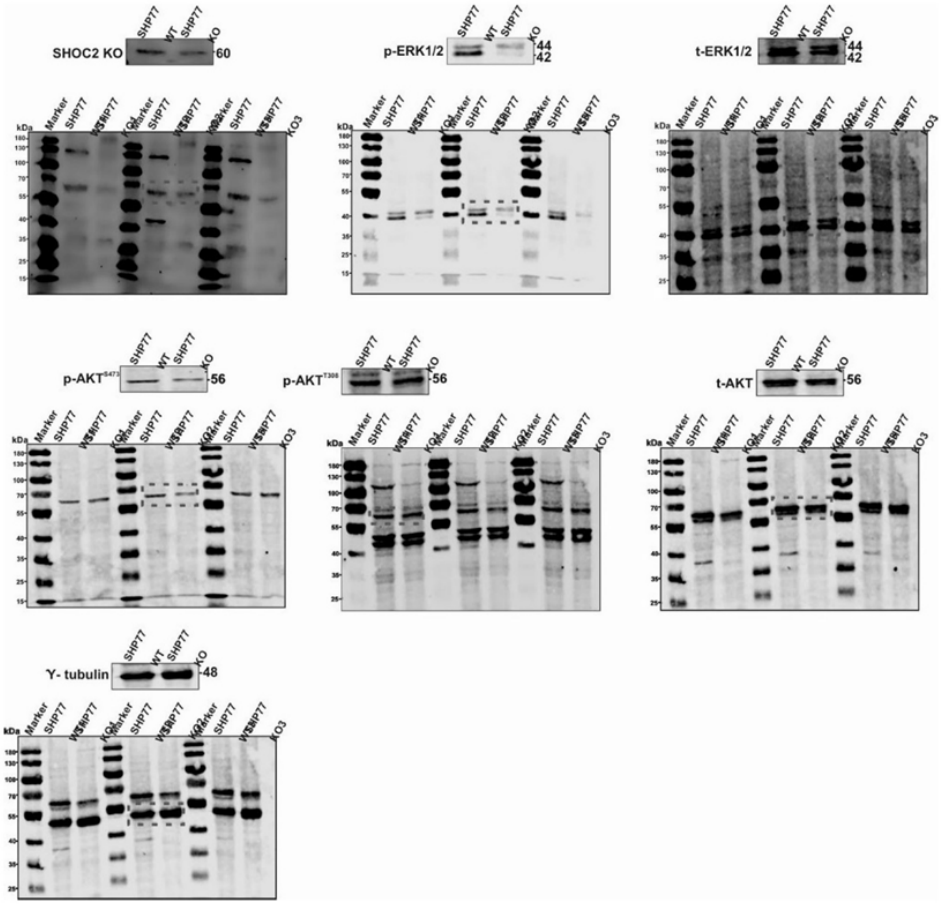

Figure S6. Original blots of *SHOC2* WT and KO SHP-77 cells. See Figure 6 for more details.

Chapter X. Distinct Regulatory and Interaction Networks of RIT GTPases

Authors: Amin Mirzaiebadizi, Frahad Bazgir, Niloufar Mosaddeghzadeh, Silke Pudewell, Radovan Dvorsky, , Mohammad Reza Ahmadian

DOI: …

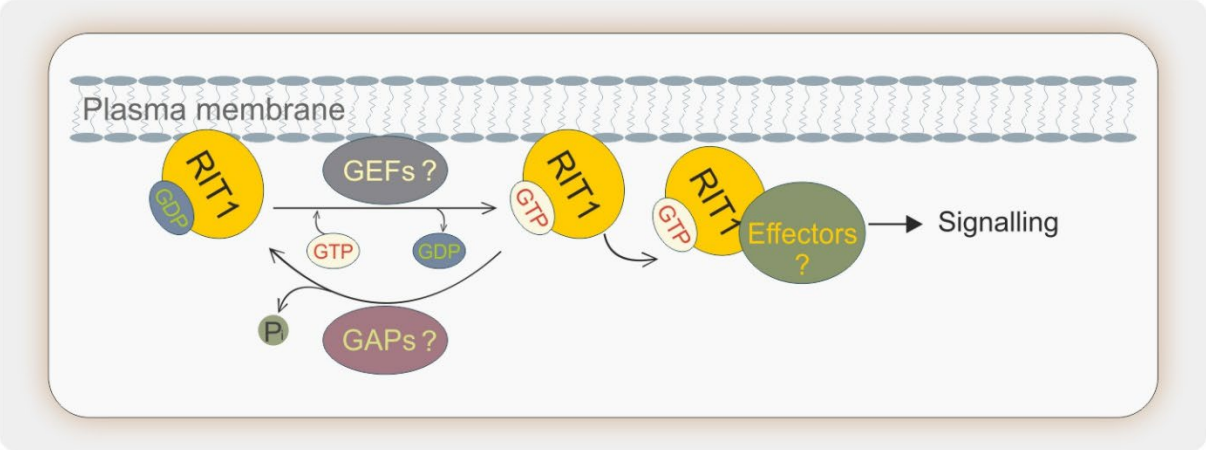

Status: To be Submitted

Journal: …
JIF: …
Contribution: ≈40%

A.M. prepared expression constructs for RIT1/2 C-terminal regions, as well as full-length RIT1(G30V/Q70L) and RIT1(S35N) variants by designing in silico mutations, obtaining the corresponding plasmids, and transforming bacterial stocks. He performed expression testing and successfully expressed and purified full-length RIT1 and RIT2, RIT1 and RIT2 C-terminal regions, and five RIT1 C-terminal mutants. He purified and prepared fluorescently labeled forms of RIT1(G30V/Q70L) and RIT1(S35N), and conducted PIP strip assays. He re-established the liposome preparation protocol and performed liposome sedimentation assays and surface plasmon resonance (SPR) kinetic analysis. A.M. contributed to manuscript writing, critical reviewing, and editing.

Distinct Regulatory Mechanisms and Interaction Networks of RIT GTPases

Amin Mirzaiebadizi [1], Frahad Bazgir [1], Niloufar Mosaddeghzadeh [1], Silke Pudewell [1], Radovan Dvorsky [1], Mohammad R. Ahmadian [1*]

[1] Institute of Biochemistry and Molecular Biology II, Medical Faculty and University Hospital Düsseldorf, Heinrich Heine University, Düsseldorf, Germany

[*] Correspondence: reza.ahmadian@hhu.de; +49-211-8112384 (M.R.A.)

Abstract: RIT1, a ubiquitously expressed small GTPase, and its neuron-specific paralog RIT2 are members of the RAS superfamily involved in the regulation of cell survival, proliferation, differentiation, and morphogenesis. Dysregulation of RIT proteins has been linked to various cancers and developmental disorders, including Parkinson's disease, autism, schizophrenia, and Noonan syndrome. Although frequently equated with classical RAS proteins, RIT1 and RIT2 exhibit distinct regulatory properties. This study demonstrates that RIT1 undergoes classical GTPase cycling but exhibits remarkably slow intrinsic nucleotide exchange and GTP hydrolysis, and is unresponsive to canonical RAS regulators, such as SOS1 and p120GAP. Most pathogenic RIT1 mutations cluster near the P-loop and switch II region, potentially interfering with GAP-mediated GTP hydrolysis. Functionally, germline RIT1 mutations have only a limited effect on canonical MAPK, PI3K/AKT, and JNK signaling pathways. Unlike classical RAS proteins, RIT1 interacts with galectin-1 rather than typical RAS effectors. Moreover, the C-terminal extension of RIT1 and RIT2 mediates membrane association via direct binding to phosphoinositides, independent of prenylation. These findings highlight RIT1 and RIT2 as structurally and functionally distinct RAS family members, regulated through unique mechanisms involving both specialized effectors and terminal extension-mediated membrane targeting.

Keywords: RIT1; RIT2; small GTPases; RAS superfamily; non-canonical regulation; membrane targeting; phosphoinositide binding; galectin-1; MAPK signaling; neurodevelopmental disorder

Introduction

Small GTPases of the RAS family function as molecular switches within cells by cycling between an active GTP-bound and an inactive GDP-bound state [1]. These proteins mediate intracellular responses to extracellular signals transmitted via receptors or adaptor proteins, ultimately influencing diverse downstream targets. Through this signaling relay, RAS proteins regulate essential cellular processes, including gene expression, metabolism, cell cycle progression, proliferation, survival, and differentiation. Somatic or germline mutations in RAS family genes or their regulators are frequently associated with cancer and developmental disorders, collectively termed RASopathies [2]. The latter are typically driven by germline mutations in components of the highly conserved RAS-MAPK pathway. Mild hyperactivation of this pathway is considered the central pathogenic feature of clinically overlapping syndromes such as Noonan syndrome, Costello syndrome, and cardiofaciocutaneous syndrome [3].

Among the best-characterized RAS proteins are HRAS, NRAS, and KRAS4B, which exhibit overlapping functions yet differ in expression patterns, regulators, and subcellular localization, underscoring both functional specificity and redundancy [4, 5]. Most RAS proteins undergo posttranslational modification at a conserved C-terminal CAAX motif (C for cysteine, A for aliphatic amino acid, and X for any amino acid), which enables membrane anchoring through prenylation. In contrast, RIT1 (also called RIT, RIBB, ROC1) and RIT2 (also called RIN, ROC2) lack this motif and instead associate with membranes through a distinct mechanism involving their positively charged C-terminal extensions [1, 6]. The individual functions of the remaining 22 members of the RAS family, including RIT1 and RIT2, remain incompletely characterized. RIT1, which is ubiquitously expressed, and its neuron-specific paralog RIT2 were first identified in the mouse retina in 1996 as a distinct RAS-related subfamily [7]. Since then, various animal models have highlighted their roles in regulating cell survival, proliferation, differentiation, and morphogenesis (Figure 1) [1, 8]. RIT1 and RIT2 also contribute to neurogenesis, neurite outgrowth, and branching [8]. Genetic studies link RIT1 and RIT2 signaling to both malignancies and developmental syndromes, including Parkinson's disease, autism, schizophrenia, and Noonan syndrome [8-14].

For instance, HIF-1α drives RIT1 overexpression in hepatocellular carcinoma under hypoxic conditions, promoting tumor migration, invasion, and drug resistance [15].

Although the upstream signals converging on RIT1 and RIT2 appear broadly similar, the precise mechanisms of regulation remain poorly defined. A variety of extracellular stimuli, including EGF, NGF, IGF1, and PACAP38, activate RIT1 and RIT2 in both neuronal and non-neuronal contexts [16-18]. To date, no guanine nucleotide exchange factors (GEFs) or GTPase-activating proteins (GAPs) have been identified that directly regulate RIT1 or RIT2. EPAC1, a cAMP-dependent RAPGEF, has been shown to link PACAP38 signaling to RIT1 activation, although it does not exhibit direct catalytic activity on RIT1 [19]. EPAC1 was later shown to activate SRC-dependent TRKA, which may in turn activate RIT1 through SOS1 and SOS2 [20]. However, neither EPAC1 nor SOS1 demonstrates direct GEF activity on RIT1 under cell-free conditions [20].

Effector binding and downstream pathway activation are central to RAS-family signaling, and several pathways have been proposed for RIT1 and RIT2 through potential interactions with known RAS effectors (Figure 1) [1, 8, 9]. For instance, RIT1 is suggested to interact with RALGDS family members such as RALGDS and RGL3, potentially linking it to RAL signaling [21]. A GST-tagged RGL3 RAS-association domain (residues 610 to 709) has proven useful for detecting GTP-bound RIT1 in cell lysates. RIT1 also activates a p38 MAPK-dependent stress resistance pathway that promotes cell survival [22]. This and other studies support a unique cytoprotective role for RIT1 not shared by other RAS family members. Additionally, RIT1 activates the p38-MSK1-CREB pathway to induce anti-apoptotic proteins such as BCL-2 and BCL-XL [23], and drives c-JUN transcription via the MKK3 and MKK6-p38γ axis. RIT1 also promotes AKT activation and BAD phosphorylation through the p38-MK2-HSP27 cascade, thereby suppressing ROS-induced apoptosis [22]. In neuronal contexts, RIT1 links NGF signaling to the MEK-ERK pathway via BRAF and p38, but not through PI3K-AKT [16, 24, 25]. It regulates the proliferation and differentiation of adult brain neural progenitors via the SIN1–mTORC2–AKT axis, which also mediates SOX2 phosphorylation, a key stem cell transcription factor [26]. RIT1 binds to SIN1 and may regulate mTORC2-mediated AKT phosphorylation [27]. On the other hand, RIT2 is implicated in PACAP38–Gαs–SRC signaling, controlling neuronal differentiation via RAC1 and CDC42, as well as actin cytoskeleton remodeling [28]. RIT2 regulates RAC1 and CDC42 activation via PAR6, influencing neurite outgrowth [29]. RIT1 also modulates actin dynamics through complex formation with RAC1 and CDC42 and PAK1 [29, 30]. iven this diversity in downstream signaling, it is plausible that RIT proteins function through scaffold proteins capable of coordinating multiple pathways (Figure 1).

In this study, we investigated the molecular regulation and interaction networks of RIT1 and RIT2 to better understand their disease-associated mechanisms. These insights are critical for developing targeted therapies for patients with RIT1 and RIT2 mutations that drive developmental disorders and malignancies.

Materials and Methods

Constructs and proteins. pGEX vectors were used for bacterial expression of full-length RIT1 wild-type, HRAS wild-type, and RIT1 mutants (K23N, G31R, A57G, Q79L, F82L, M90V, and G95A), and were transformed into *Escherichia coli* BL21 (Rosetta) for protein production. To investigate membrane targeting, the C-terminal extensions of RIT1 and RIT2 were cloned into pGEX-4T-1 and expressed in the same strain. The following constructs were used: RIT1-WT (183–219: RRKEKEAVLAMEKKSKPKNSVWKRLKSPFRKKKDSVT), RIT1-M1 (EEKEKEAVLAM EKKSKPKNSVWKRLKSPFRKKKDSVT), RIT1-M2 (RRKEKEAVLAMEKKSEPENSVWKRLK SPFRKKKDSVT), RIT1-M3 (RRKEKEAVLAMEKKSKPKNSVWEELESPFRKKKDSVT), RIT1-M4 (RRKEKEAVLAMEKKSKPKNSVWKRLKSPFREEEDSVT), RIT1-M5 (EEKEKEAVLAMEKK SEPENSVWEELESPFREEEDSVT), and RIT2-WT (182–217: RKKESMPSLMEKKLKRKDSL WKKLKGSLKKKRENMT). Protein expression was induced in bacterial cultures, and cell pellets were lysed by sonication in buffer containing DNase I, lysozyme, Triton X-100, and a protease inhibitor cocktail. Clarified lysates were used for purification of GST-tagged fusion proteins via glutathione-Sepharose. Where applicable, GST tags were cleaved using thrombin. Proteins were

then buffer-exchanged into a solution containing 30 mM HEPES or Tris-HCl, 150–500 mM NaCl, 5–10 mM $MgCl_2$, 3 mM DTT, and 0.1 mM GDP, with the pH adjusted to approximately one unit above or below each protein's isoelectric point. Nucleotide-free and fluorescently labeled proteins were prepared enzymatically using alkaline phosphatase (Roche) and phosphodiesterase (Sigma-Aldrich) at 4 °C. Fluorescent nucleotides included mant-GppNHp, mant-dGDP, and EDA-GTP-5/6-TAMRA. Excess unbound nucleotide was removed using NAP-5 desalting columns. Protein quality was assessed by SDS-PAGE, and aliquots were stored at −80 °C. For mammalian expression, HA-tagged RIT1 constructs were cloned into pMT2 vectors and transfected into HEK293T cells.

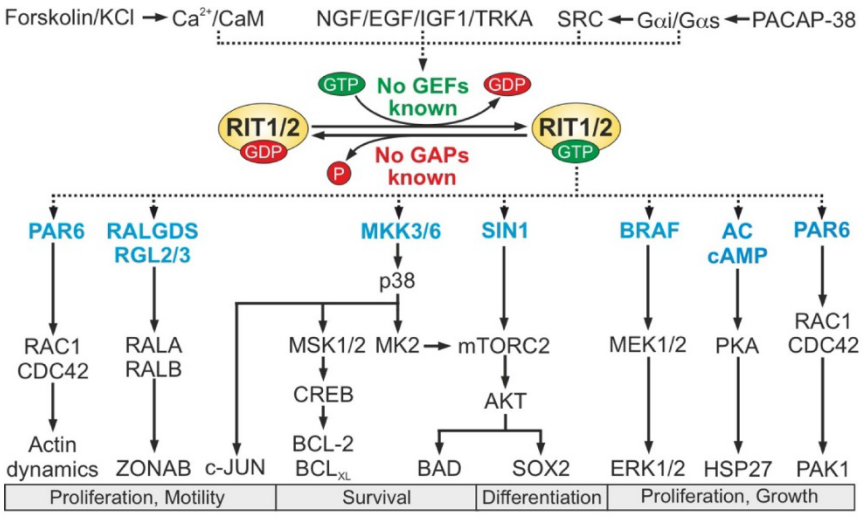

Figure 1. Putative RIT1 and RIT2 signal transduction pathways. RIT1 and RIT2 function as molecular switches by cycling between an inactive GDP-bound (off) state and an active GTP-bound (on) state. Their activation is mediated by specific guanine nucleotide exchange factors (GEFs) and inactivation by GTPase-activating proteins (GAPs), although the relevant regulators for RIT1 and RIT2 have not yet been identified. Multiple upstream signals are known to influence RIT1 and RIT2 activities through proposed effector proteins (indicated in blue), thereby regulating different cellular processes. Further details are provided in the main text.

Cell culture and lysis. HEK293T cells were seeded in 10 cm culture dishes and maintained in Dulbecco's Modified Eagle Medium (DMEM; #12320032, Thermo Fisher Scientific, Waltham, MA, USA) supplemented with 10% fetal bovine serum (FBS) and 1% penicillin/streptomycin. Cells were incubated at 37 °C in a humidified atmosphere containing 5% CO_2. Twelve hours before transfection, fresh medium was added. When cells reached approximately 70% confluency, they were transfected using TurboFect transfection reagent (Thermo Fisher, #R0532). After 24 hours, cells were washed with ice-cold phosphate-buffered saline (PBS) and lysed on ice for 5 minutes in lysis buffer containing 50 mM Tris-HCl (pH 7.5), 5 mM $MgCl_2$, 100 mM NaCl, 1% Igepal CA-630, 10% glycerol, 20 mM β-glycerophosphate, 1 mM sodium orthovanadate, and one EDTA-free protease inhibitor tablet per 50 mL. Lysates were cleared by centrifugation at 12,000 × g for 10 minutes at 4 °C, and the supernatants were collected for analysis.

Western blotting. Western blotting was performed to assess protein expression and phosphorylation states in HEK293T cells after transfection. Lysates were mixed with Laemmli sample buffer, resolved on 12.5% SDS–polyacrylamide gels, and transferred to PVDF membranes. Membranes were blocked and incubated with the following primary antibodies: anti-HA (Cell Signaling Technology, Cat# 2367) for detection of HA-tagged RIT1 and RIT2, anti-RIT1 (Abcam, Cat# ab53720), anti-RIT2 (Thermo Fisher Scientific, Cat# PA1-25559), anti-phospho-ERK1/2 (Thr202/Tyr204, CST, Cat# 4370), anti-total ERK1/2 (CST, Cat# 4696), anti-phospho-

AKT (Ser473, CST, Cat# 4060), anti-phospho-AKT (Thr308, CST, Cat# 2965), anti-total AKT (CST, Cat# 2920), anti-phospho-JNK (CST, Cat# 9251), anti-total JNK (CST, Cat# 9252), anti-phospho-p38 MAPK (Thr180/Tyr182, CST, Cat# 9211), anti-total p38 MAPK (CST, Cat# 8690), anti-γ-tubulin (Sigma Aldrich, Cat# T5326), and anti-GAPDH (CST, Cat# 2118). GST-tagged proteins were detected using an in-house anti-GST antibody. Secondary detection was carried out using IRDye 680RD or 800CW-conjugated antibodies (LI-COR: anti-rabbit Cat# 926-68073 and 926-32213; anti-mouse Cat# 926-68072 and 926-32212). Immunoreactive bands were visualized using the Odyssey Fc Imaging System (LI-COR Biosciences), and quantified by densitometry relative to the appropriate loading controls.

Structural modeling. Structural modeling and sequence analysis were performed to investigate the conserved and variant features of RIT1 and its disease-associated mutations. Amino acid alignments of RIT1, RIT2, HRAS, and KRAS were carried out using the ClustalW algorithm within the BioEdit software suite to identify conserved G-motifs (G1–G5) and map mutational hotspots across paralogs. The refined GDP-bound structure of RIT1 (PDB ID: 4KLZ) was used to visualize the secondary structure elements, including α-helices, β-strands, and switch regions I and II, as well as the clustering of germline and somatic mutations found in cancers and RASopathies. Mutational residues were displayed on the RIT1 surface using PyMOL molecular viewer, and their spatial proximity to functional motifs was analyzed. The alignment revealed that key residues involved in GTP binding and hydrolysis (such as G31, K34, and S35) are conserved, while deviations in switch regions and at specific sites (e.g., F82, corresponding to Y64 in HRAS) may underlie the insensitivity of RIT1 to canonical RAS regulators. Comparative surface representations highlighted the distribution of disease-related mutations and their localization at structurally tolerant regions or near functionally relevant pockets, providing a framework to explain their biochemical consequences. All structural figures were rendered using PyMOL and annotated according to the domain architecture identified from the crystallographic model.

Liposome preparation and sedimentation. For liposome sedimentation assays, multilamellar vesicles were prepared using a defined mixture of synthetic lipids. Each sample contained 100 µg of total lipid, combined at the following weight ratios: 37% phosphatidylserine (PS), 20% phosphatidic acid (PA), 2% NBD-labeled phosphatidylethanolamine (NBD-PE), 10.5% phosphatidylethanolamine (PE), 20% phosphatidylcholine (PC), and a phosphoinositide mix comprising 2% PIP3, 2% $PI(4,5)P_2$, 1.5% $PI(3,5)P_2$, 1.5% $PI(3,4)P_2$, 1.5% $PI(3,4,5)P_3$, and 1% each of PI3, PI4, and PI5. Lipids were dried overnight under a laminar flow hood to form a thin film. The dried film was rehydrated in buffer containing 20 mM HEPES-NaOH (pH 7.4) and 100 mM NaCl, followed by three cycles of snap-freezing and thawing. Lipid dispersion was further enhanced by 5 minutes of bath sonication. To produce uniformly sized unilamellar vesicles, the suspension was passed 21 times through a 100 nm polycarbonate filter using an Avanti extruder. For sedimentation assays, purified proteins were incubated with the prepared liposomes for 30 minutes on ice. Samples were then centrifuged at 180,000 × g for 30 minutes at 4 °C. Supernatant and pellet fractions were collected separately and analyzed by SDS-PAGE, followed by immunoblotting.

Surface plasmon resonance. Surface plasmon resonance (SPR) measurements were performed using a Biacore X100 instrument (GE Healthcare) equipped with an L1 sensor chip to evaluate the lipid membrane binding properties of full-length RIT1 and its C-terminal extension. All experiments were carried out at 25 °C using a running buffer consisting of 20 mM HEPES-NaOH (pH 7.4) and 150 mM NaCl. Prior to liposome immobilization, the chip surface was conditioned by sequential injection of 20 mM CHAPS and 40 mM octyl-β-D-glucopyranoside (octylglucoside). Liposomes were prepared as described above and immobilized onto the L1 chip surface by injecting 0.5 mM liposome suspensions at a flow rate of 5 µL/min for 900 seconds. Unbound vesicles were removed by washing with 10 mM NaOH at 30 µL/min for 30 seconds. Binding of purified RIT1 proteins to immobilized liposomes was assessed by single-cycle injection at increasing concentrations. Each protein injection was performed at a flow rate of 30 µL/min for 180 seconds, followed by dissociation in running buffer for up to 600 seconds. Sensorgrams were double-referenced using a blank flow cell and buffer-only controls. Kinetic parameters and

apparent affinities were determined by fitting the response curves to a 1:1 Langmuir binding model using Biacore X100 Evaluation Software (version 2.0.1).

Nucleotide exchange and binding assays. Nucleotide exchange and binding kinetics of RIT1 variants and HRAS were analyzed using a Horiba Fluoromax-4 fluorimeter and an SX20 stopped-flow spectrometer (Applied Photophysics). Intrinsic and GEF-stimulated reactions were performed in buffer containing 30 mM Tris-HCl (pH 7.5), 10 mM KH_2PO_4/K_2HPO_4, 5 mM $MgCl_2$, and 3 mM DTT at 25 °C. For intrinsic exchange, 0.1 µM mant-dGDP–loaded protein was rapidly mixed with a 200-fold excess of unlabeled GDP. GEF-mediated exchange was initiated by adding 10 µM of the DH–PH domain of SOS1 under identical conditions. Fluorescence changes were monitored with excitation at 355 nm and emission above 408 nm, and k_obs values were determined by fitting the curves to a single-exponential model using OriginLab software. For nucleotide binding assays, varying concentrations of nucleotide-free protein (0.2–0.8 µM) were mixed with 0.2 µM mant-dGDP. Association rate constants (k_{on}) were calculated from linear plots of k_{obs} versus protein concentration, and dissociation rate constants (k_{off}) were determined by displacement with excess unlabeled nucleotide. Equilibrium dissociation constants (K_d) were calculated as the ratio of k_{off} to k_{on}.

GTP hydrolysis measurements. Intrinsic and GAP-stimulated GTP hydrolysis rates of RIT1 variants and HRAS were measured using fluorescence-based assays on a Fluoromax-4 spectrofluorometer (Horiba Scientific, Loos, France). For intrinsic measurements, 1 µM of TAMRA-labeled GTP (TAMRA-GTP) preloaded onto purified proteins was diluted into a final volume of 200 µL in a quartz cuvette containing assay buffer composed of 30 mM Tris-HCl (pH 7.5), 150 mM NaCl, 5 mM $MgCl_2$, and 3 mM dithiothreitol (DTT). Reactions were conducted at 25 °C, and TAMRA fluorescence was recorded over time to monitor nucleotide hydrolysis. Excitation and emission wavelengths were set to 543 nm and 580 nm, respectively, using slit widths of 8 nm (excitation) and 10 nm (emission). For GAP-stimulated assays, 1 µM of TAMRA-GTP-loaded protein was incubated with 1 µM of the catalytic domain of p120GAP under the same buffer and temperature conditions. Fluorescence decay was continuously monitored, and the observed rate constants (k_{obs}) were obtained by fitting the decay curves to a single exponential function using OriginLab software.

Fluorescence polarization. Fluorescence polarization assays were performed to determine the dissociation constants (K_d) of direct protein–protein interactions involving RIT1 and RAS effectors. Measurements were carried out using a Fluoromax-4 fluorimeter (Horiba Scientific) operated in polarization mode. Purified RIT1 proteins, preloaded with mant-GppNHp, were used at a fixed concentration in a total volume of 200 µL. Binding reactions were conducted in quartz cuvettes at 25 °C in buffer containing 30 mM Tris-HCl (pH 7.5), 50 mM NaCl, 5 mM $MgCl_2$, and 3 mM DTT. Increasing concentrations of binding partners were titrated into the solution, and polarization changes were monitored over time using an excitation wavelength of 360 nm (slit width: 8 nm) and an emission wavelength of 450 nm (slit width: 10 nm). The resulting binding curves were analyzed in GraFit 5 by fitting the data to a quadratic ligand-binding equation to determine apparent K_d values.

Results and Discussions

RIT1 and RIT2 are subject to classical regulation. Extensive advances in the study of small GTPases have provided key insights into their structural features, regulatory mechanisms, and roles in diverse cellular functions and diseases. These frameworks now offer a valuable basis to explore the lesser-known RIT proteins. Like other RAS family members, RIT1 and RIT2 contain a conserved GDP/GTP-binding domain (G domain) that governs their conformational switching between active and inactive states. This domain comprises five conserved motifs (G1 to G5), which are essential for guanine nucleotide binding, hydrolysis, and interaction with regulatory proteins such as GEFs, GAPs, and effectors (Figure 2a). Structural differences between the GDP- and GTP-bound states are primarily localized to two dynamic regions: switch I (residues 48–58) and switch II (residues 77–86) (Figure 2a) [31]. While the switching mechanism is universally conserved among RAS GTPases, the structural and functional adaptations of the G domain allow for interaction with distinct sets of regulators and effectors, thereby enabling diverse signaling

outcomes (Figure 1) [32]. The crystal structure of the RIT1 G domain reveals a similar fold and secondary structure architecture to that of classical RAS proteins (Figure 2a). These conserved structural features support the conclusion that RIT1 and RIT2 undergo classical RAS-like regulation and participate in comparable molecular switching mechanisms.

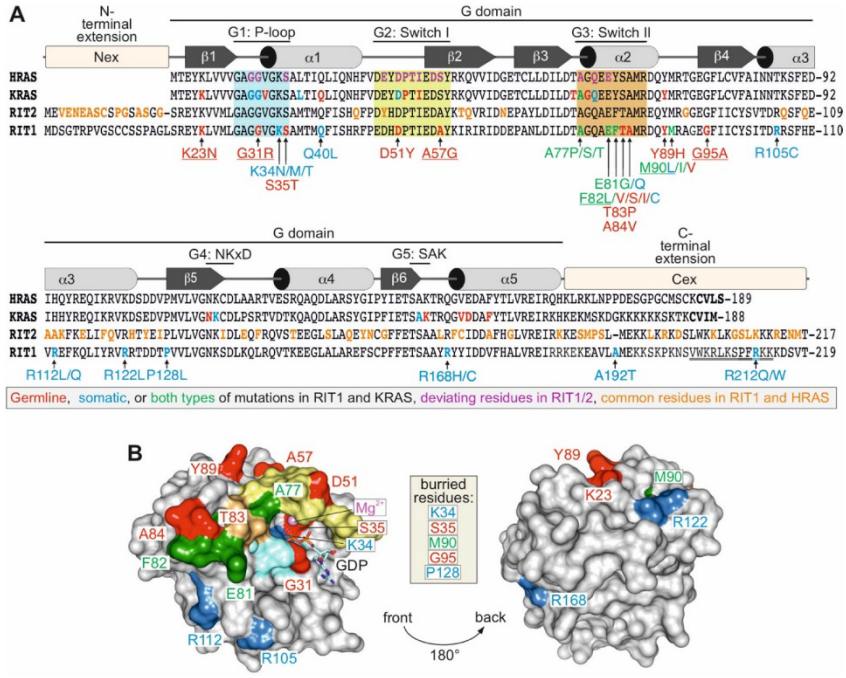

Figure 2. Disease-causing RIT1 mutations are conservative and located at permissible structural sites. (**a**) Schematic of the RIT1 G-domain highlighting secondary structure elements (α-helices and β-strands) and five conserved motifs critical for guanine nucleotide binding and hydrolysis: G1 or P-loop (aquamarine), G2 or switch I (pale yellow), G3 or switch II (light orange), G4 (NKxD), and G5 (SAK). Positions of germline and somatic RIT1 mutations identified in individuals with malignancies or developmental disorders are mapped onto the linear domain representation. Secondary structure elements are derived from the RIT1•GDP structure (PDB ID: 4KLZ). In both KRAS and RIT1, germline mutations are shown in red, somatic mutations in blue, and mutations reported in both contexts are marked in green (adapted from Van *et al.*, 2020 [9]). Orange-colored residues in RIT2 indicate positions that differ from RIT1, while purple residues in HRAS denote positions that are conserved with RIT1 and implicated in intrinsic and GAP-stimulated GTP hydrolysis. Underlined mutations represent those experimentally analyzed in Figure 4a. Unlike HRAS (CVLS) and KRAS (CVIM), RIT1 and RIT2 lack a canonical C-terminal CAAX box yet retain membrane-binding capacity, likely through residues 203–214 (double-underlined). (**b**) Surface representation of the refined RIT1•GDP structure (PDB ID: 4KLZ) illustrating the spatial distribution of disease-associated mutations. Mutations linked to malignancies are shown in blue, developmental disorders in red, and those associated with both conditions in green. Front and back views of the structure, rotated by 180 degrees, are presented. The P-loop (aquamarine), switch I (pale yellow), and switch II (light orange) are highlighted to show the clustering of mutations in these regions. Residues buried within the hydrophobic core are boxed in yellow.

RIT1 displays slow intrinsic nucleotide exchange and GTP hydrolysis rates and does not respond to the classical HRAS regulators SOS1 and p120GAP. Biochemical comparisons of RIT1 and RIT2 with classical RAS family members such as HRAS and KRAS revealed notable sequence differences, particularly within the conserved G-domain motifs G2, G3, and G5 (Figure 2). These deviations suggest that RIT1 and RIT2 have selective biochemical behaviors, especially in terms of GDP/GTP exchange, GTP hydrolysis, and interactions with regulators and effectors.

To explore the functional consequences of these substitutions, we analyzed the nucleotide-binding characteristics of RIT1 in direct comparison with HRAS, the archetypal RAS GTPase.

Using fluorescence spectroscopy with mant-dGDP, we found that RIT1 binds nucleotide with substantially lower affinity than HRAS. As shown in Figures 3a–g, RIT1 displayed a 30-fold lower association rate (k_{on}), a 6.5-fold faster dissociation rate (k_{off}), and an overall 190-fold higher dissociation constant (K_d). These data indicate that the diminished nucleotide affinity of RIT1 is predominantly driven by its reduced association rate rather than enhanced nucleotide release. This suggests that RIT1 activation in cells is unlikely to occur spontaneously and instead requires a specific guanine nucleotide exchange factor (GEF). Given additional sequence divergence between RIT1 and RIT2 across the G1–G5 motifs (Figure 2), we anticipate distinct biochemical behaviors for RIT2, which will be investigated in future studies.

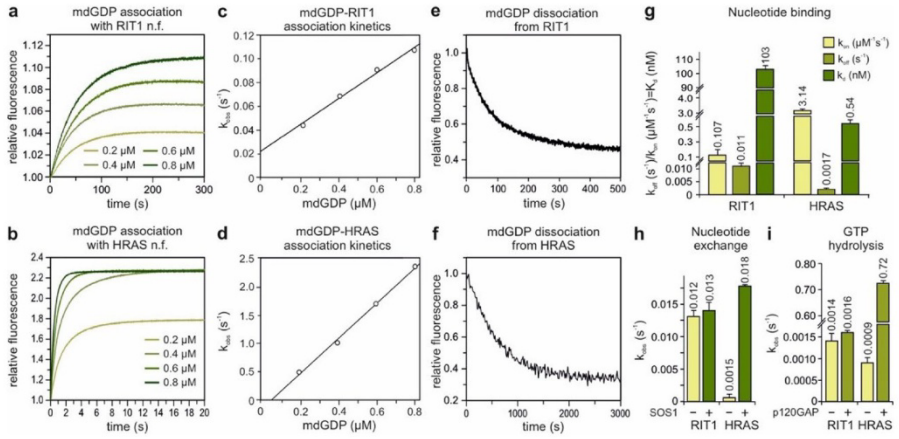

Figure 3. RIT1 GDP binding and GTP hydrolysis kinetics. (**a**, **b**) Rapid association of increasing concentrations of fluorescent mant-dGDP with 0.2 µM nucleotide-free RIT1 (**a**) and HRAS (**b**) was measured using stopped-flow fluorimetry. Association rate constants (k_{on}) were determined by linear fitting of the observed rate constants (k_{obs}) at increasing ligand concentrations (**c**, **d**). Intrinsic nucleotide dissociation from RIT1 and HRAS was monitored by following mant-dGDP release in the presence of excess unlabeled GDP, and the dissociation rate constants (k_{off}) were obtained by fitting the data to a single exponential function (**e**, **f**). Calculated values for k_{on}, k_{off}, and dissociation constant Kd (k_{off}/k_{on}) are presented as bar graphs for comparison between RIT1 and HRAS (**g**). Nucleotide exchange (h) and GTP hydrolysis (**i**) rates were assessed using 0.2 µM mant-dGDP–bound or TAMRA-GTP–loaded RIT1 and HRAS in the absence or presence of 10 µM SOS1 catalytic domain (residues 601–1020) or 1 µM p120GAP catalytic domain (residues 714–1049). All kinetic parameters were calculated by single-exponential fitting of the fluorescence of the data. Data are expressed as the mean ± S.D.

We next tested whether RIT1 is responsive to canonical RAS regulators. The catalytic core of SOS1, comprising the CDC25 and REM domains (SOS1-Cat), robustly stimulated nucleotide dissociation from HRAS but had no effect on RIT1 (Figure 3h). This suggests that RIT1 is not a substrate for SOS1. One possible explanation lies in the sequence difference at residue F82 in RIT1, which corresponds to Y64 in HRAS, a critical contact site for SOS1. Mutation of Y64 in HRAS has previously been shown to abolish SOS1-mediated exchange activity [32, 33]. We then examined GTP hydrolysis in the presence of the GAP protein p120GAP. TAMRA-GTP hydrolysis by HRAS was strongly accelerated by the catalytic domain of p120GAP, whereas RIT1 remained unresponsive (Figure 3i). Although most RAS-GAP interaction residues are conserved in RIT1 and RIT2, key substitutions at H50 (Y32 in HRAS) in switch I and A80 and F82 (E62 and Y64 in HRAS) in switch II may impair GAP recognition. Similar results were observed for the catalytic domain of Neurofibromin (NF1), although data are not shown. Together, these results

demonstrate that RIT1 does not respond to canonical RAS regulators and likely requires its own dedicated GEFs and GAPs, which remain to be identified.

Disease-associated RIT1 mutations cluster near critical regulatory regions and may interfere with GAP-stimulated GTP hydrolysis. The overall location and spatial orientation of Pathogenic RIT1 mutations are predominantly located near the P-loop and switch II region, suggesting that they may impair GAP-stimulated GTP hydrolysis. Structural localization and spatial orientation of these altered residues were deduced based on the available GDP-bound RIT1 crystal structure (PDB ID: 4KLZ). Since the structure lacks certain regions, we performed additional modeling and refinement. To evaluate whether specific mutations might directly affect nucleotide binding or hydrolysis, we analyzed their proximity to the bound GDP. Three residues in particular are positioned at key contact points: G31 and K34 interact with the β-phosphate of GDP, while S35 coordinates the essential Mg^{2+} ion (Figure 2b). Substitution of S35 with asparagine (S35N) may sterically disrupt Mg^{2+} binding, leading to reduced nucleotide affinity. This effect mirrors that seen in HRAS, where such mutations abolish nucleotide binding and produce a dominant-negative phenotype by sequestering native GEFs and preventing activation of endogenous RAS [34]. However, the majority of germline and somatic RIT1 mutations reside on the protein surface near the P-loop and switch II (Figure 2), suggesting that they more likely affect interactions with GAPs or downstream effectors [32, 50]. While effector-binding interfaces vary substantially between RIT1 and HRAS, the core residues involved in GAP recognition and catalysis are nearly identical (Figure 2a, magenta), supporting the idea that RIT1 shares a conserved mechanism of GAP-mediated inactivation with HRAS.

Functional characterization of germline and somatic RIT1 mutations reveals only weak MAPK activation and suggests distinct signaling properties. Germline RIT1 mutations result in only weak activation of the MAPK, PI3K/AKT, and JNK pathways. Previous studies have shown that germline mutations in genes such as HRAS, NRAS, KRAS, RRAS2 (TC21), and MRAS (RRAS1) typically lead to a mild gain-of-function phenotype [2, 35, 36]. Biochemical analyses of various RAS and RAS-related germline mutations have allowed classification into five mechanistic categories, most of which differ markedly from classical oncogenic RAS mutations. These functional alterations include enhanced intrinsic or GEF-stimulated nucleotide exchange, impaired GAP-mediated GTP hydrolysis, or reduced effector interaction. Despite often presenting with overlapping developmental phenotypes, these mutations can cause highly variable biochemical effects, ultimately resulting in a relatively moderate gain-of-function output.

Beyond their role in cancer [12, 13, 37, 38], RIT1's developmental importance was underscored by the identification of germline mutations in individuals with Noonan syndrome. This RASopathy is characterized by craniofacial abnormalities, congenital heart defects, and lymphatic dysfunction [11, 13, 39-41]. Compared to other Noonan subtypes, individuals with RIT1 mutations exhibit a higher frequency of cardiovascular and lymphatic anomalies [10, 42]. Notably, the RIT1 P128L mutation was identified in a patient with lung adenocarcinoma and was linked to resistance to the KRAS G12C inhibitor adagrasib [43]

To explore the functional consequences of somatic and germline RIT1 mutations found in cancer and developmental disorders, we mapped their structural positions and compared them to known KRAS mutations (Figure 2). Most mutational hotspots in both RIT1 and KRAS are located near the G1 to G3 motifs, which are critical for nucleotide binding, hydrolysis, and interaction with regulatory proteins and effectors. This pattern suggests functional parallels with previously studied NRAS mutants [2, 44]. Since gain-of-function RIT1 mutations have been implicated in Noonan syndrome, a disorder associated with MAPK signaling, we investigated their ability to modulate MAPK and related pathways [9, 11, 39, 41].

We overexpressed various RIT1 mutants in HEK-293T cells, including S35N (a dominant-negative mutant) and Q79L (a constitutively active mutant), and assessed downstream activation of MEK/ERK, JNK, and p38 kinases in comparison to wild-type RIT1 (Figure 4a). Unlike KRAS mutations, which strongly activate MEK and ERK [2, 44], most RIT1 mutants showed only mild or no increase in MEK1/2 and ERK1/2 phosphorylation. This effect was restricted to a subset of

variants. Overexpression of wild-type RIT1 alone increased phosphorylation of MEK1/2, ERK1/2, AKT^{308}, and JNK1/2, but expression of the mutants did not further enhance this activity.

Although the Q79L variant is predicted to be constitutively active based on its impaired GTP hydrolysis and reduced GAP sensitivity [35], its expression in HEK-293T cells did not result in enhanced MAPK signaling compared to wild-type. A previous study using PC6 cells, a neuron-like pheochromocytoma cell line, reported elevated ERK1/2 and p38 phosphorylation in response to GFP-tagged RIT1 Q79L [16, 45]. However, in HEK-293T cells, both Q79L and wild-type RIT1 exhibited comparable GTP loading under serum-starved conditions [46]. This discrepancy may reflect saturating activation of MAPK signaling due to overexpression of wild-type RIT1, potentially masking any additional effect of Q79L. Verification of protein levels and dose-response analysis in future experiments could clarify this. Furthermore, HEK-293T cells may lack neuronal or context-specific cofactors required for full engagement of RIT1 signaling, which could explain the stronger effects observed in PC6 cells. These findings collectively suggest that RIT1 does not mimic classical RAS signaling and likely engages a distinct set of effectors and regulatory pathways [9]

The dominant-negative RIT1 S35N mutant sequesters endogenous RIT1-specific GEFs. A particularly informative observation was made with the RIT1 S35N variant, which exhibited markedly reduced phosphorylation of MEK, ERK, and AKT^{T308}, but not of AKT^{S473}, JNK, or p38, despite showing lower protein expression levels (Figure 4a). This variant harbors a mutation at a conserved residue within the P-loop (Figure 2a, b), resulting in a nucleotide-free form of RIT1 that displays dominant-negative behavior by forming a stable complex with endogenous GEFs [34]. Supporting this mechanism, expression of RIT1 S35N led to significant suppression of MAPK and AKT^{T308} signaling, consistent with sequestration of a limiting pool of upstream RIT1-specific GEFs. Importantly, the degree of signaling inhibition appeared disproportionate to the observed reduction in S35N protein levels, further supporting a dominant-negative mechanism rather than a simple expression loss. This dominant-negative property highlights S35N as a useful molecular tool, and future experiments should help elucidate the identity of RIT1-specific GEFs.

RIT1 interacts with non-classical effectors, including galectin-1. Previous studies have implicated several proteins, such as CRAF, PAR6, PAK1, SIN1, RALGDS, RGL3, and calmodulin (CaM), as potential RIT1 effectors [7, 27, 29, 30, 45, 47, 48]. This is surprising, given the considerable diversity in both structure and function among these proteins, and their roles in signaling pathways that do not converge. However, in most cases, these interactions were predicted based on indirect evidence such as co-expression, in silico screening, or analogies to classical RAS proteins, rather than direct binding assays. To experimentally assess binding specificity, we tested several candidate effectors using purified proteins and fluorescence polarization assays.

We recently reported that the RASSF family members RASSF7 and RASSF9 bind to mGppNHp-loaded RIT1 with dissociation constants (K_d) of 34 µM and 27 µM, respectively (Figure 4b) [49]. These values were determined by titrating increasing concentrations of RASSF proteins against fluorescently labeled RIT1 in its active conformation. The results are presented in Figure 4c.

Because galectin-1 (GAL1) and CaM have previously been reported to interact with HRAS and KRAS and influence their membrane targeting [50], we included GAL1 as a positive control in our experiments exploring the RIT1–CaM interaction [7]. Unexpectedly, GAL1 bound to RIT1 with a K_d of 35 µM, whereas no significant interaction was observed for CaM under these assay conditions. Whether CaM binding to RIT1 requires calcium ions or membrane association remains to be experimentally verified. These findings raise the possibility that GAL1 may modulate RIT1 localization or function, although this will need to be confirmed through additional cellular assays.

We also assessed the binding of RIT1 to several classical RAS effectors (Figure 4c). While most interactions were weak, RGL3 bound with an affinity comparable to GAL1 and RASSF7/9. Notably, binding of the isolated Ras-binding domain (RBD) of CRAF was modest, but improved approximately 2.5-fold when combined with the cysteine-rich domain (CRD) in a tandem RBD-

CRD construct. Although these interactions are detectable, none fall within the nanomolar affinity range typical of strong, biologically significant RAS-effector interactions.

Based on these data, we propose that RIT1 and RIT2 operate through a distinct set of downstream signaling pathways not shared with classical RAS proteins. Proteomic profiling, ideally under conditions mimicking cellular membranes or signaling activation, will be necessary to identify high-confidence RIT1 effectors. Furthermore, sequence differences between RIT1 and RIT2 (Figure 2) support the hypothesis that they may differ in effector selectivity, but this prediction should be validated by performing similar binding assays with RIT2.

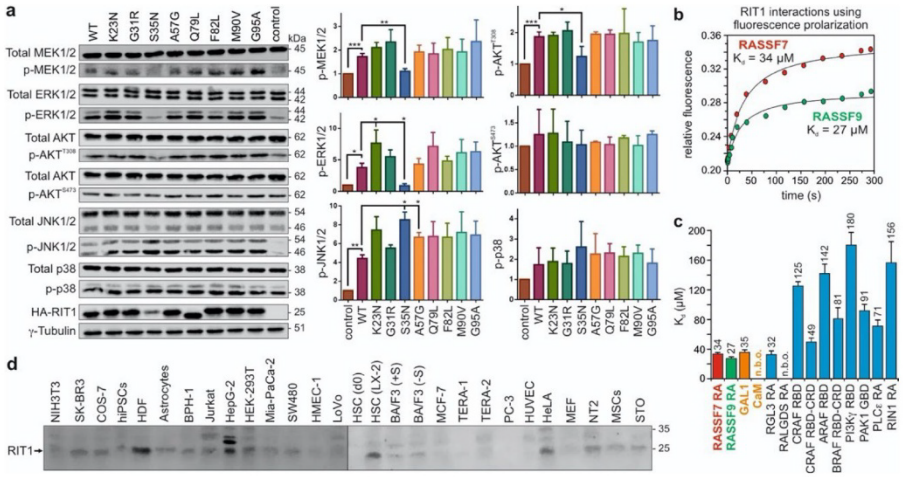

Figure 4. RIT1 signaling and effector binding characteristics. (**a**) HEK-293T cells were transfected with RIT1 variants and assessed for activation of MAPK, PI3K/AKT, and JNK signaling via Western blotting. Phosphorylation levels of MEK1/2, ERK1/2, AKT (Ser473 and Thr308), JNK1/2, and p38 were analyzed, with γ-tubulin as a loading control. Quantification was normalized to loading controls, and data represent mean ± SD from triplicate experiments. Statistical significance was determined using an unpaired t-test (*p < 0.05, **p < 0.01, ***p < 0.001). (**b**, **c**) Fluorescence polarization was used to measure dissociation constants (Kd) between mGppNHp-bound RIT1 and various effector proteins. Representative binding curves for RASSF7 and RASSF9 are shown in (b), and Kd values for all tested interactions are presented in (**c**) as bar charts with fitting errors indicated. "n.b.o." denotes no binding observed. Abbreviations: CaM, calmodulin; CRD, cysteine-rich domain; GAL1, galectin-1; GBD, GTPase-binding domain; RA, RAS-association domain; RBD, RAS-binding domain. (**d**) Immunoblot analysis of endogenous RIT1 (Abcam #ab53720) across various human and mouse cell lines including fibroblasts, stem cells, carcinoma lines, primary cells, and immortalized lines. All lanes were loaded with 20 µg of total lysate.

RIT1 has been implicated in a range of cellular processes, including proliferation, differentiation, and migration, suggesting that it functions through specific regulatory mechanisms and engages with a distinct set of effectors. Despite multiple reports proposing candidate RIT1-binding proteins [16, 46, 48], direct effectors capable of mediating its downstream functions remain poorly defined. A comprehensive, multidirectional strategy to map the regulatory and effector landscape of RIT1 is still lacking. To address this gap, a systematic approach is needed to identify and validate novel RIT1-associated signaling proteins. Rather than relying solely on overexpression systems, future studies should examine endogenous RIT1 in physiologically relevant models, such as primary human dermal fibroblasts (Figure 4b), employing a combination of biophysical, proteomic, and cellular assays. In particular, gel overlay assays represent a highly sensitive technique for detecting direct protein–protein interactions and have been effectively applied in the context of small GTPase-binding protein studies [51].

The C-terminal extension of RIT1 mediates plasma membrane localization through phosphoinositide binding. Although RIT1 and RIT2 share a conserved G domain, they differ markedly in sequence and structure outside this region. In particular, their N-terminal (Nex) and

C-terminal (Cex) extensions display the highest variability, contributing to their functional specificity (Figure 2). While the overall sequence identity between RIT1 and RIT2 is approximately 73%, most differences lie outside the canonical G1–G5 motifs. Such extensions are not unique to RIT1 and RIT2 but are also found in other RAS family proteins. Classical RAS proteins rely on posttranslational modifications (e.g., prenylation) for membrane association, which typically occurs via a C-terminal CAAX box. However, RIT1 and RIT2 lack a CAAX motif (Figure 2), and RIT2 membrane localization has been previously attributed to its C-terminal extension (Cex) [1, 6, 51].

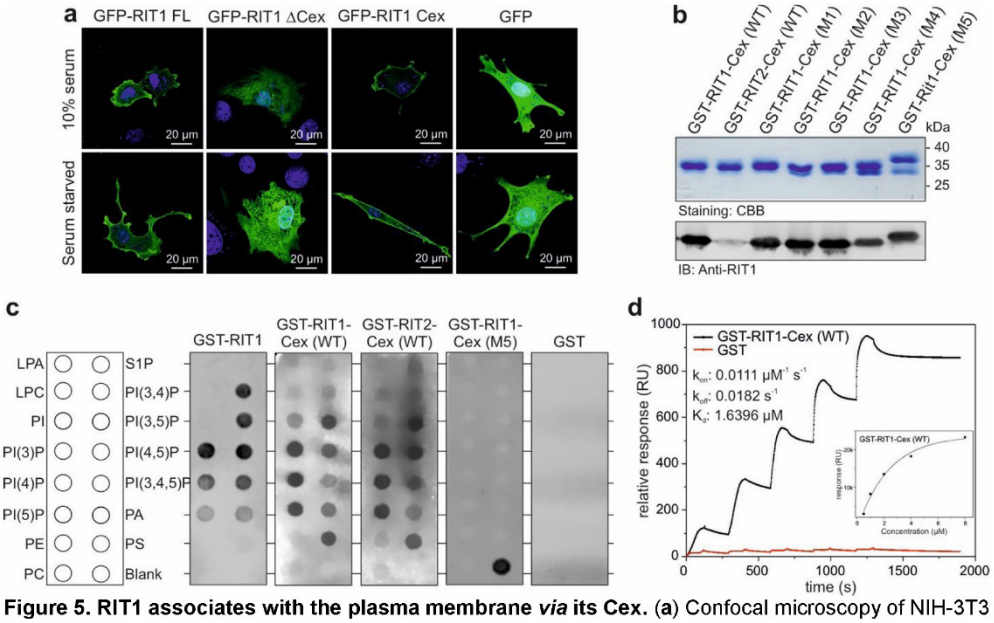

Figure 5. RIT1 associates with the plasma membrane *via* its Cex. (**a**) Confocal microscopy of NIH-3T3 fibroblasts transiently expressing GFP-tagged RIT1 variants shows that both full-length RIT1 (FL; residues 1–219) and the isolated C-terminal extension (Cex; residues 186–219) localize predominantly to the plasma membrane under serum-starved and serum-stimulated conditions, whereas the Cex-deleted variant (ΔCex; residues 1–185) remains cytoplasmic, similar to GFP alone. Nuclei were stained with DAPI (blue). Images were acquired using an LSM 510-Meta microscope (Zeiss); scale bars, 20 μm. (**b**) Immunoblotting confirmed the expression and purification of GST-tagged Cex constructs for wild-type RIT1 and RIT2, as well as RIT1 charge-reversal mutants (M1–M5; see Figure 6), using an anti-RIT1 antibody (Abcam, Cat# ab53720). (**c**) Lipid-binding specificity was assessed using phosphoinositide (PIP) strip overlay assays. Membranes were incubated with 200 ng/mL of purified GST-tagged constructs. GST-RIT1, GST-RIT1-Cex(WT), and GST-RIT2-Cex(WT) bound specifically to phosphoinositides, while no signal was detected for GST-RIT1-Cex(M5) or GST alone. (**d**) Surface plasmon resonance (SPR) analysis using an L1 sensor chip with immobilized liposomes revealed that GST-RIT1-Cex(WT) directly interacts with lipid bilayers. Kinetic analysis yielded a k_{on} of 0.0111 $\mu M^{-1}s^{-1}$, a k_{off} of 0.0182 s^{-1}, and a K_d of 1.6396 μM. The inset shows the concentration-dependent binding of GST-RIT1-Cex(WT), ranging from 0.5 μM to 8 μM. GST was used as a negative control. Notably, incomplete dissociation was observed during the wash phase, suggesting that RIT1 may be retained on membranes. This supports the possibility that accessory proteins, such as galectin-1, may modulate RIT1's membrane localization and dynamics. Lipid abbreviations: PA, phosphatidic acid; PC, phosphatidylcholine; PE, phosphatidylethanolamine; PI, phosphatidylinositol; PI3P, PtdIns(3)P; PI4P, PtdIns(4)P; PI5P, PtdIns(5)P; $PI(3,4)P_2$, PtdIns(3,4)P; $PI(3,5)P_2$, PtdIns(3,5)P; $PI(4,5)P_2$, PtdIns(4,5)P; $PI(3,4,5)P_3$, PtdIns(3,4,5)P; LPA, lysophosphatidic acid; LPC, lysophosphocholine; PS, phosphatidylserine; S1P, sphingosine 1-phosphate.

To evaluate whether the Cex region is responsible for RIT1 membrane targeting, we examined the subcellular localization of GFP-tagged RIT1 variants in NIH-3T3 fibroblasts. As shown in

Figure 5a, full-length RIT1 (FL) localized predominantly at the plasma membrane, while a ΔCex variant (residues 1–185) did not. In contrast, a construct containing only the Cex region (residues 186–219) also localized to the membrane, suggesting that the Cex is sufficient for plasma membrane association.

Two major structural classes of membrane-binding peptides exist: amphipathic α-helices and unstructured polybasic regions. The Cex regions of RIT1 and RIT2 fall into the latter category, each containing 15 lysine and arginine residues within 35 amino acids, forming a strongly basic stretch that facilitates electrostatic interaction with negatively charged phospholipids (Figure 2a) [52]. Molecular dynamics simulations have proposed a mechanism by which RIT1 engages with lipid bilayers via a stretch of 12 basic residues (residues 203–214; Figure 2a, double-underlined) [53].

To test lipid specificity, we expressed and purified full-length and truncated GST-RIT1 proteins and performed lipid-binding assays using phosphoinositide (PIP) strips (Figure 5b, c) [47]. Full-length RIT1, as well as isolated Cex constructs of RIT1 and RIT2, bound selectively to phosphoinositides but not to other membrane lipids. This binding was abolished in a GST-RIT1 Cex mutant (M5), which harbors charge-reversing mutations (Figure 5c), and in GST-only controls. These results demonstrate that RIT1 and RIT2 specifically associate with membranes through their C-terminal polybasic regions.

In addition, we analyzed the interaction of RIT1 with lipid bilayers using surface plasmon resonance (SPR). Using an L1 sensor chip coated with immobilized liposomes, we observed direct binding of RIT1 C-terminal constructs to lipid membranes. Kinetic analysis revealed a k_{on} of 0.0111 $\mu M^{-1}s^{-1}$, a k_{off} of 0.0182 s^{-1}, and a dissociation constant (K_d) of 1.6396 μM. No binding was observed for GST alone, which served as a negative control. Notably, RIT1 did not fully dissociate from the liposome surface during the dissociation phase, suggesting that membrane detachment may be regulated by accessory proteins. This observation supports a potential role for galectin-1, previously shown to interact with RIT1, as a modulator of membrane retention. These findings underscore a non-canonical membrane association mechanism within the RIT subfamily. This distinguishes RIT1 from classical RAS proteins and provides a basis for future investigations into Cex-mediated membrane interactions.

Conclusions and future Perspectives

This study provides new insights into the regulatory and membrane-associating mechanisms of RIT1 and RIT2, two understudied members of the RAS superfamily. Our findings reveal that RIT1 and RIT2 diverge significantly from classical RAS proteins in their regulatory behavior, effector interactions, and mechanisms of membrane localization. These distinctions suggest that RIT proteins are governed by unique molecular principles rather than following the canonical RAS signaling pathways. Specifically, the functional roles of their terminal extensions and their distinct responsiveness to guanine nucleotide exchange and hydrolysis imply a separate regulatory axis that remains to be fully characterized [35, 36].

A key finding of this study is that RIT1 is largely unresponsive to known RAS regulators such as SOS1 and p120GAP. Our biochemical and structural data suggest the involvement of yet unidentified GEFs and GAPs that specifically regulate RIT1 function. Furthermore, the use of dominant-negative and GTPase-deficient RIT1 variants has proven valuable in dissecting these regulatory pathways and offers a foundation for future proteomic efforts aimed at isolating native regulators. Continued investigation of these proteins in relevant cellular systems, such as human dermal fibroblasts, where endogenous RIT1 is expressed, will be essential to identify context-specific regulatory partners.

Additionally, our data indicate that RIT1 interacts with candidate effectors such as RGL3, RASSF7, and RASSF9, though with only low affinity. These interactions alone cannot explain the biological impact of disease-associated RIT1 mutations. High-affinity, functionally relevant effectors likely exist and should be identified using state-specific RIT1 mutants that mimic the persistently GTP-bound form. Further studies should also investigate the impact of these

interactions in signaling contexts relevant to development, cancer, and neurodevelopmental disorders.

An important distinguishing feature of RIT1 and RIT2 is their mode of membrane association. Unlike prenylated RAS proteins, both RIT1 and RIT2 lack a CAAX motif and instead utilize a highly basic C-terminal extension to associate with phosphoinositide-enriched membranes. We showed that this region is both necessary and sufficient for plasma membrane targeting. Mutational analysis further confirmed the importance of positively charged residues within this region, and PIP strip assays identified a strong preference for specific phosphoinositides. These findings underscore the functional specificity of the RIT1 C-terminal domain in lipid recognition.

The ability of RIT1 to bind membranes independently of prenylation raises important questions about its regulation by accessory proteins. Our observation that galectin-1, but not calmodulin, binds to RIT1 and may influence its membrane association introduces a new layer of complexity. Although the exact role of galectin-1 in modulating RIT1's subcellular localization remains to be elucidated, future studies should examine whether this interaction promotes membrane retention or facilitates spatial compartmentalization of signaling.

Biophysical analyses, including surface plasmon resonance with defined synthetic liposomes, represent a powerful approach for quantitatively assessing the binding kinetics of RIT1 and RIT2. Our preliminary SPR experiments suggest that RIT1 exhibits incomplete dissociation from liposomes, implying that additional factors may stabilize its membrane association. Follow-up studies should focus on determining the lipid specificity of the RIT C-terminal domains under controlled conditions and on exploring the influence of accessory proteins such as galectin-1 in this context.

In summary, our findings establish RIT1 as a functionally distinct small GTPase with non-canonical regulatory mechanisms, membrane interactions, and potential effector pathways. Understanding these processes in greater detail will not only clarify the physiological and pathological roles of RIT1 and RIT2 but also provide opportunities to target their pathways in diseases where their dysregulation plays a critical role.

Author Contributions: A.M.: Conceptualization, investigation, writing of the original draft. R.D., and N.M.: Analysis of protein sequence and structure. A.M. and N.M.: Expression and purification of proteins. A.M. and F.B.: Analysis of protein and liposome interactions. S.P.: Cell-based analysis by confocal microscopy. F.B. and N.M.: Cell-based analysis by Western blotting. M.R.A.: Conceptualization, resources, funding acquisition, supervision. All authors: review and editing of the manuscript.

Funding: This study was supported by the German Research Foundation (DFG; grant number: AH 92/8-1).

Informed Consent Statement: Not applicable.

Data Availability Statement: It is affirmed that no new data were generated while compiling this manuscript. All referenced data sources are openly accessible and appropriately cited within the manuscript. Please do not hesitate to contact the corresponding author if any additional information or clarification is required.

Acknowledgments: We thank our colleagues from the Institute of Biochemistry and Molecular Biology II for their support.

Conflicts of Interest: The authors declare no conflicts of interest.

Abbreviations

AKT: Protein kinase B
CAAX: Cysteine–aliphatic–aliphatic–X motif
CaM: Calmodulin
CBB: Coomassie Brilliant Blue
Cex: C-terminal extension
CRD: Cysteine-rich domain
DMEM: Dulbecco's Modified Eagle Medium
DTT: Dithiothreitol
EGF: Epidermal growth factor
EPAC1: Exchange protein directly activated by cAMP 1
FBS: Fetal bovine serum
GAL1: Galectin-1
GAP: GTPase-activating protein
GBD: GTPase-binding domain
GDP: Guanosine diphosphate
GEF: Guanine nucleotide exchange factor
GTP: Guanosine triphosphate
HA: Hemagglutinin
HDF: Human dermal fibroblasts
HRAS: Harvey rat sarcoma viral oncogene homolog
IGF1: Insulin-like growth factor 1
JNK: c-Jun N-terminal kinase
Kd: Dissociation constant
kon: Association rate constant
koff: Dissociation rate constant
MAPK: Mitogen-activated protein kinase
mGppNHp: Non-hydrolyzable GTP analog
MSK1: Mitogen- and stress-activated kinase
Nex: N-terminal extension
NGF: Nerve growth factor
PACAP38: Pituitary adenylate cyclase-activating polypeptide 38
PAR6: Partitioning defective protein 6
PAK1: p21-activated kinase 1
PBS: Phosphate-buffered saline
PC: Phosphatidylcholine
PE: Phosphatidylethanolamine
PI: Phosphatidylinositol
PI3K: Phosphoinositide 3-kinase
PIP: Phosphatidylinositol phosphate
PKA: Protein kinase A
PS: Phosphatidylserine
PVDF: Polyvinylidene difluoride
RA: RAS-association domain
RAS: Rat sarcoma
RBD: RAS-binding domain
RGL3: Ral guanine nucleotide dissociation stimulator-like 3
RIT1: Ras-like without CAAX 1
RIT2: Ras-like without CAAX 2
ROSS: Ras of small size
S1P: Sphingosine 1-phosphate
SIN1: Stress-activated protein kinase-interacting protein 1
SOS1: Son of sevenless homolog 1
SPR: Surface plasmon resonance
TAMRA: Tetramethylrhodamine
WT: Wild type

References

1. Nakhaei-Rad, S., et al., *Structural fingerprints, interactions, and signaling networks of RAS family proteins beyond RAS isoforms.* Critical reviews in biochemistry and molecular biology, 2018. **53**(2): p. 130-156.
2. Cirstea, I.C., et al., *Diverging gain-of-function mechanisms of two novel KRAS mutations associated with Noonan and cardio-facio-cutaneous syndromes.* Human molecular genetics, 2013. **22**(2): p. 262-270.
3. Gelb, B.D., et al. *New prospectives on treatment opportunities in RASopathies.* in *American Journal of Medical Genetics Part C: Seminars in Medical Genetics.* 2022. Wiley Online Library.
4. Lau, K.S. and K.M. Haigis, *Non-redundancy within the RAS oncogene family: insights into mutational disparities in cancer.* Molecules and cells, 2009. **28**(4): p. 315-320.
5. Castellano, E. and E. Santos, *Functional specificity of ras isoforms: so similar but so different.* Genes & cancer, 2011. **2**(3): p. 216-231.
6. Herrero, A., D. Matallanas, and W. Kolch, *The spatiotemporal regulation of RAS signalling.* Biochemical Society Transactions, 2016. **44**(5): p. 1517-1522.
7. Lee, C.-H.J., et al., *Rin, a neuron-specific and calmodulin-binding small G-protein, and Rit define a novel subfamily of ras proteins.* Journal of Neuroscience, 1996. **16**(21): p. 6784-6794.
8. Shi, G.-X., W. Cai, and D.A. Andres, *Rit subfamily small GTPases: regulators in neuronal differentiation and survival.* Cellular signalling, 2013. **25**(10): p. 2060-2068.
9. Van, R., et al., *The molecular functions of RIT1 and its contribution to human disease.* Biochemical Journal, 2020. **477**(15): p. 2755-2770.
10. Cavé, H., et al., *Mutations in RIT1 cause Noonan syndrome with possible juvenile myelomonocytic leukemia but are not involved in acute lymphoblastic leukemia.* European journal of human genetics, 2016. **24**(8): p. 1124-1131.
11. Yaoita, M., et al., *Spectrum of mutations and genotype–phenotype analysis in Noonan syndrome patients with RIT1 mutations.* Human genetics, 2016. **135**(2): p. 209-222.
12. Che, M. and Q. Lan, *RIT1 Promotes Glioma Proliferation and Invasion via the AKT/ERK/NF-κB Signaling Pathway.* Journal of Molecular Neuroscience, 2022: p. 1-10.
13. Berger, A., et al., *Oncogenic RIT1 mutations in lung adenocarcinoma.* Oncogene, 2014. **33**(35): p. 4418-4423.
14. Pankratz, N., et al., *Meta-analysis of Parkinson's disease: identification of a novel locus, RIT2.* Annals of neurology, 2012. **71**(3): p. 370-384.
15. Song, Z., et al., *HIF-1α-induced RIT1 promotes liver cancer growth and metastasis and its deficiency increases sensitivity to sorafenib.* Cancer letters, 2019. **460**: p. 96-107.
16. Shi, G.-X. and D.A. Andres, *Rit contributes to nerve growth factor-induced neuronal differentiation via activation of B-Raf-extracellular signal-regulated kinase and p38 mitogen-activated protein kinase cascades.* Molecular and cellular biology, 2005. **25**(2): p. 830-846.
17. Spencer, M.L., et al., *Nerve growth factor-dependent activation of the small GTPase Rin.* Journal of Biological Chemistry, 2002. **277**(20): p. 17605-17615.
18. Onoue, S., J. Hanato, and S. Yamada, *Pituitary adenylate cyclase-activating polypeptide attenuates streptozotocin-induced apoptotic death of RIN-m5F cells through regulation of Bcl-2 family protein mRNA expression.* The FEBS Journal, 2008. **275**(22): p. 5542-5551.
19. Shi, G.-X., H. Rehmann, and D.A. Andres, *A novel cyclic AMP-dependent Epac-Rit signaling pathway contributes to PACAP38-mediated neuronal differentiation.* Molecular and cellular biology, 2006. **26**(23): p. 9136-9147.
20. Shi, G.-X., L. Jin, and D.A. Andres, *Src-dependent TrkA transactivation is required for pituitary adenylate cyclase-activating polypeptide 38-mediated Rit activation and neuronal differentiation.* Molecular biology of the cell, 2010. **21**(9): p. 1597-1608.
21. Ferro, E. and L. Trabalzini, *RalGDS family members couple Ras to Ral signalling and that's not all.* Cellular signalling, 2010. **22**(12): p. 1804-1810.
22. Cai, W., et al., *Rit GTPase regulates a p38 MAPK-dependent neuronal survival pathway.* Neuroscience letters, 2012. **531**(2): p. 125-130.
23. Shi, G.-X., L. Jin, and D.A. Andres, *A rit GTPase-p38 mitogen-activated protein kinase survival pathway confers resistance to cellular stress.* Molecular and cellular biology, 2011. **31**(10): p. 1938-1948.
24. Spencer, M.L., H. Shao, and D.A. Andres, *Induction of neurite extension and survival in pheochromocytoma cells by the Rit GTPase.* Journal of Biological Chemistry, 2002. **277**(23): p. 20160-20168.
25. Hynds, D.L., et al., *Rit promotes MEK-independent neurite branching in human neuroblastoma cells.* Journal of cell science, 2003. **116**(10): p. 1925-1935.
26. Mir, S., et al., *IGF-1 mediated neurogenesis involves a novel RIT1/Akt/Sox2 cascade.* Scientific reports, 2017. **7**(1): p. 1-14.
27. Cai, W. and D.A. Andres, *mTORC2 is required for rit-mediated oxidative stress resistance.* PloS one, 2014. **9**(12): p. e115602.
28. Shi, G.-X., L. Jin, and D.A. Andres, *Pituitary adenylate cyclase-activating polypeptide 38-mediated Rin activation requires Src and contributes to the regulation of HSP27 signaling during neuronal differentiation.* Molecular and cellular biology, 2008. **28**(16): p. 4940-4951.
29. Hoshino, M., T. Yoshimori, and S. Nakamura, *Small GTPase proteins Rin and Rit Bind to PAR6 GTP-dependently and regulate cell transformation.* Journal of Biological Chemistry, 2005. **280**(24): p. 22868-22874.
30. Meyer zum Büschenfelde, U., et al., *RIT1 controls actin dynamics via complex formation with RAC1/CDC42 and PAK1.* PLoS genetics, 2018. **14**(5): p. e1007370.
31. Vetter, I.R. and A. Wittinghofer, *The guanine nucleotide-binding switch in three dimensions.* Science, 2001. **294**(5545): p. 1299-1304.

32. Hall, B.E., et al., *Structure-based mutagenesis reveals distinct functions for Ras switch 1 and switch 2 in Sos-catalyzed guanine nucleotide exchange.* Journal of Biological Chemistry, 2001. **276**(29): p. 27629-27637.
33. Freedman, T.S., et al., *A Ras-induced conformational switch in the Ras activator Son of sevenless.* Proceedings of the National Academy of Sciences, 2006. **103**(45): p. 16692-16697.
34. Feig, L.A., *Tools of the trade: use of dominant-inhibitory mutants of Ras-family GTPases.* Nature cell biology, 1999. **1**(2): p. E25-E27.
35. Flex, E., et al., *Activating mutations in RRAS underlie a phenotype within the RASopathy spectrum and contribute to leukaemogenesis.* Human molecular genetics, 2014. **23**(16): p. 4315-4327.
36. Nauth, T., et al., *Cutaneous manifestations in Costello syndrome: HRAS p. Gly12Ser affects RIN1-mediated integrin trafficking in immortalized epidermal keratinocytes.* Human Molecular Genetics, 2022.
37. Gomez-Segui, I., et al., *Novel recurrent mutations in the RAS-like GTP-binding gene RIT1 in myeloid malignancies.* Leukemia, 2013. **27**(9): p. 1943-1946.
38. Lo, A., et al., *Multiomic characterization of oncogenic signaling mediated by wild-type and mutant RIT1.* Science signaling, 2021. **14**(711): p. eabc4520.
39. Aoki, Y., et al., *Gain-of-function mutations in RIT1 cause Noonan syndrome, a RAS/MAPK pathway syndrome.* The American Journal of Human Genetics, 2013. **93**(1): p. 173-180.
40. Takahara, S., et al., *New Noonan syndrome model mice with RIT1 mutation exhibit cardiac hypertrophy and susceptibility to β-adrenergic stimulation-induced cardiac fibrosis.* EBioMedicine, 2019. **42**: p. 43-53.
41. Kouz, K., et al., *Genotype and phenotype in patients with Noonan syndrome and a RIT1 mutation.* Genetics in Medicine, 2016. **18**(12): p. 1226-1234.
42. Calcagni, G., et al., *Congenital heart defects in Noonan syndrome and RIT1 mutation.* Genetics in Medicine, 2016. **18**(12): p. 1320-1320.
43. Awad, M.M., et al., *Acquired resistance to KRASG12C inhibition in cancer.* New England Journal of Medicine, 2021. **384**(25): p. 2382-2393.
44. Gremer, L., et al., *Germline KRAS mutations cause aberrant biochemical and physical properties leading to developmental disorders.* Human mutation, 2011. **32**(1): p. 33-43.
45. Shao, H., et al., *Biochemical characterization of the Ras-related GTPases Rit and Rin.* Archives of biochemistry and biophysics, 1999. **371**(2): p. 207-219.
46. Castel, P., et al., *RIT1 oncoproteins escape LZTR1-mediated proteolysis.* Science, 2019. **363**(6432): p. 1226-1230.
47. Pudewell, S., et al., *New mechanistic insights into the RAS-SIN1 interaction at the membrane.* Frontiers in Cell and Developmental Biology, 2022. **10**.
48. Shao, H. and D.A. Andres, *A novel RalGEF-like protein, RGL3, as a candidate effector for rit and Ras.* Journal of Biological Chemistry, 2000. **275**(35): p. 26914-26924.
49. Adariani, S.R., et al., *A comprehensive analysis of RAS-effector interactions reveals interaction hotspots and new binding partners.* Journal of Biological Chemistry, 2021. **296**.
50. Pudewell, S., et al., *Accessory proteins of the RAS-MAPK pathway: Moving from the side line to the front line.* Communications biology, 2021. **4**(1): p. 1-10.
51. Navaroli, D.M., et al., *The plasma membrane-associated GTPase Rin interacts with the dopamine transporter and is required for protein kinase C-regulated dopamine transporter trafficking.* Journal of Neuroscience, 2011. **31**(39): p. 13758-13770.
52. Giménez-Andrés, M., A. Čopič, and B. Antonny, *The many faces of amphipathic helices.* Biomolecules, 2018. **8**(3): p. 45.
53. Migliori, A.D., L.A. Patel, and C. Neale, *The RIT1 C-terminus associates with lipid bilayers via charge complementarity.* Computational Biology and Chemistry, 2021. **91**: p. 107437.

3 Discussion

Small GTPases are evolutionarily conserved molecular switches that regulate key aspects of cellular behavior, including cytoskeletal dynamics, intracellular trafficking, signal transduction, and gene expression [1, 9]. Their activity is precisely controlled by regulatory elements such as GEFs, GAPs, GDIs, as well as more recently characterized modulators including accessory proteins and long noncoding RNAs [9, 10, 106, 145, 146]. Dysregulation of these signaling networks contributes to a wide range of diseases, including cancer, developmental syndromes, and infections, making small GTPases central to biological and biomedical research.

This thesis presents a comprehensive biochemical investigation of small GTPases and their modulators across human, plant, and bacterial systems. It covers both canonical and non-canonical GTPases, including RAC1, RIT1, and the plant-specific GTPase TTN5, integrating mechanistic insights with cellular and molecular function [63, 125, 131]. A major focus was placed on the melanoma-associated $RAC1^{P29S}$ hotspot mutation, which was biochemically characterized to uncover its altered regulation by upstream factors and changes in effector interactions and signaling output [63]. In the plant system, TTN5 was studied for its atypical nucleotide cycling properties, providing insight into plant-specific adaptations of GTPase regulation [125]. In the bacterial context, the effector protein SemD from *Chlamydia pneumoniae* was shown to structurally and functionally mimic active CDC42, thereby hijacking the host endocytic machinery [87].

Beyond the GTPases themselves, this thesis examines key modulators such as LZTR1 [218], long noncoding RNAs [145, 146], and a range of accessory proteins that shape small GTPase signaling through spatial and temporal regulation [106]. Collectively, these studies map a multilayered regulatory architecture that governs small GTPase function across different biological systems. The following subsections provide a detailed discussion of each chapter, highlighting conserved principles of regulation alongside context-specific adaptations. This work aims to deepen our understanding of how cells achieve precise and dynamic signal regulation across the tree of life, and how disruption of these mechanisms leads to pathologies ranging from cancer to infection and developmental disorders.

3.1 Oncogenic Characterization of the RAC1 P29S Hotspot Mutation in Melanoma

This study presents a comprehensive biochemical characterization of the melanoma-associated $RAC1^{P29S}$ hotspot mutation in comparison to $RAC1^{WT}$, $RAC1^{T17N}$, and $RAC1^{F28L}$ [63]. The findings reveal that $RAC1^{P29S}$ exhibits impaired nucleotide binding, accelerated intrinsic nucleotide exchange, and severely reduced sensitivity to GAP-mediated GTP hydrolysis, while maintaining activation via DOCK2 but not canonical DBL family GEFs. These combined properties promote the persistent accumulation of $RAC1^{P29S}$ in its active GTP-bound state, resulting in the hyperactivation of downstream signaling pathways including ERK1/2 and p38 MAPK. This persistent activation, together with altered effector binding, most notably enhanced interaction with IQGAP1 over PAK1, supports its classification as a constitutively active, gain-of-function mutant and oncogenic driver [63].

Kinetic analyses demonstrate that the P29S mutation increases intrinsic GDP dissociation and GTP loading rates. Despite this behavior, the mutant shows reduced nucleotide-binding affinity, likely due to conformational changes induced by increased flexibility in the switch I region. While the intrinsic exchange rate of $RAC1^{P29S}$ is faster than that of $RAC1^{WT}$, it remains insufficient to

drive the rapid activation required for real cell signaling without GEF support. The data show that RAC1^{P29S} is primarily activated by DOCK2, a GEF from the DOCK family, while DBL family GEFs such as TIAM1, PREX1, and VAV2 exhibit minimal activity. These observations underscore the specificity of RAC1^{P29S} regulatory interactions and suggest that DOCK2 may serve as a critical upstream activator in melanoma and other RAC1^{P29S}-driven cancers [63].

GDI1 binding assays reveal that RAC1^{P29S} retains moderate affinity for GDI1, indicating that GDI1 may still modulate its localization and recycling. In contrast, RAC1^{T17N} shows reduced GDI1 binding and impaired GEF responsiveness, consistent with its slow-cycling active behavior. RAC1^{F28L} shares a similar GEF activation profile to RAC1^{P29S}, suggesting that both mutations may affect the same GEF-binding interface [63].

The data reveal that RAC1^{P29S} exhibits approximately 30-fold higher binding affinity for IQGAP1 than for PAK1 in stopped-flow fluorimetry assays. This was further corroborated by increased binding in cell lysates under both serum-stimulated and serum-starved conditions. The stronger affinity for IQGAP1 positions it as a key effector downstream of RAC1^{P29S}, linking RAC1 signaling to cytoskeletal remodeling, adhesion, and migration. While PAK1 is a well-established kinase effector of RAC1, the relatively lower affinity of RAC1^{P29S} for PAK1 in biochemical assays compared to cell lysates suggests that other cellular components may influence its interaction in vivo [63]. These findings highlight the critical role of scaffolding proteins such as IQGAP1 in spatially modulating RAC1^{P29S}-driven signaling, particularly in the RAF/MEK/ERK pathway [10].

Functionally, the accumulation of GTP-bound RAC1^{P29S} leads to robust phosphorylation of ERK1/2 and p38 MAPK [63]. ERK hyperactivation promotes uncontrolled proliferation, while p38 MAPK activation supports cellular adaptation to stress and contributes to tumor invasion and therapy resistance. Although AKT and STAT1 phosphorylation were also observed, their effects were less pronounced, suggesting possible context-dependent roles. Notably, RAC1^{P29S} remains GTP-bound even under serum-starved conditions, where most GTPases are inactive, further reinforcing its constitutive activity [63].

Importantly, the intrinsic GTP hydrolysis rate of RAC1^{P29S} is similar to RAC1^{WT}. However, the mutation severely impairs GAP-stimulated GTP hydrolysis. Specifically, the catalytic activity of p50GAP is reduced more than 200-fold in the context of RAC1^{P29S}, leading to prolonged retention in the GTP-bound form. This impaired negative regulation is a key oncogenic mechanism based not solely on enhanced exchange but also on defective inactivation. It enables RAC1^{P29S} to drive sustained signaling and tumorigenic processes, including proliferation, survival, invasion, and epithelial-mesenchymal transition [63].

In summary, RAC1^{P29S} is a causative oncogenic driver with a unique biochemical signature: impaired nucleotide binding, accelerated nucleotide exchange, resistance to GAP-mediated inactivation, and altered effector selectivity. These features result in persistent GTP loading and hyperactivation of cancer-related signaling cascades. The identification of DOCK2 as a preferred GEF, p50GAP resistance as a key mechanism of inactivation failure, and IQGAP1 as a dominant effector provides multiple avenues for therapeutic targeting in melanoma and other cancers harboring RAC1^{P29S} mutations. mutations [63].

3.2 Characterization of TTN5: A Non-classical ARL-type GTPase in *Arabidopsis thaliana*

This study identifies TTN5 as a functional member of the ARF-like (ARL) GTPase family in *Arabidopsis thaliana*, exhibiting distinctive features that set it apart from canonical small GTPases [125]. TTN5 displays unusually rapid nucleotide exchange kinetics, a strong preference for GTP over GDP, and a notably slow GTP hydrolysis rate. These biochemical properties indicate that TTN5 predominantly exists in a GTP-bound, active state. Sequence and functional comparisons reveal a high degree of similarity to human ARL2, supporting its classification as a non-classical ARL-type GTPase [125].

Biochemical analysis demonstrated that TTN5 and its variants can bind guanine nucleotides [125]. The Q70L mutant exhibited the highest affinity for GTP and a faster exchange rate than the wild-type protein, while the T30N mutant, commonly used as a dominant-negative variant, displayed reduced GDP affinity and altered exchange kinetics. Compared to small GTPases such as HRAS and RAC1, TTN5 exhibits a nucleotide exchange rate approaching that of other non-classical GTPases like RHOD and RIF [220]. These observations suggest that TTN5 likely functions independently of canonical GEF-mediated activation [125].

Subcellular localization studies using fluorescently tagged TTN5 variants revealed associations with the plasma membrane, Golgi apparatus, multivesicular bodies, and endosomes [125]. The distribution patterns were dependent on the nucleotide-bound state of the protein, with Q70L showing preferential localization to intracellular compartments compared to the T30N mutant. Notably, TTN5 lacks N-myristoylation, similar to ARL2, and is predicted to associate with membranes via an N-terminal amphipathic helix [221, 222]. This mode of membrane interaction appears to be largely nucleotide-independent, further supporting its non-canonical regulatory behavior[125].

Colocalization analyses confirmed overlap between TTN5 and organelle markers, especially with the Golgi and multivesicular bodies (MVBs) in its GTP-bound form. TTN5 also localized to ARA7-positive compartments and FM4-64-labeled vesicles, suggesting a role in endocytic trafficking and plasma membrane material recycling [223]. These observations point to a broader role for TTN5 in vesicle transport, protein degradation, and endomembrane dynamics. The altered localization and signaling behavior of the T30N variant also underscore the importance of nucleotide binding and exchange in TTN5 function [125].

In summary, TTN5 represents a plant-specific, non-classical ARL-type GTPase that accumulates in the active GTP-bound state due to its intrinsic kinetic properties. Its association with key trafficking compartments and membrane systems suggests a role in endomembrane organization and vesicular transport. These findings expand our understanding of small GTPase regulation in plant systems and illustrate how conserved GTPase modules have been evolutionarily adapted to meet the functional demands of plant development. Future studies will be essential to identify TTN5's specific GEFs, GAPs, effectors, and cargoes to fully define its role in intracellular trafficking and plant physiology [125].

3.3 RIT GTPases: Molecular Regulation, Interaction Networks, and Membrane dynamics

This study provides comprehensive insights into the biochemical and regulatory features of RIT1 and RIT2, two less-characterized members of the RAS family. Although RIT proteins have often

been grouped with classical RAS proteins, the data presented here emphasize their unique regulatory profile. Structural analysis confirms that RIT1 shares the conserved G-domain architecture of canonical RAS proteins, including the G1–G5 motifs and switch I and II regions, suggesting conserved GDP/GTP cycling mechanisms [33, 35, 41]. However, fluorescence-based kinetic assays reveal that RIT1 exhibits significantly lower nucleotide binding affinity due to a markedly reduced association rate despite an increased dissociation rate, distinguishing it from HRAS. These results indicate that RIT1 activation in cells likely requires a specific GEF that remains to be identified, as the canonical RAS GEF SOS1 [224] shows no activity toward RIT1.

Likewise, p120GAP [225], a known GAP for HRAS, fails to stimulate GTP hydrolysis in RIT1, indicating that RIT1 may also rely on a distinct GAP. Mutational analysis shows that germline mutations associated with developmental syndromes, such as Noonan syndrome, cluster near the P-loop and switch II regions. These mutations may impair GAP binding or catalytic efficiency rather than causing direct constitutive activation as observed in classical oncogenic RAS mutations. Notably, the RIT1 Q79L variant, despite its predicted GTPase deficiency, did not exhibit elevated basal GTP loading or significant downstream activation of MAPK, PI3K/AKT, or JNK pathways in HEK-293T cells. In contrast, the S35N mutant exhibited a dominant-negative effect by reducing phosphorylation of MEK, ERK, and AKT, likely through sequestration of endogenous RIT1-specific GEFs.

Effector-binding studies using fluorescence polarization revealed only low-affinity interactions between RIT1 and previously proposed RAS effectors, including RGL3, RASSF7/9, and CRAF [35, 88, 226]. Surprisingly, galectin-1 [227], but not calmodulin, bound to RIT1 with a dissociation constant of ~35 μM. These results suggest that RIT1 may signal through unconventional effectors, distinct from the classical RAS effectors [4].

In addition to its regulatory distinctions, RIT1 exhibits a unique mode of membrane association. Unlike most RAS proteins, RIT1 lacks a C-terminal CAAX motif required for prenylation [35]. Instead, its C-terminal extension (Cex) is rich in basic residues and binds directly to phosphoinositides. Confocal imaging and PIP strip assays confirm that both full-length RIT1 and its Cex fragment associate with the plasma membrane via electrostatic interactions. This membrane association is abolished in Cex-deleted or charge-reversed mutants, and galectin-1 binding may modulate this interaction.

Together, these findings position RIT1 and RIT2 as distinct RAS family members with canonical GDP/GTP cycling mechanisms but unique regulatory and membrane-targeting features. The study supports a model in which RIT proteins integrate classical G-domain regulation with lineage-specific membrane localization. Future identification of specific GEFs, GAPs, and physiological effectors will be crucial to understand RIT1 and RIT2's roles in developmental disorders and tumorigenesis.

3.4 HSC Activation and Fibrosis: The RAS–RHO Axis in Hepatic Stellate Cells

This study explores the reciprocal regulation of RAS and RHO family GTPases in hepatic stellate cells (HSCs), providing new insights into their roles in maintaining quiescence and driving activation and differentiation [131]. In quiescent HSCs, elevated levels of ERAS and RND3 correlate with enhanced PI3K–AKT and NOTCH signaling activity. In contrast, activated HSCs exhibit increased expression of MRAS and RHOC, which is associated with the activation of the MAPK and ROCK signaling pathways [131].

ERAS is selectively expressed in quiescent HSCs and contributes to the maintenance of their undifferentiated state by activating the PI3K–AKT signaling axis [132]. Its downregulation during HSC activation is accompanied by reduced phosphorylation of AKT and FOXO1, indicating a decline in survival and homeostatic signaling. In parallel, MRAS expression rises in activated HSCs and promotes MAPK signaling via the SHOC2–PP1–RAF1 complex, leading to ERK phosphorylation and fostering transdifferentiation [131].

A similar reciprocal pattern is observed in the RHO family: RND3, enriched in quiescent HSCs, antagonizes RHOC–ROCK signaling and stabilizes the cytoskeleton, whereas RHOC predominates in activated HSCs. This switch supports the induction of α-SMA expression and cytoskeletal remodeling, hallmark features of the myofibroblastic phenotype. Both immunoblotting and mRNA profiling confirm these reciprocal expression patterns [131].

NOTCH1 signaling also plays a critical role in sustaining quiescence [228]. Its intracellular domain (N1ICD) and downstream target gene HES1 suppress pro-fibrotic markers. The cytosolic localization of NOTCH1/N1ICD in quiescent HSCs, along with sustained HES1 expression, supports its transcriptionally active, anti-fibrotic function downstream of ERAS [131].

Pharmacological inhibition of ROCK using Y-27632 maintains the quiescent morphology of HSCs, further validating the role of RHOC–ROCK signaling in promoting activation. Together, these findings support a regulatory model in which the ERAS–PI3K–AKT and NOTCH1–RND3 axis preserves quiescence, while the MRAS–MAPK and RHOC–ROCK pathways drive activation [131].

Additionally, the ERAS–ARG1–polyamine axis emerges as a critical regulator of HSC homeostasis. ARG1 is co-expressed with ERAS and catalyzes polyamine biosynthesis, including spermidine, which supports autophagy and self-renewal. Inhibition of ARG1 or polyamine synthesis accelerates HSC activation, as demonstrated by the loss of stellate morphology and lipid droplet reservoirs [143] [131].

In conclusion, this study proposes a reciprocal regulatory model in which ERAS, RND3, and NOTCH1 define the quiescent state through PI3K–AKT and anti-fibrotic signaling, while MRAS, RHOC, and ROCK signaling drive HSC activation. This dynamic switch represents a central mechanism controlling HSC fate and offers promising therapeutic targets for the treatment of chronic liver disease and fibrosis [131, 132].

3.5 Structural and Functional Mimicry of CDC42 by *Chlamydia pneumoniae* effector SemD in N-WASP Activation

This study provides detailed structural and biochemical insights into the host-cell subversion mechanism employed by the early-secreted *Chlamydia pneumoniae* effector protein SemD [87]. As an obligate intracellular pathogen, *C. pneumoniae* relies on a precisely coordinated internalization process to enter non-phagocytic epithelial cells [114]. The successful uptake of its large elementary body (EB) requires extensive remodeling of the plasma membrane and actin cytoskeleton [115]. Our findings demonstrate that SemD plays a central role in orchestrating these events by functioning as a multifunctional adaptor protein that mimics key features of the host RHO GTPase CDC42 in order to directly activate N-WASP and facilitate Arp2/3-dependent actin nucleation and branching [87].

Structurally, SemD is composed of multiple functional domains connected by flexible intrinsically disordered linker sequences, allowing it to simultaneously engage several host proteins [87]. Its

C-terminal rigid core contains a negatively charged surface that mimics the effector-binding interface of CDC42·GTP, thereby enabling high-affinity binding to the basic region (BR) and CRIB domain of N-WASP. This interaction releases the autoinhibited VCA domain of N-WASP, promoting actin polymerization at the site of bacterial entry. Biochemical assays, including pulldown and stopped-flow experiments, confirm that SemD binds N-WASP with significantly stronger and faster interaction than CDC42·GTP and can displace N-WASP from preformed CDC42·GTP–N-WASP complexes, highlighting its ability to outcompete endogenous host regulators [87].

Importantly, SemD selectively activates N-WASP without binding other CDC42 effectors such as FMNL2, indicating a level of substrate specificity that maximizes efficiency while avoiding unintended activation of competing pathways. This selectivity is likely enabled by structural differences between CDC42–N-WASP and CDC42–FMNL2 complexes, where SemD reproduces the electrostatic features of CDC42 required for N-WASP activation but lacks the hydrophobic interface necessary for FMNL2 binding [87, 118].

In addition to activating N-WASP, SemD coordinates the recruitment of other essential components of the endocytic machinery [87]. Its proline-rich domain (PRD1) interacts specifically with the SH3 domain of the membrane-remodeling protein SNX9 [229], while its N-terminal amphipathic helix anchors the protein to the cytosolic leaflet of the plasma membrane. Together, these interactions facilitate the spatial organization of SemD into a membrane-associated hub capable of synchronously recruiting N-WASP, SNX9, and monomeric G-actin. Structural modeling and experimental validation using GUV systems further support this simultaneous interaction model.

Moreover, SemD carries two WH2 motifs predicted to bind G-actin, with WH2_1 located on α-helix 1 of the core domain being structurally accessible. This domain likely contributes to the local enrichment of actin monomers at the site of bacterial entry, further enhancing SemD-mediated actin polymerization. The combined action of SemD on membrane curvature (via SNX9), actin recruitment (via WH2 domains), and actin nucleation (via N-WASP activation) enables the efficient formation of a branched actin network that drives the engulfment of the chlamydial EB [87].

Unlike many other bacterial effectors that regulate host RHO GTPases through covalent modification or enzymatic activity targeting upstream regulators (GEFs, GAPs, GDIs) [90] [9], SemD operates as a direct structural mimic [87]. This positions SemD as a unique effector that bypasses host signaling cascades by directly engaging and activating a central actin nucleator. Its action also differs from that of the EHEC effector EspFU [230], which mimics N-WASP's own VCA domain to relieve autoinhibition, or the chlamydial effector TmeA [231], which may act through a similar mechanism. In contrast, SemD directly substitutes for CDC42·GTP in a structurally resolved manner [87].

Collectively, these findings highlight SemD as a highly specialized and efficient effector that has evolved to perform multiple coordinated functions within a compact framework. By structurally and functionally mimicking host proteins, SemD maximizes its impact on the host endocytic machinery despite the limited coding capacity of the C. pneumoniae genome. This multifunctional mimicry not only facilitates bacterial entry but may also represent a broader strategy employed by intracellular pathogens to subvert host-cellular processes using compact, domain-rich effectors [87].

3.6 Modulators of Small GTPases localization, function, and regulation: Long Noncoding RNAs and Accessory Proteins

This section explores how small GTPases are regulated not only by classical modulators such as GEFs, GAPs, and GDIs, but also by emerging noncanonical regulators including long noncoding RNAs (lncRNAs) [145, 146] and accessory proteins [10, 106, 174, 218]. While the classical regulators control the activation state, membrane association, and signal fidelity of GTPases, accumulating evidence highlights additional layers of regulation that modulate expression levels, subcellular localization, protein complex assembly, and spatiotemporal signaling coordination. LncRNAs contribute by regulating gene expression at both transcriptional and post-transcriptional levels, often through microRNA sequestration in competing endogenous RNA (ceRNA) networks or by scaffolding chromatin remodeling and signaling complexes [145, 146]. Accessory proteins, including scaffolds, adaptors, anchors, and docking factors, help spatially organize and stabilize GTPase–effector complexes, ensuring precise signaling fidelity through mechanisms such as multivalent binding and compartmentalization, sometimes involving liquid-phase separation [10, 106, 218]. Collectively, these modulators fine-tune small GTPase signaling with remarkable specificity and flexibility, contributing to diverse biological outcomes including development, immune responses, cancer progression, and host–pathogen interactions. Their integration into small GTPase regulatory networks underscores the complexity and adaptability of intracellular signaling, and highlights promising avenues for both fundamental research and therapeutic targeting. [1, 10, 106, 145, 146, 218].

KRAS mutations represent some of the most prevalent oncogenic alterations across human cancers, particularly in hematologic malignancies such as juvenile myelomonocytic leukemia (JMML) [232]. While their role in activating canonical signaling cascades is well established, recent transcriptomic studies have revealed significant remodeling of the noncoding RNA landscape in KRAS-driven cancers [145]. Multiple KRAS-associated lncRNAs have emerged as critical regulators of leukemogenesis, often through their capacity to modulate apoptosis, cell survival, and signaling feedback. For instance, comparative analyses in JMML have identified MORRBID as a lncRNA that supports myeloid cell survival by repressing pro-apoptotic regulators like BIM [162]. These lncRNAs frequently function by sequestering tumor-suppressive miRNAs, thereby stabilizing oncogenic transcripts and promoting persistent KRAS pathway activation. MALAT1, for example, sponges miR-101 to preserve MCL1 expression, contributing to drug resistance [233]. Beyond competing endogenous RNA mechanisms, KRAS-related lncRNAs also engage in chromatin remodeling, control mRNA stability, facilitate the localization of signaling components, and scaffold ribonucleoprotein complexes [234] . Notably, some of these transcripts encode small peptides with signaling regulatory potential, further expanding their functional regulatory impact. Through both direct modulation of KRAS mRNA and indirect control of pathway components, these lncRNAs exert broad regulatory influence [149, 151, 152, 234]. Their high specificity and multifunctionality render them attractive therapeutic targets. Strategies such as antisense oligonucleotides, RNA interference, CRISPR-based gene silencing, and aptamer-guided targeting have shown potential in disrupting oncogenic lncRNA functions. Conversely, reintroduction of tumor-suppressive lncRNAs via synthetic mimics or viral delivery may help restore signaling balance. Targeting lncRNA–protein complexes or their encoded peptides also presents novel avenues for therapeutic intervention. Advancing our understanding of the spatial, temporal, and mechanistic roles of KRAS-associated lncRNAs will be essential for identifying effective treatment strategies in KRAS-driven cancers and beyond [145, 234].

LncRNAs modulate RHO GTPase signaling through both post-transcriptional and epigenetic mechanisms that impact upstream regulators, downstream effectors, and core family members such as RHOA, RAC1, CDC42 [146]. One key mechanism involves miRNA sequestration, where

lncRNAs relieve repression on signaling mediators. For example, the lncRNA CTC-497E21.4 promotes RHOA activation by sponging miR-22, thereby upregulating NET1, a RHOA-specific GEF. Similarly, MALAT1 enhances osteosarcoma cell invasion by upregulating ROCK1 and ROCK2, two major effectors downstream of RHOA [146]. Beyond cytoplasmic interactions, nuclear-localized lncRNAs regulate gene expression through chromatin remodeling. TUG1, for instance, recruits the histone methyltransferase EZH2 to the RND3 promoter, silencing its transcription, while m6A modification of GAS5 accelerates its degradation and indirectly sustains YAP signaling by lifting RHOB-mediated suppression TUG1 [166, 171]. These examples underscore the dual roles of lncRNAs as both regulators and downstream targets within RHO GTPase signaling pathways. Despite growing interest, functional studies remain limited, particularly for lncRNAs associated with less-characterized RHO family members. Further investigation is required to map their interactions with miRNAs, epigenetic modifiers, and signaling proteins [146]. Therapeutically, several approaches are under exploration, including antisense oligonucleotides, siRNAs, ribozymes, CRISPR/Cas9-based editing, and small molecules that disrupt lncRNA structure or lncRNA–protein interactions [146]. Notably, antisense oligonucleotides targeting MALAT1 have shown tumor-suppressive effects in preclinical models [173, 233]. Additional strategies include lncRNA promoter-driven cytotoxic gene expression, such as the H19-regulated BC-819 plasmid used in clinical trials [160, 170]. The tissue-specific expression profiles of many lncRNAs further support their potential as selective therapeutic targets [146]. However, challenges remain, including delivery efficiency, off-target effects, and limited understanding of their context-dependent functions. Advancing the systematic characterization of RHO-related lncRNAs, aided by high-throughput sequencing, proteomics, and functional screening, will be key to uncovering how they contribute to spatiotemporal regulation of cytoskeletal dynamics, cell migration, differentiation, and disease progression [146].

Accessory proteins play critical roles in shaping the signaling dynamics of the KRAS pathway, acting as spatial and temporal modulators of complex molecular interactions [10]. Although traditional research has focused on the core components of the RTK–RAS–MAPK cascade, growing evidence shows that accessory proteins, often operating at the periphery, are equally important in refining signaling specificity and output [174]. These proteins primarily function as scaffolds, adaptors, or docking modules that regulate the localization, activation, and clustering of signaling molecules within defined subcellular compartments [10, 174]. In cancer, dysregulation of accessory proteins contributes to aberrant KRAS signaling and therapy resistance. Mutations in scaffold proteins such as IQGAP1, KSR, and SHOC2 have been linked to tumor progression, invasion, and poor clinical outcomes [10, 235-237]. Our experimental findings reveal distinct consequences of accessory protein loss in KRAS(G12V)-driven cancer cells. Specifically, CRISPR-Cas9 knockout of GAL3 or PDEδ in KRAS-mutant lung cancer models interferes with membrane-associated signaling and reduces downstream activation of ERK and AKT, whereas loss of IQGAP1 unexpectedly increases AKT signaling, suggesting a context-dependent regulatory role. SHOC2 knockout selectively reduces MAPK signaling while leaving PI3K–AKT activity unaffected and sensitizes cells to MEK inhibition, indicating a therapeutic opportunity for combination treatments. The significance of accessory proteins is further supported by their role in RASopathies, where germline mutations in SHOC2, SPRED1, and SHP2 cause hyperactive MAPK signaling and developmental abnormalities [10, 188, 190, 194, 238]. Therapeutic strategies increasingly focus on targeting accessory proteins rather than the central components of KRAS signaling. Approaches include antisense oligonucleotides, peptide inhibitors, small molecules that block protein–protein interactions, and proteolysis-targeting chimeras (PROTACs) [10, 106]. For example, IQGAP1-derived peptides and KSR inhibitors like APS-2-79 have been shown to reduce ERK activation and inhibit tumor growth in preclinical models [185, 193]. Accessory proteins are also involved in immune regulation, as illustrated by SHP2's role in both RAS signaling and PD-1 checkpoint pathways [189]. Taken together, accessory proteins represent a mechanistically

diverse and therapeutically promising group of regulators, offering new opportunities to target KRAS-driven cancers with improved specificity and reduced toxicity [10].

PAK1 is a key downstream effector of RAC1 and CDC42, integrating upstream signals to regulate actin cytoskeletal remodeling, cell migration, proliferation, and survival [84, 106, 195]. In several cancers, including melanoma, non-small cell lung cancer, and estrogen receptor–positive breast cancer, PAK1 hyperactivation correlates with poor prognosis, therapeutic resistance, and increased tumor aggressiveness. Although direct pharmacological inhibition of PAK1 has been explored, it often leads to toxicity and compensatory signaling due to the protein's essential roles in normal physiology [106]. As an alternative, targeting accessory proteins that control the spatial and temporal activation of PAK1 offers a more refined therapeutic strategy. These include scaffolding proteins such as PIX and Paxillin, which guide PAK1 localization to membrane compartments and focal adhesions; adaptor proteins like NCK and GRB2, which mediate upstream interactions; and additional scaffolds such as CKIP1 and RIT1, which influence PAK1 recruitment and engagement with GTPase inputs [106]. Disrupting these interactions, for example, with small-molecule inhibitors like AX-024 targeting NCK1, can attenuate PAK1-driven cytoskeletal remodeling and invasion [208]. Moreover, a PAK1-selective degrader, BJG-05-039, has been shown to inhibit both catalytic and scaffolding functions of PAK1, improving the response to therapies such as BRAF, MEK, and CDK4/6 inhibitors [106, 239]. Transcriptomic regulation also contributes to PAK1 modulation; lncRNAs such as H19 and MALAT1 enhance CDC42/PAK1 signaling by sequestering miRNAs or scaffolding upstream activators, linking noncoding RNA function to protein signaling networks [170]. Collectively, these accessory components form a regulatory hub that ensures the spatial and temporal precision of PAK1 signaling. Their targeted manipulation presents a promising avenue for suppressing oncogenic outputs, overcoming drug resistance, and minimizing side effects associated with direct inhibition of core pathway components [106].

LZTR1 has emerged as a key accessory protein acting as a negative regulator of RAS-MAPK signaling through its role as an adaptor in the cullin 3 ubiquitin ligase complex [147, 217, 219]. By promoting ubiquitin-mediated degradation of RAS GTPases, LZTR1 controls the availability and signaling output of various RAS isoforms[218]. Initially associated with both autosomal dominant and recessive forms of Noonan syndrome, recent studies have revealed mutation-specific mechanisms that disrupt its regulatory function [218]. Notably, the $LZTR1^{L580P}$ missense variant, located in the BACK1 domain, induces aberrant polymerization of LZTR1, impairing the formation of functional ubiquitination complexes. This leads to reduced degradation and pathological accumulation of RAS proteins, particularly MRAS and RIT1, resulting in MAPK pathway hyperactivation. These findings were validated in patient-derived cardiomyocytes, where homozygous expression of $LZTR1^{L580P}$ reproduced key molecular and cellular disease features, including elevated RAS signaling, cytoskeletal abnormalities, and a hypertrophic phenotype. Correction of a single allele restored homeostasis, underscoring both the recessive impact of this variant and its therapeutic potential [218]. Although LZTR1 can bind multiple RAS isoforms, current evidence suggests a preference for degrading MRAS and RIT1 over HRAS, KRAS, and NRAS, indicating cell type- and context-specific substrate specificity [218]. Domain-specific mutations also yield distinct outcomes: Kelch domain variants impair substrate recognition, while BTB-BACK mutations like $LZTR1^{L580P}$ disrupt complex assembly and localization. The discovery that disease-associated polymerization alters LZTR1's spatial organization introduces a novel mechanism of signaling disruption [218]. These insights position LZTR1 as a finely tuned regulator of RAS pathway dynamics with important implications for developmental disorders, cardiac hypertrophy, and therapeutic targeting in RASopathies and RAS-driven malignancies [218].

In summary, this thesis presents an integrated biochemical and mechanistic dissection of small GTPases and their modulators across diverse biological contexts, spanning human, plant, and bacterial systems. From canonical signaling alterations caused by oncogenic mutations like

RAC1^{P29S} and KRAS-associated regulatory RNAs to atypical regulatory mechanisms observed in TTN5 and RIT1, the work highlights both conserved and context-specific strategies that fine-tune small GTPase activity [63, 125]. It further emphasizes the reciprocal regulation between RAS and RHO GTPases in controlling cell fate decisions, such as hepatic stellate cell activation[131]. In parallel, the study of the *Chlamydia pneumoniae* effector SemD uncovers a unique example of structural and functional mimicry, demonstrating how pathogens can hijack host actin remodeling by imitating CDC42 [87]. The thesis also underscores the emerging significance of accessory proteins and lncRNAs in orchestrating the spatial and temporal control of small GTPase signaling [106, 145, 146]. These noncanonical modulators, including KRAS and PAK1 accessory proteins as well as the RAS-degrading adaptor LZTR1, offer new insights into disease mechanisms and therapeutic vulnerabilities in cancers, RASopathies, and infectious diseases [106, 218]. Together, these findings map a multilayered regulatory landscape in which classical regulators and accessory components converge to direct GTPase-mediated signaling, reinforcing the therapeutic potential of targeting this network and its value as a framework for understanding cellular signaling dynamics.

4 Conclusions and future perspectives

This thesis presents a comprehensive investigation of selected small GTPases of the RAS superfamily, including the RAS, RHO, and ARF families, and their regulatory networks across human, plant, and bacterial systems, with a focus on their biochemical properties and molecular mechanisms. The work begins by characterizing the melanoma-associated RAC1 P29S mutation, demonstrating its predominant activation by DOCK2 GEF, resistance to GAP-mediated inactivation, and enhanced effector interaction with IQGAP1, establishing its role in driving oncogenic signaling. The plant-specific ARF-like GTPase TITAN5 (TTN5) from *Arabidopsis thaliana* is identified as a non-classical GTPase with rapid nucleotide exchange and slow hydrolysis, accumulating in its active state and localizing to vesicle trafficking compartments, highlighting its role in plant development. RIT1 is studied as a structurally canonical but functionally distinct RAS-family member with unique membrane-binding properties and low nucleotide turnover, requiring the identification of its specific GEFs, GAPs, and effectors. The *Chlamydia pneumoniae* effector SemD is shown to mimic CDC42, directly activating N-WASP to promote actin polymerization and pathogen entry, exemplifying bacterial exploitation of host GTPase signaling. In hepatic stellate cells, a reciprocal signaling model between RAS and RHO GTPases is revealed, with ERAS and RND3 supporting quiescence and MRAS and RHOC promoting fibrogenic activation, offering insight into cell state transitions relevant to liver disease.

The second part of this work focuses on the regulatory complexity introduced by noncanonical modulators. Literature-based analyses identified and categorized long noncoding RNAs (lncRNAs) involved in KRAS and RHOA signaling, highlighting their roles in transcriptional control, miRNA sequestration, and spatial regulation of signaling complexes. Similarly, accessory regulators of PAK1 were reviewed, emphasizing their therapeutic potential in PAK1-related diseases including cancer cell invasion. Experimentally, key accessory proteins such as IQGAP1, Galectin-3, PDEδ, SHOC2, and NPM1 were investigated in the context of KRAS-driven signaling. The thesis also examines the LZTR1 L580P mutation, showing that this accessory adaptor impairs CUL3-mediated degradation of RIT1 and MRAS, leading to MAPK hyperactivation and cardiomyocyte hypertrophy.

Together, these findings map a multilayered regulatory framework governing small GTPase signaling across distinct biological systems. Yet, fundamental questions remain: How are RAS signaling networks coordinated in space and time to optimize strength, efficiency, and specificity? How is the pre-assembly of protein complexes encoded to ensure accurate signaling? How do cells transmit rapid and precise signals within a densely packed cytoplasm? To what extent are these principles conserved across evolution? And ultimately, can we define a unifying rule that governs the spatiotemporal organization of signaling pathways such as RAS across the tree of life? Addressing these questions will guide future efforts to unravel the dynamic regulation of intracellular signaling.

References

1. Wittinghofer, A., *Ras superfamily small G proteins: biology and mechanisms*. 2014: Springer.
2. Trabalzini, L. and S.F. Retta, *Ras signaling: methods and protocols*. 2014: Springer.
3. Alesi, N. and E.P. Henske, *Keeping up with the Rag GTPases.* Nature Cell Biology, 2022. **24**(9): p. 1330-1331.
4. Nakhaei-Rad, S., et al., *Structural fingerprints, interactions, and signaling networks of RAS family proteins beyond RAS isoforms.* Critical reviews in biochemistry and molecular biology, 2018. **53**(2): p. 130-156.
5. Bourne, H.R., D.A. Sanders, and F. McCormick, *The GTPase superfamily: conserved structure and molecular mechanism.* nature, 1991. **349**(6305): p. 117-127.
6. Jaiswal, M., R. Dvorsky, and M.R. Ahmadian, *Deciphering the Molecular and Functional Basis of Dbl Family Proteins: A NOVEL SYSTEMATIC APPROACH TOWARD CLASSIFICATION OF SELECTIVE ACTIVATION OF THE Rho FAMILY PROTEINS*.* Journal of Biological Chemistry, 2013. **288**(6): p. 4486-4500.
7. Amin, E., et al., *Deciphering the molecular and functional basis of RHOGAP family proteins: a systematic approach toward selective inactivation of RHO family proteins.* Journal of Biological Chemistry, 2016. **291**(39): p. 20353-20371.
8. Dovas, A. and J.R. Couchman, *RhoGDI: multiple functions in the regulation of Rho family GTPase activities.* Biochemical Journal, 2005. **390**(1): p. 1-9.
9. Mosaddeghzadeh, N. and M.R. Ahmadian, *The RHO family GTPases: mechanisms of regulation and signaling.* Cells, 2021. **10**(7): p. 1831.
10. Pudewell, S., et al., *Accessory proteins of the RAS-MAPK pathway: moving from the side line to the front line.* Communications biology, 2021. **4**(1): p. 696.
11. Malumbres, M. and M. Barbacid, *RAS oncogenes: the first 30 years.* Nature Reviews Cancer, 2003. **3**(6): p. 459-465.
12. Vetter, I.R. and A. Wittinghofer, *The guanine nucleotide-binding switch in three dimensions.* Science, 2001. **294**(5545): p. 1299-1304.
13. Kontani, K., et al., *Di-Ras, a distinct subgroup of ras family GTPases with unique biochemical properties.* Journal of Biological Chemistry, 2002. **277**(43): p. 41070-41078.
14. Aksamitiene, E., A. Kiyatkin, and B.N. Kholodenko, *Cross-talk between mitogenic Ras/MAPK and survival PI3K/Akt pathways: a fine balance.* Biochemical Society Transactions, 2012. **40**(1): p. 139-146.
15. Ehrhardt, A., et al., *Distinct mechanisms determine the patterns of differential activation of H-Ras, N-Ras, K-Ras 4B, and M-Ras by receptors for growth factors or antigen.* Molecular and cellular biology, 2004. **24**(14): p. 6311-6323.
16. Spencer, M.L., H. Shao, and D.A. Andres, *Induction of neurite extension and survival in pheochromocytoma cells by the Rit GTPase.* Journal of Biological Chemistry, 2002. **277**(23): p. 20160-20168.
17. Scheffzek, K. and M.R. Ahmadian, *GTPase activating proteins: structural and functional insights 18 years after discovery.* Cellular and Molecular Life Sciences CMLS, 2005. **62**: p. 3014-3038.
18. Gureasko, J., et al., *Membrane-dependent signal integration by the Ras activator Son of sevenless.* Nature structural & molecular biology, 2008. **15**(5): p. 452-461.
19. Desideri, E., A.L. Cavallo, and M. Baccarini, *Alike but different: RAF paralogs and their signaling outputs.* Cell, 2015. **161**(5): p. 967-970.
20. Ünal, E.B., F. Uhlitz, and N. Blüthgen, *A compendium of ERK targets.* FEBS letters, 2017. **591**(17): p. 2607-2615.
21. Vanhaesebroeck, B., et al., *Synthesis and function of 3-phosphorylated inositol lipids.* Annual review of biochemistry, 2001. **70**(1): p. 535-602.

22. Ferro, E. and L. Trabalzini, *RalGDS family members couple Ras to Ral signalling and that's not all.* Cellular signalling, 2010. **22**(12): p. 1804-1810.
23. Carloni, V., et al., *Tyrosine phosphorylation of focal adhesion kinase by PDGF is dependent on ras in human hepatic stellate cells.* Hepatology, 2000. **31**(1): p. 131-140.
24. Hynds, D.L., et al., *Rit promotes MEK-independent neurite branching in human neuroblastoma cells.* Journal of cell science, 2003. **116**(10): p. 1925-1935.
25. Simanshu, D.K., D.V. Nissley, and F. McCormick, *RAS proteins and their regulators in human disease.* Cell, 2017. **170**(1): p. 17-33.
26. Ligon, A.H., et al., *Identification of a novel gene product, RIG, that is down-regulated in human glioblastoma.* Oncogene, 1997. **14**(9): p. 1075-1081.
27. Ellis, C.A., et al., *Rig is a novel Ras-related protein and potential neural tumor suppressor.* Proceedings of the National Academy of Sciences, 2002. **99**(15): p. 9876-9881.
28. Harrison, L.M., *Rhes: a GTP-binding protein integral to striatal physiology and pathology.* Cellular and molecular neurobiology, 2012. **32**: p. 907-918.
29. Navaroli, D.M., et al., *The plasma membrane-associated GTPase Rin interacts with the dopamine transporter and is required for protein kinase C-regulated dopamine transporter trafficking.* Journal of Neuroscience, 2011. **31**(39): p. 13758-13770.
30. Wes, P.D., M. Yu, and C. Montell, *RIC, a calmodulin-binding Ras-like GTPase.* The EMBO journal, 1996. **15**(21): p. 5839-5848.
31. Berger, A., et al., *Oncogenic RIT1 mutations in lung adenocarcinoma.* Oncogene, 2014. **33**(35): p. 4418-4423.
32. Aoki, Y., et al., *Gain-of-function mutations in RIT1 cause Noonan syndrome, a RAS/MAPK pathway syndrome.* The American Journal of Human Genetics, 2013. **93**(1): p. 173-180.
33. Van, R., et al., *The molecular functions of RIT1 and its contribution to human disease.* Biochemical Journal, 2020. **477**(15): p. 2755-2770.
34. Shao, H., et al., *Biochemical characterization of the Ras-related GTPases Rit and Rin.* Archives of biochemistry and biophysics, 1999. **371**(2): p. 207-219.
35. Cuevas-Navarro, A., et al., *RAS-dependent RAF-MAPK hyperactivation by pathogenic RIT1 is a therapeutic target in Noonan syndrome–associated cardiac hypertrophy.* Science Advances, 2023. **9**(28): p. eadf4766.
36. Lee, C.-H.J., et al., *Rin, a neuron-specific and calmodulin-binding small G-protein, and Rit define a novel subfamily of ras proteins.* Journal of Neuroscience, 1996. **16**(21): p. 6784-6794.
37. Fang, Z., et al., *Biochemical classification of disease-associated mutants of RAS-like protein expressed in many tissues (RIT1).* Journal of Biological Chemistry, 2016. **291**(30): p. 15641-15652.
38. Montuori, N., et al., *Urokinase-type plasminogen activator up-regulates the expression of its cellular receptor.* FEBS letters, 2000. **476**(3): p. 166-170.
39. Hoshino, M., T. Yoshimori, and S. Nakamura, *Small GTPase proteins Rin and Rit Bind to PAR6 GTP-dependently and regulate cell transformation.* Journal of Biological Chemistry, 2005. **280**(24): p. 22868-22874.
40. Meyer zum Büschenfelde, U., et al., *RIT1 controls actin dynamics via complex formation with RAC1/CDC42 and PAK1.* PLoS genetics, 2018. **14**(5): p. e1007370.
41. Castel, P., et al., *RIT1 oncoproteins escape LZTR1-mediated proteolysis.* Science, 2019. **363**(6432): p. 1226-1230.
42. Kapp, F.G., et al., *Somatic RIT1 delins in arteriovenous malformations hyperactivate RAS-MAPK signaling amenable to MEK inhibition.* Angiogenesis, 2024: p. 1-14.
43. Li, J.-T., et al., *Amplification of RIT1 in hepatocellular carcinoma and its clinical significance.* Ai zheng= Aizheng= Chinese journal of cancer, 2003. **22**(7): p. 695-699.
44. Song, Z., et al., *HIF-1α-induced RIT1 promotes liver cancer growth and metastasis and its deficiency increases sensitivity to sorafenib.* Cancer letters, 2019. **460**: p. 96-107.

45. Feng, Y.-F., et al., *RIT1 suppresses esophageal squamous cell carcinoma growth and metastasis and predicts good prognosis.* Cell death & disease, 2018. **9**(11): p. 1085.
46. Gomez-Segui, I., et al., *Novel recurrent mutations in the RAS-like GTP-binding gene RIT1 in myeloid malignancies.* Leukemia, 2013. **27**(9): p. 1943-1946.
47. Hall, A., *Rho GTPases and the actin cytoskeleton.* Science, 1998. **279**(5350): p. 509-514.
48. Wheeler, A.P. and A.J. Ridley, *Why three Rho proteins? RhoA, RhoB, RhoC, and cell motility.* Experimental cell research, 2004. **301**(1): p. 43-49.
49. Burridge, K. and K. Wennerberg, *Rho and Rac take center stage.* Cell, 2004. **116**(2): p. 167-179.
50. Shi, J., et al., *Distinct roles for ROCK1 and ROCK2 in the regulation of cell detachment.* Cell death & disease, 2013. **4**(2): p. e483-e483.
51. Wallar, B.J. and A.S. Alberts, *The formins: active scaffolds that remodel the cytoskeleton.* Trends in cell biology, 2003. **13**(8): p. 435-446.
52. Fujisawa, K., et al., *Different regions of Rho determine Rho-selective binding of different classes of Rho target molecules.* Journal of Biological Chemistry, 1998. **273**(30): p. 18943-18949.
53. Madaule, P., et al., *Role of citron kinase as a target of the small GTPase Rho in cytokinesis.* Nature, 1998. **394**(6692): p. 491-494.
54. Haeusler, L.C., et al., *Purification and biochemical properties of Rac1, 2, 3 and the splice variant Rac1b.* Methods in enzymology, 2006. **406**: p. 1-11.
55. Gu, Y., et al., *Hematopoietic cell regulation by Rac1 and Rac2 guanosine triphosphatases.* Science, 2003. **302**(5644): p. 445-449.
56. de Curtis, I., *The Rac3 GTPase in neuronal development, neurodevelopmental disorders, and cancer.* Cells, 2019. **8**(9): p. 1063.
57. Chan, A.Y., et al., *Roles of the Rac1 and Rac3 GTPases in human tumor cell invasion.* Oncogene, 2005. **24**(53): p. 7821-7829.
58. Wennerberg, K. and C.J. Der, *Rho-family GTPases: it's not only Rac and Rho (and I like it).* Journal of cell science, 2004. **117**(8): p. 1301-1312.
59. Haeusler, L.C., et al., *Comparative functional analysis of the Rac GTPases.* FEBS letters, 2003. **555**(3): p. 556-560.
60. Hodge, R.G., et al., *RAS and RHO family GTPase mutations in cancer: twin sons of different mothers?* Critical reviews in biochemistry and molecular biology, 2020. **55**(4): p. 386-407.
61. Halaban, R., *RAC1 and melanoma.* Clinical therapeutics, 2015. **37**(3): p. 682-685.
62. Krauthammer, M., et al., *Exome sequencing identifies recurrent somatic RAC1 mutations in melanoma.* Nature genetics, 2012. **44**(9): p. 1006-1014.
63. Mirzaiebadizi, A. and M.R. Ahmadian, *New insights into the classification of the RAC1 P29S hotspot mutation in melanoma as an oncogene.* bioRxiv, 2025: p. 2025.03. 04.637030.
64. Davis, M.J., et al., *RAC1P29S is a spontaneously activating cancer-associated GTPase.* Proceedings of the National Academy of Sciences, 2013. **110**(3): p. 912-917.
65. Toyama, Y., et al., *Conformational landscape alternations promote oncogenic activities of Ras-related C3 botulinum toxin substrate 1 as revealed by NMR.* Science advances, 2019. **5**(3): p. eaav8945.
66. Kawazu, M., et al., *Transforming mutations of RAC guanosine triphosphatases in human cancers.* Proceedings of the National Academy of Sciences, 2013. **110**(8): p. 3029-3034.
67. Senyuz, S., et al., *Mechanistic differences of activation of Rac1P29S and Rac1A159V.* The Journal of Physical Chemistry B, 2021. **125**(15): p. 3790-3802.
68. Hodis, E., et al., *A landscape of driver mutations in melanoma.* Cell, 2012. **150**(2): p. 251-263.
69. Mohan, A.S., et al., *Enhanced dendritic actin network formation in extended lamellipodia drives proliferation in growth-challenged Rac1P29S melanoma cells.* Developmental cell, 2019. **49**(3): p. 444-460. e9.

70. Cannon, A.C., et al., *Unique vulnerability of RAC1-mutant melanoma to combined inhibition of CDK9 and immune checkpoints.* Oncogene, 2024. **43**(10): p. 729-743.
71. Watson, I.R., et al., *The RAC1 P29S hotspot mutation in melanoma confers resistance to pharmacological inhibition of RAF.* Cancer research, 2014. **74**(17): p. 4845-4852.
72. Lionarons, D.A., et al., *RAC1P29S induces a mesenchymal phenotypic switch via serum response factor to promote melanoma development and therapy resistance.* Cancer cell, 2019. **36**(1): p. 68-83. e9.
73. Zhu, E.Y., et al., *Understanding cancer drug resistance with Sleeping Beauty functional genomic screens: Application to MAPK inhibition in cutaneous melanoma.* Iscience, 2023. **26**(10).
74. Vu, H.L., et al., *RAC 1 P29S regulates PD-L1 expression in melanoma.* Pigment cell & melanoma research, 2015. **28**(5): p. 590-598.
75. Araiza-Olivera, D., et al., *Suppression of RAC1-driven malignant melanoma by group A PAK inhibitors.* Oncogene, 2018. **37**(7): p. 944-952.
76. Foth, M., et al., *RAC1mutation is not a predictive biomarker for PI3'-kinase-β-selective pathway-targeted therapy.* Pigment Cell & Melanoma Research, 2020. **33**(5): p. 719-730.
77. González, N., et al., *Computational and in vitro pharmacodynamics characterization of 1A-116 Rac1 inhibitor: relevance of Trp56 in its biological activity.* Frontiers in Cell and Developmental Biology, 2020. **8**: p. 240.
78. Uribe-Alvarez, C., et al., *Targeting effector pathways in RAC1P29S-driven malignant melanoma.* Small GTPases, 2021. **12**(4): p. 273-281.
79. Tomino, T., et al., *DOCK1 inhibition suppresses cancer cell invasion and macropinocytosis induced by self-activating Rac1P29S mutation.* Biochemical and biophysical research communications, 2018. **497**(1): p. 298-304.
80. Immisch, L., et al., *Targeting the recurrent Rac1P29S neoepitope in melanoma with heterologous high-affinity T cell receptors.* Frontiers in Immunology, 2023. **14**: p. 1119498.
81. Etienne-Manneville, S., *Cdc42-the centre of polarity.* Journal of cell science, 2004. **117**(8): p. 1291-1300.
82. Miller, K.E., P.J. Kang, and H.-O. Park, *Regulation of Cdc42 for polarized growth in budding yeast.* Microbial cell, 2020. **7**(7): p. 175.
83. Johnson, D.I., *Cdc42: an essential Rho-type GTPase controlling eukaryotic cell polarity.* Microbiology and Molecular Biology Reviews, 1999. **63**(1): p. 54-105.
84. Tu, H. and M. Wigler, *Genetic evidence for Pak1 autoinhibition and its release by Cdc42.* Molecular and cellular biology, 1999. **19**(1): p. 602-611.
85. Stengel, K. and Y. Zheng, *Cdc42 in oncogenic transformation, invasion, and tumorigenesis.* Cellular signalling, 2011. **23**(9): p. 1415-1423.
86. Nouri, K., D.J. Timson, and M.R. Ahmadian, *New model for the interaction of IQGAP1 with CDC42 and RAC1.* Small GTPases, 2020. **11**(1): p. 16-22.
87. Kocher, F., et al., *The C hlamydia pneumoniae effector SemD exploits its host's endocytic machinery by structural and functional mimicry.* Nature Communications, 2024. **15**(1): p. 7294.
88. Adariani, S.R., et al., *A comprehensive analysis of RAS-effector interactions reveals interaction hotspots and new binding partners.* Journal of Biological Chemistry, 2021. **296**.
89. Bishop, A.L. and A. Hall, *Rho GTPases and their effector proteins.* Biochemical Journal, 2000. **348**(2): p. 241-255.
90. Jaffe, A.B. and A. Hall, *Rho GTPases: biochemistry and biology.* Annu. Rev. Cell Dev. Biol., 2005. **21**(1): p. 247-269.
91. Truebestein, L., et al., *A molecular ruler regulates cytoskeletal remodelling by the Rho kinases.* Nature communications, 2015. **6**(1): p. 10029.
92. Zhao, Z.-s. and E. Manser, *PAK and other Rho-associated kinases–effectors with surprisingly diverse mechanisms of regulation.* Biochemical Journal, 2005. **386**(2): p. 201-214.

93. Bernard, O., *Lim kinases, regulators of actin dynamics.* The international journal of biochemistry & cell biology, 2007. **39**(6): p. 1071-1076.
94. Gallo, K.A. and G.L. Johnson, *Mixed-lineage kinase control of JNK and p38 MAPK pathways.* Nature reviews Molecular cell biology, 2002. **3**(9): p. 663-672.
95. Watanabe, G., et al., *Protein kinase N (PKN) and PKN-related protein rhophilin as targets of small GTPase Rho.* Science, 1996. **271**(5249): p. 645-648.
96. Watanabe, N., et al., *Cooperation between mDia1 and ROCK in Rho-induced actin reorganization.* Nature cell biology, 1999. **1**(3): p. 136-143.
97. Rohatgi, R., H.-y.H. Ho, and M.W. Kirschner, *Mechanism of N-WASP activation by CDC42 and phosphatidylinositol 4, 5-bisphosphate.* The Journal of cell biology, 2000. **150**(6): p. 1299-1310.
98. Miki, H., et al., *IRSp53 is an essential intermediate between Rac and WAVE in the regulation of membrane ruffling.* Nature, 2000. **408**(6813): p. 732-735.
99. Liu, C.-A., et al., *Rho/Rhotekin-mediated NF-κB activation confers resistance to apoptosis.* Oncogene, 2004. **23**(54): p. 8731-8742.
100. Brown, M.D. and D.B. Sacks, *IQGAP1 in cellular signaling: bridging the GAP.* Trends in cell biology, 2006. **16**(5): p. 242-249.
101. Mosaddeghzadeh, N., et al., *Selectivity determinants of RHO GTPase binding to IQGAPs.* International Journal of Molecular Sciences, 2021. **22**(22): p. 12596.
102. Maekawa, M., et al., *Signaling from Rho to the actin cytoskeleton through protein kinases ROCK and LIM-kinase.* Science, 1999. **285**(5429): p. 895-898.
103. Totsukawa, G., et al., *Distinct roles of ROCK (Rho-kinase) and MLCK in spatial regulation of MLC phosphorylation for assembly of stress fibers and focal adhesions in 3T3 fibroblasts.* The Journal of cell biology, 2000. **150**(4): p. 797-806.
104. Ding, B., et al., *Structures reveal a key mechanism of WAVE regulatory complex activation by Rac1 GTPase.* Nature Communications, 2022. **13**(1): p. 5444.
105. Shibasaki, Y., et al., *Massive actin polymerization induced by phosphatidylinositol-4-phosphate 5-kinase in vivo.* Journal of Biological Chemistry, 1997. **272**(12): p. 7578-7581.
106. Mirzaiebadizi, A., R. Shafabakhsh, and M.R. Ahmadian, *Modulating PAK1: Accessory Proteins as Promising Therapeutic Targets.* Biomolecules, 2025. **15**(2): p. 242.
107. Garrard, S.M., et al., *Structure of Cdc42 in a complex with the GTPase-binding domain of the cell polarity protein, Par6.* The EMBO journal, 2003.
108. Rolland, Y., et al., *The CDC42-interacting protein 4 controls epithelial cell cohesion and tumor dissemination.* Developmental Cell, 2014. **30**(5): p. 553-568.
109. Modzelewska, K., et al., *Ack1 mediates Cdc42-dependent cell migration and signaling to p130Cas.* Journal of Biological Chemistry, 2006. **281**(49): p. 37527-37535.
110. Miyano, K. and H. Sumimoto, *Role of the small GTPase Rac in p22phox-dependent NADPH oxidases.* Biochimie, 2007. **89**(9): p. 1133-1144.
111. Teramoto, H., et al., *Signaling from the small GTP-binding proteins Rac1 and Cdc42 to the c-Jun N-terminal kinase/stress-activated protein kinase pathway: a role for mixed lineage kinase 3/protein-tyrosine kinase 1, a novel member of the mixed lineage kinase family.* Journal of Biological Chemistry, 1996. **271**(44): p. 27225-27228.
112. Miralles, F., et al., *Actin dynamics control SRF activity by regulation of its coactivator MAL.* Cell, 2003. **113**(3): p. 329-342.
113. Blumenstein, L. and M.R. Ahmadian, *Models of the cooperative mechanism for Rho effector recognition: implications for RhoA-mediated effector activation.* Journal of Biological Chemistry, 2004. **279**(51): p. 53419-53426.
114. Nans, A., C. Ford, and R.D. Hayward, *Host-pathogen reorganisation during host cell entry by Chlamydia trachomatis.* Microbes and infection, 2015. **17**(11-12): p. 727-731.

115. Hahn, D.L., *Chlamydia pneumoniae and chronic asthma: updated systematic review and meta-analysis of population attributable risk.* PLoS One, 2021. **16**(4): p. e0250034.
116. Shin, N., et al., *Sorting nexin 9 interacts with dynamin 1 and N-WASP and coordinates synaptic vesicle endocytosis.* Journal of Biological Chemistry, 2007. **282**(39): p. 28939-28950.
117. Prehoda, K.E., et al., *Integration of multiple signals through cooperative regulation of the N-WASP-Arp2/3 complex.* Science, 2000. **290**(5492): p. 801-806.
118. Kühn, S., et al., *The structure of FMNL2–Cdc42 yields insights into the mechanism of lamellipodia and filopodia formation.* Nature communications, 2015. **6**(1): p. 7088.
119. Sztul, E., et al., *ARF GTPases and their GEFs and GAPs: concepts and challenges.* Molecular biology of the cell, 2019. **30**(11): p. 1249-1271.
120. Cherfils, J., *Arf GTPases and their effectors: assembling multivalent membrane-binding platforms.* Current opinion in structural biology, 2014. **29**: p. 67-76.
121. Burd, C.G., T.I. Strochlic, and S.R.G. Setty, *Arf-like GTPases: not so Arf-like after all.* Trends in cell biology, 2004. **14**(12): p. 687-694.
122. D'Souza-Schorey, C. and P. Chavrier, *ARF proteins: roles in membrane traffic and beyond.* Nature reviews Molecular cell biology, 2006. **7**(5): p. 347-358.
123. Donaldson, J.G. and C.L. Jackson, *ARF family G proteins and their regulators: roles in membrane transport, development and disease.* Nature reviews Molecular cell biology, 2011. **12**(6): p. 362-375.
124. Nagai, H., et al., *A bacterial guanine nucleotide exchange factor activates ARF on Legionella phagosomes.* Science, 2002. **295**(5555): p. 679-682.
125. Mohr, I., et al., *Characterization of the small Arabidopsis thaliana GTPase and ADP-ribosylation factor-like 2 protein TITAN 5.* Journal of Cell Science, 2024. **137**(15).
126. McElver, J., et al., *The TITAN5 gene of Arabidopsis encodes a protein related to the ADP ribosylation factor family of GTP binding proteins.* The Plant Cell, 2000. **12**(8): p. 1379-1392.
127. Veltel, S., et al., *Specificity of Arl2/Arl3 signaling is mediated by a ternary Arl3-effector-GAP complex.* Febs Letters, 2008. **582**(17): p. 2501-2507.
128. Lloyd, J. and D. Meinke, *A comprehensive dataset of genes with a loss-of-function mutant phenotype in Arabidopsis.* Plant physiology, 2012. **158**(3): p. 1115-1129.
129. Bhamidipati, A., S.A. Lewis, and N.J. Cowan, *ADP ribosylation factor-like protein 2 (Arl2) regulates the interaction of tubulin-folding cofactor D with native tubulin.* The Journal of cell biology, 2000. **149**(5): p. 1087-1096.
130. Friedman, S.L., *Hepatic stellate cells: protean, multifunctional, and enigmatic cells of the liver.* Physiological reviews, 2008. **88**(1): p. 125-172.
131. Nakhaei-Rad, S., et al., *From Quiescence to Activation: The Reciprocal Regulation of Ras and Rho Signaling in Hepatic Stellate Cells.* Cells, 2025. **14**(9): p. 674.
132. Nakhaei-Rad, S., et al., *The role of embryonic stem cell-expressed RAS (ERAS) in the maintenance of quiescent hepatic stellate cells.* Journal of Biological Chemistry, 2016. **291**(16): p. 8399-8413.
133. Barry, A.E., et al., *Hepatic stellate cells and hepatocarcinogenesis.* Frontiers in cell and developmental biology, 2020. **8**: p. 709.
134. Klein, S., et al., *Rho-kinase inhibitor coupled to peptide-modified albumin carrier reduces portal pressure and increases renal perfusion in cirrhotic rats.* Scientific reports, 2019. **9**(1): p. 2256.
135. Kordes, C., I. Sawitza, and D. Häussinger, *Canonical Wnt signaling maintains the quiescent stage of hepatic stellate cells.* Biochemical and biophysical research communications, 2008. **367**(1): p. 116-123.
136. Huang, Z., et al., *Hydrostatic pressure induces profibrotic properties in hepatic stellate cells via the RhoA/ROCK signaling pathway.* FEBS Open Bio, 2022. **12**(6): p. 1230-1240.
137. Carloni, V., et al., *Cell adhesion regulates platelet-derived growth factor-induced MAP kinase and PI-3 kinase activation in stellate cells.* Hepatology, 2002. **36**(3): p. 582-591.

138. Xie, G., et al., *Cross-talk between Notch and Hedgehog regulates hepatic stellate cell fate in mice.* Hepatology, 2013. **58**(5): p. 1801-1813.
139. Kato, M., et al., *Role of Rho small GTP binding protein in the regulation of actin cytoskeleton in hepatic stellate cells.* Journal of hepatology, 1999. **31**(1): p. 91-99.
140. Li, L., et al., *Effect of Rho A on transforming growth factor β1-induced rat hepatic stellate cell migration.* Liver International, 2012. **32**(7): p. 1093-1102.
141. Lakner, A.M., et al., *Daily genetic profiling indicates JAK/STAT signaling promotes early hepatic stellate cell transdifferentiation.* World journal of gastroenterology: WJG, 2010. **16**(40): p. 5047.
142. Mannaerts, I., et al., *The Hippo pathway effector YAP controls mouse hepatic stellate cell activation.* Journal of hepatology, 2015. **63**(3): p. 679-688.
143. Pudewell, S., et al., *Physical interaction between embryonic stem cell-expressed Ras (ERas) and arginase-1 in quiescent hepatic stellate cells.* Cells, 2022. **11**(3): p. 508.
144. Cherfils, J. and M. Zeghouf, *Regulation of small gtpases by gefs, gaps, and gdis.* Physiological reviews, 2013. **93**(1): p. 269-309.
145. Saliani, M., et al., *KRAS-related long noncoding RNAs in human cancers.* Cancer gene therapy, 2022. **29**(5): p. 418-427.
146. Saliani, M., et al., *RHO GTPase-related long noncoding RNAs in human cancers.* Cancers, 2021. **13**(21): p. 5386.
147. Abe, T., et al., *LZTR1 facilitates polyubiquitination and degradation of RAS-GTPases.* Cell Death & Differentiation, 2020. **27**(3): p. 1023-1035.
148. Mattick, J.S., et al., *Long non-coding RNAs: definitions, functions, challenges and recommendations.* Nature reviews Molecular cell biology, 2023. **24**(6): p. 430-447.
149. Quinn, J.J. and H.Y. Chang, *Unique features of long non-coding RNA biogenesis and function.* Nature reviews genetics, 2016. **17**(1): p. 47-62.
150. Uszczynska-Ratajczak, B., et al., *Towards a complete map of the human long non-coding RNA transcriptome.* Nature Reviews Genetics, 2018. **19**(9): p. 535-548.
151. Mercer, T.R., M.E. Dinger, and J.S. Mattick, *Long non-coding RNAs: insights into functions.* Nature reviews genetics, 2009. **10**(3): p. 155-159.
152. Luo, J., et al., *LncRNAs: architectural scaffolds or more potential roles in phase separation.* Frontiers in Genetics, 2021. **12**: p. 626234.
153. Yao, Z.T., et al., *New insights into the interplay between long non-coding RNAs and RNA-binding proteins in cancer.* Cancer communications, 2022. **42**(2): p. 117-140.
154. Xu, W., et al., *Ribosome profiling analysis identified a KRAS-interacting microprotein that represses oncogenic signaling in hepatocellular carcinoma cells.* Science China Life Sciences, 2020. **63**: p. 529-542.
155. Liu, P., et al., *The lncRNA MALAT1 acts as a competing endogenous RNA to regulate KRAS expression by sponging miR-217 in pancreatic ductal adenocarcinoma.* Scientific Reports, 2017. **7**(1): p. 5186.
156. Chu, J., et al., *LncRNA MIR31HG functions as a ceRNA to regulate c-Met function by sponging miR-34a in esophageal squamous cell carcinoma.* Biomedicine & Pharmacotherapy, 2020. **128**: p. 110313.
157. Yang, L., et al., *Long non-coding RNA BCYRN1 exerts an oncogenic role in colorectal cancer by regulating the miR-204-3p/KRAS axis.* Cancer cell international, 2020. **20**: p. 1-13.
158. Poliseno, L., et al., *A coding-independent function of gene and pseudogene mRNAs regulates tumour biology.* Nature, 2010. **465**(7301): p. 1033-1038.
159. Li, X., et al., *Hypoxia-induced lncRNA-NUTF2P3-001 contributes to tumorigenesis of pancreatic cancer by derepressing the miR-3923/KRAS pathway.* Oncotarget, 2016. **7**(5): p. 6000.
160. Lim, Y.W.S., et al., *The double-edged sword of H19 lncRNA: Insights into cancer therapy.* Cancer Letters, 2021. **500**: p. 253-262.

161. Hofmans, M., et al., *Long non-coding RNAs as novel therapeutic targets in juvenile myelomonocytic leukemia.* Scientific reports, 2021. **11**(1): p. 2801.
162. Cai, Z., et al., *Role of lncRNA Morrbid in PTPN11 (Shp2) E76K-driven juvenile myelomonocytic leukemia.* Blood Advances, 2020. **4**(14): p. 3246-3251.
163. Xiao, H., Q. Zhu, and J. Zhou, *Long non-coding RNA MALAT1 interaction with miR-429 regulates the proliferation and EMT of lung adenocarcinoma cells through RhoA.* International journal of clinical and experimental pathology, 2019. **12**(2): p. 419.
164. Li, H., et al., *Long noncoding RNA NORAD, a novel competing endogenous RNA, enhances the hypoxia-induced epithelial-mesenchymal transition to promote metastasis in pancreatic cancer.* Molecular cancer, 2017. **16**: p. 1-14.
165. Liu, J., Y. Zhu, and C. Ge, *LncRNA ZFAS1 promotes pancreatic adenocarcinoma metastasis via the RHOA/ROCK2 pathway by sponging miR-3924.* Cancer cell international, 2020. **20**: p. 1-15.
166. Yao, X., et al., *LncRNA GAS5 regulates osteosarcoma cell proliferation, migration, and invasion by regulating RHOB via sponging miR-663a.* Cancer Management and Research, 2020: p. 8253-8261.
167. Chen, S., et al., *The role of the long non-coding RNA TDRG1 in epithelial ovarian carcinoma tumorigenesis and progression through miR-93/RhoC pathway.* Molecular Carcinogenesis, 2018. **57**(2): p. 225-234.
168. Liu, Y., et al., *The role of long non-coding RNA PCA3 in epithelial ovarian carcinoma tumorigenesis and progression.* Gene, 2017. **633**: p. 42-47.
169. Li, J., et al., *Long noncoding RNA AURKAPS1 potentiates malignant hepatocellular carcinoma progression by regulating miR-142, miR-155 and miR-182.* Scientific reports, 2019. **9**(1): p. 19645.
170. Zhou, Y., et al., *LncRNA-H19 activates CDC42/PAK1 pathway to promote cell proliferation, migration and invasion by targeting miR-15b in hepatocellular carcinoma.* Genomics, 2019. **111**(6): p. 1862-1872.
171. Xu, Y., et al., *The lncRNA TUG1 modulates proliferation in trophoblast cells via epigenetic suppression of RND3.* Cell death & disease, 2017. **8**(10): p. e3104-e3104.
172. Li, Z., et al., *FTO plays an oncogenic role in acute myeloid leukemia as a N6-methyladenosine RNA demethylase.* Cancer cell, 2017. **31**(1): p. 127-141.
173. Amodio, N., et al., *Drugging the lncRNA MALAT1 via LNA gapmeR ASO inhibits gene expression of proteasome subunits and triggers anti-multiple myeloma activity.* Leukemia, 2018. **32**(9): p. 1948-1957.
174. Pudewell, S. and M.R. Ahmadian, *Spotlight on accessory proteins: RTK-RAS-MAPK modulators as new therapeutic targets.* Biomolecules, 2021. **11**(6): p. 895.
175. Buday, L., L. Wunderlich, and P. Tamás, *The Nck family of adapter proteins: regulators of actin cytoskeleton.* Cellular signalling, 2002. **14**(9): p. 723-731.
176. McKay, M.M., D.A. Ritt, and D.K. Morrison, *Signaling dynamics of the KSR1 scaffold complex.* Proceedings of the National Academy of Sciences, 2009. **106**(27): p. 11022-11027.
177. McNulty, D.E., et al., *MAPK scaffold IQGAP1 binds the EGF receptor and modulates its activation.* Journal of biological chemistry, 2011. **286**(17): p. 15010-15021.
178. Sheikh, F., et al., *An FHL1-containing complex within the cardiomyocyte sarcomere mediates hypertrophic biomechanical stress responses in mice.* The Journal of clinical investigation, 2008. **118**(12): p. 3870-3880.
179. MacDonald, J.I., et al., *Direct binding of the signaling adapter protein Grb2 to the activation loop tyrosines on the nerve growth factor receptor tyrosine kinase, TrkA.* Journal of Biological Chemistry, 2000. **275**(24): p. 18225-18233.
180. Therrien, M., et al., *Functional analysis of CNK in RAS signaling.* Proceedings of the National Academy of Sciences, 1999. **96**(23): p. 13259-13263.

181. Amaddii, M., et al., *Flotillin-1/reggie-2 protein plays dual role in activation of receptor-tyrosine kinase/mitogen-activated protein kinase signaling.* Journal of Biological Chemistry, 2012. **287**(10): p. 7265-7278.
182. Melillo, R., et al., *Docking protein FRS2 links the protein tyrosine kinase RET and its oncogenic forms with the mitogen-activated protein kinase signaling cascade.* Molecular and Cellular Biology, 2001.
183. Mackinnon, A.C., et al., *Paxillin expression and amplification in early lung lesions of high-risk patients, lung adenocarcinoma and metastatic disease.* Journal of clinical pathology, 2011. **64**(1): p. 16-24.
184. Yoshida, T., et al., *Spreds, inhibitors of the Ras/ERK signal transduction, are dysregulated in human hepatocellular carcinoma and linked to the malignant phenotype of tumors.* Oncogene, 2006. **25**(45): p. 6056-6066.
185. Jameson, K.L., et al., *IQGAP1 scaffold-kinase interaction blockade selectively targets RAS-MAP kinase–driven tumors.* Nature medicine, 2013. **19**(5): p. 626-630.
186. Young, L.C., et al., *SHOC2–MRAS–PP1 complex positively regulates RAF activity and contributes to Noonan syndrome pathogenesis.* Proceedings of the National Academy of Sciences, 2018. **115**(45): p. E10576-E10585.
187. Martinelli, S., et al., *Molecular diversity and associated phenotypic spectrum of germline CBL mutations.* Human mutation, 2015. **36**(8): p. 787-796.
188. Brems, H. and E. Legius, *Legius syndrome, an update. Molecular pathology of mutations in SPRED1.* The Keio Journal of Medicine, 2013. **62**(4): p. 107-112.
189. Zhao, M., et al., *SHP2 inhibition triggers anti-tumor immunity and synergizes with PD-1 blockade.* Acta Pharmaceutica Sinica B, 2019. **9**(2): p. 304-315.
190. Jones, G.G., et al., *SHOC2 phosphatase-dependent RAF dimerization mediates resistance to MEK inhibition in RAS-mutant cancers.* Nature communications, 2019. **10**(1): p. 2532.
191. Indarte, M., et al., *An inhibitor of the pleckstrin homology domain of CNK1 selectively blocks the growth of mutant KRAS cells and tumors.* Cancer research, 2019. **79**(12): p. 3100-3111.
192. Tari, A.M., et al., *Liposome-incorporated Grb2 antisense oligodeoxynucleotide increases the survival of mice bearing bcr-abl-positive leukemia xenografts.* International journal of oncology, 2007. **31**(5): p. 1243-1250.
193. Dhawan, N.S., A.P. Scopton, and A.C. Dar, *Small molecule stabilization of the KSR inactive state antagonizes oncogenic Ras signalling.* Nature, 2016. **537**(7618): p. 112-116.
194. Xie, J., et al., *Allosteric inhibitors of SHP2 with therapeutic potential for cancer treatment.* Journal of medicinal chemistry, 2017. **60**(24): p. 10205-10219.
195. Kichina, J.V., et al., *PAK1 as a therapeutic target.* Expert opinion on therapeutic targets, 2010. **14**(7): p. 703-725.
196. Manser, E., et al., *A brain serine/threonine protein kinase activated by Cdc42 and Rac1.* Nature, 1994. **367**(6458): p. 40-46.
197. Manser, E., et al., *PAK kinases are directly coupled to the PIX family of nucleotide exchange factors.* Molecular cell, 1998. **1**(2): p. 183-192.
198. Nayal, A., et al., *Paxillin phosphorylation at Ser273 localizes a GIT1–PIX–PAK complex and regulates adhesion and protrusion dynamics.* The Journal of cell biology, 2006. **173**(4): p. 587-589.
199. Kim, Y.-B., et al., *The role of the pleckstrin homology domain-containing protein CKIP-1 in activation of p21-activated kinase 1 (PAK1).* Journal of Biological Chemistry, 2015. **290**(34): p. 21076-21085.
200. Puto, L.A., et al., *p21-activated kinase 1 (PAK1) interacts with the Grb2 adapter protein to couple to growth factor signaling.* Journal of Biological Chemistry, 2003. **278**(11): p. 9388-9393.

201. Galisteo, M.L., et al., *The adaptor protein Nck links receptor tyrosine kinases with the serine-threonine kinase Pak1.* Journal of Biological Chemistry, 1996. **271**(35): p. 20997-21000.
202. Turner, C.E., et al., *Paxillin LD4 motif binds PAK and PIX through a novel 95-kD ankyrin repeat, ARF–GAP protein: a role in cytoskeletal remodeling.* The Journal of cell biology, 1999. **145**(4): p. 851-863.
203. Talukder, A., Q. Meng, and R. Kumar, *CRIPak, a novel endogenous Pak1 inhibitor.* Oncogene, 2006. **25**(9): p. 1311-1319.
204. Kissil, J.L., et al., *Merlin, the product of the Nf2 tumor suppressor gene, is an inhibitor of the p21-activated kinase, Pak1.* Molecular cell, 2003. **12**(4): p. 841-849.
205. Alahari, S.K., P.J. Reddig, and R.L. Juliano, *The integrin-binding protein Nischarin regulates cell migration by inhibiting PAK.* The EMBO journal, 2004. **23**(14): p. 2777-2788.
206. Xia, C., et al., *Regulation of the p21-activated kinase (PAK) by a human Gβ-like WD-repeat protein, hPIP1.* Proceedings of the National Academy of Sciences, 2001. **98**(11): p. 6174-6179.
207. Ijuin, T. and T. Takenawa, *Regulation of insulin signaling and glucose transporter 4 (GLUT4) exocytosis by phosphatidylinositol 3, 4, 5-trisphosphate (PIP3) phosphatase, skeletal muscle, and kidney enriched inositol polyphosphate phosphatase (SKIP).* Journal of Biological Chemistry, 2012. **287**(10): p. 6991-6999.
208. Alarcon, B. and A. Borroto, *Small molecule AX-024 targets T cell receptor signaling by disrupting CD3ε-Nck interaction.* The Journal of Biological Chemistry, 2020. **295**(29): p. 10076.
209. Sun, X., L. Luo, and J. Li, *LncRNA MALAT1 facilitates BM-MSCs differentiation into endothelial cells via targeting miR-206/VEGFA axis.* Cell Cycle, 2020. **19**(22): p. 3018-3028.
210. Johnson, M., M. Sharma, and B.R. Henderson, *IQGAP1 regulation and roles in cancer.* Cellular signalling, 2009. **21**(10): p. 1471-1478.
211. Fukata, M., et al., *Cdc42 and Rac1 regulate the interaction of IQGAP1 with β-catenin.* Journal of Biological Chemistry, 1999. **274**(37): p. 26044-26050.
212. Hu, W., et al., *IQGAP1 promotes pancreatic cancer progression and epithelial-mesenchymal transition (EMT) through Wnt/β-catenin signaling.* Scientific reports, 2019. **9**(1): p. 7539.
213. Le Clainche, C., et al., *IQGAP1 stimulates actin assembly through the N-WASP-Arp2/3 pathway.* Journal of Biological Chemistry, 2007. **282**(1): p. 426-435.
214. Jin, S.H., et al., *IQGAP2 inactivation through aberrant promoter methylation and promotion of invasion in gastric cancer cells.* International journal of cancer, 2008. **122**(5): p. 1040-1046.
215. Stylli, S.S., A.H. Kaye, and P. Lock, *Invadopodia: at the cutting edge of tumour invasion.* Journal of clinical neuroscience, 2008. **15**(7): p. 725-737.
216. Sakurai-Yageta, M., et al., *The interaction of IQGAP1 with the exocyst complex is required for tumor cell invasion downstream of Cdc42 and RhoA.* The Journal of cell biology, 2008. **181**(6): p. 985-998.
217. Bigenzahn, J.W., et al., *LZTR1 is a regulator of RAS ubiquitination and signaling.* Science, 2018. **362**(6419): p. 1171-1177.
218. Busley, A.V., et al., *Mutation-induced LZTR1 polymerization provokes cardiac pathology in recessive Noonan syndrome.* Cell reports, 2024. **43**(7).
219. Zhang, H., et al., *LZTR1: A promising adaptor of the CUL3 family.* Oncology Letters, 2021. **22**(1): p. 564.
220. Jaiswal, M., et al., *New insight into the molecular switch mechanism of human Rho family proteins: shifting a paradigm.* Biological Chemistry, 2013. **394**(1): p. 89-95.
221. Lee, M.C., et al., *Sar1p N-terminal helix initiates membrane curvature and completes the fission of a COPII vesicle.* Cell, 2005. **122**(4): p. 605-617.
222. Kapoor, S., et al., *Effect of the N-terminal helix and nucleotide loading on the membrane and effector binding of Arl2/3.* Biophysical journal, 2015. **109**(8): p. 1619-1629.

223. Lee, G.-J., et al., *The Arabidopsis rab5 homologs rha1 and ara7 localize to the prevacuolar compartment.* Plant and Cell Physiology, 2004. **45**(9): p. 1211-1220.
224. Freedman, T.S., et al., *A Ras-induced conformational switch in the Ras activator Son of sevenless.* Proceedings of the National Academy of Sciences, 2006. **103**(45): p. 16692-16697.
225. Ahmadian, M.R., et al., *Confirmation of the arginine-finger hypothesis for the GAP-stimulated GTP-hydrolysis reaction of Ras.* Nature structural biology, 1997. **4**(9): p. 686-689.
226. Shao, H. and D.A. Andres, *A novel RalGEF-like protein, RGL3, as a candidate effector for rit and Ras.* Journal of Biological Chemistry, 2000. **275**(35): p. 26914-26924.
227. Blaževitš, O., et al., *Galectin-1 dimers can scaffold Raf-effectors to increase H-ras nanoclustering.* Scientific reports, 2016. **6**(1): p. 24165.
228. Duncan, A.W., et al., *Integration of Notch and Wnt signaling in hematopoietic stem cell maintenance.* Nature immunology, 2005. **6**(3): p. 314-322.
229. Lundmark, R. and S.R. Carlsson, *SNX9–a prelude to vesicle release.* Journal of cell science, 2009. **122**(1): p. 5-11.
230. Sallee, N.A., et al., *The pathogen protein EspFU hijacks actin polymerization using mimicry and multivalency.* Nature, 2008. **454**(7207): p. 1005-1008.
231. Keb, G., et al., *Chlamydia trachomatis TmeA directly activates N-WASP to promote actin polymerization and functions synergistically with TarP during invasion.* Mbio, 2021. **12**(1): p. 10.1128/mbio. 02861-20.
232. Flotho, C., et al., *RAS mutations and clonality analysis in children with juvenile myelomonocytic leukemia (JMML).* Leukemia, 1999. **13**(1): p. 32-37.
233. Wang, X., et al., *Silencing of long noncoding RNA MALAT1 by miR-101 and miR-217 inhibits proliferation, migration, and invasion of esophageal squamous cell carcinoma cells.* Journal of biological chemistry, 2015. **290**(7): p. 3925-3935.
234. Han, P. and C.-P. Chang, *Long non-coding RNA and chromatin remodeling.* RNA biology, 2015. **12**(10): p. 1094-1098.
235. Wei, T. and P.F. Lambert, *Role of IQGAP1 in Carcinogenesis.* Cancers, 2021. **13**(16): p. 3940.
236. Neilsen, B.K., et al., *KSR as a therapeutic target for Ras-dependent cancers.* Expert opinion on therapeutic targets, 2017. **21**(5): p. 499-509.
237. Hauseman, Z.J., et al., *Targeting the SHOC2–RAS interaction in RAS-mutant cancers.* Nature, 2025: p. 1-10.
238. Zhang, J., F. Zhang, and R. Niu, *Functions of Shp2 in cancer.* Journal of cellular and molecular medicine, 2015. **19**(9): p. 2075-2083.
239. Kichina, J.V., A. Maslov, and E.S. Kandel, *PAK1 and therapy resistance in melanoma.* Cells, 2023. **12**(19): p. 2373.

Acknowledgements

Firstly, I would like to express my deepest gratitude to my supervisor, Prof. Reza Ahmadian, for his continuous guidance, scientific insight, and unwavering support throughout the course of my Ph.D. His deep knowledge, scientific curiosity, and relentless motivation have profoundly shaped my research direction and scientific growth. Without you, Reza, finalizing this Ph.D. journey would not have been possible. Thank you for everything. You opened the path, threw me into the ocean, and trusted that I would survive and reach the goal. I am deeply grateful for your incredible trust. I am proud to be your last Ph.D. student and will carry that pride with me for the rest of my life.

I am also sincerely thankful to Prof. Dieter Willbold for serving as my second supervisor and for giving me the opportunity to access and work in his laboratory. I am grateful for his support and his contribution as the second reviewer of this thesis.

My sincere thanks go to Prof. Petra Bauer for her valuable collaboration and insightful input on the TTN5 project.

I would like to extend my heartfelt appreciation to Dr. Lothar Gremer for his exceptional mindset, generosity, and extraordinary scientific quality. His innovative thinking, deep passion for protein biochemistry, and constant enthusiasm for science have been a continuous source of motivation throughout my Ph.D. journey and beyond.

I am grateful to Prof. Johannes H. Hegemann for his trust in me and to Prof. Sander H. J. Smits as well, for their inspiring collaboration on the SemD project.

I am also sincerely thankful to Dr. Lukas Cyganek for our collaboration on the LZTR1 project.

I also wish to thank the entire team at the Institute of Biochemistry and Molecular Biology II at Heinrich Heine University Düsseldorf for providing a supportive environment for my doctoral research. Special thanks to Prof. Jürgen Scheller, Dr. Roland Piekorz, and Dr. Doreen M. Floß for managing the institute and creating an atmosphere in which we could work, grow, and accomplish what we set out to do.

I am especially grateful to all colleagues and friends who have contributed to this journey with their scientific input, encouragement, and friendship. In particular, Petra, your kindness gave me the feeling that I could truly trust people, even far from home. Carmen, thank you for all your support and for always being there to listen when I needed it. I will never forget your generosity and compassion. Fereshteh and Yvonne, your support was always appreciated. Niloufar, your presence at the beginning of this journey made the early days easier. Thank you for your help and for the memories from the first month of my Ph.D. Julia, I could always count on you to discuss science and technical matters, and you helped make the work environment better. Vanshika, Parmis, and Assma, supporting you in your thesis work was a rewarding start to my mentorship experience. Hamid Agha and Puyan, your friendship in Germany was a true gift, and I thank you both for everything.

I would like to thank my father, Hamid, who worked tirelessly to give us a better life until the very last moment of his own. I dedicate this work to you, and I hope I have made you proud. Your strength and sacrifices mean everything to me. I will always be proud of you and truly believe that no one could have been a better father. To my mother, Shahnaz, thank you for your endless prayers, your values, and for teaching me that being a good human matters more than wealth or

academic achievement. I hope I have been a good son to you. To my brother Iman and sister Azam, thank you for reminding me what it means to have a family. Azam, your warmth and support since childhood have always been a comfort. There is truly nothing more valuable in life than family.

Thank you to my parents-in-law, whose kindness and support made me feel like a true part of their family. I never felt like a son-in-law, but like a son. I am proud to have you in my life.

Finally, I thank my wife, my best friend and partner, with whom I have grown and built the life we now share. Thank you for being the wonderful mother of the most fascinating little being in the world, our son Mehrad. There are no words to express what you mean to me or how deeply I value you. Without you, I would not be where I am or who I have become.

And above all, I thank the source of all existence, the light that guided me, the beginning and the end, the origin of every cell and molecule in me, the one whose mercy has never ceased. I thank you for my existence, for the vision, for who I am, and for everything. There are no words to describe how kind and loving you are. I love you, and I wish to draw ever closer to you, to reach clarity, to feel you more fully, and to walk toward you always. I long for the moment when you are satisfied, and I am in the limitless realm where there is only you. Though this truth is already present, I long for the moment when I can fully feel it and find redemption.

Eidesstattliche Erklärung

Ich versichere an Eides Statt, dass die Dissertation von mir selbständig und ohne unzulässige fremde Hilfe unter Beachtung der „Grundsätze zur Sicherung guter wissenschaftlicher Praxis an der Heinrich-Heine-Universität Düsseldorf“ erstellt worden ist. Diese Dissertation wurde in der vorgelegten oder einer ähnlichen Form noch bei keiner anderen Institution eingereicht und es wurden bisher keine erfolglosen Promotionsversuche von mir unternommen.

Düsseldorf, May 2025

Amin Mirzaiebadizi